

**HETEROGENEOUS NO_x CHEMISTRY IN POLLUTED URBAN ATMOSPHERES:
IMPLICATIONS FOR THE FORMATION OF PARTICLES AND OZONE AND
CONTROL STRATEGY DEVELOPMENT**

Final Report
Contract No. 00-323

Prepared for:

California Air Resources Board and the
California Environmental Protection Agency
Research Division
P.O. Box 2815
Sacramento, CA 95812

Prepared by:

Principal Investigator: Barbara J. Finlayson-Pitts
Principal Scientist: Lisa M. Wingen

Researchers: Yael Dubowski
Kevin A. Ramazan
Armando M. Rivera-Figueroa
Ann Louise Sumner
Dennis Syomin

Donald Dabdub (Department of Mechanical and
Aerospace Engineering)
Angel Jimenez-Aranda
Eladio Knipping

Department of Chemistry
University of California, Irvine
Irvine, CA 92697-2025

January 30, 2004

Disclaimer

The statements and conclusions in this Report are those of the contractor and not necessarily those of the California Air Resources Board. The mention of commercial products, their source, or their use in connection with material reported herein is not to be construed as actual or implied endorsement of such products.

ACKNOWLEDGEMENTS

The authors are grateful to the California Air Resources Board (Contract No. 00-323) for support of this work. Kevin Ramazan was also supported for one quarter by the GAANN fellowship (Graduate Assistance in Areas of National Need) from the Department of Energy. The authors would like to thank Professor Ken Shea, D. Batra and K. R. Muroya for assistance with the BET surface area measurements, Erik Menke and Professor Reg Penner for the AFM images, John Newberg and Professor John Hemminger for the XPS data, Professor Jim Rutledge for loan of the contact angle apparatus, Dr. Rachel Hoffman for providing mass spectrometry data on water uptake, and Jorg Meyer for glassblowing. The authors would also like to thank P. R. Griffiths, J. P. Devlin, G. E. Ewing, G. Lammel, V. Grassian, N. Saliba, and J. N. Pitts, Jr. for helpful discussions.

This Report was submitted in fulfillment of ARB Contract No. 00-323, "Heterogeneous NO_x Chemistry in Polluted Urban Atmospheres: Implications for the Formation of Particles and Ozone and Control Strategy Development", under the sponsorship of the California Air Resources Board. Work was completed as of January 30, 2004.

TABLE OF CONTENTS

	Page
LIST OF FIGURES	i
LIST OF TABLES	vi
ABSTRACT	vii
EXECUTIVE SUMMARY	viii
1. INTRODUCTION	1
2. METHODS AND MATERIALS	7
I. ANALYTICAL METHODS AND EQUIPMENT	7
I.A. Water Uptake Cell	7
I.B. Long Path Infrared Cells	7
I.C. Porous Glass Cell Used for Porous Glass and Silica Pellet Studies	8
I.D. ATR Probe	9
I.E. LP-ATR Chamber	9
II. EXPERIMENTAL PROCEDURES	11
II.A. Water Uptake on Surfaces Relevant to Laboratory Studies	11
II.A.1. Water Contact Angle	11
II.A.2. Surface Characterization	11
II.A.3. Water Uptake Measurements	11
II.A.4. X-Ray Photoelectron Spectroscopy	13
II.B. Heterogeneous NO ₂ Hydrolysis Experiments	13
II.B.1. Gas Phase Measurements	13
II.B.2. Surface Species Measurements	14
II.C. LP-ATR Studies of NO ₂ Hydrolysis	14
II.D. Photochemical Production of HONO	15
II.D.1. Experimental Procedures	15
II.D.2. Modeling	18
II.E. HONO Decomposition Experiments	22
II.F. Studies of the Renoxification of Nitric Acid	22
III. MATERIALS	24
3. RESULTS	28

I.	WATER UPTAKE ON SURFACES RELEVANT TO LABORATORY STUDIES	28
I.A.	Contact Angles for the Surfaces with Water.....	29
I.B.	AFM Measurements of the Surface Morphology	30
I.C.	Infrared Measurements of Water Uptake.....	33
I.D.	XPS Analysis of Surfaces	38
I.E.	Discussion.....	39
I.F.	Atmospheric Implications.....	43
II.	MECHANISM OF THE HETEROGENEOUS REACTION OF NO ₂ WITH WATER	44
II.A.	Background.....	44
II.B.	A New Mechanism for HONO Formation from the Reaction of NO ₂ with Water on Surfaces.....	45
II.C.	Present and Prior Observations: Testing the Mechanism	46
II.C.1.	Products, Intermediates, and Mass Balance	46
II.C.1a.	Gas Phase Products.....	46
II.C.1b.	Surface Species.....	48
i.	N ₂ O ₄	48
ii.	Nitric acid and Nitric Acid-Water Hydrates.....	50
II.C.2.	Kinetics.....	55
II.C.2a.	Rate of NO ₂ Hydrolysis Reaction.....	55
II.C.2b.	Reaction Order.....	57
i.	Reaction Order with Respect to Water Vapor	57
ii.	Reaction Order with Respect to NO ₂	59
II.D.	Mechanisms and Models.....	65
II.E.	Atmospheric Implications.....	74
II.E.1.	Polluted Urban Environments.....	74
II.E.2.	Airborne Particles and Clouds	79
II.E.3.	Indoors	80
II.E.4.	Snowpacks	80
III.	THE USE OF ATTENUATED TOTAL REFLECTANCE SPECTROSCOPY TO PROBE INTERFACE SPECIES	81
IV.	LP-ATR STUDIES OF NO ₂ HYDROLYSIS.....	81
V.	HONO DECOMPOSITION	86
V.A.	Introduction.....	86
V.B.	Experiments in an HNO ₃ -Conditioned Cell.....	88
V.C.	Experiments in an Unconditioned Cell.....	89
V.D.	Discussion.....	93
V.E.	Atmospheric Implications.....	100
VI.	PHOTOCHEMICAL PRODUCTION OF HONO.....	100
VI.A.	Introduction.....	100

VI.B. Results and Discussion	102
VI.C. Conclusions.....	107
VII. LABORATORY STUDIES OF POTENTIAL MECHANISMS OF RENOXIFICATION OF TROPOSPHERIC NITRIC ACID	107
VII.A. Introduction.....	107
VII.B. Heterogeneous Reaction of NO with HNO ₃ on Silica Surfaces	109
VII.C. Heterogeneous Reactions of CO, CH ₄ and SO ₂ with Adsorbed HNO ₃	113
VII.D. Role of Surface Materials in Renoxification in the Boundary Layer ...	115
VIII. MODELING THE IMPACTS OF RENOXIFICATION ON TROPOSPHERIC OZONE	117
4. DISCUSSION	121
5. SUMMARY AND CONCLUSIONS	125
6. RECOMMENDATIONS.....	128
REFERENCES	129
LIST OF PUBLICATIONS	139
GLOSSARY OF TERMS, ABBREVIATIONS, AND SYMBOLS	140
APPENDIX.....	144

LIST OF FIGURES

1. INTRODUCTION

Figure 1.1.	Summary of some of the literature reported rates for the heterogeneous hydrolysis of NO_2 as a function of the surface-to-volume (S/V) ratio of the reactor.....	4
-------------	---	---

2. METHODS AND MATERIALS

Figure 2.1.	Glass cell used for measurements of water uptake on glass and other surfaces.....	7
Figure 2.2.	Schematic diagram of the ATR probe used for FTIR characterization of thin films.....	9
Figure 2.3.	Schematic of the LP-ATR chamber used to study the kinetics and mechanisms of heterogeneous reactions.....	10
Figure 2.4.	Typical data for the loss of NO_2 during photolysis plotted in the form of equation (I).....	17
Figure 2.5.	A typical first order plot for the photolysis of 1.2 ppm HONO in the presence of 135 ppm of cyclohexane.....	18

3. RESULTS

Figure 3.1.	Loss of NO_2 and formation of HONO from the heterogeneous hydrolysis of NO_2 on the surface of a 561 L chamber at 24°C coated with halocarbon wax using the dip method. Measurements were made using differential optical absorption spectrometry (DOAS). Initial concentration of NO_2 was 38.6 ppm and the RH was 85%.....	29
Figure 3.2.	Contact angle measurements of a $1\mu\text{L}$ water droplet on three typical surfaces: (a) halocarbon wax coated using the dip method, (b) untreated borosilicate glass, and (c) plasma-cleaned borosilicate glass.....	30
Figure 3.3.	AFM measurements (in non-contact mode) of the surface morphology for (a) untreated borosilicate glass; (b) untreated quartz; (c) borosilicate glass cleaned using hot H_2O_2 ; (d) borosilicate glass coated with the C8 SAM.....	32
Figure 3.4.	AFM measurements (in non-contact mode) of the surface morphology for (a) borosilicate glass coated with halocarbon-wax using the dip method; (b) borosilicate glass coated using the solvent method and (c) FEP Teflon film.....	33
Figure 3.5.	Infrared spectra of surfaces in contact with N_2 at 80% RH and, for comparison, the spectrum of bulk liquid water: (1) bulk water (a, right axis), untreated glass (b), quartz (c); (2) H_2O_2 cleaned glass (d), plasma cleaned glass (e), and water rinsed glass (f); (3) dip method halocarbon wax	

	(g, right axis), solvent method halocarbon wax (h), C8 monolayer (i), and FEP Teflon film (j). The bulk water spectrum (1a) was obtained by measuring the IR transmission through a drop of water “sandwiched” between two ZnSe windows ratioed to the bare windows34
Figure 3.6.	Water uptake isotherms for (a) smooth untreated glass (solid circles) and quartz (open triangles); (b) water rinsed glass (open diamonds), and plasma cleaned glass (solid squares); and (c) dip method (open circles) and solvent method (asterisks) halocarbon wax coated glass. An exponential fit of the untreated borosilicate glass data in (a) is included in each panel (dashed black line) as a guide to the eye. The solid lines are fits to each set of data, excluding the solvent method halocarbon wax, which falls on the fit for untreated glass. The dip method halocarbon wax data points (panel (c)) were taken after two hours equilibration time, although water uptake was still increasing for the high RH experiments (see text and Figure 3.8)....36
Figure 3.7.	Relative intensity of the liquid water peak, integrated from 2600 - 4000 cm^{-1} , on H_2O_2 -cleaned borosilicate glass surface (triangles) as a function of relative humidity. The solid line is a fit to the data. Also shown for comparison is the isotherm for water uptake on untreated glass and the fit shown in Figure 3.6a as a guide37
Figure 3.8.	Water uptake on halocarbon wax, (dip method) as a function of the exposure time to humidified nitrogen between 20% and 81% RH. The lines show fits to the data37
Figure 3.9.	XPS analysis of the surfaces of quartz, untreated borosilicate glass, borosilicate glass rinsed with Nanopure water, plasma-cleaned borosilicate glass, and H_2O_2 -cleaned borosilicate glass. The molar ratios of various elements relative to oxygen are shown.....38
Figure 3.10.	Model Type II ($c_B = 20$) and Type III ($c_B = 0.1$) BET isotherms described by equation (III).....40
Figure 3.11.	AFM images of (a) a green ivy leaf surface with an RMS surface roughness of 195 Å and (b) a <i>Vinca minor</i> flower petal with an RMS surface roughness of 51 Å.....43
Figure 3.12.	Schematic diagram of proposed mechanism of heterogeneous hydrolysis of NO_245
Figure 3.13.	Concentration-time profiles for NO_2 hydrolysis experiments in this laboratory at (a) 21% RH, $[\text{NO}_2]_0 = 1.5 \times 10^{15}$ molecule cm^{-3} , (b) 48% RH, $[\text{NO}_2]_0 = 1.4 \times 10^{15}$ molecule cm^{-3} , (c) 80% RH, $[\text{NO}_2]_0 = 2.5 \times 10^{15}$ molecule cm^{-3} . The corresponding yields of gas phase HONO, NO and N_2O , expressed relative to the measured losses of NO_2 , are shown in parts (d-f). As discussed in the text, the experiments at 21% and 48% RH were carried out in the 7.4 L cell and that at 80% in the 19.4 L cell47
Figure 3.14.	Spectra of porous glass discs:(a) Exposed to gaseous HNO_3 followed by pumping and then adding 1.2 Torr NO_2 ; (b) Porous glass exposed to 1.3 Torr NO_2 only; (c) Difference spectrum (a - 0.92b). All experiments carried out in 1 atm N_2 using 64 scans at 1 cm^{-1} resolution. Background used for spectra was that of the unexposed porous glass50

Figure 3.15.	Spectra of porous glass exposed to (a) water vapor and (b) water vapor and nitric acid after pumping times of 0, 5, 10, and 35 s. The insets show expanded regions for absorptions by (c) H ₂ O and (d) HNO ₃ , H ₂ O and complexes between the two.....	53
Figure 3.16.	Spectra of NO ₂ ⁺ on porous glass surface (a) during heterogeneous NO ₂ hydrolysis; (b) after exposure to gaseous HNO ₃ , and (c) after exposure to H ¹⁵ NO ₃	54
Figure 3.17.	Initial rates of HONO (□) formation (in 19.4 L cell) and NO (Δ) formation (in 7.4 L cell) as a function of relative humidity at 295 ± 2 K. The NO rates have been multiplied by 10 ⁻⁷ to adjust to scale. The solid line is a fit through the combined data sets for the rates of HONO and NO formation. The number of effective layers of water measured on a smooth borosilicate glass surface are shown for comparison (right axis and × symbols) (<i>Sumner et al., 2004</i>).....	58
Figure 3.18.	First and second order Type A kinetics plots for the loss of NO ₂ at (a) 21% RH, [NO ₂] ₀ = 1.5×10 ¹⁵ molecule cm ⁻³ , (b) 48% RH, [NO ₂] ₀ = 1.4×10 ¹⁵ molecule cm ⁻³ , (c) 80% RH, [NO ₂] ₀ = 2.4×10 ¹⁵ molecule cm ⁻³ . As discussed in the text, the experiments at 21% and 48% RH were carried out in the 7.4 L cell and that at 80% in the 19.4 L cell.....	63
Figure 3.19.	Plots of (a) log(d[HONO]/dt) and (b) log(-d[NO ₂]/dt) vs log[NO ₂] ₀ for experiments carried out in the 19.4 L glass long path cell in this laboratory at 21% (◆), 48% (▲), and 80% (●) RH. The slopes (± 2s) are reaction order in NO ₂ calculated using the initial rates of HONO formation or NO ₂ loss (see text).....	64
Figure 3.20.	Comparison of model predicted loss of NO ₂ and formation of HONO and NO to experimental data for typical runs at (a) 20% RH, (b) 50% RH and (c) 80% RH	73
Figure 3.21.	Water uptake on some common materials found in the boundary layer. Adapted from Lammel (<i>1999</i>).....	76
Figure 3.22.	Initial rates of generation of HONO measured in several studies, normalized to a S/V of 3.4 m ⁻¹ and water vapor concentration of 3.6 × 10 ¹⁷ cm ⁻³ used in the studies by Pitts <i>et al.</i> (<i>1984</i>) • Pitts <i>et al.</i> (<i>1984</i>); □ Sakamaki <i>et al.</i> (<i>1983</i>); + Svensson <i>et al.</i> (<i>1987</i>) rates divided by 10; × Svensson <i>et al.</i> (<i>1987</i>) experiment at 54% RH; ◆ This work, 19.4 L cell; ♦ This work, 7.4 L cell.....	77
Figure 3.23.	Gas phase data (time profiles and yields) obtained during NO ₂ hydrolysis experiments in the LP-ATR chamber at 20 % RH (a – b), 50% RH (c – d), and 80% RH (e – f).....	83
Figure 3.24.	ATR surface data corresponding to Fig. 3.37 obtained during NO ₂ hydrolysis experiments in the LP-ATR chamber at (a) 20%, (b) 50%, and (c) 80% RH.....	84
Figure 3.25.	Comparison of ATR spectra in the presence (a) and absence of organics (b) with HNO ₃ and NO ₃ ⁻ reference spectra. (a) Solid spectrum taken at t = 30 min. during 50% RH NO ₂ hydrolysis experiment in the LP-ATR chamber with organics present on the walls (left axis), (b) Solid spectrum taken at t = 30 min. during 50% RH NO ₂ hydrolysis experiment in a clean 1.75 L	

	glass chamber (left axis). The dotted line is a dry HNO ₃ reference ATR spectrum (right axis). The dash-dotted line is an ATR spectrum of aqueous NO ₃ ⁻ (0.1 M NaNO ₃) (right axis)	85
Figure 3.26.	Concentration time-profiles of HONO (◆), NO ₂ (●) and NO (Δ) and corresponding plots of log(-d[HONO] _o /dt) vs. log[HONO] _o of HONO decay experiments at ~0% (a, b), 20% (c, d) and 50% RH (e, f) in the HNO ₃ conditioned cell. Based on the known equilibrium constant for 2 HONO ↔ NO + NO ₂ + H ₂ O (<i>Chan et al., 1976a, b</i>) equilibrium is not attained within the reaction times used here	88
Figure 3.27.	Concentration time-profiles of HONO (◆), NO ₂ (●) and NO (Δ) and corresponding plots of log(-d[HONO] _o /dt) vs. log[HONO] _o of HONO decay experiments at ~0% (a, b), 20% (c, d) and 50% (e, f) RH in the unconditioned cell. Based on the known equilibrium constant for 2 HONO ↔ NO + NO ₂ + H ₂ O (<i>Chan et al., 1976a, b</i>), equilibrium is not attained within the reaction times used here	90
Figure 3.28.	Concentration-time profile of HONO in the HONO-conditioned cell at 50% RH and 1 atm in N ₂ . Before the experiment, the cell was exposed at 50% RH for 1 hour to 13 ppm of HONO that contained 28 ppm of NO ₂ and 60 ppm of NO as impurities. The cell was then pumped out before the water vapor-N ₂ mixture was added	93
Figure 3.29.	Schematic of the reaction mechanism of the heterogeneous hydrolysis of NO ₂ proposed by Finlayson-Pitts <i>et al. (2003)</i> with the inclusion of competitive adsorption between water and HONO (<i>Syomin and Finlayson-Pitts, 2003</i>)	101
Figure 3.30.	Experimental concentration-time profiles for NO ₂ (●), HONO (◆), and NO (▼) with 46 ppm initial [NO ₂] and 39% RH in 1 atm N ₂ at 296 K. The error bar on the HONO concentration is ± 2s	102
Figure 3.31.	Comparison of experimental data (symbols) and model-predicted (solid lines) concentration-time profiles for NO ₂ (●), HONO (◆), and NO (▼) with (a) 20 ppm initial [NO ₂] and 33% RH in N ₂ (b) 46 ppm initial [NO ₂] and 39% RH in N ₂ (c) and 54 ppm initial [NO ₂] and 57% RH in N ₂	103
Figure 3.32.	Experimental data (symbols) and model-predicted (lines) concentration-time profiles for NO ₂ (●), HONO (◆), and NO (▼) with 46 ppm initial [NO ₂] and 39% RH in N ₂ . The dotted line indicates the model prediction for HONO with the inclusion of photolysis of adsorbed HNO ₃ , reaction (35). The error bar on the HONO concentration is ± 2s.....	104
Figure 3.33.	Experimental data (symbols) and model-predicted (lines) concentration-time profiles for NO ₂ (●), HONO (◆), and NO (▼) of (a) 45 ppm initial [NO ₂] and 46% RH in N ₂ and (b) 46 ppm initial [NO ₂] and 48% RH in air. The dotted line indicates the concentration of HONO with the inclusion of surface-adsorbed HNO ₃ photolysis in model. The error bar on the HONO concentration is ± 2s.....	106
Figure 3.34.	(a) Spectrum of the gas phase plus surface adsorbed HNO ₃ on silica in the 1300 – 1800 cm ⁻¹ region. Bands at 1677, 1400, and 1313 cm ⁻¹ are due to molecular HNO ₃ adsorbed on the surface, and the broad peak at the low	

wavenumber side of the 1677 cm^{-1} peak is due to adsorbed water. The peaks at 1352 and 1525 cm^{-1} are due to the ν_3 asymmetric stretching vibration of NO_3^- ; (b) Immediately after the introduction of 9.7×10^{16} NO molecule cm^{-3} , and (c) 65 minutes later. Gas phase NO_2 (1617 cm^{-1}) and surface N_2O_4 (1745 cm^{-1}) are observed upon reaction 110

- Figure 3.35. (a) Spectrum from 65 min. reaction time (Figure 3.32c) after subtraction of the initial spectrum of adsorbed HNO_3 ($0.07 \times$ initial spectrum, Fig. 3.32a); also shown is a reference spectrum of gas phase NO_2 (3.2×10^{16} molecule cm^{-3}). (b) Difference spectrum after subtraction of gaseous NO_2 ($1.35 \times$ reference spectrum in Fig. 3.33a). (c) Spectrum of water adsorbed on silica pellet 112
- Figure 3.36. Modeled and observed ozone concentrations in the South Coast air basin for Aug. 27 – 28, 1987 with and without renoxification for (a) central Los Angeles, CA, (b) Riverside, CA, and (c) San Bernardino, CA 119
- Figure 3.37. Modeled and observed maximum ozone concentrations as a function of NO_x “scaling factor” (see text) in the South Coast air basin for Aug. 28, 1987 with and without renoxification for (a) central Los Angeles, CA and (b) Riverside, CA 120

LIST OF TABLES

2. METHODS AND MATERIALS

Table 2.1.	Volume and surface area measurements of the long path cells.....	8
Table 2.2.	Chemical reactions in model	20
Table 2.3.	Samples used for water uptake measurements and surface characterization	25

3. RESULTS

Table 3.1.	Summary of contact angle and AFM measurements.....	31
Table 3.2.	Reanalysis of some kinetics data reported in the literature on heterogeneous NO ₂ hydrolysis on the surfaces of laboratory systems (Teflon, glass, quartz, acid solutions, aerosol particles)	60
Table 3.3.	Comparison of rates of HONO generation in this work with some previous studies as a function of the initial NO ₂ concentration	78
Table 3.4.	Summary of HONO decomposition experiments	91

ABSTRACT

Experimental laboratory studies of heterogeneous reactions of oxides of nitrogen were carried out using a variety of spectroscopic techniques. This included the development and application of a new chamber that combines long path infrared analysis for gases with attenuated total reflectance infrared analysis for simultaneous measurement of the chemistry occurring in the thin surface film. The reactions studied included the heterogeneous hydrolysis of NO_2 to form gas phase HONO and surface-adsorbed HNO_3 , “renoxification” reactions of adsorbed nitric acid with NO to regenerate NO_2 and the effects of light on the production of gas phase HONO. The nature of the thin water film on the surface that provides the milieu for this chemistry was also explored and the changes in the film characterized as a function of relative humidity. Finally, the interactions of gas phase HONO itself with surfaces were explored and it was shown that a competition between HONO and water for surface sites is a major determinant of how much HONO is released to the gas phase. Preliminary airshed modeling of the renoxification process suggests that such chemistry may be significant in determining ozone and particle concentrations in polluted urban atmospheres and highlights the importance of including heterogeneous reactions in the boundary layer in current airshed models.

EXECUTIVE SUMMARY

Background. Oxides of nitrogen play a central role in air pollution in California, and indeed, worldwide. Not only do many of the chemical compounds that fall into this category have health effects themselves, but they also react in air to form ozone (O_3), particles and a host of other secondary air pollutants. Accurate modeling of the formation of these secondary air pollutants requires accurate and detailed knowledge of the chemistry involved, both in terms of the rates of the reactions as well as the intermediates and products formed. Without such knowledge, the application of models to determine air pollution control strategies is doomed to have unacceptably large uncertainties. The gas phase chemistry of oxides of nitrogen and volatile organic compounds is reasonably well known and represented in airshed models. However, the same is not true for heterogeneous reactions on surfaces found in the boundary layer. For example, it is known that reactions of oxides of nitrogen on surfaces are the major source of nitrous acid (HONO) in air. Nitrous acid is the major source at dawn of the highly reactive hydroxyl free radical that initiates photochemical smog formation; in fact, HONO is a major source of hydroxyl radicals even when all sources are considered over an entire day. Unfortunately, because such heterogeneous reactions have not been understood, they are not included in airshed models, despite the critical role they play in the formation of photochemical air pollution. The overall goal of this research was to provide some of the fundamental kinetic and mechanistic data for heterogeneous oxides of nitrogen that are needed to assess their importance in urban areas in California.

Methods. The methodology involved experimental studies of the reactions of oxides of nitrogen on surfaces that are characteristic of those used in laboratory systems (*e.g.*, smog chambers) as well as those found in urban areas. The loss of reactants and the formation of intermediates and products were followed in laboratory studies using spectroscopic methods. In some studies, the techniques were such that the gases could be measured and in others, species adsorbed on the surface were followed. A major advance was the development and application of a chamber in which both the gas phase and the surface could be followed simultaneously. In addition, studies using several different methods that can provide information on the physical morphology of surfaces and on their chemical composition were carried out in collaborative work with colleagues in the Department of Chemistry at UCI at no cost to this contract. The combination of these methods were applied to studying (1) the heterogeneous hydrolysis of nitrogen dioxide (NO_2) to form HONO; (2) the formation of nitric acid (HNO_3) on the surface during the heterogeneous NO_2 hydrolysis; (3) the reaction of HNO_3 on the surface with nitric oxide (NO) to regenerate NO_2 , a "renoxification" process with important control strategy implications; (4) the nature of the thin water film on the surface that provides the milieu for this chemistry; (5) the potential for the formation of HONO through photochemical reactions on surfaces; and (6) the nature of the interaction of HONO with surfaces. Some preliminary airshed modeling studies were also carried out to investigate the importance of the renoxification reaction.

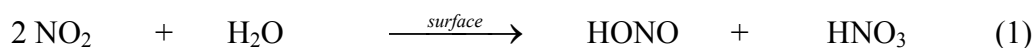
Results. These studies provide the most comprehensive treatment of the heterogeneous reactions of oxides of nitrogen carried out to date. This work establishes that there are a number of important intermediates on the surface that are involved in the formation of HONO; these include the NO_2 dimer, N_2O_4 , undissociated molecular HNO_3 and its complexes with water, the

nitrosonium and nitronium ions, adsorbed HONO and nitrate ions. The simultaneous presence of organic compounds on the surface does not significantly change the chemistry. The relative amounts of the various surface species depends critically on the amount of water on the surface, and this is determined by the gas phase water vapor concentration, i.e., the relative humidity (RH). For example, at intermediate RH (~50%), the HNO₃ on the surface reacts with NO to regenerate NO₂. This renoxification process converts HNO₃ back to photochemically active forms, so that deposition of HNO₃ is no longer a permanent sink as assumed in current models. This will lead to increased levels of O₃, particles and associated secondary air pollutants. Preliminary airshed modeling that includes this renoxification suggests that it will lead to significantly higher O₃ levels throughout the Southern California air basin, and may change the shape of the VOC-NO_x isopleths compared to those without this heterogeneous chemistry. This research also established that the heterogeneous hydrolysis of NO₂ on surfaces to form HONO is not itself enhanced by light, as had been suggested by earlier studies. However, it appears likely that light does interact with the intermediates of this reaction on surfaces, likely HNO₃ or its associated species, to generate HONO during the day as suggested by recent studies by Zhou *et al.* Finally, this research has shown that HONO is not only formed by reactions on surfaces, but also reacts further on surfaces to generate gas phase NO, NO₂ and likely surface species such as HNO₃ as well. An important finding is that there appears to be a competition between HONO and water for adsorption sites on the surface; this means that HONO can remain adsorbed on surfaces and subsequently be released into the gas phase when the RH increases. Thus, surfaces in the urban boundary layer likely act as reservoirs of HONO so that it is not only real-time heterogeneous chemistry that determines the amount of gas phase HONO, but also the previous history of the surface itself and in particular, its capacity to store HONO.

Conclusions. Reactions of oxides of nitrogen on surfaces play a critical role in the formation of photochemical air pollution, including O₃, particles and a host of secondary air pollutants. While these reactions are not included in current airshed models, preliminary modeling results suggest they could be quite significant. Of particular interest from these studies are the renoxification of HNO₃ adsorbed on surfaces back to photochemically active forms, the photolysis of adsorbed HNO₃ and/or associated species to form gas phase HONO and the ability of surfaces to act as reservoirs of HONO. Recommendations for future work include more detailed studies of the ability of various surfaces to act as HONO reservoirs, of the mechanism of NO formation from the surface reaction of HONO, of the mechanism and kinetics of the light-induced HONO formation by photolysis of surface-adsorbed oxides of nitrogen such as HNO₃, and introduction of all of this heterogeneous chemistry of oxides of nitrogen into airshed models in order to probe fully the impacts on the formation of O₃, acids and associated secondary air pollutants.

1. INTRODUCTION

It has been known for more than half a century that a number of reactions of nitrogen oxides that are slow in the gas phase do occur at significant rates on the surfaces of laboratory systems. One of the best known examples is the reaction of hydrolysis of nitrogen dioxide (NO₂), where the overall stoichiometry is represented by reaction (1):



This reaction is of particular interest in atmospheric chemistry because it generates nitrous acid (HONO), a major source of hydroxyl radical (OH) in polluted urban atmospheres (*Perner and Platt, 1979; Platt et al., 1980; Calvert et al., 1994; Winer and Biermann, 1994; Harrison et al., 1996; Lammel and Cape, 1996; Lammel, 1999; Finlayson-Pitts and Pitts, 2000; Kotamarthi et al., 2001; Schiller et al., 2001; Aliche et al., 2002; Stutz et al., 2002a*). Since OH initiates the chemistry that leads to the formation of ozone (O₃) and other air pollutants, it is important to determine which OH precursors are significant in order to accurately model urban airsheds and to develop regional control strategies. A number of studies have shown that HONO is a major OH source when compared to other well known sources of OH such as the photolysis of O₃ and formaldehyde (HCHO), and the dark reaction of O₃ with alkenes; this is the case not only at dawn, but even when averaged over the entire day. The formation of HONO by reaction (1) indoors has also been observed (*Pitts et al., 1985; 1989; Brauer et al., 1990; Febo and Perrino, 1991; Spengler et al., 1993; Spicer et al., 1993; Vecera and Dasgupta, 1994; Weschler et al., 1994; Wainman et al., 2001*) and is of concern since it can lead to human respiratory tract irritation (*Rasmussen et al., 1995*) and can react with amines in air to form carcinogenic nitrosamines (*Pitts et al., 1978*).

There are a number of excellent reviews of potential mechanisms of HONO formation in the troposphere (*Calvert et al., 1994; Harrison et al., 1996; Lammel and Cape, 1996; Lammel, 1999*). While reaction (1) is believed to be a major contributor to HONO formation in air, there are other sources, including direct emissions from fossil fuel combustion (*Pitts et al., 1984b; 1989; Brauer et al., 1990; Febo and Perrino, 1991; Spicer et al., 1993; Vecera and Dasgupta, 1994; Kirchstetter et al., 1996; Kurtenbach et al., 2001*). Another potential source is the reaction of soot surfaces with NO₂ (*Ammann et al., 1998; Gerecke et al., 1998; Kalberer et al., 1999; Kleffmann et al., 1999; Longfellow et al., 1999; Al-Abadleh and Grassian, 2000; Alcalá-Jornod et al., 2000; Stadler and Rossi, 2000; Arens et al., 2001*). However, it appears that the soot surface deactivates with time, which would limit the amount of HONO that can be generated from this reaction. A recent study suggests that it is the semi-volatile and/or water-soluble organics generated in diesel exhaust that lead to significant HONO formation from NO₂, rather than the soot surface itself (*Gutzwiller et al., 2002*).

Modeling studies combined with measurements of HONO and its precursors in urban areas suggest that the reaction (2) of NO, NO₂ and water is a HONO source (*Calvert et al., 1994*).



In contrast, the addition of NO to the NO₂-H₂O mixture in laboratory studies does not affect the reaction and, therefore, it is generally thought that reaction (2) is not important (*Wayne and Yost, 1951; Graham and Tyler, 1972; Carter et al., 1982; Sakamaki et al., 1983; Pitts et al., 1984a; Svensson et al., 1987; Jenkin et al., 1988; Perrino et al., 1988; Wiesen et al., 1995; Gerecke et al., 1998; Kleffmann et al., 1998a*).

The gas phase reaction of OH with NO also generates HONO. However, since most of the OH sources are photolytic, this reaction is most important during the day when HONO efficiently photolyzes back to OH + NO (*Finlayson-Pitts and Pitts, 2000*). Similarly, the reaction of HO₂ with NO₂ generates HONO, but is not likely to be a significant source of atmospheric HONO due to its small rate constant (*Tyndall et al., 1995*) and competing daytime photolysis.

Photochemical formation of HONO in snowpacks has been identified in the Arctic following irradiation of surface snow with either natural sunlight or a xenon arc lamp with a Pyrex glass filter ($\lambda > 280$ nm) (*Zhou et al., 2001; Dibb et al., 2002*). *Zhou et al. (2001)* proposed that photolysis of NO₃⁻ present in the snow forms predominantly O⁻ and NO₂ at the air-ice interface, with the NO₂ hydrolyzing to nitrite and nitrate ions in a reaction equivalent to reaction (1):



When the snow surface is acidic, NO₂⁻ is converted to HONO which then escapes to the gas phase. Despite the fast photolysis of HONO occurring during daylight hours, the researchers observed up to 10 ppt HONO near the surface under ambient conditions. The generation of OH in snowpacks, either through the reaction of O⁻ with water or the photolysis of HONO, is important since it leads to oxidation of organics and the generation of such species as HCHO (*Sumner and Shepson, 1999*).

There are also several reports of enhanced HONO formation in the presence of UV radiation. A photoenhancement of HONO formation from heterogeneous NO₂ hydrolysis was reported by *Akimoto et al. (1987)* using a Teflon-coated smog chamber. More recently, *Zhou et al. (2002; 2003)* reported evidence for a photochemical production of HONO from HNO₃ adsorbed on silicate surfaces. Such enhancements would lead to increased OH and, hence, O₃ production during the daytime, and are clearly important to include in airshed models which aim to predict O₃. However, little is known about the mechanism(s) of these additional sources of HONO.

In summary, it is generally believed that reaction (1) is a significant source of HONO, and hence OH. Current urban airshed models often include a simple parameterization of reaction (1) based on rates observed experimentally in some laboratory systems. However, this treatment may not be appropriate given the complexity of the reaction, the important role of the surface and species adsorbed on it, and how the surface composition changes during experiments. It is clearly critical to understand the reaction on a molecular level in order to accurately include it in airshed models that are used to develop air pollution control strategies. In addition, understanding this chemistry will contribute to the elucidation of the photochemistry in snowpacks. Finally, this chemistry may occur on surfaces of airborne dust particles that are known to be transported globally and to play a role in the chemistry of the global troposphere (*Prospero and Nees, 1977; Prospero et al., 1981; Prospero and Nees, 1986; Dentener et al., 1996; Gillette, 1997; Perry et al., 1997; Zhang et al., 1997; Prospero, 1999; Zhang and Carmichael, 1999; deReus et al., 2000; Clarke et al., 2001*).

A number of studies have established that reaction (1) is negligible in the gas phase but occurs in the presence of surfaces (*Wayne and Yost, 1951; Cathala and Weinrich, 1952; Peters and Holman, 1955; Goyer, 1963; England and Corcoran, 1974; TenBrink et al., 1978; Sakamaki et al., 1983; Pitts et al., 1984a; Akimoto et al., 1987; Svensson et al., 1987; Jenkin et al., 1988; Perrino et al., 1988; Febo and Perrino, 1991; Bambauer et al., 1994; Wiesen et al., 1995; Harrison and Collins, 1998; Kleffmann et al., 1998a, b; Chou et al., 1999; Goodman et al., 1999; Barney and Finlayson-Pitts, 2000; Kurtenbach et al., 2001*). Figure 1.1 summarizes the results of a number of these studies in terms of the measured rates of reaction as a function of the surface-to-volume (S/V) ratio of the reaction cells used. This plot shows the combined formation rates of HONO plus NO (a secondary reaction product of HONO) normalized for the different initial NO₂ and water vapor concentrations used in the various studies. An increase in the rates with S/V is expected for a surface reaction where there are a given number of product molecules formed per second per unit surface area. For large reactors (small S/V), the product is diluted into a larger volume, giving a smaller increase in the product *concentration* per unit time compared to smaller reaction chambers. Thus, the trend to larger reaction rates with larger S/V ratios seen in the data shown in Figure 1.1 is consistent with expectations for a heterogeneous reaction on the chamber surface.

While the experimental results are not uniformly in quantitative agreement, there are a number of common observations of NO₂ studies in the dark:

- (1) Three gas phase products have been observed. The major gas phase product is HONO, but the yield is usually less than the 50% expected from reaction (1) (*TenBrink et al., 1978; Sakamaki et al., 1983; Pitts et al., 1984a; 1985; Svensson et al., 1987; Jenkin et al., 1988; Perrino et al., 1988; Wiesen et al., 1995; Kleffmann et al., 1998a, b; Wainman et al., 2001*). NO is the other significant gaseous product (*England and Corcoran, 1974; TenBrink et al., 1978; Sakamaki et al., 1983; Pitts et al., 1984a; Svensson et al., 1987; Wainman et al., 2001*); in some studies (*Sakamaki et al., 1983*), NO was reported to be formed simultaneously with HONO, while in others (*Pitts et al., 1984a*) it was observed only at longer reaction times. Small quantities of N₂O are also formed (*Wiesen et al., 1995; Kleffmann et al., 1998a*).

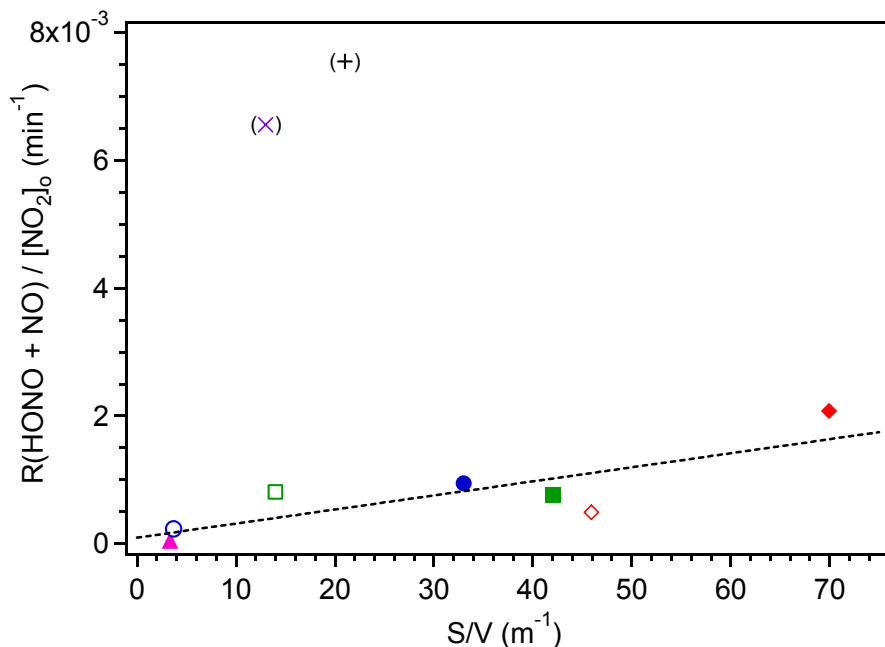


Figure 1.1. Summary of some of the literature reported rates for the heterogeneous hydrolysis of NO₂ as a function of the surface-to-volume (S/V) ratio of the reactor. The Y-axis is the total rate of HONO plus NO formation normalized to 1 ppm NO₂ and 50% relative humidity. ▲ Pitts *et al.* (1984): Teflon-coated chamber at 24°C and 50% RH (S/V=3.4 m⁻¹); ○ Sakamaki *et al.* (1983): PFA-coated chamber at 30°C and 49% RH (S/V=3.7 m⁻¹); ● Sakamaki *et al.* (1983): quartz cell at 22°C and 15% RH (S/V=33 m⁻¹); □ Svensson *et al.* (1987): Teflon-lined chamber at 22°C and 54% RH (S/V=14 m⁻¹); ■ Svensson *et al.* (1987): Teflon-lined chamber at 22°C and 29% RH with Teflon foil added (S/V=42 m⁻¹); × Jenkin *et al.* (1988): Pyrex chamber at 23°C and 29% RH (S/V=13 m⁻¹); + Wiesen *et al.* (1995): Quartz reactor with dry, synthetic air (S/V=21 m⁻¹). ◇ Data from this laboratory: 19.4 L glass cell at 23°C and 50% RH (S/V=46 m⁻¹); ◆ Data from this laboratory: 7.4 L glass cell at 23°C and 50% RH (S/V=70 m⁻¹).

- (2) The rate of generation of HONO has been reported in most studies of this reaction to be first order in nitrogen dioxide (Sakamaki *et al.*, 1983; Pitts *et al.*, 1984a; Pitts *et al.*, 1985; Svensson *et al.*, 1987; Jenkin *et al.*, 1988; Perrino *et al.*, 1988; Febo and Perrino, 1991; Wiesen *et al.*, 1995; Harrison and Collins, 1998; Kleffmann *et al.*, 1998a) and first order in water vapor (England and Corcoran, 1974; Sakamaki *et al.*, 1983; Pitts *et al.*, 1984a; 1985; Svensson *et al.*, 1987; Jenkin *et al.*, 1988; Perrino *et al.*, 1988; Febo and Perrino, 1991; Harrison and Collins, 1998).
- (3) Nitric acid has not been observed in the gas phase but nitrate is measured in washings from the surface (Svensson *et al.*, 1987) and on denuder surfaces (Febo and Perrino, 1991), and molecular nitric acid has been observed on silica surfaces in the presence of

NO₂ and water (Goodman *et al.*, 1999; Barney and Finlayson-Pitts, 2000). Presumably, as the reaction proceeds, the surfaces become more acidic.

- (4) The rates of NO₂ loss and HONO formation in clean chambers are higher than those in “conditioned chambers” (*i.e.* “dirty” chambers contaminated from previous experiments) (Pitts *et al.*, 1984a; Svensson *et al.*, 1987).
- (5) The rates in conditioned chambers are relatively insensitive to the nature of the *underlying* surface. For example, Svensson *et al.* reported similar rate constants for HONO formation on glass and smooth FEP Teflon film, and Pitts *et al.* showed that the rates of HONO production in two environmental chambers and in a mobile home were relatively consistent over a wide range of initial NO₂ concentrations (0.05 – 20 ppm) (Pitts *et al.*, 1984a; 1985; Svensson *et al.*, 1987). The data in Figure 1.1 also illustrate that the rates measured using different surfaces are relatively consistent, again suggesting that the nature of the underlying surface does not play a critical role in the reaction.
- (6) Use of H₂¹⁸O generates H¹⁸ONO and, at very low water vapor concentrations, HON¹⁸O is also generated. For example, Sakamaki *et al.* showed that NO₂ reacts in a small quartz cell at room temperature with H₂¹⁸O at 15% RH to generate exclusively H¹⁸ONO (Sakamaki *et al.*, 1983). Svensson *et al.* reported a similar observation for relative humidities in the range of ~20 – 40% RH; however, at a relative humidity of ~4% RH, HON¹⁸O was also formed (Svensson *et al.*, 1987).

While the HONO produced in (1) is released to the gas phase, the HNO₃ remains adsorbed on the surface (Goodman *et al.*, 1999; Barney and Finlayson-Pitts, 2000). Initial studies in this laboratory have shown that adsorbed HNO₃ reacts with gaseous NO leading to NO₂ and HONO formation, reaction (4) (Mochida and Finlayson-Pitts, 2000; Saliba *et al.*, 2000; 2001):



This regeneration of photochemically active forms of oxides of nitrogen from HNO₃ is known as “renoxification” and is potentially a very important recycling step that is currently left out of current airshed models.

The goals of this project were to examine these sources of HONO and its subsequent reactions, including the role of adsorbed HNO₃ in the chemistry. Specific goals were as follows:

1. To investigate the kinetics and mechanisms by which HONO, HNO₃ and NO form during heterogeneous NO₂ hydrolysis and determine the role played by N₂O₄. Although many studies have reported that reaction (1) is first order with respect to NO₂ (Sakamaki *et al.*, 1983; Pitts *et al.*, 1984a; 1985; Svensson *et al.*, 1987; Jenkin *et al.*, 1988; Febo and

Perrino, 1991; Wiesen et al., 1995; Harrison and Collins, 1998; Kleffmann et al., 1998a), there is evidence that N_2O_4 is enhanced on silica surfaces and is likely to play an important role in reaction (1) (*Goodman et al., 1999; Barney and Finlayson-Pitts, 2000*).

2. To investigate the water adsorbed on surfaces typically used in laboratory studies and found in the troposphere. Most laboratory studies have reported that the rate of reaction (1) is first order with respect to water vapor (*England and Corcoran, 1974; Sakamaki et al., 1983; Pitts et al., 1984a; Svensson et al., 1987; Jenkin et al., 1988*). However, the reaction is known to be heterogeneous, *i.e.*, it occurs on the surfaces in the reaction chamber which are in equilibrium with water vapor. Hence understanding the amount and nature of the water on these surfaces is essential for elucidating the kinetics and mechanisms of the heterogeneous reactions.
3. As part of the first two goals, to develop and apply a new chamber in which both long path FTIR and attenuated total reflectance are incorporated in order to measure gas phase and surface species simultaneously during the heterogeneous hydrolysis of NO_2 .
4. To study heterogeneous NO_2 hydrolysis in the presence of UV radiation to determine if HONO production is enhanced as reported by several other groups.
5. To understand the decomposition of HONO in clean chambers as well as those that have HNO_3 on the walls. We also investigated the forms of HNO_3 adsorbed on surfaces and its reactions with gaseous HONO and NO.
6. To incorporate these results into an airshed model to assess their impacts on the formation of O_3 in the troposphere.

2. METHODS AND MATERIALS

I. ANALYTICAL METHODS AND EQUIPMENT

I.A. Water Uptake Cell

Water uptake experiments were carried out using transmission Fourier transform infrared spectroscopy (FTIR). The samples of interest were positioned within a borosilicate glass cell enclosed with 32 mm diameter ZnSe windows, as shown in Figure 2.1. The cell had an 11 cm path length and could accommodate thin, disc-shaped, samples with a diameter up to 25 mm. The center o-ring permitted installation and removal of the samples, which were positioned an average of ~6 mm apart in thin slots cut in a glass holder and secured with small amounts of halocarbon wax. Up to ten samples could be mounted in the cell, allowing for the measurement of water uptake on a total of 20 surfaces. All gas flows through the cell were set using calibrated flow meters (Matheson TF 1050). A type-K thermocouple with an Omega HH202A digital readout ($\pm 0.25\%$ reading + 0.2°C) was positioned inside the cell to monitor the cell temperature during experiments. All measurements were conducted at atmospheric pressure under dynamic conditions with a total flow rate of 200 mL min^{-1} .

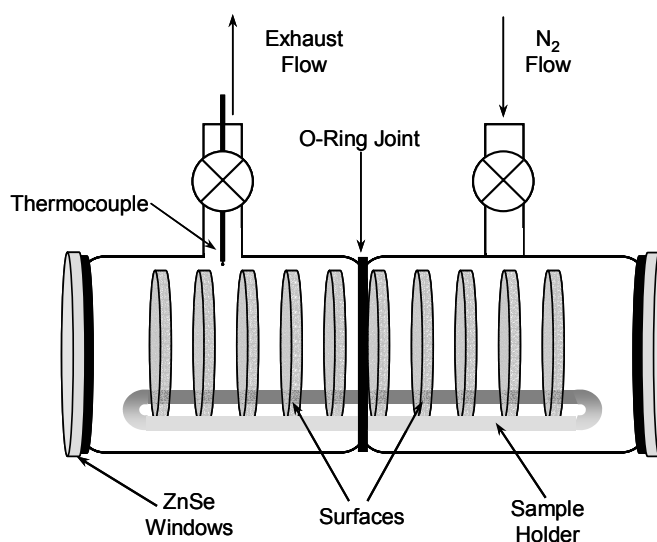


Figure 2.1. Glass cell used for measurements of water uptake on glass and other surfaces.

I.B. Long Path Infrared Cells

Two long path infrared cells were used during this research, both made of borosilicate glass. Each cell has a set of three gold-coated White optics (*White, 1942*) with a protective layer of silicon monoxide. The first cell was described in detail in the Final Report of the

previous contract (Contract 97-311); the relevant details of this cell are given in Table 2.1. The second cell is surrounded by UV lamps (Sylvania, 30 W, F30T8 / 350BL, $\lambda = 320 - 400$ nm) for photolysis experiments. The pathlength of the cell, which is specified in each section, varied depending on the project. The internal flanges and mounts of both cells were coated with a thin coating of halocarbon wax (Halocarbon Products, Inc., Series 1500) to prevent contact of gases with the metal surfaces. We have shown in recent studies (*Sumner et al., 2004*) that halocarbon wax takes up water in amounts similar to borosilicate glass over a broad range of relative humidities. Thus, for reactions occurring on the cell surfaces, such as those described here, the total surface area including the optics is most relevant. Both values are shown in Table 1 for comparison.

Table 2.1. Volume and surface areas for the long path cells.

Measurement	LP Cell 1	LP Cell 2
Base Path	0.8 m	1.0 m
Volume	7.4 L	19.4 L
Total Path Length(s) Used	32 m	48, 72, 84, and 112 m
Surface Area of Cell Walls Only	0.31 m ²	0.58 m ²
Surface Area to Volume Ratio (S/V) of Cell Walls Only	42 m ⁻¹	30 m ⁻¹
Total Surface Area Including Internal Mirrors, Mounts, and Flanges	0.52 m ²	0.89 m ²
Total S/V Including Internal Mirrors, Mounts, and Flanges	70 m ⁻¹	46 m ⁻¹

I.C. Porous Glass Cell Used for Porous Glass and Silica Pellet Studies

The cell used to investigate the heterogeneous reactions of various gases with adsorbed nitric acid by following the changes in species adsorbed on porous glass or pressed silica discs is described in detail in the Final Report for the previous contract. The solid substrates were suspended in the center of the borosilicate glass cell using a glass holder. The cell had ZnSe windows, a volume of 79 cm³, a surface area of 232 cm², and a path length for the infrared beam of 6.3 cm. The holder could be moved out of the beam into a sidearm to characterize gas-phase species or positioned in the infrared beam for characterization of

the combination of the gas-phase plus surface species. The spectrum of the surface species alone was obtained from the difference of these two spectra.

I.D. ATR Probe

Infrared spectra of thin films were measured using an ATR probe (Axiom Analytical Inc., DPR-111) interfaced to an FTIR spectrometer (Thermo-Nicolet, Nexus 670 or Avatar 370) with a commercial beam-directing module. The module reflects the FTIR beam down a hollow gold-coated light guide to the probe head holding the cylindrical ATR crystal (AMTIR (AsSeGe), 3.2 mm diameter \times 40 mm length), in which the beam undergoes nine effective internal reflections. The light intensity is attenuated at each reflection due to penetration of the beam $\sim 0.1 - 1 \mu\text{m}$ into the crystal-air interface, depending on wavelength and angle of incidence, before exiting the crystal (Harrick, 1967). The beam is then redirected up the probe with a gold retro-reflecting cone through a second light guide and finally to an MCT detector. The probe was inserted through a 1-in. vacuum tight fitting into either a 1.75 L glass chamber or into a 100 L chamber described in the following section. Figure 2.2 shows the path of the IR beam through the ATR probe.

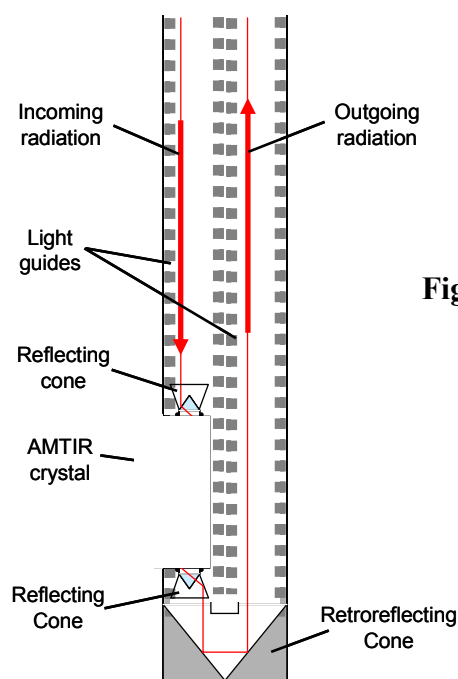


Figure 2.2. Schematic diagram of the ATR probe used for FTIR characterization of thin films.

I.E. LP-ATR Chamber

The LP-ATR chamber is designed to investigate heterogeneous reactions by measuring both gas phase and adsorbed species simultaneously and in real time. A diagram of the chamber is shown in Figure 2.3. The body of the chamber is a borosilicate glass tube, ~ 30 cm diameter and 1.4 m length, which is sealed with o-rings at each end to stainless steel end plates. Each endplate is actually a set of two circular plates (not shown in Fig. 2.3): the

inner endplate seals to the glass tube and holds the optics, while the other endplate is an outer cover which can be removed to access the backs of the optics mounts for alignment. The covers seal to the inner endplate with o-rings. One of the end plates has a 6 in. extended stainless steel flange to which a variety of ports are positioned for addition of diluent gas, reactants, a pressure gauge, and the ATR probe (described in the previous section). The chamber can be evacuated to $\sim 5 \times 10^{-3}$ Torr using a dry pumping system (BOC Edwards, QDP80 / QMB250F) and pressure is monitored with a 1000 Torr diaphragm gauge (Leybold CTR91) and a thermal conductivity gauge (Leybold TTR 216S) to measure the pressure of the evacuated chamber. Humidity and temperature are measured using a probe (Vaisala, HMP238) which extends through a fitting on the endplate into the chamber. A quartz tube runs down the center of the chamber and through both endplates, sealed with o-ring fittings at each end, so that photolysis experiments can be carried out using a lamp tube (wavelengths > 200 nm) which fits inside the quartz tube.

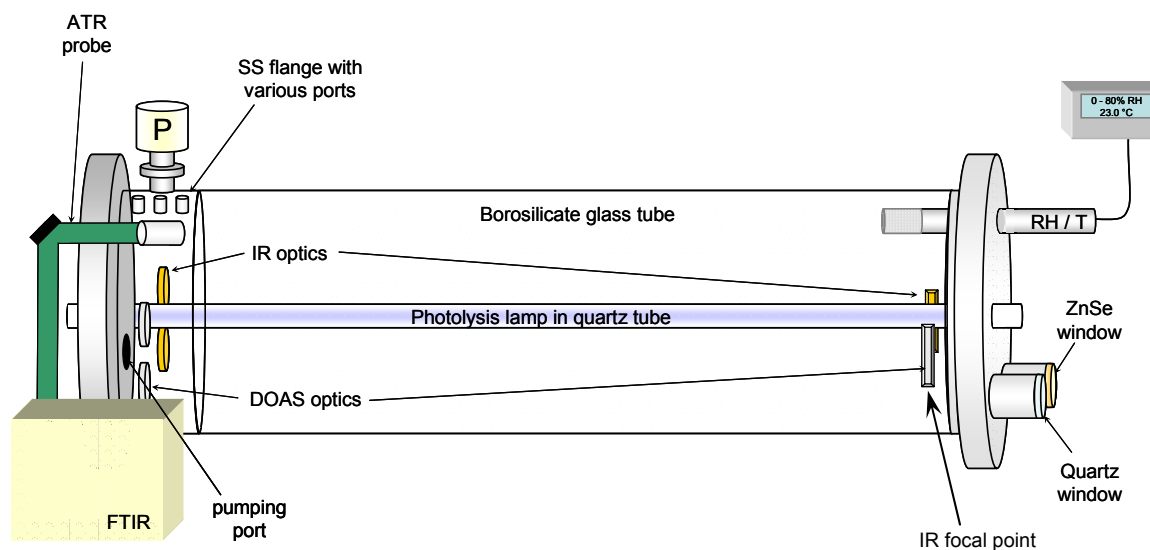


Figure 2.3. Schematic of the LP-ATR chamber used to study the kinetics and mechanisms of heterogeneous reactions.

Two sets of White optics (*White, 1942*) are mounted to the endplates; one set is coated with protected gold for long path IR, while the other has a high reflectance coating for a future long path differential optical absorption spectroscopy (DOAS) system using UV/visible light. For long path IR, the collimated, external beam from an FTIR (Thermo-Nicolet, Nexus 670) is focused with gold-coated mirrors to a point directly under the rectangular mirror in the chamber through a ZnSe window. The beam diverges as it travels the base path length (1.25 m) to the first internal (round) mirror. Adjustment of the internal mirrors for multiple reflections is carried out by removing the end covers.

The ATR probe extends through a bored-through o-ring compression fitting on the stainless steel flange. It is interfaced to an FTIR (Thermo-Nicolet, Avatar 370) typically run at $1 - 4 \text{ cm}^{-1}$ resolution.

II. EXPERIMENTAL PROCEDURES

II.A. Water Uptake on Surfaces Relevant to Laboratory Studies

II.A.1. Water Contact Angle

Surface wettability of the materials described above was probed by contact angle measurements using water droplets. Quasi-equilibrium contact angles of sessile 1 μ L Nanopure water droplets were measured under ambient conditions with a Kodak DCS 315 camera equipped with a long-range microscope (Infinity Optics). The shape of the droplet depends on its interaction with the surface (*Ulman, 1991*). The line tangent to the curve of the droplet to the point where it intersects the solid surface forms the contact angle. A water droplet resting on a hydrophobic surface would form a spherical droplet having a high contact angle, but would have a much smaller contact angle when placed on a more hydrophilic surface. These studies were carried out in the laboratory of Professor Jim Rutledge of the UCI Department of Physics, and represent additional work at no cost to CARB that was not included in the original contract.

II.A.2. Surface Characterization

Atomic force microscopy (AFM) was used to probe the physical topography of the air/solid interface of the samples described above. Samples were imaged with a Park Scientific Instruments (PSI) Autoprobe LS Atomic Force Microscope under ambient conditions. The images were obtained in either contact mode with PSI Ultralever B tips, with the tip force set to approximately 25 nN, or in non-contact mode with PSI Ultralever C tips. In contact mode, each 256 \times 256 pixel image took approximately 5 min to obtain, with a scan rate of 1 Hz in the fast (horizontal) direction. In non-contact mode, each 256 \times 256 pixel image took approximately 10 minutes, with a scan rate of 0.5 Hz. Root Mean Square (RMS) surface roughness values were calculated using the PSI ProScan software on background corrected AFM images. Background correction involved the fitting of each scan line in an AFM image with a second order polynomial, and the subtraction of this best fit curve from the raw data. This procedure left intact all surface roughness on a length scale smaller than one-half the image size, but it removed lower frequency noise and the tube curvature artifact from the data. No Fourier filtering of AFM images was carried out. These studies were carried out by Erik Menke and Professor Reg Penner in the Department of Chemistry at UCI and also represent additional research not originally proposed but carried out at no additional cost to CARB.

II.A.3. Water Uptake Measurements

The amount of liquid water adsorbed on the surfaces was determined as a function of relative humidity (RH) by transmission FTIR. The samples of interest were studied in the cell described above.

The RH in the cell was set by mixing flows of dry and 100% RH nitrogen, obtained by passing N₂ through Nanopure water in two borosilicate glass fritted bubblers, in series. The bubblers were kept in a water bath set at 22.0 ± 0.2 °C (MGW Lauda MT) to reduce the effects of evaporative cooling. The temperature of the cell in the FTIR sample compartment, which was normally ~3 °C warmer than the room, was cooled by passing the spectrometer purge gas (25 L min⁻¹ flow rate) through a stainless steel coil in a temperature controlled bath (MGW Lauda RCS) set at -8 °C. Heat tape was wrapped around the glass cell and used to fine-tune the cell temperature, which was maintained at 22.0 ± 0.2 °C. The use of Teflon tubing was minimized in favor of non-porous materials including glass and stainless steel. This was intended to reduce the degassing of water vapor from within the porous Teflon walls and also the permeation of room air through the tubing. The KBr windows separating the spectrometer's sample and interferometer/detector compartments were removed; even under fast dry nitrogen purge, the KBr windows held variable amounts of liquid water, which generated an irreproducible signal that was often significant compared to the water adsorbed on the samples of interest.

Spectra of the glass and other materials in equilibrium with humidified N₂ were obtained as interferograms at 1 cm⁻¹ resolution on an FTIR spectrometer (Mattson, Galaxy 5020) equipped with a liquid nitrogen cooled mercury cadmium telluride detector. The samples were dried in the cell overnight under a flow of dry N₂ (200 mL min⁻¹) at 40 °C. To ensure that the nitrogen was completely dry, the vapor above liquid N₂ (Airgas, 55 psi) was used. After cooling the cell to 22 °C, a background spectrum of 2048 scans was obtained each day, with a flow of dry nitrogen through the cell. The dry and humid nitrogen flows were then set to the desired relative humidity and flow through the cell was established. Sample spectra of 1024 scans were obtained at each RH after an equilibration time of 15 min.

Water vapor spectra for subtraction were measured with the samples removed from the glass cell. During water vapor spectra collection, an optical filter was used to remove IR radiation below 2000 cm⁻¹. Infrared radiation was reflected off the cell windows and returned to the interferometer where it was remodulated and its phase shifted by 180°. This phenomenon has been described by Griffiths and de Haseth (1986) and was observed in this system as negative peaks in the 3200 cm⁻¹ region; the peaks resulted from the water bend in the 1600 cm⁻¹ region that were frequency-doubled upon remodulation. The optical filter was constructed from three borosilicate glass discs (described above) that were held together with halocarbon wax. The outer surfaces were covered with FEP Teflon film to minimize water uptake on the filter. The FEP film was roughened with 1 μm diamond polishing paper to eliminate multiple reflections within the film, as described below. The optical filter efficiently absorbed the IR radiation at wavenumbers below 2000 cm⁻¹ that had caused the interference. Any small amounts of liquid water that may have been present on the ZnSe windows or the optical filter were subtracted from the sample spectra, along with water vapor.

A problem that often arises with the use of thin parallel surfaces in transmission IR spectroscopy is multiple reflection of the IR radiation between the two surfaces (*Griffiths and de Haseth, 1986*). The multiple reflections cause interference fringes on either side of the centerburst in the interferograms and result in sinusoidal noise peaks in the single beam and

absorbance spectra. Replacing these fringes in the interferogram with zeros before the Fourier transform is performed has the effect of removing the interference pattern from the single beam spectrum (*Griffiths and de Haseth, 1986*). While this zero-filling procedure adds small amounts of noise to the spectrum, the final result is much more useful. Thus, interference fringes were typically removed from the interferogram before performing the Fourier transform, for which 5064 interferogram data points were used to calculate 4 cm^{-1} resolution single beam spectra. Absorbance spectra were obtained by ratioing the single beam spectrum for a given RH to the background spectrum from that day. Although the noise that resulted from the internal reflections in the quartz samples was apparent in the single beam spectra, it was not visible in the ratioed absorbance spectra. Interference fringes were not produced for the halocarbon wax dip method samples whose surfaces were not smooth, and hence did not have interference from multiple internal reflections.

II.A.4. X-Ray Photoelectron Spectroscopy

To understand the effects different surface treatments on glass and quartz, X-ray photoelectron spectroscopy (XPS) was used to probe the elemental composition of the air/solid interface of the glass and quartz samples. These studies were carried out by John Newberg and Professor Hemminger as additional experiments not originally included in the contract but carried out at no additional cost to CARB. X-ray photoelectron spectra of the surfaces were obtained in an ESCALAB MKII ultra-high vacuum (UHV) instrument (VG Scientific) equipped with three individually pumped chambers, allowing for rapid transfer (< 1 hr.) of samples from atmospheric to UHV pressures. Sample surfaces were irradiated under UHV ($\sim 5 \times 10^{-10}$ Torr) with 1486.6 eV X-rays from an aluminum anode at 15 keV and 20 mA. The kinetic energies of the ejected photoelectrons were analyzed using a 150 mm hemispherical electron energy analyzer. Data collection and analysis were carried out using the software package PISCES (Dayta Systems Ltd.). XPS peak areas were integrated after a linear background subtraction. The surface concentrations were determined by dividing the integrated areas by standard sensitivity factors (relative to an F(1s) sensitivity factor of 1.0) (*Wagner et al., 1981; Hemminger et al., 1990*). The sensitivity factors used are as follows: O(1s), 0.721; Si(2p), 0.355; C(1s), 0.306; B(1s), 0.165; Zn(2p_{3/2}), 3.734; K(2p_{3/2}), 1.013; Na(1s), 1.655; Ti(2p_{3/2}), 1.360; Al(2p), 0.246. Due to the uncertainty in the sampling depth for each element, the surface composition should be considered semi-quantitative.

II.B. Heterogeneous NO₂ Hydrolysis Experiments

II.B.1. Gas Phase Measurements

Gaseous products of the heterogeneous nitrogen dioxide (NO₂) hydrolysis were studied by adding a dilute NO₂/N₂ mixture to a long path cell and then bringing the cell to atmospheric pressure at the desired RH (~20, 50, or 80%) using the appropriate combination of flows of H₂O/N₂ and dry N₂. Some studies were also carried out using Ultrahigh Purity air; the results were indistinguishable from the experiments carried out in N₂. To avoid the possible oxidation of NO by O₂, most experiments were carried out in N₂. The reactants and products were measured by FTIR (Mattson, Research Series or Cygnus) in the dark for

reaction times up to 15 hr. using a path length of 32 m in the smaller cell and either 84 m or 112 m in the larger cell.

Absorption spectra were quantitatively analyzed for each gaseous species using two approaches. The first was based on the net absorbances of the peaks at selected wavenumbers. The second used a least squares fitting procedure, MFC (*Gomer et al., 1995*) which determines the ratio of the species in the spectrum of interest relative to a reference spectrum of known concentration. This fitting procedure uses all of the data over a selected spectral region, rather than the absorbance at a single peak height. MFC was used in conjunction with an in-house calibration or literature reference spectrum (*EPA, 2002*) at the same resolution and total pressure. Nitrogen dioxide was quantified using the band centered at 2910 cm^{-1} for the MFC analysis as well as the net absorbance of the peak at 2917 cm^{-1} . Calibrations were carried out using an authentic sample of NO_2 ; although the 2910 cm^{-1} band is much weaker than that in the 1600 cm^{-1} region, it does not overlap with water absorption bands and hence provides more precise analysis. Nitrous acid (HONO) was quantified using its ν_3 (*trans*-HONO) absorption at 1263 cm^{-1} and the published effective cross section (base 10) of $3.7 \times 10^{-19}\text{ cm}^2\text{ molecule}^{-1}$ (*Barney et al., 2000*). *Trans*-HONO is in equilibrium with the *cis* form, and the effective absorption cross section takes this ratio into account to give the total (*trans* plus *cis*) HONO concentration. The value of the effective cross section cited assumes the ratio of *trans/cis* at room temperature to be 2.3 (*Barney et al., 2000*). Nitrous oxide (N_2O) was quantified using the rotational line of the ν_3 band at 2236 cm^{-1} with the calibration from an authentic sample or, when using MFC, a published reference spectrum using the entire band centered at 2223 cm^{-1} at the same resolution.

The small absorption lines of nitric oxide (NO) are particularly difficult to observe due to the strong water vapor absorptions in this region and the weak absorption cross section for NO in the infrared. Both the Q branch at 1876 cm^{-1} and a second vibration-rotation line at 1900 cm^{-1} , which are not overlapped by water vapor lines, were compared with a calculated reference spectrum for quantification (*EPA, 2002*). The detection limits in the 7.4 L cell were the following (in units of molecules cm^{-3}): 5×10^{13} for NO_2 , 1.5×10^{13} for HONO, 3.5×10^{13} for NO, and 2.5×10^{12} for N_2O . In the 19.4 L cell, they were 2.8×10^{13} for NO_2 , 6.2×10^{12} for HONO, 4.3×10^{13} for NO, and 2.3×10^{12} for N_2O .

II.B.2. Surface Species Measurements

Several experiments were conducted using the small cell that had a holder for porous glass and silica pellets in order to characterize surface species formed during heterogeneous NO_2 hydrolysis. Transmission FTIR spectra were taken through porous glass pieces (Vycor 7930, 14 mm \times 0.24 mm thick discs of mass 59 mg and an internal (BET) surface area of $90\text{ m}^2\text{ g}^{-1}$, Advanced Glass and Ceramics, Holden, MA) which hold adsorbed water. Each of these experiments is described in the Results section of this report.

II.C. LP-ATR Studies of NO_2 Hydrolysis

Heterogeneous NO_2 hydrolysis experiments were performed in the new chamber that has been designed with both long path FTIR for gases and ATR-FTIR for analysis of the thin

water film on the surface. These were carried out immediately after fabrication to examine the effects of organics on the formation rates and yields of the products. The stainless steel surfaces were left uncoated, but still held some organics which were used during fabrication. The reason for not cleaning the chamber first was to investigate the possible effects of small amounts of surface-adsorbed organics on the heterogeneous NO₂ hydrolysis. For example, one proposal is that the formation of N₂O occurs via reactions involving adsorbed organics (Barlow, 2003). The gas phase path length was aligned to 47.5 or 72.5 m. In each NO₂ hydrolysis experiment, the desired RH was added to the chamber by mixing dry N₂ with humid N₂ to a pressure of ~700 Torr. Initial spectra were taken at this RH using both the long path FTIR and ATR-FTIR to use as background spectra. Approximately 14 – 15 Torr of pure NO₂ was added to a small flow cell (553 mL) and was then flushed with dry N₂ into the chamber to give ~100 ppm NO₂ at 760 Torr. Upon addition of the NO₂ to the chamber, scanning was initiated for both using the long path FTIR and the ATR-FTIR. Experiments were carried out in the dark at ~298 K and continued for ~10 hrs. Long path spectra were collected continuously at 1 cm⁻¹ resolution and 86 co-added scans over ~1 min. Net absorbances were determined for gaseous NO₂, HONO, NO, and N₂O for their bands at 2917, 1264, 1875, and 2213 cm⁻¹, respectively. Calibrations were performed to quantify NO₂, NO, and N₂O, while the published absorption cross section was used for HONO (Barney *et al.*, 2000). ATR spectra were collected simultaneously and continuously at 1 cm⁻¹ resolution and 160 scans over ~1 min.

II.D. Photochemical Production of HONO

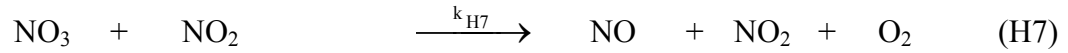
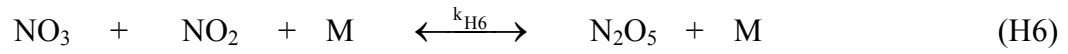
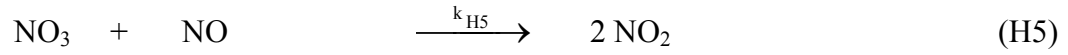
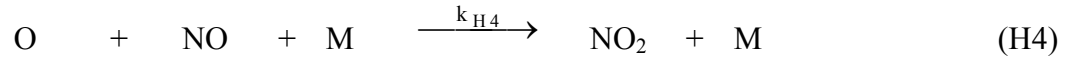
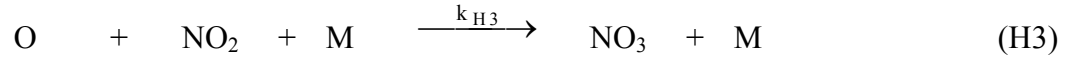
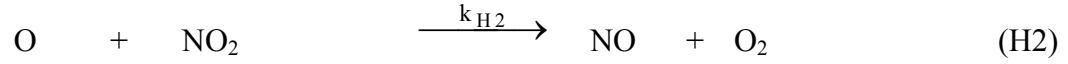
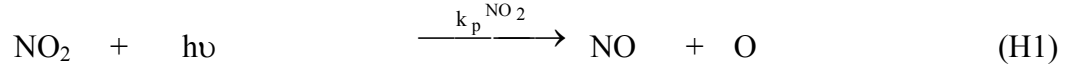
II.D.1. Experimental Procedures

Concentrations of NO₂, HONO, and NO in the 19.4 L long path cell aligned to 84 or 48 m cell were measured using FTIR (Mattson, Research Series). Spectra were typically collected at a resolution of 1 cm⁻¹, and consisted of 64 co-added scans over 30 seconds. Gas phase NO₂, HONO, and NO were quantified by the net absorbance of their bands at 2917, 1263, and 1875 cm⁻¹, respectively. Concentrations of NO₂ and NO were determined as discussed above. Concentrations of H₂O were determined using a calibration obtained by flowing a known concentration of water vapor through the cell and measuring rotational lines at 1174 cm⁻¹ and 1187 cm⁻¹.

In each NO₂ hydrolysis experiment, ~20 – 50 ppm NO₂ was introduced to the cell as a mixture in nitrogen. The cell was filled to atmospheric pressure from a collapsible Teflon chamber that contained a water-carrier gas mixture obtained by flowing N₂ or air through a bubbler containing Nanopure water and mixing it with dry N₂ or air. This method quickly brought the cell pressure to 1 atm at the desired RH. Nitrous acid accumulated for 2 – 3 hr via the hydrolysis of NO₂ before irradiation began. Photolysis periods typically lasted for 2 – 3 hr. All experiments were performed at 296 ± 1 K.

In order to model the system quantitatively, the photolysis rate constants for NO₂ and HONO in this system were acquired. For NO₂, this was determined experimentally by adding NO₂ to the cell in concentrations similar to those in the hydrolysis experiments. The cell was filled to 1 atm with N₂, irradiated with UV light, and the decay of NO₂ measured.

The NO₂ photolysis rate constant was calculated using the method of Holmes *et al.* (1973) based on the following mechanism (H1 – H7):



With the appropriate steady state assumptions for NO, NO₃, and N₂O₅ in an O₂ deficient environment, the photolysis rate constant for NO₂ ($k_p^{\text{NO}_2}$) was calculated using the following relationship (Holmes *et al.*, 1973):

$$k_p^{\text{NO}_2} = \frac{Z}{2t} \quad (\text{I})$$

where t is time and Z is given by equation (II):

$$Z = \left\{ \left(1 + \frac{k_{\text{H3}}[M]}{k_{\text{H2}}} - \frac{k_{\text{H4}}[M]}{k_{\text{H2}}} \right) \ln \frac{[\text{NO}_2]_0}{[\text{NO}_2]} + \frac{k_{\text{H4}}[M]}{k_{\text{H2}}} \left(\frac{[\text{NO}_2]_0}{[\text{NO}_2]} - 1 \right) \right\} \quad (\text{II})$$

Here [NO₂]₀ is the initial NO₂ concentration, [NO₂] is the concentration at time t , k_{H2} , k_{H3} , and k_{H4} are the rate constants for reactions (H2), (H3), and (H4) respectively, and M is the required third body, in this case N₂.

The NO₂ photolysis rate constant was obtained from the slope of a plot of Z versus time. From data such as that shown in Figure 2.4, the NO₂ photolysis rate constant ($k_p^{\text{NO}_2}$) was determined to be $(1.6 \pm 0.1) \times 10^{-3} \text{ s}^{-1}$ (2s).

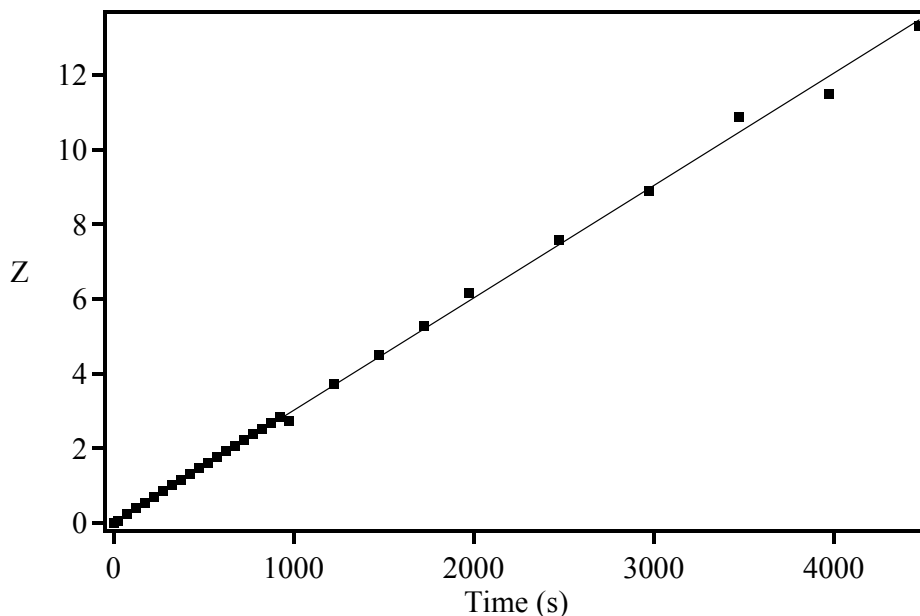


Figure 2.4. Typical data for the loss of NO₂ during photolysis plotted in the form of equation (I).

To determine the HONO photolysis rate constant, 100 – 200 ppm of cyclohexane was added to a mixture of HONO (0.2 – 1.8 ppm) in N₂ in order to scavenge the OH and prevent the regeneration of HONO from the OH + NO recombination reaction and the loss of HONO from secondary reactions, such as HONO + OH. The HONO decay was treated as first order and the HONO photolysis rate constant obtained from equation (III):

$$\ln \frac{[\text{HONO}]_o}{[\text{HONO}]} = k_p^{\text{HONO}} t \quad (\text{III})$$

The photolysis rate constant for HONO (k_p^{HONO}) was determined from data such as that shown in Figure 2.5 to be $(4.9 \pm 1.4) \times 10^{-4} \text{ s}^{-1}$ (2s).

As a further check on the experimentally determined HONO photolysis rate constant, equation (IV) was also used to calculate k_p^{HONO} based on the measured value of $k_p^{\text{NO}_2}$:

$$\frac{k_p^{\text{HONO}}}{k_p^{\text{NO}_2}} = \frac{\int_{320 \text{ nm}}^{400 \text{ nm}} \Phi_{\text{HONO}}(\lambda) \sigma_{\text{HONO}}(\lambda) F(\lambda) d\lambda}{\int_{320 \text{ nm}}^{400 \text{ nm}} \Phi_{\text{NO}_2}(\lambda) \sigma_{\text{NO}_2}(\lambda) F(\lambda) d\lambda} \quad (\text{IV})$$

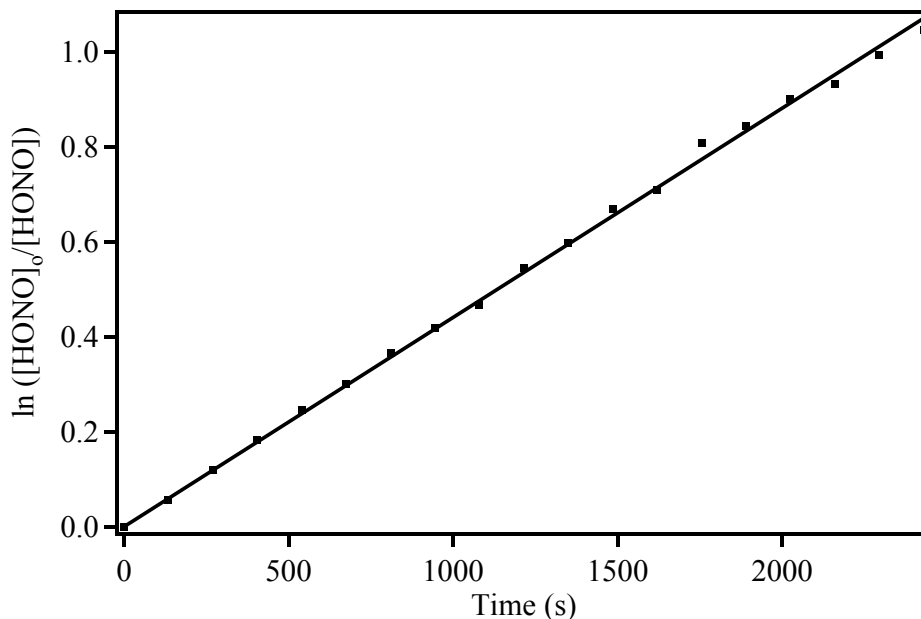


Figure 2.5. A typical first order plot for the photolysis of 1.2 ppm HONO in the presence of 135 ppm of cyclohexane.

In equation (IV), σ is the relevant base e absorption cross section, Φ is the corresponding quantum yield, and F is the intensity of light (*Finlayson-Pitts and Pitts, 2000; Sander et al., 2003*). This calculation yielded a value of $k_p^{\text{HONO}} = 4.8 \times 10^{-4} \text{ s}^{-1}$, in excellent agreement with the measured value. This agreement establishes that additional sources of HONO, such as photolysis of surface-adsorbed species, are not significant under the conditions that k_p^{HONO} was measured.

II.D.2. Modeling

A computer kinetics modeling program (REACT for Windows v.1.2) (*Braun et al., 1988; Bozzelli, 2000; Manka, 2001*) was used to simulate the gas phase chemistry as well as the hydrolysis of NO_2 in the cell. This program numerically integrates the differential rate equations representing the reaction kinetics. The model for the dark period includes the gas phase and surface chemistry, given in sections A and C of Table 2.2. The gas phase model includes the relevant gas phase reactions available from current databases (*Tsang and Herron, 1991; Sander et al., 2000; Atkinson et al., 2001; 2003*). To represent the chemistry during irradiation, photolysis reactions listed in section B of Table 2.2 were included. The surface reactions were parameterized as gas phase rate processes for simplicity. Because the details of the NO_2 heterogeneous hydrolysis mechanism are uncertain, this portion of the model is simplified to have the least number of unknown variables and yet still capture the essence of what is known about the heterogeneous hydrolysis of NO_2 : the reaction is first order in NO_2 and water vapor (*Sakamaki et al., 1983; Pitts, 1984; Svensson et al., 1987; Jenkin et al., 1988; Perrino et al., 1988; Febo and Perrino, 1991; Mertes and Wahner, 1995; Wiesen et al., 1995; Harrison and Collins, 1998; Kleffmann et al., 1998a; Finlayson-Pitts et al., 2003*), there is a competitive adsorption between H_2O and HONO (*Syomin and*

Finlayson-Pitts, 2003), and HONO undergoes heterogeneous reactions on the cell walls to generate NO (*Syomin and Finlayson-Pitts, 2003*). A more complex mechanism involving N₂O₄ can also be used, but since the rate constants for the individual steps are not known, it does not add to the data interpretation during photolysis. Hence, we have chosen to use this more simplified mechanism in this case.

Rate constants for the surface reactions were adjusted within the constraints of the mechanism to provide a best fit of the observed decay of NO₂ and formation of HONO during the dark period. By accurately predicting the chemistry in the dark and having measured the photolysis rate constants for NO₂ and HONO, the chemistry should be accurately predicted during the irradiation period. The rate constant for the NO₂ heterogeneous hydrolysis was allowed to vary slightly from experiment to experiment to give the best fit to the data in the dark portion of the experiment; this value was then used for the photolysis portion of the experiment. This enabled the model to reproduce the HONO concentrations at the beginning of the photolysis. All other rate constants in section C of Table 2.2 remained constant.

Table 2.2. Chemical reactions in model used for photoenhancement studies

Reaction	Rate Constant (k^{298}) ^a	Reference
A. Gas Phase Reactions		
$2 \text{NO}_2 \xrightarrow{M} \text{N}_2\text{O}_4$	2.5×10^{-14}	Atkinson et al., 2002
$\text{N}_2\text{O}_4 \longrightarrow 2 \text{NO}_2$	1.1×10^5	Atkinson et al., 2002
$\text{NO}_3 + \text{NO} \longrightarrow 2 \text{NO}_2$	2.6×10^{-11}	Sander et al., 2003
$\text{NO}_2 + \text{NO}_3 \xrightarrow{M} \text{N}_2\text{O}_5$	1.2×10^{-12}	Sander et al., 2003
$\text{N}_2\text{O}_5 \longrightarrow \text{NO}_2 + \text{NO}_3$	3.8×10^{-2}	Sander et al., 2003
$\text{NO}_2 + \text{O}(^3\text{P}) \longrightarrow \text{NO} + \text{O}_2$	1.0×10^{-11}	Sander et al., 2003
$\text{NO}_2 + \text{O}(^3\text{P}) \xrightarrow{M} \text{NO}_3$	3.3×10^{-12}	Sander et al., 2003
$\text{NO}_2 + \text{O}_3 \longrightarrow \text{NO}_3 + \text{O}_2$	3.2×10^{-17}	Sander et al., 2003
$\text{NO}_2 + \text{OH} \xrightarrow{M} \text{HNO}_3$	1.0×10^{-11}	Sander et al., 2003
$\text{NO}_2 + \text{OH} \xrightarrow{M} \text{HOONO}$	2.1×10^{-12}	Sander et al., 2003
$\text{HOONO} \longrightarrow \text{NO}_2 + \text{OH}$	1.1	Sander et al., 2003
$\text{NO}_2 + \text{HO}_2 \xrightarrow{M} \text{HO}_2\text{NO}_2$	1.4×10^{-12}	Sander et al., 2003
$\text{HO}_2\text{NO}_2 \longrightarrow \text{NO}_2 + \text{HO}_2$	8.6×10^{-2}	Sander et al., 2003
$\text{NO} + \text{NO}_2 \xrightarrow{M} \text{N}_2\text{O}_3$	7.2×10^{-15}	Atkinson et al., 2002
$\text{N}_2\text{O}_3 \longrightarrow \text{NO} + \text{NO}_2$	3.8×10^5	Atkinson et al., 2002
$\text{NO} + \text{O}(^3\text{P}) \xrightarrow{M} \text{NO}_2$	1.7×10^{-12}	Sander et al., 2003
$2 \text{NO} + \text{O}_2 \longrightarrow 2 \text{NO}_2$	2.0×10^{-38}	Atkinson et al., 2002
$\text{NO} + \text{O}_3 \longrightarrow \text{NO}_2 + \text{O}_2$	1.9×10^{-14}	Sander et al., 2003
$\text{NO} + \text{OH} \xrightarrow{M} \text{HONO}$	7.4×10^{-12}	Sander et al., 2003
$\text{NO} + \text{HO}_2 \longrightarrow \text{OH} + \text{NO}_2$	8.1×10^{-12}	Sander et al., 2003
$\text{NO}_3 + \text{O}(^3\text{P}) \longrightarrow \text{O}_2 + \text{NO}_2$	1.0×10^{-11}	Sander et al., 2003
$\text{NO}_3 + \text{OH} \longrightarrow \text{HO}_2 + \text{NO}_2$	2.2×10^{-11}	Sander et al., 2003
$\text{NO}_3 + \text{HO}_2 \longrightarrow \text{OH} + \text{NO}_2 + \text{O}_2$	3.5×10^{-12}	Sander et al., 2003
$\text{N}_2\text{O} + \text{O}(^1\text{D}) \longrightarrow \text{N}_2 + \text{O}_2$	4.9×10^{-11}	Sander et al., 2003
$\text{O}(^1\text{D}) + \text{O}_2 \longrightarrow \text{O}(^3\text{P}) + \text{O}_2$	4.0×10^{-11}	Sander et al., 2003
$\text{HONO} + \text{OH} \longrightarrow \text{H}_2\text{O} + \text{NO}_2$	4.5×10^{-12}	Sander et al., 2003
$\text{HONO} + \text{O}(^3\text{P}) \longrightarrow \text{NO}_2 + \text{OH}$	9.1×10^{-16}	Tsang and Herron, 1991
$\text{N}_2\text{O} + \text{O}(^1\text{D}) \longrightarrow 2 \text{NO}$	6.7×10^{-11}	Sander et al., 2003
$\text{O}(^3\text{P}) + \text{O}_2 \xrightarrow{M} \text{O}_3$	1.5×10^{-14}	Sander et al., 2003
$\text{O}(^1\text{D}) + \text{O}_3 \longrightarrow 2 \text{O}_2$	1.2×10^{-10}	Sander et al., 2003
$\text{O}(^1\text{D}) + \text{O}_3 \longrightarrow 2 \text{O}(^3\text{P}) + \text{O}_2$	1.2×10^{-10}	Sander et al., 2003
$\text{O}(^3\text{P}) + \text{O}_3 \longrightarrow 2 \text{O}_2$	8.0×10^{-15}	Sander et al., 2003
$\text{H} + \text{O}_2 \xrightarrow{M} \text{HO}_2$	1.2×10^{-12}	Sander et al., 2003

Reaction	Rate Constant ^a	Reference	
$O(^1D) + H_2O \longrightarrow 2 OH$	2.2×10^{-10}	Sander et al., 2003	
$O(^3P) + H_2O_2 \longrightarrow OH + HO_2$	1.7×10^{-15}	Sander et al., 2003	
$OH + O_3 \longrightarrow HO_2 + O_2$	7.3×10^{-14}	Sander et al., 2003	
$2 OH \longrightarrow O(^3P) + H_2O$	1.9×10^{-12}	Sander et al., 2003	
$2 OH \xrightarrow{M} H_2O_2$	6.3×10^{-12}	Sander et al., 2003	
$OH + HO_2 \longrightarrow O_2 + H_2O$	1.1×10^{-10}	Sander et al., 2002	
$H + O_3 \longrightarrow OH + O_2$	2.9×10^{-11}	Sander et al., 2003	
$OH + H_2O_2 \longrightarrow HO_2 + H_2O$	1.7×10^{-12}	Sander et al., 2003	
$HO_2 + O_3 \longrightarrow OH + 2 O_2$	1.9×10^{-15}	Sander et al., 2003	
$O(^3P) + OH \longrightarrow O_2 + H$	3.3×10^{-11}	Sander et al., 2003	
$O(^3P) + HO_2 \longrightarrow OH + O_2$	5.9×10^{-11}	Sander et al., 2003	
$OH + HNO_3 \longrightarrow H_2O + NO_3$	1.5×10^{-13}	Sander et al., 2003	
$2 HO_2 \longrightarrow H_2O_2 + O_2$	0 % RH	2.9×10^{-12}	Sander et al., 2003
	50 % RH	5.4×10^{-12}	Sander et al., 2003
	80 % RH	6.9×10^{-12}	Sander et al., 2003
$NO_2 + H \longrightarrow OH + NO$	1.3×10^{-10}	Sander et al., 2003	
B. Photolysis Reactions			
$NO_2 \xrightarrow{h\nu} NO + O(^3P)$	$(1.6 \pm 0.1) \times 10^{-3}$	Measured ^b	
$HONO \xrightarrow{h\nu} NO + OH$	$(4.9 \pm 1.4) \times 10^{-4}$	Measured ^c	
$HONO_{(wall)} \xrightarrow{h\nu} NO + OH$	$(4.9 \pm 1.4) \times 10^{-4}$	Estimated	
$O_3 \xrightarrow{h\nu} O_2 + O(^1D)$	$(4.7 \pm 0.1) \times 10^{-5}$	Calculated ^d	
$HNO_{3(wall)} \xrightarrow{h\nu} HONO$	$(1.1 \pm 0.9) \times 10^{-5}$	Model Fit ^e	
C. Surface Reactions			
$NO_{2(g)} + H_2O_{(g)} \longrightarrow HONO_{(wall)}$	$(2.4 \pm 0.4) \times 10^{-23}$	Model Fit ^f	
$NO_{2(g)} + H_2O_{(g)} \longrightarrow HNO_{3(wall)}$	$(2.4 \pm 0.4) \times 10^{-23}$	Model Fit ^f	
$HONO_{(wall)} + H_2O_{(g)} \longrightarrow HONO_{(gas)} + H_2O_{(g)}$	1.35×10^{-20}	Model Fit	
$HONO_{(wall)} \longrightarrow NO_{(g)}$	8.0×10^{-4}	Model Fit	
$HONO_{(g)} \longrightarrow HONO_{(wall)}$	2.0×10^{-4}	Measured	
$HONO_{(wall)} + HNO_{3(wall)} \longrightarrow \text{Products}$	1.0×10^{-17}	Model Fit	
$N_2O_5 \longrightarrow 2 HNO_{3(wall)}$	83	Calculated ^g	
<p>a. Termolecular reactions with a third body are accounted for in the rate constants using $[M] = 2.46 \times 10^{19}$ molecule cm^{-3} to match experimental conditions. Rate constants are in the units of $cm^3 \text{ molecule}^{-1} s^{-1}$ or s^{-1}.</p> <p>b. Experimentally measured as described in the text. Errors shown are 2s.</p> <p>c. Experimentally measured in the cell using cyclohexane as an OH scavenger. Errors shown are 2s.</p> <p>d. Calculated using an analogue of equation (IV).</p> <p>e. Included only at longer photolysis times; see text in Results section.</p> <p>f. The rates of these reactions were always taken as being equal; by expressing the production of HONO and HNO_3 separately, the first order kinetics in NO_2 and H_2O was captured.</p> <p>g. Equivalent to a reaction probability of 0.03 (Hu and Abbatt, 1997).</p>			

II.E. HONO Decomposition Experiments

Experiments were conducted at 296 K in the 19.4 L long path cell with 72 m path length. Gas phase species were monitored using FTIR (Mattson, Research Series). In a typical HONO decomposition experiment, 4 – 50 Torr of a mixture of HONO in N₂ was introduced into the cell using the HONO generator described below. The pressure was then brought up to 1 atm with N₂ at the desired RH. Nitrogen was used as the diluent gas to minimize the potential for thermal oxidation of NO in the system by oxygen. The RH was adjusted by varying the ratio of humid and dry N₂ during filling of the chamber. The humid N₂ was obtained by flowing N₂ gas through a bubbler containing Nanopure water and held at 296 K. All HONO decomposition experiments were conducted at 296 K.

Concentrations of HONO, NO₂, and NO in the cell were measured as a function of time using FTIR spectroscopy. Spectra were collected at a resolution of 1 cm⁻¹, and 64 scans collected over 30 seconds were averaged for each data point. Gas phase HONO, NO₂ and NO were quantified by the net absorbance of their bands at 1263, 2917 and 1875 cm⁻¹, respectively. Absolute concentrations of NO₂ and NO were based on calibrations using authentic samples in the cell. Nitrous acid concentrations were calculated from absorbances (base 10) using an effective cross section of $(3.7 \pm 0.4) \times 10^{-19}$ cm² molecule⁻¹ at 1263 cm⁻¹ (Barney *et al.*, 2000). Use of the effective cross section gives the total HONO concentration (*cis* and *trans* isomers, which are in equilibrium). (The 1263 cm⁻¹ band that was measured is only due to the *trans* form.)

Two sets of studies were carried out using different treatments of the surfaces of the cell. In the first series, the cell walls were conditioned with gas phase nitric acid (HNO₃) by introducing approximately 2 Torr of dry gaseous HNO₃ into the cell. After ~15 min., the cell was evacuated with a diffusion-pump for several hours. The HONO and humid N₂ were then added as described above. In the second series, the cell walls were unconditioned. At the beginning of this set of experiments the cell was thoroughly rinsed first with distilled and then with Nanopure water to remove soluble contaminants. Subsequent experiments in this series were carried out after simply evacuating the cell for several hours with a diffusion pump, due to the impracticality of disassembling the cell, rinsing it and realigning the optics for individual experiments.

II.F. Studies of the Renoxification of Nitric Acid

Experiments to investigate the renoxification of HNO₃ were conducted using the cell designed to hold the porous glass and silica discs. For reactions on relatively dry surfaces, the reaction surface was raised in the side arm and heated to ~320 °C for 30 – 60 min. while under vacuum. This treatment removed some of the water that was adsorbed from room air. Nitric acid (~1 × 10¹⁷ molecule cm⁻³) was introduced into the reaction cell and then pumped out for 5 minutes. This HNO₃ dosing was repeated three times followed by pumping for ~30 min. after the last treatment. Nitric acid remains adsorbed on the surface after this procedure, as indicated by its infrared absorption bands discussed in detail below. Finally, the reactant gas (NO, CO, CH₄ or SO₂) was introduced into the cell at concentrations ranging between (1

$- 26) \times 10^{16}$ molecule cm^{-3} . In some cases, N_2 was added to a total pressure of 1 atm. For experiments carried out with RH higher than 0%, N_2 flowed through a bubbler holding water and was diluted with dry N_2 to obtain the desired RH.

Experiments with adsorbed ammonium nitrate (NH_4NO_3) were also conducted in order to determine if it reacts in a manner similar to HNO_3 . The NH_4NO_3 was formed by dosing the silica with dry HNO_3 as described above, followed by the addition of excess NH_3 vapor. After evacuating the cell to remove any remaining gas-phase species, NO was added. The experiments with NH_4NO_3 were performed at reduced pressure, *i.e.* no addition of N_2 .

Reaction progress was monitored with time using FTIR. First, the single beam background spectra were collected with the cell evacuated by moving the surface out of, and then into, the infrared beam. In order to obtain an absorbance spectrum of the surface species and the gas together, the reactants were added to the cell and the single beam spectrum was recorded with the surface in the beam. The spectrum was then ratioed to that of the evacuated cell with the surface in the beam to give the absorbance spectrum of the gas plus adsorbed species. This procedure cancelled out the absorptions due to the silica itself, which occur below 2000 cm^{-1} and in the $3000 - 3600 \text{ cm}^{-1}$ region. The absorbance spectrum of the gases was obtained by ratioing the single beam spectrum to that of the cell under vacuum, both with the surface out of the infrared beam. Finally, the spectrum of the gas phase species was subtracted from the gas plus surface to obtain the spectrum of species on the surface. Spectra were collected using 32 co-added scans at a resolution of 1 cm^{-1} unless otherwise specified. All experiments were conducted at $296 \pm 1 \text{ K}$.

Two different types of silica surfaces, a porous glass plate and pressed pellets of untreated fumed silica powder, were used. The $2 \times 3 \text{ cm}$ plate of porous glass (Corning) was $\sim 1 \text{ mm}$ thick as provided by the manufacturer. The normal infrared cutoff for porous glass is 2000 cm^{-1} (*Kiselev and Lygin, 1975*). In order to shift the cutoff down to 1550 cm^{-1} , the porous glass plate was thinned in the center by etching using HF as described elsewhere (*Barney and Finlayson-Pitts, 2000*). The total porous glass surface area, measured using a commercial instrument (Accelerated Surface Area and Porosimetry System – ASAP 2000, Micromeritics; N_2 adsorbate) based on the Brunauer-Emmett-Teller (BET) method (*Brunauer et al., 1938*), was $71.2 \text{ m}^2 \text{ g}^{-1}$ resulting in a total surface area of 28.5 m^2 averaged over the thinner etched section and the surrounding unetched glass. The chemical composition of porous glass is 96.3% SiO_2 , 2.95% B_2O_3 , 0.04% Na_2O and 0.72% $\text{Al}_2\text{O}_3 + \text{ZrO}_2$ (*Elmer, 1992*). The porous glass plate was cleaned by rinsing with Nanopure water after each experiment.

The pressed silica pellets were prepared with Cab-O-Sil[®] (Cabot Corp.) and have an infrared cutoff at $\sim 1300 \text{ cm}^{-1}$ (*Low and Ramasubramanian, 1966; Papirer, 2000*). Cab-O-Sil[®] is untreated fumed silica powder of high purity ($\geq 99.8\% \text{ SiO}_2$), with particle sizes ranging from 0.2 to $0.3 \mu\text{m}$ (*CABOT, 1999*). Approximately 0.02 g of the silica powder was pressed into a 13 mm diameter pellet, with a thickness of $\sim 0.05 \text{ mm}$. The surface area, measured in the same way as for the porous glass plate, was $329 \pm 3 (2s) \text{ m}^2 \text{ g}^{-1}$, resulting in a total surface area of 6.6 m^2 per pellet. A new pellet was used for each experiment.

Ion chromatography (IC, Alltech Odyssey) was used to quantify the HNO₃ adsorbed on the surfaces. After the dosing procedure described above, an infrared spectrum of the adsorbed HNO₃ on the surface was recorded. The pellet was removed from the cell, rinsed with Nanopure water and analyzed for nitrate (NO₃⁻). The mobile phase was a 1:10 (v:v) mixture of 1.7 mM NaHCO₃/1.8 mM Na₂CO₃ in Nanopure water with a constant flow rate of 1.20 mL min⁻¹. A 150 mm × 4.6 mm Novosep A-1 Anion column, equipped with a 7.5 mm × 4.6 mm guard column, was used for separation at a constant temperature of 35 °C. An auto suppressor (DS-PLUSTM) was used to improve sensitivity. A conductivity detector (Alltech 550) with positive polarity, a detection range of 10 μS (S = Ω⁻¹), and a time-constant of 1 s was used for the NO₃⁻ analysis. The IC was calibrated for NO₃⁻ using aqueous solutions prepared from sodium nitrate powder.

III. MATERIALS

The surfaces studied in the water uptake studies are summarized in Table 2.3. They include both hydrophilic and hydrophobic materials. The hydrophilic materials are thin cover slips of smooth glass (VWR Micro Cover Glasses) and quartz (Quartz Plus, Inc.). Cover glass discs were used because they were sufficiently thin that they did not significantly attenuate the infrared beam in the region of interest (above 2000 cm⁻¹). Standard borosilicate laboratory glass (Type I, Class A, ASTM, 2001) used in many laboratory studies of heterogeneous reactions has a higher silica content, but like the cover slips, also contains small amounts of boron, sodium and aluminum oxides (see Table 2.3). The overall similarity between the Type I, Class A glass and the cover slips is such that using the latter to probe interactions with water is reasonable.

Measurements were conducted on the hydrophilic glass as received from the manufacturer, and also after employing three different treatments. In the first case, the glass discs were rinsed with Nanopure water (Barnstead, 18.1 MΩ cm) and dried in N₂ (Oxygen Service Co., ≥ 99.999%). In the second case, the discs were cleaned for 35 minutes with an argon plasma discharge (Harrick Scientific Plasma Cleaner/Sterilizer PDC-32G, medium power). For the third treatment, which has been suggested for cleaning porous glass surfaces (*Elmer, 1992*), the discs were submerged in hot (~85 °C) H₂O₂ (30%, Electron Microscopy Sciences, ACS Reagent Grade) for approximately 10 minutes, followed by thorough rinsing with Nanopure water and drying in the cell in a stream of dry nitrogen gas at 40°C overnight.

A variety of hydrophobic materials were also analyzed for their water uptake characteristics. Halocarbon wax (Halocarbon Products Corp., Series 1500) samples were prepared in two ways, each utilizing the smooth glass discs as the substrate. For the “dip method,” the glass discs were dipped into melted halocarbon wax and mounted in the sample holder. The coated discs were then gently warmed with a heat gun until the wax appeared to flow freely to reduce the impact of air bubbles on the surface. The coated discs were cloudy to the eye but appeared to have a smooth and quite thick coating. The “solvent method” involved submerging the glass discs in a warm solution of halocarbon wax dissolved in dichloromethane (EM Science, 99.8%). The samples were also gently heated with a heat

Table 2.3. Samples used for water uptake measurements and surface characterization.

Material	Description	Chemical Composition	Source
Smooth Glass	Micro Cover Glasses, No. 1, 25 mm diameter × 0.13 – 0.17 mm	64% SiO ₂ , 9% B ₂ O ₃ , 7% ZnO, 7% K ₂ O, 7% Na ₂ O, 3% TiO ₂ , 3% Al ₂ O ₃	VWR Scientific, Inc., Buffalo Grove, IL
Laboratory Glass ^a	Designation E438-92: Specification for Type I, Class A (ASTM, 2001)	81% SiO ₂ , 13% B ₂ O ₃ , 4% Na ₂ O, 2% Al ₂ O ₃	ASTM International West Conshohocken, PA
Quartz	Quartz Cover Slips substrate grade, 25 mm dia. × 0.16 mm	Corning 7980 Synthetic Fused Silica: >99.9% SiO ₂	Quartz Plus, Inc. Brookline, NH
Halocarbon Wax	Series 1500	Polychloro-trifluoroethylene	Halocarbon Products Corp. River Edge, NJ
FEP Film	2 mil FEP Teflon Film	Fluoropolymer	Livingstone Coating Corp., Wayne, NJ
Organic SAM	C8 Self Assembled Monolayer	<i>n</i> -octyltrichlorosilane: 95%	Geselt
FEP Coating	FEP Teflon Coating CCI-109	fluoropolymer	Crest Coating, Inc. Anaheim, CA
PFA Coating	PFA Teflon Coating	fluoropolymer	Crest Coating, Inc. Anaheim, CA
Fluoropolymer Coating	FluoroPel PFC801A	fluoropolymer	Cytonix Corp. Beltsville, MD

^aData provided for comparison.

gun. The resulting coating was hazy to the eye, but obviously much thinner than the coating using the dip method.

Samples of thin FEP Teflon film (Norton High Performance Films) were supported by thin halocarbon wax-coated aluminum washers for the infrared study. The Teflon film was pressed onto the warm halocarbon wax coating, which held the film firmly in place, and the excess film removed.

Self-assembled monolayers (SAMs) of *n*-octyltrichlorosilane (Geselt, 95%) were deposited on borosilicate glass discs according to a well-established technique (*Sagiv, 1980*). These are designated C8 SAMs throughout. Briefly, the glass discs were cleaned with boiling ethanol, then with boiling chloroform. The dry glass was further cleaned with an argon plasma discharge for ~30 minutes. Upon removal from the plasma cleaner, the substrates were stored in Nanopure water until deposition of the monolayer was carried out. After drying the surfaces with nitrogen, the discs were placed in a mM solution of *n*-octyltrichlorosilane in dodecane for 10 min. The C8 SAM-coated discs were then placed in boiling chloroform to remove any physisorbed material. The coating and chloroform extraction steps were repeated two additional times to ensure a smooth, well-ordered coating.

Three additional hydrophobic materials, two Teflon spray-coated materials and a fluoropolymer coating, were also studied. Such coatings are commonly used in laboratory systems, such as in smog chambers in which many studies of atmospheric reactions have been carried out (*Sakamaki et al., 1983; Pitts et al., 1984a*). Due to the substrate material (metal and thick glass), these materials could not be probed by infrared spectroscopy. However, analysis of the wetting and surface characteristics could still be studied as described above in sections II.A.1 and II.A.2, respectively. The Teflon spray-coated materials, Teflon FEP CCI-109 and PFA Teflon, were used as received from the manufacturer. The third material, a fluoropolymer coating, was applied as a 1% FluoroPel PFC 801A emulsion in a fluoropolymer to a glass microscope slide (*P. Wennberg, personal communication*). The coating was then annealed at 90°C and the solvent evaporated.

Nitrous acid was synthesized by reacting hydrochloric acid (HCl) with sodium nitrite (NaNO₂):



Prior to reaction, the solid NaNO₂ (Aldrich, 99.5%) was exposed to humid N₂ (80-100% RH) for 15 – 20 minutes to moisten the salt surface. The flow of humid N₂ was stopped and replaced by a flow of gaseous HCl prepared by passing dry N₂ over a HCl solution (Fisher, Certified ACS Plus, 12.1 M diluted ~ 1:3 (v:v) using Nanopure water (Barnstead, 18.2 MΩ cm).

Nitric oxide (Matheson, 99%) was purified by passing it through a liquid nitrogen trap to remove impurities such as NO₂ and HNO₃. Nitrogen dioxide was synthesized by reacting purified NO with excess (>2:1) O₂ (Oxygen Service Co., 99.993%) for ≥ 2 hr. The

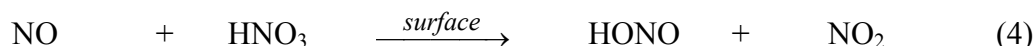
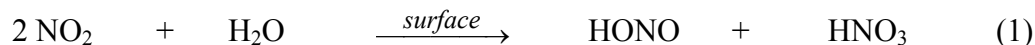
NO₂ was then purified by condensing in a cold finger at 195 K and pumping away the excess O₂. Gaseous NH₃ was produced using the vapor above a 29.5% ammonium hydroxide solution (NH₄OH, Fisher Certified ACS Plus) that was purified by one freeze-pump-thaw cycle. FeCl₃ (Fisher Scientific, Laboratory Grade, Anhydrous) and sodium nitrate (NaNO₃, Aldrich ACS Reagent Grade) were used as received. The 1.7 mM sodium bicarbonate/1.8 mM sodium carbonate used for IC was EZ-LUTE (Alltech). Gaseous carbon monoxide (CO, Matheson, 99.99%), methane (CH₄, Matheson, 99.999 %), and anhydrous sulfur dioxide (SO₂, Matheson, 99.98 %) were used directly from the cylinders without further purification. The vapor over a bulb of cyclohexane (C₆H₁₂, Fisher, 99.9%, purified by freeze-pump-thaw cycles) was used for scavenging OH radicals in some experiments.

Nitrogen was humidified by bubbling N₂ through Nanopure water and diluting with dry N₂. Dry, gaseous HNO₃ used for conditioning the long path cell and for adsorbing to silica surfaces was taken from the vapor above a mixture of 2:1 H₂SO₄:HNO₃ (Fisher Scientific 95.7% H₂SO₄, 69.9% HNO₃) that was purified by three freeze-pump-thaw cycles. Isotopically substituted H¹⁵NO₃ (Sigma-Aldrich, 40 wt. % solution in H₂O, 98 atom % ¹⁵N), used for peak assignments, was also purified by freeze-pump-thaw cycles. N₂O (Liquid Carbonic, 99.99%), used for calibrations, was used as received.

3. RESULTS

I. WATER UPTAKE ON SURFACES RELEVANT TO LABORATORY STUDIES

As discussed in the Introduction, a number of heterogeneous reactions, including the nitrogen dioxide hydrolysis reaction (1) and the reaction (4) of adsorbed nitric acid with gaseous nitric oxide,



occur in thin water films present on surfaces. These reactions have been observed to depend on the water vapor concentration (*Pitts et al., 1984a; Svensson et al., 1987; Jenkin et al., 1988; Saliba et al., 2001; Finlayson-Pitts et al., 2003*), which is reasonable since the relative humidity determines the equilibrium concentration of water on the surface. What is perhaps surprising is that such reactions do not appear to be very sensitive to the nature of the substrate. For example, Figure 3.1 shows data from a study of reaction (1) carried out in this laboratory (*Sumner et al., 2004*) at 85% RH and 24°C in a 561 L chamber, described previously (*DeHaan et al., 1999*), whose internal surfaces were coated with hydrophobic halocarbon wax. This coating is often used in laboratory studies as it is chemically inert, like Teflon, but can be easily applied and removed. Despite the fact that only small amounts of water would be expected on such a hydrophobic surface, loss of NO₂ and formation of HONO does indeed occur. Furthermore, when corrected to a common reaction chamber surface-to-volume ratio (S/V) and to an RH of 50%, the rate of HONO formation (4.5×10^{-2} ppb min⁻¹ per ppm NO₂) is in good agreement with rates measured in larger (5800 L) Teflon-coated smog chambers (3.9×10^{-2} ppb min⁻¹ per ppm NO₂) and in smaller (7 – 19 L) borosilicate glass cells [$(2 - 4 \times 10^{-2}$ ppb min⁻¹ per ppm NO₂)] (*Finlayson-Pitts et al., 2003*). This agreement is remarkable, given the very different nature of the chamber materials ranging from hydrophobic (Teflon, halocarbon wax) to hydrophilic (glass), for which different amounts of water might be expected to be available on the surface for reaction.

A prerequisite to fully understanding such heterogeneous processes is elucidating the amount and nature of water on the surfaces. The goal of this work is therefore to elucidate the interaction of water at room temperature with some surfaces typically used in laboratory systems, and related materials, that can provide insight into the role of these thin films in atmospheric reactions. The materials studied include the following: (1) borosilicate glass as provided by the manufacturer, (2) borosilicate glass cleaned using water, hot H₂O₂, or an argon plasma discharge, (3) quartz, (4) thin FEP Teflon film, (5) halocarbon wax-coated glass using two different coating methods, (6) glass coated with a C8 organic self-assembled monolayer (SAM), and (7) several thick Teflon coatings applied to solid substrates. Four different types of measurements were made that provide insights from the macroscopic to

molecular level. On a macroscopic scale, contact angle measurements of water droplets on these surfaces were obtained to examine the wettability of the surfaces. On a micron to sub-micron scale, atomic force microscopy (AFM) measurements provide insight into the surface structure. On the molecular level, transmission FTIR of the surfaces in the presence of increasing water vapor concentrations was used to probe the nature and amounts of water on the surfaces. Finally, X-ray photoelectron spectroscopy (XPS) was used to study the elemental surface composition of the glass and quartz samples for which water uptake measurements were made.

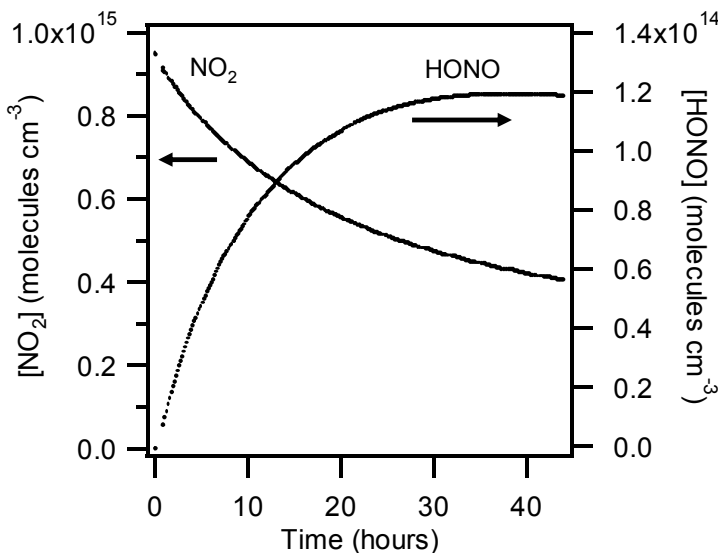


Figure 3.1. Loss of NO₂ and formation of HONO from the heterogeneous hydrolysis of NO₂ on the surface of a 561 L chamber at 24°C coated with halocarbon wax using the dip method. Measurements were made using differential optical absorption spectrometry (DOAS). Initial concentration of NO₂ was 38.6 ppm and the RH was 85%.

I.A. Contact Angles for the Surfaces with Water

Interaction of water with the surfaces studied here on a macroscopic scale can be characterized by the contact angle. It became clear during the course of this research that measurement of contact angles for water on the various surfaces would be helpful. We were fortunate to be able to access an instrument to do this in the laboratory of Professor Rutledge, and report here the data for these measurements. These were not proposed in the original contract and were carried out at no additional cost to CARB.

Figure 3.2 shows the results of three typical contact angle measurements made for a hydrophobic surface (halocarbon wax, Fig. 3.2a), a hydrophilic surface (plasma-cleaned borosilicate glass, Fig. 3.2c) and an intermediate surface (untreated borosilicate glass, Fig. 3.2b). As expected, the contact angle is large for the hydrophobic surface and small for the hydrophilic surface. The intermediate contact angle measured for the untreated borosilicate

glass is indicative of organic contamination on the surface, as supported by XPS measurements discussed below.

Table 3.1 summarizes the measured contact angles for the various materials. They can be grouped into three categories: (1) high contact angles ($>80^\circ$) measured for the halocarbon wax, Teflon coatings and a C8 SAM on solid substrates, (2) low contact angles ($<10^\circ$) exemplified by the cleaned borosilicate glass, and (3) intermediate values represented by the untreated borosilicate glass, the water-rinsed glass and quartz.

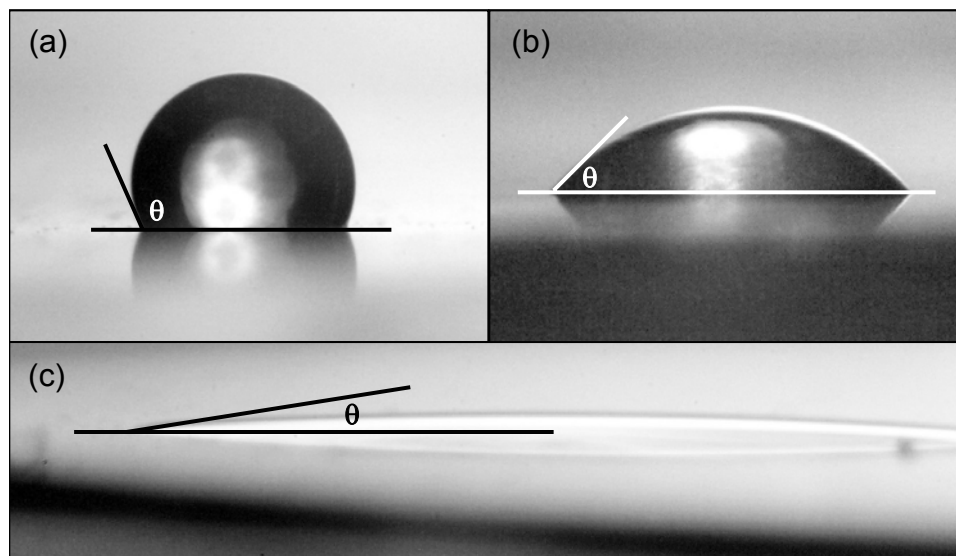


Figure 3.2. Contact angle measurements of a $1\mu\text{L}$ water droplet on three typical surfaces: (a) halocarbon wax coated using the dip method, (b) untreated borosilicate glass, and (c) plasma-cleaned borosilicate glass.

I.B. AFM Measurements of the Surface Morphology

It also became evident during the course of these studies that knowledge of the morphology of the surfaces would be important in understanding water uptake. We were fortunate to develop a collaboration with Professor Penner and his research group to carry out atomic force microscopy measurements of the surfaces, again at no additional cost to this contract. Figures 3.3 and 3.4 show typical AFM images of representative surfaces.

Table 3.1. Summary of contact angle and AFM measurements.

Sample	Water Contact Angle (degrees)	Surface Roughness^a Average \pm 1s (\AA)
<i>Hydrophilic Samples</i>		
Untreated glass	32 ± 2 (1s)	10 ± 5
Water-rinsed glass	25	9 ± 3
Plasma-cleaned glass	<10	11 ± 2
H ₂ O ₂ -cleaned glass	<10	20 ± 1
Quartz	22 ± 4 (1s)	62 ± 0.3
<i>Hydrophobic Samples</i>		
Halocarbon wax: dip method	92	$>145 \pm 13^b$
Halocarbon wax: solvent method	83	$>24^{b,c}$
Thin FEP Teflon film	109	72 ± 1
C8 SAM	98	9 ± 1
FEP Teflon film	102	$(160 \pm 24)^d$
PFA Teflon coating	112	$(699 \pm 18)^d$
FluoroPel PFC 801A coating	111	$(126 \pm 18)^d$

^a Measured in non-contact mode on $5 \mu\text{m} \times 5 \mu\text{m}$ sections.

^b Minimum value since AFM image (Fig. 3.4) suggests tip may not fully probe the minimum depth of the pores.

^c Much of the surface had what appeared to be particles embedded in the film, which could have been dust picked up during the coating. If these regions are included, the average roughness increases to $77 \pm 76 \text{\AA}$. This is again a minimum value since the AFM tip may not fully probe the depth of pores.

^d Contact mode measurements made on $2 \mu\text{m} \times 2 \mu\text{m}$ sections. Smaller surface roughness is typically measured in contact mode because topographic features that are associated with weakly adsorbed species such as water, surface structures etc. are swept away by the tip which exerts appreciable force on the surface and thus wipes the surface as the image is being acquired.

For each sample the root mean square (RMS) surface roughness (R) was calculated as follows:

$$R_{RMS} = \sqrt{\frac{\sum_{n=1}^N (z_n - \bar{z})^2}{N - 1}} \quad (\text{V})$$

where \bar{z} is the average z height and N is the number of points sampled. However, it should be noted that these are minimum values since, in many cases, the pores on the surfaces appear to be quite deep and the tip may not have fully probed the depth of such pores. In addition, the values obtained depend on the particular portion of the surface scanned, and for irregular surfaces, this may vary from region to region. In general, as the size of the surface that is scanned increases, larger corrections for the low-frequency undulations of the surface are required. This increases the uncertainty of the RMS roughness value. As a result, these values can also be sensitive to the size of the area that is scanned. The average and standard deviation (1s) values of surface roughness are summarized in Table 3.1, along with the areas used in each case.

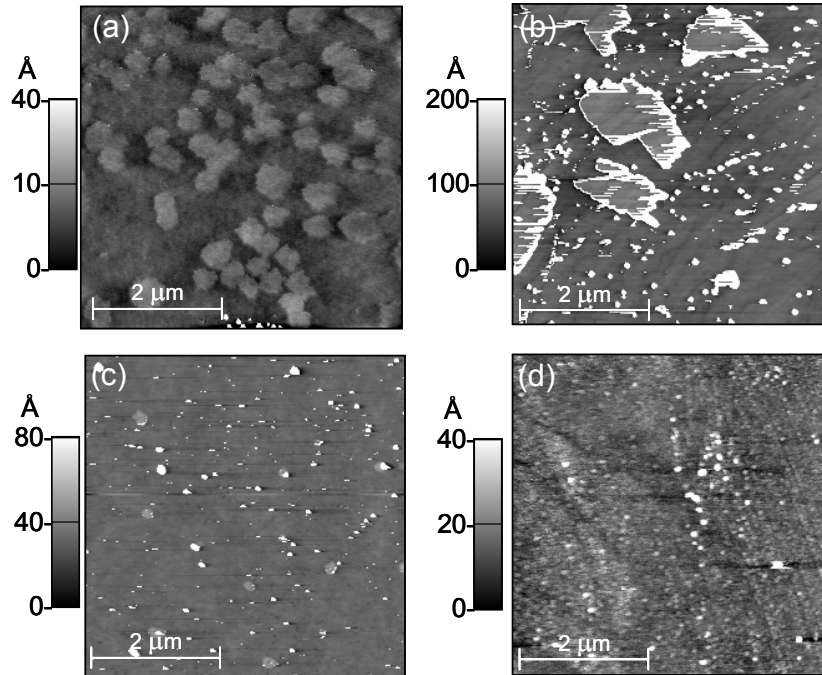


Figure 3.3. AFM measurements (in non-contact mode) of the surface morphology for (a) untreated borosilicate glass; (b) untreated quartz; (c) borosilicate glass cleaned using hot H₂O₂; (d) borosilicate glass coated with the C8 SAM.

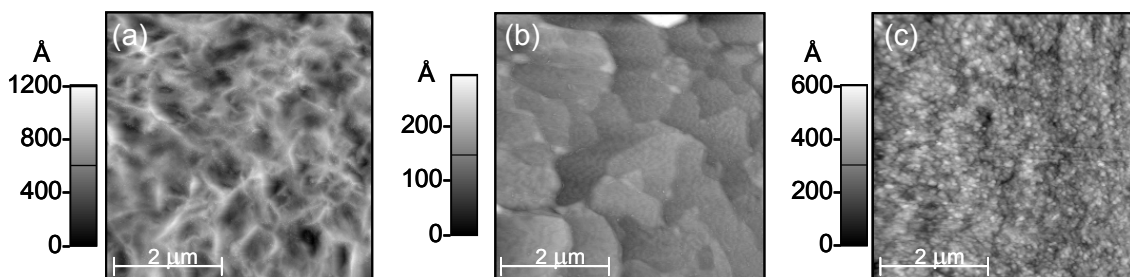


Figure 3.4. AFM measurements (in non-contact mode) of the surface morphology for (a) borosilicate glass coated with halocarbon-wax using the dip method; (b) borosilicate glass coated using the solvent method and (c) FEP Teflon film.

I.C. Infrared Measurements of Water Uptake

Figure 3.5 shows typical infrared spectra for samples through which there was sufficient transmission of the infrared beam to make measurements of the weak absorptions due to water on the surface. The broad features from $2800 - 3800 \text{ cm}^{-1}$ are due to OH stretching vibrations in condensed phase water (*Herzberg, 1945; Du et al., 1994a, b; Shultz et al., 2000; Richmond, 2001*). The sharp peaks from $3500 - 3900 \text{ cm}^{-1}$ are residuals due to subtraction of gas phase water. It has been shown that small thermal instabilities in the HeNe laser of the spectrometer, to which the absorption wavenumbers are referenced, can lead to shifts of up to $\pm 0.034 \text{ cm}^{-1}$ in the sharp rotational lines of gas phase water (*Weis and Ewing, 1998*). This made complete subtraction of the water impossible. However, this imperfect subtraction does not contribute significantly to the liquid water peak area since these sharp peaks are approximately equally positive and negative.

For comparison, the spectrum of bulk liquid water, obtained by placing a drop of water between two ZnSe windows, is also shown in Figure 3.5a. At 80% RH, the peak positions and band shapes of water adsorbed on quartz, untreated glass, water-rinsed glass, and plasma-cleaned glass as well as the halocarbon wax coatings are similar to that of bulk liquid water. The peak on the H_2O_2 cleaned glass (Fig. 3.5d) is red-shifted significantly to $\sim 3200 \text{ cm}^{-1}$. The C8 SAM and FEP Teflon film (Fig. 3.5i and j) take up much smaller amounts of water; the peak for the water film on the C8 SAM is also red-shifted.

The liquid water peak can be used to estimate the number of water layers present on the surface as a function of relative humidity. The water coverage, Θ , in number of layers, is calculated from the absorbance spectra using Equation II, a modified form of Beer's law (*Foster and Ewing, 2000*),

$$\Theta = \frac{2.303 A}{N \times S_{\text{H}_2\text{O}} \times \bar{\sigma}} \quad (\text{VI})$$

where N is the number of surfaces in the infrared beam and $S_{\text{H}_2\text{O}}$ is the surface density of one water monolayer (1.0×10^{15} molecule cm^{-2}). The base-10 integrated absorbance, A , of the liquid water peak ($2800 - 4000 \text{ cm}^{-1}$) is determined from the absorbance spectra. The integrated cross section, $\bar{\sigma}$ (base- e) was calculated for the same range to be $1.43 \times 10^{-16} \text{ cm molecule}^{-1}$ from optical constants reported by Downing and Williams (1975).

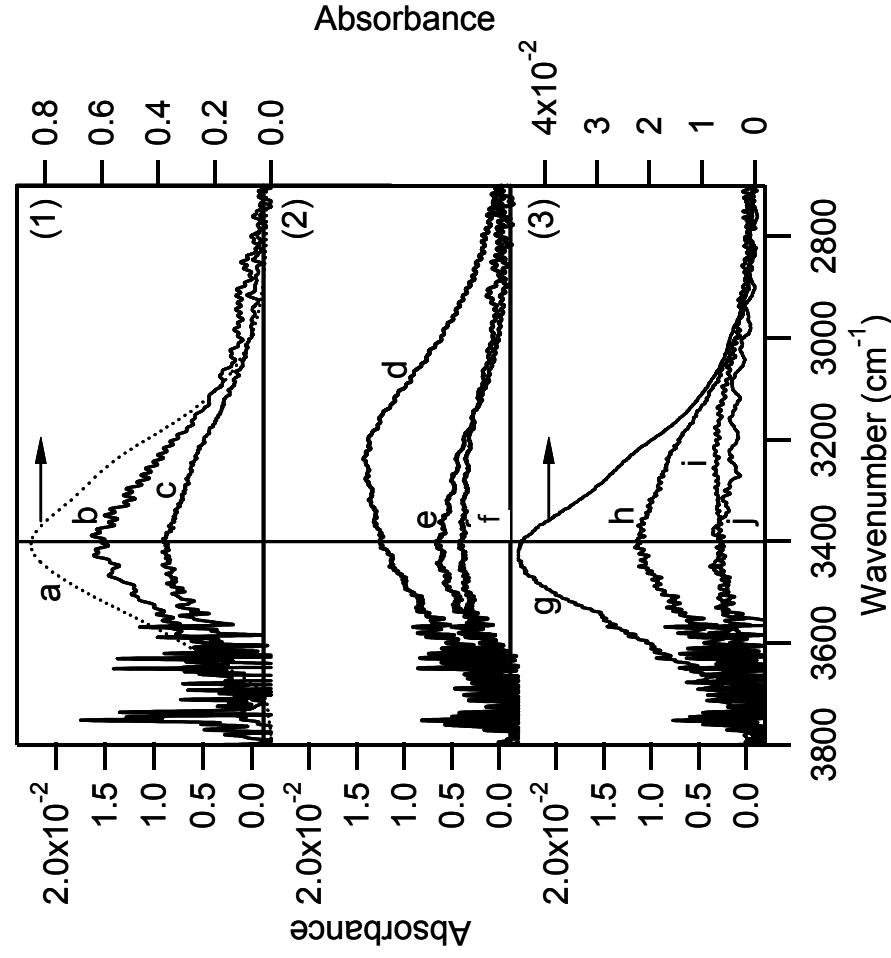


Figure 3.5. Infrared spectra of surfaces in contact with N_2 at 80% RH and, for comparison, the spectrum of bulk liquid water: (1) bulk water (a, right axis), untreated glass (b), quartz (c); (2) H_2O_2 cleaned glass (d), plasma cleaned glass (e), and water rinsed glass (f); (3) dip method halocarbon wax (g, right axis), solvent method halocarbon wax (h), C8 monolayer (i), and FEP Teflon film (j). The bulk water spectrum (1a) was obtained by measuring the IR transmission through a drop of water “sandwiched” between two ZnSe windows ratioed to the bare windows.

As shown in previous studies (Saliba *et al.*, 2001) and observed again in the present work (data not shown), the shape and peak position of the infrared spectrum of water on borosilicate glass change as the relative humidity is lowered. The peak becomes broader and shifts to higher wavenumbers. This is similar to observations of water uptake on other solids such as NaCl (Foster and Ewing, 1999, 2000; Cantrell and Ewing, 2001), where the peak

due to water condensed on the surface blue-shifts towards the gas phase absorption peak at low water coverages. This indicates disruptions in the 3-D hydrogen bonding network and strong interactions of the adsorbed water with the surface (*Drost-Hansen, 1971; Papirer, 2000*). Similar results were observed in the present studies for water on plasma-cleaned glass, quartz, halocarbon wax, and Teflon film.

The absorption coefficients of water increase by approximately an order of magnitude from gas phase to bulk liquid water, and again from liquid to ice (*Pimentel and McClelland, 1960; Irvine and Pollack, 1968*). The true value of the integrated cross section for a structured, thin water film on a surface is likely to be different from the bulk water value and to vary with coverage. However, the island-like features in the AFM data (Fig. 3.3a) provide additional insight into the amount of liquid water present on glass, at least at RH above ~60%, and further analysis indicates that the estimate using the infrared absorption coefficient for liquid water is reasonable. Island-like features similar to those shown in Fig. 3.3a have been observed on surfaces such as mica in the presence of water vapor and have been attributed to islands of water on the surface (*Xu et al., 1998*). The features in Fig. 3.3a are typically ~1.2 nm in height, corresponding to islands of water about 3 layers high. (The fraction of the surface covered with such islands was somewhat variable, likely reflecting variability in the relative humidity in the laboratory from day to day). The estimated number of layers of water using FTIR under similar conditions is 1.4, but this assumes an equal distribution of water over the surface. Given that AFM indicates that about half of the surface is covered with water islands, the amounts of water on the surface estimated using AFM and FTIR are consistent. To emphasize that the water measured using FTIR is not necessarily equally distributed over the surface, we express these data in terms of an “equivalent number of water monolayers”.

For the H₂O₂-cleaned glass, there is a significant red-shift in the infrared peak at all relative humidities, in contrast to the other surfaces. Such a shift is characteristic of water with a more ice-like structure (*Herzberg, 1945; Du et al., 1994a, b; Shultz et al., 2000; Richmond, 2001*). There may be shoulders on the low wavenumber side of the water peaks for plasma-cleaned glass, quartz and the solvent-coated halocarbon wax as well (Fig. 3.5).

Figure 3.6 shows the equivalent number of water monolayers on the glass after various treatments, on quartz, and on halocarbon wax coatings prepared by different methods. The results for water uptake on quartz are in excellent agreement with the previously reported results of Awakuni and Calderwood (*1972*). Figure 3.6b shows data for two of the treated glass samples. (The isotherm for H₂O₂-cleaned glass is shown later.) Water coverage of these surfaces is similar to that of the untreated borosilicate glass up to approximately 60% RH, but is significantly smaller above 80% RH and does not show evidence of condensation as 100% RH is approached. Figure 3.6c shows comparable data for the halocarbon wax coated surfaces. The halocarbon wax coating prepared by both the dip and solvent methods show evidence of multilayer adsorption similar to the untreated borosilicate glass.

As seen from the spectra in Fig. 3.5, the peak for the H₂O₂-treated glass is red-shifted quite substantially from that for bulk liquid water. This increases the uncertainty of the

application of absorption coefficients for bulk, liquid water sufficiently that we chose not to estimate the number of monolayers using equation (VI). However, one can examine the shape of the isotherm by using the measured absorbance of the band as a function of RH, as shown in Figure 3.7 along with the isotherm for untreated glass. The dependence of the water uptake on RH is quite different than for the untreated borosilicate glass, with the shape of water uptake on H₂O₂-treated glass resembling a Langmuir isotherm (Adamson, 1990; Masel, 1996; Adamson and Gast, 1997).

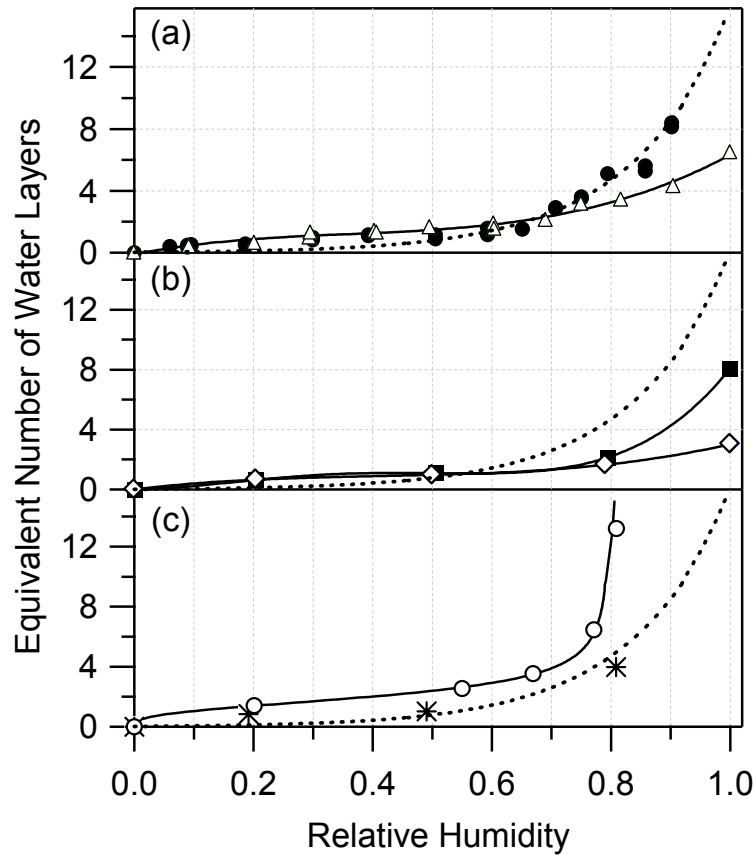


Figure 3.6. Water uptake isotherms for (a) smooth untreated glass (solid circles) and quartz (open triangles); (b) water rinsed glass (open diamonds), and plasma cleaned glass (solid squares); and (c) dip method (open circles) and solvent method (asterisks) halocarbon wax coated glass. An exponential fit of the untreated borosilicate glass data in (a) is included in each panel (dashed black line) as a guide to the eye. The solid lines are fits to each set of data, excluding the solvent method halocarbon wax, which falls on the fit for untreated glass. The dip method halocarbon wax data points (panel (c)) were taken after two hours equilibration time, although water uptake was still increasing for the high RH experiments (see text and Figure 3.8).

While most surfaces came to equilibrium with water vapor within 15 minutes, the dipped halocarbon wax coating continued to take up water over more than an hour at higher relative humidities, as shown in Figure 3.8. This is especially apparent at 81% RH, as water continued to adsorb to the surface even after 2 hours of exposure.

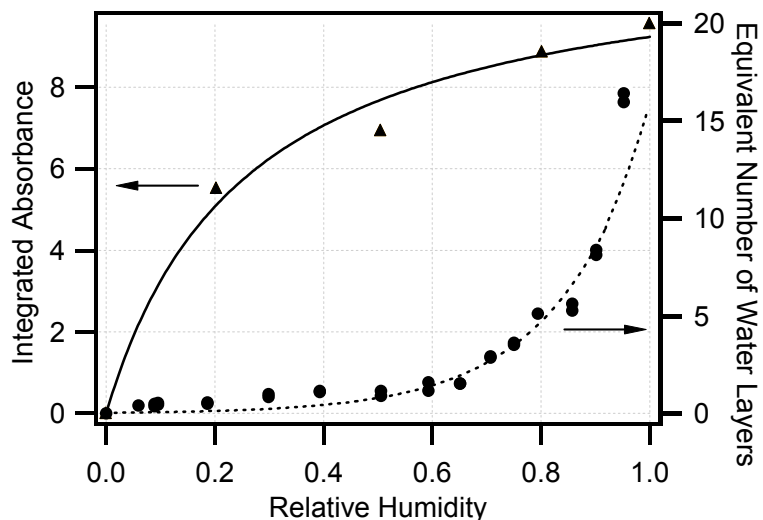


Figure 3.7. Relative intensity of the liquid water peak, integrated from 2600 - 4000 cm^{-1} , on H_2O_2 -cleaned borosilicate glass surface (triangles) as a function of relative humidity. The solid line is a fit to the data. Also shown for comparison is the isotherm for water uptake on untreated glass and the fit shown in Figure 3.6a as a guide.

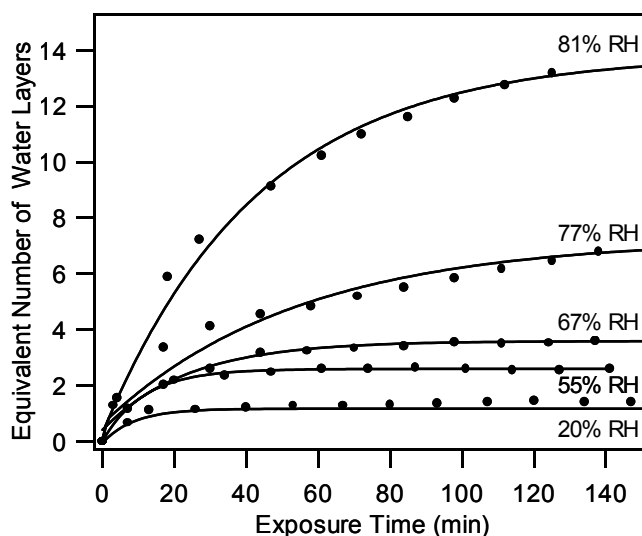


Figure 3.8. Water uptake on halocarbon wax, (dip method) as a function of the exposure time to humidified nitrogen between 20% and 81% RH. The lines show fits to the data.

I.D. XPS Analysis of Surfaces

The results of the water uptake measurements were sufficiently unusual in many respects that measurements of the change in surface composition due to the various treatments seemed appropriate. In order to assess the impact of the three cleaning methods applied to borosilicate glass, XPS measurements were made on the glass samples and, for comparison, the quartz sample. These studies were carried out by John Newberg and Professor John Hemminger at no additional cost to CARB. Figure 3.9 shows the molar ratio of the major elements to the oxygen peak in each case. In the case of the quartz sample, the Si:O ratio is within experimental uncertainty of the expected SiO_2 stoichiometry. The more complex borosilicate glass samples show the expected large number of elements at the surface. As is common with surface analysis, there is always some adventitious carbon on the surfaces. However, clearly the H_2O_2 and plasma cleaning removed significant amounts of carbon from the surface.

As expected, quartz consists primarily of silica; small amounts of Na and Mg were also observed but may arise from contamination during sample handling and preparation. The borosilicate glass has substantial amounts of Na, B, K, and Zn. The surface of water-rinsed glass is similar in composition to that of untreated glass, with somewhat smaller Na. The increase in sodium for the plasma cleaned sample may result from the deposition of sodium from the inner chamber of the plasma cleaner, which is made of glass. Cleaning using H_2O_2 removes the B and K from the surface and substantially decreases the surface Zn and Na.

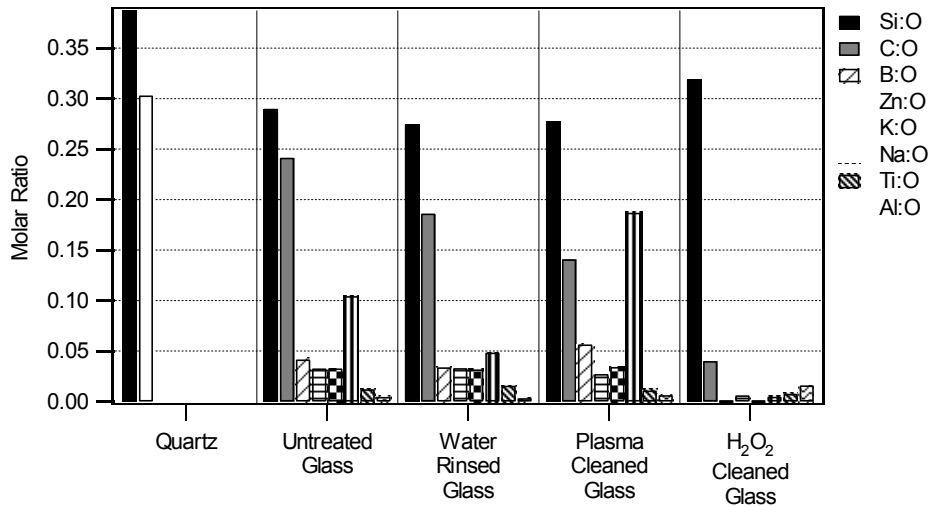


Figure 3.9. XPS analysis of the surfaces of quartz, untreated borosilicate glass, borosilicate glass rinsed with Nanopure water, plasma-cleaned borosilicate glass, and H_2O_2 -cleaned borosilicate glass. The molar ratios of various elements relative to oxygen are shown.

I.E. Discussion

The goal of this work is to understand the interaction of water with various surfaces often used in laboratory studies of heterogeneous reactions that occur in thin water surface films at room temperature. As discussed in detail elsewhere (*Finlayson-Pitts et al., 2003*), rates of NO₂ hydrolysis calculated for experiments, such as that shown in Figure 3.1, conducted in chambers of various sizes and wall composition can be compared after normalizing the rate for the surface-to-volume ratios of the reactors, the initial NO₂ concentrations, and the RH. Interestingly, the normalized rates of the heterogeneous hydrolysis of gaseous NO₂ that were measured in large smog chambers coated with hydrophobic Teflon (*Sakamaki et al., 1983; Pitts et al., 1984a*) and in much smaller hydrophilic Pyrex cells (*Finlayson-Pitts et al., 2003*) were similar. The data presented here provide some insights into why this is the case.

Borosilicate glass reactors are commonly used in many laboratory systems, and are known to adsorb water on their polar surface, which is terminated by Si-OH groups (*Langmuir, 1918; Derjaguin and Zorin, 1957; Adamson, 1967; Gregg and Sing, 1982; Saliba et al., 2001*). The multilayer uptake of gases on solids is commonly described by the BET model, which predicts that the fractional coverage of the surface can be described by the BET equation (VII) (*Gregg and Sing, 1982; Adamson, 1990; Masel, 1996; Adamson and Gast, 1997*),

$$\text{fractional coverage} = \frac{c_B \times \text{RH}}{(1 - \text{RH}) \times [1 + (c_B - 1) \times \text{RH}]} \quad (\text{VII})$$

where the constant $c_B \sim e^{(Q_1 - Q_v) / RT}$ and Q_1 and Q_v are the enthalpy of adsorption of water on the substrate and on water itself (*i.e.* the enthalpy of condensation of water), respectively (*Adamson and Gast, 1997*), and RH represents the partial pressure of the adsorbate. The shape of the isotherm is therefore determined by the value of the constant c_B , which reflects the strength of the interaction of the gas with the substrate. Model BET isotherms are shown in Figure 3.10 for c_B equal to 0.1 and 20. For c_B values larger than about 10, there is a “knee” in the isotherm at low RH; such isotherms are classified as Type II, and are typified by the uptake of water on polar surfaces (*Gregg and Sing, 1982*). For weak interactions between the gas and the surface, c_B is significantly smaller and the isotherms, classified as Type III, are smoothly concave with increasing relative humidity (*Adamson, 1967; Gregg and Sing, 1982; Adamson, 1990; Masel, 1996; Adamson and Gast, 1997*). Type III isotherms are often observed for water on non-polar surfaces (*Gregg and Sing, 1982*), where it forms islands (*Masel, 1996*). The AFM image in Fig. 3.3a does indeed show islands on the surface, which we attribute to water. While the AFM and infrared data are in reasonable agreement on the amount of water on the surface at relative humidities above ~60%, the smaller amounts of water at lower RH and the increased uncertainty in the appropriate infrared absorption coefficient in this region preclude definitively classifying the water uptake as Type II or Type III.

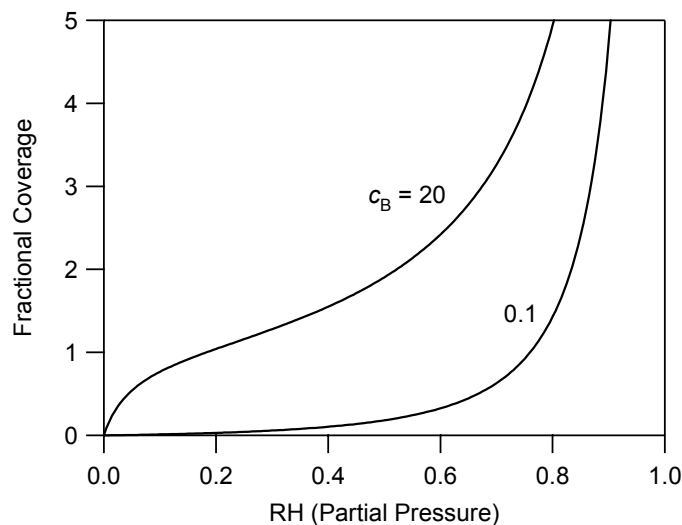


Figure 3.10. Model Type II ($c_B = 20$) and Type III ($c_B = 0.1$) BET isotherms described by equation (VII).

The BET isotherm (equation VII) predicts that, as the vapor pressure of the adsorbate is approached, the number of adsorbed layers should approach infinity, *i.e.* the surface should become fully covered with liquid water. However, as seen in Fig. 3.2b, water on the untreated borosilicate glass has a finite contact angle so that a drop of the bulk liquid is present at the same time that there is a thin film of water on the surface. As discussed in detail by Adamson (1968), this situation is best described by Type VI and VII isotherms. On a molecular level, these isotherms occur in situations in which the structure of the adsorbate molecules closest to the surface is highly perturbed compared to the bulk liquid. A variety of evidence in the literature shows that water at the solid/water interface is structured and has properties different from bulk water; the structured orientation of surface water may extend anywhere from three monolayers to many molecular diameters (Drost-Hansen, 1971; Parks, 1984). It is also supported by the red-shift in the infrared spectrum of water adsorbed on borosilicate glass reported from earlier studies in this laboratory (Saliba *et al.*, 2001) and also observed in the present work.

The amount of adsorbed water on untreated glass in the present study is somewhat smaller than reported in earlier, preliminary studies in this laboratory (Saliba *et al.*, 2001). This may be due to improved temperature control in the present experiments, variable degrees of organic contamination on the surfaces, or both. In any event, in typical laboratory glass vacuum systems, organic contamination from room air or backstreaming from pumps cannot be completely avoided and hence, the water uptake measured for the untreated borosilicate glass here should be comparable to that in such glass vacuum systems. It should be noted that surfaces in ambient air upon which heterogeneous chemistry occurs will also hold adsorbed organics.

The amount of water present on treated borosilicate glass shown in Fig. 3.6b demonstrates that the water uptake at higher RH is sensitive to the pretreatment of the

surface, with less water uptake if the glass has been plasma-cleaned or even just rinsed with Nanopure water prior to the experiments. XPS analysis (Fig. 3.9) indicates that the inorganic surface composition of these samples is similar to that of the untreated glass. However, there is less carbon on the plasma-cleaned sample as expected, and perhaps on the water-rinsed glass. This suggests that some of the organic material on the untreated glass is comprised of oxidized, polar organics that can be removed by rinsing with water. Such polar organics may also help to adsorb water onto the surface. Although these samples show differences in sodium, the water-rinsed glass has less Na and the plasma-cleaned more than the untreated glass, there is no observed correlation between water uptake and the surface sodium. This is not surprising since there is also no obvious reason to expect sodium to be involved in water uptake. Derjaguin and Zorin (1957) measured the thickness of water layers on cleaned smooth glass surfaces to be from a few Å to ~62 Å over the range from 95 – 100% RH; this would correspond to ~ 1 – 18 layers of water, consistent with the measurements reported here.

The H₂O₂-cleaned borosilicate glass is quite different from the other borosilicate glass samples in all of the characteristics studied here. The surface is now primarily composed of silica, with B, Zn, K and Na having been largely removed (Fig. 3.9), showing that the surface of the glass has been modified by the H₂O₂ treatment. The bulk most likely is not modified. The AFM image (Fig. 3.3c) does not show the large islands of water seen on the untreated glass. The water uptake (Fig. 3.7) is similar to a Type I Langmuir adsorption isotherm for which there are a fixed number of surface sites that become saturated at high adsorbate gas concentrations, or alternatively, a microporous surface in which the pores become progressively filled with water (Gregg and Sing, 1982; Adamson, 1990; Adamson and Gast, 1997). The shift in the infrared absorption peak to ~3200 cm⁻¹ suggests a more ice-like structure of the adsorbed water (Herzberg, 1945; Du et al., 1994a, b; Shultz et al., 2000; Richmond, 2001). The combination of all of these data suggest that the H₂O₂ forms micropores on leaching the trace metals, and these provide the major sites for water uptake.

Perhaps most interesting is the interaction of water with halocarbon wax, Teflon and the C8 SAM. Although these materials are classically considered to be hydrophobic, which is supported by the large measured contact angles (Table 3.1), the water uptake measurements indicate that a significant amount of water, similar to that on untreated borosilicate glass, can be taken up on the halocarbon wax coated glass, and to a lesser extent, on the smooth FEP Teflon film and C8 SAM (Fig. 3.5i). It is known that, on single crystal surfaces, water tends to adsorb at surface defects (Dai et al., 1995; Hoffman et al., 2003; 2004). Thus, adsorption of water onto solid surfaces may be dependent on the roughness of the surface, in addition to its chemical properties. For example, Rudich et al. (2000), showed that the corrugation of hydrophobic surfaces impacted the interaction with water and that more corrugated surfaces did, in fact, hold more water than the smooth organic films.

The AFM images support the hypothesis that surface roughness plays a major role in water uptake on the surfaces that are hydrophobic on a macroscopic scale. The halocarbon wax sample coated using the dip method is seen in Fig. 3.4a to have a very porous, web-like structure with deep and tortuous channels. The increased time to come to equilibrium with gas phase water (Fig. 3.8) is therefore not surprising. This highly irregular and porous

surface leads to significant amounts of water uptake, indeed, more than that on the untreated borosilicate glass surface (Fig. 3.6c). The solvent-coated halocarbon wax (Fig. 3.4b) has less surface roughness and does not appear to be as porous, but is still much more irregular than the glass and quartz (Table 3.1 and Fig. 3.3) so that uptake on surface discontinuities may occur. As seen in Fig. 3.6, the water uptake on the solvent-coated halocarbon wax surface (3.6c) is similar to that on the untreated borosilicate glass (3.6a). It is possible that the halocarbon wax coatings also have some adsorbed polar organics that assist in water uptake.

The thin FEP Teflon film also takes up some water (Fig. 3.5j), estimated to be ~2 equivalent layers of water at 80% RH and rising to ~6 equivalent layers at 100% RH, significantly less than the halocarbon wax coatings. Awakuni and Calderwood (1972) reported uptake of three layers of water by Teflon film at 100% RH. Svensson *et al.* (1987) reported two layers on Teflon film at 5% relative humidity, with condensation on the surface at 90% RH; however, it is not clear that the surface structure of the material in those studies is comparable to the Teflon film used here. The AFM image of our Teflon film sample (Fig. 3.4c) shows very small pores that may be responsible for water uptake. The depth of these pores is greater on average than those in the C8 SAM, as indicated by a surface roughness of 72 Å compared to 9 Å for the SAM. The smooth, relatively defect-free nature of the C8 SAM is likely responsible not only for the small amounts of water it takes up, but also for the shift in the infrared spectrum (Fig. 3.5i) to a more ice-like structure. The small amounts of water that are adsorbed on the C8 SAM may be taken up in defects in the coating which expose small regions of the underlying glass substrate, and/or on some of the elevated features on the surface seen in Fig. 3.3d.

As discussed earlier, laboratory studies of heterogeneous atmospheric reactions in thin aqueous films have typically used reactors made of glass, quartz, Teflon-coated glass or metal, and thin FEP Teflon films. The similarity in kinetics and mechanisms for the NO₂ heterogeneous hydrolysis in a halocarbon wax coated chamber (Fig. 3.1) to that in borosilicate glass chambers (Finlayson-Pitts *et al.*, 2003) can now be understood since the two surfaces have now been shown to adsorb similar amounts of water (Fig. 3.6c, halocarbon wax dip method). Given the importance of surface structure (*e.g.* roughness and porosity) for water adsorption, it is expected that the FEP and PFA Teflon coatings, which also have quite high surface roughness values (Table 3.1), would behave in a similar manner to the halocarbon wax coatings. Thus, the agreement with studies carried out in Teflon-coated smog chambers (Sakamaki *et al.*, 1983; Pitts *et al.*, 1984a) is also understandable.

Thin films of FEP Teflon adsorb substantially less water than the halocarbon wax, and presumably less than the similarly rough Teflon coatings as well. The much smaller water uptake on smooth FEP Teflon films is consistent with the smaller rates of NO₂ heterogeneous hydrolysis measured by Pitts *et al.* (1984a). However, it should be noted that in experiments using chambers constructed of such films, other materials inside the chambers such as optics and sampling lines may contribute significantly to the uptake of water and hence the surface available for heterogeneous chemistry.

I.F. Atmospheric Implications

As discussed in more detail elsewhere (Finlayson-Pitts *et al.*, 2003; Rivera-Figueroa *et al.*, 2003), silicates are common components of many surfaces found in building materials, including concrete, asphalt, and window glass (Diamant, 1970). In addition, silica has been identified as a major component of soil and soil derived dust (Gillette, 1997; Finlayson-Pitts and Pitts, 2000). The uptake of water on such surfaces is known to promote heterogeneous chemistry not only in laboratory systems (Saliba *et al.*, 2001; Finlayson-Pitts *et al.*, 2003), but also on surfaces found in the tropospheric boundary layer. Therefore, our measurements of water uptake on borosilicate glass and quartz are relevant and useful for understanding chemistry on these tropospheric surfaces.

Given our measurements showing that water adsorbs even to hydrophobic materials if their surfaces have appropriate roughness, it is likely that other hydrophobic materials, such as vegetation, may also hold water in quantities sufficient to support heterogeneous chemistry. Figure 3.11 shows AFM images of the surfaces of an ivy leaf and a *Vinca minor* flower petal. Clearly there are surface irregularities that, despite the hydrophobic nature of the surfaces, should lead to water uptake in a manner similar to the halocarbon wax. The surface roughness values for a $1\ \mu\text{m} \times 1\ \mu\text{m}$ section of each sample were $195\ \text{\AA}$ for an ivy leaf and $51\ \text{\AA}$ for the *Vinca minor* petal, similar to the values for halocarbon wax and Teflon in Table 3.1. Water uptake on vegetation and its participation in heterogeneous reactions in the atmosphere is supported by the observation of HONO production over a variety of surface types, including vegetation (Perner and Platt, 1979; Platt *et al.*, 1980; Winer and Biermann, 1994; Harrison *et al.*, 1996; Lammel and Cape, 1996; Lammel, 1999; Finlayson-Pitts and Pitts, 2000; Aliche *et al.*, 2002; Stutz *et al.*, 2002a).

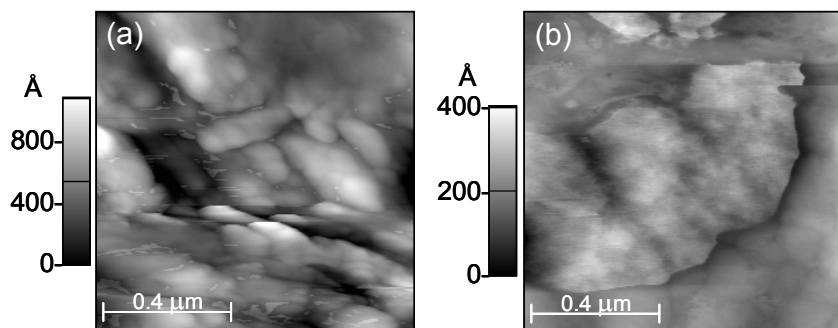


Figure 3.11. AFM images of (a) a green ivy leaf surface with an RMS surface roughness of $195\ \text{\AA}$ and (b) a *Vinca minor* flower petal with an RMS surface roughness of $51\ \text{\AA}$.

The results presented here give a strong indication that most, if not all, surfaces in contact with the atmosphere will hold water in sufficient amounts to promote heterogeneous reactions. Further field investigations of surface chemistry and elucidation of the impact of including heterogeneous reactions (*e.g.* reactions (1) and (4)) in atmospheric models are necessary to determine the full role played by heterogeneous chemistry in the atmosphere.

II. MECHANISM OF THE HETEROGENEOUS REACTION OF NO₂ WITH WATER

II.A. Background

Once the nature of water on the surfaces and its relationship to gas phase water had been elucidated, this knowledge was applied to understanding the role of surface water in the heterogeneous NO₂ hydrolysis. Here we present new experimental data for this heterogeneous hydrolysis and discuss them in light of earlier studies. We outline major features of a new mechanism for reaction (1) that is consistent not only with our experiments but also with many of the previous observations.

The studies reported here have been carried out using borosilicate glass, which is relevant to understanding the mechanism in laboratory systems. This is an essential first step for extrapolating to processes in urban airsheds. As discussed in the previous section, silicates are atmospherically relevant as they are major components of building materials and soils (*Gillette, 1997; BNZ Materials, 1999a, b; Portland Cement Association, 1999; USGS, 1999*). The surface area available in soils and buildings may be comparable to, or larger than, the surface area of airborne particles in the planetary boundary layer. Thus, it is expected that heterogeneous chemistry in the boundary layer, where measurements of HONO and other oxides of nitrogen are often made, will have a significant contribution from reactions on soils, buildings, roads, and other such materials (*Harrison et al., 1996; Lammel and Cape, 1996; Lammel, 1999*). There is some evidence for this from field studies. For example, Harrison and coworkers observed fluxes of HONO upward from the surface when NO₂ concentrations were >10 ppb, but downward fluxes at smaller NO₂ concentrations; they attributed this to competition between generation at the surface and the deposition of HONO (*Harrison and Kitto, 1994; Harrison et al., 1996*). Andrés-Hernández *et al.* concluded that the relatively large HONO/NO_x ratios they observed in Milan compared to less polluted non-urban regions were due to heterogeneous chemistry on urban surfaces such as buildings, aided by a low inversion layer (*Andrés-Hernández et al., 1996*).

In short, given the contribution of silicates to the composition of soils and many building materials, the chemistry discussed below may extrapolate in a reasonable fashion to the lowest portion of the atmosphere in urban areas. In addition, as discussed below, this chemistry may occur on airborne dust particles that are transported globally. Finally, the mechanistic insights obtained from room temperature studies on surfaces will also aid in understanding the chemistry and photochemistry reported on ice surfaces.

We focus here on studies of heterogeneous NO₂ hydrolysis that have been carried out using water vapor, gas phase NO₂ and a solid surface. The potential relevance to the reactions on liquid aerosol particles, fogs and clouds is discussed briefly in Section 3.II.E.

II.B. A New Mechanism for HONO Formation from the Reaction of NO₂ with Water on Surfaces

Figure 3.12 is a schematic diagram of the major components of our proposed mechanism. The key features are as follows:

1. The dimer of nitrogen dioxide, N₂O₄, is an important precursor surface species in the reaction.
2. The reactive surface species is proposed to be asymmetric dinitrogen tetroxide, ONONO₂, formed by isomerization of symmetric N₂O₄.
3. The asymmetric ONONO₂ autoionizes to generate NO⁺NO₃⁻, this is in competition with a back reaction with gas phase NO₂ to form symmetric N₂O₄. The NO⁺NO₃⁻ complex reacts with water to generate HONO that escapes, at least in part, from the surface in a process that involves water, as well as nitric acid that remains on the surface.
4. The HNO₃ on the surface generates NO₂⁺, a well known reaction in concentrated solutions of HNO₃.
5. Nitric oxide is generated by the reaction of HONO with NO₂⁺. Nitrous acid also reacts with HNO₃ to generate NO⁺ on the surface.

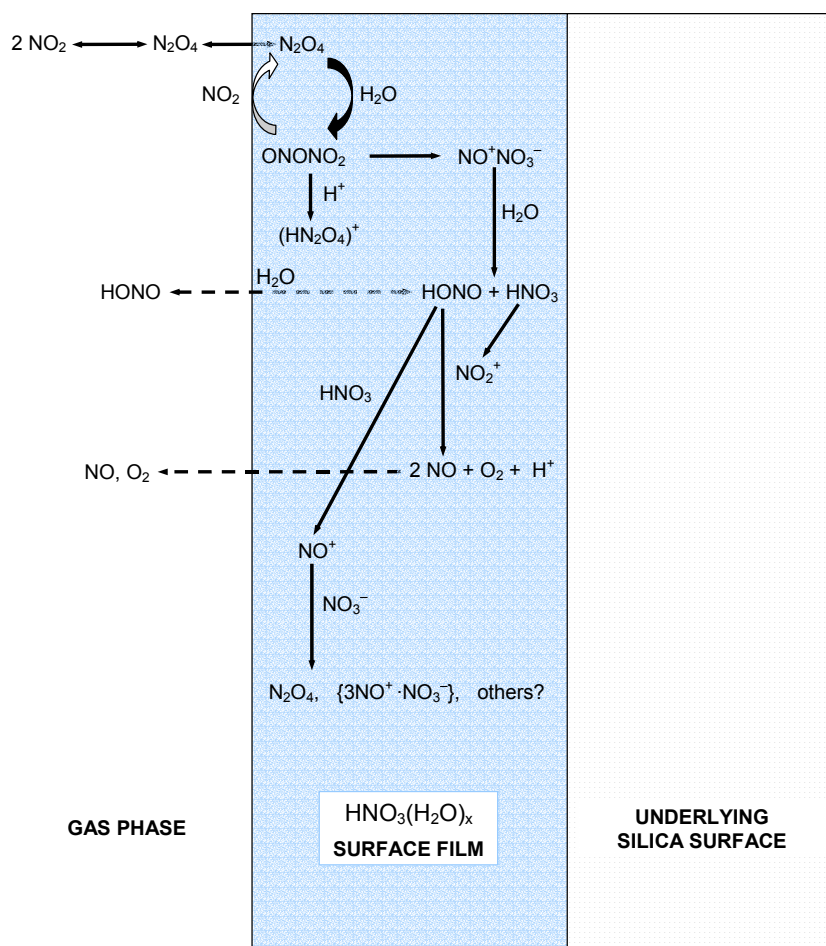


Figure 3.12. Schematic diagram of proposed mechanism of heterogeneous hydrolysis of NO₂.

We describe in the following sections a variety of experimental data from this laboratory and show that this mechanism is consistent with these data as well as with many observations from previous studies of the heterogeneous hydrolysis of NO₂.

II.C. Present and Prior Observations: Testing the Mechanism

II.C.1. Products, Intermediates, and Mass Balance

II.C.1a. Gas Phase Products.

Product formation in heterogeneous NO₂ hydrolysis experiments has been studied in this laboratory using Fourier transform infrared spectroscopy (FTIR) to measure gaseous species in two borosilicate glass long path cells with multi-reflection White cell optics (*White, 1942*). The characteristics of these cells are summarized in Table 2.1. The experiments were carried out by first adding a low pressure of a dilute NO₂/N₂ mixture to the cell and then bringing the cell to atmospheric pressure at the desired relative humidity (~20, 50, or 80%) using the appropriate combination of flows of H₂O/N₂ and dry N₂. The reactants and products were measured by FTIR in the dark for reaction times up to 15 hr.

Throughout this section, we use a combination of units for concentration: molecule cm⁻³ or ppm for NO₂, HONO, NO and N₂O, and either relative humidity (RH) or molecule cm⁻³ for water vapor. Because concentrations have been reported both ways in the previous literature, we prefer to report our data using both conventions for ease of comparison with the various studies.

Typical concentration-time profiles for these experiments are shown in Figure 3.13 at three different relative humidities. The experiments at ~20% and ~50% RH were carried out in the smaller cell (S/V = 70 m⁻¹) with an initial NO₂ concentration of 60 ppm. Runs were also carried out at 80% RH in the smaller cell, but there was a large uncertainty in quantification of the loss of NO₂ that may have been caused by significant amounts of liquid water at this high relative humidity on the optical mirrors as they aged. The experiment shown at 80% RH was carried out using the larger cell (S/V = 46 m⁻¹) and an initial NO₂ concentration of 100 ppm. The reaction occurs on the surface and hence depends on the S/V ratio of the reaction chamber; as discussed in more detail below, the rate of HONO formation also depends linearly on the initial NO₂ concentration. Experiments in these two cells under conditions where the *product* of the S/V ratio and the initial NO₂ concentration are similar, as is the case for the data in Figure 3.13a-c, should thus be directly comparable and, indeed, as discussed in more detail below, they are consistent.

In agreement with previous studies of this reaction, HONO and NO are the two major gaseous products observed (*England and Corcoran, 1974; TenBrink et al., 1978; Sakamaki et al., 1983; Pitts et al., 1984a; 1985; Akimoto et al., 1987; Svensson et al., 1987; Jenkin et al., 1988; Perrino et al., 1988; Wiesen et al., 1995; Kleffmann et al., 1998a; Wainman et al., 2001*). Small amounts of N₂O are also formed at the higher relative humidities and longer reaction times. The rates of loss of NO₂ and the formation of products clearly increase as the

Under all conditions, nitrous acid increases initially, reaches a plateau, and then decreases. This behavior suggests that HONO undergoes secondary chemistry in the cell.

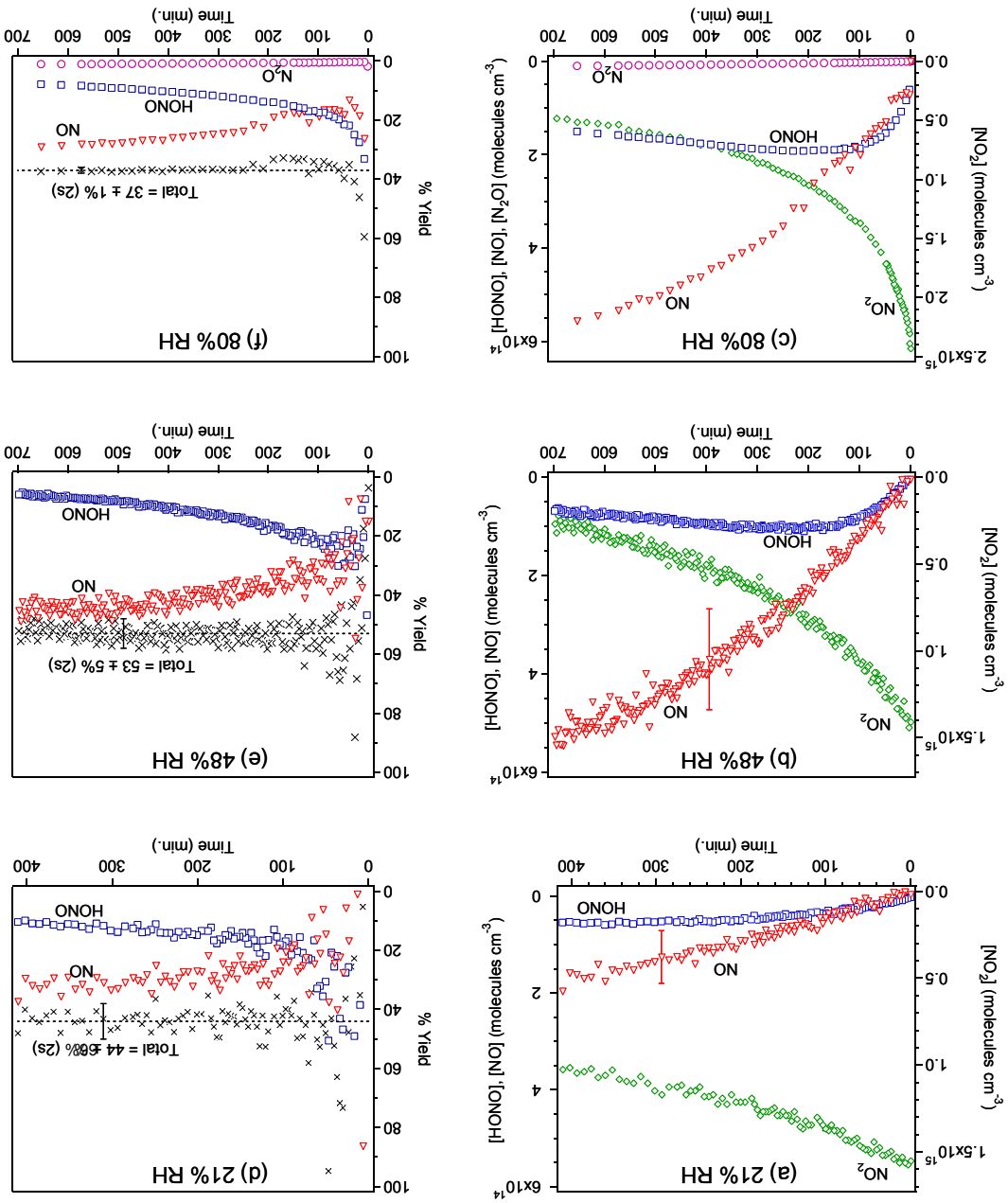


Figure 3.13. Concentration-time profiles for NO_2 hydrolysis experiments in this laboratory at (a) 21% RH, $[\text{NO}_2]_0 = 1.5 \times 10^{15} \text{ molecule cm}^{-3}$, (b) 48% RH, $[\text{NO}_2]_0 = 1.4 \times 10^{15} \text{ molecule cm}^{-3}$, (c) 80% RH, $[\text{NO}_2]_0 = 2.5 \times 10^{15} \text{ molecule cm}^{-3}$. The corresponding yields of gas phase HONO, NO and N_2O , expressed relative to the measured losses of NO_2 , are shown in parts (d-f). As discussed in the text, the yields for each gaseous product were determined as a function of time and are also shown in Figure 3.13d-f. The yield of HONO is much less than 50% of the NO_2 loss, the experiments at 21% and 48% RH were carried out in the 7.4 L cell and particularly at longer reaction times where secondary chemistry becomes more important that at 80% in the 19.4 L cell.

The yield of NO relative to HONO increases with time, and NO becomes the major product after several hours. The formation of small amounts of N₂O is in agreement with the studies of Wiesen *et al.* and Kleffmann *et al.* who reported N₂O formation during hydrolysis of NO₂ on the acidic surfaces of quartz reaction chambers and on perchloric acid/air interfaces using a bubbler apparatus (Wiesen *et al.*, 1995; Kleffmann *et al.*, 1998a, b).

For the overall reaction (1), the yield of gaseous HONO plus its secondary reaction products such as NO should be 50%. This is consistent with our measurements (Figure 3.13d-f) when the experimental uncertainties, particularly in the NO concentrations, are taken into account. The scatter in the yield plots at shorter reaction times is due to two factors: (1) the products are present in concentrations near their detection limits, and (2) the change in the NO₂ concentration is small.

The variation in the yields of NO and HONO in the previous laboratory studies in the literature suggests that the nature of the surface film plays an important role in determining the relative amounts of NO and HONO generated (England and Corcoran, 1974; TenBrink *et al.*, 1978; Sakamaki *et al.*, 1983; Pitts *et al.*, 1984a; 1985; Svensson *et al.*, 1987; Jenkin *et al.*, 1988). The initial yields of HONO approached 50% in the studies of Pitts *et al.* where the initial NO₂ concentrations were, for the most part, below 1 ppm (Pitts *et al.*, 1984a). Sakamaki *et al.* used a reaction chamber that was very similar in size (see Table 3.2) and surface materials, but observed significant yields of NO (about 30% of the HONO yields) even at short reaction times; however, their initial NO₂ concentrations were larger, from 0.78 ppm to 20 ppm (Sakamaki *et al.*, 1983). This was also the case for our studies, as well as those of a number of other researchers (England and Corcoran, 1974; TenBrink *et al.*, 1978; Svensson *et al.*, 1987), which were carried out using initial NO₂ concentrations above one ppm. The use of higher reactant concentrations will result in more rapid accumulation of HNO₃ on the walls of the reactor and hence accelerate secondary surface reactions involving HNO₃. Perhaps relevant to this is the work of Febo and Perrino which, in contrast to the other studies, was carried out under flow conditions; they observed equimolar production of nitrite and nitrate, with the sum equal to the NO₂ loss (Febo and Perrino, 1991). Under flow conditions, HONO would be swept away from the acidic surface as it is formed, minimizing secondary reactions on the walls. The body of evidence therefore suggests that the NO that is observed results from secondary reactions of HONO on the walls of the reactor.

II.C.1b. Surface Species.

i. N₂O₄. Infrared spectroscopic studies show that adsorbed N₂O₄ is formed on the reaction surface immediately upon exposure of silica surfaces to gaseous NO₂ at room temperature (Goodman *et al.*, 1999; Barney and Finlayson-Pitts, 2000). There is no evidence for detectable amounts of NO₂ adsorbed on the surface. This is reasonable since the Henry's law coefficient for N₂O₄ in water and sulfuric acid is approximately two orders of magnitude larger than that for NO₂ (Schwartz and White, 1981, 1983; Langenberg *et al.*, 1998; Finlayson-Pitts and Pitts, 2000). Although we show below that these reactions cannot be thought of as occurring in bulk aqueous solutions, the relative values of the Henry's law constants do indicate that the interaction of water with N₂O₄ is more favorable than with NO₂. Chou *et al.* (1999) have shown by *ab initio* calculations that complexes between N₂O₄

and one or two water molecules are stabilized by 4.3 kcal mol⁻¹ and 11.5 kcal mol⁻¹, respectively, relative to separated N₂O₄ and water; the complexes of NO₂ with one or two water molecules were shown to be stabilized by only 0.9 kcal mol⁻¹ and 8.3 kcal mol⁻¹ relative to the separated reactants. Thus, both the relative values of the N₂O₄ and NO₂ Henry's law constants and *ab initio* calculations show that N₂O₄ interacts more strongly with water and would be more likely present in the surface water film than NO₂.

Although N₂O₄ is observed on the surface immediately upon exposure to NO₂, it is not known how N₂O₄ interacts with the surface film. Possible interactions include association with one or more H₂O molecules (*Chou et al., 1999*), with undissociated HNO₃ molecules, or with HNO₃-H₂O complexes or hydrates. Nitric acid does appear to be involved as our experiments show that it enhances the amount of N₂O₄ adsorbed on the surface. Figure 3.14 shows the transmission spectra of clean pieces of porous glass (Vycor 7930, 14 mm diameter × 0.24 mm thick discs of mass 59 mg and an internal (BET) surface area of 90 m² g⁻¹, Advanced Glass and Ceramics, Holden, MA) exposed in a cell described elsewhere (*Barney and Finlayson-Pitts, 2000*) to NO₂ with and without prior adsorption of HNO₃ on the glass surface. The porous glass had been exposed to the water vapor in room air and not heated during the initial cell evacuation. Under these conditions, water remains adsorbed on the surface.

In Figure 3.14a, the glass has been “conditioned” with dry gaseous HNO₃ by adding 2 – 3 Torr of HNO₃ vapor from above a mixture of 2:1 H₂SO₄:HNO₃ to the cell, and then pumping it out; this procedure was repeated three times followed by pumping for 30 min. before 1.2 Torr NO₂ was added. Figure 3.14b is the spectrum for porous glass that was exposed to 1.3 Torr of gaseous NO₂ alone. In both cases, the cell was filled with N₂ to atmospheric pressure. The band at 1680 cm⁻¹ is due to molecular nitric acid on the surface and that at 1740 cm⁻¹ is due to adsorbed N₂O₄ (*Hisatsune et al., 1960; Koch et al., 1995; Goodman et al., 1999; Barney and Finlayson-Pitts, 2000*). Figure 3.14c is the difference spectrum, (a – 0.92b), where the factor 0.92 takes into account the slightly larger NO₂ pressure when the spectrum in Figure 3.14b was taken. These data show that not only is N₂O₄ taken up on the porous glass surface, but also that the amount adsorbed increases with the amount of nitric acid on the surface. This suggests that N₂O₄ is interacting with HNO₃ and/or HNO₃-H₂O water complexes on the surface, perhaps in addition to the interactions with H₂O.

In the long path cell studies shown in Figure 3.13 surface species could not be measured and so it was not known if NO₂/N₂O₄ was taken up on the surface. However, given the rapid appearance of N₂O₄ on silica surfaces (*Goodman et al., 1999; Barney and Finlayson-Pitts, 2000*), it is likely that a similar process occurs on the borosilicate glass cell walls.

N₂O₄ has generally been ignored as being important in the atmosphere because of its small concentrations and relatively slow reactions in the gas phase. For example, at an NO₂ concentration of 0.1 ppm (2.5 × 10¹² molecule cm⁻³), the equilibrium concentration of N₂O₄ is only 1.5 × 10⁶ molecule cm⁻³, based on the well-known 2 NO₂ ↔ N₂O₄ equilibrium constant (*DeMore et al., 1997*). Although our studies were carried out at much higher

concentrations of NO_2 , and hence N_2O_4 , than found in the atmosphere, they demonstrate that N_2O_4 is preferentially taken up on surfaces compared to NO_2 . Given that the kinetics on surfaces may be quite different than in the gas phase and that the relevant chemistry forming HONO in the atmosphere occurs rather slowly (*e.g.*, overnight), it is reasonable that N_2O_4 could play a role under atmospheric conditions.

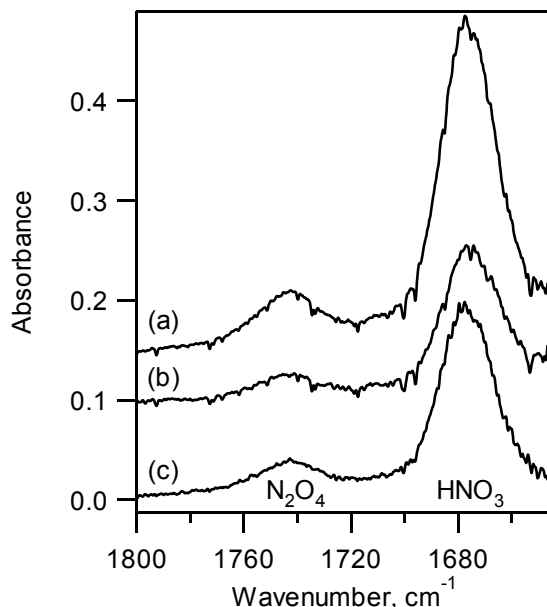


Figure 3.14. Spectra of porous glass discs: (a) Exposed to gaseous HNO_3 followed by pumping and then adding 1.2 Torr NO_2 ; (b) Porous glass exposed to 1.3 Torr NO_2 only; (c) Difference spectrum (a-0.92b). All experiments carried out in 1 atm N_2 using 64 scans at 1 cm^{-1} resolution. Background used for spectra was that of the unexposed porous glass.

ii. Nitric acid and Nitric Acid-Water Hydrates. While a number of groups report that HNO_3 production is not observed in the gas phase (*Sakamaki et al., 1983; Pitts et al., 1984a; Svensson et al., 1987; Febo and Perrino, 1991*), a variety of both indirect as well as direct evidence indicates that HNO_3 is indeed formed and remains on the surface. For example, *Svensson et al.* rinsed the walls of their chamber with water after NO_2 hydrolysis experiments and analyzed the washings by ion chromatography (IC); the nitrate concentration was shown to be consistent with the stoichiometry of reaction (1) (*Svensson et al., 1987*). *Febo and Perrino* used a glass flow reactor to study the products of NO_2 hydrolysis (*Febo and Perrino, 1991*). The HNO_3 and HONO that remained on the walls after reaction were collected and measured by IC as NO_3^- and NO_2^- , respectively, while gaseous HONO was measured using a chemiluminescence analyzer in combination with denuders to remove HNO_3 and HONO, or HNO_3 only. In their experiments, equal rates of formation of nitrite and nitrate were observed, and the sum was equal to the NO_2 decay rate.

More recently, infrared studies have confirmed the formation of HNO_3 and NO_3^- during the reaction of NO_2 on silica surfaces (*Goodman et al., 1999; Barney and Finlayson-*

Pitts, 2000). For example, Goodman *et al.* (1999) showed by transmission FTIR that addition of gaseous NO₂ to dehydrated silica particles (heated to 673 K) yields oxide-coordinated NO₃⁻. In contrast, the use of hydrated silica particles, prepared by exposure to ≥ 10 Torr H₂O followed by evacuation (yielding a coverage of 0.08 H₂O monolayers), resulted in the formation of undissociated HNO₃ upon addition of gaseous NO₂. The authors suggest that water on hydrated silica particles interacts with undissociated HNO₃ via hydrogen bonding which may be observed as a broad absorption in the 2700 – 3700 cm⁻¹ region. Similar observations of the formation of undissociated HNO₃ during the reaction of NO₂ on porous glass were also made in this laboratory (*Barney and Finlayson-Pitts, 2000*); the infrared cutoff of porous glass at ~1550 cm⁻¹ did not allow the observation of nitrate ions, but subsequent studies using pressed discs of silica powder where the cutoff is extended to ~1300 cm⁻¹ revealed small peaks due to NO₃⁻ (*Rivera-Figueroa et al., 2003*).

It should be noted that the surface nitric acid observed is largely *undissociated* HNO₃ which, as discussed below, has unique reactivity compared to the dissociated H⁺ and NO₃⁻ ions. Thin films of water on silica surfaces do not have the same spectroscopic signatures as bulk water, so it is perhaps not surprising to find undissociated HNO₃ associated with these thin water films. For example, transmission FTIR spectroscopy experiments on water uptake on borosilicate glass discussed earlier show that at the water vapor concentrations used in these experiments, one to twelve monolayers of water (corresponding to film thicknesses of 0.35 to 4 nm) would be present on the surface in the absence of nitric acid (*Saliba et al., 2001; Sumner et al., 2004*). These thin water films exhibit blue-shifted O-H stretching vibrations relative to bulk, liquid water, indicating that the thin films are less hydrogen-bonded than in the bulk liquid. This is similar to the observations of Ewing and coworkers on solids such as mica and NaCl, and has been interpreted as reflecting either a two-dimensional water network or islands of water on the surface (*Foster and Ewing, 1999, 2000; Cantrell and Ewing, 2001*). While it has been suggested that water films have properties approaching bulk water at approximately 3 water monolayers (*Parks, 1984*), the data of Saliba *et al.* and Sumner *et al.* show that the O-H stretch of adsorbed water is blue-shifted relative to bulk water even at 5 water monolayers (*Saliba et al., 2001; Sumner et al., 2004*). This suggests that it may be more appropriate to consider the mechanism of the NO₂ heterogeneous hydrolysis as occurring in a 2-D surface film or in small islands, rather than in a bulk, 3-D liquid.

However, this surface film is not simply comprised of water, since nitric acid is formed simultaneously during the reaction and remains on the surface. In addition, as discussed in more detail below, even after pumping and moderate heating, nitric acid from previous experiments remains on the surface. Thus, the thin film is, at the very least, comprised of nitric acid and water. An experimental observation common to researchers handling nitric acid in glass vacuum systems is that HNO₃ is very “sticky” and difficult to pump out, even with extensive heating and pumping. However, experiments in this and other (*Goodman et al., 2001*) laboratories show that nitric acid can be readily pumped off dry silica surfaces. The role of water must be to form very stable nitric acid-water complexes or hydrates. Nitric acid is well known to form hydrates with water both in aqueous solution (*Chédin, 1952; Högfeldt, 1963; Addison, 1980*) and on ice (*Tolbert and Middlebrook, 1990; Ritzhaupt and Devlin, 1991; Koch et al., 1996; Tisdale et al., 1999*). In aqueous solution, as

the concentration of nitric acid increases, the composition changes from the dissociated ions to the trihydrate and then the monohydrate, and finally pure HNO₃ (Chédin, 1952; Högfeldt, 1963; Addison, 1980). On ice, the dihydrate is also observed (Tolbert and Middlebrook, 1990; Ritzhaupt and Devlin, 1991; Koch et al., 1996; Tisdale et al., 1999). Different forms of the monohydrate such as H₂O...HONO₂, (H₂OH)⁺....(ONO₂)⁻ and 4HNO₃·H₂O have also been observed using Raman spectroscopy (Herzog-Cance et al., 1978; Thi et al., 1981).

There is also theoretical evidence for nitric acid-water complexes. *Ab initio* calculations of the 1:1 nitric acid-water complex in the gas phase have been carried out showing that two hydrogen bonds form between HNO₃ and H₂O with a binding energy for the complex of 9.5 kcal mol⁻¹ (Tao et al., 1996; Staikova and Donaldson, 2001; McCurdy et al., 2002). Although such *ab initio* calculations are for a gas phase environment, these calculations show that undissociated HNO₃ is stabilized upon formation of the HNO₃-H₂O complex. Studies of water clusters with HNO₃ have shown that four water molecules are required for dissociation of nitric acid (Kay et al., 1981; Zhang et al., 1994; Gilligan and Castleman, 2001). Thus, complexation of nitric acid with the relatively small amounts of water present in thin films on the surfaces, and limited dissociation to H⁺ and NO₃⁻ is reasonable.

It should be noted that, in our experiments as well as those of other researchers, the reaction chambers are typically pumped on after each experiment, sometimes with heating. However, at least in the case of borosilicate glass, some nitric acid and water remains on the surface. As a result, the surface layer already contains adsorbed acid when the next experiment is initiated. This is likely responsible for the “dirty chamber” effect on the rates reported by some groups (Pitts et al., 1984a; Svensson et al., 1987).

Experiments were conducted on porous glass to determine the relative strengths of interaction of HNO₃ and H₂O with a silica surface and how pumping affects the relative magnitudes of water and nitric acid. Figure 3.15a is a spectrum of water adsorbed on the porous glass, obtained by first heating the porous glass to 400 K to drive off adsorbed water, cooling to room temperature and then exposing to 10 Torr water vapor in 723 Torr N₂ for 30 min.; the gas phase water peaks have been subtracted. Absorption bands due to water at 1620 cm⁻¹ (ν₂ bending mode), 3400 cm⁻¹ (ν₁ and ν₃ stretching modes) and a weak combination band (ν₂ + ν₃) at 5272 cm⁻¹ are evident. The negative peak at 3750 cm⁻¹ is due to the free (non-hydrogen bonded) SiO-H stretch, indicating that free SiO-H groups decrease on exposure to water vapor. This is believed to be due to clustering of water to these groups via hydrogen bonding interactions; on pumping off the water, this peak recovers, indicating that the interaction is reversible.

Figure 3.15b shows spectra of porous glass after it had been heated to 420 K, cooled and exposed to 1.5 Torr HNO₃ followed by 10 Torr of water vapor. The first spectrum (black) was taken 10 min. later (the gas phase has been subtracted). The peak at 3400 cm⁻¹ has red-shifted by ~70 cm⁻¹ to 3330 cm⁻¹, and a new peak at 1680 cm⁻¹ appears. The latter is assigned to undissociated HNO₃ (Goodman et al., 1999; Barney and Finlayson-Pitts, 2000; Goodman et al., 2001). The peak at 1620 cm⁻¹ has broadened. *Ab initio* calculations show that the formation of a 1:1 HNO₃-H₂O complex in the gas phase results in a band at ~ 3300

cm^{-1} due to the hydrogen-bonded OH ν_1 stretch in nitric acid; this band is red-shifted by ~ 300 cm^{-1} from the OH stretch in the uncomplexed gas phase HNO_3 (Tao *et al.*, 1996; Staikova and Donaldson, 2001; McCurdy *et al.*, 2002). As more water is complexed to nitric acid, this band continues to red-shift (McCurdy *et al.*, 2002). These calculations are consistent with the infrared spectra of nitric acid hydrates, which typically have strong bands in this region (Tolbert and Middlebrook, 1990; Ritzhaupt and Devlin, 1991; Koch *et al.*, 1996; Tisdale *et al.*, 1999). However, the bending mode of water in the 1600 cm^{-1} region does not change significantly on binding to nitric acid, which is consistent with our observations (Tao *et al.*, 1996; Staikova and Donaldson, 2001; McCurdy *et al.*, 2002). We therefore assign the peaks at 3300 cm^{-1} and 1620 cm^{-1} in Figure 3.15b to a combination of liquid water and nitric acid-water complexes.

The subsequent spectra were taken after pumping times of 5 s, 10 s and 35 s. During these initial stages of pumping, it can be seen that the water peak at 5272 cm^{-1} decreases, indicating water is being pumped off the surface. The peaks at 1680 cm^{-1} due to HNO_3 and 1620 cm^{-1} due to water, or water complexed to nitric acid, also decrease; however, the 1620 cm^{-1} band decreases more rapidly than that at 1680 cm^{-1} (Fig. 3.15d). These indicate a change in the composition of the surface film, consistent with the preferential removal of water, and may reflect a change from the trihydrate through the dihydrate to the monohydrate and perhaps ultimately species such as $4\text{HNO}_3 \cdot \text{H}_2\text{O}$ as observed in solid and liquid mixtures of HNO_3 and water by Raman spectroscopy (Herzog-Cance *et al.*, 1978).

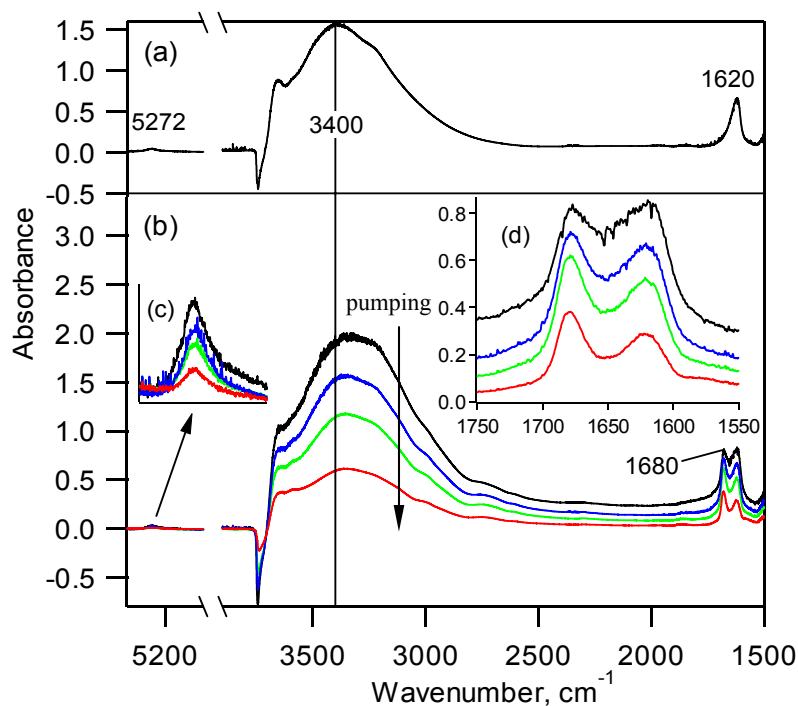


Figure 3.15. Spectra of porous glass exposed to (a) water vapor and (b) water vapor and nitric acid after pumping times of 0, 5, 10, and 35 s. The insets show expanded regions for absorptions by (c) H_2O and (d) HNO_3 , H_2O and complexes between the two.

The combination of data suggests that there are significant amounts of undissociated nitric acid on the surface, perhaps in part in the form of hydrates. In concentrated HNO₃ solutions, NO₂⁺ is also generated via a self-reaction of HNO₃ (Addison, 1980):



These reactions are in equilibrium so that, in the presence of sufficient water, NO₂⁺ converts back to HNO₃. Experimental studies have shown that, in the gas phase, this conversion of NO₂⁺ to HNO₃ occurs in clusters of NO₂⁺ with four or more water molecules (Fehsenfeld and Howard, 1973; Fehsenfeld et al., 1975; Cao et al., 1993; Sunderlin and Squires, 1993; Cao et al., 1994).

A search was made for NO₂⁺ on porous glass during an NO₂ hydrolysis experiment, and, for comparison, porous glass was exposed to gaseous HNO₃ alone. Figure 3.16a shows the spectrum in the 2200 to 2400 cm⁻¹ region of porous glass upon exposure to 1.3 Torr NO₂ and addition of N₂ to atmospheric pressure; the porous glass had been exposed to room air and evacuated but not heated, so there are significant amounts of water on the surface to participate in the hydrolysis. The broad peak at 2297 cm⁻¹ is consistent with that reported in the literature for NO₂⁺ (Forney et al., 1993; Koch et al., 1995; Agreiter et al., 2001). Figure 3.16b is the spectrum in the same region of a similar piece of porous glass that had been exposed to HNO₃ and then the gas phase pumped off; the peak at 2297 cm⁻¹ is also present, as expected for NO₂⁺ formed from concentrated HNO₃. To confirm this assignment, a fresh piece of porous glass was exposed to ¹⁵N-labelled nitric acid; it is seen in Figure 3.16c that the peak has red-shifted by 33 cm⁻¹, to 2265 cm⁻¹, confirming the assignment of this band as NO₂⁺ (Forney et al., 1993).

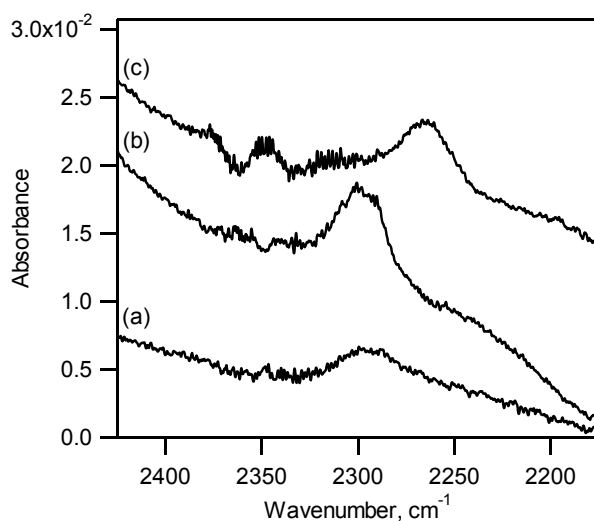


Figure 3.16. Spectra of NO₂⁺ on porous glass surface (a) during heterogeneous NO₂ hydrolysis; (b) after exposure to gaseous HNO₃, and (c) after exposure to H¹⁵NO₃.

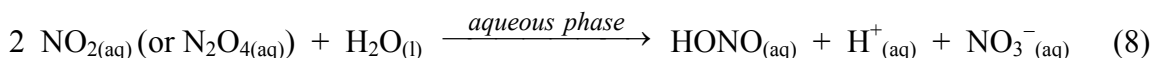
In summary, the composition of nitric acid-water thin films on silicate and other surfaces is clearly complex, but cannot be thought of as simply nitric acid-water aqueous solutions. The composition of these thin films under atmospheric conditions is not known, but clearly is an area that warrants both theoretical and experimental investigation. Despite the complexity, however, we have observed in laboratory studies many of the gas phase as well as surface intermediates and products proposed in the mechanism shown in Figure 3.12. These include HONO and NO in the gas phase, and on the surface, HNO₃, water-nitric acid complexes, NO₂⁺ and N₂O₄.

II.C.2. Kinetics

II.C.2a. Rate of NO₂ Hydrolysis Reaction.

It is clear from the combination of data discussed above that a thin film of water with nitric acid on the surface provides the reaction medium for the heterogeneous NO₂ hydrolysis. Although the infrared data show that this film does not, at least spectroscopically, behave like a bulk liquid, it is worthwhile to compare the measured rates of HONO generation with those expected *if* the film could be treated as a bulk aqueous solution. The bulk aqueous phase kinetics for uptake and reaction of NO₂ in aqueous solutions are well known (*Schwartz and White, 1981, 1983; Cheung et al., 2000*). It can be readily shown that the observed rates of HONO formation from NO₂ hydrolysis in our long path cell experiments as well as those reported in previous studies by other researchers are much larger than those predicted by bulk aqueous phase kinetics.

For example, consider a typical experiment carried out at 50% RH and an initial [NO₂] of 50 ppm in the 7.4 L long path cell (S/V = 70 m⁻¹). The number of water monolayers on the surface at 50% RH is ~3 (*Saliba et al., 2001; Sumner et al., 2004*); taking monolayer water coverage to be 1.0 × 10¹⁵ molecule cm⁻², the available volume of water on the reaction chamber walls is ~5 × 10⁻⁷ L (assuming there is also water on the halocarbon wax coated optics mounts). The aqueous phase reaction of NO₂ with bulk liquid water has been studied in detail (*Schwartz and White, 1981, 1983; Cheung et al., 2000*). As discussed by Schwartz and White (*1983*) studies of this reaction cannot distinguish between NO₂ and N₂O₄ as the reactant, and it can be written either way, with appropriate adjustment of the rate constant:



A recent measurement of the second order rate constant for NO₂ taken as the reactant is 3.0 × 10⁷ M⁻¹ s⁻¹ (*Cheung et al., 2000*). Using a Henry's law constant for NO₂ of 1.4 × 10⁻² M atm⁻¹ (*Cheung et al., 2000*), the concentration of aqueous phase NO₂ in equilibrium with 50 ppm gaseous NO₂ is 7.0 × 10⁻⁷ M. The calculated rate of HONO formation in the aqueous phase, proportional to the square of [NO_{2(aq)}], is thus 1.5 × 10⁻⁵ M s⁻¹. If it is assumed that all of this aqueous HONO escapes into the gas phase, the maximum rate of HONO formation would be 4 × 10¹² molecule s⁻¹ in a volume of 7.4 L, or 5 × 10⁸ molecule

$\text{cm}^{-3} \text{s}^{-1}$. The average observed HONO formation rate in a typical long path cell experiment carried out at 50% RH and an initial NO_2 concentration of 50 ppm in the 7.4 L long path cell was $\sim 2 \times 10^{10} \text{ molecule cm}^{-3} \text{ s}^{-1}$, a factor of 40 larger than expected based on chemistry in the bulk aqueous phase. When the simultaneous production of NO, which is at least in part from secondary reactions of HONO, is taken into account, the discrepancy is close to two orders of magnitude.

A similar conclusion can be reached from the data of other researchers, for example, from the larger (5800 L) chamber used by Pitts *et al.* (1984a). A question is how much water would have been on the Teflon-coated walls of their chamber at 50% RH. In the separate experiments in our laboratory discussed above, the amount of water on a halocarbon wax surface at 50% RH measured using transmission FTIR spectroscopy was about the same as that on glass (Sumner *et al.*, 2004). We therefore assume that the Teflon-coated surface of the large environmental chamber of Pitts and coworkers takes up water in the discontinuities on roughened hydrophobic surface in a manner similar to our measurements for a halocarbon wax coating. This assumption is supported by the similar rates in the generation of gas phase products between the studies of Pitts *et al.* (1984a) and ours, when differences in the S/V of the reactors are taken into account.

Application of calculations similar to those described above for potential HONO formation in the aqueous phase on walls of the environmental chamber of Pitts and coworkers then shows that the observed HONO formation rate is about four orders of magnitude larger than expected for the aqueous phase reaction (Pitts *et al.*, 1984a). For example, for an initial NO_2 concentration of 530 ppb and 50% RH (their run # 757), the calculated rate of gas phase HONO formation from a reaction in a bulk aqueous phase on the walls equivalent to 3 layers of water is $9 \times 10^{-6} \text{ ppb min}^{-1}$, compared to their measured rate of $6 \times 10^{-2} \text{ ppb min}^{-1}$ of HONO.

These comparisons assume that the volume of water on the cell walls is not altered by the presence of HNO_3 . However, this may not be the case, at least at low relative humidities. Bogdan and Kulmala (1997) reported increased water uptake by pyrogenic silica powders under some conditions when exposed simultaneously to gas phase nitric acid. Thus, the amount of adsorbed water was 0.02 g per g of SiO_2 at 55% RH when exposed to pure water vapor, while 0.10 g H_2O per g of SiO_2 was adsorbed when exposed to the vapor over a 45 % (w/w) HNO_3 - H_2O solution whose relative humidity was estimated to be 53 %. Svensson *et al.* observed that approximately a factor of two times more water was taken up on a Teflon surface at $\sim 10\%$ relative humidity when the Teflon had been first exposed to HNO_3 (Svensson *et al.*, 1987). In both studies, however, there was no significant increase in water uptake at higher relative humidities.

These observations are consistent with surfaces retaining nitric acid even on pumping. Subsequent exposure to water vapor leads to uptake of water on the surface and the formation of nitric acid-water thin films. At the lower relative humidities, the increased water uptake may be related to the water needed to form a particular hydrate of nitric acid, *e.g.* the trihydrate. However, at the higher relative humidities, there may be sufficient water

on the surface to dissociate the HNO₃, leading to water uptake that is similar to that for water alone.

However, with respect to the kinetics in the thin films, even a factor of five increase in water uptake measured for silica powders (*Bogdan and Kulmala, 1997*) does not reconcile the large discrepancies in the measured rates of HONO production compared to that calculated for reaction in a bulk aqueous layer on the surface.

II.C.2b. Reaction Order.

Kinetics studies can be helpful in assessing which mechanisms are, or particularly are not, feasible based on the experimental data. The dependence of the rates of NO₂ loss and of product formation on the concentrations of the reactants has been studied by a number of groups (*England and Corcoran, 1974; Sakamaki et al., 1983; Pitts et al., 1984a; Svensson et al., 1987; Jenkin et al., 1988; Perrino et al., 1988; Febo and Perrino, 1991; Wiesen et al., 1995; Harrison and Collins, 1998; Kleffmann et al., 1998b*). For reaction (1) as written, the overall rate law is given by equation (VIII):

$$\text{Rate} = R = -\frac{1}{2} \frac{d[\text{NO}_2]}{dt} = \frac{d[\text{HONO}]}{dt} = k [\text{NO}_2]^a [\text{H}_2\text{O}]^b \quad (\text{VIII})$$

If the reaction is first order in NO₂, then a plot of the initial rate of NO₂ loss or HONO formation against the initial NO₂ concentration should be linear. Similarly, the analogous plot as a function of the gas phase water concentration should be linear if the reaction is first order in water vapor. This analytical approach has been taken in many of the kinetics analyses of the heterogeneous NO₂ hydrolysis, and it is generally reported that the reaction is first order in NO₂ and first order in gaseous H₂O. We treat the dependence of the rates on water vapor first, followed by the dependence on the NO₂ concentration.

i. Reaction Order with Respect to Water Vapor. Figure 3.17 shows the dependence of the initial HONO and NO rates of formation on the concentration of water vapor measured in this laboratory. Consistent with the earlier studies, the rates of HONO and NO formation increase with water vapor concentration. However, the current studies were carried out to 80% RH, a higher water vapor concentration than used in most previous studies. While there is a significant increase in the rates of HONO and NO formation from 20 to 50% relative humidity, the increase from 50% to 80% RH is much larger than expected for a linear relationship. Also shown for comparison are recent measurements in this laboratory (*Sumner et al., 2004*) of the uptake of water on borosilicate glass cover slips (0.13 – 0.17 mm thickness, 25 mm diameter, Micro Cover Glass, Number 1, VWR Scientific). It is clear that the shapes of plots of d[HONO]/dt and d[NO]/dt versus relative humidity are similar in shape to the water uptake isotherm. These results show that the rates of HONO and NO formation are determined by the amount of water on the surface, rather than the gas phase water concentration.

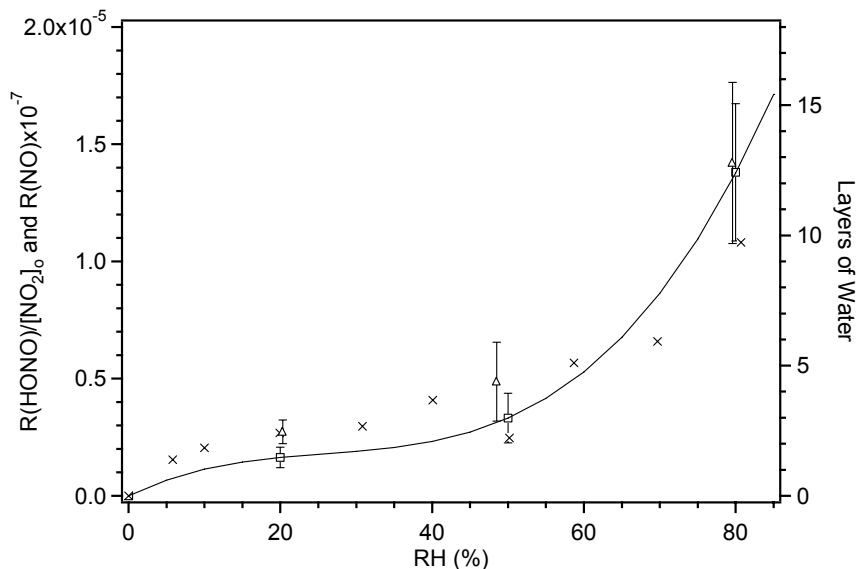


Figure 3.17. Initial rates of HONO (□) formation (in 19.4 L cell) and NO (Δ) formation (in 7.4 L cell) as a function of relative humidity at 295 ± 2 K. The NO rates have been multiplied by 10^{-7} to adjust to scale. The solid line is a fit through the combined data sets for the rates of HONO and NO formation. The number of effective layers of water measured on a smooth borosilicate glass surface are shown for comparison (right axis and × symbols) (*Sumner et al., 2004*).

In previous studies, the rates of formation of HONO, and NO where they have been measured, have generally been reported to be linear in the concentration of water vapor (*England and Corcoran, 1974; Sakamaki et al., 1983; Pitts et al., 1984a; Svensson et al., 1987; Jenkin et al., 1988*), although *Svensson et al. (1987)* reported a steep increase in the rate of NO production at 77% RH ($[\text{H}_2\text{O}] = 5 \times 10^{17}$ molecule cm^{-3}) in their experiments. The data of *Pitts et al. (1984a)* for HONO generation increase more than expected based on a linear relationship for experiments at 305 K and 60% RH ($[\text{H}_2\text{O}] = 7 \times 10^{17}$ molecule cm^{-3}), although they state that, within the scatter of the data, no firm conclusions can be drawn. *Kleffmann et al.* observed that HONO formation was “almost independent” of water vapor at low NO_2 concentrations, and attributed this to an excess of water present on the reactor surfaces (*Kleffmann et al., 1998a*).

In short, over a limited range of relative humidities, the relationship between the rate of HONO formation and water vapor concentration appears to be linear. However, our data clearly show that, on a borosilicate glass surface, the rate of formation follows the shape of the isotherm for water uptake on the surface. This again is consistent with the mechanism in Figure 3.12 in that it is water on the surface that is the reactant, rather than the collision of a water molecule from the gas phase with HONO precursors on the surface such as asymmetric ONONO_2 .

One important aspect of the amount of water on the surface is its impact on the dissociation of nitric acid. As discussed above, with small amounts of water on the surface, nitric acid is largely undissociated. This is important because it is clear that the chemistry of undissociated nitric acid compared to nitrate ions on surfaces is quite different. For example, gaseous NO reacts (*Smith, 1947; Jaffe and Ford, 1967; Kaiser and Wu, 1977b; McKinnon et al., 1979; Streit et al., 1979; Besemer and Nieboer, 1985; Svensson and Ljungström, 1988; Fairbrother et al., 1997; Mochida and Finlayson-Pitts, 2000; Saliba et al., 2000; 2001; Rivera-Figueroa et al., 2003*) with undissociated HNO₃ on silica surfaces to generate HONO and NO₂, but does not react with nitrate ions (*Rivera-Figueroa et al., 2003*).

ii. Reaction Order with Respect to NO₂. The reaction order with respect to NO₂ was examined from data such as those in Figure 3.13 first by examining the rates of NO₂ decay. For a first order reaction, a plot of ln [NO₂] versus time should be linear, while for a second order reaction, a plot of 1/[NO₂] as a function of time should be linear. We designate these Type A plots. Figure 3.18 shows typical data from this laboratory plotted in this manner. In all cases, plots of ln [NO₂] and 1/[NO₂] versus time are both reasonably linear in the initial stages of the reaction where secondary chemistry is less important. This precludes distinguishing between first order and second order kinetics in a definitive manner.

These results prompted us to examine the reaction order data from some earlier studies. Where available, data from our experiments and previous NO₂ hydrolysis studies were plotted in two different ways to determine the reaction order. The first, Type A, is as described above, in which either ln [NO₂] or 1/[NO₂] are plotted versus time; these plots utilize the rate of NO₂ decay during an individual experiment.

A second approach utilizes the rate law, equation (VIII) above, where the reaction order can be obtained from plots of the log of the initial rate of NO₂ loss or of product formation versus log of the initial NO₂ concentration:

$$\log (R) = \log k + a \log [\text{NO}_2] + b \log [\text{H}_2\text{O}] \quad (\text{IX})$$

We designate these Type B plots; the reaction orders in NO₂ and H₂O, *a* and *b*, respectively, are obtained from the slopes of the appropriate log-log plots.

Table 3.2 summarizes our analysis of some of the previously reported laboratory studies of reaction (1) where sufficient data are available in the published paper for such an examination. For Type A plots, the time-dependence of the loss of NO₂ in a number of studies is similar to that reported here (*England and Corcoran, 1974; Wiesen et al., 1995; Harrison and Collins, 1998; Kleffmann et al., 1998a*). That is, when we constructed Type A plots from their data, no clear distinctions between first and second order in NO₂ could be made, especially at early reaction times before secondary chemistry became apparent.

Table 3.2. Reanalysis of some kinetics data reported in the literature on heterogeneous NO₂ hydrolysis on the surfaces of laboratory systems (Teflon, glass, quartz, acid solutions, aerosol particles)

Reference	<u>Type A Plots</u>		<u>Type B Plots^a</u>		Reactor type	Reported reaction order
	ln[NO ₂] vs Time	1/[NO ₂] vs Time	Slope of log -d([NO ₂]/dt) vs log [NO ₂] _o (±2s)	Slope of log d([HONO]/dt) vs log [NO ₂] _o (±2s)		
England and Corcoran, 1974	Linear in first 500 min.	Linear in first 500 min.	N/A ^b	N/A	4.4 L Pyrex (S/V 36 m ⁻¹)	Authors reported second order in NO ₂ at 25 - 40°C using NO ₂ decay at H ₂ O concentrations of (0.7 - 2.8) × 10 ¹⁷ molecule cm ⁻³
Sakamaki <i>et al.</i> , 1983	N/A(a)	N/A ^b	1.2 ± 0.2	0.74 ± 0.37	6065 L PFA-coated (S/V 3.7 m ⁻¹)	Authors reported first order in NO ₂ using NO ₂ decay rate or HONO and NO formation rates at 30 °C and [H ₂ O] of 2.3 × 10 ¹⁷ molecule cm ⁻³
Pitts <i>et al.</i> , 1984	N/A	N/A	1.0 ± 0.2 ^c	0.85 ± 0.15 ^c	5800 L Teflon-coated chamber (S/V 3.4 m ⁻¹)	Authors reported that slope of HONO formation in Type B plot was close to unity at 297 K and [H ₂ O] of 3.7 × 10 ¹⁷ cm ⁻³ and at 305 K and [H ₂ O] of 5.9 × 10 ¹⁷ molecule cm ⁻³
Svensson <i>et al.</i> , 1987	N/A	N/A	1.1 ± 0.04	0.59 ± 0.25	153 L Glass reactor lined with Teflon film (S/V 14 m ⁻¹)	Authors reported first order for NO ₂ decay at [H ₂ O] = 2.5 × 10 ¹⁶ molecule cm ⁻³ using data after first 60 min. of reaction

Jenkin <i>et al.</i> , 1988 ^d	N/A	N/A	1.2 ± 0.5	N/A	19.8 L PTFE-coated glass cylinder with stainless steel endplates (S/V 13 m ⁻¹)	^d Authors reported first order for NO ₂ loss at 292 K and [H ₂ O] = 1.2×10^{17} molecule cm ⁻³
Febo and Perrino, 1991 ^e	N/A	N/A	N/A	1.5 ± 0.2	Frosted Pyrex glass flow reactor	^e Authors reported first order in NO ₂ by NO ₂ decay or HONO formation at 5×10^{17} molecule cm ⁻³ H ₂ O
Wiesen <i>et al.</i> , 1995	Linear in first 50 min.	Linear in first 50 min.	N/A	N/A	64 L quartz reactor Pyrex cell (S/V 21 m ⁻¹) and bubbler connected to 11 L Pyrex cell (S/V 22 m ⁻¹)	Authors reported HONO formation was first order in NO ₂ in quartz reactor and dry synthetic air and when gases were passed through a bubbler containing various solutions
Harrison and Collins, 1998	Linear in first 2 min.	Linear in first 2 min.	N/A	N/A	Flow tube in presence of aerosol particles	Authors reported NO ₂ loss was first order in NO ₂ at 279 K and [H ₂ O] = 2×10^{17} molecule cm ⁻³
Kleffmann <i>et al.</i> , 1998a	Linear in first 100 min.	Linear in first 100 min.	N/A	N/A	64 L quartz reactor (S/V 21 m ⁻¹) and bubbler containing sulfuric acid/water solutions	Both NO ₂ decay and HONO formation were reported first order in NO ₂ on quartz surface at [NO ₂] = (0.05 - 5) × 10 ¹² molecule cm ⁻³ and [H ₂ O] = (10 ¹² - 10 ¹⁷ molecule cm ⁻³). NO ₂ loss was first order when bubbled through sulfuric acid solutions. Authors reported that NO ₂ decay was second order in NO ₂ at high [NO ₂] and 248 K in bubbler apparatus.

This Work	Linear in first 200 min.	Linear in first 200 min.	1.6 ± 0.2	1.2 ± 0.4	20 L glass cell (S/V 30 m^{-1})
-----------	--------------------------------	--------------------------------	---------------	---------------	---

^a Values for slopes calculated here based on data presented in those papers.

^b N/A = Data not reported in paper in such a manner that this value could be calculated.

^c Calculated using the 297 K data.

^d Most experiments were performed at <10 Torr total pressure, with four experiments performed at ~300 Torr.

^e The authors did not report the temperature; we presumed 25°C to calculate that their RH \cong 64%.

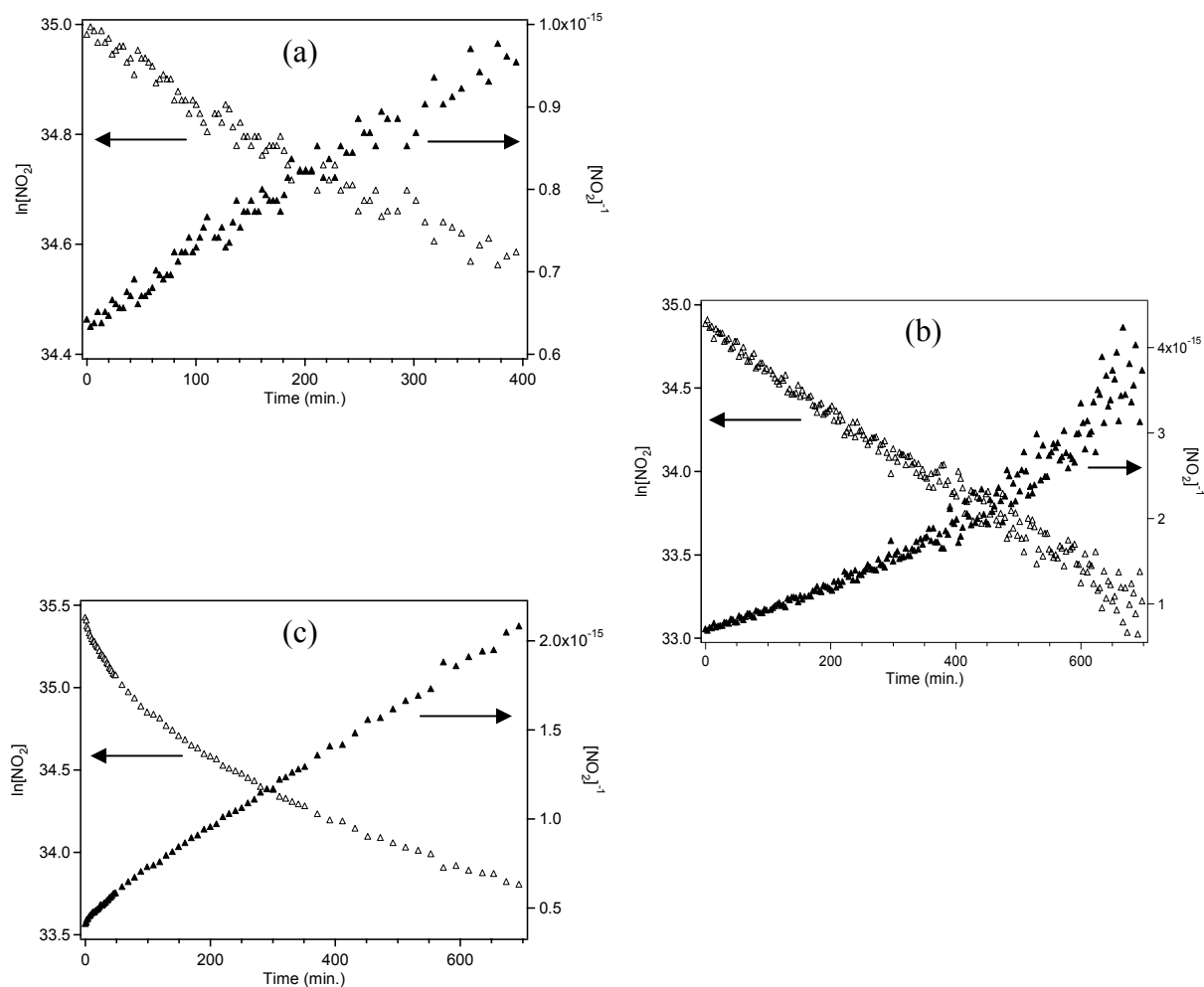


Figure 3.18. First and second order Type A kinetics plots for the loss of NO_2 at (a) 21% RH, $[\text{NO}_2]_0 = 1.5 \times 10^{15}$ molecule cm^{-3} , (b) 48% RH, $[\text{NO}_2]_0 = 1.4 \times 10^{15}$ molecule cm^{-3} , (c) 80% RH, $[\text{NO}_2]_0 = 2.4 \times 10^{15}$ molecule cm^{-3} . As discussed in the text, the experiments at 21% and 48% RH were carried out in the 7.4 L cell and that at 80% in the 19.4 L cell.

Type B plots could be constructed for four studies carried out in chambers similar to those used here (Sakamaki *et al.*, 1983; Pitts *et al.*, 1984a; Svensson *et al.*, 1987; Jenkin *et al.*, 1988). As Table 3.2 shows, the slopes of these Type B plots for the loss of NO_2 fall within the range from 1.0 to 1.2, supporting first order kinetics for the removal of NO_2 from the gas phase. The HONO data are more scattered, with slopes of the log-log plots falling in the range from 0.59 to 1.5. The lowest value, 0.59 ± 0.25 (2s) was obtained from the published rates which were calculated using the data after the first 60 minutes of reaction. This could be due to larger impacts of secondary chemistry on the apparent reaction rate. The largest value was obtained using a glass flow tube that, as discussed earlier, may have minimized the impacts of secondary chemistry (Febo and Perrino, 1991).

Figure 3.19 shows Type B plots for experiments carried out in this laboratory in the 19.4 L glass long path cell. The data for HONO formation have an average slope of 1.2 ± 0.4 (2s), in agreement with previous studies in other laboratories in which HONO formation was reported to be first order in NO_2 (Sakamaki *et al.*, 1983; Pitts *et al.*, 1984a; Pitts *et al.*, 1985; Svensson *et al.*, 1987; Jenkin *et al.*, 1988; Febo and Perrino, 1991; Wiesen *et al.*, 1995; Harrison and Collins, 1998; Kleffmann *et al.*, 1998a). The reaction order for loss of NO_2 is somewhat higher, 1.6 ± 0.2 ; the reasons for the discrepancy between this and the values of ~ 1.0 (Table 3.2) are not clear.

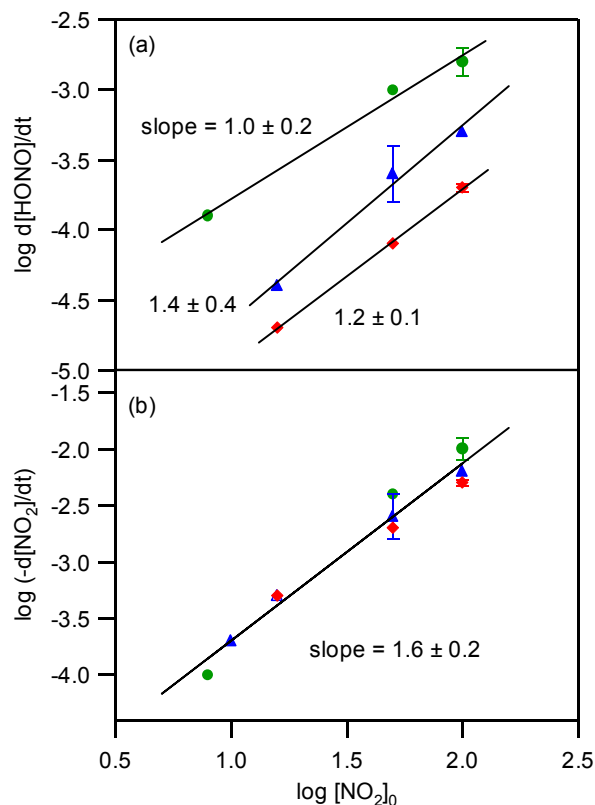
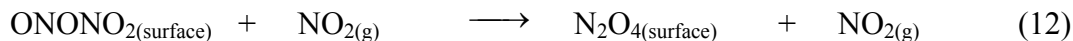


Figure 3.19. Plots of (a) $\log(d[\text{HONO}]/dt)$ and (b) $\log(-d[\text{NO}_2]/dt)$ vs $\log[\text{NO}_2]_0$ for experiments carried out in the 19.4 L glass long path cell in this laboratory at 21% (\blacklozenge), 48% (\blacktriangle), and 80% (\bullet) RH. The slopes ($\pm 2s$) are reaction order in NO_2 calculated using the initial rates of HONO formation or NO_2 loss (see text).

Although the reaction requires a surface and water, as discussed above, it cannot be treated as if it occurred in an aqueous bulk water solution on the walls of the reactor. Rather, a thin film as shown in Figure 3.12 is a more appropriate model for the medium in which this chemistry occurs. This mechanism predicts that HONO formation is first order in gas phase NO_2 despite N_2O_4 being a key precursor to HONO. This arises from the back reaction of asymmetric ONONO_2 with gas phase NO_2 . The key steps for HONO in Figure 3.12 can be summarized as follows:



If the rate of reaction of ONONO₂ with NO₂ to regenerate N₂O₄ on the surface is faster than its reaction with water, (*i.e.* $k_{12}[\text{NO}_2] \gg k_{13}[\text{H}_2\text{O}]$), the steady-state concentration of ONONO₂ on the surface is given by:

$$[\text{ONONO}_2]_{\text{ss}} = \frac{k_{11}K_9K_{10}[\text{NO}_2]^2}{k_{12}[\text{NO}_2]} = C[\text{NO}_2] \quad (\text{X})$$

where k_{11} and k_{12} are the rate constants for reactions (11) and (12), K_9 and K_{10} are the equilibrium constants for reactions (9) and (10), and C is the combination of rate and equilibrium constants $\{k_{11}K_9K_{10}/k_{12}\}$. The rate of HONO generation is given by

$$\frac{d[\text{HONO}]}{dt} = k_{13}[\text{ONONO}_2][\text{H}_2\text{O}_{(\text{surface})}] = k_{13}C[\text{H}_2\text{O}_{(\text{surface})}][\text{NO}_2] \quad (\text{XI})$$

and hence is first order in NO₂. An alternate portion of the mechanism that would be consistent with HONO production being first order in NO₂ is also considered briefly in the following section.

II.D. Mechanisms and Models

A key step in Figure 3.12 is uptake of gaseous N₂O₄ on the surface and its isomerization to surface asymmetric ONONO₂. This isomerization is known to occur in solid matrices at low temperatures or high pressures, on ice and in solution (*Parts and Miller, 1965; Addison, 1980; Bolduan and Jodl, 1982; Agnew et al., 1983; Bolduan et al., 1984; Jones et al., 1985; Givan and Loewenschuss, 1989a, b, 1990a, b, 1991a, b; Pinnick et al., 1993; Wang et al., 1997; Wang et al., 1998a; Wang and Koel, 1998, 1999*), although one study observed only the symmetric form of N₂O₄ on ice films (*Sato et al., 2000*). Koel and

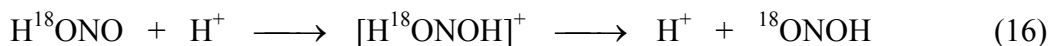
water and/or nitric acid. For example, the complex $3\text{NO}^+\cdot\text{NO}_3^-$ has been observed by Raman spectroscopy in solutions of N_2O_4 in HNO_3 (Addison, 1980; Harrar *et al.*, 1997). Similar considerations apply to the other surface species. For example, in the gas phase, clusters of NO_3^- with HNO_3 and H_2O are well known and it seems likely that similar complexes would form on the surface (Davidson *et al.*, 1977; Herzog-Cance *et al.*, 1978; Lee *et al.*, 1980; Wlodek *et al.*, 1980; D'Auria and Turco, 2001). Oligomer $(\text{HNO}_3)_x$ chains as well as complexes such as $(\text{NO}_3\cdot 3\text{HNO}_3)^-$ have been reported in liquid and solid anhydrous HNO_3 (Herzog-Cance *et al.*, 1978; Herzog-Cance *et al.*, 1985; Jirsak and Rodriguez, 2000).

Given the apparent complexity of the species in the surface film, it would clearly be of great interest to detect intermediates such as asymmetric ONONO_2 (including the protonated form), autoionized NO^+NO_3^- , or other complexes of NO^+ on these surfaces.

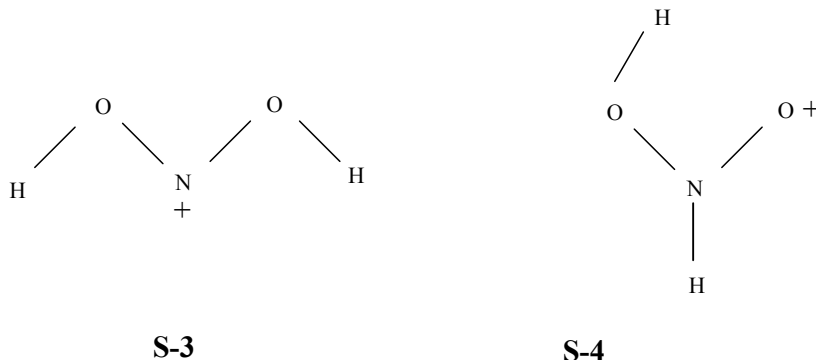
This mechanism for formation of HONO is also consistent with isotope labeling experiments. Sakamaki *et al.* (1983) showed that NO_2 reacts in a small quartz cell at room temperature with H_2^{18}O at 15% RH to generate exclusively H^{18}ONO . Svensson *et al.* (1987) reported a similar observation for relative humidities in the range of ~20 – 40%; however, at a relative humidity of ~4%, HON^{18}O was also formed. The formation of H^{18}ONO is easily explained by the mechanism in Figure 3.12. Once the asymmetric ONONO_2 has autoionized to NO^+NO_3^- , reaction of H_2^{18}O will lead to H^{18}ONO :



The formation of the HON^{18}O may be due to a proton-exchange reaction of HONO:

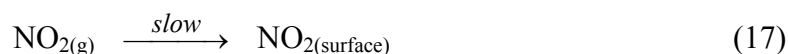


Ab initio calculations of protonated nitrous acid show that the most stable form is a cluster of NO^+ with water, $\text{NO}^+(\text{H}_2\text{O})$ (DePetris *et al.*, 1991; Choi *et al.*, 1994). However, there are two higher energy forms (by ~30 - 40 kcal mol⁻¹) corresponding to protonation at the terminal oxygen or at the nitrogen, respectively:



The observation of HON¹⁸O only at very low relative humidities (*Svensson et al., 1987*) is not surprising in that the ratio of nitric acid to water on the surface is likely quite high, giving a very acidic surface film that would enhance reaction (16).

All of the previous studies reported that the formation of HONO was first order in NO₂ (*Sakamaki et al., 1983; Pitts et al., 1984a; Pitts et al., 1985; Svensson et al., 1987; Jenkin et al., 1988; Febo and Perrino, 1991; Wiesen et al., 1995; Harrison and Collins, 1998; Kleffmann et al., 1998a*). This led to the conclusion that N₂O₄ cannot be the reactive species, since its concentration varies with [NO₂]². Based on experiments performed at 50% RH in large chambers (~4 – 6 m³) that were Teflon or Teflon-coated, *Pitts et al. (1984a)* proposed several mechanisms consistent with the observed first order NO₂ kinetics. One hypothesis was that adsorption of NO₂ on the surface is rate-determining:



Formation of HONO was proposed to occur either by the direct reaction of surface-adsorbed NO₂ with water on the surface,



or through the formation of an NO₂–water complex at the interface, followed by reaction with a second NO₂ molecule:



For both of these mechanisms, uptake of NO₂ on the surface is rate-determining.

An alternate proposed mechanism involved rapid uptake of NO₂ from the gas phase, with the slow formation of a surface NO₂-H₂O complex as the rate-determining step (*Pitts et al., 1984a; Jenkin et al., 1988*):



followed by reaction (20). In all cases, the HONO is released into the gas phase while the HNO₃ was proposed to remain on the surface.

Further evidence for the formation of a complex of NO₂ with water at the interface was obtained in studies of the uptake of gaseous NO₂ on liquid water where the uptake was measured to be much faster than expected based on bulk phase solubility and reaction (Ponche *et al.*, 1993; Mertes and Wahner, 1995). However, direct measurement of surface species was not carried out in these studies.

Cheung *et al.* (2000) studied the uptake and reaction of NO₂ with liquid water in a falling droplet apparatus and a bubble apparatus. Similar experiments have in the past generated evidence for the formation of complexes at the air-water interface as part of the mechanism of reaction, *e.g.*, of gaseous Cl₂ with bromide ion in aqueous solution (Hu *et al.*, 1995). In the case of the NO₂ studies, Cheung *et al.* (2000) found no evidence for a reactive NO₂ complex at the interface. There is one report of an NO₂-H₂O adduct on ice surfaces with only the symmetric N₂O₄ being observed (Sato *et al.*, 2000); the reason for the discrepancy between this and the studies that have reported isomerization is unclear (Parts and Miller, 1965; Addison, 1980; Bolduan and Jodl, 1982; Agnew *et al.*, 1983; Bolduan *et al.*, 1984; Jones *et al.*, 1985; Givan and Loewenschuss, 1989a, b, 1990a, b, 1991a, b; Pinnick *et al.*, 1993; Wang *et al.*, 1997; Wang *et al.*, 1998a; Wang and Koel, 1998, 1999).

An analogous system involving SO₂ may be relevant for examining whether the formation of a complex of NO₂ with water at the interface is a viable mechanism for heterogeneous NO₂ hydrolysis. There are data from studies of the uptake of SO₂ into aqueous solutions (Jayne *et al.*, 1990; Boniface *et al.*, 2000) and from sum frequency generation studies (Donaldson *et al.*, 1995) that a complex of SO₂ exists at the interface and plays a role in its uptake and oxidation. In addition, a significant decrease in the surface tension of bisulfite solutions was reported and attributed to this complex (Donaldson *et al.*, 1995). However, ATR-FTIR studies of SO₂ uptake into thin water films on an infrared-transmitting crystal, interpreted with the aid of *ab initio* calculations, failed to find evidence for an interface complex of SO₂ with water (Yang *et al.*, 2002). It may be that the surface complex was present at concentrations below the detection limit of $4 \times 10^{14} \text{ cm}^{-2}$ or that in this case, the complex is an ion-water cluster (Jayne *et al.*, 1990; Shi *et al.*, 1999; Clegg and Abbatt, 2001), for which the detection limits were higher, rather than a complex with the unionized gas molecule.

Ab initio calculations give a binding energy for an SO₂-H₂O complex (the most stable “open-faced sandwich” structure in which the planes of SO₂ and H₂O molecules are parallel) of $\sim 4 - 5 \text{ kcal mol}^{-1}$ compared to the separated reactants (Donaldson *et al.*, 1995; Yang *et al.*, 2002). Chou *et al.* (1999) have calculated that the binding energy for NO₂ with one water molecule is only $0.90 \text{ kcal mol}^{-1}$. Thus, the interaction between NO₂ and one water molecule is weaker than between SO₂ and water (and the latter is not particularly strong). Based on this information, it seems unlikely that NO₂ would form a complex at the surface with water. Certainly, there is no definitive evidence in favor of such a complex at the interface of air with thin films of water or water-nitric acid on surfaces.

Based on this and the other evidence presented, we therefore favor the more complex, multi-step mechanism in Figure 3.12. As discussed in the previous section, HONO generation by the mechanism in Figure 3.12 will be first order in NO₂ if the conversion of ONONO₂ back to N₂O₄ by reaction with gas phase NO₂ is rapid compared to the reaction of ONONO₂ with water. It should be noted that, while Figure 3.12 captures the major features of our proposed mechanism, there are alternatives to particular steps in the overall process that may also be consistent with the experimental observations. For example, one possibility is that there is a fixed amount of N₂O₄ that can be accommodated on the surface per unit area. In this scenario, N₂O_{4(surface)} is not in equilibrium with the gas phase dimer but rather, there is a maximum amount that the surface can hold; increased concentrations of the dimer in the gas phase would not lead to increased surface concentrations of N₂O₄ once the surface sites were filled. Under this scenario, the following reactions would also predict HONO generation that is first order in NO₂:



If reaction (22) were the rate-determining step and the concentration of N₂O_{4(surface)} was at its maximum, independent of gas phase N₂O₄, the steady-state concentration of ONONO₂ and hence the rate of generation of HONO would be first order in gas phase NO₂. In experiments using the porous glass surface and gas phase NO₂ concentrations in the 0.6 – 1.3 Torr range, the intensity of the 1740 cm⁻¹ infrared absorption band of N₂O₄ on the surface increased with the NO₂ pressure, suggesting that this alternate mechanism is less likely than that shown in Figure 3.12. Because HNO₃ on the surface also impacts the amount of surface N₂O₄ as seen in Figure 3.14, it has not yet been possible to definitively determine whether the surface N₂O₄ varies with the gas phase concentration of [NO₂] or [NO₂]², *i.e.* N₂O₄. However, it is possible that these porous glass experiments do not extrapolate directly to smooth glass because of the much larger internal surface area of the porous glass and pore geometry (*Gelb and Gubbins, 1998*). In addition, there is some difference in the composition of the porous glass (96.3% SiO₂, 2.95% B₂O₃, 0.04% Na₂O and 0.72% Al₂O₃ + ZrO₂) compared to the smooth glass of the long path cells (81% SiO₂, 13% B₂O₃, 4% Na₂O and 2% Al₂O₃). Hence we cannot definitively rule out alternative steps in the overall mechanism.

Nitric oxide has been observed in this and a number of other studies (*England and Corcoran, 1974; TenBrink et al., 1978; Sakamaki et al., 1983; Pitts et al., 1984a; Svensson et al., 1987; Wainman et al., 2001*) to be generated simultaneously with HONO, although Pitts *et al.* (1984a) reported that NO was observed only at longer reaction times after an induction period. Since the concentration of HONO decreases at larger extents of reaction (Figure 3.13), it is likely that secondary reactions of HONO on the cell walls generate NO. There have been a number of studies of the loss of HONO in laboratory reaction chambers that indicate that this chemistry also occurs on the reactor surfaces (*Wayne and Yost, 1951; Graham and Tyler, 1972; England and Corcoran, 1975; Chan et al., 1976a, b; Cox and Derwent, 1976/77; Kaiser and Wu, 1977b; Mebel et al., 1998; TenBrink and Spoelstra,*

1998). The formation of both NO and NO₂ was observed in a manner consistent with reaction (-2) in terms of the reaction products as well as second order kinetics in the initial HONO concentration:



The production of NO by the bimolecular reaction of HONO on the surface is one possibility in the NO₂ hydrolysis system, *i.e.* HONO is generated in the gas phase and then undergoes secondary reaction (-2) on the walls. In this case, production of NO would be expected to be a very sensitive function of the HONO concentration, and to have an induction time. While an induction time for NO generation was reported in the studies of Pitts *et al.* (1984a), NO was generated immediately in our experiments and those of Sakamaki *et al.* (1983) and Svensson *et al.* (1987). A major difference between the latter experiments and those of Pitts *et al.* (1984a) is the range of initial NO₂ concentrations used; in the former cases, NO₂ was typically in the 1 – 100 ppm range, whereas most of the Pitts *et al.* (1984a) experiments were carried out in the sub-ppm range. At higher NO₂ concentrations, the reaction is faster and HNO₃ builds up more rapidly on the walls. This suggests that the secondary chemistry that converts HONO to NO on the surface involves either HNO₃ or species derived from it. Studies described in the next section address this issue.

There may also be additional secondary chemistry that *forms* HONO at longer reaction times. For example, gaseous NO reacts with HNO₃ on silica surfaces to generate NO₂ as the major product (Smith, 1947; Jaffe and Ford, 1967; Kaiser and Wu, 1977b; McKinnon *et al.*, 1979; Streit *et al.*, 1979; Besemer and Nieboer, 1985; Svensson and Ljungström, 1988; Fairbrother *et al.*, 1997; Mochida and Finlayson-Pitts, 2000; Saliba *et al.*, 2000; 2001; Rivera-Figueroa *et al.*, 2003). It is likely that HONO is first formed (reaction 4),



and that HONO is then removed by secondary chemistry on the surface as discussed above. The generation of NO₂ in reaction (4) and the secondary HONO chemistry complicate interpretations of the kinetics and mass balance, particularly at larger extents of reaction, *i.e.*, higher initial concentrations and longer reaction times.

In order to provide an initial test of our proposed mechanism, we used the REACT version (Bozzelli, 2000; Manka, 2001) of the ACUCHEM model (Braun *et al.*, 1988) to predict the formation of HONO and NO, and the loss of NO₂ under the conditions of the experiments in Figure 3.13. The gas phase chemistry is reasonably well known (Tsang and Herron, 1991; DeMore *et al.*, 1997; Sander *et al.*, 2000; Atkinson *et al.*, 2001). This model does not explicitly treat uptake and reactions on surfaces, so the surface reactions

summarized in Figure 3.12 were parameterized as gas phase reactions. Rate constants for the surface reactions were adjusted within the constraints of the proposed mechanism (*e.g.*, the back reaction of ONONO₂ must be faster than its reaction with water) to obtain a best fit to the data for a typical experiment at 50% RH and an initial concentration of 60 ppm NO₂, similar to the conditions in Figure 3.13b. Based on our experimental observations described above, it was assumed that there was N₂O₄ and HNO₃ present on the walls initially. The model was then run for typical 20% and 80% RH experiments.

While this model gave reasonable fits to the HONO and NO production, NO₂ concentrations were over-predicted at longer reaction times. The addition of a reaction (23) of HONO with HNO₃ on the surface that generates an intermediate that slowly gives N₂O₄



gave a reasonable fit to all of the gas phase measurements. This reaction, which was proposed in earlier studies of the decomposition of nitric acid (*Johnston et al., 1955*), can be thought of as a reaction of NO₃⁻ with NO⁺ formed from the reaction of HONO with the acid, *i.e.*, the reverse of the overall NO₂ hydrolysis reaction. As discussed in the following section, after this modeling was completed, experimental evidence for such a reaction was indeed developed.

Figure 3.20 shows the model predictions compared to the measured losses of NO₂ and production of HONO and NO at 20%, 50% and 80% RH. While the match is not perfect, it provides a reasonable fit, given the unknown rate constants and details of the mechanism. Furthermore, this mechanism predicts that the reaction order (obtained from a plot of log of the initial rate versus log of the initial NO₂ concentration) for the initial formation of HONO is in the range of 0.9 to 1.1 and that for loss of NO₂ is in the range of 1.8 to 2.1, in reasonable agreement with our measured values of 1.2 ± 0.4 and 1.6 ± 0.2, respectively. Further studies are planned using a model that is designed to treat both gas and surface species specifically in a heterogeneous chemical system.

Several studies have concluded that, in a “dirty” chamber, the nature of the underlying surface does not significantly alter the chemistry (*Pitts et al., 1984a; Svensson et al., 1987*). This is not surprising if a thin surface film of nitric acid and water is the reactive medium in which the chemistry takes place. The underlying surface provides the support for this film but apparently does not change its composition substantially, at least for relatively unreactive surfaces.

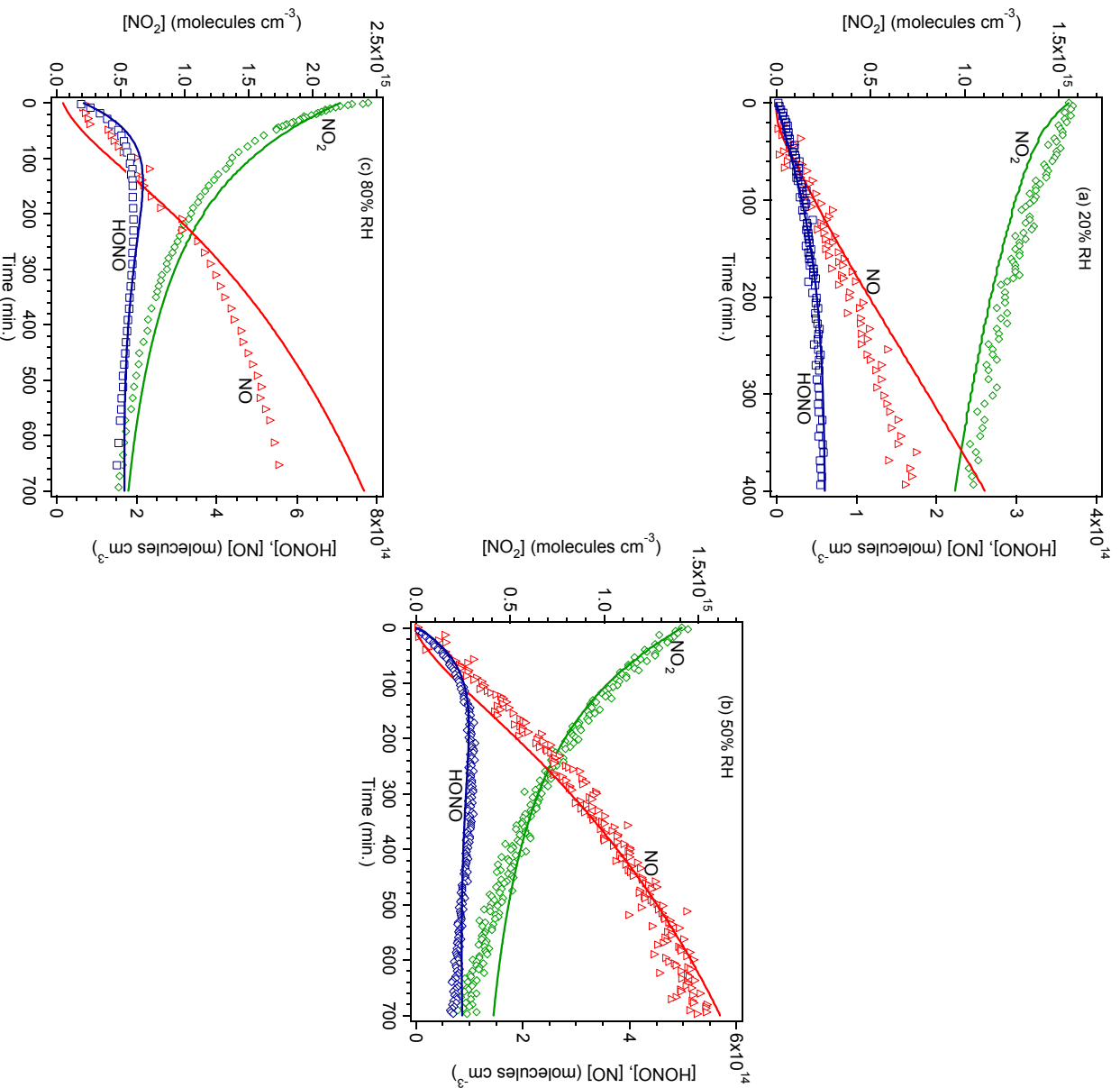


Figure 3.20. Comparison of model predicted loss of NO_2 and formation of HONO and NO to experimental data for typical runs at (a) 20% RH, (b) 50% RH and (c) 80% RH.

Finally, a common observation in the literature is that the initial rate of HONO formation and loss rate for NO_2 are faster on a clean surface. For example, Pits *et al.* (1984*d*) reported that the observed rate of HONO formation was doubled after cleaning their Teflon-coated evacuable chamber by the irradiation of Cl_2 and subsequent heating during evacuation for several hours. The HONO formation rate was no longer elevated after several more experiments were performed. Svensson *et al.* (1987) reported similar behavior for

clean compared to contaminated surfaces. There are several possible explanations for this effect, based on our proposed mechanism. As discussed earlier, acid present on a contaminated surface is likely to protonate both N_2O_4 and/or $ONONO_2$; if protonation decreases the rates of conversion of N_2O_4 to $ONONO_2$, and/or the autoionization of $ONONO_2$ to $NO^+NO_3^-$, the rate of HONO generation would decrease. Another possibility is that nitric acid already present on the walls ties up some of the water on the surface in the form of nitric acid-water complexes. Hence the amount of “free” water available to play a role in isomerizing the N_2O_4 and to react with $NO^+NO_3^-$ to form HONO will be decreased, leading to reduced rates of HONO formation.

Our mechanism does not address the formation of N_2O . The available data strongly suggest that it is formed by secondary reactions of HONO on the acidic surface (*Wiesen et al., 1995; Kleffmann et al., 1998a, b*). Hyponitrous acid, $HON=NOH$, is known to decompose to N_2O over a wide pH range, including under highly acidic conditions (*Buchholz and Powell, 1963; Hughes and Stedman, 1964*), and HON is known to self-react in solution to form N_2O (*Akhtar et al., 1982; Akhtar et al., 1985; Bazylinski and Hollocher, 1985; Loechler et al., 1987*):



This suggests that the N_2O precursors ($HON=NOH$ and/or HON) are formed by reactions of the protonated forms of HONO (structures **S-3** and **S-4** above) or possibly NO^+ , and that these generate N_2O . Similar chemistry has been proposed for the formation of N_2O under acidic conditions in the presence of SO_2 (*Pires and Rossi, 1997*). Clearly, this area awaits further study.

II.E. Atmospheric Implications

II.E.1. Polluted Urban Environments

An important aspect of atmospheric chemistry in the boundary layer of urban areas that has not received much attention is the heterogeneous chemistry occurring on buildings, structures, soils and vegetation. Such surfaces have been proposed in the past to be important substrates for the heterogeneous NO_2 hydrolysis (*Harrison and Kitto, 1994; Andrés-Hernández et al., 1996; Harrison et al., 1996; Lammel and Cape, 1996; Lammel, 1999*), but may also be important in other processes such as renoxification of nitric acid (*Mochida and Finlayson-Pitts, 2000; Saliba et al., 2000; 2001; Rivera-Figueroa et al., 2003*). Also consistent with reactions at the surface is the recent observation of increased HONO/ NO_2 ratios at ground level compared to higher altitudes (*Stutz et al., 2002b*). There is also evidence that windows, for example, adsorb organics in urban areas (*Diamond et al., 2000; Gingrich et al., 2001*), and may provide a support on which their oxidation occurs. This area of reactions in thin films on surfaces (**SURFACE = Surfaces, Urban and Remote: Films As a Chemical Environment**) has the potential to contribute significantly to the chemistry of this portion of the earth's atmosphere. The resulting impacts can be substantial,

since the chemistry occurs in the physical location in which people are exposed to air pollutants. This is also the region in which many measurements of atmospheric species are taken for regulatory purposes, and hence the chemistry of the lower boundary layer significantly influences our understanding of atmospheric processes, the development of computer kinetics models, and their application to the promulgation of control strategies.

It is clear from our studies that the nature of the surface film is a key determinant of the kinetics and mechanism of the heterogeneous hydrolysis of NO_2 . The experiments reported here were carried out on borosilicate glass; many urban building materials contain silicates so that surface characteristics may be similar to the glass walls of laboratory reactors. Regardless, the evidence from the combination of the many different studies of this reaction suggests that the reaction is not very sensitive to the nature of the underlying surface. Based on the work presented here, one would expect the surface film of water and nitric acid to be the determining factor. Hence, it is the amount of water on the surfaces as a function of relative humidity that is likely to be important rather than the water vapor concentration or chemical nature of the underlying surface.

Figure 3.21 shows a summary prepared by Lammel (1999) of the number of water layers taken up on various surfaces found in urban regions as a function of relative humidity. It is seen that the water uptake isotherms measured in this laboratory for borosilicate glass are similar to those for stone and soil materials. While vegetation takes up less water, a monolayer or more is present at relative humidities above 50%. Hence, all of these surfaces are likely to participate in HONO and NO formation in urban areas where significant NO_2 levels are present.

Our mechanism predicts that the asymmetric dimer ONONO_2 reacts with water to generate HONO, and the latter reacts on the surface to form NO. As a result, the rate of NO formation from secondary HONO reactions should be sensitive to the relative concentrations of water and acid on the surface. Different amounts of acid on the walls of reaction chambers in laboratory studies may be the reason for different amounts of NO production relative to HONO reported in previous studies. It is not known what the form of nitric acid is on surfaces in urban environments nor what the ratio of HONO to NO production will be under typical atmospheric conditions. In addition, accurately representing the mechanism in Figure 3.12 in airshed models will not be possible until the individual steps are known. Still, one can compare the rates of HONO and NO generation in various laboratory studies to obtain a likely range of maximum HONO production rates.

Figure 3.22 shows such a comparison of the rates of HONO generation reported by Sakamaki *et al.* (1983), Pitts *et al.* (1984a), Svensson *et al.* (1987), as well as in the present work. Different relative humidities, temperature and S/V ratios were used in the various studies. We have chosen data that were measured at 50% RH, or the closest RH studied to 50%, and normalized the reported rates of HONO generation for both the S/V ratio of 3.4 m^{-1} and to the water vapor concentration of $3.6 \times 10^{17} \text{ molecule cm}^{-3}$ used in the Pitts *et al.* (1984a) studies. This normalization involved a simple multiplication of the reported rates of HONO generation by the S/V ratio ($R_{\text{HONO}} \times 3.4 \text{ m}^{-1} \div (\text{S/V used in that study})$) and by the ratio of water vapor in the Pitts *et al.* (1984a) study to that in the comparison experiments.

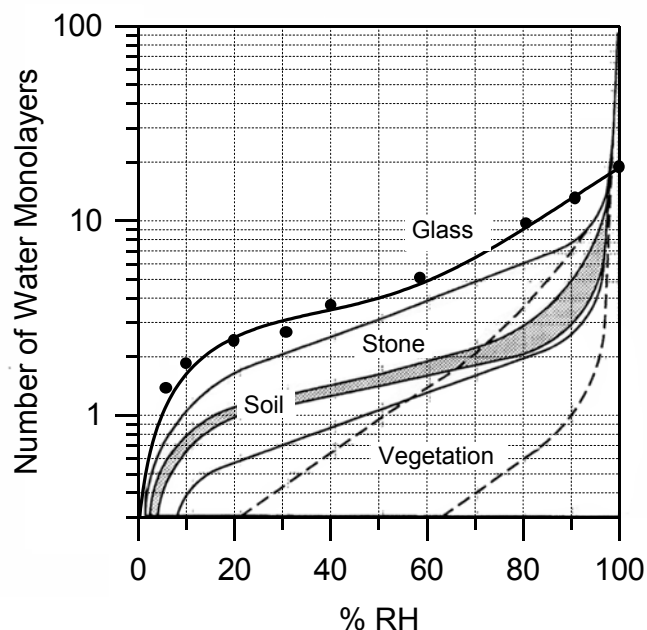


Figure 3.21. Water uptake on some common materials found in the boundary layer. Adapted from Lammel (1999).

A correction also needs to be made for different methods of HONO measurement. Nitrous acid was measured by FTIR in the studies of Sakamaki *et al.* (1983), Svensson *et al.* (1987) and this work, but different absorption cross sections were used, giving different HONO concentrations for a given measured absorbance, which leads to different measured formation rates. In the Pitts *et al.* studies, HONO was measured by DOAS (Pitts *et al.*, 1984a). The HONO infrared absorption cross section we used (Barney *et al.*, 2000) was determined by simultaneous measurement of HONO concentrations by DOAS so our data should be directly comparable to those of Pitts *et al.* (1984a). We have therefore corrected the rates of HONO formation reported by Sakamaki *et al.* (1983) and Svensson *et al.* (1987) to our effective absorption cross section of $3.7 \times 10^{-19} \text{ cm}^2 \text{ molecule}^{-1}$ (measured for the *trans* form at 1264 cm^{-1} but taking into account the *cis* form in equilibrium with it); the values of the absorption cross sections used in the Sakamaki *et al.* (1983) and Svensson *et al.* (1987) studies were $2.8 \times 10^{-19} \text{ cm}^2 \text{ molecule}^{-1}$ and $4.8 \times 10^{-19} \text{ cm}^2 \text{ molecule}^{-1}$, respectively.

Table 3.3 summarizes the slopes of the plots of HONO generation in Figure 3.22, normalized to the initial NO_2 . Pitts *et al.* (1984a) only observed NO at longer reaction times, and their initial rates of HONO production accounted for 40 – 50% of the NO_2 loss as expected if HONO were the only gas phase product. However, significant rates of NO production were observed simultaneously in this work and that of Sakamaki *et al.* (1983) and Svensson *et al.* (1987) with the relative rates of NO to HONO generation varying from about 0.3 to 1.0. Table 3.3, therefore, also shows the estimated *total* rates of production of HONO plus NO.

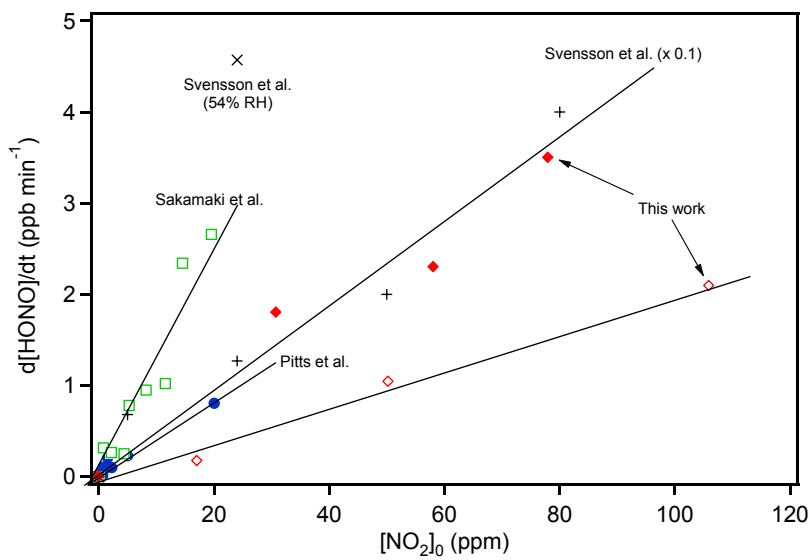


Figure 3.22. Initial rates of generation of HONO measured in several studies, normalized to a S/V of 3.4 m^{-1} and water vapor concentration of $3.6 \times 10^{17} \text{ cm}^{-3}$ used in the studies by Pitts *et al.* (1984a) • Pitts *et al.* (1984a); □ Sakamaki *et al.* (1983); + Svensson *et al.* (1987) rates divided by 10; × Svensson *et al.* (1987) experiment at 54% RH; ◇ This work, 19.4 L cell; ◆ This work, 7.4 L cell.

Comparison of these laboratory rates of HONO production in Table 3.3 shows that the dependence of the rate of (HONO + NO) formation in the present studies is in reasonable agreement with that of Pitts *et al.* (1984a) but smaller than measured by Sakamaki *et al.* (1983). One reason for the latter discrepancy may be that their studies were carried out at a temperature of $30 \text{ }^\circ\text{C}$, about $5 - 10 \text{ }^\circ\text{C}$ higher than the other three studies (although Svensson *et al.* (1987) reported a negative temperature dependence). The rates of HONO generation reported by Svensson and Ljungström (1988) are substantially higher than those in the other three studies. The experiments used for the rate calculation were carried out at very small water vapor concentrations, 1000 ppm, which correspond to 3.8% RH at their temperature of 22°C ; the correction to their data for the water vapor was more than an order of magnitude. Given the complex nature of the surface film, such a linear extrapolation may not be justified and hence the apparent discrepancy not surprising. Also shown is the result of a single experiment from their studies that was carried out at a relative humidity of $\sim 50\%$ (Svensson *et al.*, 1987); this is in better agreement with the other studies shown.

Table 3.3. Comparison of rates of HONO generation in this work with some previous studies as a function of the initial NO₂ concentration.

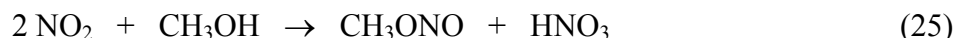
Reference	$\{1/[\text{NO}_2]_0\} \times d[\text{HONO}]/dt$ (ppb min ⁻¹ per ppm NO ₂) (± 2s)	Typical Ratio of Initial Rate of NO Production to that of HONO	Approximate Rate of Production of HONO Plus NO per ppm NO ₂ (ppb min ⁻¹ per ppm NO ₂)
This work (19.4 L cell)	$(2.1 \pm 0.4) \times 10^{-2}$	1.0	4×10^{-2}
This work (7.4 L cell)	$(4.2 \pm 1.2) \times 10^{-2}$	1.0	8×10^{-2}
Sakamaki <i>et al.</i> (1983)	$(14 \pm 4) \times 10^{-2}$	0.3	18×10^{-2}
Pitts <i>et al.</i> (1984a)	$(3.9 \pm 0.4) \times 10^{-2}$	0	4×10^{-2}
Svensson <i>et al.</i> (1987)	0.43 ± 0.14	0.6	0.7
Svensson <i>et al.</i> (1987) at 54%RH	0.2	0.6	0.3

Given the very different chamber sizes (*i.e.*, S/V) and composition of the chamber walls, the agreement in the rates of production of HONO for our studies at 50% RH compared to those of Pitts *et al.* (1984a) is quite good. The average HONO production rate per ppm of NO₂ at 50% RH from our study and that of Pitts *et al.* (1984a) which were carried out at similar temperatures and relative humidities, is 4×10^{-2} ppb min⁻¹ per ppm of NO₂, normalized to a S/V ratio of 3.4 m⁻¹. This corresponds to an emission rate from the chamber surface of 3×10^{10} HONO cm⁻² min⁻¹ at an NO₂ concentration of 1 ppm.

For the purposes of examining whether this rate is consistent with concentrations of HONO measured in the boundary layer in polluted urban atmospheres, we shall assume an NO₂ concentration of 0.1 ppm. From the results of the laboratory studies, the emission rate of HONO will be 3×10^9 HONO cm⁻² min⁻¹ at 50% RH and 0.1 ppm NO₂. However, the surfaces on which the reaction occurs are not geometrically flat. Typical BET surface areas for soil are 1 – 15 m²g⁻¹ (Hodson *et al.*, 1998). We have measured the mass of a quantity of sand (Norway Bay, Quebec) that would visually cover a known surface area with a very thin layer and find a coverage of 0.2 g of sand per cm² of geometric area. Thus, the available surface area of sand and soils per cm² of geometric area may be on the order of 2000 – 30,000 cm² per cm² geometric area. The emission rate of HONO from 1 cm² geometric area would then be in the range of $(0.6 - 9) \times 10^{13}$ HONO min⁻¹. Taking the height of the boundary layer to be 38.5 m, the height often used in one airshed model for a polluted urban area (Knipping and Dabdub, 2002), the total HONO concentration formed in 10 hours (*e.g.* overnight) would be in the range of 40 – 600 ppb. However, this assumes that the reaction is not limited by diffusion of NO₂ to the soil surface, that the entire BET surface area is available for reaction, and that all of the HONO is released to the gas phase without any subsequent deposition or secondary reactions on the surfaces. Thus, while such calculations

are quite approximate, they demonstrate that this chemistry is more than adequate to generate the typical range of HONO concentrations of a few ppb measured under such conditions (*Perner and Platt, 1979; Platt et al., 1980; Winer and Biermann, 1994; Harrison et al., 1996; Lammel and Cape, 1996; Lammel, 1999; Finlayson-Pitts and Pitts, 2000; Alicke et al., 2002; Stutz et al., 2002a*).

While this paper has focused on the heterogeneous reaction of NO₂ with water, it should be noted that a similar reaction occurs with alcohols (*Koda et al., 1985; Akimoto and Takagi, 1986; Takagi et al., 1986; Butler et al., 1992; Finlayson-Pitts et al., 1992*):



The organic nitrites such as CH₃ONO also photolyze readily, leading to the formation of HO₂ and OH via reactions of the alkoxy radical that is generated (*Finlayson-Pitts and Pitts, 2000*). This chemistry may become important if the use of alcohol fuels or additives to gasoline increases, particularly with the phase-out of MTBE as a fuel additive.

II.E.2. Airborne Particles and Clouds

There are a variety of solid airborne particles that could serve as substrates for this chemistry as well, including sea salt and windblown dust (*Finlayson-Pitts and Pitts, 2000*). It has been known for many years that dust particles that become airborne through windstorms can be transported long distances and may impact chemistry on a global scale (*Prospero and Nees, 1977; Prospero et al., 1981; Prospero and Nees, 1986; Dentener et al., 1996; Gillette, 1997; Perry et al., 1997; Zhang et al., 1997; Prospero, 1999; Zhang and Carmichael, 1999; deReus et al., 2000; Clarke et al., 2001*). For example, dust particles remove oxides of nitrogen such as N₂O₅ that might otherwise lead to ozone formation. The present work and the previous studies of heterogeneous NO₂ hydrolysis suggest that the surfaces of SiO₂ in such particles may also help to generate OH via the formation of HONO. Indeed, increased HONO production has been observed during a dust storm in Phoenix, Arizona (*Wang et al., 2002*).

The components of dust particles include not only silicates, but also a number of other components such as Fe₂O₃, Al₂O₃, and TiO₂ (*Finlayson-Pitts and Pitts, 2000*). Nitric oxide has been reported as the major gas phase product from the heterogeneous reaction of NO₂ on these surfaces in the absence of water vapor by Grassian and coworkers (*Goodman et al., 1998; Miller and Grassian, 1998; Underwood et al., 1999; Grassian, 2001, 2002*); HONO may be a major gaseous product when there are significant amounts of water on the surface. Börensen *et al.* (2000) reported the formation and subsequent loss of nitrite ions on the surface of Al₂O₃ during its reaction with NO₂ in the absence of water vapor and proposed that the loss was due to acidification of the surface that converts surface nitrite to gas phase HONO. However, gas phase products could not be directly measured in those studies.

Aerosol particles in urban areas have a complex composition and can act as condensation nuclei for fog and cloud formation. There is evidence from field studies for the generation of HONO in aerosols and clouds (*Cape et al., 1992; Notholt et al., 1992; Andrés-Hernández et al., 1996; Harrison et al., 1996; Lammel and Cape, 1996; Lammel, 1999; Acker et al., 2001*). How the mechanism of formation of HONO in these liquid media is related to those in thin films on solid substrates such as those studied here is not known, but clearly an area of interest.

II.E.3. Indoors

Nitrous acid has been observed indoors in a number of studies (*Pitts et al., 1985; Pitts et al., 1989; Brauer et al., 1990; Febo and Perrino, 1991; Spengler et al., 1993; Spicer et al., 1993; Weschler et al., 1994; Wainman et al., 2001*). Although HONO is generated during combustion, for example in gas stoves and space heaters (*Pitts et al., 1989; Brauer et al., 1990; Febo and Perrino, 1991; Spicer et al., 1993; Vecera and Dasgupta, 1994*), it is clear that the heterogeneous hydrolysis of NO₂ on the materials inside homes plays a significant role. High levels of nitrogen dioxide are often found inside commercial facilities such as ice skating rinks (*Brauer et al., 1997*) and hence formation of nitrous acid is expected in these cases as well.

The uptake of NO₂ on various materials used inside and outside buildings has been shown to vary over a wide range (*Nishimura et al., 1986; Spicer et al., 1989; Kirkitsos and Sikiotis, 1996; Wainman et al., 2001*). In the studies of *Spicer et al. (1989)* wallboard, cement blocks, wool carpets, brick and masonite had the highest uptake rates, which may reflect their ability to adsorb water and form a surface film. These were greater than window glass by more than an order of magnitude. Similarly, *Wainman et al. (2001)* showed that carpets made of synthetic fibers increased both the NO₂ removal rate and the formation of HONO. Thus, HONO and NO production rates may be greater on residential materials compared to borosilicate glass used in the present studies. However, clearly one needs to understand the nature of the surface film on such materials in order to accurately extrapolate from laboratory studies to indoor air environments.

II.E.4. Snowpacks

Over the past few years, there have been some intriguing observations made regarding photochemistry in snowpacks. For example, *Sumner and Shepson (1999)* reported the photochemical production of HCHO, and enhanced production of NO and NO₂ that is associated with light has also been observed (*Honrath et al., 1999; Jones et al., 2000; 2001*). *Zhou et al. (2001)* and *Dibb et al. (2002)* measured HONO production in the Arctic snowpack, and this may be a major source of OH that leads to the formation of such species as HCHO. The mechanism proposed is the photolysis of NO₃⁻ to generate NO₂, followed by the heterogeneous hydrolysis of NO₂ to form HONO. In this case, the chemistry may be similar to that proposed here for the reaction on silica surfaces at room temperature.

If the formation of HONO involves N₂O₄, it may be enhanced on the surface of ice due to the temperature dependence of the NO₂-N₂O₄ equilibrium. The temperature

dependence of the equilibrium constant is known (*DeMore et al., 1997*), and it increases by a factor of 124 from a temperature of 298 K to 245 K, typical of the Arctic in the spring. This increase in the fraction of NO₂ that is N₂O₄ in the gas phase, combined with increasing solubility with decreasing temperatures, may therefore enhance the amount of N₂O₄ on the ice surface and hence the generation of HONO. Of course, the nature of the surface of ice, where a quasi-liquid layer exists, is quite different from that of a solid silicate that holds adsorbed water, so a direct extrapolation of the present results is not possible. However, there are likely to be substantial similarities in the chemistry so that understanding the room temperature reaction on silica surfaces will be helpful in elucidating the snowpack chemistry as well.

III. THE USE OF ATTENUATED TOTAL REFLECTANCE SPECTROSCOPY TO PROBE INTERFACE SPECIES

Measurement of species formed at interfaces is clearly an important part of the study of heterogeneous chemistry. In order to fully explore such heterogeneous processes, an analytical technique is needed that can (a) provide *in situ* selective detection of surface species and (b) be used in combination with long path FTIR spectroscopy for gas phase measurements. Initial investigations using an attenuated total reflectance (ATR)-FTIR probe were carried out in separate experiments to verify its suitability in studying species in and on thin films.

Sulfur dioxide (SO₂) was one of the first species for which experimental evidence for the existence of a surface complex was obtained in surface films of water solutions (*Jayne et al., 1990; Boniface et al., 2000*) and from sum frequency generation studies (*Donaldson et al., 1995*). The uptake of SO₂ has been proposed to involve an uncharged surface complex which subsequently converts into ionic species. A search was made for this SO₂-water complex at or near the surface using ATR at 298 K with complementary *ab initio* calculations of a 1:1 SO₂-H₂O complex (*Yang et al., 2002*). Bands attributable to SO₂ (aq) at 1330 and 1145 cm⁻¹ were identified. However, no infrared absorption bands attributable to such a complex of SO₂ were observed experimentally in the expected region (1150 cm⁻¹). An upper bound was determined of 4×10^{14} SO₂ cm⁻² to the concentration of neutral SO₂ molecules weakly sorbed to the surface in equilibrium with ~1 atm SO₂ (g) (*Yang et al., 2002*). ATR-FTIR was found to provide a powerful means of searching for surface species and complexes using well-developed and readily available spectroscopic methods. ATR-FTIR was then applied to thin water films containing nitric acid and other species formed from heterogeneous NO₂ hydrolysis while simultaneously measuring gaseous species using long path FTIR.

IV. LP-ATR STUDIES OF NO₂ HYDROLYSIS

As seen in sections 3.I and 3.II, separate experiments in which either the gas phase or the surface could be followed provided a great deal of information on the kinetics and mechanisms of the heterogeneous hydrolysis of NO₂. However, it is clearly highly desirable

to be able to monitor both the gas phase and the surface film simultaneously during one experiment. This was made possible through the development of a new and unique apparatus described earlier in which both long path FTIR for gases and ATR-FTIR for the surface film were incorporated into one chamber.

The gas phase data (time profiles and yields) from experiments carried out in the LP-ATR chamber at 20, 50, and 80% RH with $[\text{NO}_2]_0 \cong 100$ ppm are shown in Figure 3.23. As discussed in Section 2.II.F. (Methods and Materials), these experiments were carried out just after fabrication of the chamber, so that the surfaces retained some organics which were used during machining. The reason for carrying out the experiments without first removing the organics was to explore whether their presence would modify the kinetics or mechanism of the heterogeneous hydrolysis in a significant manner. For example, one proposal is that organics are involved in the production of N_2O (*Barlow, 2003*). Since organics are present on surfaces in air, these experiments are directly relevant to conditions in the polluted urban boundary layer.

In preliminary experiments, the yields of gas phase HONO, NO, and N_2O (Fig. 3.23b,d,f) remain at approximately 50% of the NO_2 loss, as was the case in the absence of organics, in agreement with the stoichiometry of reaction (1) (*Finlayson-Pitts et al., 2003*) with NO becoming the dominant product due to secondary chemistry of HONO.

The LP-ATR chamber allows simultaneous collection of surface data using an ATR probe. Selected surface spectra at various extents of reaction are shown in Figure 3.24 for the same experiments of Figure 3.23.

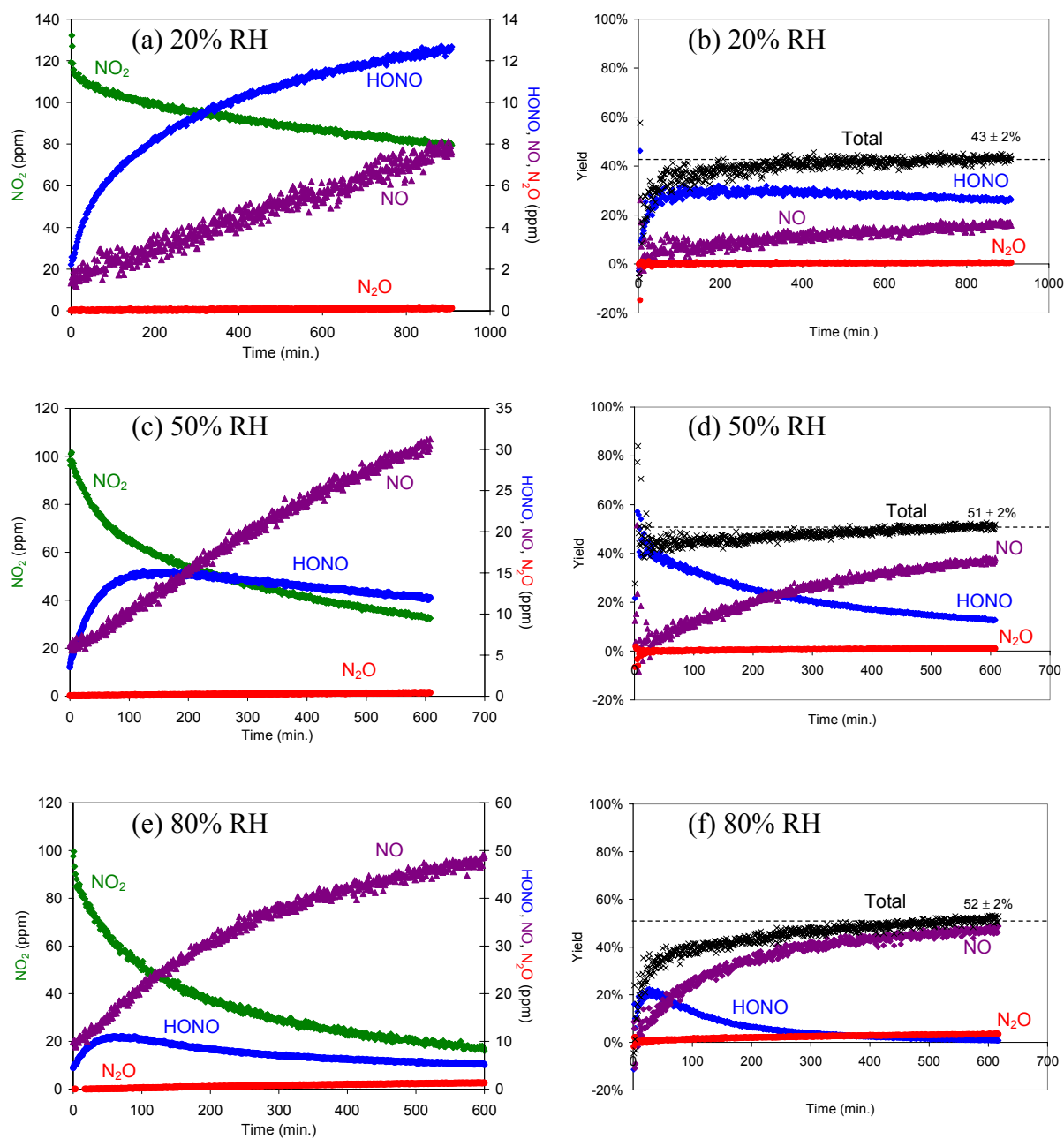


Figure 3.23. Gas phase data (time profiles and yields) obtained during NO_2 hydrolysis experiments in the LP-ATR chamber at 20 % RH (a, b), 50% RH (c, d), and 80% RH (e, f).

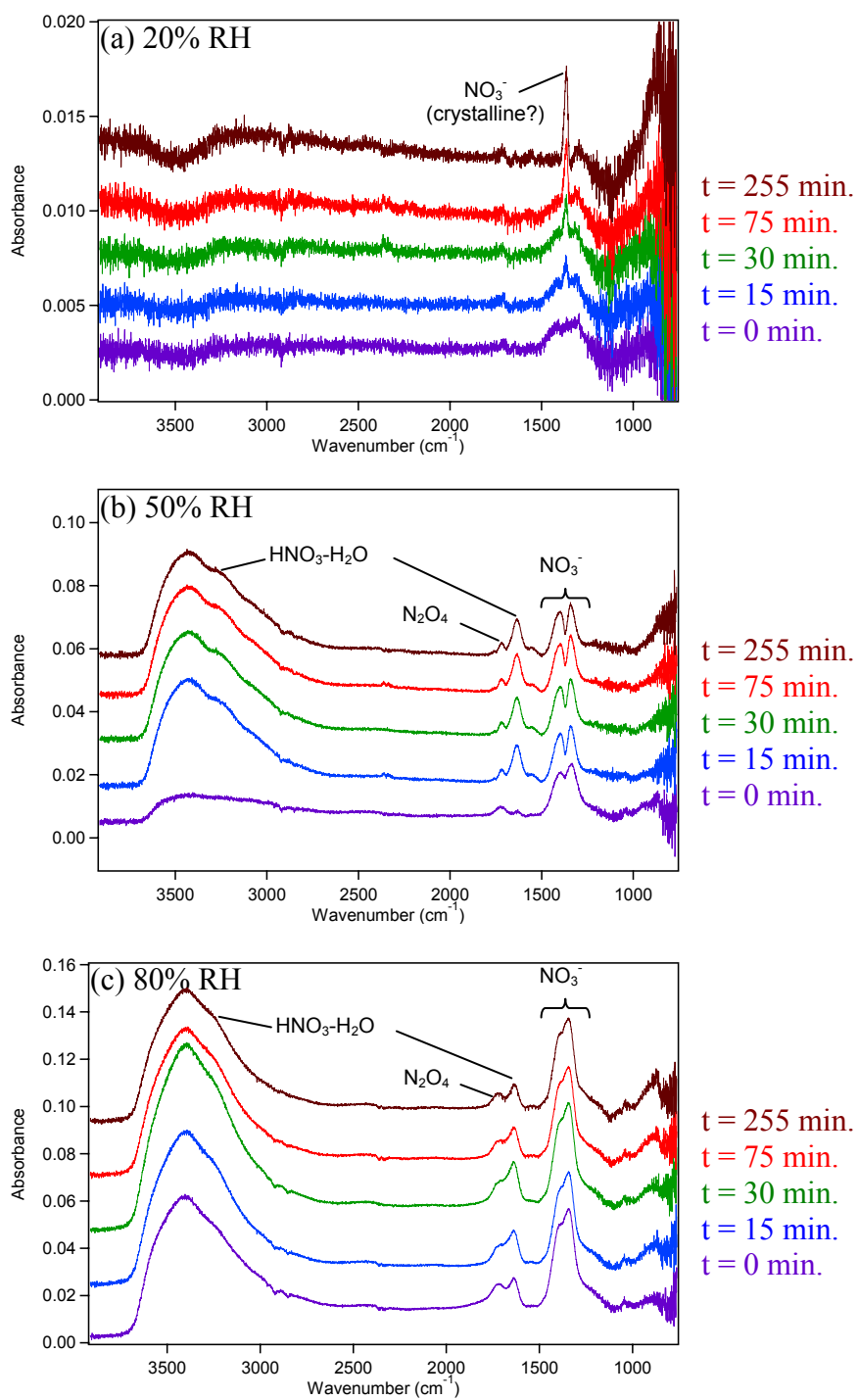


Figure 3.24. ATR surface data corresponding to Fig. 3.23 obtained during NO₂ hydrolysis experiments in the LP-ATR chamber at (a) 20%, (b) 50%, and (c) 80% RH.

Several surface species have been observed including NO_3^- (1340 and 1420 cm^{-1}), N_2O_4 (1740 cm^{-1}), and a $\text{HNO}_3\text{-H}_2\text{O}$ complex (3200 and 1640 cm^{-1}). At 20% RH, the reaction is slower and much less of each surface species were formed (note the y-axis range). In addition, a peak appears at $\sim 1365\text{ cm}^{-1}$ in the nitrate region but that is sharper than typical aqueous nitrate peaks. In addition, the liquid water peak near 3400 cm^{-1} decreases with time. This suggests that crystalline NO_3^- has formed on the ATR element, which is not surprising given the lower relative humidity.

Figure 3.25 shows the effects of the presence of organics on the surface species observed during experiments carried out at 50% RH.

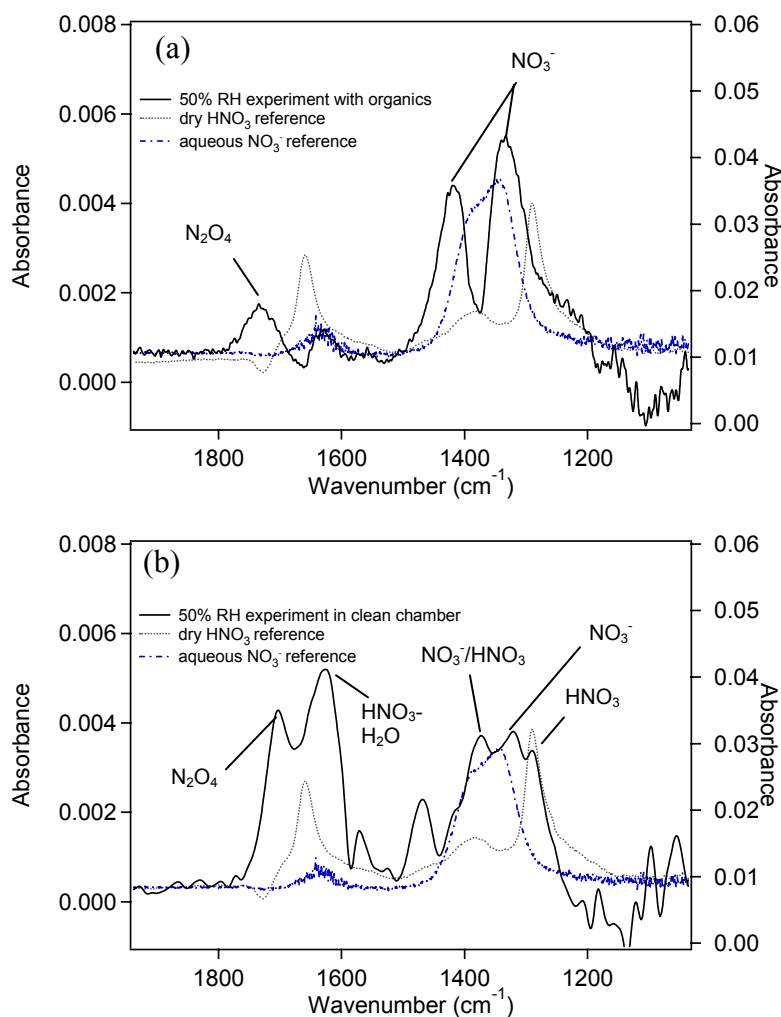


Figure 3.25. Comparison of ATR spectra in the presence (a) and absence of organics (b) with HNO_3 and NO_3^- reference spectra. (a) Solid spectrum taken at $t = 30$ min. during 50% RH NO_2 hydrolysis experiment in the LP-ATR chamber with organics present on the walls (left axis), (b) Solid spectrum taken at $t = 30$ min. during 50% RH NO_2 hydrolysis experiment in a clean 1.75 L glass chamber (left axis). The dotted line is a dry HNO_3 reference ATR spectrum (right axis). The dash-dotted line is an ATR spectrum of aqueous NO_3^- (0.1 M NaNO_3) (right axis).

Figure 3.25a shows an ATR spectrum taken in the “dirty” chamber (solid line) in which NO_3^- was observed at 1340 and 1420 cm^{-1} (same experiment as Fig. 3.24b). A reference spectrum of aqueous NO_3^- (0.1 M NaNO_3 , dash-dotted line) is included to show the location of aqueous nitrate bands. The nitrate bands formed on the surface in this experiment are more structured than the broad peaks of aqueous nitrate; this is typical of nitrate ions on surfaces (*Vogt and Finlayson-Pitts, 1994; Sporleder and Ewing, 2001*). A reference spectrum of dry adsorbed HNO_3 is also included (dotted line) to show the absence of the molecular HNO_3 band at 1300 cm^{-1} . However, Figure 3.25b shows the formation of molecular HNO_3 in an experiment at the same RH, but in a chamber with no organics present. Experiments are planned in which organics are added to the chamber in a more controlled fashion. However, since significantly less molecular HNO_3 is formed when organics are present, these preliminary data suggest that a reaction between HNO_3 and organics may occur on surfaces, which has significant implications for the measurement of organic films on urban surfaces such as those carried out by Diamond and coworkers (*Diamond et al., 2000*).

V. HONO DECOMPOSITION

V.A. Introduction

Understanding the reactions of HONO on surfaces is important not only from a fundamental chemistry standpoint, but also for interpreting field and environmental chamber studies. Measurements of HONO and its precursor NO_2 in ambient air allow one to probe the contribution of heterogeneous reactions at the earth's surface to the production of HONO, and ultimately of OH, provided both the production and loss processes for HONO are understood.

In environmental chambers used to simulate reactions in air, the production of HONO has been observed from chamber walls even when oxides of nitrogen have not been included in the reaction mixture (*Carter et al., 1981, 1982; Sakamaki and Akimoto, 1988; Glasson and Dunker, 1989; Killus and Whitten, 1990; Finlayson-Pitts and Pitts, 2000*). Additionally, there have been several studies of the loss of HONO in laboratory systems (*Chan et al., 1976a, b; Kaiser and Wu, 1977a, b; Jenkin et al., 1988; Wallington and Japar, 1989; TenBrink and Spoelstra, 1998*). *Chan et al. (1976a; 1976b)* studied the decomposition in a stainless steel reactor ($S/V = 5.3 \text{ m}^{-1}$) at concentrations of HONO ranging from 2 – 9 ppm and at water vapor concentrations corresponding to 0.7 – 15% RH. They reported that the reaction is second order in HONO and occurs in the gas phase to generate NO and NO_2 :



In a number of subsequent studies, other groups also observed NO and NO_2 as products, but concluded that the reaction occurred heterogeneously on the reactor walls. For example, *Kaiser and Wu (1977a)* reported that the reaction occurred on the walls of a Pyrex reactor ($S/V = 63 \text{ m}^{-1}$) at RH from 0.2 to 5%, with a reaction order between one and two with

respect to HONO. The rate of HONO loss decreased with increasing water vapor, with an apparent reaction order in water vapor of about -0.6. The production of NO and NO₂ were not consistent with reaction (-2) alone and for analysis of the data, the reactions of HONO and NO with HNO₃ were included in their mechanism. These researchers found that prior exposure of the reactor walls to a mixture of NO, NO₂ and H₂O decreased the rate of HONO decomposition as the surface “aged,” but that coating the reactor surface with boric acid increased the decomposition rate. In a separate study, Kaiser and Wu (1977b) studied the loss of HONO in the reactor in the presence of HNO₃, and concluded that the chamber walls play a role in the reaction between HONO and HNO₃. They observed the reaction to be first order in HONO as well as gas phase HNO₃, and the reaction rate decreased when the water vapor pressure was increased from 0.1 to 5 Torr, corresponding to a RH from 0.5 to 22% RH.

Jenkin *et al.* (1988) studied the loss of HONO in a glass cell (S/V = 13 m⁻¹) in conjunction with studies of the HONO formation by reaction (1). They reported that the loss of HONO was first order at water vapor concentrations corresponding to 3.2 and 9.5% RH. Wallington and Japar (1989) studied the decomposition of HONO in a similar reactor. They reported that the rate of disappearance of HONO increased in the presence of HNO₃ and could be modeled by a first order process in HONO. Ten Brink and Spoelstra (1998) followed the loss of HONO in a Pyrex chamber at 80% RH. The decay of HONO was observed to be second order, with the major initial gas phase product being NO. At much longer reaction times (~60 hrs), NO₂ was also observed as a product. They reported that the results were the same at 50% RH.

In summary, the preponderance of evidence shows that the loss of HONO in laboratory systems occurs via reactions on the chamber walls. This is in agreement with theoretical studies of reaction (-2), which show that this reaction in the gas phase should be very slow, with a rate constant of ~10⁻²⁵ cm³ molecule⁻¹ s⁻¹ (Mebel *et al.*, 1998). Furthermore, the rate and mechanism might depend on the nature and amounts of co-adsorbed species, including water.

With the exception of the Ten Brink and Spoelstra (1998) experiments, previous studies have been carried out at relative humidities that are much lower than those found in the troposphere. In addition, there has been no comprehensive study of the heterogeneous decomposition of HONO in which the concentrations of HONO and co-adsorbed species such as water and nitric acid were systematically varied over a wide range. We report here the results of such experiments, using the walls of a borosilicate glass chamber as the surface, as in many of the previous studies. However, this material is also relevant to many surfaces found in the boundary layer, since windows, buildings, concrete etc. have high silicate contents (Diamant, 1970; Finlayson-Pitts *et al.*, 2003; Rivera-Figueroa *et al.*, 2003). We show that both water and HNO₃ compete with HONO for sites on the surface, which affects the kinetics, the products, and the mechanism of heterogeneous HONO uptake and reaction. This result has significant implications for HONO measurements in environmental chambers as well as in ambient air.

V.B. Experiments in an HNO₃-Conditioned Cell

In the first set of experiments, the cell walls were first conditioned with dry HNO₃ prior to adding HONO in order to provide reproducible surface conditions in which HNO₃ was present on the walls. Figure 3.26 shows typical concentration-time profiles for HONO decay in an HNO₃ conditioned cell at 0 (Fig. 3.26a), 20 (Fig. 3.26c) and 50 % RH (Fig. 3.26e), along with profiles for the gas phase products, NO and NO₂. Both NO₂ and NO are unavoidably present at the beginning of each experiment due to HONO decomposition during its generation and handling in the glass manifold. This was particularly significant in these experiments because the walls of the vacuum line used to introduce HONO into the cell had also been exposed to nitric acid. The data in Fig. 3.26 show that the only gas phase product observed in measurable yield is NO₂. The concentration of nitric oxide, present initially as an impurity, does not change significantly with time.

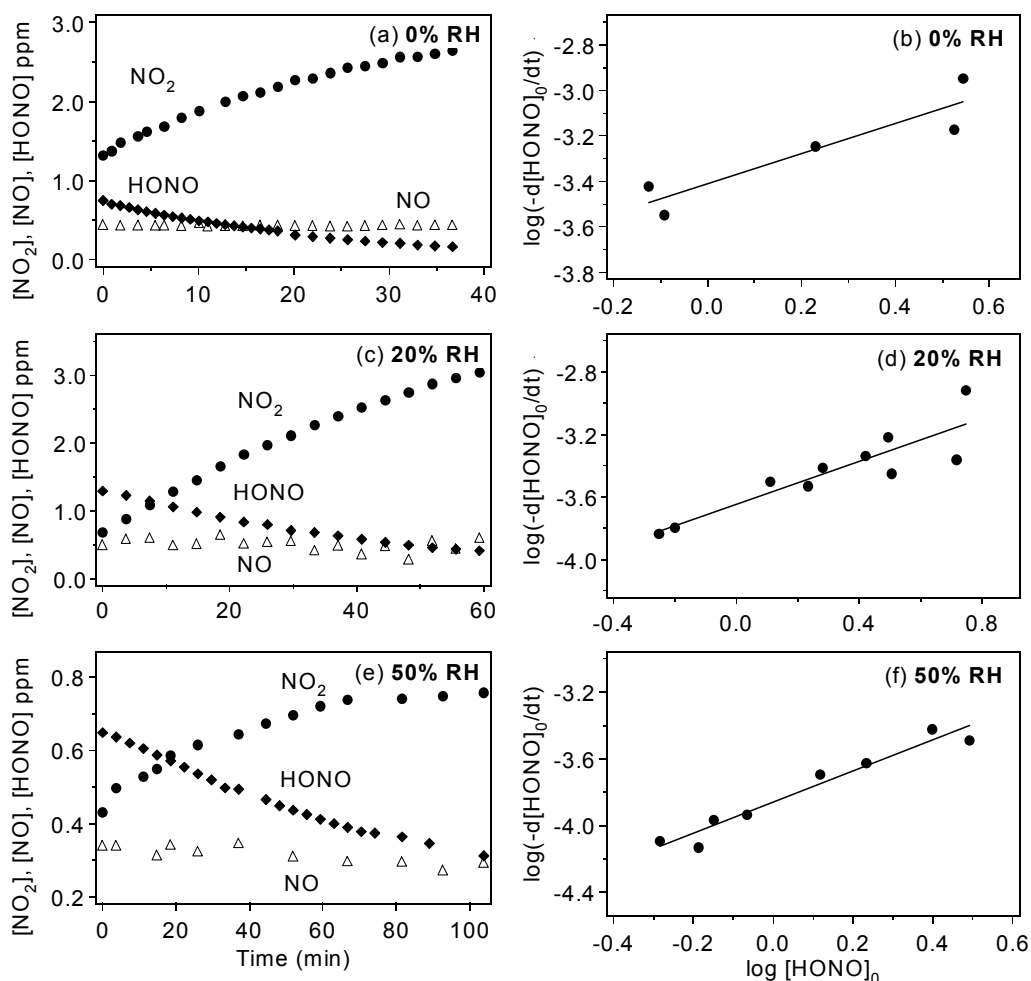


Figure 3.26. Concentration time-profiles of HONO (◆), NO₂ (●) and NO (Δ) and corresponding plots of log(-d[HONO]₀/dt) vs. log[HONO]₀ of HONO decay experiments at ~0 % (a, b), 20% (c, d) and 50% RH (e, f) in the HNO₃ conditioned cell. Based on the known equilibrium constant for $2 \text{HONO} \leftrightarrow \text{NO} + \text{NO}_2 + \text{H}_2\text{O}$ (Chan et al., 1976a, b) equilibrium is not attained within the reaction times used here.

For each experiment, the initial rate of HONO loss and the corresponding rate of NO₂ formation were measured. The rate of HONO loss can be expressed by equation (XII),

$$-\frac{d[\text{HONO}]}{dt} = k_d [\text{HONO}]^n \quad (\text{XII})$$

where n is the reaction order with respect to HONO and k_d the rate constant for HONO loss. This assumes that other species than HONO are not involved in the HONO loss (or that if they are, their concentrations are constant). The reaction order and rate constants for HONO decay were obtained from the slope and intercepts respectively of log-log plots of the initial rate of HONO loss versus the initial HONO concentration:

$$\log (-d[\text{HONO}]_0 / dt) = \log k_d + n \log [\text{HONO}]_0 \quad (\text{XIII})$$

Figures 3.26b, d and f show the log-log plots for 0, 20 and 50% RH, respectively. In all cases the reaction is approximately first order in HONO.

The data are summarized in Table 3.4. The first order rate constants (k_d) for loss of HONO decrease by a factor of approximately three in the range from 0 to 50% RH. The yield of NO₂ formed relative to HONO removed is between two and three at 0 and 20% RH, but falls to one at 50% RH.

V.C. Experiments in an Unconditioned Cell

In a second set of experiments, the cell was thoroughly cleaned first. Due to the impracticality of cleaning after each run and aligning the optics (which necessitates extensive gas recalibrations), the cell was then diffusion pumped between runs. Figure 3.27a, c and e shows typical concentration-time profiles for the decay of HONO and the formation of NO and NO₂ in the unconditioned cell at 0, 20 and 50% RH. At 0% RH, equal amounts of NO and NO₂ are produced. However, as the RH increases the relative yield of NO increases and that of NO₂ decreases.

Figures 3.27b, d, and f show the log-log plots (equation XIII) used to obtain the reaction order. The reaction is first order at 0% RH but changes to approximately second order at 50% RH. Table 3.4 also includes the data for these experiments. Because the reaction is first order only at 0% RH, the rate constant k_d is shown only for this set of experiments. However, it is clear from Figures 3.27a, c and e that, as the RH increases, the rate of loss of HONO decreases.

Studies of the formation of HONO by the heterogeneous hydrolysis of NO₂, reaction (1), were previously carried out in this cell at values of RH up to 80% (*Finlayson-Pitts et al.*,

2003). Based on these earlier experiments, HONO formation by heterogeneous NO_2 hydrolysis is negligible in comparison with the rate of HONO loss.

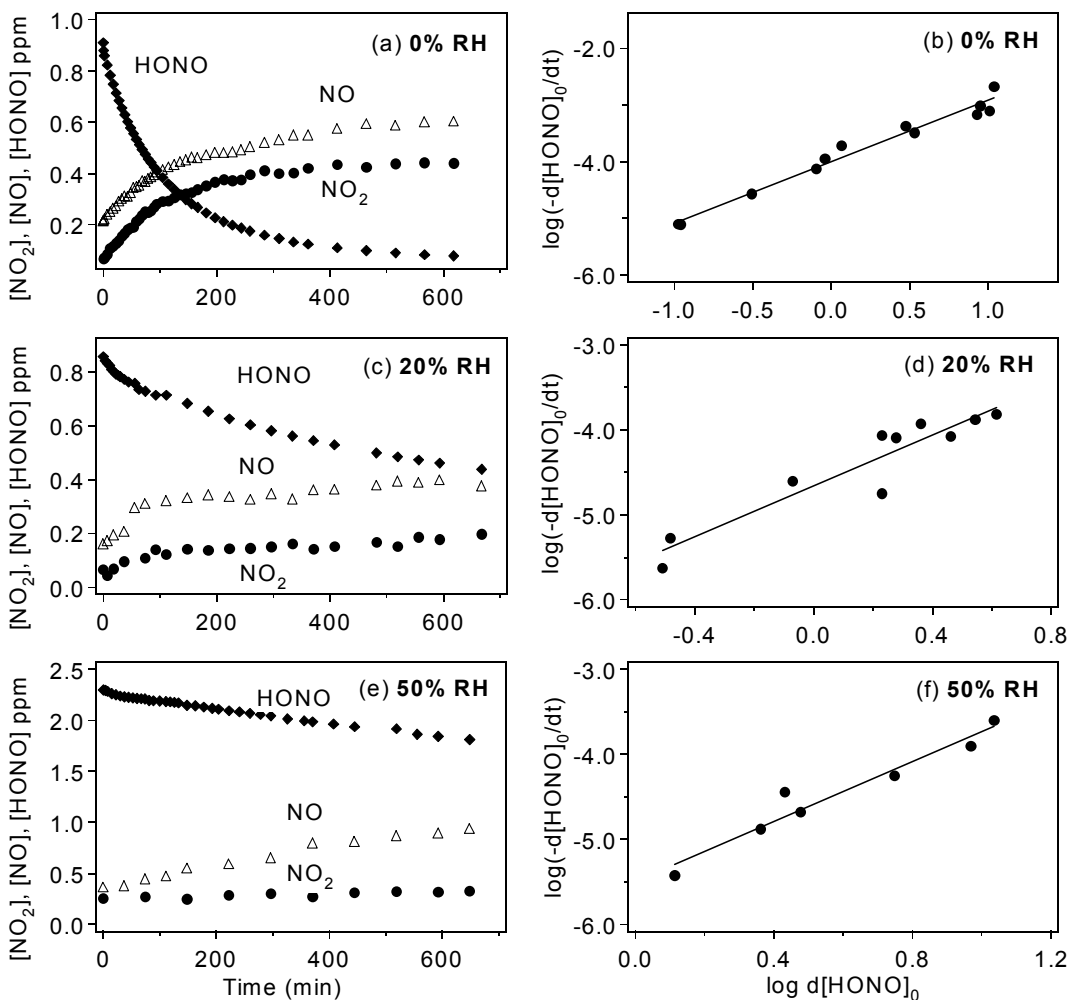


Figure 3.27. Concentration time-profiles of HONO (\blacklozenge), NO_2 (\bullet) and NO (Δ) and corresponding plots of $\log(-d[\text{HONO}]_0/dt)$ vs. $\log[\text{HONO}]_0$ of HONO decay experiments at ~0% (a, b), 20% (c, d) and 50% (e, f) RH in the unconditioned cell. Based on the known equilibrium constant for $2 \text{HONO} \leftrightarrow \text{NO} + \text{NO}_2 + \text{H}_2\text{O}$ (Chan et al., 1976a, b), equilibrium is not attained within the reaction times used here.

Table 3.4. Summary of HONO decomposition experiments.

Conditioning of RH cell walls (%)	No. of Expts	Range of initial [HONO] ₀ (ppm)	Reaction order in [HONO] ₀	First-order rate constant for HONO loss k_d (units of 10^{-4} s^{-1})	Yield of NO ₂ ^c	Yield of NO ^d
HNO ₃						
0	5	0.75 – 3.5	0.7 ± 0.3^a	3.9 ± 1.1^a	2.3 ± 1.0^b	0
20	10	0.56 – 5.6	0.7 ± 0.2	2.3 ± 0.6	2.8 ± 0.5	0
50	8	0.52 – 3.1	0.9 ± 0.2	1.4 ± 0.2	1.1 ± 0.3	0
Unconditioned						
0	12	0.11 – 10.9	1.1 ± 0.1	1.0 ± 0.2	0.59 ± 0.20	0.57 ± 0.13^b
20	10	0.31 – 4.1	1.5 ± 0.4	^c See footnote	0.26 ± 0.26	0.67 ± 0.56
50	7	1.3 – 1 0.9	1.8 ± 0.4	^c See footnote	0.1 ± 0.1	1.1 ± 0.2

^a Errors represent $\pm 2s$.

^b Errors represent 95% confidence limits (CL) using the *t*-test. The 95 % CL is given by $\frac{ts}{\sqrt{N}}$ where the standard deviation $s =$

$$\sqrt{\frac{\sum(x_i - x_{av})^2}{N-1}}$$

and *N* is the number of data points in the mean.

^c For the HNO₃-conditioned cell, the yield of NO₂ was calculated from the initial rates of NO₂ formation and HONO loss, *i.e.* from $(d[\text{NO}_2]/dt) / (-d[\text{HONO}]/dt)$. For the unconditioned cell where the rates of reaction were significantly slower, the yields were calculated from $\Delta[\text{NO}_2] / \Delta[\text{HONO}]$ at the end of each run; this was judged to be more accurate than using rates for the slower HONO losses.

^d The yields were calculated from $\Delta[\text{NO}] / \Delta[\text{HONO}]$ at the end of each run.

^e Since the reaction order is significantly greater than one, a first-order rate constant cannot be reported. However, as seen in Figure 3.27, the rate of loss of HONO decreased with increasing RH.

At low HONO concentrations (<0.9 ppm) and 50% RH in the unconditioned cell, HONO concentrations initially increased upon addition of the humid N₂, rather than decreased as was the case under all other conditions. This suggests that water competes with HONO for surface sites and displaces some HONO that was previously adsorbed onto the walls into the gas phase. To test this point, experiments were carried out in which the cell was first exposed for one hour at 50% RH to 13 ppm HONO and then pumped for 60 min. Dry N₂ was added up to 1 atm pressure and the gas composition monitored for 9.5 hours. No production of gaseous HONO was observed during this time. The cell was then pumped out and N₂ at 50% RH added. Figure 3.28 shows the concentration-time profile for HONO. Clearly, HONO is being produced in the gas phase, and the only available source is displacement by the competitive adsorption of water on the surface.

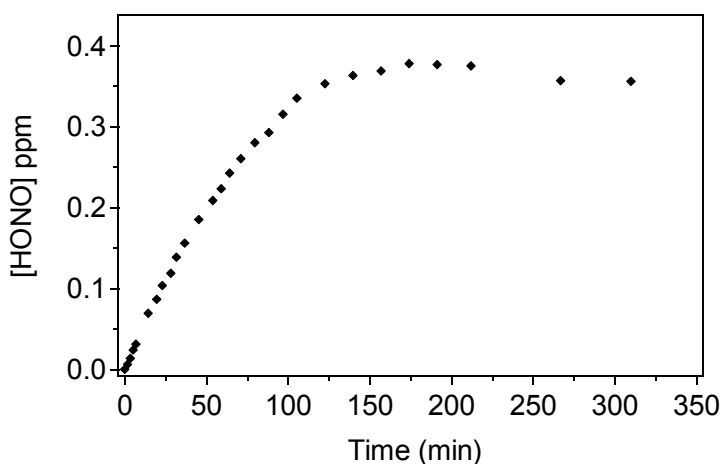
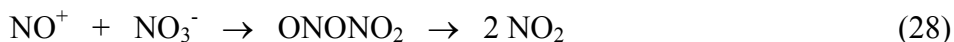


Figure 3.28. Concentration-time profile of HONO in the HONO-conditioned cell at 50% RH and 1 atm in N₂. Before the experiment, the cell was exposed at 50% RH for 1 hour to 13 ppm of HONO that contained 28 ppm of NO₂ and 60 ppm of NO as impurities. The cell was then pumped out before the water vapor-N₂ mixture was added.

V.D. Discussion

For the reaction in the cell that had been pretreated with HNO₃, the reaction is approximately first order in HONO (Fig. 3.26), and NO₂ is the only gas phase product. Because the loss of HONO occurs on the surface of the cell, it is expected to be sensitive to the nature of the thin film of co-adsorbed species on the chamber walls. It is known from other studies in this laboratory that after exposing borosilicate glass to gas phase HNO₃, some of it remains adsorbed even after prolonged pumping (*Finlayson-Pitts et al., 2003; Rivera-Figueroa et al., 2003; Dubowski et al., 2004*). The form of the acid on the surface is not known, but it is likely to be, at least in part, complexed to water (*Finlayson-Pitts et al., 2003; Dubowski et al., 2004*).

The production of NO₂ as the only gas phase product in the experiments where the walls were conditioned with HNO₃ is consistent with the uptake of HONO on the chamber walls, followed by its protonation by adsorbed nitric acid:

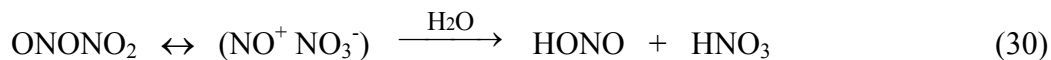


If the HNO₃ adsorbed on the cell walls is constant, the rate of reaction of HONO should be first order in HONO, in agreement with observations.

Reactions (26) - (28) are the reverse of the heterogeneous hydrolysis of NO₂, reaction (1), which we proposed to occur via formation of the asymmetric NO₂ dimer (*Finlayson-Pitts et al., 2003*):



The ONONO₂ then autoionizes and reacts with adsorbed water to generate HONO and HNO₃:



This sequence can be driven in reverse by high initial concentrations of HONO and HNO₃ as used in the present study. The stoichiometry from reactions (26) – (28) is expected to be $\Delta[\text{NO}_2] / \Delta[\text{HONO}] = 2$. Our measured yields of NO₂ are 2.3 ± 1.0 and 2.8 ± 0.5 at 0 and 20 % RH, respectively; the latter value is slightly larger than anticipated on the basis of the proposed mechanism. The yield of NO₂ at 50% RH falls to approximately one, and no additional gas phase products are observed. This suggests that, for every two HONO molecules that are taken up on the surface, one reacts to form NO₂ via the mechanism described above, while one remains on the surface as undissociated HONO, as the dissociated form of HONO (H⁺ + NO₂⁻), or as some as yet unidentified involatile product.

Nitrogen dioxide is known to be generated in the decomposition of pure nitric acid (*Chédin, 1952; Högfeltdt, 1963; Addison, 1980; Crowley et al., 1993*), and indeed, some NO₂ formation was observed over time after the cell was pumped following the HNO₃ conditioning procedure. At 0% RH, the increase was small and represented less than 10% of the NO₂ formed in experiments where HONO was added. At 50% RH, significant amounts of NO₂ were generated, up to several ppm in 100 min. However, when HONO is present in the cell, its uptake and reaction with HNO₃ on the walls must compete with the generation of NO₂ from the self-reactions of adsorbed HNO₃. Thus, the NO₂ observed in the absence of HONO is an upper limit for the case where HONO is present. The fact that the yield of NO₂ falls to approximately one at 50% RH, compared to two at 0% RH, suggests that the

contribution from the self-reactions of HNO₃ on the wall at the higher RH is not a major contributor to the measured NO₂ in the presence of added HONO.

A possible explanation for the low NO yields in the HNO₃-conditioned cell is that both NO and NO₂ are generated initially, but the NO reacts with adsorbed HNO₃ (*Smith, 1947; Jaffe and Ford, 1967; Kaiser and Wu, 1977b; McKinnon et al., 1979; Streit et al., 1979; Besemer and Nieboer, 1985; Svensson and Ljungström, 1988; Fairbrother et al., 1997; Mochida and Finlayson-Pitts, 2000; Saliba et al., 2000; 2001; Rivera-Figueroa et al., 2003*),



Based on earlier experiments in this laboratory in a different cell, this process is expected to be too slow to be significant under the present experimental conditions (*Saliba et al., 2000; 2001*). As a further check on this point, experiments were carried out at 0 and 50% RH in which 12 ppm of NO were added to the HNO₃ conditioned cell and the concentrations of gases monitored for 6 hours. The observed rates of loss of NO and formation of NO₂ were confirmed to be too slow to be consistent with an initial formation of NO followed by reaction (31).

The data in Table 3.4 and in Figures 3.26 and 3.27 show that the rate constant for HONO decomposition decreases with increasing relative humidity. As the partial pressure of water vapor increases, the amount of water on the surface increases relative to the amount of adsorbed nitric acid. The decreased rate constant at higher RH might be due to increased competition for the reaction of NO⁺NO₃⁻ with water to generate HONO and HNO₃. Alternatively, or perhaps in addition, increased adsorbed water could change the nature of nitric acid on the surface. Nitric acid exists in the undissociated, molecular form at low RH on silica surfaces (*Goodman et al., 1999; Barney and Finlayson-Pitts, 2000; Goodman et al., 2001*). Upon addition of water, dissociation to H⁺ and NO₃⁻ occurs. This is consistent with gas-phase studies of complexes of nitric acid with water, where ionization of the acid occurs when there are four or more water molecules in the cluster with one nitric acid molecule (*Kay et al., 1981; Zhang et al., 1994; Gilligan and Castleman, 2001*). A decrease in the rate constant with increasing RH would also result if molecular HNO₃ is the reactant, while the dissociated ionic form, whose concentration increases with more water on the surface, is unreactive.

In the unconditioned cell, the reaction was first order in HONO (Fig. 3.27b) at 0% RH with a rate constant that was about a factor of three slower than in the HNO₃-conditioned cell. In this case, nitric oxide and nitrogen dioxide were generated in equal yields, in contrast to the HNO₃ conditioned chamber where NO₂ was the sole gas phase product. As the RH increases to 50%, the rate of HONO loss decreases, the reaction order increases and the product changes to NO with a yield greater than 90%. This is in contrast to the reaction on the HNO₃-conditioned cell walls where the reaction order remained one and NO₂ was the only product over the 0 – 50% range of RH.

We propose that the experimental observations in the unconditioned cell are attributable to competition between HONO and H₂O for the available surface sites. Thus, as the water vapor concentration increases, the coverage of surface-adsorbed water increases. This leads to a decrease in the amount of adsorbed HONO, and hence in the rate of reaction. This conclusion is supported by the data in Figure 3.28, where the addition of water to a cell previously exposed to HONO and then pumped out leads to an increase in HONO in the gas phase.

Further, a competition between water and HONO for surface sites is consistent with the change in reaction order from one to two as the water vapor concentration increases. Thus, in a system where both HONO and H₂O can be adsorbed on a surface, the fraction of the surface covered by HONO (θ_{HONO}) is given by equation (XIV) (Masel, 1996),

$$\theta_{HONO} = \frac{K^{HONO} [HONO]}{1 + K^{HONO} [HONO] + K^{H2O} [H_2O]} \quad (XIV)$$

where K^{HONO} is the equilibrium constant for the surface uptake and desorption of HONO (*i.e.* $K^{HONO} = k_{26}/k_{-26}$ for reaction (26) above), K^{H2O} is the corresponding equilibrium constant for adsorption of water, and [HONO] and [H₂O] are the gas phase concentrations. In the absence of water vapor, equation (XIV) becomes

$$\theta_{HONO} = \frac{K^{HONO} [HONO]}{1 + K^{HONO} [HONO]} \quad (XV)$$

and if $K^{HONO} [HONO] \gg 1$, the fractional coverage of the surface by HONO becomes constant at one, *i.e.* the surface is saturated with HONO. In this case, the rate of reaction of gas phase HONO with adsorbed HONO is given by

$$-\frac{d[HONO]}{dt} = k' [HONO]_g [HONO]_{ads} = k' [HONO] \times S \times \theta_{HONO} = k' [HONO] \times S \quad (XVI)$$

where k' is the rate constant for the gas-surface reaction and S is the surface density of one HONO monolayer (molecule per cm²). Because of the saturation of the surface by HONO, the reaction is predicted to be first-order in gas-phase HONO, which is consistent with our experimental observations.

At high relative humidities, water partially displaces HONO from the surface. Under conditions where $K^{H_2O}[H_2O] \gg K^{HONO}[HONO]$, equation (XV) becomes

$$\theta_{HONO} = \frac{K^{HONO}[HONO]}{1 + K^{H_2O}[H_2O]} \quad (XVII)$$

The rate of reaction of gas phase HONO with adsorbed HONO is then given by equation (XVIII):

$$-\frac{d[HONO]}{dt} = k'[HONO] \times S \times \theta_{HONO} = \frac{k'K[HONO]^2 \times S}{1 + K^{H_2O}[H_2O]} \quad (XVIII)$$

That is, the loss of HONO from the gas phase decreases with increasing RH and becomes second order in HONO at constant RH, consistent with the experimental observations at 50% RH (Fig. 3.27e).

The fact that the rate appears to be between first and second order at intermediate relative humidities implies that the terms $K^{HONO}[HONO]$ and $K^{H_2O}[H_2O]$ are comparable under these conditions. Consider 20% RH, for example, where the water vapor concentration is about 5×10^3 ppm, and a 5 ppm HONO concentration. For the two terms $K^{HONO}[HONO]$ and $K^{H_2O}[H_2O]$ to be of comparable magnitude, K^{HONO} must be greater than K^{H_2O} by a factor of approximately 10^3 .

The equilibrium constants for uptake of HONO and H₂O onto surfaces are related to the enthalpy and entropy of adsorption through the free energy. If it is assumed that the entropy of adsorption is similar for HONO and H₂O, then the ratio of the equilibrium constants is given by

$$K^{HONO}/K^{H_2O} = \exp [-(\Delta H_{ads}^{HONO} - \Delta H_{ads}^{H_2O})/RT] \quad (XIX)$$

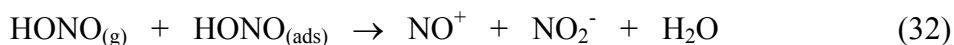
where ΔH_{ads}^{HONO} and $\Delta H_{ads}^{H_2O}$ are the enthalpies of adsorption of HONO and water on the surface. If $K^{HONO}/K^{H_2O} \sim 10^3$, the difference between the enthalpies of adsorption of HONO and H₂O ($\Delta H_{ads}^{HONO} - \Delta H_{ads}^{H_2O}$) must be approximately -17 kJ mol^{-1} .

Thompson and Margey (2003) recently calculated enthalpies for formation of complexes of silica molecules (SiH₃OH or Si(OH)₄), taken as proxies for a silica surface, with HONO, water, HNO₃, NO₂ and N₂O₄. The enthalpy of formation for the complex of HONO with SiH₃OH was calculated to be $-25.1 \text{ kJ mol}^{-1}$, and for the complex of H₂O with SiH₃OH, the enthalpy was calculated to be in the range from -15.5 to $-23.2 \text{ kJ mol}^{-1}$,

depending on the particular orientation of water to the silicate. This calculation shows that the difference in the enthalpies of adsorption for these complexes of HONO or H₂O is in the range of - (2 – 10) kJ mol⁻¹. The difference for binding of HONO compared to H₂O to Si(OH)₄ was also small, ~2 kJ mol⁻¹. These differences are much smaller than our estimate of -17 kJ mol⁻¹. The apparent discrepancy could be due to several factors. First, the isolated SiH₃OH or Si(OH)₄ molecules used as proxies might not be truly representative of silica surfaces. This is particularly the case for borosilicate glass, which contains small amounts of oxides of metals such as Na, Zn, B, Al and Ti. Also, HONO may not adsorb in the molecular form by hydrogen bonding, as assumed in the calculations. For example, partial or full ionization to H⁺ and NO₂⁻ would provide strong electrostatic interactions, with larger associated heats of adsorption.

This work also predicted that nitric acid would form much stronger complexes with SiH₃OH and Si(OH)₄ than HONO (*Thompson and Margey, 2003*). This might be the reason why HONO does not compete with HNO₃ for surface sites in the HNO₃-conditioned experiments, where the data are consistent with saturation of the surface sites by HNO₃.

The formation of equal amounts of NO and NO₂ as products is consistent with an autoionization reaction between gas-phase and adsorbed HONO:



Such autoionization reactions are known for HNO₃ (*Chédin, 1952; Högfeltdt, 1963; Addison, 1980*) as well as for N₂O₅ (*Mozurkewich and Calvert, 1988; Fried et al., 1994; George et al., 1994; Behnke et al., 1997; Robinson et al., 1997; Schweitzer et al., 1998; Wahner et al., 1998*) and N₂O₄ on ice (*Wang et al., 1998a; Wang and Koel, 1998, 1999*). In the case of HONO, the relatively large enthalpy of adsorption on the surface relative to water as discussed above suggests that the adsorbed species might already be partially or fully ionized.

As the RH increases in the unconditioned cell, the yield of NO increases and that of NO₂ decreases. At 50% RH, the yield of NO is greater than 90% (Table 3.4 and Fig. 3.27e). These observations are similar to those of Ten Brink and Spoelstra (*1998*), who studied the decay of HONO in a Pyrex chamber at 80% RH and 1 – 10 ppm HONO. Typical data in Fig. 3 of that paper show NO as the major gas phase product in the first ~7 hours of the reaction.

The mechanistic basis for the change in products as the RH increases in the unconditioned cell is not clear. In earlier studies of the NO₂ heterogeneous hydrolysis we reported that the yield of HONO was less than 0.5 as expected from reaction (1), and that the “missing HONO” was replaced by gas phase NO (*Finlayson-Pitts et al., 2003*). We proposed that this was due to the reaction of HONO with NO₂⁺ on the surface,



If this is the source of NO in the present experiments in the unconditioned cell at 50% RH, the NO_2^+ would have to be generated from adsorbed HONO if the reaction is to be second order as experimentally observed. However, the mechanism of formation of NO_2^+ on the surface from HONO is not clear.

In summary, most of the experiments reported here are consistent with our proposed mechanisms. The only observation for which a clear explanation is not available is the change in the product distribution in the unconditioned cell from equal amounts of NO and NO_2 at 0% RH to primarily NO at 50% RH.

To the best of our knowledge, this is the first comprehensive study of HONO reactions on a borosilicate glass surface in which both the initial HONO concentration and the RH were varied over a relatively wide range, including the impact of coadsorption of HNO_3 . The data reported here agree in large part with previous studies carried out over a more limited set of conditions. For example, Chan *et al.* reported that at low relative humidities in an unconditioned cell, NO and NO_2 are both generated and the rate of HONO loss decreases with RH, consistent with our experiments (Chan *et al.*, 1976a, b). We observed that the presence of HNO_3 increases the rate significantly and that the loss of HONO is first order under these conditions, in agreement with Kaiser and Wu (1977a) and Wallington and Japar (1989). Reaction orders between one and two have been reported, depending on the conditions and presence of HNO_3 (Chan *et al.*, 1976a, b; Kaiser and Wu, 1977a, b; Jenkin *et al.*, 1988; Wallington and Japar, 1989; TenBrink and Spoelstra, 1998). Our measured reaction orders are generally in agreement with these previous studies when comparisons are made under similar experimental conditions. For example, Jenkin *et al.* (1988) measured the rate of HONO decay in a glass chamber of similar size to the one used in these studies and reported the loss was first order at RH corresponding to 3.2 and 9.5% and the absolute value of the first order rate constant was $3.7 \times 10^{-4} \text{ s}^{-1}$. This is in excellent agreement with the value of $(3.9 \pm 1.1) \times 10^{-4} \text{ s}^{-1}$ measured in the present studies where the loss was also first order.

Finally, the results presented here provide some insight into laboratory studies of the heterogeneous hydrolysis of NO_2 in which yields of HONO have been frequently measured to be less than expected based on reaction (1). The observation of increasing yields of NO with decreasing HONO yields at intermediate to high relative humidities in such studies of reaction (1) (England and Corcoran, 1974; TenBrink *et al.*, 1978; Sakamaki *et al.*, 1983; Pitts *et al.*, 1984a; Svensson *et al.*, 1987; Wainman *et al.*, 2001; Finlayson-Pitts *et al.*, 2003) is consistent with the formation of HONO followed by its conversion to NO on the “unconditioned” walls of the reactor as illustrated, for example, by the data in Figure 3.27e.

V.E. Atmospheric Implications

Nitrous acid production from the surfaces of environmental (“smog”) chambers used for studying atmospheric reactions has been observed in many studies using different chambers (*Carter et al., 1981, 1982; Sakamaki and Akimoto, 1988; Glasson and Dunker, 1989; Killus and Whitten, 1990*). This has been observed even when oxides of nitrogen have not been added during the experiment, implying that it must have arisen from contamination from previous experiments. Our studies show that the competition between water and HONO for surface sites leads to desorption of adsorbed HONO from the surface as the RH increases. This suggests that contamination of the walls of environmental chambers in previous experiments leaves adsorbed HONO (or comparable species such as H^+ and NO_2^-) on the surface, and that HONO is displaced by water when the RH value is increased. Hence, if this point is accepted, generation of HONO in such chambers will be unavoidable once the chamber walls have been exposed to oxides of nitrogen. Consistent with this explanation is the observation that the rate of generation of HONO in such chambers increases with RH (*Killus and Whitten, 1990*).

Nitrous acid has been measured in many field experiments, and it is clear from such studies that surface reactions act both as a source and as a sink for HONO. Separating the production and loss processes for HONO requires that the kinetics and mechanisms of this uptake be understood. In the tropospheric boundary layer there are a variety of surfaces of different chemical composition (*e.g.* vegetation, building materials etc.) available that might participate in uptake of HONO. Since many building materials are silicates (*Diamant, 1970*), our experiments using borosilicate glass are relevant to such surfaces in urban areas.

The results presented here suggest that the loss of HONO can vary from first to second order, depending on the RH and presence of reactive co-adsorbed species such as HNO_3 . These experiments also show that HONO can be displaced from surfaces by water vapor, leading to an apparent increase in HONO as a function of RH. However, the formation of HONO from the NO_2 heterogeneous hydrolysis also increases with RH (*Finlayson-Pitts et al., 2003*) so that measurements of HONO in air at different RH may be affected both by the dependence of reaction (1) on water and by the displacement of HONO from the surface through preferential adsorption of water.

Stutz and coworkers (*2003*) have measured HONO and NO_2 in urban areas and find that their data are consistent with a first-order loss of HONO at RH from 10 to 100%. This suggests that urban surfaces may have sufficient deposited HNO_3 (or other species that are reactive towards HONO) that the kinetics for the loss of HONO are determined by the collision rate of HONO with the surface.

VI. PHOTOCHEMICAL PRODUCTION OF HONO

VI.A. Introduction

A photoenhancement of the generation of HONO from the heterogeneous hydrolysis of NO_2 was reported by Akimoto *et al.* (1987). The HONO formed in a 6065-L Teflon coated smog chamber did not decay as rapidly as predicted by a model of the chemistry when the mixture in air was irradiated with a filtered Xe lamp ($\lambda > 290 \text{ nm}$). The difference between the model-predicted and experimental data was attributed to a photoenhancement of the heterogeneous NO_2 hydrolysis reaction. Recently Zhou *et al.* (2002; 2003) reported evidence for a photochemical production of HONO from HNO_3 deposited on surfaces. This HONO production was first observed in a “dirty” glass sampling line exposed to sunlight during a field study, and was confirmed in subsequent laboratory experiments (Zhou *et al.*, 2002; 2003). Killus and Whitten (1990) reviewed data from various smog chambers to suggest that photoenhanced HONO production occurs on quartz and glass surfaces but significantly less on Teflon surfaces, such as that used by Akimoto *et al.* (1987).

In the present study, HONO formation from NO_2 hydrolysis in a borosilicate glass cell has been studied in the presence and absence of UV radiation (320 – 400 nm) in 1 atm of N_2 or air. The data are interpreted in the framework of a simplified mechanism represented by a kinetics model developed to describe the reaction in both the dark and the light periods. The photolysis rate constants for HONO and NO_2 were measured independently in the same system for inclusion in the model. A comparison of the experimental data to the model predictions clearly establishes that there is no photoenhancement of the fundamental mechanism of NO_2 hydrolysis. Our experiments do show evidence of a secondary photochemical HONO production at longer photolysis times.

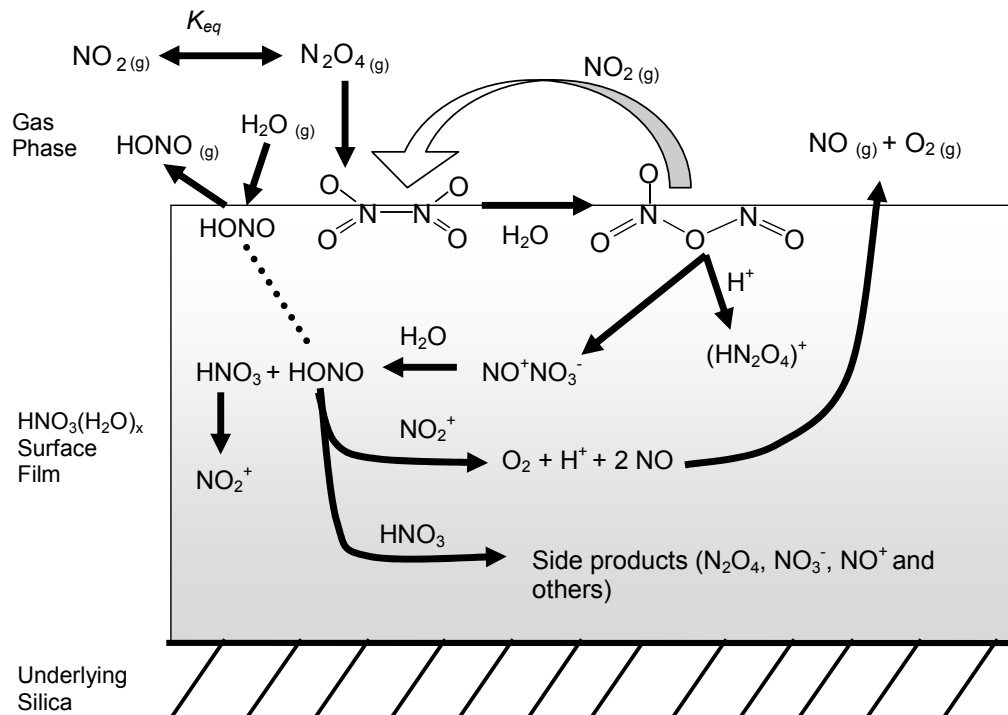


Figure 3.29 Schematic of the reaction mechanism of the heterogeneous hydrolysis of NO_2 proposed by Finlayson-Pitts *et al.* (2003) with the inclusion of competitive adsorption between water and HONO (Syomin and Finlayson-Pitts, 2003).

VI.B. Results and Discussion

Figure 3.30 shows a typical concentration-time profile for the gaseous reactants and products for the reaction of 46 ppm NO_2 at 39% RH in 1 atm of N_2 . In the dark period (region I), the NO_2 concentration slowly decays while HONO and, to a lesser extent, NO increase. At ~ 6500 s, the contents of the cell were irradiated (region II). As expected from the large absorption cross sections and quantum yields for NO_2 and HONO in the 300 – 400 nm region (*Finlayson-Pitts and Pitts, 2000*), the concentrations of both compounds decrease rapidly. Nitric oxide, the primary photolysis product of these reactions, rapidly increases. After ~ 650 seconds of photolysis (region III), the HONO concentration begins to level off and less than 25% of the initial NO_2 concentration remains.

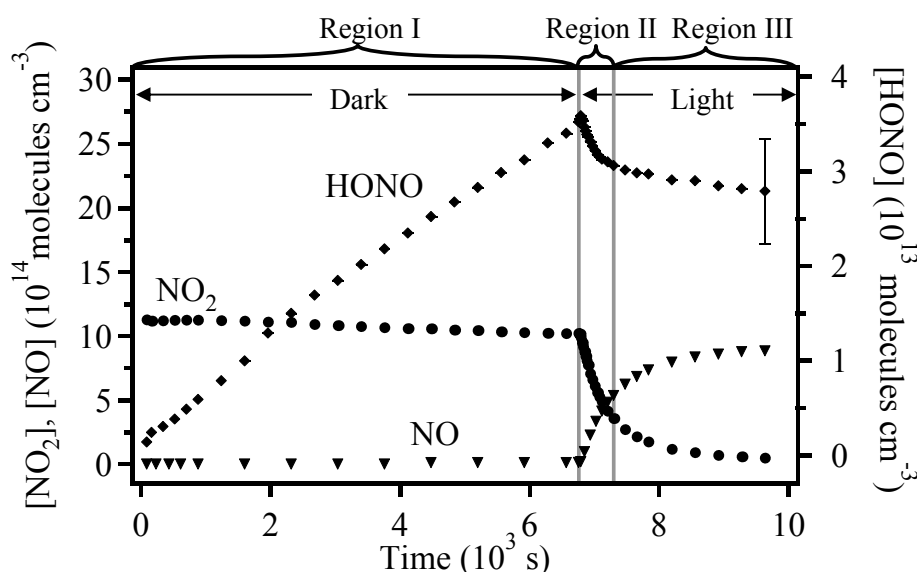


Figure 3.30. Experimental concentration-time profiles for NO_2 (\bullet), HONO (\blacklozenge), and NO (\blacktriangledown) with 46 ppm initial $[\text{NO}_2]$ and 39% RH in 1 atm N_2 at 296 K. The error bar on the HONO concentration is $\pm 2\text{s}$.

Figure 3.31 shows expanded plots for the concentration-time profiles for three NO_2 hydrolysis experiments at different relative humidities and initial concentrations of NO_2 . The x-axis time is referenced to the irradiation period with zero designated as the start of irradiation. In the dark period, there is excellent agreement between the measured (symbols) and model predicted concentrations (solid lines), allowing for accurate initial concentrations for the photolysis period. The photolysis period was modeled by including the photodissociation of NO_2 , HONO, and O_3 in the model (section B of Table 2.2), along with the secondary chemistry of $\text{O}(^1\text{D})$, $\text{O}(^3\text{P})$, and OH (included in section A of Table 2.2) generated by photolysis. The agreement between the experimentally measured HONO concentrations and model predictions is excellent in this initial period of irradiation (region II) without including any photoenhancement of the NO_2 heterogeneous hydrolysis reaction.

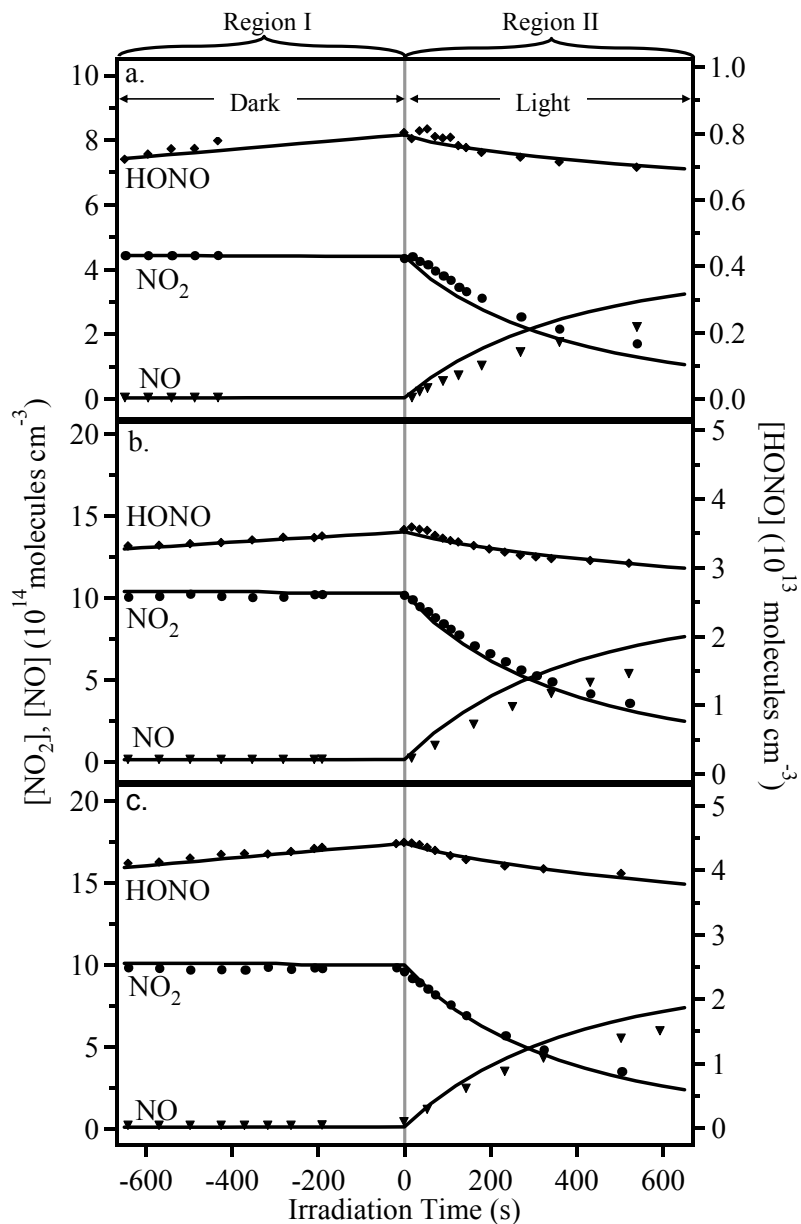


Figure 3.31. Comparison of experimental data (symbols) and model-predicted (solid lines) concentration-time profiles for NO_2 (\bullet), HONO (\blacklozenge), and NO (\blacktriangledown) with (a) 20 ppm initial $[\text{NO}_2]$ and 33% RH in N_2 (b) 46 ppm initial $[\text{NO}_2]$ and 39% RH in N_2 (c) and 54 ppm initial $[\text{NO}_2]$ and 57% RH in N_2 .

As shown in Figure 3.32, the model begins to underestimate the HONO concentrations at longer photolysis times (region III). Although the 2s error bars on the HONO concentrations (which is due primarily to the uncertainty in the measured absorption cross section) overlaps the model predictions in region III, the model provides a good match to the data at shorter photolysis times (region II). This suggests that an additional source of

HONO exists at the longer irradiation times, which is not included in the well-known chemistry shown in Table 2.2. Indeed, there is experimental evidence from other laboratories for such a photochemical production of HONO. Thus, Zhou *et al.* (2002) recently reported significant production of HONO when a “dirty” glass sampling manifold was exposed to sunlight, and hypothesized that photolysis of HNO₃ on the surface was the source of the additional HONO. In a later laboratory experiment, significant HONO and NO_x production was observed when 0 – 80% RH air was irradiated with a filtered mercury arc lamp (>290 nm) in a glass flow cell which had been previously conditioned with gaseous HNO₃ (Zhou *et al.*, 2003).

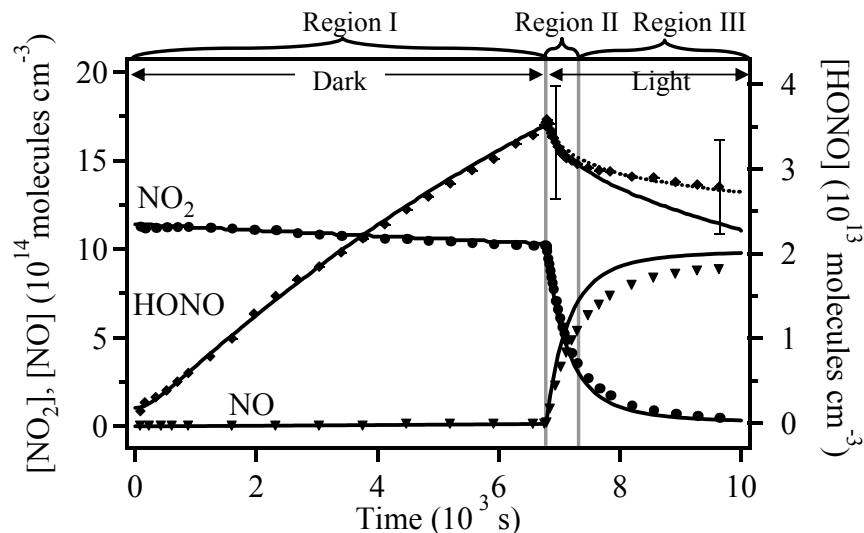


Figure 3.32. Experimental data (symbols) and model-predicted (lines) concentration-time profiles for NO₂ (●), HONO (◆), and NO (▼) with 46 ppm initial [NO₂] and 39% RH in N₂. The dotted line indicates the model prediction for HONO with the inclusion of photolysis of adsorbed HNO₃, reaction (35). The error bar on the HONO concentration is ± 2s.

To test whether the photolysis of adsorbed HNO₃ was a possible source of the additional HONO in Region (III), reaction (35) was added to the model.



As seen by the dotted line in Figure 3.32, including this reaction in the model with a rate constant of $2 \times 10^{-5} \text{ s}^{-1}$ brings the model predicted HONO concentrations into agreement with the data in both regions II and III.

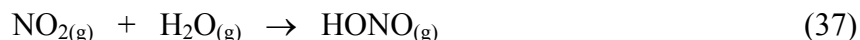
To test for reaction (35) in our system, the cell walls were conditioned by filling the reaction cell with ~2 Torr of dry gaseous HNO₃ and pumping out three times. The cell was

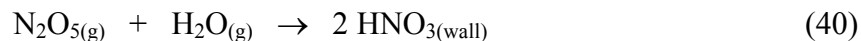
then filled with 139 ppm cyclohexane in 1 atm of dry air and the system exposed to 320 – 400 nm radiation for 90 min. Any gas phase HONO produced by photolysis of adsorbed HNO₃ would photolyze to form NO and OH. In the presence of oxygen, OH will react with cyclohexane to form cyclohexanone with a yield of 0.321 (*Aschmann et al., 1997*). In our experiments, no cyclohexanone production was observed. Based on the measured cyclohexanone detection limit in our system of 2.2 ppm, we calculated an upper limit for the rate constant for reaction (35) in our system of $\leq 3 \times 10^{-4} \text{ s}^{-1}$. This value is an order of magnitude larger than that used to obtain model agreement with our data, and hence a contribution from reaction (35) is not inconsistent with our data.

It should be noted that the technique used by Zhou *et al.* (2002; 2003) to measure HONO has ppt sensitivity. However, it is based on uptake into an aqueous solution and measurement of the nitrite. While he has been very careful in testing for possible interferences, any species that forms nitrite in solution will be measured as HONO and there is therefore some possibility of unrecognized artifacts in the identification of HONO as a product of adsorbed HNO₃ photolysis.

A complementary set of runs was performed after the cyclohexane experiments using similar initial conditions in air and then N₂ to probe for unanticipated effects of O₂ on the heterogeneous chemistry. Figure 3.33 shows that, as expected, the decay of NO₂ upon irradiation in air is slower than that in N₂ due to the regeneration of NO₂ by gas phase chemistry involving NO_x and O₂. However, the model fits the data during the dark and initial photolysis period for experiments in both N₂ and air. Again these results indicate that there is no photoenhancement of the NO₂ heterogeneous hydrolysis itself. (The decay of HONO in Region III in these experiments is somewhat faster than observed in earlier experiments carried out before cyclohexane/cyclohexanone was used in this system, which is attributed to increased OH scavenging by organics adsorbed on the cell walls). The dotted lines in Figure 3.33 show HONO concentrations when the rate constant for reaction (35) is $1.2 \times 10^{-5} \text{ s}^{-1}$ for the experiment in air and $5 \times 10^{-6} \text{ s}^{-1}$ for that in N₂. The variability in the rate constants for the photolysis of adsorbed HNO₃ that provide best fits to the data is not surprising, given that the surface conditions will change, particularly after carrying out the experiments using cyclohexane. The data suggests that there is still some photochemical production of HONO from a species adsorbed on the wall, such as HNO₃, consistent with the reports of Zhou *et al.* (2002; 2003).

The earlier studies in which a photoenhancement of the heterogeneous hydrolysis was reported were performed in air using a much larger (6065 L) chamber that was coated with Teflon, with a filtered (> 290 nm) high pressure Xe lamp as the light source (*Akimoto et al., 1987*). The surface reaction mechanism used in their model was as follows:





Despite these differences in the experimental conditions, our data are quite similar to those of Akimoto and coworkers (1987). It seems likely, based on the present results, that the source of the additional HONO observed in their experiments was photochemical production of HONO from species adsorbed on the cell walls, as we have observed at longer photolysis times. Studies in this laboratory (Dubowski *et al.*, 2004) have shown that nitric acid adsorbs onto both glass and Teflon surfaces in the presence of water vapor and hence photochemical production of HONO from photolysis of adsorbed HNO_3 might be expected from both their Teflon-lined chamber and our borosilicate glass cell.

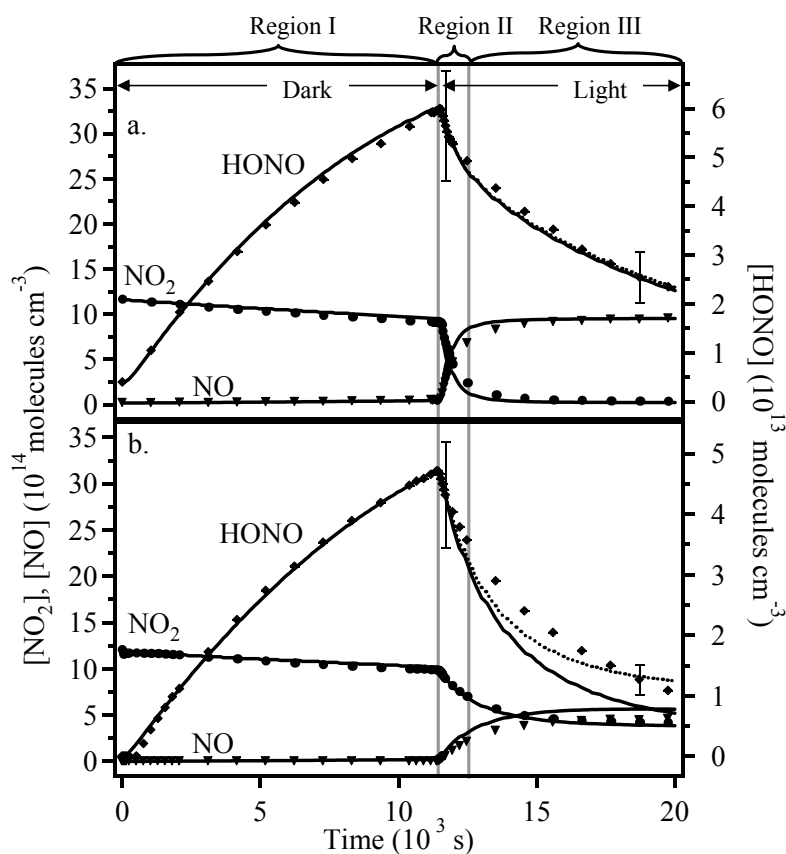


Figure 3.33. Experimental data (symbols) and model-predicted (lines) concentration-time profiles for NO_2 (\bullet), HONO (\blacklozenge), and NO (\blacktriangledown) of (a) 45 ppm initial $[\text{NO}_2]$ and 46% RH in N_2 and (b) 46 ppm initial $[\text{NO}_2]$ and 48% RH in air. The dotted line indicates the concentration of HONO with the inclusion of surface-adsorbed HNO_3 photolysis in model. The error bar on the HONO concentration is $\pm 2\text{s}$.

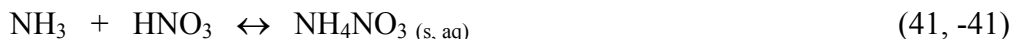
VI.C. Conclusions

The effect of UV (320 – 400 nm) irradiation on HONO production during the heterogeneous hydrolysis of NO₂ has been investigated. The fundamental NO₂ heterogeneous hydrolysis is **not** photoenhanced. However, the experimental decay of HONO was slower than expected at longer photolysis times, suggesting that there is a secondary photochemical source of HONO such as the photolysis of adsorbed HNO₃ which is formed by the heterogeneous hydrolysis. As proposed by Zhou and coworkers (2002; 2003) such a reaction could be an important source of HONO in the atmosphere during the day.

VII. LABORATORY STUDIES OF POTENTIAL MECHANISMS OF RENOXIFICATION OF TROPOSPHERIC NITRIC ACID

VII.A. Introduction

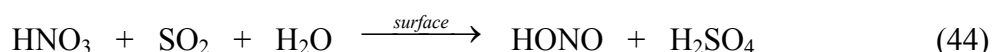
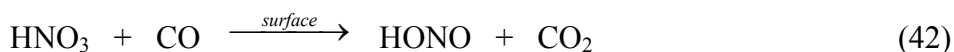
Reactive nitrogen oxides, particularly NO_x (NO + NO₂), are well known to be oxidized in the atmosphere to nitric acid (HNO₃) (Finlayson-Pitts and Pitts, 2000). Nitric acid is removed from the atmosphere by wet and dry deposition, or through reaction with ammonia (NH₃):



Ammonium nitrate (NH₄NO₃), an important component of atmospheric particulate matter in polluted atmospheres (Finlayson-Pitts and Pitts, 2000; Grassian, 2002), may also undergo deposition. As a result, the formation of HNO₃ is generally considered to result in the permanent removal of NO_x from the troposphere.

The reduction of HNO₃ back to photochemically active nitrogen (*e.g.* NO, NO₂, HONO), so-called “renoxification”, could alter the concentration of a number of important atmospheric species, including ozone, and hence impact air pollution control strategies. Surfaces on which such processes may occur include not only airborne particles, but also soils, building materials and vegetation. These surfaces may potentially be quite important in promoting heterogeneous chemistry in the boundary layer. For example, Diamond *et al.* (2000) and Gingrich *et al.* (2001) have shown that windows on buildings in both urban and rural areas have organic films that include both low vapor pressure organic compounds as well as semi-volatile organics. This issue of heterogeneous chemistry on soil and structures in urban atmospheres is one that has not received a great deal of attention, but that may prove to be quite significant, given that this is the region where many atmospheric measurements are made and human exposure is the greatest. While we focus here on chemistry relevant to the boundary layer, it should be noted that renoxification processes have also been proposed for the upper troposphere and lower stratosphere where the NO_x/HNO₃ ratio has frequently been measured to be higher than predicted by models of the gas phase chemistry (Chatfield, 1994; Singh *et al.*, 1998; WMO, 1998; Gao *et al.*, 1999; Osterman *et al.*, 1999; Lary and Shallcross, 2000; Perkins *et al.*, 2001).

Fairbrother *et al.* (1997) suggested that nitric oxide (NO), carbon monoxide (CO), methane (CH₄), and sulfur dioxide (SO₂) might influence renoxification in the atmosphere via reactions with HNO₃ on surfaces:



These reactions were proposed based on their thermodynamic feasibility. Heterogeneous reactions with HCHO and H₂O₂ were also considered and shown to be thermodynamically feasible as well (Fairbrother *et al.*, 1997); the reaction of HCHO with HNO₃ in the liquid phase was suggested earlier by Chatfield (1994) to resolve discrepancies between measured and modeled NO_x/HNO₃ ratios in the free troposphere. While modeling studies by Lary and Shallcross (2000) suggested that the agreement between the measured and modeled NO_x/HNO₃ ratio in the upper troposphere would improve significantly if the reaction of CO with HNO₃ occurs with a reaction probability of $\gamma \geq 1 \times 10^{-4}$, there have been no experimental studies of the feasibility of this reaction, nor of reactions (43) and (44).

These reactions may also be important sources of HONO (Saliba *et al.*, 2000), which is the major source of OH at dawn in polluted urban areas (Pitts *et al.*, 1984a; Winer and Biermann, 1994; Finlayson-Pitts and Pitts, 2000; Alicke *et al.*, 2002; Stutz *et al.*, 2002a). Reaction of OH with organics generates RO₂ and HO₂ free radicals that convert NO to NO₂. Photolysis of NO₂ then forms O(³P) that leads to O₃ formation (Finlayson-Pitts and Pitts, 2000). This heterogeneous chemistry thus has the potential to impact the formation of ozone and associated photochemical air pollutants in polluted urban areas.

Previous studies in this laboratory showed that NO does react with HNO₃ adsorbed on porous glass in the absence of added water vapor (Mochida and Finlayson-Pitts, 2000), as well as on smooth borosilicate glass at ~50% RH (Saliba *et al.*, 2000; Saliba *et al.*, 2001). Porous glass is a high surface area quartz material whose surface is terminated in –SiOH groups (Kiselev and Lygin, 1975; Elmer, 1992). These polar –OH groups on the surface physisorb water readily, and hence porous glass is also known as "thirsty glass". As a result, water is observed spectroscopically on these surfaces when placed in a cell and pumped on briefly. In contrast, smooth borosilicate glass holds very little water unless in contact with water vapor. At 20% RH for example, an amount of water equivalent to only about 1 – 2 layers is present on the surface (Saliba *et al.*, 2001; Sumner *et al.*, 2004); the infrared spectrum indicates that this is likely not a smooth film similar to bulk water, but rather islands or a 2-D water network. As a result, chemistry that occurs on porous glass in the

absence of significant amounts of gas phase water vapor will occur only at higher relative humidities on smooth glass.

In our earlier studies, only small concentrations of gaseous HONO were observed and the major gaseous reaction product was NO₂. This was proposed to be due to reaction (4), followed by secondary reactions of HONO on the surface, such as reaction (45),



or the self-reaction of HONO on the surface. However, whether the HNO₃-NO reaction occurs on different substrates was not investigated in these previous studies. For example, the composition of the porous glass used in those studies was 96.3% SiO₂, 2.95% B₂O₃, 0.04% Na₂O and 0.72% Al₂O₃ + ZrO₂ (Elmer, 1992), so catalysis by trace components such as the metal oxides may have played a role in the reaction. In addition, whether other species associated with HNO₃ on the surface such as nitrate ions (NO₃⁻) participated in the chemistry was not known; if NO₃⁻ also undergoes such a reaction, additional nitrate sources, such as airborne nitrate particles and ammonium nitrate fertilizer applied to vegetation and soils (Pacific Environmental Services, 1996), could also contribute to “renoxification.”

We therefore also carried out experimental studies using Fourier transform infrared (FTIR) transmission spectroscopy to examine whether CO, CH₄ and SO₂ react with adsorbed HNO₃ as proposed (Fairbrother *et al.*, 1997; Lary and Shallcross, 2000), and whether NH₄NO₃ reacts with NO in a manner similar to HNO₃. In addition, the possible catalysis by Fe³⁺ (the most common oxidation state of iron in the atmosphere (Dedik *et al.*, 1992; Erel *et al.*, 1993; Zhu *et al.*, 1997; Siefert *et al.*, 1998)) as proposed by Lary and Shallcross (2000) and effects of sulfuric acid (H₂SO₄) on the surface were investigated for the reaction of CO with HNO₃. Further studies of the reaction of gaseous NO with adsorbed HNO₃ were carried out on pure silica to probe whether trace components of glass played a role in the chemistry, and to elucidate the nature of the reactive form of HNO₃. We show that, while the reaction of HNO₃ with CO, CH₄ and SO₂ does not occur, the HNO₃-NO reaction does take place on pure silica, establishing that it is likely that it is the existence of thin water films on the surface that is important, rather than catalysis by trace components of borosilicate glasses. We show, based on the lower limit measured for the reaction probability, that the HNO₃-NO reaction in thin water films on terrestrial surfaces such as soils may be important in renoxification in the urban boundary layer.

VII.B. Heterogeneous Reaction of NO with HNO₃ on Silica Surfaces

Studies of the reaction of NO with adsorbed HNO₃ on silica pellets were conducted using nitric oxide concentrations in the range from (2 – 14) × 10¹⁶ molecule cm⁻³. Figure 3.34 shows typical spectra of the gas phase plus the surface in the 1300 – 1800 cm⁻¹ region before (Figure 3.34a) and after addition of NO (Figure 3.34b, c). In this case, the pellet was not heated prior to the reaction; while no additional water vapor was added to the cell, water adsorbed from room air was present initially as expected (Kiselev and Lygin, 1975; Elmer,

1992) and as evidenced by the overlapping band on the low wavenumber side of the HNO₃ peak. Ion chromatography measurements show that the initial nitrate (HNO₃ + NO₃⁻) on the silica pellet for a band of this intensity at 1677 cm⁻¹ is a total of 2.4 × 10¹⁸ molecules or 3.7 × 10¹³ molecule cm⁻², corresponding to ~ 10% of a monolayer; this is consistent with Goodman *et al.* (2001) who report a saturation coverage of HNO₃ on silica powder of (7 ± 3) × 10¹³ molecule cm⁻².

Upon addition of NO (Figure 3.34b), surface HNO₃ decreases and peaks attributable to N₂O₄ and NO₂ increase. Lifting the pellet out of the infrared beam shows that the N₂O₄ is primarily on the surface and the NO₂ is entirely in the gas phase. After 65 minutes of reaction time (Figure 3.34c), most of the surface HNO₃ has reacted, gas phase NO₂ has increased, and the surface N₂O₄ has decreased. These observations are consistent with the study of Mochida and Finlayson-Pitts (2000) in which NO was observed to react with HNO₃ adsorbed on porous glass, generating NO₂ as the major gaseous product. Independent experiments in this laboratory have shown that surface N₂O₄ is enhanced by the presence of HNO₃ (Finlayson-Pitts *et al.*, 2003). Thus, when the HNO₃ has reacted almost completely, N₂O₄ on the surface also decreases as observed in Figure 3.34c.

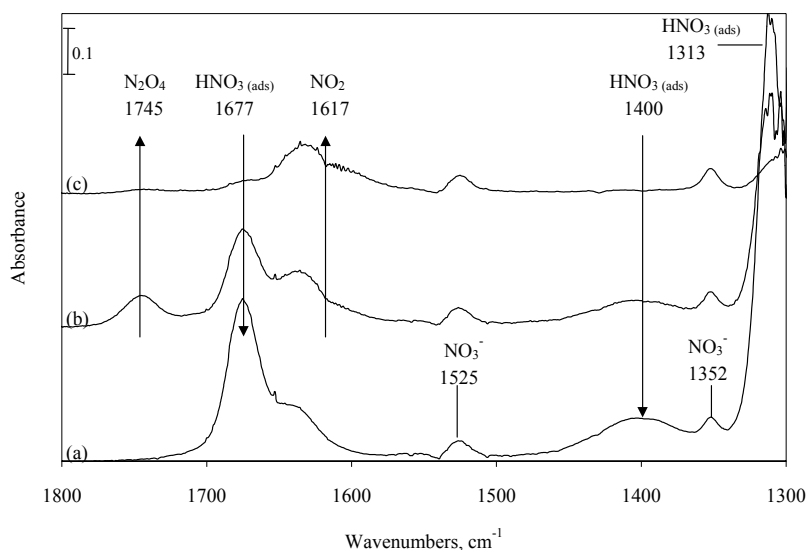


Figure 3.34. (a) Spectrum of the gas phase plus surface adsorbed HNO₃ on silica in the 1300 – 1800 cm⁻¹ region. Bands at 1677, 1400, and 1313 cm⁻¹ are due to molecular HNO₃ adsorbed on the surface, and the broad peak at the low wavenumber side of the 1677 cm⁻¹ peak is due to adsorbed water. The peaks at 1352 and 1525 cm⁻¹ are due to the ν₃ asymmetric stretching vibration of NO₃⁻; (b) Immediately after the introduction of 9.7 × 10¹⁶ NO molecule cm⁻³, and (c) 65 minutes later. Gas phase NO₂ (1617 cm⁻¹) and surface N₂O₄ (1745 cm⁻¹) are observed upon reaction.

If it were the case that NO_3^- reacts with gaseous NO, the reaction could also occur on nitrate-fertilized soils, where NO is generated by biological processes and is also present by contact with polluted air in the boundary layer. Such a reaction may also occur on atmospheric particles containing nitrate. The peaks assigned to NO_3^- observed in this study did not change during the reaction (Fig. 3.34), suggesting that nitrate does not react. To probe this further, studies were conducted using adsorbed NH_4NO_3 , which is a major form of NO_3^- in atmospheric particles (*Finlayson-Pitts and Pitts, 2000*) as well as in fertilizer (*Pacific Environmental Services, 1996*). Experiments were conducted on a silica pellet and on the porous glass plate, which were allowed to come to equilibrium with water vapor at ~50% RH and then evacuated. The formation of NH_4NO_3 on the silica surfaces by reaction of adsorbed HNO_3 with gaseous NH_3 was confirmed spectroscopically by the disappearance of the molecular HNO_3 bands, and the appearance of N-H stretches in the 2800 – 3300 cm^{-1} and 1420-1450 cm^{-1} regions, and the NO_3^- stretch at 1360 cm^{-1} , in agreement with the literature (*Shen et al., 1993; Cziczo and Abbatt, 2000*). Gaseous NO was added to the cell at concentrations of $(1 - 2) \times 10^{17}$ molecule cm^{-3} . The infrared absorption bands due to NH_4NO_3 on the silica surfaces were too intense to quantify small changes, if they occurred; however, NH_4NO_3 was also formed on the ZnSe windows of the cell during the dosing procedure and could be monitored quantitatively. No change in these bands nor a decrease in NO or increase in NO_2 was observed after 1 hour reaction time.

Water could potentially affect these reactions through hydration of and/or reaction with intermediates and products. For example, NO^+ and NO_2^+ have been recently proposed as key intermediates in the heterogeneous hydrolysis of NO_2 on silica surfaces (*Finlayson-Pitts et al., 2003*) and may be common to other NO_x heterogeneous reactions such as those studied here. It has been shown in studies of the reactions of NO^+ and NO_2^+ clustered with water molecules in the gas phase, that at least four water molecules are needed in order to convert these species to HONO (*Fehsenfeld et al., 1969; Choi et al., 1994; Hamman et al., 2000*) and HNO_3 (*Fehsenfeld and Howard, 1973; Fehsenfeld et al., 1975; Cao et al., 1993; Sunderlin and Squires, 1993; Cao et al., 1994*), respectively. On the other hand, water can also inhibit the reactions, for example by enhancing the dissociation of the reactive molecular form of HNO_3 to unreactive ions; in the presence of four or more water molecules in a gas phase cluster with HNO_3 , dissociation occurs (*Kay et al., 1981; Zhang et al., 1994; Gilligan and Castleman, 2001*).

To investigate whether the reaction might be affected by water, $\sim 4.9 \times 10^{17}$ molecule cm^{-3} water vapor was then added to the cell and the reaction monitored for another 20 hours. Neither the loss of NH_4NO_3 on the cell windows nor the formation of gas-phase products was observed, even for the long reaction times. These results indicate that NH_4NO_3 does not react with gaseous NO and, therefore, NO_3^- is not the form of HNO_3 that is reactive with NO. It also confirms that NH_4NO_3 will not undergo renoxification in the troposphere, unless it is first converted back to HNO_3 through thermal decomposition, reaction (-41).

Figure 3.35a shows the spectrum from the HNO_3 -NO reaction after 65 min (Fig. 3.34c), from which the HNO_3 band has been subtracted using the initial spectrum of adsorbed HNO_3 (prior to addition of NO); for comparison, a reference spectrum of gaseous NO_2 is shown. Subtraction of the NO_2 gives the spectrum shown in Figure 3.35b. (The small

structure remaining around 1600 cm^{-1} is likely due to changes in the gas phase water, which has strong infrared bands in this region, in the purge gas during the experiment). Figure 3.35c is the spectrum of water adsorbed on the silica. Comparison of Fig. 3.35b and 3.35c shows that the remaining band at $\sim 1640\text{ cm}^{-1}$ in Figure 3.35b is shifted from that for pure water at 1628 cm^{-1} by $\sim 12\text{ cm}^{-1}$. *Ab initio* calculations show that the band due to this bending mode of water in a 1:1 gaseous nitric acid-water complex should shift by $\sim 10\text{ cm}^{-1}$ compared to water (Tao *et al.*, 1996; Staikova and Donaldson, 2001; McCurdy *et al.*, 2002). We therefore assign the 1640 cm^{-1} band to the bending mode of water in a nitric acid-water complex.

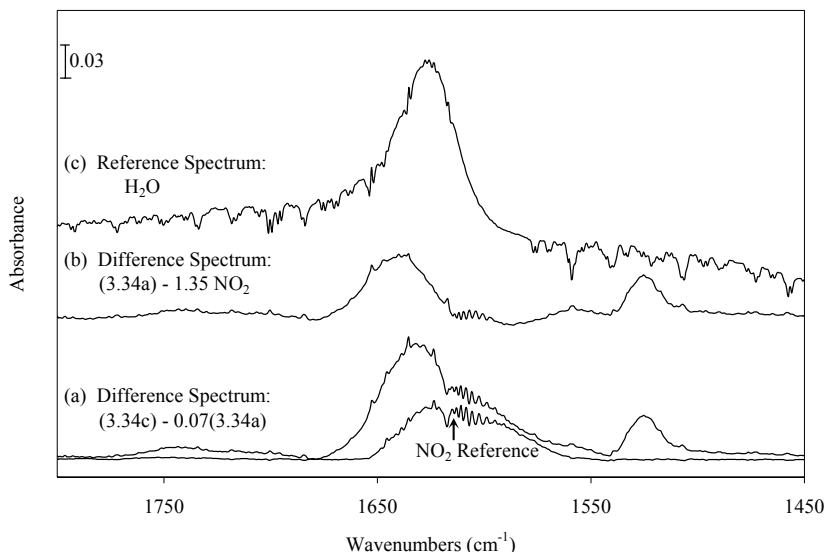


Figure 3.35. (a) Spectrum from 65 min. reaction time (Figure 3.34c) after subtraction of the initial spectrum of adsorbed HNO_3 ($0.07 \times$ initial spectrum, Fig. 3.34a); also shown is a reference spectrum of gas phase NO_2 (3.2×10^{16} molecule cm^{-3}). (b) Difference spectrum after subtraction of gaseous NO_2 ($1.35 \times$ reference spectrum in Fig. 3.35a) from spectrum in part (a); (c) Spectrum of water adsorbed on silica pellet.

These and previous experiments (Mochida and Finlayson-Pitts, 2000; Saliba *et al.*, 2000; 2001) indicate that reaction (4) followed by the secondary reaction (45) (or the self-reaction) of HONO gives the net reaction (31):



Thus, for each NO reacted, two molecules of HNO_3 should be consumed and three molecules of NO_2 generated. In the experiment shown here, the total amount of NO available for reaction in the cell initially is 7.7×10^{18} molecules; this is in significant excess over the HNO_3 on the surface which was measured by IC to be 2.4×10^{18} molecules. Thus, HNO_3 is

the limiting reagent under these conditions. The concentration of HNO₃ remaining on the surface after 65 min. is 7% of the initial value. This reaction of the surface HNO₃ should generate 3.3×10^{18} NO₂, giving a concentration of 4.2×10^{16} molecule cm⁻³ in the 79 cm³ cell. The concentration of gas phase NO₂ in Figure 3.34 was measured using an independent calibration for NO₂ in the cell to be 4.4×10^{16} molecule cm⁻³, in excellent agreement with the stoichiometry of the overall reaction (31).

The reaction probability (γ) for NO reacting with surface-adsorbed HNO₃ can in principle be calculated using the initial rate of loss of NO ($-d[\text{NO}]/dt$), the cell volume (V_{cell}) and the surface area (A) of the pressed silica pellet,

$$\gamma = \frac{\left(\frac{-d[\text{NO}]}{dt}\right) \times V_{\text{cell}}}{A[\text{NO}]_0 \sqrt{\frac{RT}{2\pi M}}} \quad (\text{XX})$$

where M is the molecular weight of NO. However, the NO is in significant excess over the available HNO₃ and so measuring the small changes in its concentration in the early stages of the reaction is not feasible. As an alternative, we use half of the initial rate of loss of surface-adsorbed HNO₃, based on the stoichiometry of the overall reaction (31), as a measure of $d[\text{NO}]/dt$. The reaction is sufficiently fast that, under the conditions of Figure 3.34, 43% of the initial HNO₃ reacts by the time the first spectrum is obtained (2 scans in 2.2 s) giving an average reaction time of 1.1 s. This change in the HNO₃ concentration leads to a calculated reaction probability of $\gamma^{\text{NO}} = 7 \times 10^{-9}$. The average reaction probability over seven experiments using silica pellets was $(6 \pm 2) \times 10^{-9}$ (2s). However, these are lower limits since the initial rate of HNO₃ loss was sufficiently fast that its loss could not be monitored continuously in the initial stages of the reaction. Thus, the lower limit to the reaction probability is $\gamma^{\text{NO}} \geq (6 \pm 2) \times 10^{-9}$. This is similar to the results of Saliba *et al.* (2001) for the reaction of NO with HNO₃ on a smooth borosilicate glass surface at 50% RH, where the reaction probability was estimated to be on the order of 10^{-8} .

The present studies show that the heterogeneous reaction of gaseous NO with HNO₃ occurs not only on porous and smooth glass, but also on pure silica. Thus, catalysis by trace constituents in the borosilicate materials is not important in this reaction. The key to the chemistry is the presence of undissociated nitric acid in a thin water “film”, and hence the chemical composition of the underlying surface is important primarily with respect to the amount of water it holds under atmospheric conditions. Figure 3.21 (section 3.II.E.) shows the amount of water on various terrestrial surfaces as a function of relative humidity (Lammel, 1999). Soil and stone typically have from one to a few layers of water over the range of relative humidities from 30 to 90%, with vegetation taking up less water, as expected from its hydrophobic surface. The water uptake by soil and stone is similar to that of borosilicate glass (Saliba *et al.*, 2001; Sumner *et al.*, 2004) where the HNO₃-NO reaction has been observed to occur at intermediate relative humidities (~40 – 60% RH) in a manner

similar to that observed here on hydrated silica surfaces. Thus, the chemistry occurring in thin water films on soil, sand and other silicate materials in the boundary layer is expected to be similar to that observed in these laboratory studies.

These studies also show that the undissociated form of HNO₃ must be the reactive species, and not the nitrate anion. This also indicates that the treatment of soils with nitrate fertilizer will not play a role in “renoxification”. In short, in addition to deposition and reaction with NH₃ and mineral components such as CaCO₃, HNO₃ may be in part removed by heterogeneous reaction with NO in thin water films on solid surfaces in the boundary layer.

VII.C. Heterogeneous Reactions of CO, CH₄ and SO₂ with Adsorbed HNO₃

The reaction of CO with adsorbed HNO₃ was studied using CO concentrations from $(3 - 26) \times 10^{16}$ molecule cm⁻³. Adsorbed HNO₃ and gaseous CO were monitored for 60 minutes. No statistically significant decrease was observed in surface HNO₃ or gaseous CO, and no bands due to the expected products, such as CO₂, HONO, or NO₂/N₂O₄ from HONO secondary reactions were observed. The addition of water vapor corresponding to 50% RH had no effect on the reaction.

Lary and Shallcross (2000) suggested that this reaction may be feasible in particles containing iron, which can act as a catalyst. While both Fe³⁺ and Fe²⁺ have been observed in airborne particles, Fe³⁺ is the most common oxidation state present under atmospheric conditions (Dedik *et al.*, 1992; Erel *et al.*, 1993; Zhu *et al.*, 1997; Siefert *et al.*, 1998). To probe for a catalytic effect of Fe³⁺ in the dark, one experiment was carried out using a pellet prepared from the mixture of silica and iron chloride (FeCl₃) (10:1 w:w). No reaction, *i.e.* disappearance of reactants or appearance of products, was identified over time. Therefore, Fe³⁺ does not catalyze the reaction of gaseous CO with HNO₃ on surfaces.

Sulfuric acid is a common component of particles in the atmosphere (Finlayson-Pitts and Pitts, 2000). To test for the effects of H₂SO₄ on the proposed reaction (42), an experiment was carried out under the same conditions using a silica pellet that had been previously submerged in concentrated H₂SO₄. Because of its low vapor pressure, H₂SO₄ does not desorb from the surface under our conditions and there was insufficient transmission of the infrared beam to observe species on the surface. Thus, the surface was moved out of the infrared beam and the gas phase was monitored. No gaseous products were observed, indicating that the presence of H₂SO₄ does not enhance the reaction of CO with HNO₃.

Although no significant decrease in CO was observed, we conducted a least-squares analysis of the CO concentration versus time to obtain the maximum possible loss of CO under these experimental conditions, and hence to calculate an upper limit of the value for the reaction probability. We define the maximum loss rate as the lower 95% confidence limit of the slope of [CO] *versus* time. The maximum loss obtained shows no statistical difference when compared to blank experiments without HNO₃ treatment, confirming the lack of reaction. This approach gives an upper limit for the reaction probability of $\gamma^{\text{CO}} \leq 10^{-10}$. This upper limit is six orders of magnitude smaller than the reaction probability used by Lary and

Shallcross in their modeling studies (*Lary and Shallcross, 2000*). This reaction therefore seems unlikely to be responsible for the discrepancy between the measured and modeled NO_x/HNO_3 ratios.

The reaction (43) of gaseous CH_4 with adsorbed HNO_3 was studied using the porous glass plate or pressed silica pellets, with methane concentrations in the range of $(1 - 19) \times 10^{16}$ molecule cm^{-3} . Peaks for adsorbed HNO_3 and gaseous CH_4 (3017 cm^{-1}) were monitored for 120 minutes. Again, no change in the reactants or appearance of products was observed. Using the same approach as described above for CO, an upper limit to the reaction probability for reaction (43) of $\gamma^{\text{CH}_4} \leq 10^{-12}$ was obtained.

Finally, the reaction of gaseous SO_2 with adsorbed HNO_3 was studied using the porous glass plate and pressed silica pellets, respectively. For one porous glass plate experiment, a water vapor concentration equivalent to 40% RH was added. SO_2 concentrations of $(5 - 18) \times 10^{16}$ molecule cm^{-3} were used and the reaction was monitored for 120 minutes. In one experiment, gas phase SO_2 was monitored for 180 minutes with the porous glass out of the IR beam since it has a 1550 cm^{-1} cutoff that prevents detection of the gas phase SO_2 bands at 1360 cm^{-1} and 1152 cm^{-1} simultaneously with the surface bands. Again, no decrease in the adsorbed HNO_3 or gaseous SO_2 was observed, and no bands due to any of the expected products, such as H_2SO_4 (1196 and 1053 cm^{-1}), appeared (*Yang and Finlayson-Pitts, 2001*), including in the experiment in which additional water vapor was added. From these observations, an upper limit of $\gamma^{\text{SO}_2} \leq 10^{-10}$ was calculated. The reaction of fuming nitric acid with SO_2 in solution to form nitrososulfuric acid has been reported, but requires the presence of nitrogen dioxide (*Coleman et al., 1939*). *Martin et al. (1981)* reported that nitric acid in solution does not react with dissolved SO_2 , and that the reaction was not catalyzed by a variety of metals, including Fe^{3+} . The results of the present experiments, where HNO_3 is present in a thin water film on a surface and NO_2 is absent, are therefore consistent with the solution results.

VII.D. Role of Surface Materials in Renoxification in the Boundary Layer

The tropospheric boundary layer contains appreciable areas of natural and artificial surfaces. While two well-characterized model silicate surfaces were used in these studies, there are many surfaces in the lowest region of the atmosphere that also contain significant amounts of silicates, *e.g.* soils and the surfaces of buildings, including windows (*BNZ Materials, 1999a, b; Portland Cement Association, 1999; USGS, 1999*). It is likely that the available area on these surfaces exceeds that on airborne particles in the boundary layer. As a result, these surfaces may play a significant role in the uptake and reaction of air pollutants in the region closest to the earth's surface where many air quality measurements are made, and human exposure to atmospheric constituents is maximized.

Such surfaces may promote heterogeneous reactions, such as (4) and (42) – (44), that are not kinetically favored in the gas phase but may occur on surfaces. If this were the case for HNO_3 adsorbed on surfaces, then the deposition of HNO_3 would become a part of the active nitrogen oxides cycle, rather than act as a permanent sink as previously believed. These studies show that the reactions of HNO_3 adsorbed on silica surfaces with gaseous CO,

CH₄, and SO₂ do not occur at measurable rates. As a result, these reactions are not expected to participate in “renoxification” in the boundary layer and seem highly unlikely to be responsible for the discrepancy between the measured and modeled NO_x/HNO₃ ratios as proposed by model studies (*Lary and Shallcross, 2000*).

However, the reaction of adsorbed HNO₃ with gaseous NO does occur, with a lower limit to the reaction probability of $\gamma^{\text{NO}} \geq (6 \pm 2) \times 10^{-9}$ (2s). While this lower limit is relatively slow, such chemistry may occur over hours to days in the boundary layer of polluted urban atmospheres. Consider a column of air 1 cm × 1 cm and 38.5 m high, the height of the lowest box in a well-known airshed model (*Knipping and Dabdub, 2002*). At an NO concentration of 100 ppb that is found in polluted urban atmospheres, the rate of generation of additional NO₂ via the overall reaction (31) can be calculated to be 9×10^4 molecule cm⁻³ s⁻¹. In 1 hour, an additional NO_x concentration of ~0.014 ppb would result from this renoxification. However, this assumes the surface is geometrically flat; this is certainly not the case for soil, where the available surface area can be much larger, *e.g.* ~1 – 15 m² g⁻¹ (*Hodson et al., 1998*). We have measured the mass per geometric area of a thin layer of sand to be 0.2 g cm⁻². With a surface area in the range of 1 – 15 m² g⁻¹, this thin layer of sand with geometric area 1 cm² would have a surface for uptake and reaction of gases in the range of $(0.2 - 3) \times 10^4$ cm², *i.e.* a factor of 2000 to 30,000 greater than the flat geometrical area. If the HNO₃-NO renoxification reaction occurred at the lower limit to the rate as measured in these laboratory studies, it would lead to the generation of additional NO_x of ~30 – 400 ppb, if transport of NO to the surface were not limiting. Diffusion and biological production of NO within the soil could also contribute to renoxification processes. On the other hand, the availability of HNO₃ on soils and other surfaces in the polluted boundary layer is not known, but is likely to be less than that used in the present studies, and transport of NO to the surface from the boundary layer may be limiting.

Knipping and Dabdub (*2002*) have shown that inclusion of renoxification reactions, specifically reaction (46), in the airshed model for the South Coast Air Basin in Southern California may help to resolve some long-standing discrepancies between observations and model-predictions for species such as ozone. In this initial assessment carried out prior to the present experimental studies, the reaction probability was taken to be unity and the reaction limited by either the deposition rate of gas phase HNO₃ or of turbulent diffusion/collision of nitric oxide with an idealized geometrically flat area at the earth’s surface. While the reaction probability is likely substantially less than unity, the area at the surface available for such chemistry is much larger than the assumed flat surface as discussed above. These model studies gave much better agreement for the peak O₃ concentrations measured at the Central Los Angeles monitoring station. While it is not confirmed that the HNO₃-NO reaction is indeed responsible for resolving the discrepancy between the model predictions and field observations, it is intriguing and suggestive that such renoxification processes reproduce the observations in a manner that other known chemistry cannot. Additional airshed model results are shown in the next section (3.VIII.).

Clearly, renoxification processes need to be considered further as potentially important in polluted urban atmospheres. In addition, the role of structures such as buildings,

roads etc., as well as natural materials such as soils and vegetation (*SURFACE*), in promoting heterogeneous reactions needs to be explored.

VIII. MODELING THE IMPACTS OF RENOXIFICATION ON TROPOSPHERIC OZONE

A description of the California Institute of Technology (CIT) Airshed model was included in the Final Report to the previous contract (97-311) and can be found elsewhere (*Meng et al., 1998*). The model includes the chemistry (LCC mechanism) and physics of 42 gas phase species and 19 aerosol species distributed into 8 bin sizes. It also includes a size-resolved and chemically resolved aerosol model within the three-dimensional detailed gas-phase model. The model was applied to the South Coast Air Basin of California to simulate the conditions during the 1987 South Coast Air Quality Study (SCAQS) on August 27 – 28, 1987. The *Base Case* model was run to simulate the SCAQS episode using a standard VOC-NO_x gas-phase chemical mechanism coupled with a detailed dynamic inorganic/organic aerosol model, but without the renoxification of adsorbed HNO₃. Renoxification was then added, reaction (4) of NO with HNO₃, in order to assess its effect on the ozone concentration over a 48 hour period and as a function of changes in the NO_x emissions.

These model runs are preliminary in that they contain a number of simplifying assumptions. These include a reaction probability for the reaction of NO with adsorbed HNO₃ of unity, which will overestimate the importance of this reaction; the actual reaction probability is not known, and only a *lower* limit of $\sim 10^{-8}$ is available from the experimental studies. Second, the geometric surface area is assumed for deposition; this will underestimate the importance of this reaction. For example, measurements of the molecular (BET) surface areas of materials found in the boundary layer such as sand and asphalt are about two to three orders of magnitude larger than the corresponding geometric surface area. The third assumption is that only the nitric acid formed during these model runs is available to participate in the renoxification reactions; this will underestimate the importance of this chemistry since there is likely to be a reservoir of nitric acid on surfaces that can also react.

Time series plots for modeled ozone are presented in Figure 3.36a – c for three regions of California's South Coast air basin during the SCAQS episode with and without renoxification. The observations during that period are also shown in the plots. It was previously reported for the Riverside and San Bernardino cases that including renoxification caused the model to predict a "double peak" for ozone, which was not present in the base case model. However, specification of the initial conditions aloft for the second day have been revised and now even the base case model predicts double ozone peaks, consistent with observations of multiple peaks at downwind locations (Fig. 3.36 b-c, second day). The results show that in all three regions (central Los Angeles, Riverside, and San Bernardino, CA), including renoxification in the model increases ozone production and improves the match between modeled and observed peak ozone.

Figure 3.37 shows plots of the modeled maximum ozone concentration as the NO_x emissions are changed for cases with and without renoxification. These plots are intended to show the effect of decreasing NO_x emissions on the maximum O₃ concentrations. The x-

axis, the NO_x “scaling factor”, represents the emissions of NO_x relative to those on August 28, 1987. Thus, a scaling factor of 1.0 represents the NO_x emitted on that day, while NO_x scaling factors <1.0 represent lower NO_x emissions; this is particularly useful in determining the impacts of NO_x controls. In Los Angeles (Fig. 3.37a), a decrease in NO_x initially causes an increase in O_3 followed by a rapid decline when NO_x reaches ≤ 0.5 its value on that day (without renoxification, in direction of the arrow). This behavior is typical of urban regions with low VOC/NO_x ratios, such as Los Angeles (*Finlayson-Pitts and Pitts, 2000*). The initial increase in O_3 when NO_x is decreased is due to the rapid reaction of NO with O_3 as well as the reaction of NO_2 with OH (in competition with VOC) to form HNO_3 . However, it is interesting that the relative increase in ozone predicted as the NO decreases is smaller than for the base case, *i.e.* with renoxification, the important control strategy controversy of predicted increasing ozone with decreasing NO_x is less pronounced. In Riverside (Fig. 3.37b), ozone is not very sensitive to NO_x as expected for downwind regions which typically have high VOC/NO_x ratios.

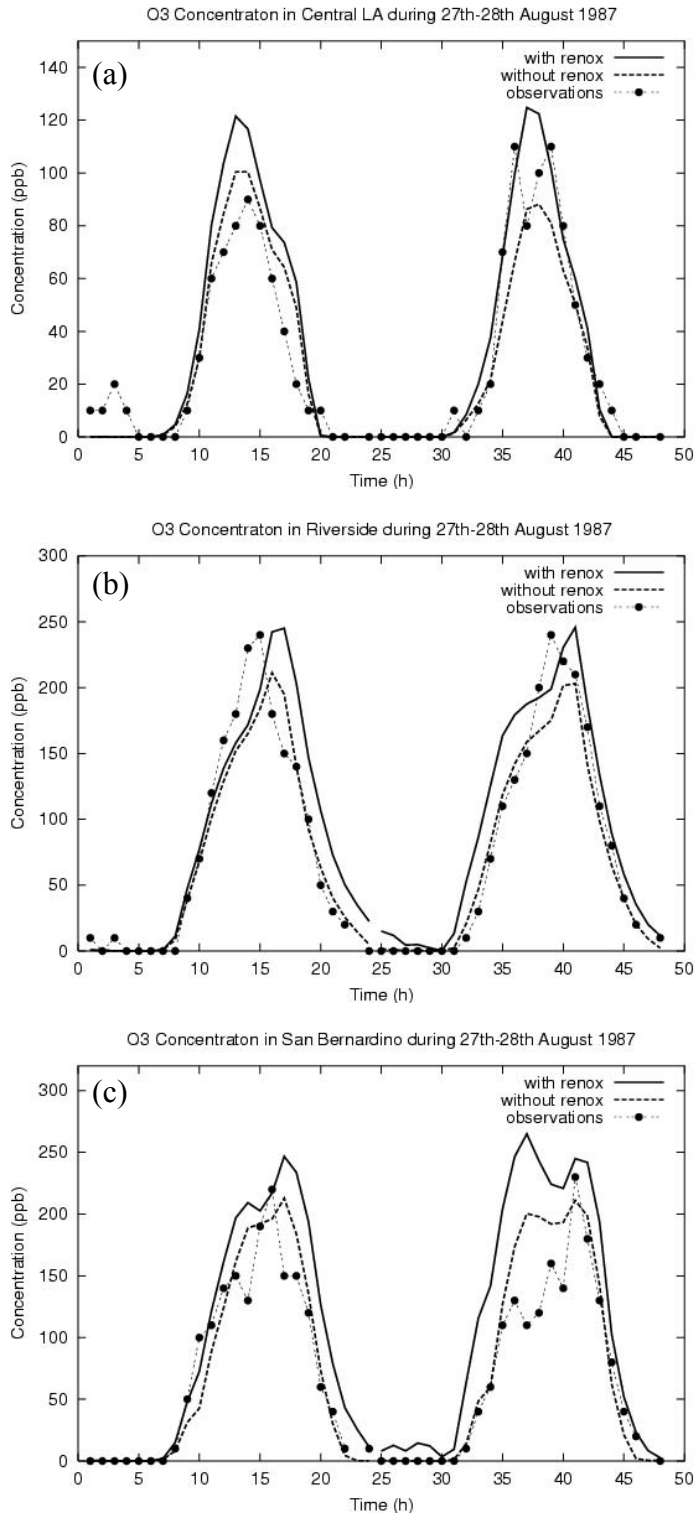


Figure 3.36. Modeled and observed ozone concentrations in the South Coast air basin for Aug. 27 – 28, 1987 with and without renoxification for (a) central Los Angeles, CA, (b) Riverside, CA, and (c) San Bernardino, CA.

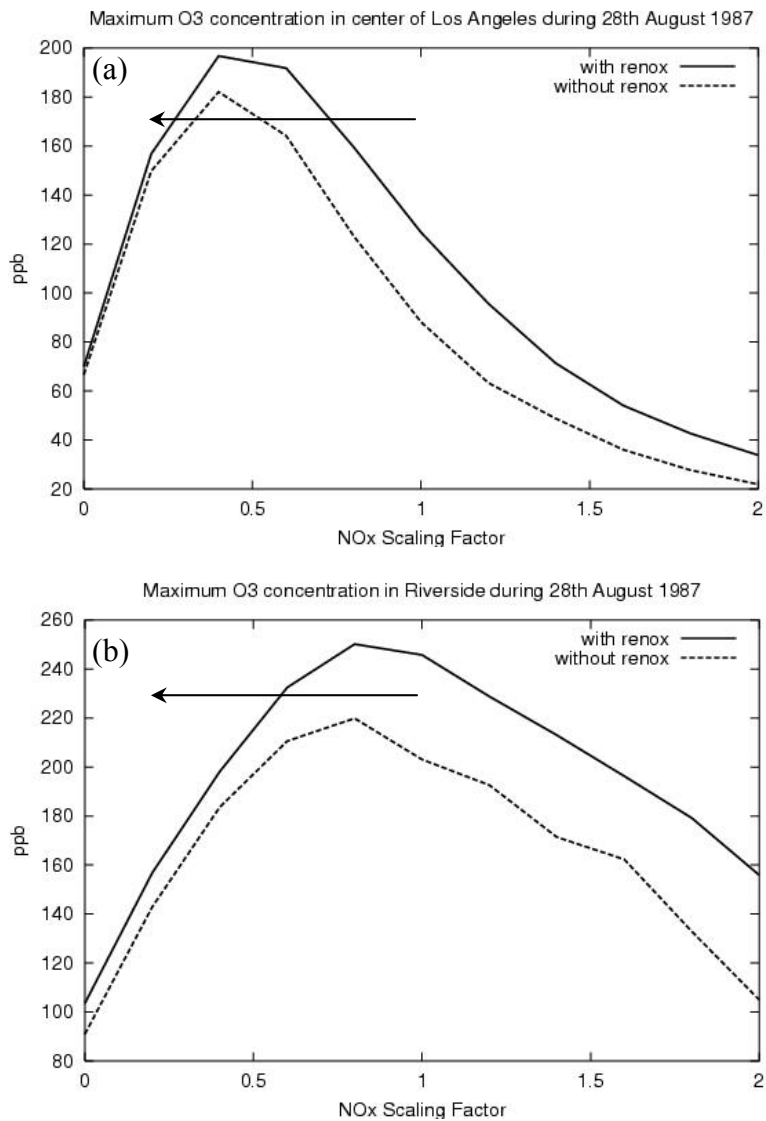


Figure 3.37. Modeled and observed maximum ozone concentrations as a function of NO_x “scaling factor” (see text) in the South Coast air basin for Aug. 28, 1987 with and without renoxification for (a) central Los Angeles, CA and (b) Riverside, CA.

4. DISCUSSION

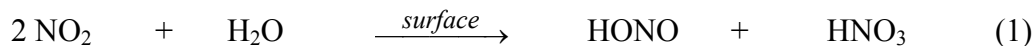
The major atmospheric sources and sinks of nitrous acid were addressed in this research project since it is considered a key determinant of tropospheric ozone and fine particle pollution. The results of the individual experiments are discussed in detail in the previous section. A discussion of the major points and their atmospheric implications are provided here.

The reactions considered throughout this research are heterogeneous, occurring on the walls of the reaction chambers used. The rates of these reactions change with the relative humidity, which is reasonable since the relative humidity determines the amount of water in equilibrium with the surface. An important result from this work is that the Teflon, halocarbon wax, and C8 SAM samples, which are hydrophobic as indicated by the large contact angles measured, all exhibited significant amounts of water uptake. The water uptake on these hydrophobic materials was similar to that on quartz and uncleaned borosilicate glass. AFM measurements showed that the high surface roughness of these surfaces plays a major role in water adsorption. This result is useful in understanding the results of previous laboratory studies of NO₂ hydrolysis that showed similar rates of HONO formation in chambers made of glass, quartz, Teflon-coated glass and metal, and thin Teflon films. For example, the study of NO₂ hydrolysis carried out in a halocarbon wax coated chamber had a rather surprisingly similar rate of HONO formation to that in borosilicate glass chambers (*Finlayson-Pitts et al., 2003; Sumner et al., 2004*). This result is reasonable, given that the two surfaces were observed to adsorb similar amounts of water.

The water uptake studies suggest that other hydrophobic materials, such as vegetation, may contain sufficient adsorbed water to allow the same heterogeneous chemistry to occur in the tropospheric boundary layer. Thus, AFM images were collected of the surfaces of an ivy leaf and a *Vinca minor* flower petal to demonstrate that the surface roughness of vegetation is similar to halocarbon wax and FEP Teflon film and will likely hold similar amounts of water (*Sumner et al., 2004*). Indeed, there are many reports of HONO production over various surface types in the troposphere, including vegetation (*Perner and Platt, 1979; Platt et al., 1980; Winer and Biermann, 1994; Harrison et al., 1996; Lammel and Cape, 1996; Lammel, 1999; Finlayson-Pitts and Pitts, 2000; Alicke et al., 2002; Stutz et al., 2002a*). In addition, silicates are common components of many surfaces found in the tropospheric boundary layer, including soil and soil derived dust (*Gillette, 1997; Finlayson-Pitts et al., 2003*) and, in urban areas, concrete, asphalt, and window glass (*Diamant, 1970*). Therefore, the measurements of water uptake on borosilicate glass and quartz are useful for understanding chemistry on these tropospheric surfaces as well.

Significant advances were made in understanding heterogeneous NO₂ hydrolysis and a mechanism is proposed that is consistent with our laboratory data and with many observations from previous studies. For example, the yields of HONO are often less than the 50% expected from reaction (1) (*TenBrink et al., 1978; Sakamaki et al., 1983; Pitts et*

al., 1984a; 1985; Svensson *et al.*, 1987; Jenkin *et al.*, 1988; Perrino *et al.*, 1988; Wiesen *et al.*, 1995; Kleffmann *et al.*, 1998a, b; Wainman *et al.*, 2001).



This was found to be due to the secondary chemistry of HONO on the walls of the chamber. The other major product, NO, becomes dominant after several hours; the relative amounts of NO and HONO produced vary widely in the literature, suggesting that the changing surface film plays an important role in reaction (1).

Several surface species that are intermediates in our proposed mechanism were observed during NO₂ hydrolysis on silica surfaces which held adsorbed water. Although the reaction is shown to be first order in NO₂, our studies show that N₂O₄ interacts more strongly with adsorbed water on silica surfaces than NO₂, especially in the presence of nitric acid. Our mechanism proposes that HONO is formed from N₂O₄ as the key reactant, but the overall kinetics are consistent with a process that is first order with respect to NO₂ due to secondary reactions of the NO₂ dimer on the surface. Surface-adsorbed HNO₃ was identified to exist largely as undissociated HNO₃. This is not surprising given the very thin films of water present on the surfaces which do not behave as bulk water (*Sumner et al.*, 2004). In addition, a nitric acid-water complex was identified. Nitric acid is known to form these hydrates in aqueous solutions (*Chédin*, 1952; *Högfeldt*, 1963; *Addison*, 1980) and on ice (*Tolbert and Middlebrook*, 1990; *Ritzhaupt and Devlin*, 1991; *Koch et al.*, 1996; *Tisdale et al.*, 1999); *ab initio* calculations support this stable complex formation (*Tao et al.*, 1996; *Staikova and Donaldson*, 2001; *McCurdy et al.*, 2002; *Escribano et al.*, 2003). The nitronium ion, NO₂⁺, was also identified, which is known to be formed via the self-reaction of HNO₃ in concentrated solutions (*Addison*, 1980). Therefore, thin surface films on silica surfaces, and likely in the troposphere as well, contain many species that strongly suggest they cannot be thought of as conventional aqueous solutions of acids.

A new chamber, which has the ability to simultaneously measure gas phase species and surface species using long path FTIR spectroscopy and attenuated total reflectance (ATR) – FTIR spectroscopy, was applied to the study of heterogeneous NO₂ hydrolysis in the presence of organics adsorbed on the walls of the chamber. Our preliminary studies show that the presence of organics does not change the gas phase products or their yields; the sum of the NO, HONO, and N₂O produced account for ~50% of the NO₂ loss, as expected from reaction (1) and in agreement with studies in clean chambers. Several surface species have been identified with the simultaneous use of the ATR probe, including N₂O₄, NO₃⁻, and an HNO₃-H₂O complex. While undissociated HNO₃ was observed in NO₂ hydrolysis experiments in a clean chamber at 50% RH, it was not observed in the chamber with organics present. Studies are underway to determine if reactions of organics with HNO₃ on the surface play a role in the formation of NO or N₂O.

The key steps in the proposed mechanism are (*Finlayson-Pitts et al., 2003*):

- The dimer of N_2O_4 is an important precursor surface species in the reaction.
- The reactive surface species is proposed to be *asymmetric* dinitrogen tetroxide, ONONO_2 , formed by isomerization of symmetric N_2O_4 .
- The asymmetric ONONO_2 autoionizes to generate NO^+NO_3^- . This is in competition with a back reaction with gas phase NO_2 to form symmetric N_2O_4 ; the overall rate equation is therefore consistent with a process that is first order in NO_2 .
- The NO^+NO_3^- complex reacts with water to generate HONO that escapes, at least in part, from the surface, as well as nitric acid that remains on the surface.
- The amount of HONO that escapes into the gas phase is determined by the relative humidity due to a competition between HONO and H_2O for available surface sites.
- The HNO_3 on the surface generates NO_2^+ , a well known reaction in concentrated solutions of HNO_3 .
- Nitric oxide is generated by the reaction of HONO with NO_2^+ . Nitrous acid also reacts with HNO_3 to generate NO^+ on the surface.

As a result of this comprehensive study of NO_2 hydrolysis, it is clear that much of the heterogeneous chemistry in laboratory systems as well as in the boundary layer as well, is determined by the nature of the surface film containing water, nitric acid, and other nitrogen oxide complexes and ions, such as NO_2^+ . This is consistent with direct measurements of increased HONO/ NO_2 ratios at ground level compared to higher altitudes (*Stutz et al., 2002a*).

Heterogeneous NO_2 hydrolysis was also examined in the presence of UV radiation due to the report of a photoenhancement of HONO formation from heterogeneous NO_2 hydrolysis by Akimoto *et al.* (1987) using a Teflon-coated smog chamber. Zhou *et al.* (2002; 2003) also reported a photochemical production of HONO from HNO_3 deposited on surfaces. Long path FTIR experiments were carried out in the absence and presence of UV radiation (320 – 400 nm). The experimental data were examined using a kinetics model to describe the reaction using a simplified mechanism similar to that proposed above. Excellent agreement was obtained between the measured HONO concentrations and model predictions in the early irradiation period of the reaction before secondary chemistry became apparent, without including a photoenhancement of the heterogeneous NO_2 hydrolysis. At longer times, however, the HONO decay was slower than the model predicted, indicating an additional photochemical source of HONO. This additional photochemical HONO source may be the photolysis of adsorbed HNO_3 , as proposed by Zhou *et al.* (2002; 2003), which is formed during heterogeneous NO_2 hydrolysis, rather than an enhancement of the NO_2 hydrolysis itself.

Considerable progress was made in understanding the interactions of gaseous nitrogen oxides with surfaces containing adsorbed nitric acid. The decomposition of gaseous HONO was measured in a borosilicate glass cell that had been conditioned with

nitric acid and in the “clean” cell which had not been conditioned, but contained small amounts of nitric acid due to its production in previous experiments. Substantial differences in the production of NO and NO₂ and their rates in the conditioned versus unconditioned cell were observed. A key result of this work is that the addition of HONO to an unconditioned cell followed by exposure to water vapor leads to displacement of the HONO from the surface. This suggests that water competes with HONO for surface sites and displaces some HONO that was previously adsorbed on the walls. An important implication of this is that HONO can remain adsorbed on surfaces in the troposphere and subsequently desorb into the gas phase when the relative humidity increases. These pre-exposed surfaces can therefore act as reservoirs of nitrous acid; indeed, field studies have shown that tropospheric surfaces can act as both sources and sinks of HONO (*Stutz et al., 2002a; 2003*).

Also considered was the reduction of adsorbed HNO₃ back to HONO by nitric oxide, carbon monoxide (CO), methane (CH₄), and sulfur dioxide (SO₂). Reaction of HNO₃ with CO, CH₄, and SO₂ was not observed, and upper limits to their reaction probabilities were reported. Previous studies in this laboratory showed that NO reacts with HNO₃ adsorbed on silica surfaces containing adsorbed water (*Mochida and Finlayson-Pitts, 2000; Saliba et al., 2000; 2001*). In the current study, the reactive form of the adsorbed nitric acid (nitrate or undissociated HNO₃) was examined. Ammonium nitrate (NH₄NO₃), which is a major form of nitrate in atmospheric particles and in fertilizer, was adsorbed onto silica pellets and exposed to gaseous NO. Transmission FTIR through the pellet and gaseous surroundings showed no detectable changes in NO or increases in NO₂ or HONO. These studies show that the undissociated form of HNO₃ must be the reactive species, and not the nitrate anion. Hence, the treatment of soils with nitrate fertilizer will not play a role in recycling HNO₃ back into reactive gaseous nitrogen oxides, or “renoxification”.

The potential impacts of renoxification of undissociated adsorbed HNO₃ on ozone formation were predicted using the CIT airshed model for the South Coast Air Basin in Southern California. Addition of the renoxification led to much better agreement for the peak ozone concentrations measured at the central Los Angeles, Riverside, and San Bernardino monitoring stations. Although it cannot be confirmed that this particular renoxification chemistry is responsible for the discrepancy, the significant improvement between observed and modeled ozone concentrations shows the substantial impacts that heterogeneous chemistry can have on ozone and other air pollutants.

5. SUMMARY AND CONCLUSIONS

It has been recognized for more than five decades that oxides of nitrogen play a central role in air pollution because they react in air to form ozone, particles and a host of other secondary air pollutants. The gas phase chemistry of oxides of nitrogen and volatile organic compounds is reasonably well known and represented in airshed models. Relatively little is known about potential heterogeneous reactions of oxides of nitrogen on surfaces found in the boundary layer. For example, it is known that reactions of oxides of nitrogen on surfaces are the major source of nitrous acid (HONO) in air. Nitrous acid is the major source at dawn of the highly reactive hydroxyl free radical that initiates photochemical smog formation; in fact, nitrous acid is a major source of hydroxyl radicals even when all sources are considered over an entire day. Unfortunately, because such heterogeneous reactions have not been understood, they are not included in airshed models, despite the critical role they play in the formation of photochemical air pollution. The overall goal of this research was to provide some of the fundamental kinetic and mechanistic data for heterogeneous oxides of nitrogen that are needed to assess their importance in urban areas in California.

These studies consisted of experimental studies of the reactions of oxides of nitrogen on surfaces that are characteristic of those used in laboratory systems (*e.g.*, smog chambers) as well as those found in urban areas. The loss of reactants and the formation of intermediates and products were followed in laboratory studies using spectroscopic methods. These included long-path Fourier transform infrared spectrometry (FTIR) for gases and attenuated total reflectance (ATR)-FTIR for species adsorbed on the surface. In addition, transmission FTIR was used to study species on silica surfaces. Because it is the water on the surface that determines the chemistry, the uptake of water on a variety of different surfaces was studied as a function of relative humidity. A major advance was the development and application of a chamber in which both the gas phase and the surface could be followed simultaneously by the incorporation of both long path FTIR and ATR-FTIR into one apparatus. In addition, studies using several different methods that can provide information on the physical morphology of surfaces and on their chemical composition were carried out in collaborative work with colleagues in the Department of Chemistry at UCI at no cost to this contract. These methods include atomic force microscopy (AFM) carried out by Professor Penner and his group, and X-ray photoelectron spectroscopy (XPS) carried out by Professor Hemminger and his group.

The combination of these methods were applied to studying (1) the heterogeneous hydrolysis of nitrogen dioxide (NO_2) to form HONO; (2) the formation of nitric acid on the surface during the heterogeneous NO_2 hydrolysis; (3) the reaction of nitric acid on the surface with nitric oxide to regenerate NO_2 , a "renoxification" process with important control strategy implications; (4) the nature of the thin water film on the surface that provides the milieu for this chemistry; (5) the potential for the formation of HONO through photochemical reactions on surfaces; and (6) the nature of the interaction of

HONO with surfaces. Some preliminary airshed modeling studies were also carried out to investigate the importance of the renoxification reaction.

This work establishes that there are a number of important intermediates on the surface that are involved in the formation of nitrous acid from the hydrolysis of NO_2 on surfaces. These studies suggest that the NO_2 dimer (N_2O_4) is likely the key intermediate in this chemistry. In addition, undissociated molecular nitric acid and its complexes with water, the nitrosonium and nitronium ions, adsorbed nitrous acid and nitrate ions are believed to be important. The simultaneous presence of organic compounds on the surface does not significantly change the chemistry.

The relative amounts of the various surface species depend critically on the amount of water on the surface, and this is determined by the gas phase water vapor concentration, *i.e.*, the relative humidity (RH). For example, at intermediate RH ($\sim 50\%$), the nitric acid on the surface reacts with nitric oxide to regenerate NO_2 . This renoxification process converts nitric acid back to photochemically active forms, so that deposition of nitric acid is no longer a permanent sink as assumed in current models. This will lead to increased levels of ozone, particles and associated secondary air pollutants. Preliminary airshed modeling that includes this renoxification suggests that it will lead to significantly higher ozone levels throughout the Southern California air basin, and may change the shape of the VOC- NO_x isopleths compared to those without this heterogeneous chemistry.

A key finding of this research is that the amount of water available on surfaces to participate in this heterogeneous chemistry does not vary dramatically from surface to surface, even when comparing surfaces that are expected to be hydrophilic (*e.g.* borosilicate glass) to those that are hydrophobic (*e.g.* Teflon, the surfaces of vegetation). Despite the fact that the measured contact angles are consistent with the classification of surfaces as hydrophobic or hydrophilic, the infrared spectroscopic measurements show that this is not a good indicator of whether or not there is water on the surface available for heterogeneous chemistry. For example, hydrophobic halocarbon wax took up as much or more water than borosilicate glass. The key seems to be surface roughness, and given that this is characteristic of many surfaces in the boundary layer such as vegetation, it is expected that this heterogeneous chemistry will be pervasive.

This research also established that the heterogeneous hydrolysis of NO_2 on surfaces to form HONO is not itself enhanced by light, as had been suggested by earlier studies. However, it appears likely that light does interact with the intermediates of this reaction on surfaces, likely nitric acid or its associated species, to generate HONO during the day as suggested by recent studies by Zhou *et al.* Finally, this research has shown that nitrous acid is not only formed by reactions on surfaces, but it also reacts further on surfaces to generate gas phase nitric oxide, nitrogen dioxide and likely surface species such as nitric acid as well. An important finding is that there appears to be a competition between nitrous acid and water for adsorption sites on the surface; this means that nitrous acid can remain adsorbed on surfaces and subsequently be released into the gas phase when the RH increases. Thus, surfaces in the urban boundary layer likely act as

reservoirs of nitrous acid so that it is not only real-time heterogeneous chemistry that determines the amount of gas phase HONO, but also the previous history of the surface itself and in particular, its capacity to store HONO.

In conclusion, reactions of oxides of nitrogen on surfaces play a critical role in the formation of photochemical air pollution, including ozone, particles and a host of secondary air pollutants. While these reactions are not included in current airshed models, preliminary modeling results suggest they could be quite significant. Of particular interest from these studies are the renoxification of nitric acid adsorbed on surfaces back to photochemically active forms, the photolysis of adsorbed nitric acid and/or associated species to form gas phase HONO and the ability of surfaces to act as reservoirs of HONO.

6. RECOMMENDATIONS

Recommendations for future work include more detailed studies of the ability of various surfaces to act as HONO reservoirs. Without a detailed understanding of the interplay between adsorbed nitrous acid, water and the gas phase concentrations of HONO, it will be difficult to interpret field measurements and to incorporate the chemistry accurately into airshed models. Further work is also needed on the chemistry of HONO on surfaces, particularly the mechanism by which NO is generated from adsorbed HONO. Third, the mechanism and kinetics of the light-induced HONO formation by photolysis of surface-adsorbed oxides of nitrogen such as nitric acid needs much further work to understand exactly what the surface species is that is generating HONO. Finally, introduction of all of this heterogeneous chemistry of oxides of nitrogen into airshed models is needed in order to probe fully the impacts on the formation of ozone, acids and associated secondary air pollutants.

REFERENCES

- Acker, K., D. Moller, W. Wieprecht, R. Auel, D. Kalass and W. Tschewenka, *Water Air Soil Pollut.*, 2001, **130**, 331.
- Adamson, A. W., *The Physical Chemistry of Surfaces*, John Wiley & Sons, 1967.
- Adamson, A. W., *J. Coll. Interf. Sci.*, 1968, **27**, 180.
- Adamson, A. W., *Physical Chemistry of Surfaces*, John Wiley & Sons, 1990.
- Adamson, A. W. and A. P. Gast, *Physical Chemistry of Surfaces*, John Wiley & Sons, 1997.
- Addison, C. C., *Chem. Rev.*, 1980, **80**, 21.
- Agnew, S. F., B. I. Swanson, L. H. Jones and D. Schiferl, *J. Phys. Chem.*, 1983, **87**, 5065.
- Agreiter, J., M. Frankowski and V. E. Bondybey, *Low Temperature Physics*, 2001, **27**, 890.
- Akhtar, M. J., J. A. Balschi and F. T. Bonner, *Inorg. Chem.*, 1982, **21**, 2216.
- Akhtar, M. J., F. T. Bonner and M. N. Hughes, *Inorg. Chem.*, 1985, **24**, 1934.
- Akimoto, H. and H. Takagi, *Environ. Sci. Technol.*, 1986, **20**, 393.
- Akimoto, H., H. Takagi and F. Sakamaki, *Int. J. Chem. Kinet.*, 1987, **19**, 539.
- Al-Abadleh, H. A. and V. H. Grassian, *J. Phys. Chem. A*, 2000, **104**, 11926.
- Alcala-Jornod, C., H. VandenBergh and M. J. Rossi, *Phys. Chem. Chem. Phys.*, 2000, **2**, 5584.
- Alicke, B., U. Platt and J. Stutz, *J. Geophys. Res. Atmos.*, 2002, **107**, DOI: 10.1029/2000JD000075.
- Ammann, M., M. Kalberer, D. T. Jost, L. Tobler, E. Rossler, D. Piguet, H. W. Gaggeler and U. Baltensperger, *Nature*, 1998, **395**, 157.
- Andrés-Hernández, M. D., J. Notholt, J. Hjorth and O. Schrems, *Atmos. Environ.*, 1996, **30**, 175.
- Arens, F., L. Gutzwiller, U. Baltensperger, H. Gaggeler and M. Ammann, *Environ. Sci. Technol.*, 2001, **35**, 2191.
- Aschmann, S. M., A. A. Chew, J. Arey and R. Atkinson, *J. Phys. Chem. A*, 1997, **101**, 8042.
- Atkinson, R., D. L. Baulch, R. A. Cox, J. N. Crowley, R. F. Hampson, J. A. Kerr, M. J. Rossi and J. Troe, *Summary of Evaluated Kinetic and Photochemical Data for Atmospheric Chemistry, IUPAC Subcommittee on Gas Kinetic Data Evaluation for Atmospheric Chemistry*, Web version, <http://www.iupac-kinetic.ch.cam.ac.uk/>, 2001.
- Awakuni, Y. and J. H. Calderwood, *J. Phys. D*, 1972, **5**, 1038.
- Bambauer, A., B. Brantner, M. Paige and T. Novakov, *Atmos. Environ.*, 1994, **28**, 3225.
- Barlow, S., personal communication, 2003.
- Barney, W. S. and B. J. Finlayson-Pitts, *J. Phys. Chem. A*, 2000, **104**, 171.
- Barney, W. S., L. M. Wingen, M. J. Lakin, T. Brauers, J. Stutz and B. J. Finlayson-Pitts, *J. Phys. Chem. A*, 2000, **104**, 1692.
- Bazylinski, D. A. and T. C. Hollocher, *Inorg. Chem.*, 1985, **24**, 4285.
- Behnke, W., C. George, V. Scheer and C. Zetzsch, *J. Geophys. Res.*, 1997, **102**, 3795.
- Bernardi, F., F. Cacace, G. dePetris, F. Pepi and I. Rossi, *J. Phys. Chem. A*, 1998, **102**, 1987.

- Besemer, A. C. and H. Nieboer, *Atmos. Environ.*, 1985, **19**, 507.
- BNZ Materials, I., *Silica Brick and Mortar*, BNZ Materials, Inc., Littleton, CO, 1999a.
- BNZ Materials, I., *Insulating Fire Brick - Material Safety Data Sheet*, BNZ Materials, Inc., Littleton, CO, 1999b.
- Bogdan, A. and M. Kulmala, *J. Colloid Interfac. Sci.*, 1997, **191**, 95.
- Bolduan, F. and H. J. Jodl, *Chem. Phys. Lett.*, 1982, **85**, 283.
- Bolduan, F., H. J. Jodl and A. Loewenschuss, *J. Chem. Phys.*, 1984, **80**, 1739.
- Boniface, J., Q. Shi, Y. Q. Li, J. L. Cheung, O. V. Rattigan, P. Davidovits, D. R. Worsnop, J. T. Jayne and C. E. Kolb, *J. Phys. Chem A*, 2000, **104**, 7502.
- Borensen, C., U. Kirchner, V. Scheer, R. Vogt and R. Zellner, *J. Phys. Chem. A*, 2000, **104**, 5036.
- Bozzelli, J. W., *J. Chem. Ed.*, 2000, **77**, 165.
- Brauer, M., P. B. Ryan, H. H. Suh, P. Koutrakis, J. D. Spengler, N. P. Leslie and I. H. Billick, *Environ. Sci. Technol.*, 1990, **24**, 1521.
- Brauer, M., L. Lee, J. D. Spengler, R. O. Salonen, A. Pennanen, O. A. Braathen, E. Mihalikova, P. Miskovic, A. Nozaki, T. Tsuzuki, S. Rui-Jin, Y. Xu, A. Qing-Xiang, H. Drahonovska and S. Kjaergaard, *Air & Waste Manage. Assoc.*, 1997, **47**, 1095.
- Braun, W., J. T. Herron and D. K. Kahaner, *Int. J. Chem. Kinet.*, 1988, **20**, 51.
- Brunauer, S., P. H. Emmett and E. Teller, *J. Am. Chem. Soc.*, 1938, **60**, 309.
- Buchholz, J. R. and R. E. Powell, *J. Am. Chem. Soc.*, 1963, **85**, 509.
- Butler, J. W., J. M. Andino and S. M. Japar, *Environ. Sci. Technol.*, 1992, **26**, 1670.
- CABOT, *CAB-O-SIL(R) HS-5 Untreated Fumed Silica*, CABOT Corporation: Tuscola, IL, 1999.
- Calvert, J. G., G. Yarwood and A. M. Dunker, *Res. Chem. Intermed.*, 1994, **20**, 463.
- Cantrell, W. and G. E. Ewing, *J. Phys. Chem. B*, 2001, **105**, 5434.
- Cao, Y., J.-H. Choi, B.-M. Haas, M. S. Johnson and M. Okamura, *J. Chem. Phys.*, 1993, **99**, 9307.
- Cao, Y., J.-H. Choi, B.-M. Haas and M. Okamura, *J. Phys. Chem.*, 1994, **98**, 12176.
- Cape, J. N., K. J. Hargreaves, R. Storeton-West, D. Fowler, R. N. Colville, T. W. Choularton and M. W. Gallagher, *Atmos. Environ.*, 1992, **26A**, 2301.
- Carter, W. P. L., R. Atkinson, A. M. Winer and J. N. J. Pitts, *Int. J. Chem. Kinet.*, 1981, **13**, 735.
- Carter, W. P. L., R. Atkinson, A. M. Winer and J. N. J. Pitts, *Int. J. Chem. Kinet.*, 1982, **14**, 1071.
- Cathala, J. and G. Weinrich, *Compt. Rend.*, 1952, **244**, 1502.
- Chan, W. H., R. J. Nordstrom, J. G. Calvert and J. H. Shaw, *Chem. Phys. Lett.*, 1976a, **37**, 441.
- Chan, W. H., R. J. Nordstrom, J. G. Calvert and J. H. Shaw, *Env. Sci. Technol.*, 1976b, **10**, 674.
- Chatfield, R. B., *Geophys. Res. Lett.*, 1994, **21**, 2705.
- Chédin, J., *J. Chim. Physique*, 1952, **49**, 109.
- Cheung, J. L., Y. Q. Li, J. Boniface, Q. Shi, P. Davidovits, D. R. Worsnop, J. T. Jayne and C. E. Kolb, *J. Phys. Chem. A*, 2000, **104**, 2655.
- Choi, J.-H., K. T. Kuwata, B.-M. Haas, Y. Cao, M. S. Johnson and M. Okamura, *J. Chem. Phys.*, 1994, **100**, 7153.

- Chou, A., Z. Li and F.-M. Tao, *J. Phys. Chem. A*, 1999, **103**, 7848.
- Clarke, A. D., W. G. Collins, P. J. Rasch, V. N. Kapustin, K. Moore, S. Howell and H. E. Fuelberg, *J. Geophys. Res.*, 2001, **106**, 32555.
- Clegg, S. M. and J. P. D. Abbatt, *J. Phys. Chem. A*, 2001, **105**, 6630.
- Cox, R. A. and R. G. Derwent, *J. Photochem.*, 1976/77, **6**, 23.
- Crowley, J. N., J. P. Burrows, G. K. Moortgat, G. Poulet and G. LeBras, *Int. J. Chem. Kinet.*, 1993, **25**, 795.
- Cziczko, D. J. and J. P. D. Abbatt, *J. Phys. Chem.*, 2000, **104**, 2038.
- Dai, D., S. J. Peters and G. E. Ewing, *J. Phys. Chem.*, 1995, **99**, 10299.
- Davidson, J. A., F. C. Fehsenfeld and C. J. Howard, *Int. J. Chem. Kinet.*, 1977, **9**, 17.
- Dedik, A. N., P. Hoffmann and J. Ensling, *Atmos. Environ.*, 1992, **26A**, 2545.
- DeHaan, D. O., T. Brauers, K. Oums, J. Stutz, T. Nordmeyer and B. J. Finlayson-Pitts, *Int. Rev. Phys. Chem.*, 1999, **18**, 343.
- Dentener, F. J., G. R. Carmichael, Y. Zhang, J. Lelieveld and P. J. Crutzen, *J. Geophys. Res.*, 1996, **101**, 22.
- DePetris, G., A. D. Marzio and F. Grandinetti, *J. Phys. Chem.*, 1991, **95**, 9782.
- deReus, M., F. Dentener, A. Thomas, S. Borrmann, J. Ström and J. Lelieveld, *J. Geophys. Res.*, 2000, **105**, 15263.
- Derjaguin, B. V. and Z. M. Zorin, *2nd Proc. Intern. Congr. Surface Activity (London)*, 1957, **2**, 145.
- Diamant, R. M. E., *The Chemistry of Building Materials*, Business Books Limited, 1970.
- Diamond, M. L., S. E. Gingrich, K. Fertuck, B. E. McCarry, G. A. Stern, B. Billeck, B. Grift, D. Brooker and T. D. Yager, *Environ. Sci. Technol.*, 2000, **34**, 2900.
- Dibb, J. E., M. Arsenault, M. C. Peterson and R. E. Honrath, *Atmos. Environ.*, 2002, **36**, 2501.
- Donaldson, D. J., J. A. Guest and M. C. Goh, *J. Phys. Chem.*, 1995, **99**, 9313.
- Downing, H. D. and D. Williams, *J. Geophys. Res.*, 1975, **80**, 1656.
- Du, Q., E. Freysz and Y. R. Shen, *Phys. Rev. Lett.*, 1994a, **72**, 238.
- Du, Q., E. Freysz and Y. R. Shen, *Science*, 1994b, **264**, 826.
- Dubowski, Y., A. L. Sumner, E. Menke, D. J. Gaspar, J. T. Newberg, R. C. Hoffman, R. M. Penner, J. C. Hemminger and B. J. Finlayson-Pitts, *Phys. Chem. Chem. Phys.*, 2004, **submitted**.
- England, C. and W. H. Corcoran, *Ind. Eng. Chem. Fundam.*, 1974, **13**, 373.
- England, C. and W. H. Corcoran, *Ind. Eng. Chem. Fundam.*, 1975, **14**, 55.
- EPA, *Office of Air Quality Planning & Standards, Emission Measurement Center, AEDC Calculated Spectra*, Technology Transfer Network Emission Measurement Center., <http://www.epa.gov/ttn/emc/ftir/aedcdat1.html>, 2002.
- Erel, Y., S. O. Pehkonen and M. R. Hoffmann, *J. Geophys. Res.*, 1993, **98**, 18423.
- Escribano, R., M. Couceiro, P. C. Gómez, E. Carrasco, M. A. Moreno and V. J. Herrero, *J. Phys. Chem. A*, 2003, **107**, 651.
- Fairbrother, D. H., D. J. D. Sullivan and H. S. Johnston, *J. Phys. Chem. A*, 1997, **101**, 7350.
- Febo, A. and C. Perrino, *Atmos. Environ.*, 1991, **25A**, 1055.
- Fehsenfeld, F. C., E. E. Ferguson and M. Mosesman, *Chem. Phys. Lett.*, 1969, **4**, 73.
- Fehsenfeld, F. C. and C. J. Howard, *J. Chem. Phys.*, 1973, **59**, 6272.
- Fehsenfeld, F. C., C. J. Howard and A. L. Schmeltekopf, *J. Chem. Phys.*, 1975, **63**, 2835.

- Finlayson-Pitts, B. J., J. N. Pitts and A. C. Lloyd, *Environ. Sci. Technol.*, 1992, **26**, 1668.
- Finlayson-Pitts, B. J. and J. N. Pitts, *Chemistry of the Upper and Lower Atmosphere: Theory, Experiments and Applications*, Academic Press, 2000.
- Finlayson-Pitts, B. J., L. M. Wingen, A. L. Sumner, D. Syomin and K. A. Ramazan, *Phys. Chem. Chem. Phys.*, 2003, **5**, 223.
- Forney, D., W. E. Thompson and M. E. Jacox, *J. Chem. Phys.*, 1993, **99**, 7393.
- Foster, M. C. and G. E. Ewing, *Surf. Sci.*, 1999, **428**, 102.
- Foster, M. C. and G. E. Ewing, *J. Chem. Phys.*, 2000, **112**, 6817.
- Fried, A., B. E. Henry and J. G. Calvert, *J. Geophys. Res.*, 1994, **99**, 3517.
- Gao, R. S., D. W. Fahey, L. A. Del Negro, S. G. Donnelly, E. R. Keim, J. A. Neuman, E. Teverovskaia, P. O. Wennberg, T. F. Hanisco, E. J. Lanzendorf, M. H. Proffitt, J. J. Margitan, J. C. Wilson, J. W. Elkins, R. M. Stimpfle, R. C. Cohen, C. T. McElroy, T. P. Bui, R. J. Salawitch, S. S. Brown, A. R. Ravishankara, R. W. Portmann, M. K. W. Ko, D. K. Weisenstein and P. A. Newman, *Geophys. Res. Lett.*, 1999, **26**, 1153
- Gelb, L. D. and K. E. Gubbins, *Langmuir*, 1998, **14**, 2097.
- George, C., J. L. Ponche, P. Mirabel, W. Behnke, V. Scheer and C. Zetzsch, *J. Phys. Chem.*, 1994, **98**, 8780.
- Gerecke, A., A. Thielmann, L. Gutzwiller and M. J. Rossi, *Geophys. Res. Lett.*, 1998, **25**, 2453.
- Gillette, D., *J. Expos. Anal. Environ. Epidemiol.*, 1997, **7**, 303.
- Gilligan, J. J. and A. W. J. Castleman, *J. Phys. Chem. A*, 2001, **105**, 5601.
- Gingrich, S. E., M. L. Diamond, G. A. Stern and B. E. McCarry, *Environ. Sci. Technol.*, 2001, **35**, 4031.
- Givan, A. and A. Loewenschuss, *J. Chem. Phys.*, 1989a, **91**, 5126.
- Givan, A. and A. Loewenschuss, *J. Chem. Phys.*, 1989b, **90**, 6135.
- Givan, A. and A. Loewenschuss, *J. Chem. Phys.*, 1990a, **93**, 866.
- Givan, A. and A. Loewenschuss, *Struct. Chem.*, 1990b, **1**, 579.
- Givan, A. and A. Loewenschuss, *J. Chem. Phys.*, 1991a, **94**, 7592.
- Givan, A. and A. Loewenschuss, *J. Chem. Phys.*, 1991b, **94**, 7562.
- Glasson, W. A. and A. M. Dunker, *Environ. Sci. Technol.*, 1989, **23**, 970.
- Gomer, T., T. Brauers, F. Heintz, J. Stutz and U. Platt, *University of Heidelberg*, 1995,
- Goodman, A. L., T. M. Miller and V. H. Grassian, *J. Vacuum Sci. & Technol.*, 1998, **16**, 2585.
- Goodman, A. L., G. M. Underwood and V. H. Grassian, *J. Phys. Chem. A.*, 1999, **103**, 7217.
- Goodman, A. L., E. T. Bernard and V. H. Grassian, *J. Phys. Chem. A*, 2001, **105**, 6443.
- Goyer, G. G., *J. Colloid Sci.*, 1963, **18**, 616.
- Graham, R. F. and B. J. Tyler, *J. Chem. Soc., Faraday Trans. I*, 1972, **68**, 683.
- Grassian, V. H., *Intern. Rev. Phys. Chem.*, 2001, **20**, 467.
- Grassian, V. H., *J. Phys. Chem. A*, 2002, **106**, 860.
- Gregg, S. J. and K. S. W. Sing, *Adsorption, Surface Area and Porosity*, Academic Press, 1982.
- Griffiths, P. R. and J. A. de Haseth, *Fourier Transform Infrared Spectrometry*, Wiley, 1986.

- Gutzwiller, L., F. Arens, U. Baltensperger, H. W. Gäggeler and M. Ammann, *Environ. Sci. Technol.*, 2002, **36**, 677.
- Hamman, E., E. P. F. Lee and J. M. Dyke, *J. Phys. Chem. A*, 2000, **104**, 4571.
- Harrar, J. E., L. P. Rigdon and S. F. Rice, *J. Raman Spectrosc.*, 1997, **28**, 891.
- Harrick, N. J., *Internal Reflection Spectroscopy*, Interscience Publishers, 1967.
- Harrison, R. M. and A.-M. N. Kitto, *Atmos. Environ.*, 1994, **28**, 1089.
- Harrison, R. M., J. D. Peak and G. M. Collins, *J. Geophys. Res.*, 1996, **101**, 14429.
- Harrison, R. M. and G. M. Collins, *J. Atmos. Chem.*, 1998, **30**, 397.
- Hemminger, C. S., T. A. Land, A. Christie and J. C. Hemminger, *Surf. Interf. Anal.*, 1990, **15**, 323.
- Herzberg, G., *Molecular Spectra and Molecular Structure. II. Infrared and Raman Spectra of Polyatomic Molecules*, D. Van Nostrand Company, Inc., 1945.
- Herzog-Cance, M. H., J. Potier, A. Potier, P. Dhamelincourt, B. Sombret and F. Wallart, *J. Raman Spectrosc.*, 1978, **7**, 303.
- Herzog-Cance, M.-H., A. Potier and J. Potier, *Can. J. Chem.*, 1985, **63**, 1492.
- Hisatsune, I. C., J. P. Devlin and Y. Wada, *J. Chem. Phys.*, 1960, **33**, 714.
- Hodson, M. E., S. J. Langan, F. M. Kennedy and D. C. Bain, *Geoderma*, 1998, **85**, 1.
- Hoffman, R. C., M. Kaleuati and B. J. Finlayson-Pitts, *J. Phys. Chem. A*, 2003, **107**, 7818.
- Hoffman, R. C., A. L. Laskin and B. J. Finlayson-Pitts, *J. Aerosol Sci.*, 2004, **in press**.
- Högfeldt, E., *Acta Chem. Scandinavica*, 1963, **17**, 785.
- Holmes, J. R., R. J. O'Brien, J. H. Crabtree, T. A. Hecht and J. H. Seinfeld, *Environ. Sci. Technol.*, 1973, **7**, 519.
- Honrath, R. E., M. C. Peterson, S. Guo, J. E. Dibb, P. B. Shepson and B. Campbell, *Geophys. Res. Lett.*, 1999, **26**, 695.
- Hu, J. H., Q. Shi, P. Davidovits, D. R. Worsnop, M. S. Zahniser and C. E. Kolb, *J. Phys. Chem.*, 1995, **99**, 8768.
- Hu, J. H. and J. P. D. Abbatt, *J. Phys. Chem. A.*, 1997, **101**, 871.
- Hughes, M. N. and G. Stedman, *J. Chem. Soc.*, 1964, 163.
- Irvine, W. M. and J. B. Pollack, *Icarus*, 1968, **8**, 324.
- Jaffe, S. and H. W. Ford, *J. Phys. Chem.*, 1967, **71**, 1832.
- Jayne, J. T., P. Davidovits, D. R. Worsnop, M. S. Zahniser and C. E. Kolb, *J. Phys. Chem.*, 1990, **94**, 6041.
- Jenkin, M. E., R. A. Cox and D. J. Williams, *Atmos. Environ.*, 1988, **22**, 487.
- Jirsak, T. and J. A. Rodriguez, *Langmuir*, 2000, **16**, 10287.
- Johnston, H. S., L. Foering and J. R. White, *J. Am. Chem. Soc.*, 1955, **77**, 4208.
- Jones, A. E., R. Weller, E. W. Wolff and H. W. Jacobi, *Geophys. Res. Lett.*, 2000, **27**, 345.
- Jones, A. E., R. Weller, P. S. Anderson, H. W. Jacobi, E. W. Wolff, O. Schrems and H. Miller, *Geophys. Res. Lett.*, 2001, **28**, 1499.
- Jones, L. H., B. I. Swanson and S. F. Agnew, *J. Chem. Phys.*, 1985, **82**, 4389.
- Kaiser, E. W. and C. H. Wu, *J. Phys. Chem.*, 1977a, **81**, 1701.
- Kaiser, E. W. and C. H. Wu, *J. Phys. Chem.*, 1977b, **81**, 187.
- Kalberer, M., M. Ammann, F. Arens, H. W. Gaggeler and U. Baltensperger, *J. Geophys. Res.*, 1999, **104**, 13825.
- Kay, B. D., V. Hermann and A. W. J. Castleman, *Chem. Phys. Lett.*, 1981, **80**, 469.

- Killus, J. P. and G. Z. Whitten, *Int. J. Chem. Kinet.*, 1990, **22**, 547.
- Kirchstetter, T. W., R. A. Harley and D. Littlejohn, *Environ. Sci. Technol.*, 1996, **30**, 2843.
- Kirkitsos, P. and D. Sikiotis, *Atmos. Environ.*, 1996, **30**, 941.
- Kiselev, A. V. and V. I. Lygin, *Infrared Spectra of Surface Compounds*, John Wiley & Sons, Inc., 1975.
- Kleffmann, J., K. H. Becker and P. Wiesen, *Atmos. Environ.*, 1998a, **32**, 2721.
- Kleffmann, J., K. H. Becker and P. Wiesen, *J. Chem. Soc., Faraday Trans.*, 1998b, **94**, 3289.
- Kleffmann, J., K. H. Becker, M. Lackhoff and P. Wiesen, *Phys. Chem. Chem. Phys.*, 1999, **1**, 5443.
- Knipping, E. M. and D. Dabdub, *Atmos. Environ.*, 2002, **36**, 5741.
- Koch, T. G., A. B. Horn, M. A. Chesters, M. R. S. McCoustra and J. R. Sodeau, *J. Phys. Chem.*, 1995, **99**, 8362.
- Koch, T. G., N. S. Holmes, T. B. Roddis and J. R. Sodeau, *J. Phys. Chem.*, 1996, **100**, 11402.
- Koda, S., K. Yoshikawa, J. Okada and K. Akita, *Environ. Sci. Technol.*, 1985, **19**, 262.
- Kotamarthi, V. R., J. S. Gaffney, N. A. Marley and P. V. Doskey, *Atmos. Environ.*, 2001, **35**, 4489.
- Kurtenbach, R., K. H. Becker, J. A. G. Gomes, J. Kleffmann, J. C. Lörzer, M. Spittler, P. Wiesen, R. Ackermann, A. Geyer and U. Platt, *Atmos. Environ.*, 2001, **35**, 3385.
- Lammel, G. and J. N. Cape, *Chem. Soc. Rev.*, 1996, **25**, 361.
- Lammel, G., *Formation of Nitrous Acid: Parameterization and Comparison with Observations, Report No. 286*, 36, Max-Planck-Institut-für Meteorologie, Hamburg, 1999.
- Langenberg, S., V. Proksch and U. Schurath, *Atmos. Environ.*, 1998, **32**, 3129.
- Langmuir, I., *J. Amer. Chem. Soc.*, 1918, **40**, 1361.
- Lary, D. J. and D. E. Shallcross, *J. Geophys. Res.*, 2000, **105**, 11617.
- Lee, N., R. G. Keese and A. W. J. Castleman, *J. Chem. Phys.*, 1980, **72**, 1089.
- Loechler, E. L., A. M. Schneider, D. B. Schwartz and T. C. Hollocher, *J. Am. Chem. Soc.*, 1987, **109**, 3076.
- Longfellow, C. A., A. R. Ravishankara and D. R. Hanson, *J. Geophys. Res.*, 1999, **104**, 13833.
- Low, M. J. D. and N. Ramasubramanian, *J. Phys. Chem.*, 1966, **70**, 2740.
- Manka, M. J., *Alchemy Software*, 2001, Wesley Chapel.
- Martin, L. R., D. E. Damschen and H. S. Judeikis, *Atmos. Environ.*, 1981, **15**, 191.
- Masel, R. I., *Principles of Adsorption and Reaction on Solid Surfaces*, John Wiley & Sons, 1996.
- McCurdy, P. R., W. P. Hess and S. S. Xantheas, *J. Phys. Chem. A*, 2002, **106**, 7628.
- McKinnon, I. R., J. G. Mathieson and I. R. Wilson, *J. Phys. Chem.*, 1979, **83**, 779.
- Mebel, A. A., M. C. Lin and C. F. Melius, *J. Phys. Chem. A*, 1998, **102**, 1803.
- Meng, Z., D. Dabdub and J. H. Seinfeld, *J. Geophys. Res.*, 1998, **103**, 3419.
- Mertes, S. and A. Wahner, *J. Phys. Chem.*, 1995, **99**, 14000.
- Miller, T. M. and V. H. Grassian, *Geophys. Res. Lett.*, 1998, **25**, 3835.
- Mochida, M. and B. J. Finlayson-Pitts, *J. Phys. Chem. A*, 2000, **104**, 9705.
- Mozurkewich, M. and J. Calvert, *J. Geophys. Res.*, 1988, **93**, 15889.

- Nishimura, H., T. Hayamizu and Y. Yanagisawa, *Environ. Sci. Technol.*, 1986, **20**, 413.
- Notholt, J., J. Hjorth and F. Raest, *Atmos. Environ.*, 1992, **26A**, 211.
- Osterman, G. B., B. Sen, G. C. Toon, R. J. Salawich, J. J. Margitan and J.-F. Blavier, *Geophys. Res. Lett.*, 1999, **26**, 1157.
- Pacific Environmental Services, *Background Report, AP-42 Section 6.8, Ammonium Nitrate Fertilizer*, 1, U. S. Environmental Protection Agency, Research Triangle Park, 1996.
- Parks, G. A., *J. Geophys. Res.*, 1984, **89**, 3997.
- Parts, L. and J. T. Miller, *J. Chem. Phys.*, 1965, **43**, 136.
- Perkins, K. K., T. F. Hanisco, R. C. Cohen, L. C. Koch, R. M. Stimpfle, P. B. Voss, G. P. Bonne, E. J. Lanzendorf, J. G. Anderson, P. O. Wennberg, R. S. Gao, L. A. Del Negro, R. J. Salawitch, C. T. McElroy, E. J. Hints, M. Loewenstein and T. P. Bui, *J. Phys. Chem. A*, 2001, **105**, 1521
- Perner, D. and U. Platt, *Geophys. Res. Lett.*, 1979, **6**, 917.
- Perrino, C., F. DeSantis and A. Febo, *Atmos. Environ.*, 1988, **22**, 1925.
- Perry, K. D., T. A. Cahill, R. A. Eldred, D. D. Dutcher and T. E. Gill, *J. Geophys. Res.*, 1997, **102**, 11225.
- Peters, M. S. and J. L. Holman, *Ind. Eng. Chem.*, 1955, **47**, 2536.
- Pimentel, G. C. and A. L. McClelland, *The Hydrogen Bond*, W. H. Freeman, 1960.
- Pinnick, D. A., S. F. Agnew and B. I. Swanson, *J. Phys. Chem.*, 1993, **96**, 7092.
- Pires, M. and M. J. Rossi, *Int. J. Chem. Kinet.*, 1997, **29**, 869.
- Pitts, J. N., D. Grosjean, K. vanCauwenberghe, J. P. Schmid and D. R. Fitz, *Environ. Sci. Technol.*, 1978, **12**, 946.
- Pitts, J. N., E. Sanhueza, R. Atkinson, W. P. L. Carter, A. M. Winer, G. W. Harris and C. N. Plum, *Int. J. Chem. Kinet.*, 1984a, **16**, 919.
- Pitts, J. N., H. W. Biermann, A. M. Winer and E. C. Tuazon, *Atmos. Environ.*, 1984b, **18**, 847.
- Pitts, J. N., T. J. Wallington, H. W. Biermann and A. M. Winer, *Atmos. Environ.*, 1985, **19**, 763.
- Pitts, J. N., H. W. Biermann, E. C. Tuazon, M. Green, W. D. Long and A. M. Winer, *J. Air Pollut. Control Assoc.*, 1989, **39**, 1344.
- Pitts, J. N., Sanhueza, E., Atkinson, R., Carter, W., Winer, A., Harris, W., and Plum, C., *Int. J. Chem. Kinet.*, 1984, **16**, 919.
- Platt, U., D. Perner, G. W. Harris, A. M. Winer and J. N. P. Jr., *Nature*, 1980, **285**, 312.
- Ponche, J. L., C. George and P. Mirabel, *J. Atmos. Chem.*, 1993, **16**, 1.
- Portland Cement Association, *Scientific Principles*, Portland Cement Association, 1999.
- Prospero, J. M. and R. T. Nees, *Science*, 1977, **196**, 1196.
- Prospero, J. M., R. A. Glaccum and R. T. Nees, *Nature*, 1981, **289**, 570.
- Prospero, J. M. and R. T. Nees, *Nature*, 1986, **320**, 735.
- Prospero, J. M., *J. Geophys. Res.*, 1999, **104**, 15917.
- Rasmussen, T. R., M. Brauer and S. Kjaergaard, *Am. J. Crit. Care Med.*, 1995, **151**, 1504.
- Richmond, G. L., *Annu. Rev. Phys. Chem.*, 2001, **52**, 357.
- Ritzhaupt, G. and J. P. Devlin, *J. Phys. Chem.*, 1991, **95**, 90.
- Rivera-Figueroa, A., A. L. Sumner and B. J. Finlayson-Pitts, *Environ. Sci. Technol.*, 2003, **37**, 548.

- Robinson, G. N., D. R. Worsnop, J. T. Jayne, C. E. Kolb and P. Davidovits, *J. Geophys. Res.*, 1997, **102**, 3583.
- Rudich, Y., I. Benjamin, R. Naaman, E. Thomas, S. Trakhtenberg and R. Ussyshkin, *J. Phys. Chem. A*, 2000, **104**, 5238.
- Sagiv, J., *J. Am. Chem. Soc.*, 1980, **102**, 92.
- Sakamaki, F., S. Hatakeyama and H. Akimoto, *Int. J. Chem. Kinet.*, 1983, **15**, 1013.
- Sakamaki, F. and H. Akimoto, *Int. J. Chem. Kinet.*, 1988, **20**, 111.
- Saliba, N., M. Mochida and B. J. Finlayson-Pitts, *Geophys. Res. Lett.*, 2000, **27**, 3229.
- Saliba, N. A., H. Yang and B. J. Finlayson-Pitts, *J. Phys. Chem. A*, 2001, **105**, 10339.
- Sander, S. P., R. R. Friedl, W. B. DeMore, D. M. Golden, M. J. Kurylo, R. F. Hampson, R. E. Huie, G. K. Moortgat, A. R. Ravishankara, C. E. Kolb and M. J. Molina, *Chemical Kinetics and Photochemical Data for Use in Stratospheric Modeling, Evaluation No. 13*, Jet Propulsion Laboratory, California Institute of Technology, Pasadena, CA, 2000.
- Sander, S. P., A. R. Ravishankara, R. R. Friedl, D. M. Golden, C. E. Kolb, M. J. Kurylo, M. J. Molina, R. E. Huie, V. L. Orkin, G. K. Moortgat and B. J. Finlayson-Pitts, *Chemical Kinetics and Photochemical Data for Use in Atmospheric Studies, Evaluation Number 14*, Jet Propulsion Laboratory, California Institute of Technology, Pasadena, 2003.
- Sato, S., D. Yamaguchi, K. Nakagawa, Y. Inoue, A. Yabushita and M. Kawasaki, *Langmuir*, 2000, **16**, 9533.
- Schiller, C. L., S. Locquiao, T. J. Johnson and G. W. Harris, *J. Atmos. Chem.*, 2001, **40**, 275.
- Schweitzer, F., P. Mirabel and C. George, *J. Phys. Chem. A*, 1998, **102**, 3942.
- Shen, Z. X., M. H. Kuok and S. H. Tang, *Spectrochim. Acta*, 1993, **49A**, 21.
- Shi, Q., Y. Q. Li, P. Davidovits, J. T. Jayne, D. R. Worsnop, M. Mozurkewich and C. E. Kolb, *J. Phys. Chem. B*, 1999, **103**, 2417.
- Shultz, M. J., C. Schnitzer, D. Simonelli and S. Baldelli, *Int. Rev. Phys. Chem.*, 2000, **19**, 123.
- Siefert, R. L., A. M. Johansen, M. R. Hoffmann and S. P. Pehkonen, *J. Air Waste Manage. Assoc.*, 1998, **48**, 128.
- Singh, H. B., W. Viezee, Y. Chen, A. N. Thakur, Y. Kondo, R. W. Talbot, G. L. Gregory, G. W. Sachse, D. R. Blake, J. D. Bradshaw, Y. Wang and D. J. Jacob, *J. Geophys. Res.*, 1998, **103**, 28237.
- Smith, J. H., *J. Amer. Chem. Soc.*, 1947, **69**, 1741.
- Spengler, J. D., M. Brauer, J. M. Samet and W. E. Lambert, *Environ. Sci. Technol.*, 1993, **27**, 841.
- Spicer, C. W., R. W. Coutant, G. F. Ward, D. W. Joseph, A. J. Gaynor and I. H. Billick, *Environment Intern.*, 1989, **15**, 643.
- Spicer, C. W., D. V. Kenny, G. F. Ward and I. H. Billick, *J. Air Waste Manage. Assoc.*, 1993, **43**, 1479.
- Sporleder, D. and G. E. Ewing, *J. Phys. Chem. A*, 2001, **105**, 1838.
- Stadler, D. and M. J. Rossi, *Phys. Chem. Chem. Phys.*, 2000, **2**, 5420.
- Staikova, M. and D. J. Donaldson, *Phys. Chem. Chem. Phys.*, 2001, **3**, 1999.
- Streit, G. E., J. S. Wells, F. C. Fehsenfeld and C. J. Howard, *J. Chem. Phys.*, 1979, **70**, 3439.

- Stutz, J., B. Aliche and A. Neftel, *J. Geophys. Res. Atmos.*, 2002a, **107**, DOI: 10.1029/2001JD000390.
- Stutz, J., *personal communication*, 2003,
- Sumner, A. L. and P. B. Shepson, *Nature*, 1999, **398**, 230.
- Sumner, A. L., E. J. Menke, Y. Dubowski, J. T. Newberg, R. M. Penner, J. C. Hemminger, L. M. Wingen, T. Brauers and B. J. Finlayson-Pitts, *Phys. Chem. Chem. Phys.*, 2004, **6**, 604.
- Sunderlin, L. S. and R. R. Squires, *Chem. Phys. Lett.*, 1993, **212**, 307.
- Svensson, R., E. Ljungstrom and O. Lindqvist, *Atmos. Environ.*, 1987, **21**, 1529.
- Svensson, R. and E. Ljungström, *Int. J. Chem. Kinet.*, 1988, **20**, 857.
- Syomin, D. and B. J. Finlayson-Pitts, *Phys. Chem. Chem. Phys.*, 2003, **5**, 5236.
- Takagi, H., S. Hatakeyama, H. Akimoto and S. Koda, *Environ. Sci. Technol.*, 1986, **20**, 387.
- Tao, F.-M., K. Higgins, W. Klemperer and D. D. Nelson, *Geophys. Res. Lett.*, 1996, **23**, 1797.
- TenBrink, H. M. and H. Spoelstra, *Atmos. Environ.*, 1998, **32**, 247.
- Thi, M. P., M. H. Herzog-Cance, A. Potier and J. Potier, *J. Raman Spectros.*, 1981, **11**, 96.
- Thompson, K. C. and P. Margey, *Phys. Chem. Chem. Phys.*, 2003, **5**, 2970.
- Tisdale, R. T., A. J. Prenni, L. T. Iraci and M. A. Tolbert, *Geophys. Res. Lett.*, 1999, **26**, 707.
- Tolbert, M. A. and A. M. Middlebrook, *J. Geophys. Res.*, 1990, **95**, 22.
- Tsang, W. and J. T. Herron, *J. Phys. Chem. Ref. Data*, 1991, **20**, 609.
- Tyndall, G. S., J. J. Orlando and J. G. Calvert, *Environ. Sci. Technol.*, 1995, **29**, 202.
- Ulman, A., *An Introduction to Ultrathin Organic Films from Langmuir-Blodgett to Self Assembly*, Academic Press, 1991.
- Underwood, G. M., T. M. Miller and V. H. Grassian, *J. Phys. Chem. A*, 1999, **103**, 6184.
- USGS, *Sediment*, U.S. Geological Survey, National Park Service, Department of Interior, Washington, DC, 1999.
- Vecera, Z. and P. K. Dasgupta, *Intern. J. Environ. Anal. Chem.*, 1994, **56**, 311.
- Vogt, R. and B. J. Finlayson-Pitts, *J. Phys. Chem.*, 1994, **98**, 3747.
- Wagner, C. D., L. E. Davis, M. V. Zeller, J. A. Taylor, R. H. Raymond and L. H. Gale, *Surf. Interf. Anal.*, 1981, **3**, 211.
- Wahner, A., T. F. Mentel, M. Sohn and J. Stier, *J. Geophys. Res.*, 1998, **103**, 31103.
- Wainman, T., C. J. Weschler, P. J. Lioy and J. Zhang, *Environ. Sci. Technol.*, 2001, **35**, 2200.
- Wallington, T. J. and S. M. Japar, *J. Atmos. Chem.*, 1989, **9**, 399.
- Wang, J., M. R. Voss, H. Busse and B. E. Koel, *J. Phys. Chem. B*, 1998a, **102**, 4693.
- Wang, J. and B. E. Koel, *J. Phys. Chem. A*, 1998, **102**, 8573.
- Wang, J. and B. E. Koel, *Surf. Sci.*, 1999, **436**, 15.
- Wang, X., Q. Zheng and K. Fan, *J. Molec. Structure*, 1997, **403**, 245.
- Wang, X., Q.-Z. Qin and K. Fan, *J. Molec. Structure*, 1998b, **432**, 55.
- Wayne, L. G. and D. M. Yost, *J. Chem. Phys.*, 1951, **19**, 41.
- Weis, D. D. and G. E. Ewing, *Anal. Chem.*, 1998, **70**, 3175.
- Weschler, C. J., H. C. Shields and D. V. Naik, *Environ. Sci. Technol.*, 1994, **28**, 2120.
- White, J. U., *J. Opt. Soc. Am.*, 1942, **32**, 285.

- Wiesen, P., J. Kleffmann, R. Kurtenbach and K. H. Becker, *Faraday Discuss.*, 1995, **100**, 121.
- Winer, A. M. and H. W. Biermann, *Res. Chem. Intermed.*, 1994, **20**, 423.
- Wlodek, S., Z. Luczynski and H. Wincel, *Int. J. Mass Spectrom. Ion Phys.*, 1980, **35**, 39.
- WMO, *Scientific Assessment of Ozone Depletion: 1998*, World Meteorological Organization, Geneva, Switzerland, 1998.
- Xu, L., A. Lio, J. Hu, D. F. Ogletree and M. Salmeron, *J. Phys. Chem. B*, 1998, **102**, 540.
- Yang, H. and B. J. Finlayson-Pitts, *J. Phys. Chem. A*, 2001, **105**, 1890.
- Yang, H., N. J. Wright, A. M. Gagnon, R. B. Gerber and B. J. Finlayson-Pitts, *Phys. Chem. Chem. Phys.*, 2002, **4**, 1832.
- Zhang, X., E. Mereand and A. W. J. Castleman, *J. Phys. Chem.*, 1994, **98**, 3554.
- Zhang, X. Y., R. Arimoto and Z. S. An, *J. Geophys. Res.*, 1997, **102**, 28041.
- Zhang, Y. and G. R. Carmichael, *J. Appl. Meteorol.*, 1999, **38**, 353.
- Zhou, X., H. J. Beine, R. E. Honrath, J. D. Fuentes, W. Simpson, P. B. Shepson and J. W. Bottenheim, *Geophys. Res. Lett.*, 2001, **28**, 4087.
- Zhou, X., H. Gao, Y. He, G. Huang, S. B. Bertman, K. Civerolo and J. Schwab, *Geophys. Res. Lett.*, 2003, **30**, ASC12.
- Zhou, X. L., Y. He, G. Huang, T. D. Thornberry, M. A. Carroll and S. B. Bertman, *Geophys. Res. Lett.*, 2002, **29**, 1681.
- Zhu, X., J. M. Prospero and F. J. Millero, *J. Geophys. Res.*, 1997, **102**, 21297.

LIST OF PUBLICATIONS

1. Ramazan, K. A.; Syomin, D.; Finlayson-Pitts, B. J., "The photochemical production of HONO during the heterogeneous hydrolysis of NO₂," submitted to *Phys. Chem. Chem. Phys.*, **2004**.
2. Sumner, A. L.; Menke, E. J.; Dubowski, Y.; Newberg, J. T.; Penner, R. M.; Hemminger, J. C.; Wingen, L. M.; Brauers, T.; Finlayson-Pitts, B. J., "The nature of water on surfaces of laboratory systems and implications for heterogeneous chemistry in the troposphere," *Phys. Chem. Chem. Phys.*, **2004**, 6, 604-613.
3. Rivera-Figueroa, A. M.; Sumner, A. L.; Finlayson-Pitts, B. J. "Laboratory Studies of Potential Mechanisms of Renoxification of Tropospheric Nitric Acid," *Environ. Sci. Technol.*, **2003**, 37, 548-554.
4. Finlayson-Pitts, B. J.; Wingen, L. M.; Sumner, A. L.; Syomin, D.; Ramazan, K. A., "The heterogeneous hydrolysis of NO₂ in laboratory systems and in outdoor and indoor atmospheres: An integrated mechanism, *Phys. Chem. Chem. Phys.*, **2003**, 5, 223-242.
5. Syomin, D. A.; Finlayson-Pitts, B. J. "HONO decomposition on borosilicate glass surfaces: Implications for environmental chamber studies and field experiments," *Phys. Chem. Chem. Phys.*, **2003**, 5, 5236-5242.
6. Yang, H.; Wright, N. J.; Gagnon, A. M.; Gerber, R. B.; Finlayson-Pitts, B. J., "An upper limit to the concentration of an SO₂ complex at the air-water interface at 298 K: Infrared experiments and *ab initio* calculations," *Phys. Chem. Chem. Phys.*, **2002**, 4, 1832-1838.
7. Saliba, N. A.; Yang, H.; Finlayson-Pitts, B. J. "Reaction of gaseous nitric oxide with nitric acid on silica surfaces in the presence of water at room temperature," *J. Phys. Chem. A*, **2001**, 105, 10339-10346.

GLOSSARY OF TERMS, ABBREVIATIONS AND SYMBOLS

Chemical Formulas

Al_2O_3 :	aluminum oxide
B_2O_3 :	diboron trioxide
CH_4 :	methane
CO :	carbon monoxide
CaF_2 :	calcium fluoride
FeCl_3 :	ferric chloride
HgCdTe :	mercury-cadmium-tellurium (MCT)
HCl :	hydrogen chloride
HNO_3 :	nitric acid
$\text{HNO}_3\text{-H}_2\text{O}$:	nitric acid monohydrate
$\text{HNO}_3\text{-2H}_2\text{O}$:	nitric acid dihydrate
$\text{HNO}_3\text{-3H}_2\text{O}$:	nitric acid trihydrate
$\text{HNO}_3(\text{H}_2\text{O})_x$:	any nitric acid-water complex
HO_2 :	hydroperoxy radical
HOONO :	peroxynitrous acid
HO_2NO_2 :	peroxynitric acid
HONO :	nitrous acid
H_2O :	water
H_2O_2 :	hydrogen peroxide
H_2SO_4 :	sulfuric acid
H_3O^+ :	hydronium ion
K_2O :	potassium oxide
NaCl :	sodium chloride
Na_2O :	sodium oxide
NaHCO_3 :	sodium bicarbonate
Na_2CO_3 :	sodium carbonate
NaNO_2 :	sodium nitrite
NaNO_3 :	sodium nitrate
NH_3 :	ammonia
NH_4OH :	ammonium hydroxide
NH_4NO_3 :	ammonium nitrate
NO :	nitrogen oxide
NO^+ :	nitrosonium ion
NO_2 :	nitrogen dioxide
NO_2^+ :	nitronium ion
NO_3 :	nitrate radical
NO_3^- :	nitrate ion
NO_x :	collective term for $\text{NO} + \text{NO}_2$
NO_y :	sum of nitrogen oxides, $\text{NO} + \text{NO}_2 + 2 \text{N}_2\text{O}_4 + \text{HNO}_3 + 2 \text{N}_2\text{O}_5 + \dots$
N_2 :	nitrogen
N_2O :	nitrous oxide

N ₂ O ₄ :	dinitrogen tetroxide (symmetric form, if unspecified)
N ₂ O ₅ :	dinitrogen pentoxide
O(¹ D):	excited oxygen atom
O(³ P):	ground state oxygen atom
O ₂ :	oxygen
O ₃ :	ozone
OH:	hydroxyl radical
ONONO ₂ :	asymmetric dinitrogen tetraoxide
SiO ₂ :	silicon dioxide or silica
SO ₂ :	sulfur dioxide
TiO ₂ :	titanium dioxide
ZnSe:	zinc selenide
ZnO:	zinc oxide
ZrO ₂ :	zirconium dioxide
KBr:	potassium bromide

<u>Units</u>	
cm ⁻¹ :	wavenumber
g:	grams
μL:	microliter
mL:	milliliter
L:	liter
M:	molarity
h:	hour
min:	minute
m:	meter
mm:	millimeter
MΩ cm:	megaohm centimeter
nm:	nanometer
μm:	micrometer
in:	inch
ppb:	parts per billion by volume
ppm:	parts per million by volume
mM:	millimolar
s:	second
psi:	pounds per square inch
W:	watts
nN:	nanoNewtons
Hz:	Hertz
Torr:	1 mm of mercury
eV:	electron volt
keV:	kilo electron volt
mA:	milliamp ere
K:	Kelvin
°C:	degrees Celsius
μS:	microsiemens

Ω : ohm

Acronyms

ACS: American Chemical Society
AFM: Atomic Force Microscopy
AMTIR: Amorphous Material Transmitting InfraRed: Ge-As-Se glass
ASAP: Accelerated Surface Area and Porosimetry system
ATR: Attenuated Total Reflectance
BET: Brunauer-Emmet-Teller
CIT: California Institute of Technology
C8 SAM: Self-assembled monolayer of the 8-carbon alkane (*n*-octyl) on a surface
DOAS: Differential Optical Absorption Spectroscopy
EPA: US Environmental Protection Agency
FEP: fluorinated ethylene propylene
FTIR: Fourier transform infrared
IC: Ion chromatography
IR: Infrared
M: any third molecule to remove excess energy
MCT: mercury-cadmium-tellurium
MFC: name of spectral analysis fitting software
NAM: nitric acid monohydrate
NAD: nitric acid dihydrate
NAT: nitric acid trihydrate
PM: particulate matter
PM_{2.5}: particulate matter with diameter $\leq 2.5 \mu\text{m}$
PM₁₀: particulate matter with diameter $\leq 10 \mu\text{m}$
PFA: perfluoroalkoxy
PSI: Park Scientific Instruments
RH: relative humidity
SAM: self-assembled monolayer
UHP: ultra high purity
UHV: ultra high vacuum
UV: ultraviolet
XPS: X-ray photoelectron spectroscopy

Symbols and Abbreviations

k : rate constant
 k_p : photolysis rate constant
 $h\nu$: energy of a light photon of frequency ν , where h = Planck's constant
 λ : wavelength of radiation
 ν_x : fundamental vibration, where $x = 1, 2, \dots$
 s : sample standard deviation
 S/V : ratio of surface area to volume
 t : time
 \ln : log base e
 σ : absorption cross section

F: intensity of light
 Φ : quantum yield
 Θ : coverage

APPENDIX

The following attached pages are publications resulting from this work.

The Photochemical Production of HONO During the Heterogeneous Hydrolysis of NO₂

Kevin A. Ramazan, Dennis Syomin and Barbara J. Finlayson-Pitts*

Department of Chemistry
University of California
Irvine, CA 92697-2025

For Submission to:

Physical Chemistry Chemical Physics

February 12, 2004

*Author to whom correspondence should be addressed.

Phone (949) 824-7670; Fax (949) 824-3168; email: bjfinlay@uci.edu

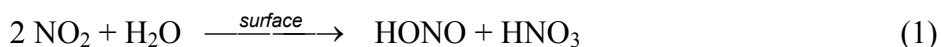
ABSTRACT

The heterogeneous hydrolysis of NO_2 on thin water films, a major source of HONO and hence OH radicals in polluted urban atmospheres, has been previously reported to be photoenhanced.¹ We report here studies of the impact of 320 – 400 nm radiation on HONO formation during the heterogeneous NO_2 hydrolysis at 296 K. The experiments were carried out using long path Fourier transform infrared radiation (FTIR) spectroscopy with three initial NO_2 concentrations (20, 46, and 54 ppm) and at relative humidities of 33, 39, and 57%, respectively, in a borosilicate glass cell. Nitrous acid was first allowed to accumulate from NO_2 hydrolysis in the dark, and then the mixture of reactants and products was irradiated. The measured concentration-time profiles of the gases were compared to the predictions of a kinetics model developed for this system. The loss of HONO upon irradiation initially was consistent with its photolysis and known secondary gas phase chemistry, and there was no evidence of a photoenhancement of the fundamental NO_2 hydrolysis as proposed earlier. At later photolysis times, HONO production was greater than the model predicted, suggesting secondary photochemical HONO production from the photolysis of a species, such as HNO_3 adsorbed on the walls as suggested by Zhou et al.^{2,3}

INTRODUCTION

Nitrous acid (HONO) was first identified spectroscopically in ambient urban air in 1979.⁴ Since then, a number of atmospheric measurements have shown that HONO accumulates during the night and undergoes photolysis in the early morning to produce a pulse of hydroxyl radicals (OH).⁵⁻¹² Indeed, HONO photolysis is the major source of OH in the early morning in high NO_x locations, and is a significant source even when averaged over 24 hours.^{6,8,11,12} Therefore, it is important to understand the sources and sinks of HONO and the mechanism of its formation since OH drives the chemistry that leads to the formation of O₃ and a variety of other secondary air pollutants.¹³

The major atmospheric source of HONO is believed to be the heterogeneous hydrolysis of NO₂, generally represented by (1):



The surfaces available for reaction include airborne particles, soils, and urban surfaces such as glass, concrete and foliage.^{7-9,14} Although reaction (1) has been extensively studied in reaction chambers by reacting gas phase NO₂ in the presence of water vapor,^{1,14-31} the mechanism of reaction (1) has been difficult to elucidate. This laboratory has recently proposed a mechanism for reaction (1) in which dinitrogen tetroxide (N₂O₄) is a key intermediate.¹⁴ A schematic diagram of the proposed mechanism is shown in Figure 1.

In this mechanism, gaseous N_2O_4 , in equilibrium with NO_2 , is taken up into the water film present on the surface. The N_2O_4 isomerizes to the asymmetric form, ONONO_2 , which autoionizes to form NO^+NO_3^- at the surface. This ion pair reacts with surface film water to form adsorbed HONO and HNO_3 . The HNO_3 remains on the surface while HONO is either displaced into the gas phase by the competitive adsorption between water and HONO,³² or undergoes secondary chemistry to produce gaseous NO, NO_2 , and small amounts of N_2O . In order for HONO production to be first order in NO_2 , as many previous studies reported,^{14,19-28} a back reaction involving NO_2 reacting with ONONO_2 must be faster than the competing reaction with water.

A photoenhancement of the generation of HONO from the heterogeneous hydrolysis of NO_2 was reported by Akimoto et al.¹ The HONO formed in a 6065-L Teflon coated smog chamber did not decay as rapidly as predicted by a model of the chemistry when the mixture in air was irradiated with a filtered Xe lamp ($\lambda > 290$ nm). The difference between the model-predicted and experimental data was attributed to a photoenhancement of the heterogeneous NO_2 hydrolysis reaction. Recently Zhou et al.^{2,3} reported evidence for a photochemical production of HONO from HNO_3 deposited surfaces. This HONO production was first observed in a “dirty” glass sampling line exposed to sunlight during a field study,² and was confirmed in subsequent laboratory experiments.³ Killus and Whitten reviewed data from various smog chambers to suggest that photoenhanced HONO production occurs on quartz and glass surfaces but significantly less on Teflon surfaces,³³ such as that used by Akimoto et al.¹

In the present study, HONO formation from NO₂ hydrolysis in a borosilicate glass cell has been studied in the presence and absence of UV radiation (320 – 400 nm) in 1 atm of N₂ or air. The data are interpreted in the framework of a simplified mechanism similar to that shown in Figure 1, along with a kinetics model developed to describe the reaction in both the dark and the light periods. The photolysis rate constants for HONO and NO₂ were measured independently in the same system for inclusion in the model. A comparison of the experimental data to the model predictions clearly establishes that there is no photoenhancement of the fundamental mechanism of NO₂ hydrolysis. Our experiments do show evidence of a secondary photochemical HONO production at longer photolysis times.

EXPERIMENTAL METHODS

A. Experimental. A cylindrical borosilicate glass long path cell (0.15 m i.d., 1 m base path, 19.4 L volume, and a surface to volume ratio of 46 m⁻¹ including optics¹⁴) was used as a reaction vessel. The cell was equipped with a set of White optics³⁴ aligned for a path length of 84 or 48 meters. The flanges and inner supports consist of anodized aluminum covered with a thin coating of halocarbon wax (Halocarbon Products, Inc., Series 1500) to avoid reactions with metal surfaces. Ultraviolet radiation (320-400 nm) from blacklamps (Sylvania, 30 W, F30T8 / 350BL) entered the cell through the borosilicate walls.

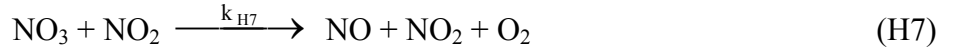
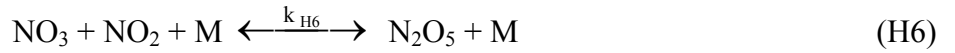
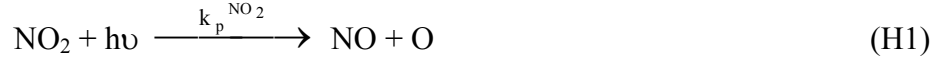
Concentrations of NO₂, HONO, and NO in the cell were measured using FTIR (Mattson, Research Series). Spectra were typically collected at a resolution of 1 cm⁻¹ and consisted of 64 co-added scans collected over 30 seconds. Gas phase NO₂, HONO, and NO were quantified by the net absorbance of their peaks at 2917, 1263, and 1875 cm⁻¹, respectively. Concentrations of

NO₂ and NO were determined based on calibrations using mixtures of known concentrations in N₂ in the cell, while the HONO concentrations were calculated using the 1263 cm⁻¹ peak due to the *trans*- isomer and applying an effective absorption cross section of $(3.7 \pm 0.4) \times 10^{-19}$ cm² molecule⁻¹ (base 10) to measure total HONO based on a *trans/cis* ratio of 2.3.^{35,36}

Concentrations of H₂O were determined using a calibration obtained by flowing a known concentration of water vapor through the cell and measuring rotational lines at 1174 cm⁻¹ and 1187 cm⁻¹.

In each NO₂ hydrolysis experiment, ~ 20 – 50 ppm NO₂ was introduced to the cell as a mixture in nitrogen (Oxygen Service Company, 99.999%) or air (Oxygen Service Company, < 0.1 ppm THC, < 0.5 ppm CO, < 2.0 ppm H₂O, < 0.5 ppm CO₂). The cell was filled to atmospheric pressure from a collapsible Teflon chamber that contained a water-carrier gas mixture obtained by flowing N₂ or air through a bubbler containing Nanopure[®] water (Barnstead, 18.2 MΩ cm) and mixing it with dry N₂ or air. This method quickly brought the cell pressure to 1 atm at the desired RH. Nitrous acid accumulated for 2 – 3 hr via the hydrolysis of NO₂ before irradiation began. Photolysis periods typically lasted for 2 – 3 hr. All experiments were performed at 296 ± 1 K.

In order to model the system quantitatively, the photolysis rate constants for NO₂ and HONO in this system were acquired. For NO₂, this was determined experimentally by adding NO₂ to the cell in concentrations similar to those in the hydrolysis experiments. The cell was filled to 1 atm with N₂, irradiated and the decay of NO₂ measured. The NO₂ photolysis rate constant was calculated using the method of Holmes et al.,³⁷ based on the following mechanism:



With the appropriate steady state assumptions for NO, NO₃, and N₂O₅ in an O₂ deficient environment, the photolysis rate constant for NO₂ ($k_p^{\text{NO}_2}$) was determined using the following relationship:³⁷

$$k_p^{\text{NO}_2} = \frac{Z}{2t} \quad (\text{I})$$

where t is time and Z is given by equation (II):

$$Z = \left\{ \left(1 + \frac{k_{\text{H3}}[\text{M}]}{k_{\text{H2}}} - \frac{k_{\text{H4}}[\text{M}]}{k_{\text{H2}}} \right) \ln \frac{[\text{NO}_2]_0}{[\text{NO}_2]} + \frac{k_{\text{H4}}[\text{M}]}{k_{\text{H2}}} \left[\frac{[\text{NO}_2]_0}{[\text{NO}_2]} - 1 \right] \right\} \quad (\text{II})$$

Here $[\text{NO}_2]_0$ is the initial NO₂ concentration, $[\text{NO}_2]$ is the concentration at time t , k_{H2} , k_{H3} , and k_{H4} are the rate constants for reactions (H2), (H3), and (H4) respectively, and M is the required third body, in this case N₂.

The NO₂ photolysis rate constant was obtained from the slope of a plot of Z versus time. From data such as that shown in Figure 2, the NO₂ photolysis rate constant ($k_p^{\text{NO}_2}$) was determined to be $(1.6 \pm 0.1) \times 10^{-3} \text{ s}^{-1}$ (2s).

To determine the HONO photolysis rate constant, 100 – 200 ppm of cyclohexane (Fisher, 99.9%) was added to mixtures of HONO (0.2 - 1.8 ppm) in N₂ in order to scavenge the OH and prevent the regeneration of HONO from the OH + NO recombination reaction and the loss of HONO from secondary reactions, such as HONO + OH. The HONO decay was treated as first order and the HONO photolysis rate constant obtained from equation (III):

$$\ln \frac{[\text{HONO}]_0}{[\text{HONO}]} = k_p^{\text{HONO}} t \quad (\text{III})$$

The photolysis rate constant for HONO (k_p^{HONO}) was determined from data such as that shown in Figure 3 to be $(4.9 \pm 1.4) \times 10^{-4} \text{ s}^{-1}$ (2s). As a further check on experimentally determined HONO photolysis rate constant, equation (IV) was also used to calculate k_p^{HONO} based on the measured value of $k_p^{\text{NO}_2}$:

$$\frac{k_p^{\text{HONO}}}{k_p^{\text{NO}_2}} = \frac{\int_{320 \text{ nm}}^{400 \text{ nm}} \Phi_{\text{HONO}}(\lambda) \sigma_{\text{HONO}}(\lambda) F(\lambda) d\lambda}{\int_{320 \text{ nm}}^{400 \text{ nm}} \Phi_{\text{NO}_2}(\lambda) \sigma_{\text{NO}_2}(\lambda) F(\lambda) d\lambda} \quad (\text{IV})$$

In equation (IV), σ is the relevant base *e* absorption cross section, Φ is the corresponding quantum yield, and *F* is the intensity of light.^{13,38} This calculation yielded a value of $k_p^{\text{HONO}} = 4.8 \times 10^{-4} \text{ s}^{-1}$, in excellent agreement with the measured value. This agreement establishes that

additional sources of HONO such as photolysis of surface-adsorbed species (see below) is not significant under the conditions that k_p^{HONO} was measured.

B. Materials. Nitric oxide (Matheson, 99%) was purified by passing it through a liquid nitrogen trap to remove impurities such as NO_2 and HNO_3 . Nitrogen dioxide was synthesized by reacting the purified NO with excess oxygen (Oxygen Service Company, 99.993%) for at least 2 hr. The NO_2 was then purified by condensing in a cold finger at 195 K and pumping away the excess O_2 .

Nitrous acid was synthesized by reacting HCl with NaNO_2 :



Solid NaNO_2 (Aldrich, 99.5%) was exposed to humid N_2 (80-100% RH) for 15 – 20 minutes to moisten the salt surface. The flow of humid N_2 was stopped and replaced with a flow of gaseous HCl prepared by passing dry N_2 over a HCl solution (Fisher, Certified ACS Plus, 12.1 M diluted ~ 1:3 (v:v) using Nanopure[®] water).

C. Modeling. A kinetics modeling program (REACT for Windows v.1.2)^{39,40,41 Fl #40} was used to simulate the gas phase chemistry as well as the hydrolysis of NO_2 in the cell. The program numerically integrates the differential rate equations representing the reaction kinetics. The model for the dark period includes the gas phase and surface chemistry, given in sections A and C of Table 1. The gas phase model includes the relevant gas phase reactions available from current databases.^{38,42,43} To represent the chemistry during irradiation, photolysis reactions listed in section B of Table 1 were included. The surface reactions were parameterized as gas phase

rate processes for simplicity. Because the details of the NO_2 heterogeneous hydrolysis mechanism are uncertain, this portion of the model is simplified to have the least number of unknown variables and yet still capture the essence of what is known about the heterogeneous hydrolysis of NO_2 : the reaction is first order in NO_2 and water vapor,^{14,19-28} there is a competitive adsorption between H_2O and HONO ,³² and HONO undergoes heterogeneous reactions on the cell walls to generate NO .³² A more complex mechanism involving N_2O_4 can also be used but since the rate constants for the individual steps are not known, it does not add to the data interpretation during photolysis and hence we have chosen to use this more simplified mechanism in this case.

Rate constants for the surface reactions were adjusted within the constraints of the mechanism to provide a best fit to the observed decay of NO_2 and the formation of HONO during the dark period. By accurately predicting the chemistry in the dark and having measured the photolysis rate constants for NO_2 and HONO , the chemistry should be accurately predicted during the irradiation period. The rate constant for the NO_2 heterogeneous hydrolysis was allowed to vary slightly from experiment to experiment to give the best fit to the data in the dark portion of the experiment; this value was then used for the photolysis portion of the experiment. This enabled the model to reproduce the HONO concentrations at the beginning of the photolysis. All other rate constants in Section C of Table 1 remained constant.

RESULTS AND DISCUSSION

Figure 4 shows a typical concentration-time profile for the gaseous reactants and products for the reaction of 46 ppm NO_2 at 39 % RH in 1 atm of N_2 . In the dark period (region I), the NO_2

concentration slowly decays while HONO and, to a lesser extent, NO increase. At ~ 6500 s, the contents of the cell were irradiated (region II). As expected from the large absorption cross sections and quantum yields for NO_2 and HONO in the 300 – 400 nm region,¹³ the concentrations of both compounds decrease rapidly. Nitric oxide, the primary photolysis product of these reactions, rapidly increases. After ~ 650 seconds of photolysis (region III), the HONO concentration begins to level off and less than 25% of the initial NO_2 concentration remains.

Figure 5 shows expanded plots for the concentration-time profiles for three NO_2 hydrolysis experiments at different relative humidities and initial concentrations of NO_2 . The x-axis time is referenced to the irradiation period with zero designated as the start of irradiation. In the dark period, there is excellent agreement between the measured (symbols) and model predicted concentrations (solid lines), allowing for accurate initial concentrations for the photolysis period. The photolysis period was modeled by including the photodissociation of NO_2 , HONO, and O_3 in the model (section B of Table 1), along with the secondary chemistry of $\text{O}(^1\text{D})$, $\text{O}(^3\text{P})$, and OH (included in section A of Table 1) generated by photolysis. The agreement between the experimentally measured HONO concentrations and model predictions is excellent in this initial period of irradiation (region II) without including any photoenhancement of the NO_2 heterogeneous hydrolysis reaction.

As shown in Figure 6, the model begins to underestimate the HONO concentrations at longer photolysis times,(region III). Although the 2s error bars on the HONO concentrations (which is due primarily to the uncertainty in the measured absorption cross section) overlaps the model predictions in region III, the model provides a good match to the data at shorter photolysis times

(region II). This suggests that an additional source of HONO exists at the longer irradiation times, which is not included in the well-known chemistry shown in Table 1. Indeed, there is experimental evidence from other laboratories for such a photochemical production of HONO. Thus, Zhou et al.² recently reported significant production of HONO when a “dirty” glass sampling manifold was exposed to sunlight, and hypothesized that photolysis of HNO₃ on the surface was the source of the additional HONO. In a later laboratory experiment,³ significant HONO and NO_x production was observed when 0 – 80 % RH air was irradiated with a filtered mercury arc lamp (>290 nm) in a glass flow cell which had been previously conditioned with gaseous HNO₃.

To test HNO₃ photolysis as a possible source of the additional HONO in Region (III), reaction (2) was added to the model.



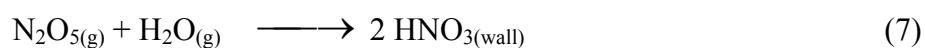
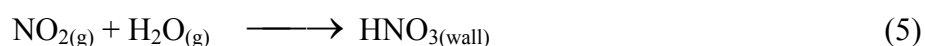
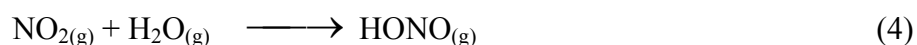
As seen by the dotted line in Figure 6, including this reaction in the model with a rate constant of $2 \times 10^{-5} \text{ s}^{-1}$ brings the model predicted HONO concentrations into agreement with the data in both regions II and III.

To test for reaction (2) in our system, the cell walls were conditioned by filling the reaction cell with ~ 2 torr of dry gaseous HNO₃ and pumping out three times. The cell was then filled with 139 ppm cyclohexane in 1 atm of dry air and the system exposed to 320 – 400 nm radiation for 90 min. Any gas phase HONO produced by photolysis of adsorbed HNO₃ would photolyze to form NO and OH. In the presence of oxygen, OH will react with cyclohexane to form

cyclohexanone with a yield of 0.321.⁴⁴ In our experiments, no cyclohexanone production was observed. Based on the measured cyclohexanone detection limit in our system of 2.2 ppm, we calculated an upper limit for the rate constant for reaction (2) in our system of $\leq 3 \times 10^{-4} \text{ s}^{-1}$. This value is an order of magnitude larger than that used to obtain model agreement with our data, and hence a contribution from reaction (2) is not inconsistent with our data.

A complementary set of runs was performed after the cyclohexane experiments using similar initial conditions in air and then N_2 to probe for unanticipated effects of O_2 on the heterogeneous chemistry. Figure 7 shows that, as expected, the decay of NO_2 upon irradiation in air is slower than that in N_2 due to the regeneration of NO_2 by gas phase chemistry involving NO_x and O_2 . However, the model fits the data during the dark and initial photolysis period for experiments in both N_2 and air. Again these results indicate that there is no photoenhancement of the NO_2 heterogeneous hydrolysis itself. (The decay of HONO in Region III in these experiments is somewhat faster than observed in earlier experiments carried out before cyclohexane/cyclohexanone was used in this system, which is attributed to increased OH scavenging by organics adsorbed on the cell walls). The dotted lines in Figure 7 show HONO concentrations when the rate constant for reaction (2) is $1.2 \times 10^{-5} \text{ s}^{-1}$ for the experiment in air and $5 \times 10^{-6} \text{ s}^{-1}$ for that in N_2 . The variability in the rate constants for the photolysis of adsorbed HNO_3 that provide best fits to the data is not surprising, given that the surface conditions will change, particularly after carrying out the experiments using cyclohexane. The data suggests that there is still some photochemical production of HONO from a species adsorbed on the wall, such as HNO_3 , consistent with the reports of Zhou et al.^{2,3}

The earlier studies in which a photoenhancement of the heterogeneous hydrolysis was reported¹ were performed in air using a much larger (6065 L) chamber that was coated with Teflon, with a filtered (> 290 nm) high pressure Xe lamp as the light source. The surface reaction mechanism used in their model was as follows:



Despite these differences in the experimental conditions, our data are quite similar to those of Akimoto and coworkers.¹ It seems likely, based on the present results, that the source of the additional HONO observed in their experiments was photochemical production of HONO from species adsorbed on the cell walls, as we have observed at longer photolysis times. Studies in this laboratory⁴⁵ have shown that nitric acid adsorbs onto both glass and Teflon surfaces in the presence of water vapor and hence photochemical production of HONO from photolysis of adsorbed HNO₃ might be expected from both their Teflon-lined chamber and our borosilicate glass cell.

CONCLUSIONS

The effect of UV (320 – 400 nm) irradiation on HONO production during the heterogeneous hydrolysis of NO₂ has been investigated. The fundamental NO₂ heterogeneous hydrolysis is not

photoenhanced. However, the experimental decay of HONO was slower than expected at longer photolysis times, suggesting that there is a secondary photochemical source of HONO such as the photolysis of adsorbed HNO₃ which is formed by the heterogeneous hydrolysis. As proposed by Zhou and coworkers,^{2,3} such a reaction could be an important source of HONO in the atmosphere during the day.

ACKNOWLEDGEMENTS

We are thankful to the California Air Resources Board (Contract No. 00-323) and the National Science Foundation (Grant No. ATM-0097573) for the support of this work. We would also like to thank J. N. Pitts Jr. and L. M. Wingen for many useful discussions.

Table 1. Chemical Reactions in Model

Reaction	Rate Constant (k^{298}) ^a	Reference
A. Gas Phase Reactions		
$2 \text{NO}_2 \xrightarrow{M} \text{N}_2\text{O}_4$	2.5×10^{-14}	Atkinson et al., 2002
$\text{N}_2\text{O}_4 \longrightarrow 2 \text{NO}_2$	1.1×10^5	Atkinson et al., 2002
$\text{NO}_3 + \text{NO} \longrightarrow 2 \text{NO}_2$	2.6×10^{-11}	Sander et al., 2003
$\text{NO}_2 + \text{NO}_3 \xrightarrow{M} \text{N}_2\text{O}_5$	1.2×10^{-12}	Sander et al., 2003
$\text{N}_2\text{O}_5 \longrightarrow \text{NO}_2 + \text{NO}_3$	3.8×10^{-2}	Sander et al., 2003
$\text{NO}_2 + \text{O}(^3\text{P}) \longrightarrow \text{NO} + \text{O}_2$	1.0×10^{-11}	Sander et al., 2003
$\text{NO}_2 + \text{O}(^3\text{P}) \xrightarrow{M} \text{NO}_3$	3.3×10^{-12}	Sander et al., 2003
$\text{NO}_2 + \text{O}_3 \longrightarrow \text{NO}_3 + \text{O}_2$	3.2×10^{-17}	Sander et al., 2003
$\text{NO}_2 + \text{OH} \xrightarrow{M} \text{HNO}_3$	1.0×10^{-11}	Sander et al., 2003
$\text{NO}_2 + \text{OH} \xrightarrow{M} \text{HOONO}$	2.1×10^{-12}	Sander et al., 2003
$\text{HOONO} \longrightarrow \text{NO}_2 + \text{OH}$	1.1	Sander et al., 2003
$\text{NO}_2 + \text{HO}_2 \xrightarrow{M} \text{HO}_2\text{NO}_2$	1.4×10^{-12}	Sander et al., 2003
$\text{HO}_2\text{NO}_2 \longrightarrow \text{NO}_2 + \text{HO}_2$	8.6×10^{-2}	Sander et al., 2003
$\text{NO} + \text{NO}_2 \xrightarrow{M} \text{N}_2\text{O}_3$	7.2×10^{-15}	Atkinson et al., 2002
$\text{N}_2\text{O}_3 \longrightarrow \text{NO} + \text{NO}_2$	3.8×10^5	Atkinson et al., 2002
$\text{NO} + \text{O}(^3\text{P}) \xrightarrow{M} \text{NO}_2$	1.7×10^{-12}	Sander et al., 2003
$2 \text{NO} + \text{O}_2 \longrightarrow 2 \text{NO}_2$	2.0×10^{-38}	Atkinson et al., 2002
$\text{NO} + \text{O}_3 \longrightarrow \text{NO}_2 + \text{O}_2$	1.9×10^{-14}	Sander et al., 2003
$\text{NO} + \text{OH} \xrightarrow{M} \text{HONO}$	7.4×10^{-12}	Sander et al., 2003
$\text{NO} + \text{HO}_2 \longrightarrow \text{OH} + \text{NO}_2$	8.1×10^{-12}	Sander et al., 2003
$\text{NO}_3 + \text{O}(^3\text{P}) \longrightarrow \text{O}_2 + \text{NO}_2$	1.0×10^{-11}	Sander et al., 2003
$\text{NO}_3 + \text{OH} \longrightarrow \text{HO}_2 + \text{NO}_2$	2.2×10^{-11}	Sander et al., 2003
$\text{NO}_3 + \text{HO}_2 \longrightarrow \text{OH} + \text{NO}_2 + \text{O}_2$	3.5×10^{-12}	Sander et al., 2003
$\text{N}_2\text{O} + \text{O}(^1\text{D}) \longrightarrow \text{N}_2 + \text{O}_2$	4.9×10^{-11}	Sander et al., 2003
$\text{O}(^1\text{D}) + \text{O}_2 \longrightarrow \text{O}(^3\text{P}) + \text{O}_2$	4.0×10^{-11}	Sander et al., 2003
$\text{HONO} + \text{OH} \longrightarrow \text{H}_2\text{O} + \text{NO}_2$	4.5×10^{-12}	Sander et al., 2003
$\text{HONO} + \text{O}(^3\text{P}) \longrightarrow \text{NO}_2 + \text{OH}$	9.1×10^{-16}	Tsang and Herron, 1991
$\text{N}_2\text{O} + \text{O}(^1\text{D}) \longrightarrow 2 \text{NO}$	6.7×10^{-11}	Sander et al., 2003
$\text{O}(^3\text{P}) + \text{O}_2 \xrightarrow{M} \text{O}_3$	1.5×10^{-14}	Sander et al., 2003
$\text{O}(^1\text{D}) + \text{O}_3 \longrightarrow 2 \text{O}_2$	1.2×10^{-10}	Sander et al., 2003
$\text{O}(^1\text{D}) + \text{O}_3 \longrightarrow 2 \text{O}(^3\text{P}) + \text{O}_2$	1.2×10^{-10}	Sander et al., 2003
$\text{O}(^3\text{P}) + \text{O}_3 \longrightarrow 2 \text{O}_2$	8.0×10^{-15}	Sander et al., 2003
$\text{H} + \text{O}_2 \xrightarrow{M} \text{HO}_2$	1.2×10^{-12}	Sander et al., 2003

$O(^1D) + H_2O \longrightarrow 2 OH$		2.2×10^{-10}	Sander et al., 2003
$O(^3P) + H_2O_2 \longrightarrow OH + HO_2$		1.7×10^{-15}	Sander et al., 2003
$OH + O_3 \longrightarrow HO_2 + O_2$		7.3×10^{-14}	Sander et al., 2003
$2 OH \longrightarrow O(^3P) + H_2O$		1.9×10^{-12}	Sander et al., 2003
$2 OH \xrightarrow{M} H_2O_2$		6.3×10^{-12}	Sander et al., 2003
$OH + HO_2 \longrightarrow O_2 + H_2O$		1.1×10^{-10}	Sander et al., 2002
$H + O_3 \longrightarrow OH + O_2$		2.9×10^{-11}	Sander et al., 2003
$OH + H_2O_2 \longrightarrow HO_2 + H_2O$		1.7×10^{-12}	Sander et al., 2003
$HO_2 + O_3 \longrightarrow OH + 2 O_2$		1.9×10^{-15}	Sander et al., 2003
$O(^3P) + OH \longrightarrow O_2 + H$		3.3×10^{-11}	Sander et al., 2003
$O(^3P) + HO_2 \longrightarrow OH + O_2$		5.9×10^{-11}	Sander et al., 2003
$OH + HNO_3 \longrightarrow H_2O + NO_3$		1.5×10^{-13}	Sander et al., 2003
$2 HO_2 \longrightarrow H_2O_2 + O_2$	0 % RH	2.9×10^{-12}	Sander et al., 2003
	50 % RH	5.4×10^{-12}	Sander et al., 2003
	80 % RH	6.9×10^{-12}	Sander et al., 2003
$NO_2 + H \longrightarrow OH + NO$		1.3×10^{-10}	Sander et al., 2003
B. Photolysis Reactions			
$NO_2 \xrightarrow{h\nu} NO + O(^3P)$		$(1.6 \pm 0.1) \times 10^{-3}$	Measured ^b
$HONO \xrightarrow{h\nu} NO + OH$		$(4.9 \pm 1.4) \times 10^{-4}$	Measured ^c
$HONO_{(wall)} \xrightarrow{h\nu} NO + OH$		$(4.9 \pm 1.4) \times 10^{-4}$	Estimated
$O_3 \xrightarrow{h\nu} O_2 + O(^1D)$		$(4.7 \pm 0.1) \times 10^{-5}$	Calculated ^d
$HNO_{3(wall)} \xrightarrow{h\nu} HONO$		$(1.1 \pm 0.9) \times 10^{-5}$	Model Fit ^e
C. Surface Reactions			
$NO_{2(g)} + H_2O_{(g)} \longrightarrow HONO_{(wall)}$		$(2.4 \pm 0.4) \times 10^{-23}$	Model Fit ^f
$NO_{2(g)} + H_2O_{(g)} \longrightarrow HNO_{3(wall)}$		$(2.4 \pm 0.4) \times 10^{-23}$	Model Fit ^f
$HONO_{(wall)} + H_2O_{(g)} \longrightarrow HONO_{(gas)} + H_2O_{(g)}$		1.35×10^{-20}	Model Fit
$HONO_{(wall)} \longrightarrow NO_{(g)}$		8.0×10^{-4}	Model Fit
$HONO_{(g)} \longrightarrow HONO_{(wall)}$		2.0×10^{-4}	Measured
$HONO_{(wall)} + HNO_{3(wall)} \longrightarrow \text{Products}$		1.0×10^{-17}	Model Fit
$N_2O_5 \longrightarrow 2 HNO_{3(wall)}$		83	Calculated ^g
<p>a. Termolecular reactions with a third body are accounted for in the rate constants using $[M] = 2.46 \times 10^{19}$ molecules cm^{-3} to match experimental conditions. Rate constants are in the units of $cm^3 \text{ molec}^{-1} s^{-1}$ or s^{-1}.</p> <p>b. Experimentally measured as described in the text. Errors shown are 2s.</p> <p>c. Experimentally measured in the cell using cyclohexane as an OH scavenger. Errors shown are 2s.</p> <p>d. Calculated using an analogue of equation (IV).</p> <p>e. Included only at longer photolysis times; see text.</p> <p>f. The rates of these reactions were always taken as being equal; by expressing the production of HONO and HNO_3 separately, the first order kinetics in NO_2 and H_2O was captured.</p> <p>g. Equivalent to a reaction probability of 0.03.⁴⁶</p>			

FIGURE CAPTIONS

Figure 1. Schematic of the reaction mechanism of the heterogeneous hydrolysis of NO_2 proposed by Finlayson-Pitts et al.¹⁴ with the inclusion of competitive adsorption between water and HONO.³²

Figure 2. Typical data for the loss of NO_2 during photolysis plotted in the form of equation (I) (see text).

Figure 3. Typical first order plot for the photolysis of 1.2 ppm HONO in the presence of 135 ppm of cyclohexane.

Figure 4. Experimental concentration-time profiles for NO_2 (●), HONO (◆), and NO (▼) with 46 ppm initial $[\text{NO}_2]$ and 39% RH in 1 atm N_2 at 296 K. Error bar on HONO concentration is $\pm 2\text{s}$.

Figure 5. Comparison of experimental data (symbols) and model-predicted (solid lines) concentration-time profiles for NO_2 (●), HONO (◆), and NO (▼) with (a) 20 ppm initial $[\text{NO}_2]$ and 33% RH in N_2 (b) 46 ppm initial $[\text{NO}_2]$ and 39% RH in N_2 (c) and 54 ppm initial $[\text{NO}_2]$ and 57% RH in N_2 .

Figure 6. Experimental data (symbols) and model-predicted (lines) concentration-time profiles for NO_2 (●), HONO (◆), and NO (▼) with 46 ppm initial $[\text{NO}_2]$ and 39% RH in N_2 . The dotted line indicates the model prediction for HONO with the inclusion of photolysis of adsorbed HNO_3 , reaction (2). Error bar on HONO concentration is $\pm 2\text{s}$.

Figure 7. Experimental data (symbols) and model-predicted (lines) concentration-time profiles for NO_2 (●), HONO (◆), and NO (▼) of (a) 45 ppm initial $[\text{NO}_2]$ and 46% RH in N_2 and (b) 46 ppm initial $[\text{NO}_2]$ and 48% RH in air. The dotted line indicates the concentration of HONO with the inclusion of surface-adsorbed HNO_3 photolysis in model. Error bar on HONO concentration is $\pm 2\text{s}$.

REFERENCES

- 1 H. Akimoto, H. Takagi and F. Sakamaki. *J. Phys. Chem. A* 1987, **19**, 539.
- 2 X. Zhou, Y. He, G. Huang, T. Thornberry, M. Carroll and S. Bertman. *Geophys. Res. Lett.* 2002, **29**, DOI: 10.1029/2002GL015080.
- 3 X. L. Zhou, H. L. Gao, Y. He, G. Huang, S. B. Bertman, K. Civerolo and J. Schwab. *Geophys. Res. Lett.* 2003, **30**, 2217 DOI:10.1029/2003GL018620.
- 4 D. Perner and U. Platt. *Geophys. Res. Lett.* 1979, **6**, 917.
- 5 U. Platt, D. Perner, G. W. Harris, A. M. Winer and J. N. Pitts Jr. *Nature* 1980, **285**, 312.
- 6 A. M. Winer and H. W. Biermann. *Res. Chem. Intermed.* 1994, **20**, 423.
- 7 G. Lammel and J. Cape. *Chem. Soc. Rev.* 1996, **25**, 361.
- 8 R. M. Harrison, J. D. Peak and G. M. Collins. *J. Geophys. Res. Atmos.* 1996, **101**, 14429.
- 9 G. Lammel "Formation of Nitrous Acid: Parameterization and Comparison with Observations," Max-Planck-Institut-für Meteorologie, 1999.
- 10 C. Schiller, S. Locquiao, T. Johnson and G. Harris. *J. Atmos. Chem* 2001, **40**, 275.
- 11 J. Stutz, B. Alicke and A. Neftel. *J. Geophys. Res. Atmos.* 2002, **107**, DOI: 10.1029/2001JD000390.
- 12 B. Alicke, U. Platt and J. Stutz. *J. Geophys. Res.* 2002, **107**, DOI:10.1029/2000JD000075.
- 13 B. J. Finlayson-Pitts and J. N. Pitts *Chemistry of the Upper and Lower Atmosphere: Theory, Experiments, and Applications*, Academic Press, 2000.
- 14 B. J. Finlayson-Pitts, L. M. Wingen, A. L. Sumner, D. Syomin and K. A. Ramazan. *Phys. Chem. Chem. Phys.* 2003, **5**, 223.
- 15 P. G. Caudle and K. G. Denbigh. *Trans. Faraday Soc.* 1953, **49**, 39.
- 16 M. S. Peters and J. L. Holman. *Ind. Eng. Chem.* 1955, **47**, 2536.
- 17 R. F. Graham and B. J. Tyler. *J. Chem. Soc., Faraday Trans. I* 1972, **68**, 683.
- 18 C. England and W. Corcoran. *Ind. Eng. Chem.* 1974, **13**, 373.
- 19 F. Sakamaki, S. Hatakeyama and H. Akimoto. *Int. J. Chem. Kinet.* 1983, **15**, 1013.
- 20 J. N. Pitts, Sanhueza, E., Atkinson, R., Carter, W., Winer, A., Harris, W., and Plum, C. *Int. J. Chem. Kinet.* 1984, **16**, 919.
- 21 R. Svensson, E. Ljungstrom and O. Lindqvist. *Atmos. Environ.* 1987, **21**, 1529.
- 22 M. Jenkin, R. Cox and D. Williams. *Atmos. Environ.* 1988, **22**, 487.
- 23 C. Perrino, F. De Santis and A. Febo. *Atmos. Environ.* 1988, **22**, 1925.
- 24 A. Febo and C. Perrino. *Atmos. Environ.* 1991, **25**, 1055.
- 25 S. Mertes and A. Wahner. *J. Phys. Chem.* 1995, **99**, 14000.
- 26 P. Wiesen, J. Kleffmann, R. Kurtenbach and K. Becker. *Faraday Discuss.* 1995, **100**, 121.
- 27 R. Harrison and G. Collins. *J. Atmos. Chem.* 1998, **30**, 397.
- 28 J. Kleffmann, K. H. Becker and P. Wiesen. *Atmos. Environ.* 1998, **32**, 2721.
- 29 A. L. Goodman, G. M. Underwood and V. H. Grassian. *J. Phys. Chem. A* 1999, **103**, 7217.
- 30 W. S. Barney and B. J. Finlayson-Pitts. *J. Phys. Chem. A* 2000, **104**, 171.
- 31 A. L. Goodman, E. T. Bernard and V. H. Grassian. *J. Phys. Chem. A* 2001, **105**, 6443.
- 32 D. A. Syomin and B. J. Finlayson-Pitts. *Phys. Chem. Chem. Phys.* 2003, **5**, 5236.
- 33 J. Killus and G. Whitten. *Int. J. Chem. Kinet.* 1990, **22**, 547
- 34 J. U. White. *J. Opt. Soc. Am.* 1942, **32**, 285.
- 35 W. S. Barney, L. M. Wingen, M. J. Lakin, T. Brauers, J. Stutz and B. J. Finlayson-Pitts. *J. Phys. Chem. A* 2001, **105**, 4166.

- 36 W. S. Barney, L. M. Wingen, M. J. Lakin, T. Brauers, J. Stutz and B. J. Finlayson-Pitts. *J. Phys. Chem. A* 2000, **104**, 1692.
- 37 J. R. Holmes, R. J. O'Brien, J. H. Crabtree, T. A. Hecht and J. H. Seinfeld. *Environ. Sci. and Technol.* 1973, **7**, 519.
- 38 S. P. Sander, A. R. Ravishankara, R. R. Friedl, D. M. Golden, C. E. Kolb, M. J. Kurylo, M. J. Molina, R. E. Huie, V. L. Orkin, G. K. Moortgat and B. J. Finlayson-Pitts "Chemical Kinetics and Photochemical Data for Use in Atmospheric Studies. Evaluation Number 14," Jet Propulsion Laboratory, California Institute of Technology, 2003.
- 39 W. Braun, J. Herron and D. Kahaner. *Int. J. Chem. Kinet.* 1988, **20**, 51.
- 40 Bozzelli. *J. Chem. Ed.* 2000, **77**, 165.
- 41 M. J. Manka. *Alchemy Software* 2001, Wesley Chapel, Fl.
- 42 R. Atkinson, D. L. Baulch, R. A. Cox, J. N. Crowley, R. F. Hampson, J. A. Kerr, M. J. Rossi and J. Troe. *IUPAC Subcommittee on Gas Kinetic Data Evaluation for Atmospheric Chemistry* 2002, Chemical Kinetics Data Center.
- 43 W. Tsang and J. T. Herron. *J. Phys. Chem. Ref. Data* 1991, **20**, 609.
- 44 S. M. Aschmann, A. A. Chew, J. Arey and R. Atkinson. *J. Phys. Chem. A* 1997, **101**, 8042.
- 45 Y. Dubowski, A. L. Sumner, E. J. Menke, D. J. Gaspar, J. Newberg, R. C. Hoffman, R. M. Penner, J. C. Hemminger and B. J. Finlayson-Pitts. *Phys. Chem. Chem. Phys.* 2004, to be submitted.
- 46 J. H. Hu and J. P. D. Abbatt. *J. Phys. Chem. A.* 1997, **101**, 871.

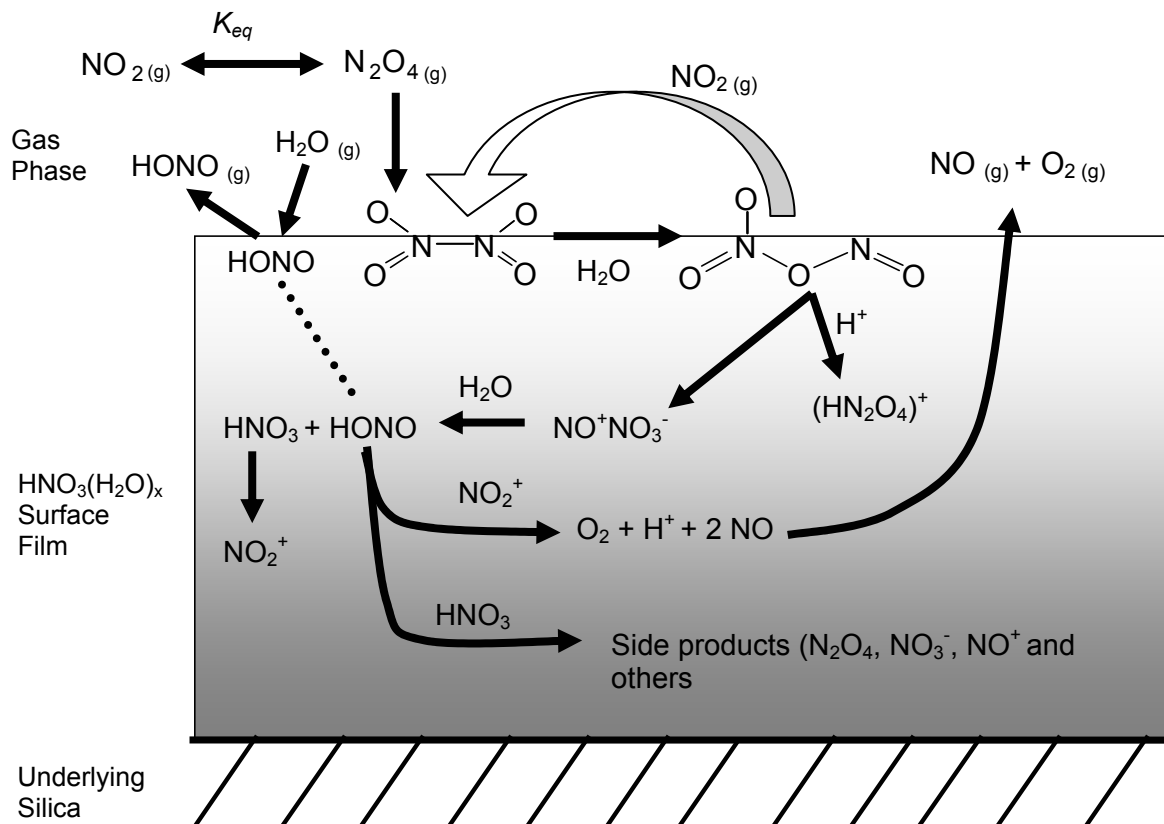


Figure 1. Schematic of the reaction mechanism of the heterogeneous hydrolysis of NO_2 proposed by Finlayson-Pitts et al.¹⁴ with the inclusion of competitive adsorption between water and HONO .³²

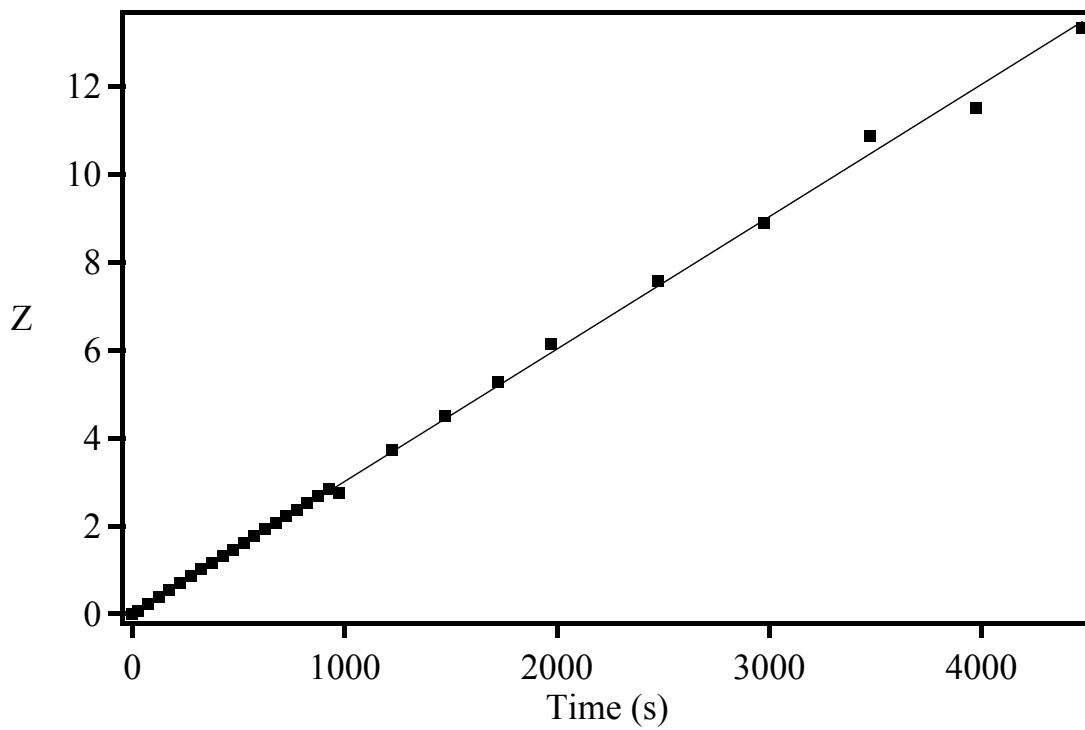


Figure 2. Typical data for the loss of NO_2 during photolysis plotted in the form of equation (I) (see text).

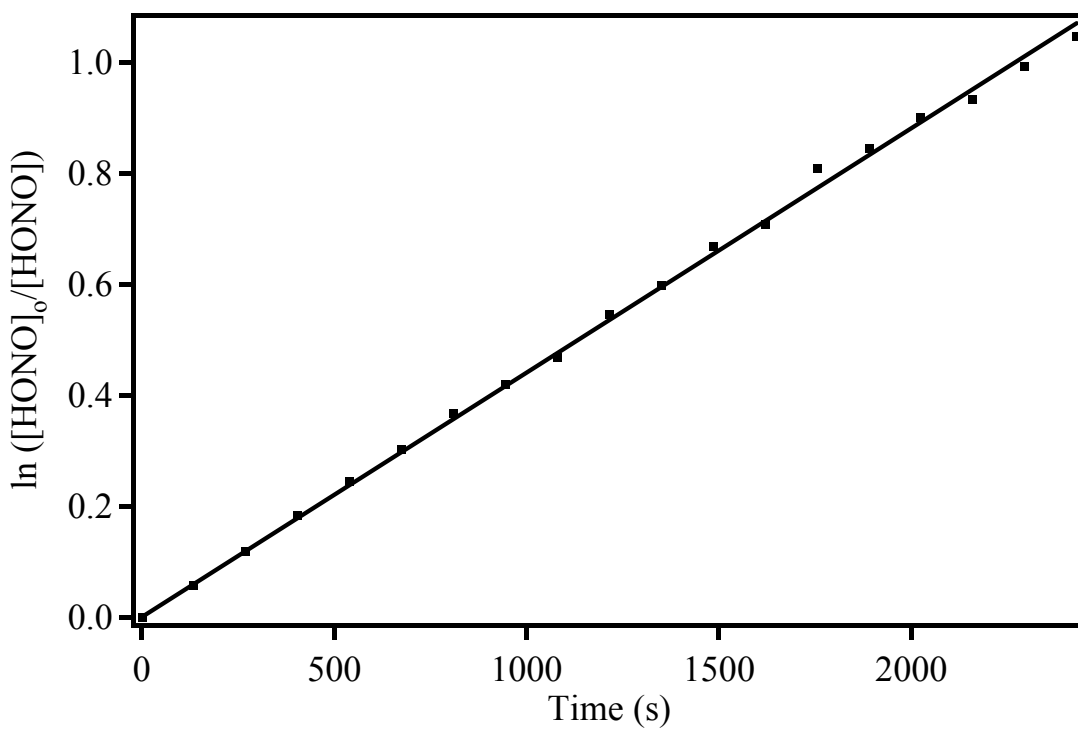


Figure 3. Typical first order plot for the photolysis of 1.2 ppm HONO in the presence of 135 ppm of cyclohexane.

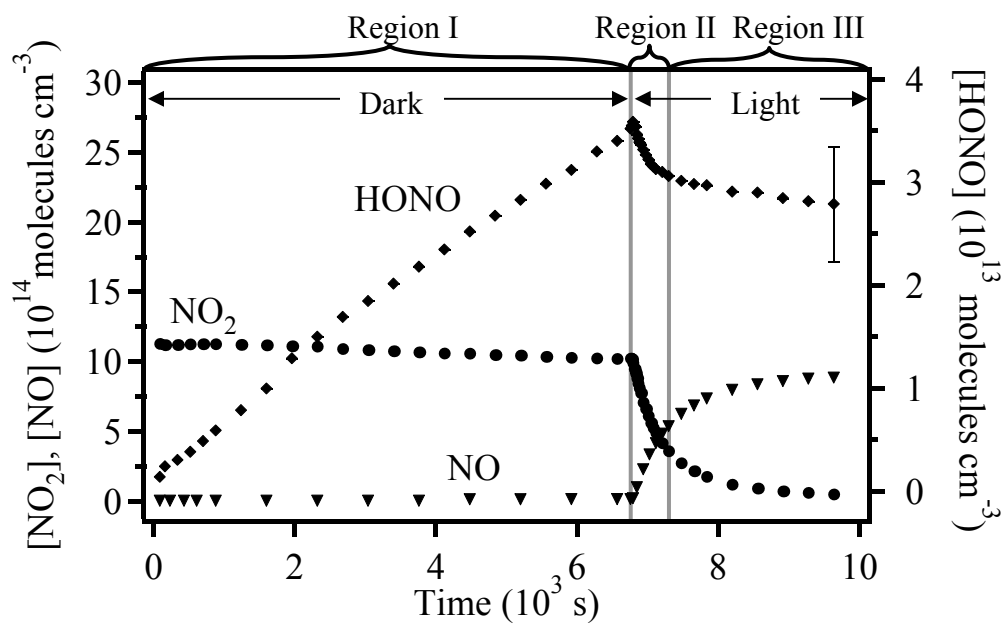


Figure 4. Experimental concentration-time profiles for NO_2 (\bullet), HONO (\blacklozenge), and NO (\blacktriangledown) with 46 ppm initial $[\text{NO}_2]$ and 39% RH in 1 atm N_2 at 296 K. Error bar on HONO concentration is ± 2 s.

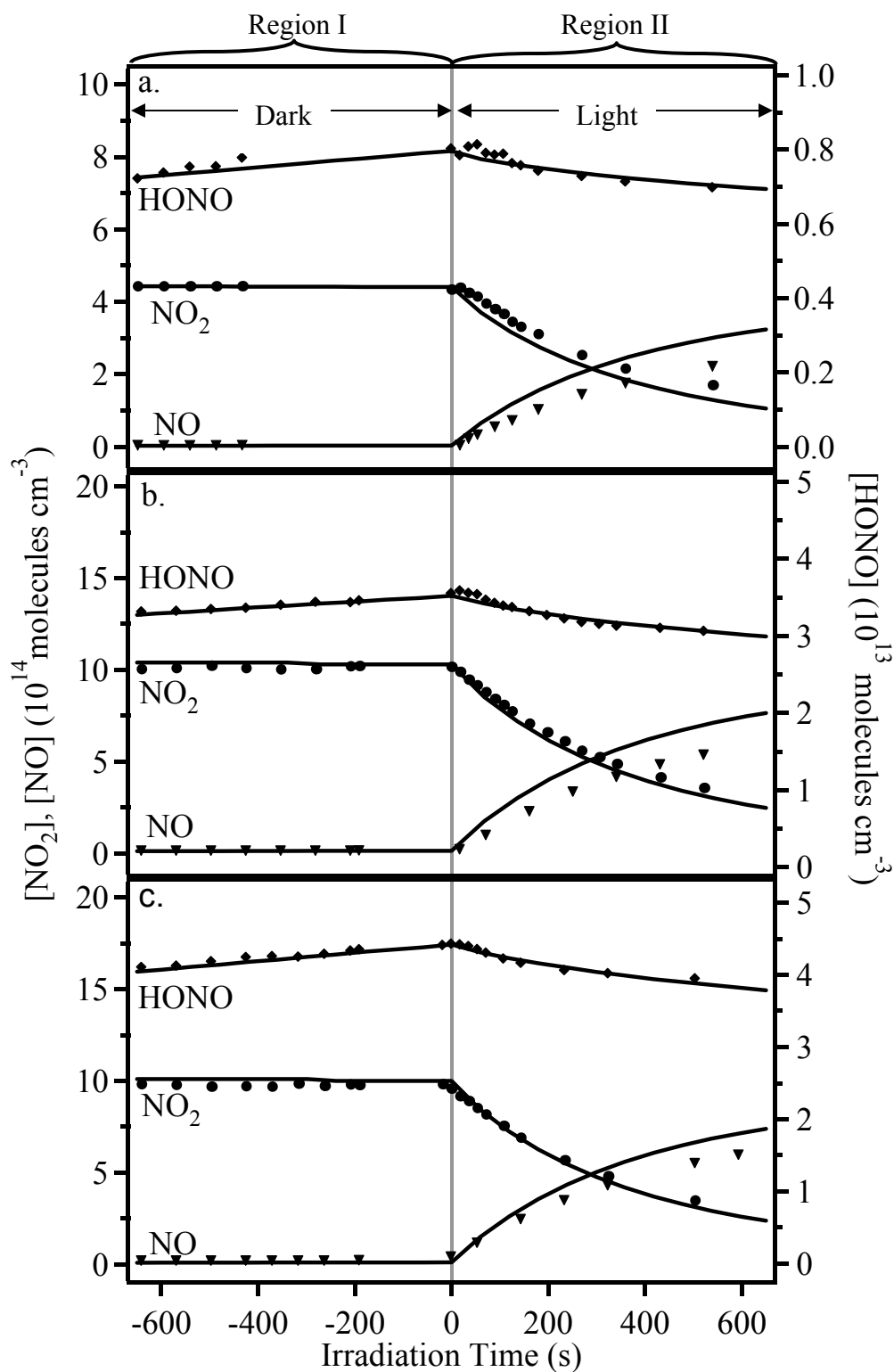


Figure 5. Comparison of experimental data (symbols) and model-predicted (solid lines) concentration-time profiles for NO_2 (\bullet), HONO (\blacklozenge), and NO (\blacktriangledown) with (a) 20 ppm initial $[\text{NO}_2]$ and 33% RH in N_2 (b) 46 ppm initial $[\text{NO}_2]$ and 39% RH in N_2 (c) and 54 ppm initial $[\text{NO}_2]$ and 57% RH in N_2 .

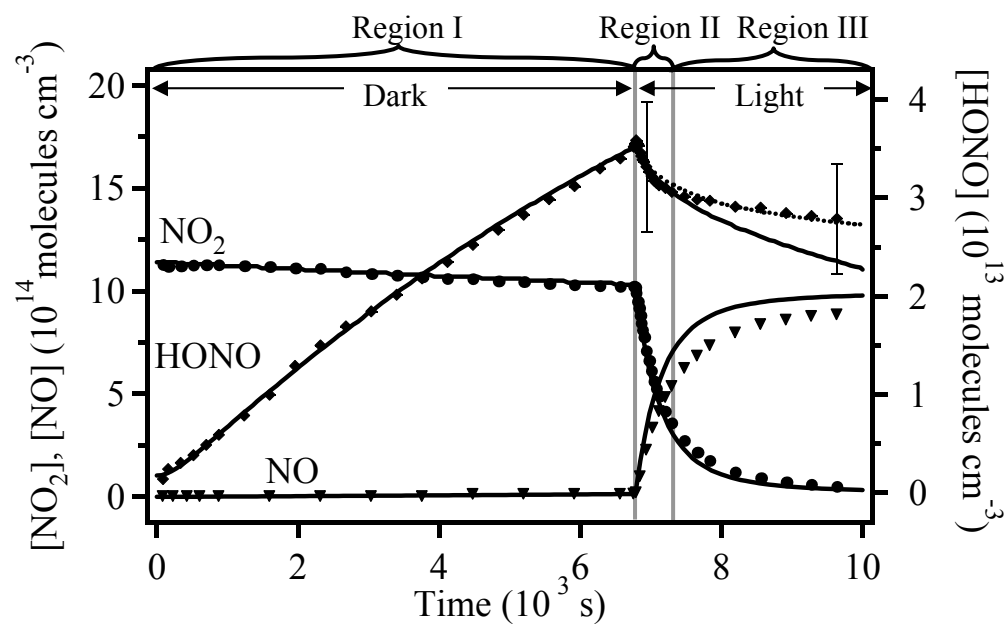


Figure 6. Experimental data (symbols) and model-predicted (lines) concentration-time profiles for NO_2 (\bullet), HONO (\blacklozenge), and NO (\blacktriangledown) with 46 ppm initial $[\text{NO}_2]$ and 39% RH in N_2 . The dotted line indicates the model prediction for HONO with the inclusion of photolysis of adsorbed HNO_3 , reaction (2). Error bar on HONO concentration is $\pm 2\text{s}$.

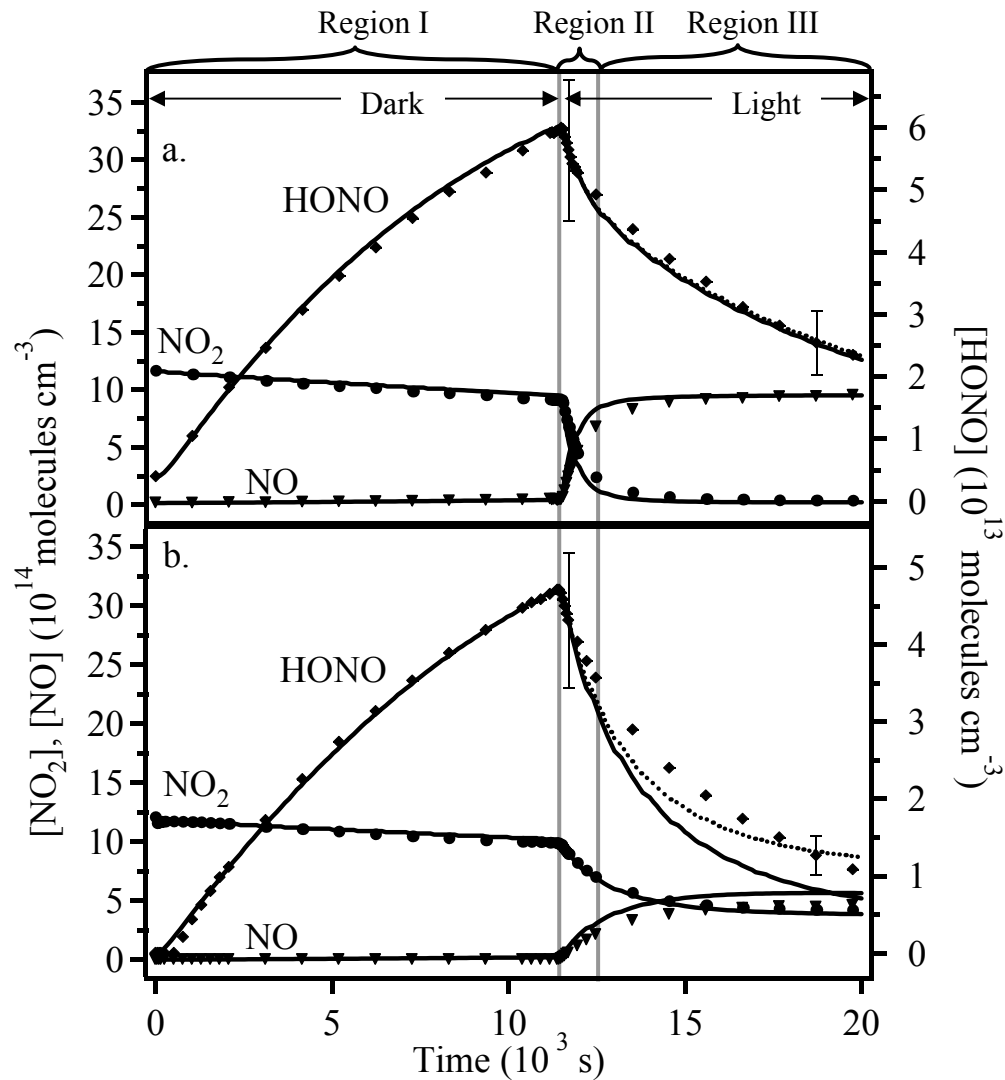


Figure 7. Experimental data (symbols) and model-predicted (lines) concentration-time profiles for NO_2 (\bullet), HONO (\blacklozenge), and NO (\blacktriangledown) of (a) 45 ppm initial $[\text{NO}_2]$ and 46% RH in N_2 and (b) 46 ppm initial $[\text{NO}_2]$ and 48% RH in air. The dotted line indicates the concentration of HONO with the inclusion of surface-adsorbed HNO_3 photolysis in model. Error bar on HONO concentration is $\pm 2\text{s}$.

The nature of water on surfaces of laboratory systems and implications for heterogeneous chemistry in the troposphere

Ann Louise Sumner,^a Erik J. Menke,^b Yael Dubowski,^b John T. Newberg,^b Reginald M. Penner,^b John C. Hemminger,^b Lisa M. Wingen,^b Theo Brauers^c and Barbara J. Finlayson-Pitts^{*b}

^a Battelle, 505 King Ave., Columbus, OH 43201-2693, USA

^b Department of Chemistry, University of California, Irvine, Irvine, CA 92697-2025, USA.

E-mail: bjfinlay@uci.edu; Fax: +1 (949) 824-3168; Tel: +1 (949) 824-7670

^c Institut für Atmosphärische Chemie (ICG3), Forschungszentrum KFA Jülich, D-52425 Jülich, Germany

Received 17th July 2003, Accepted 8th December 2003

First published as an Advance Article on the web 12th January 2004

A number of heterogeneous reactions of atmospheric importance occur in thin water films on surfaces in the earth's boundary layer. It is therefore important to understand the interaction of water with various materials, both those used to study heterogeneous chemistry in laboratory systems, as well as those found in the atmosphere. We report here studies at 22 °C to characterize the interaction of water with such materials as a function of relative humidity from 0–100%. The surfaces studied include borosilicate glass, both untreated and after cleaning by three different methods (water, hydrogen peroxide and an argon plasma discharge), quartz, FEP Teflon film, a self assembled monolayer of *n*-octyltrichlorosilane (C8 SAM) on glass, halocarbon wax coatings prepared by two different methods, and several different types of Teflon coatings on solid substrates. Four types of measurements covering the range from the macroscopic level to the molecular scale were made: (1) contact angle measurements of water droplets on these surfaces to obtain macroscopic scale data on the water-surface interaction, (2) atomic force microscopy measurements to provide micron to sub-micron level data on the surface topography, (3) transmission FTIR of the surfaces in the presence of increasing water vapor concentrations to probe the interaction with the surface at a molecular level, and (4) X-ray photoelectron spectroscopy measurements of the elemental surface composition of the glass and quartz samples. Both borosilicate glass and the halocarbon wax coatings adsorbed significantly more water than the FEP Teflon film, which can be explained by a combination of the chemical nature of the surfaces and their physical topography. The C8 SAM, which is both hydrophobic and has a low surface roughness, takes up little water. The implications for the formation of thin water films on various surfaces in contact with the atmosphere, including building materials, soil, and vegetation, are discussed.

I. Introduction

Heterogeneous processes in the troposphere have a substantial impact on trace gas concentrations. For example, a number of heterogeneous reactions, including the nitrogen dioxide hydrolysis reaction (1) and the reaction (2) of adsorbed nitric acid with gaseous nitric oxide,



occur in thin water films present on surfaces. Such reactions have been observed to depend on the water vapor concentration,^{1–5} which is reasonable since the relative humidity (RH) determines the equilibrium concentration of water on the surface.

The formation of nitrous acid in reaction (1) has been particularly well-studied in many different laboratories using a variety of reactors, surface materials, and coatings.^{2–22} HONO is a major source of the hydroxyl radical (OH) in polluted urban regions,^{23–29} which drives the chemistry of both remote and urban atmospheres. Since subsequent oxidation of organic compounds by OH radicals and other oxidants in the presence of nitrogen oxides and sunlight produce ozone as well as other secondary pollutants in the troposphere,³⁰

understanding the sources and sinks of HONO is critical for accurately modeling the troposphere and predicting future trace gas concentrations.

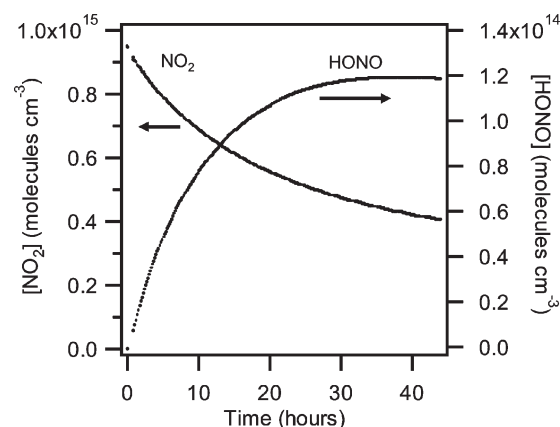


Fig. 1 Loss of NO_2 and formation of HONO at 24 °C from the heterogeneous hydrolysis of NO_2 on the surface of a 561 L chamber coated with halocarbon wax using the dip method. Measurements were made using differential optical absorption spectrometry (DOAS). Initial concentration of NO_2 was 38.6 ppm and the RH was 85%.

Fig. 1 shows an example of a study of reaction (1) carried out in this laboratory at 85% RH and 24 °C in a 561 L chamber, described previously,³¹ whose internal surfaces were coated with hydrophobic halocarbon wax. This coating is often used in laboratory studies as it is chemically inert, like Teflon, but can be easily applied and removed. Despite the fact that only small amounts of water would be expected on such a hydrophobic surface, loss of NO₂ and formation of HONO does indeed occur. Furthermore, when corrected to a common reaction chamber surface-to-volume ratio (S/V) and to an RH of 50%, the rate of HONO formation (4.5×10^{-2} ppb min⁻¹ per ppm NO₂) is in good agreement with rates measured in larger (5800 L) Teflon-coated smog chambers (3.9×10^{-2} ppb min⁻¹ per ppm NO₂),² and in smaller (7–19 L) borosilicate glass cells [$(2-4) \times 10^{-2}$ ppb min⁻¹ per ppm NO₂].⁵ This agreement is remarkable, given the very different nature of the chamber materials ranging from hydrophobic (Teflon, halocarbon wax) to hydrophilic (glass), for which different amounts of water might be expected to be available on the surface for reaction.

A prerequisite to fully understanding such heterogeneous processes is understanding the amount and nature of water on the surfaces. The goal of this work is therefore to elucidate the interaction of water at room temperature with some surfaces typically used in laboratory systems, and related materials, that can provide insight into the role of these thin films in atmospheric reactions. The materials studied include the following: (1) borosilicate glass as provided by the manufacturer; (2) borosilicate glass cleaned using water, hot H₂O₂, or an argon plasma discharge; (3) quartz; (4) thin FEP Teflon film; (5) halocarbon wax-coated glass using two different coating methods; (6) glass coated with a C8 organic self-assembled monolayer (SAM); and (7) several thick Teflon coatings applied to solid substrates. Four different types of measurements were made that provide insights from the macroscopic to molecular level. On a macroscopic scale, contact angle measurements of water droplets on these surfaces were obtained to examine the wettability of the surfaces. On a micron to sub-micron scale, atomic force microscopy (AFM) measurements provide insight into the surface structure. On the molecular level, transmission FTIR of the surfaces in the presence of increasing water vapor concentrations was used to probe the nature and amounts of water on the surfaces. Finally, X-ray photoelectron spectroscopy (XPS) was used to study the elemental surface composition of the glass and quartz samples for which water uptake measurements were made. The implications for understanding heterogeneous reactions in or on surface water films in

laboratory systems as well as extrapolation to atmospheric surfaces are discussed.

II. Experimental methods

A. Surface materials

The materials included in this study, many of which are commonly used in laboratory experiments, are summarized in Table 1. They include both hydrophilic and hydrophobic materials. The hydrophilic materials are thin cover slips of smooth glass (VWR Micro Cover Glasses) and quartz (Quartz Plus, Inc.). Cover glass discs were used because they were sufficiently thin that they did not significantly attenuate the infrared beam in the region of interest (above 2000 cm⁻¹). Standard borosilicate laboratory glass (Type I, Class A)³² used in many laboratory studies of heterogeneous reactions has a higher silica content, but like the cover slips, also contains small amounts of boron, sodium and aluminum oxides (see Table 1). The overall similarity between the Type I, Class A glass and the cover slips is such that using the latter to probe interactions with water is reasonable.

Measurements were conducted on the hydrophilic glass as received from the manufacturer, and also after employing three different treatments. In the first case, the glass discs were rinsed with Nanopure water (Barnstead, 18.1 MΩ cm) and dried in nitrogen (Oxygen Service Co., 99.999%). In the second case, the discs were cleaned for 35 minutes with an argon plasma discharge (Harrick Scientific Plasma Cleaner/Sterilizer PDC-32G, medium power). For the third treatment, which has been suggested for cleaning porous glass surfaces,³³ the discs were submerged in hot (85 °C) H₂O₂ (30%, Electron Microscopy Sciences, ACS Reagent Grade) for approximately 10 minutes, followed by thorough rinsing with Nanopure water and drying in the cell in a stream of dry nitrogen gas at 40 °C overnight.

A variety of hydrophobic materials were also analyzed for their water uptake characteristics. Halocarbon wax (Halocarbon Products Corp., Series 1500) samples were prepared in two ways, each utilizing the smooth glass discs as the substrate. For the “dip method,” the glass discs were dipped into melted halocarbon wax and mounted in the sample holder. The coated discs were then gently warmed with a heat gun until the wax appeared to flow freely to reduce the impact of air bubbles on the surface. The coated discs were cloudy to the eye but appeared to have a smooth and quite thick coating. The “solvent method” involved submerging the glass discs in a warm solution of halocarbon wax dissolved in

Table 1 Samples used for water uptake measurements and surface characterization

Material	Description	Chemical composition	Source
Smooth glass	Micro cover glasses, No. 1, 25 mm dia. × 0.13–0.17 mm	64% SiO ₂ , 9% B ₂ O ₃ , 7% ZnO, 7% K ₂ O, 7% Na ₂ O, 3% TiO ₂ , 3% Al ₂ O ₃	VWR Scientific, Inc., Buffalo Grove, IL
Laboratory glass ^a	Designation E438-92: specification for Type I, Class A ³²	81% SiO ₂ , 13% B ₂ O ₃ , 4% Na ₂ O, 2% Al ₂ O ₃	ASTM International West Conshohocken, PA
Quartz	Quartz cover slips substrate grade, 25 mm dia. × 0.16 mm	Corning 7980 Synthetic Fused Silica: > 99.9% SiO ₂	Quartz Plus, Inc. Brookline, NH
Halocarbon wax	Series 1500	Polychlorotrifluoroethylene	Halocarbon Products Corp. River Edge, NJ
FEP film	2 mil FEP Teflon film	Fluoropolymer	Norton Performance Plastics
Organic SAM	C8 self assembled monolayer	<i>n</i> -octyltrichlorosilane: 95%	Geselt
FEP coating	FEP Teflon coating CCI-109	Fluoropolymer	Crest Coating Inc. Anaheim, CA
PFA coating	PFA Teflon coating	Fluoropolymer	Crest Coating, Inc. Anaheim, CA
Fluoropolymer coating	FluoroPel PFC801A	Fluoropolymer	Cytonix Corp. Beltsville, MD

^a Data provided for comparison.

dichloromethane (EM Science, 99.8%). The samples were also gently heated with a heat gun. The resulting coating was hazy to the eye, but obviously much thinner than the coating using the dip method.

Samples of thin FEP Teflon film (Norton High Performance Films) were supported by thin halocarbon wax-coated aluminum washers for the infrared study. The Teflon film was pressed onto the warm halocarbon wax coating, which held the film firmly in place, and the excess film removed.

Self-assembled monolayers of *n*-octyltrichlorosilane (Geselt, 95%) were deposited on borosilicate glass discs according to a well-established technique.³⁴ Briefly, the glass discs were cleaned with boiling ethanol, then with boiling chloroform. The dry glass was further cleaned with an argon plasma discharge for 30 minutes. Upon removal from the plasma cleaner, the substrates were stored in Nanopure water until deposition of the monolayer was carried out. After drying the surfaces with nitrogen, the discs were placed in a mM solution of *n*-octyltrichlorosilane in dodecane for 10 min. The C8 SAM-coated discs were then placed in boiling chloroform to remove any physisorbed material. The coating and chloroform extraction steps were repeated two additional times to ensure a smooth, well-ordered coating.

Three additional hydrophobic materials, two Teflon spray-coated materials and a fluoropolymer coating, were also studied. Such coatings are commonly used in laboratory systems, such as in smog chambers,^{2,12} in which many studies of atmospheric reactions have been carried out. Due to the substrate material (metal and thick glass), these materials could not be probed by infrared spectroscopy. However, analysis of the wetting and surface characteristics could still be studied as described in sections II B and C, respectively. The Teflon spray-coated materials, Teflon FEP CCI-109 and PFA Teflon, were used as received from the manufacturer. The third material, a fluoropolymer coating, was applied as a 1% FluoroPel PFC 801A emulsion in a fluoropolymer to a glass microscope slide.³⁵ The coating was then annealed at 90 °C and the solvent evaporated.

B. Water contact angle

Surface wettability of the materials described above was probed by contact angle measurements using water droplets. Quasi-equilibrium contact angles of sessile 1 μ L Nanopure water droplets were measured under ambient conditions with a Kodak DCS 315 camera equipped with a long-range microscope (Infinity Optics). The shape of the droplet depends on its interaction with the surface.³⁶ The line tangent to the curve of the droplet to the point where it intersects the solid surface forms the contact angle. A water droplet resting on a hydrophobic surface would form a spherical droplet having a high contact angle, but would have a much smaller contact angle when placed on a more hydrophilic surface.

C. Surface characterization

Atomic force microscopy (AFM) was used to probe the physical topography of the air/solid interface of the samples described above. Samples were imaged with a Park Scientific Instruments (PSI) Autoprobe LS Atomic Force Microscope under ambient conditions. The images were obtained in either contact mode with PSI Ultralever B tips, with the tip force set to approximately 25 nN, or in non-contact mode with PSI Ultralever C tips. In contact mode, each 256 \times 256 pixel image took approximately 5 min to obtain, with a scan rate of 1 Hz in the fast (horizontal) direction. In non-contact mode, each 256 \times 256 pixel image took approximately 10 min, with a scan rate of 0.5 Hz. RMS roughness values were calculated using the PSI ProScan software on background corrected AFM images. Background correction involved the fitting of each

scan line in an AFM image with a second order polynomial, and the subtraction of this best fit curve from the raw data. This procedure left intact all surface roughness on a length scale smaller than one-half the image size, but it removed lower frequency noise and the tube curvature artifact from the data. No Fourier filtering of AFM images was carried out.

D. Water uptake measurements

The amount of liquid water adsorbed on the surfaces was determined as a function of relative humidity by transmission Fourier transform infrared spectroscopy (FTIR). The samples of interest were positioned within a glass cell enclosed with 32 mm diameter ZnSe windows, as shown in Fig. 2. The cell had an 11 cm path length and could accommodate thin, disc-shaped, samples with a diameter up to 2.5 cm. The center O-ring permitted installation and removal of the samples, which were positioned an average of 6 mm apart in thin slots cut in a glass holder and secured with small amounts of halocarbon wax. Up to ten samples could be mounted in the cell, allowing for the measurement of water uptake on a total of 20 surfaces. All gas flows through the cell were set using calibrated flow meters (Matheson TF 1050). A type-K thermocouple with an Omega HH202A digital readout ($\pm 0.25\%$ reading $+0.2^\circ\text{C}$) was positioned inside the cell to monitor the cell temperature during experiments. All measurements were conducted at atmospheric pressure under dynamic conditions with a total flow rate of 200 mL min⁻¹.

The relative humidity in the cell was set by mixing flows of dry and 100% RH nitrogen, obtained by passing N₂ through Nanopure water in two borosilicate glass fritted bubblers, in series. The bubblers were kept in a water bath set at $22.0 \pm 0.2^\circ\text{C}$ (MGW Lauda MT) to reduce the effects of evaporative cooling. The temperature of the cell in the FTIR sample compartment, which was normally 3 °C warmer than the room, was cooled by passing the spectrometer purge gas (25 L min⁻¹ flow rate) through a stainless steel coil in a temperature controlled bath (MGW Lauda RCS) set at 8 °C. Heat tape was wrapped around the glass cell and used to fine-tune the cell temperature, which was maintained at $22.0 \pm 0.2^\circ\text{C}$. The use of Teflon tubing was minimized in favor of non-porous materials including glass and stainless steel. This was intended to reduce the degassing of water vapor from within the porous Teflon walls and also the permeation of room air through the tubing. The KBr windows separating the spectrometer's sample and interferometer/detector compartments were removed; even under fast dry nitrogen purge, the KBr windows held variable amounts of liquid water, which generated an irreproducible signal that was often significant compared to the water adsorbed on the samples of interest.

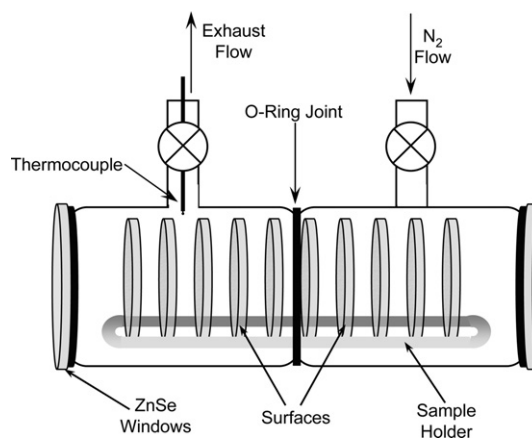


Fig. 2 Cell used for measurements of water uptake on glass and other surfaces.

Spectra of the glass and other materials in equilibrium with humidified N₂ were obtained as interferograms at 1 cm⁻¹ resolution on an FTIR spectrometer (Mattson, Galaxy 5020) equipped with a liquid nitrogen cooled mercury cadmium telluride detector. The samples were dried in the cell overnight under a flow of dry N₂ (200 mL min⁻¹) at 40 °C. To ensure that the nitrogen was completely dry, the vapor above liquid N₂ (Airgas, 55 psi) was used. After cooling the cell to 22 °C, a background spectrum of 2048 scans was obtained each day, with a flow of dry nitrogen through the cell. The dry and humid nitrogen flows were then set to the desired relative humidity and flow through the cell was established. Sample spectra of 1024 scans were obtained at each relative humidity after an equilibration time of 15 min.

Water vapor spectra for subtraction were also measured with the samples removed from the glass cell. During water vapor spectra collection, an optical filter was used to remove IR radiation below 2000 cm⁻¹. Infrared radiation was reflected off the cell windows and returned to the interferometer where it was remodulated and its phase shifted by 180°. This phenomenon has been described by Griffiths and de Haseth³⁷ and was observed in this system as negative peaks in the 3200 cm⁻¹ region; the peaks resulted from the water bend in the 1600 cm⁻¹ region that were frequency-doubled upon remodulation. The optical filter was constructed from three borosilicate glass discs (described above) that were held together with halocarbon wax. The outer surfaces were covered with FEP Teflon film to minimize water uptake on the filter. The FEP film was roughened with 1 μm diamond polishing paper to eliminate multiple reflections within the film, as described below. The optical filter efficiently absorbed the IR radiation at wavenumbers below 2000 cm⁻¹ that had caused the interference. Any small amounts of liquid water that may have been present on the ZnSe windows or the optical filter were subtracted from the sample spectra, along with water vapor.

A problem that often arises with the use of thin parallel surfaces in transmission IR spectroscopy is multiple reflection of the IR radiation between the two surfaces.³⁷ The multiple reflections cause interference fringes on either side of the centerburst in the interferograms and result in sinusoidal noise peaks in the single beam and absorbance spectra. Replacing these fringes in the interferogram with zeros before the Fourier transform is performed has the effect of removing the interference pattern from the single beam spectrum.³⁷ While this zero-filling procedure adds small amounts of noise to the spectrum, the final result is much more useful. Thus, interference fringes were typically removed from the interferogram before performing the Fourier transform, for which 5064 interferogram data points were used to calculate 4 cm⁻¹ resolution single beam spectra. Absorbance spectra were obtained by ratioing the single beam spectrum for a given relative humidity to the background spectrum from that day. Although the noise that resulted from the internal reflections in the quartz samples was apparent in the single beam spectra, it was not visible in the ratioed absorbance spectra. Interference fringes were not produced for the halocarbon wax dip method samples whose surfaces were not smooth, and hence did not have interference from multiple internal reflections.

E. X-ray photoelectron spectroscopy

X-ray photoelectron spectroscopy (XPS) was used to probe the elemental composition of the air/solid interface of the glass (both untreated and cleaned/treated) and quartz samples to provide insight into the changes induced by each treatment technique. X-ray photoelectron spectra of the surfaces were obtained in an ESCALAB MKII ultra-high vacuum (UHV) instrument (VG Scientific) equipped with three individually pumped chambers, allowing for rapid transfer (<1 h) of samples from atmospheric to UHV pressures. Sample surfaces

were irradiated under UHV (5 × 10⁻¹⁰ Torr) with 1486.6 eV X-rays from an aluminum anode at 15 keV and 20 mA. The kinetic energies of the ejected photoelectrons were analyzed using a 150 mm hemispherical electron energy analyzer. Data collection and analysis were carried out using the software package PISCES (Dayta Systems Ltd.). XPS peak areas were integrated after a linear background subtraction. The surface concentrations were determined by dividing the integrated areas by standard sensitivity factors (relative to an F(1s) sensitivity factor of 1.0).^{38,39} The sensitivity factors used are as follows: O(1s), 0.721; Si(2p), 0.355; C(1s), 0.306; B(1s), 0.165; Zn(2p_{3/2}), 3.734; K(2p_{3/2}), 1.013; Na(1s), 1.655; Ti(2p_{3/2}), 1.360; Al(2p), 0.246. Due to the uncertainty in the sampling depth for each element, the surface composition should be considered semi-quantitative.

III. Results

A. Contact angles for the surfaces with water

Interaction of water with the surfaces studied here on a macroscopic scale can be characterized by the contact angle. Fig. 3 shows the results of three typical contact angle measurements made for a hydrophobic surface (halocarbon wax, Fig. 3a), a hydrophilic surface (plasma-cleaned borosilicate glass, Fig. 3c) and an intermediate surface (untreated borosilicate glass, Fig. 3b). As expected, the contact angle is large for the hydrophobic surface and small for the hydrophilic surface. The intermediate contact angle measured for the untreated borosilicate glass is indicative of organic contamination on the surface, as supported by XPS measurements discussed below.

Table 2 summarizes the measured contact angles for the various materials. They can be grouped into three categories: (1) high contact angles (>80°) measured for the halocarbon wax, Teflon coatings and a C8 SAM on solid substrates, (2) low contact angles (<10°) exemplified by the cleaned borosilicate glass, and (3) intermediate values represented by the untreated borosilicate glass, the water-rinsed glass and quartz.

B. AFM measurements of the surface morphology

Figs. 4 and 5 show typical AFM images of representative surfaces. For each sample the root mean square (RMS) surface roughness was calculated as follows:

$$R_{\text{RMS}} = \sqrt{\frac{\sum_{n=1}^N (z_n - \bar{z})^2}{N}} \quad (1)$$

where \bar{z} is the average z height and N is the number of points sampled. However, it should be noted that these are minimum values since, in many cases, the pores on the surfaces appear to be quite deep and the tip may not have fully probed the depth

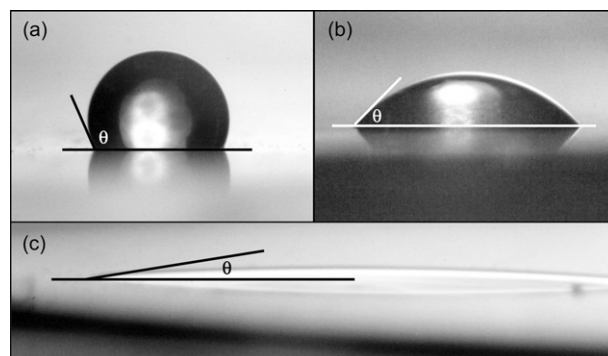


Fig. 3 Contact angle measurements of a 1 μL water droplet on three typical borosilicate glass surfaces: (a) halocarbon wax coated using the dip method, (b) untreated, and (c) plasma-cleaned.

Table 2 Summary of contact angle and AFM measurements.

Sample	Water contact angle/ $^{\circ}$	Surface roughness ^a average $\pm 1 s/\text{\AA}$
Hydrophilic samples		
Untreated glass	$32 \pm 2 (1 s)$	10 ± 5
Water-rinsed glass	25	9 ± 3
Plasma-cleaned glass	<10	11 ± 2
H ₂ O ₂ -cleaned glass	<10	20 ± 1
Quartz	$22 \pm 4 (1 s)$	62 ± 0.3
Hydrophobic samples		
Halocarbon wax: dip method	92	$> 145 \pm 13^b$
Halocarbon wax: solvent method	83	$> 24^b c$
Thin FEP Teflon film	109	$> 72 \pm 1^b$
C8 SAM	98	9 ± 1
FEP Teflon film	102	$(160 \pm 24)^d$
PFA Teflon coating	112	$(699 \pm 18)^d$
Fluorofel PFC 801A coating	111	$(126 \pm 18)^d$

^a Measured in non-contact mode on $5 \mu\text{m} \times 5 \mu\text{m}$ sections. ^b Minimum value since AFM image (Fig. 5) suggests tip may not fully probe the minimum depth of the pores. ^c Much of the surface had what appeared to be particles embedded in the film, which could have been dust picked up during the coating. If these regions are included, the average roughness increases to $77 \pm 76 \text{\AA}$. This is again a minimum value since the AFM tip may not fully probe the depth of pores. ^d Contact mode measurements made on $2 \mu\text{m} \times 2 \mu\text{m}$ sections. Smaller surface roughness is typically measured in contact mode because topographic features that are associated with weakly adsorbed species such as water, surface structures, etc. are swept away by the tip which exerts appreciable force on the surface and thus wipes the surface as the image is being acquired.

of such pores. In addition, the values obtained depend on the particular portion of the surface scanned, and for irregular surfaces, this may vary from region to region. In general, as the size of the surface that is scanned increases, larger corrections for the low-frequency undulations of the surface are required. This increases the uncertainty of the RMS roughness value. As a result, these values can also be sensitive to the size of the area that is scanned. The average and standard deviation ($1 s$) values of surface roughness are summarized in Table 2, along with the areas used in each case.

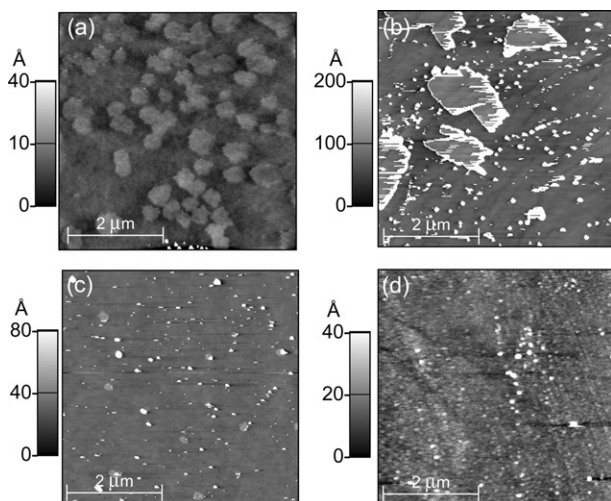


Fig. 4 AFM measurements (in non-contact mode) of the surface morphology for (a) untreated borosilicate glass; (b) untreated quartz; (c) borosilicate glass cleaned using hot H₂O₂; (d) borosilicate glass coated with the C8 SAM.

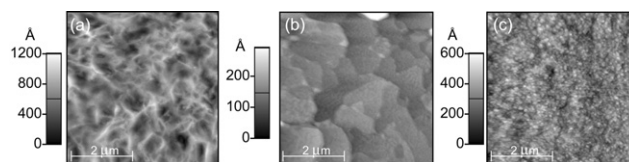


Fig. 5 AFM measurements (in non-contact mode) of the surface morphology for (a) borosilicate glass coated with halocarbon-wax using the dip method; (b) borosilicate glass coated using the solvent method and (c) FEP Teflon film.

C. Infrared measurements of water uptake

Fig. 6 shows typical infrared spectra for samples through which there was sufficient transmission of the infrared beam to make measurements of the weak absorptions due to water on the surface. The broad features from $2800\text{--}3800 \text{ cm}^{-1}$ are due to OH stretching vibrations in condensed phase water.^{40–44} The sharp peaks from $3500\text{--}3900 \text{ cm}^{-1}$ are residuals due to subtraction of gas phase water. It has been shown that small thermal instabilities in the HeNe laser of the spectrometer, to which the absorption wavenumbers are referenced, can lead to shifts of up to $\pm 0.034 \text{ cm}^{-1}$ in the sharp rotational lines of gas phase water.⁴⁵ This made complete subtraction of the water impossible. However, this imperfect subtraction does not contribute significantly to the liquid water peak area since these sharp peaks are approximately equally positive and negative.

For comparison, the spectrum of bulk liquid water, obtained by placing a drop of water between two ZnSe windows, is also shown in Fig. 6-1a. At 80% RH, the peak positions and band shapes of water adsorbed on quartz, untreated glass, water-rinsed glass, and plasma-cleaned glass as well as the halocarbon wax coatings are similar to that of bulk liquid water. The peak on the H₂O₂ cleaned glass (Fig. 6-2d) is red-shifted significantly to 3200 cm^{-1} . The C8 SAM and FEP Teflon film (Fig. 6-3i and 6-3j) take up much smaller amounts of

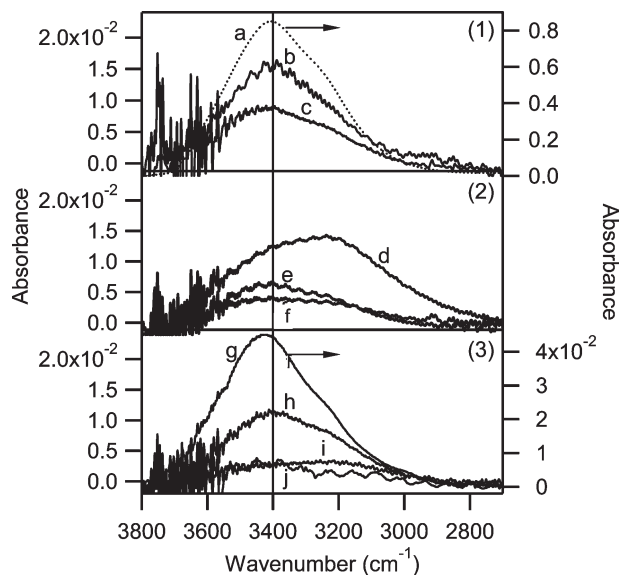


Fig. 6 Infrared spectra of surfaces in contact with N₂ at 80% RH and, for comparison, the spectrum of bulk liquid water: (1) bulk water (a, right axis), untreated glass (b), quartz (c); (2) H₂O₂ cleaned glass (d), plasma cleaned glass (e), and water rinsed glass (f); (3) dip method halocarbon wax (g, right axis), solvent method halocarbon wax (h), C₈ monolayer (i), and FEP Teflon film (j). The bulk water spectrum (1a) was obtained by measuring the IR transmission through a drop of water “sandwiched” between two ZnSe windows ratioed to the bare windows.

water; the peak for the water film on the C8 SAM is also red-shifted.

The liquid water peak can be used to estimate the number of water layers present on the surface as a function of relative humidity. The water coverage, θ , in number of layers, is calculated from the absorbance spectra using eqn. (II), a modified form of Beer's law,⁴⁶

$$\theta = \frac{2.303A}{NS_{\text{H}_2\text{O}}\bar{\sigma}} \quad (\text{II})$$

where N is the number of surfaces in the infrared beam and $S_{\text{H}_2\text{O}}$ is the surface density of one water monolayer (1.0×10^{15} molec cm^{-2}). The base-10 integrated absorbance, A , of the liquid water peak (from 2800 to 4000 cm^{-1}) is determined from the absorbance spectra. The integrated cross section, $\bar{\sigma}$ (to base e) was calculated for the same range to be 1.43×10^{16} $\text{cm}^2 \text{molecule}^{-1}$ from optical constants reported by Downing and Williams.⁴⁷

As shown in previous studies¹ and observed again in the present work (data not shown), the shape and peak position of the infrared spectrum of water on borosilicate glass change as the relative humidity is lowered. The peak becomes broader and shifts to higher wavenumbers. This is similar to observations of water uptake on other solids such as NaCl,^{46,48,49} where the peak due to water condensed on the surface blue-shifts towards the gas phase absorption peak at low water coverages. This indicates disruptions in the 3-D hydrogen bonding network and strong interactions of the adsorbed water with the surface.^{50,51} Similar results were observed in the present studies for water on plasma-cleaned glass, quartz, halocarbon wax, and Teflon film.

The absorption coefficients of water increase by approximately an order of magnitude from gas phase to bulk liquid water, and again from liquid to ice.^{52,53} The true value of the integrated cross section for a structured, thin water film on a surface is likely to be different from the bulk water value and to vary with coverage. However, the island-like features in the AFM data (Fig. 4a) provide additional insight into the amount of liquid water present on glass, at least at RH above 60%, and further analysis indicates that the estimate using the infrared absorption coefficient for liquid water is reasonable. Island-like features similar to those shown in Fig. 4a have been observed on surfaces such as mica in the presence of water vapor and have been attributed to islands of water on the surface.⁵⁴ The features in Fig. 4a are typically 1.2 nm in height, corresponding to islands of water about three layers high. (The fraction of the surface covered with such islands was somewhat variable, likely reflecting variability in the relative humidity in the laboratory from day to day). The estimated number of layers of water using FTIR under similar conditions is 1.4, but this assumes an equal distribution of water over the surface. Given that AFM indicates that about half of the surface is covered with water islands, the amounts of water on the surface estimated using AFM and FTIR are consistent. To emphasize that the water measured using FTIR is not necessarily equally distributed over the surface, we express these data in terms of an "equivalent number of water monolayers".

For the H_2O_2 -cleaned glass, there is a significant red-shift in the infrared peak at all relative humidities, in contrast to the other surfaces. Such a shift is characteristic of water with a more ice-like structure.⁴⁰⁻⁴⁴ There may be shoulders on the low wavenumber side of the water peaks for plasma-cleaned glass, quartz and the solvent-coated halocarbon wax as well (Fig. 6).

Fig. 7 shows the equivalent number of water monolayers on the glass after various treatments, on quartz, and on halocarbon wax coatings prepared by different methods.

The results for water uptake on quartz are in excellent agreement with the previously reported results of Awakuni

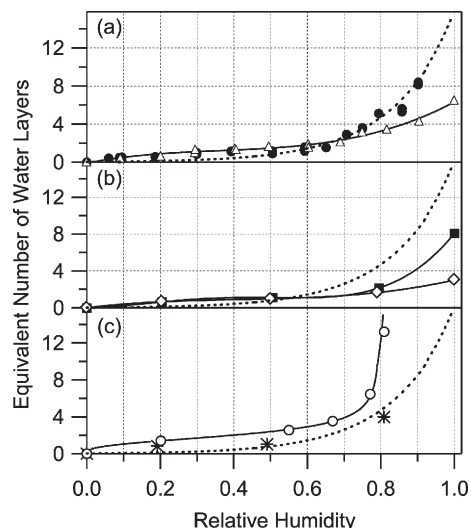


Fig. 7 Water uptake isotherms for (a) smooth untreated glass (solid circles) and quartz (open triangles); (b) water rinsed glass (open diamonds), and plasma cleaned glass (solid squares); and (c) dip method (open circles) and solvent method (asterisks) halocarbon wax coated glass. The dashed black line for the untreated borosilicate glass data in (a) is included in each panel as a guide for the eye. The solid lines are fits to each set of data, excluding the solvent method halocarbon wax, which falls on the fit for untreated glass. The dip method halocarbon wax data points (panel (c)) were taken after two hours equilibration time, although water uptake was still increasing for the high RH experiments (see text and Fig. 9).

and Calderwood.⁵⁵ Fig. 7b shows data for two of the treated glass samples. (The isotherm for H_2O_2 -cleaned glass is shown later.) Water coverage of these surfaces is similar to that of the untreated borosilicate glass up to approximately 60% RH, but is significantly smaller above 80% RH and does not show evidence of condensation as 100% RH is approached. Fig. 7c shows comparable data for the halocarbon wax coated surfaces. The halocarbon wax coating prepared by both the dip and solvent methods show evidence of multilayer adsorption similar to the untreated borosilicate glass.

As seen from the spectra in Fig. 6, the peak for the H_2O_2 -treated glass is red-shifted quite substantially from that for bulk liquid water. This increases the uncertainty of the application of absorption coefficients for bulk, liquid water sufficiently that we chose not to estimate the number of monolayers using eqn. (II). However, one can examine the shape of the isotherm by using the measured absorbance of the band as a function of RH, as shown in Fig. 8 along with the isotherm for untreated glass. The dependence of the water uptake on RH is quite

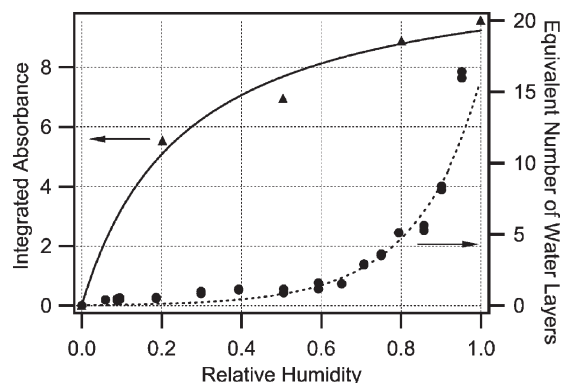


Fig. 8 Relative intensity of the liquid water peak, integrated from 2600–4000 cm^{-1} , on H_2O_2 -cleaned borosilicate glass surface (triangles) as a function of relative humidity. The solid line is a fit to the data. Also shown for comparison is the isotherm for water uptake on untreated glass and the fit shown also in Fig. 7a as a guide.

different than for the untreated borosilicate glass, with the shape of water uptake on H₂O₂-treated glass resembling a Langmuir isotherm.^{56–58}

While most surfaces came to equilibrium with water vapor within 15 minutes, the dipped halocarbon wax coating continued to take up water over more than an hour at higher relative humidities, as shown in Fig. 9. This is especially apparent at 81% RH, as water continued to adsorb to the surface even after 2 hours of exposure.

D. XPS analysis of surfaces

In order to assess the impact of the three cleaning methods applied to borosilicate glass, XPS measurements were made on the glass samples and, for comparison, the quartz sample. Fig. 10 shows the molar ratio of the major elements to the oxygen peak in each case. In the case of the quartz sample, the Si:O ratio is within experimental uncertainty of the expected SiO₂ stoichiometry. The more complex borosilicate glass samples show the expected large number of elements at the surface. As is common with surface analysis, there is always some adventitious carbon on the surfaces. However, clearly the H₂O₂ and plasma cleaning removed significant amounts of carbon from the surface.

As expected, quartz consists primarily of silica; small amounts of Na and Mg were also observed but may arise from contamination during sample handling and preparation. The borosilicate glass has substantial amounts of Na, B, K, and Zn. The surface of water-rinsed glass is similar in composition to that of untreated glass, with somewhat smaller Na. The increase in sodium for the plasma cleaned sample may result from the deposition of sodium from the inner chamber of the plasma cleaner, which is made of glass. Cleaning using H₂O₂ removes the B and K from the surface and substantially decreases the surface Zn and Na.

IV. Discussion

The goal of this work is to understand the interaction of water with various surfaces often used in laboratory studies of heterogeneous reactions that occur in thin water surface films at room temperature. As discussed in detail elsewhere,⁵ rates of NO₂ hydrolysis calculated for experiments, such as that shown in Fig. 1, conducted in chambers of various sizes and wall composition can be compared after normalizing the rate for the surface-to-volume ratios of the reactors, the initial NO₂ concentrations, and the RH. Interestingly, the normalized rates of the heterogeneous hydrolysis of gaseous NO₂ that were measured in large smog chambers coated with hydrophobic Teflon^{2,12} and in much smaller hydrophilic Pyrex cells⁵

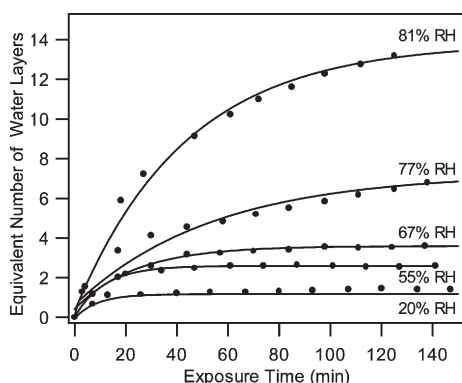


Fig. 9 Water uptake on halocarbon wax, (dip method) as a function of the exposure time to humidified nitrogen between 20% and 81% RH. The lines show exponential best fits to the data.

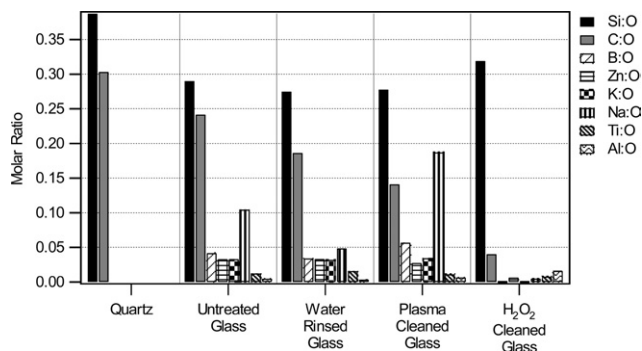


Fig. 10 XPS analysis of the surfaces of quartz, untreated borosilicate glass, borosilicate glass rinsed with Nanopure water, plasma-cleaned borosilicate glass, and H₂O₂-cleaned borosilicate glass. The molar ratios of various elements relative to oxygen are shown.

were similar. The data presented here provide some insights into why this is the case.

Borosilicate glass reactors are commonly used in many laboratory systems, and are known to adsorb water on their polar surface, which is terminated by Si–OH groups (*e.g.*, see refs. 1,59–62). The multilayer uptake of gases on solids is commonly described by the BET model, which predicts that the fractional coverage of the surface can be described by the BET eqn. (III),^{56–58,62}

$$\text{fractional coverage} = \frac{c_B RH}{(1 - RH)[1 + (c_B - 1)RH]} \quad (\text{III})$$

where the constant $c_B = \exp\{(Q_1 - Q_v)/RT\}$ and Q_1 and Q_v are the enthalpy of adsorption of water on the substrate and on water itself (*i.e.* the enthalpy of condensation of water), respectively,⁵⁸ and RH represents the partial pressure of the adsorbate. The shape of the isotherm is therefore determined by the value of the constant c_B , which reflects the strength of the interaction of the gas with the substrate. Model BET isotherms are shown in Fig. 11 for c_B equal to 0.1 and 20. For c_B values larger than about 10, there is a “knee” in the isotherm at low RH; such isotherms are classified as Type II, and are typified by the uptake of water on polar surfaces.⁶² For weak interactions between the gas and the surface, c_B is significantly smaller and the isotherms, classified as Type III, are smoothly concave with increasing relative humidity.^{56–58,61,62} Type III isotherms are often observed for water on non-polar surfaces,⁶² where it forms islands.⁵⁷ The AFM image in Fig. 4a does indeed show islands on the surface, which we attribute to water. While the AFM and infrared data are in reasonable agreement on the amount of water on the surface at relative humidities above 60%, the smaller amounts of water at lower RH and the increased uncertainty in the appropriate infrared absorption coefficient in this region

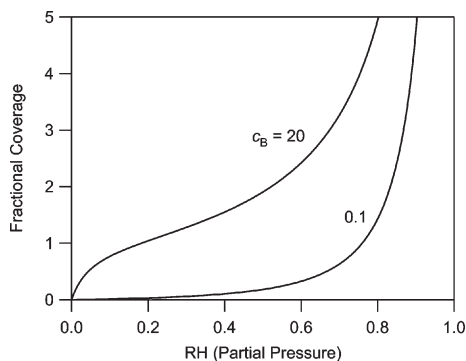


Fig. 11 Model Type II ($c_B = 20$) and Type III ($c_B = 0.1$) BET isotherms described by eqn. (III).

preclude definitively classifying the water uptake as Type II or Type III.

The BET isotherm (eqn. III) predicts that, as the vapor pressure of the adsorbate is approached, the number of adsorbed layers should approach infinity, *i.e.* the surface should become fully covered with liquid water. However, as seen in Fig. 3b, water on the untreated borosilicate glass has a finite contact angle so that a drop of the bulk liquid is present at the same time that there is a thin film of water on the surface. As discussed in detail by Adamson,⁶³ this situation is best described by Type VI and VII isotherms. On a molecular level, these isotherms occur in situations in which the structure of the adsorbate molecules closest to the surface is highly perturbed compared to the bulk liquid. A variety of evidence in the literature shows that water at the solid/water interface is structured and has properties different from bulk water; the structured orientation of surface water may extend anywhere from three monolayers to many molecular diameters.^{50,64} It is also supported by the red-shift in the infrared spectrum of water adsorbed on borosilicate glass reported from earlier studies in this laboratory¹ and also observed in the present work.

The amount of adsorbed water on untreated glass in the present study is somewhat smaller than reported in earlier, preliminary studies in this laboratory.¹ This may be due to improved temperature control in the present experiments, variable degrees of organic contamination on the surfaces, or both. In any event, in typical laboratory glass vacuum systems, organic contamination from room air or backstreaming from pumps cannot be completely avoided and hence, the water uptake measured for the untreated borosilicate glass here should be comparable to that in such glass vacuum systems. It should be noted that surfaces in ambient air upon which heterogeneous chemistry occurs will also hold adsorbed organics.

The amount of water present on treated borosilicate glass shown in Fig. 7b demonstrates that the water uptake at higher RH is sensitive to the pretreatment of the surface, with less water uptake if the glass has been plasma-cleaned or even just rinsed with Nanopure water prior to the experiments. XPS analysis (Fig. 10) indicates that the inorganic surface composition of these samples is similar to that of the untreated glass. However, there is less carbon on the plasma-cleaned sample as expected, and perhaps on the water-rinsed glass. This suggests that some of the organic material on the untreated glass is comprised of oxidized, polar organics that can be removed by rinsing with water. Such polar organics may also help to adsorb water onto the surface. Although these samples show differences in sodium, the water-rinsed glass has less Na and the plasma-cleaned more than the untreated glass, there is no observed correlation between water uptake and the surface sodium. This is not surprising since there is also no obvious reason to expect sodium to be involved in water uptake. Derjaguin and Zorin⁶⁰ measured the thickness of water layers on cleaned smooth glass surfaces to be from a few Å to 62 Å over the range from 95–100% RH; this would correspond to 1–18 layers of water, consistent with the measurements reported here.

The H₂O₂-cleaned borosilicate glass is quite different from the other borosilicate glass samples in all of the characteristics studied here. The surface is now primarily composed of silica, with B, Zn, K and Na having been largely removed (Fig. 10), showing that the surface of the glass has been modified by the H₂O₂ treatment. The bulk most likely is not modified. The AFM image (Fig. 4c) does not show the islands of water seen on the untreated glass. The water uptake (Fig. 8) is similar to a Type I Langmuir adsorption isotherm for which there are a fixed number of surface sites that become saturated at high adsorbate gas concentrations, or alternatively, a microporous surface in which the pores become progressively filled with water.^{56,58,62} The shift in the infrared absorption peak to

3200 cm⁻¹ suggests a more ice-like structure of the adsorbed water.^{40–44} The combination of all of these data suggest that the H₂O₂ forms micropores on leaching the trace metals, and these provide the major sites for water uptake.

Perhaps most interesting is the interaction of water with halocarbon wax, Teflon and the C8 SAM. Although these materials are classically considered to be hydrophobic, which is supported by the large measured contact angles (Table 2), the water uptake measurements indicate that a significant amount of water, similar to that on untreated borosilicate glass, can be taken up on the halocarbon wax coated glass, and to a lesser extent, on the smooth FEP Teflon film and C8 SAM (Fig. 6). It is known that, on single crystal surfaces, water tends to adsorb at surface defects (*e.g.* refs. 65,66). Thus, adsorption of water onto solid surfaces may be dependent on the roughness of the surface, in addition to its chemical properties. For example, Rudich *et al.*,⁶⁷ showed that the corrugation of hydrophobic surfaces impacted the interaction with water and that more corrugated surfaces did, in fact, hold more water than the smooth organic films.

The AFM images support the hypothesis that surface roughness plays a major role in water uptake on the surfaces that are hydrophobic on a macroscopic scale. The halocarbon wax sample coated using the dip method is seen in Fig. 5a to have a very porous, web-like structure with deep and tortuous channels. The increased time to come to equilibrium with gas phase water (Fig. 9) is therefore not surprising. This highly irregular and porous surface leads to significant amounts of water uptake, indeed, more than that on the untreated borosilicate glass surface (Fig. 7c). The solvent-coated halocarbon wax (Fig. 5b) has less surface roughness and does not appear to be as porous, but is still much more irregular than the glass and quartz (Table 2 and Fig. 4) so that uptake on surface discontinuities may occur. As seen in Fig. 7, the water uptake on the solvent-coated halocarbon wax surface (Fig. 7c) is similar to that on the untreated borosilicate glass (Fig. 7a). It is possible that the halocarbon wax coatings also have some adsorbed polar organics that assist in water uptake.

The thin FEP Teflon film also takes up some water (Fig. 6c), estimated to be 2 equivalent layers of water at 80% RH and rising to 6 equivalent layers at 100% RH, significantly less than the halocarbon wax coatings. Awakuni and Calderwood⁵⁵ reported uptake of three layers of water by Teflon film at 100% RH. Svensson *et al.*³ reported two layers on Teflon film at 5% relative humidity, with condensation on the surface at 90% RH; however, it is not clear that the surface structure of the material in those studies is comparable to the Teflon film used here. The AFM image of our Teflon film sample (Fig. 5c) shows very small pores that may be responsible for water uptake. The depth of these pores is greater on average than those in the C8 SAM, as indicated by a surface roughness of > 72 Å compared to 9 Å for the SAM. The smooth, relatively defect-free nature of the C8 SAM is likely responsible not only for the small amounts of water it takes up, but also for the shift in the infrared spectrum (Fig. 6c) to a more ice-like structure. The small amounts of water that are adsorbed on the C8 SAM may be taken up in defects in the coating which expose small regions of the underlying glass substrate, and/or on some of the elevated features on the surface seen in Fig. 4d.

As discussed earlier, laboratory studies of heterogeneous atmospheric reactions in thin aqueous films have typically used reactors made of glass, quartz, Teflon-coated glass or metal, and thin FEP Teflon films. The similarity in kinetics and mechanisms for the NO₂ heterogeneous hydrolysis in a halocarbon wax coated chamber (Fig. 1) to that in borosilicate glass chambers⁵ can now be understood since the two surfaces have now been shown to adsorb similar amounts of water (Fig. 7c). Given the importance of surface structure (*e.g.* roughness and porosity) for water adsorption, it is expected that the FEP and PFA Teflon coatings, which also have quite high surface

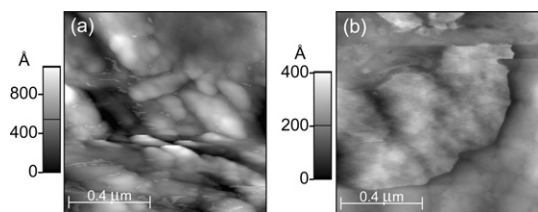


Fig. 12 AFM images of (a) a green ivy leaf surface with an RMS surface roughness of 195 Å and (b) a *Vinca minor* flower petal with an RMS surface roughness of 51 Å.

roughness values (Table 2), would behave in a similar manner to the halocarbon wax coatings. Thus, the agreement with studies carried out in Teflon-coated smog chambers^{2,12} is also understandable.

Thin films of FEP Teflon adsorb substantially less water than the halocarbon wax, and presumably less than the similarly rough Teflon coatings as well. The much smaller water uptake on smooth FEP Teflon films is consistent with the smaller rates of NO₂ heterogeneous hydrolysis measured by Pitts *et al.*² and Svensson *et al.*³ However, it should be noted that in experiments using chambers constructed of such films, other materials inside the chambers such as optics and sampling lines may contribute significantly to the uptake of water and hence the surface available for heterogeneous chemistry.

V. Atmospheric implications

As discussed in more detail elsewhere,^{5,68} silicates are common components of many surfaces found in building materials, including concrete, asphalt, and window glass.⁶⁹ In addition, silica has been identified as a major component of soil and soil derived dust.^{30,70} The uptake of water on such surfaces is known to promote heterogeneous chemistry not only in laboratory systems (*e.g.*, refs. 1,5) but also on surfaces found in the tropospheric boundary layer. Therefore, our measurements of water uptake on borosilicate glass and quartz are relevant and useful for understanding chemistry on these tropospheric surfaces.

Given our measurements showing that water adsorbs even to hydrophobic materials if their surfaces have appropriate roughness, it is likely that other hydrophobic materials, such as vegetation, may also hold water in quantities sufficient to support heterogeneous chemistry. Fig. 12 shows AFM images of the surfaces of an ivy leaf and a *Vinca minor* flower petal. Clearly there are surface irregularities that, despite the hydrophobic nature of the surfaces, should lead to water uptake in a manner similar to the halocarbon wax. The surface roughness values for a 1 μm × 1 μm section of each sample were 195 Å for an ivy leaf and 51 Å for the *V. minor* petal, similar to the values for halocarbon wax and Teflon in Table 2. Water uptake on vegetation and its participation in heterogeneous reactions in the atmosphere is supported by the observation of HONO production over a variety of surface types, including vegetation.^{19,23–30}

The results presented here give a strong indication that most, if not all, surfaces in contact with the atmosphere will hold water in sufficient amounts to promote heterogeneous reactions. Further field investigations of surface chemistry and elucidation of the impact of including heterogeneous reactions (*e.g.* reactions (1) and (2)) in atmospheric models are necessary to determine the full role played by heterogeneous chemistry in the atmosphere.

Acknowledgements

We are grateful to the California Air Resources Board (Contract No. 00-323) and the National Science Foundation (Grant No. CHE-0209719) for support of this work, and

James N. Pitts Jr. for many stimulating discussions. RMP and EJM acknowledge funding from the National Science Foundation (Grant No. CHE-011155). We also thank Husheng Yang, Theresa McIntire, and Peter Griffiths for helpful discussions, James E. Rutledge and Justin Burton for their assistance in measurement of water contact angles, and Lisa Lucio Gough for assistance with manuscript preparation. We thank Paul Wennberg as well as Crest Coating and Livingstone Coating Corp. for providing the Teflon coated samples and Teflon film.

References

- N. Saliba, H. Yang and B. J. Finlayson-Pitts, *J. Phys. Chem. A*, 2001, **105**, 10339.
- J. N. Pitts, Jr., E. Sanhueza, R. Atkinson, W. P. L. Carter, A. M. Winer, G. W. Harris and C. N. Plum, *Int. J. Chem. Kinet.*, 1984, **16**, 919.
- R. Svensson, E. Ljungstrom and O. Lindqvist, *Atmos. Environ.*, 1987, **21**, 1529.
- M. E. Jenkin, R. A. Cox and D. J. Williams, *Atmos. Environ.*, 1988, **22**, 487.
- B. J. Finlayson-Pitts, L. M. Wingen, A. L. Sumner, D. Syomin and K. A. Ramazan, *Phys. Chem. Chem. Phys.*, 2003, **5**, 223.
- L. G. Wayne and D. M. Yost, *J. Chem. Phys.*, 1951, **19**, 41.
- J. Cathala and G. Weinrich, *Compt. Rend.*, 1952, **244**, 1502.
- M. S. Peters and J. L. Holman, *Ind. Eng. Chem.*, 1955, **47**, 2536.
- G. G. Goyer, *J. Colloid Sci.*, 1963, **18**, 616.
- C. England and W. H. Corcoran, *Ind. Eng. Chem. Fundam.*, 1974, **13**, 373.
- H. M. Ten Brink, J. A. Bontje, H. Spoelstra and J. F. van deVate, in *Studies in Environmental Science*, ed. M. M. Benarie, Elsevier, Amsterdam, 1978, vol. 1, pp. 239.
- F. Sakamaki, S. Hatakeyama and H. Akimoto, *Int. J. Chem. Kinet.*, 1983, **15**, 1013.
- H. Akimoto, H. Takagi and F. Sakamaki, *Int. J. Chem. Kinet.*, 1987, **19**, 539.
- A. Febo and C. Perrino, *Atmos. Environ.*, 1991, **25A**, 1055.
- A. Bambauer, B. Brantner, M. Paige and T. Novakov, *Atmos. Environ.*, 1994, **28**, 3225.
- J. Kleffmann, K. H. Becker and P. Wiesen, *Atmos. Environ.*, 1998, **32**, 2721.
- J. Kleffmann, K. H. Becker and P. Wiesen, *J. Chem. Soc., Faraday Trans.*, 1998, **94**, 3289.
- R. M. Harrison and G. M. Collins, *J. Atmos. Chem.*, 1998, **30**, 397.
- G. Lammel, *Formation of Nitrous Acid - Parameterisation and Comparison with Observations*, Max Planck Institute for Meteorology, Hamburg, 1999, Report No. 286, pp. 1–36.
- R. Kurtenbach, K. H. Becker, J. A. G. Gomes, J. Kleffmann, J. C. Lörzer, M. Spittler, P. Wiesen, R. Ackermann, A. Geyer and U. Platt, *Atmos. Environ.*, 2001, **35**, 3385.
- A. L. Goodman, G. M. Underwood and V. H. Grassian, *J. Phys. Chem. A.*, 1999, **103**, 7217.
- W. S. Barney and B. J. Finlayson-Pitts, *J. Phys. Chem. A*, 2000, **104**, 171.
- D. Perner and U. Platt, *Geophys. Res. Lett.*, 1979, **6**, 917.
- U. Platt, D. Perner, G. W. Harris, A. M. Winer and J. N. Pitts, Jr., *Nature*, 1980, **285**, 312.
- A. M. Winer and H. W. Biermann, *Res. Chem. Intermed.*, 1994, **20**, 423.
- R. M. Harrison, J. D. Peak and G. M. Collins, *J. Geophys. Res.*, 1996, **101**, 14429.
- G. Lammel and J. N. Cape, *Chem. Soc. Rev.*, 1996, **25**, 361.
- J. Stutz, B. Alicke and A. Neff, *J. Geophys. Res.*, 2002, **107**, 8192.
- B. Alicke, U. Platt and J. Stutz, *J. Geophys. Res. Atmos.*, 2002, **107**, 8196.
- B. J. Finlayson-Pitts and J. N. Pitts, Jr., *Chemistry of the Upper and Lower Atmosphere: Theory, Experiments and Applications*, Academic Press, San Diego, 2000.
- D. O. DeHaan, T. Brauers, K. Oum, J. Stutz, T. Nordmeyer and B. J. Finlayson-Pitts, *Int. Rev. Phys. Chem.*, 1999, **18**, 343.
- Standard Specifications for Glasses in Laboratory Apparatus*, ASTM International, West Conshohocken, PA, 2001.
- T. H. Elmer, in *Engineered Materials Handbook*, vol. 4, Ceramics and Glasses, ASM International, Materials Park, OH, 1992, vol. 4, pp. 427.
- J. Sagiv, *J. Am. Chem. Soc.*, 1980, **102**, 92.

- 35 Graciously provided by Paul Wennberg.
- 36 A. Ulman, *An Introduction to Ultrathin Organic Films From Langmuir-Blodgett to Self Assembly*, Academic Press, San Diego, 1991.
- 37 P. R. Griffiths and J. A. de Haseth, *Fourier Transform Infrared Spectrometry*, Wiley, New York, 1986.
- 38 C. S. Hemminger, T. A. Land, A. Christie and J. C. Hemminger, *Surf. Interface Anal.*, 1990, **15**, 323.
- 39 C. D. Wagner, L. E. Davis, M. V. Zeller, J. A. Taylor, R. H. Raymond and L. H. Gale, *Surf. Interface Anal.*, 1981, **3**, 211.
- 40 G. Herzberg, *Molecular Spectra and Molecular Structure. II. Infrared and Raman Spectra of Polyatomic Molecules*, D. Van Nostrand Company, Inc., Princeton, N. J., 1945, vol. II.
- 41 Q. Du, E. Freysz and Y. R. Shen, *Phys. Rev. Lett.*, 1994, **72**, 238.
- 42 Q. Du, E. Freysz and Y. R. Shen, *Science*, 1994, **264**, 826.
- 43 M. J. Shultz, C. Schnitzer, D. Simonelli and S. Baldelli, *Int. Rev. Phys. Chem.*, 2000, **19**, 123.
- 44 G. L. Richmond, *Annu. Rev. Phys. Chem.*, 2001, **52**, 357.
- 45 D. D. Weis and G. E. Ewing, *Anal. Chem.*, 1998, **70**, 3175.
- 46 M. C. Foster and G. E. Ewing, *J. Chem. Phys.*, 2000, **112**, 6817.
- 47 H. D. Downing and D. Williams, *J. Geophys. Res.*, 1975, **80**, 1656.
- 48 M. C. Foster and G. E. Ewing, *Surf. Sci.*, 1999, **427–428**, 102.
- 49 W. Cantrell and G. E. Ewing, *J. Phys. Chem. B*, 2001, **105**, 5434.
- 50 W. Drost-Hansen, in *Chemistry and Physics of Interfaces*, American Chemical Society, Washington, DC, 1971, vol. 2, pp. 204.
- 51 *Adsorption on Silica Surfaces*, ed. E. Papirer, Marcel Dekker, New York, 2000.
- 52 G. C. Pimental and A. L. McClelland, *The Hydrogen Bond*, Reinhold, New York, 1960.
- 53 W. M. Irvine and J. B. Pollack, *Icarus*, 1968, **8**, 324.
- 54 L. Xu, A. Lio, J. Hu, D. F. Ogletree and M. Salmeron, *J. Phys. Chem. B*, 1998, **102**, 540.
- 55 Y. Awakuni and J. H. Calderwood, *J. Phys. D*, 1972, **5**, 1038.
- 56 A. W. Adamson, *Physical Chemistry of Surfaces*, John Wiley & Sons, New York, 5th edn., 1990.
- 57 R. I. Masel, *Principles of Adsorption and Reaction on Surfaces*, John Wiley & Sons, New York, 1996.
- 58 A. W. Adamson and A. P. Gast, *Physical Chemistry of Surfaces*, John Wiley & Sons, Inc., New York, 6th edn., 1997.
- 59 I. Langmuir, *J. Amer. Chem. Soc.*, 1918, **40**, 1361.
- 60 B. V. Derjaguin and Z. M. Zorin, *2nd Proc. Intern. Congr. Surface Activity (London)*, 1957, **2**, 145.
- 61 A. W. Adamson, *Physical Chemistry of Surfaces*, John Wiley & Sons, New York, 1967.
- 62 S. J. Gregg and K. S. W. Sing, *Adsorption, Surface Area and Porosity*, 2nd edn., Academic Press, London, 1982.
- 63 A. W. Adamson, *J. Colloid Interface Sci.*, 1968, **27**, 180.
- 64 G. A. Parks, *J. Geophys. Res.*, 1984, **89**, 3997.
- 65 D. Dai, S. J. Peters and G. E. Ewing, *J. Phys. Chem.*, 1995, **99**, 10299.
- 66 R. C. Hoffman, M. Kaleuati and B. J. Finlayson-Pitts, *J. Phys. Chem. A*, 2003, **107**, 7818.
- 67 Y. Rudich, I. Benjamin, R. Naaman, E. Thomas, S. Trakhtenberg and R. Ussyshkin, *J. Phys. Chem. A*, 2000, **104**, 5238.
- 68 A. Rivera-Figueroa, A. L. Sumner and B. J. Finlayson-Pitts, *Environ. Sci. Technol.*, 2002, **37**, 548.
- 69 R. M. E. Diamant, *The Chemistry of Building Materials*, Business Books Limited, London, 1970.
- 70 D. Gillette, *J. Exposure Anal. Environ. Epidemiol.*, 1997, **7**, 303.

Laboratory Studies of Potential Mechanisms of Renoxification of Tropospheric Nitric Acid

A. M. RIVERA-FIGUEROA, A. L. SUMNER, AND B. J. FINLAYSON-PITTS*

Department of Chemistry, University of California at Irvine, Irvine, California 92697-2025

Laboratory studies of the heterogeneous reactions between HNO₃ in thin water films on silica surfaces and gaseous NO, CO, CH₄, and SO₂, proposed as potential "renoxification" mechanisms in the atmosphere, are reported. Transmission FTIR was used to monitor reactants and products on the silica surface and in the gas phase as a function of time. No reaction of CO, CH₄, or SO₂ was observed; upper limits to the reaction probabilities (γ^{rxn}) are $\leq 10^{-10}$ for CO and SO₂ and $\leq 10^{-12}$ for CH₄. However, the reaction of HNO₃ with NO does occur with a lower limit for the reaction probability of $\gamma^{NO} \geq (6 \pm 2) \times 10^{-9}$ (2s). The experimental evidence shows that the chemistry is insensitive to whether the substrate is pure silica or borosilicate glass. Nitric acid in its molecular form, and not the nitrate anion form, was shown to be the reactive species, and NH₄NO₃ was shown not to react with NO. The HNO₃-NO reaction could be a significant means of renoxification of nitric acid on the surfaces of buildings and soils in the boundary layer of polluted urban atmospheres. This chemistry may help to resolve some discrepancies between model-predicted ozone and field observations in polluted urban atmospheres.

Introduction

Reactive nitrogen oxides, particularly NO + NO₂ (=NO_x), are well-known to be oxidized in the atmosphere to nitric acid (HNO₃) (1). Nitric acid is removed from the atmosphere by wet and dry deposition, through reaction with some components of atmospheric particles (2) such as CaCO₃, and by reaction with ammonia (NH₃):

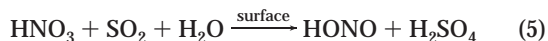


Ammonium nitrate (NH₄NO₃), an important component of atmospheric particulate matter in polluted atmospheres (1, 3), also undergoes deposition. As a result, the formation of HNO₃ is generally considered to result in the permanent removal of NO_x from the troposphere.

The reduction of HNO₃ back to photochemically active nitrogen (e.g., NO, NO₂, HONO), so-called "renoxification", could alter the concentration of a number of important atmospheric species including ozone (O₃) and hence impact air pollution control strategies. Surfaces on which such processes may occur include not only airborne particles but also soils, building materials, and vegetation. These surfaces may potentially be quite important in promoting hetero-

geneous chemistry in the boundary layer. For example, Diamond et al. (4) and Gingrich et al. (5) have shown that windows on buildings in both urban and rural areas have organic films that include both low vapor pressure organic compounds and semivolatile organics. This issue of heterogeneous chemistry on soil and structures in urban atmospheres is one that has not received a great deal of attention but that may prove to be quite significant given that this is the region where many atmospheric measurements are made and human exposure is the greatest. While we focus here on chemistry relevant to the boundary layer, it should be noted that renoxification processes have also been proposed for the upper troposphere and lower stratosphere where the NO_x/HNO₃ ratio has frequently been measured to be higher than predicted by models of the gas-phase chemistry (6–12).

Fairbrother et al. (13) suggested that nitric oxide (NO), carbon monoxide (CO), methane (CH₄), and sulfur dioxide (SO₂) might influence renoxification in the atmosphere via reactions with HNO₃ on surfaces:



These reactions were proposed based on their thermodynamic feasibility. Heterogeneous reactions with HCHO and H₂O₂ were also considered and shown to be thermodynamically feasible as well (13); the reaction of HCHO with HNO₃ in the liquid phase was suggested earlier by Chatfield (6) to resolve discrepancies between measured and modeled NO_x/HNO₃ ratios in the free troposphere. While modeling studies by Lary and Shallcross (11) suggested that the agreement between the measured and the modeled NO_x/HNO₃ ratio in the upper troposphere would improve significantly if the reaction of CO with HNO₃ occurs with a reaction probability of $\gamma \geq 1 \times 10^{-4}$, there have been no experimental studies of the feasibility of this reaction, nor of reactions 4 and 5.

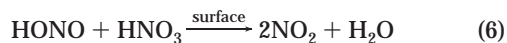
These reactions may also be important sources of HONO (14), which is the major source of OH at dawn in polluted urban areas (1, 15–18). Reaction of OH with organics generates RO₂ and HO₂ free radicals that convert NO to NO₂. Photolysis of NO₂ then forms O(³P) that leads to O₃ formation (1). This heterogeneous chemistry thus has the potential to impact the formation of ozone and associated photochemical air pollutants in urban areas.

Previous studies in this laboratory showed that NO does react with HNO₃ adsorbed on porous glass in the absence of added water vapor (19) as well as on smooth borosilicate glass at ~50% RH (14, 20). Porous glass is a high surface area quartz material whose surface is terminated in -SiOH groups (21, 22). These polar -OH groups on the surface physisorb water readily; hence, porous glass is also known as "thirsty glass". As a result, water is observed spectroscopically on these surfaces when placed in a cell and pumped on briefly. In contrast, smooth borosilicate glass holds very little water unless in contact with water vapor. At 20% RH for example, an amount of water equivalent to only about 1–2 layers is present on the surface (20, 23); the infrared spectrum indicates that this is likely not a smooth film similar to bulk

* Corresponding author e-mail: bfinlay@uci.edu; phone: (949) 824-7670; fax: (949) 824-3168.

water but rather islands or a 2-D water network. As a result, chemistry that occurs on porous glass in the absence of significant amounts of gas-phase water vapor will occur only at higher relative humidities on smooth glass.

In our earlier studies, only small concentrations of gaseous HONO were observed, and the major gaseous reaction product was NO₂. This was proposed to be due to reaction 2, followed by secondary reactions of HONO on the surface, such as reaction 6:



or the self-reaction of HONO on the surface. However, whether the HNO₃-NO reaction occurs on different substrates was not investigated in these previous studies. For example, the composition of the porous glass used in those studies was 96.3% SiO₂, 2.95% B₂O₃, 0.04% Na₂O, and 0.72% Al₂O₃ + ZrO₂ (22), so catalysis by trace components such as the metal oxides may have played a role in the reaction. In addition, whether other species associated with HNO₃ on the surface such as nitrate anions (NO₃⁻) participated in the chemistry was not known; if NO₃⁻ also undergoes such a reaction, additional nitrate anions, such as airborne nitrate particles and ammonium nitrate fertilizer applied to vegetation and soils (24), could also contribute to renoxification.

We report here experimental studies using Fourier transform infrared (FTIR) transmission spectroscopy to examine whether CO, CH₄, and SO₂ react with adsorbed HNO₃ as proposed (11, 13) and whether NH₄NO₃ reacts with NO in a manner similar to HNO₃. In addition, the possible catalysis by Fe³⁺ [the most common oxidation state of iron in the atmosphere (25-28)] as proposed by Lary and Shallcross (11) and effects of sulfuric acid (H₂SO₄) on the surface were investigated for the reaction of CO with HNO₃. Further studies of the reaction of gaseous NO with adsorbed HNO₃ were carried out on pure silica to probe whether trace components of glass played a role in the chemistry and to elucidate the nature of the reactive form of HNO₃. We show that, while the reaction of HNO₃ with CO, CH₄, and SO₂ does not occur, the HNO₃-NO reaction does take place on pure silica, establishing that it is likely that it is the existence of thin water films on the surface that is important rather than catalysis by trace components of borosilicate glasses. We show, on the basis of the lower limit measured for the reaction probability, that the HNO₃-NO reaction in thin water films on terrestrial surfaces such as soils may be important in renoxification in the urban boundary layer.

Experimental Section

The experimental apparatus used in these studies has been described previously (19, 29). Briefly, these heterogeneous reactions were studied using FTIR (Mattson Research Series). Either a porous glass plate or pressed silica pellets provided the reaction surface. These surfaces were suspended in the center of a borosilicate glass cell using a glass holder; the reaction cell had ZnSe windows, a volume of 79 cm³, a surface area of 232 cm², and a path length for the infrared beam of 6.3 cm. The holder could be moved out of the beam into a sidearm to characterize gas-phase species or positioned in the infrared beam for characterization of the combination of the gas-phase plus surface species. The spectrum of the surface species alone was obtained from the difference. Spectra were collected using 32 co-added scans at a resolution of 1 cm⁻¹ unless otherwise specified. All experiments were conducted at (23 ± 1) °C.

The reaction surface was either first pumped on or, alternatively, heated in the sidearm (cell surface was ~320 °C) for 30-60 min while pumping, followed by cooling to room temperature. In both cases, water was observed

spectroscopically to be present on the surface at the beginning of the reaction, and no difference in the chemistry for these two pretreatments was evident. Nitric acid (~ 1 × 10¹⁷ molecule cm⁻³) was introduced into the reaction cell and then pumped out for 5 min. This HNO₃ dosing was repeated three times followed by pumping for ~30 min after the last treatment. Nitric acid remains adsorbed on the surface after this procedure, as indicated by its infrared absorption bands discussed in detail below. Finally, the reactant gas (NO, CO, CH₄, or SO₂) was introduced into the cell at concentrations ranging between (1-26) × 10¹⁶ molecule cm⁻³; these relatively high concentrations were used to force the chemistry, in the event that the reactions did occur but with small reaction probabilities. In addition, it allowed us to observe not only the surface HNO₃ but also the gas-phase species. The goal was to probe the fundamental chemistry of these processes, which are most readily and commonly carried out at higher than ambient concentrations (1); once reaction probabilities are obtained from such experiments however, they can be reliably applied to atmospheric conditions. In some cases, N₂ was added to a total pressure of 1 atm. For experiments carried out with relative humidity (RH) higher than 0%, N₂ was flowed through a bubbler holding water and was diluted with dry N₂ to obtain the desired relative humidity.

Experiments with adsorbed NH₄NO₃ were also conducted in order to determine if it reacts in a manner similar to HNO₃. The NH₄NO₃ was formed by dosing the silica with dry HNO₃ as described above, followed by the addition of excess NH₃ vapor. After the cell was evacuated to remove any remaining gas-phase species, NO was added. For convenience, the experiments with NH₄NO₃ were performed at reduced pressure (i.e. no addition of N₂), which is not expected to impact the reaction.

The progress of the reaction with time was monitored using FTIR. First, the single-beam background spectra were collected with the cell evacuated by moving the surface out of, and then into, the infrared beam. To obtain an absorbance spectrum of the surface species and the gas together, the reactants were added to the cell and the single-beam spectrum was recorded with the surface in the beam. The spectrum was then ratioed to that of the evacuated cell with the surface in the beam to give the absorbance spectrum of the gas plus adsorbed species. This procedure canceled out the absorptions due to the silica itself, which occur below 2000 cm⁻¹ and in the 3000-3600-cm⁻¹ region. The absorbance spectrum of the gases was obtained by ratioing the single-beam spectrum to that of the cell under vacuum, both with the surface out of the infrared beam. Finally, the spectrum of the gas-phase species was subtracted from the gas plus surface to obtain the spectrum of species on the surface.

Two different types of silica surfaces, a porous glass plate and pressed pellets of untreated fumed silica powder, were used. The 2 × 3 cm plate of porous glass (Corning) was ~1 mm thick as provided by the manufacturer. The normal infrared cutoff for porous glass is 2000 cm⁻¹ (21). To shift the cutoff down to 1550 cm⁻¹, the porous glass plate was thinned in the center by etching with HF as described elsewhere (29). The total porous glass surface area, measured using a commercial instrument based on the Brunauer-Emmett-Teller (BET) method (30) (Accelerated Surface Area and Porosimetry System, ASAP 2000, Micromeritics; N₂ adsorbate), was 71.2 m² g⁻¹, resulting in a total surface area of 28.5 m² averaged over the thinner etched section and the surrounding unetched glass. The porous glass plate was cleaned by rinsing with Nanopure water after each experiment.

The pressed silica pellets were prepared with Cab-O-Sil (Cabot Corp.) and have an infrared cutoff at ~1300 cm⁻¹ (31, 32). Cab-O-Sil is untreated fumed silica powder of high purity

($\geq 99.8\%$ SiO₂), with particle sizes ranging from 0.2 to 0.3 μm (33). Approximately 0.02 g of the silica powder was pressed into a 13 mm diameter pellet, with a thickness of ~ 0.05 mm. The surface area, measured in the same way as for the porous glass plate, was 329 m² g⁻¹, resulting in a total surface area of 6.5 m² per pellet. A new pellet was used for each experiment.

Ion chromatography (IC) (Alltech Odyssey) was used to quantify the HNO₃ adsorbed on the surfaces. After the dosing procedure described above, an infrared spectrum of the adsorbed nitric acid on the surface was recorded. The pellet was removed from the cell, rinsed with Nanopure water, and analyzed for NO₃⁻. The mobile phase was a 1:10 (v:v) mixture of 1.7 mM NaHCO₃/1.8 mM Na₂CO₃ in Nanopure water and used at a constant flow rate of 1.20 mL min⁻¹. A 150 mm \times 4.6 mm Novosep A-1 Anion column equipped with a 7.5 mm \times 4.6 mm guard column was used for separation at a constant temperature of 35 °C. An autosuppressor (DS-PLUS) was used to improve sensitivity. A conductivity detector (Alltech 550) with positive polarity, a detection range of 10 μS ($S = \Omega^{-1}$), and a time constant of 1 s was used for the NO₃⁻ analysis. The IC was calibrated for NO₃⁻ using aqueous solutions prepared from sodium nitrate (NaNO₃) powder.

Chemicals. To obtain anhydrous gas-phase HNO₃, the vapor was drawn from a mixture of liquid HNO₃ (Fisher Scientific, 69.9%) and H₂SO₄ (Fisher Scientific, 95.7%) prepared in a ratio of 1:2 (v:v) HNO₃:H₂SO₄ and purified by three freeze-pump-thaw cycles. Gaseous NH₃ was produced using the vapor above a 29.5% ammonium hydroxide solution (Fisher Certified ACS Plus) that was purified by one freeze-pump-thaw cycle. FeCl₃ (Fisher Scientific, laboratory grade, anhydrous) and NaNO₃ (Aldrich, ACS reagent grade) were used as received. The 1.7mM sodium bicarbonate/1.8 mM sodium carbonate used for IC was EZ-LUTE (Alltech). Nitric oxide (Matheson, 99%) was purified from contaminants such as N₂O, NO₂, and HNO₃ by passing it rapidly through a liquid nitrogen trap. The gases CO (Matheson, 99.99%), CH₄ (Matheson, 99.999%), anhydrous SO₂ (Matheson, 99.98%), and N₂ (Matheson, 99.999%) were used directly from the cylinder without further purification. Nanopure water (Barnstead, 18.1 M Ω ·cm) was used to supply water vapor to the reaction cell, to clean the porous glass, and to prepare the NaNO₃ solutions for the IC calibration.

Results and Discussion

Heterogeneous Reaction of NO with HNO₃ on Silica Surfaces. Studies of the reaction of NO with adsorbed HNO₃ on silica pellets were conducted using nitric oxide concentrations in the range from (2–14) $\times 10^{16}$ molecule cm⁻³. Figure 1 shows typical spectra of the gas phase plus the surface in the 1300–1800 cm⁻¹ region before (Figure 1a) and after addition of NO (Figure 1b,c). In this case, the pellet was not heated prior to the reaction; while no additional water vapor was added to the cell, water adsorbed from room air was present initially as expected (21, 22) and as evidenced by the overlapping band on the low wavenumber side of the HNO₃ peak. Ion chromatography measurements show that the initial nitrate (HNO₃ + NO₃⁻) on the silica pellet for a band of this intensity at 1677 cm⁻¹ is a total of 2.4 $\times 10^{18}$ molecules or 3.7 $\times 10^{13}$ molecule cm⁻², corresponding to $\sim 10\%$ of a monolayer; this is consistent with Goodman et al. (34), who report a saturation coverage of HNO₃ on silica powder of (7 \pm 3) $\times 10^{13}$ molecule cm⁻².

Upon addition of NO (Figure 1b), surface HNO₃ decreases and peaks attributable to N₂O₄ and NO₂ increase. Lifting the pellet out of the infrared beam shows that the N₂O₄ is primarily on the surface and that the NO₂ is entirely in the gas phase. After 65 min of reaction time (Figure 1c), most of the surface HNO₃ has reacted, gas-phase NO₂ has increased, and the surface N₂O₄ has decreased. These observations are consistent with the study of Mochida and Finlayson-Pitts

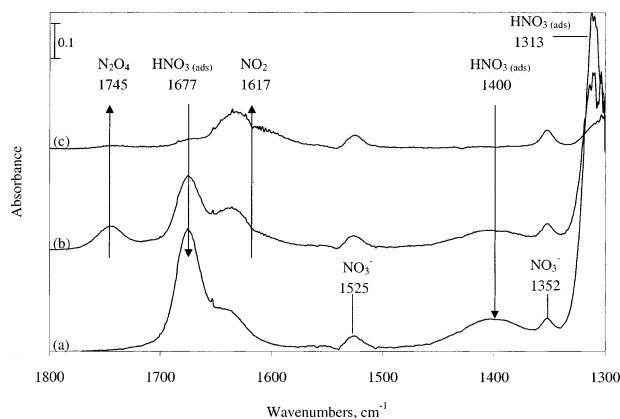


FIGURE 1. (a) Spectrum of the gas-phase plus surface-adsorbed HNO₃ on silica in the 1300–1800 cm⁻¹ region. Bands at 1677, 1400, and 1313 cm⁻¹ are due to molecular HNO₃ adsorbed on the surface (19, 29, 34, 53, 62–64), and the broad peak at the low wavenumber side of the 1677 cm⁻¹ peak is due to adsorbed water. The peaks at 1352 and 1525 cm⁻¹ are due to the ν_3 asymmetric stretching vibration of NO₃⁻. (b) Immediately after the introduction of 9.7 $\times 10^{16}$ NO cm⁻³ and (c) 65 min later. Gas-phase NO₂ (1617 cm⁻¹) and surface N₂O₄ (1745 cm⁻¹) are observed upon reaction.

(19) in which NO was observed to react with HNO₃ adsorbed on porous glass, generating NO₂ as the major gaseous product. Independent experiments in this laboratory have shown that surface N₂O₄ is enhanced by the presence of HNO₃ (35). Thus, when the HNO₃ has reacted almost completely, N₂O₄ on the surface also decreases as observed in Figure 1c.

If it were the case that NO₃⁻ reacts with gaseous NO, the reaction could also occur on nitrate-fertilized soils, where NO is generated by biological processes and is also present by contact with polluted air in the boundary layer. Such a reaction may also occur on atmospheric particles containing nitrate. The peaks assigned to NO₃⁻ observed in this study did not change during the reaction (Figure 1), suggesting that nitrate does not react. To probe this further, studies were conducted using adsorbed NH₄NO₃, which is a major form of NO₃⁻ in atmospheric particles (1) as well as in fertilizer (24). Experiments were conducted on a silica pellet and on the porous glass plate, which were allowed to come to equilibrium with water vapor at $\sim 50\%$ RH and then evacuated. The formation of NH₄NO₃ on the silica surfaces by reaction of adsorbed HNO₃ with gaseous NH₃ was confirmed spectroscopically by the disappearance of the molecular HNO₃ bands and the appearance of N–H stretches in the 2800–3300 and 1420–1450 cm⁻¹ regions and the NO₃⁻ stretch at 1360 cm⁻¹, in agreement with the literature (36, 37). Gaseous NO was added to the cell at concentrations of (1–2) $\times 10^{17}$ molecule cm⁻³. The infrared absorption bands due to NH₄NO₃ on the silica surfaces were too intense to quantify small changes, if they occurred; however, NH₄NO₃ was also formed on the ZnSe windows of the cell during the dosing procedure and could be monitored quantitatively. No change in these bands nor a decrease in NO or an increase in NO₂ was observed after 1 h reaction time.

Water could potentially affect these reactions through hydration of and/or reaction with intermediates and products. For example, NO⁺ and NO₂⁺ have been recently proposed as key intermediates in the heterogeneous hydrolysis of NO₂ on silica surfaces (35) and may be common to other NO_x heterogeneous reactions such as those studied here. It has been shown in studies of the reactions of NO⁺ and NO₂⁺ clustered with water molecules in the gas phase that at least four water molecules are needed in order to convert these species to HONO (38–40) and HNO₃ (41–45), respectively. On the other hand, water can also inhibit the

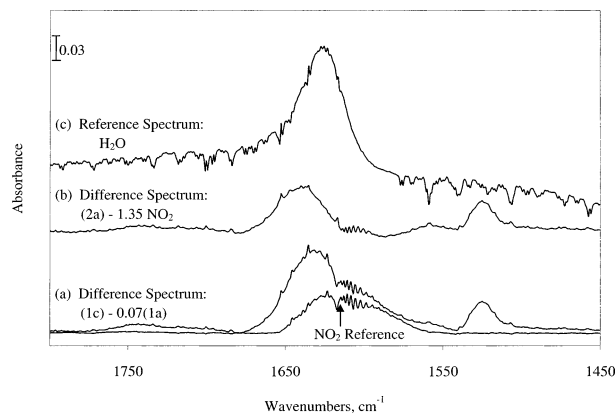


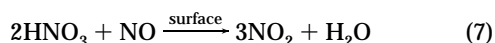
FIGURE 2. (a) Spectrum from 65 min reaction time (Figure 1c) after subtraction of the initial spectrum of adsorbed HNO_3 ($0.07 \times$ initial spectrum, Figure 1a); also shown is a reference spectrum of gas-phase NO_2 (3.2×10^{16} molecule cm^{-3}). (b) Difference spectrum after subtraction of gaseous NO_2 ($1.35 \times$ reference spectrum in Figure 2a) from spectrum a. (c) Spectrum of water adsorbed on silica pellet.

reactions, for example, by enhancing the dissociation of the reactive molecular form of HNO_3 to unreactive ions; in the presence of four or more water molecules in a gas-phase cluster with HNO_3 , dissociation occurs (46–48).

To investigate whether the reaction might be affected by water, $\sim 4.9 \times 10^{17}$ molecule cm^{-3} water vapor was then added to the cell, and the reaction was monitored for another 20 h. Neither the loss of NH_4NO_3 on the cell windows nor the formation of gas-phase products was observed even for the long reaction times. These results indicate that NH_4NO_3 does not react with gaseous NO ; therefore, NO_3^- is not the form of HNO_3 that is reactive with NO . It also confirms that NH_4NO_3 will not undergo renoxification in the troposphere unless it is first converted back to HNO_3 through thermal decomposition (reaction-1).

Figure 2a shows the spectrum from the HNO_3 – NO reaction after 65 min (Figure 1c) from which the HNO_3 band has been subtracted using the initial spectrum of adsorbed HNO_3 (prior to addition of NO); for comparison, a reference spectrum of gaseous NO_2 is shown. Subtraction of the NO_2 gives the spectrum shown in Figure 2b. (The small structure remaining around 1600 cm^{-1} is likely due to changes in the gas-phase water, which has strong infrared bands in this region, in the purge gas during the experiment.) Figure 2c is the spectrum of water adsorbed on the silica. Comparison of Figure 2, spectra b and c, shows that the remaining band at $\sim 1640 \text{ cm}^{-1}$ in Figure 2b is shifted from that for pure water at 1628 cm^{-1} by $\sim 12 \text{ cm}^{-1}$. Ab initio calculations (49–51) show that the band due to this bending mode of water in a 1:1 gaseous nitric acid–water complex should shift by $\sim 10 \text{ cm}^{-1}$ as compared to water. We therefore assign the 1640-cm^{-1} band to the bending mode of water in a nitric acid–water complex.

These and previous experiments (14, 19, 20) indicate that reaction 2 followed by the secondary reaction 6 (or the self-reaction) of HONO gives the net reaction 7:



Thus, for each NO reacted, two molecules of HNO_3 should be consumed and three molecules of NO_2 generated. In the experiment shown here, the total amount of NO available for reaction in the cell initially is 7.7×10^{18} molecules; this is in significant excess over the HNO_3 on the surface, which was measured by IC to be 2.4×10^{18} molecules. Thus, HNO_3 is the limiting reagent under these conditions. The concen-

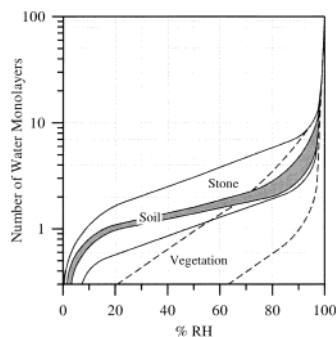


FIGURE 3. Uptake of water on some terrestrial surfaces as a function of relative humidity. From Lammel (52).

tration of HNO_3 remaining on the surface after 65 min is 7% of the initial value. This reaction of the surface HNO_3 should generate 3.3×10^{18} NO_2 , giving a concentration of 4.2×10^{16} molecule cm^{-3} in the 79-cm^3 cell. The concentration of gas-phase NO_2 in Figure 1 was measured using an independent calibration for NO_2 in the cell to be 4.4×10^{16} molecule cm^{-3} , in excellent agreement with the stoichiometry of the overall reaction 7.

The reaction probability (γ) for NO reacting with surface-adsorbed HNO_3 can in principle be calculated using the initial rate of loss of NO ($-\text{d}[\text{NO}]/\text{d}t$), the cell volume (V_{cell}), and the surface area (A) of the pressed silica pellet:

$$\gamma = \frac{\left(\frac{-\text{d}[\text{NO}]}{\text{d}t}\right) V_{\text{cell}}}{A[\text{NO}]_0 \sqrt{\frac{RT}{2\pi M}}} \quad (8)$$

where M is the molecular weight of NO . However, the NO is in significant excess over the available HNO_3 , and so measuring the small changes in its concentration in the early stages of the reaction is not feasible. As an alternative, we use half of the initial rate of loss of surface-adsorbed HNO_3 , based on the stoichiometry of the overall reaction 7, as a measure of $\text{d}[\text{NO}]/\text{d}t$. The reaction is sufficiently fast that, under the conditions of Figure 1, 43% of the initial HNO_3 reacts by the time the first spectrum is obtained (2 scans in 2.2 s), giving an average reaction time of 1.1 s. This change in the HNO_3 concentration leads to a calculated reaction probability of $\gamma^{\text{NO}} = 7 \times 10^{-9}$. The average reaction probability over seven experiments using silica pellets was $(6 \pm 2) \times 10^{-9}$ (2s). However, these are lower limits since the initial rate of HNO_3 loss was sufficiently fast that its loss could not be monitored continuously in the initial stages of the reaction. Thus, the lower limit to the reaction probability is $\gamma^{\text{NO}} \geq (6 \pm 2) \times 10^{-9}$ (2s). This is similar to the results of Saliba et al. (20) for the reaction of NO with HNO_3 on a smooth borosilicate glass surface at 50% RH, where the reaction probability was estimated to be on the order of 10^{-8} .

The present studies show that the heterogeneous reaction of gaseous NO with HNO_3 occurs not only on porous and smooth glass but also on pure silica. Thus, catalysis by trace constituents in the borosilicate materials is not important in this reaction. The key to the chemistry is the presence of undissociated nitric acid in a thin water “film”; hence, the chemical composition of the underlying surface is important primarily with respect to the amount of water it holds under atmospheric conditions. Figure 3 shows the amount of water on various terrestrial surfaces as a function of relative humidity (52). Soil and stone typically have from one to a few layers of water over the range of relative humidities from 30 to 90%, with vegetation taking up less water, as expected from its hydrophobic surface. The water uptake by soil and stone is similar to that of borosilicate glass (20, 23) where the

HNO₃-NO reaction has been observed to occur at intermediate relative humidities (~40-60% RH) in a manner similar to that observed here on hydrated silica surfaces. Thus, the chemistry occurring in thin water films on soil, sand, and other silicate materials in the boundary layer is expected to be similar to that observed in these laboratory studies.

These studies also show that the undissociated form of HNO₃ must be the reactive species and not the nitrate anion. This also indicates that the treatment of soils with nitrate fertilizer will not play a role in renoxification. In short, in addition to deposition and reaction with NH₃ and mineral components such as CaCO₃, HNO₃ may be in part removed by heterogeneous reaction with NO in thin water films on solid surfaces in the boundary layer.

Heterogeneous Reactions of CO, CH₄, and SO₂ with Adsorbed HNO₃. The reaction of CO with adsorbed HNO₃ was studied using CO concentrations from $(3-26) \times 10^{16}$ molecule cm⁻³. Adsorbed HNO₃ and gaseous CO were monitored for 60 min. No statistically significant decrease was observed in surface HNO₃ or gaseous CO, and no bands due to the expected products such as CO₂, HONO, or NO₂/N₂O₄ from HONO secondary reactions were observed. The addition of water vapor corresponding to 50% RH had no effect on the reaction.

Lary and Shallcross (11) suggested that this reaction may be feasible in particles containing iron, which can act as a catalyst. While both Fe³⁺ and Fe²⁺ have been observed in airborne particles, Fe³⁺ is the most common oxidation state present under atmospheric conditions (25-28). To probe for a catalytic effect of Fe³⁺ in the dark, one experiment was carried out using a pellet prepared from the mixture of silica and iron chloride (FeCl₃) (10:1 w:w). No reaction (i.e., disappearance of reactants or appearance of products) was identified over time. Therefore, Fe³⁺ does not catalyze the reaction of gaseous CO with HNO₃ on surfaces.

Sulfuric acid is a common component of particles in the atmosphere (1). To test for the effects of H₂SO₄ on the proposed reaction 3, an experiment was carried out under the same conditions using a silica pellet that had been previously submerged in concentrated H₂SO₄. Because of its low vapor pressure, H₂SO₄ does not desorb from the surface under our conditions, and there was insufficient transmission of the infrared beam to observe species on the surface. Thus, the surface was moved out of the infrared beam, and the gas phase was monitored. No gaseous products were observed, indicating that the presence of H₂SO₄ does not enhance the reaction of CO with HNO₃.

Although no significant decrease in CO was observed, we conducted a least-squares analysis of the CO concentration versus time to obtain the maximum possible loss of CO under these experimental conditions and hence to calculate an upper limit of the value for the reaction probability. We define the maximum loss rate as the lower 95% confidence limit of the slope of [CO] versus time. The maximum loss obtained shows no statistical difference when compared to blank experiments without HNO₃ treatment, confirming the lack of reaction. This approach gives an upper limit for the reaction probability (equation 1) of $\gamma^{\text{CO}} \leq 10^{-10}$. This upper limit is 6 orders of magnitude smaller than the reaction probability used by Lary and Shallcross in their modeling studies (11). This reaction therefore seems unlikely to be responsible for the discrepancy between the measured and the modeled NO_x/HNO₃ ratios.

Reaction 4 of gaseous CH₄ with adsorbed HNO₃ was studied using the porous glass plate and pressed silica pellets, with methane concentrations in the range of $(1-19) \times 10^{16}$ molecule cm⁻³. Peaks for adsorbed HNO₃ and gaseous CH₄ (3017 cm⁻¹) were monitored for 120 min. Again, no change in the reactants or appearance of products was observed.

Using the same approach as described above for CO, an upper limit to the reaction probability for reaction 4 of $\gamma^{\text{CH}_4} \leq 10^{-12}$ was obtained.

Finally, the reaction of gaseous SO₂ with adsorbed HNO₃ was studied using the porous glass plate and pressed silica pellets. For one porous glass plate experiment, a water vapor concentration equivalent to 40% RH was added. SO₂ concentrations of $(5-18) \times 10^{16}$ molecule cm⁻³ were used, and the reaction was monitored for 120 min. In one experiment, gas-phase SO₂ was monitored for 180 min with the porous glass out of the IR beam since it has a 1550 cm⁻¹ cutoff that prevents detection of the gas-phase SO₂ bands at 1360 and 1152 cm⁻¹ simultaneously with the surface bands. Again, no decrease in the adsorbed HNO₃ or gaseous SO₂ was observed, and no bands due to any of the expected products, such as H₂SO₄ (1196 and 1053 cm⁻¹), appeared (53) including in the experiment in which water vapor was added. From these observations, an upper limit of $\gamma^{\text{SO}_2} \leq 10^{-10}$ was calculated. The reaction of fuming nitric acid with SO₂ in solution to form nitrososulfuric acid has been reported but requires the presence of nitrogen dioxide (54). Martin et al. (55) reported that nitric acid in solution does not react with dissolved SO₂ and that the reaction was not catalyzed by a variety of metals, including Fe³⁺. The results of the present experiments, where HNO₃ is present in a thin water film on a surface and NO₂ is absent, are therefore consistent with the solution results.

Role of Surface Materials in Renoxification in the Boundary Layer. The tropospheric boundary layer contains appreciable areas of natural and artificial surfaces. While two well-characterized model silicate surfaces were used in these studies, there are many surfaces in the lowest region of the atmosphere that also contain significant amounts of silicates [e.g., soils and the surfaces of buildings, including windows (56-59)]. It is likely that the available area on these surfaces exceeds that on airborne particles in the boundary layer. As a result, these surfaces may play a significant role in the uptake and reaction of air pollutants in the region closest to the earth's surface where many air quality measurements are made, and human exposure to atmospheric constituents is maximized. We have denoted this as SURFACE: Surfaces, Urban and Remote: Films as a Chemical Environment.

Such surfaces may promote heterogeneous reactions, such as eqs 2-5, that are not kinetically favored in the gas phase but may occur on surfaces. If this were the case for HNO₃ adsorbed on surfaces, then the deposition of HNO₃ would become a part of the active nitrogen oxides cycle rather than act as a permanent sink as previously believed. These studies show that the reactions of HNO₃ adsorbed on silica surfaces with gaseous CO, CH₄, and SO₂ do not occur at measurable rates. As a result, these reactions are not expected to participate in renoxification in the boundary layer and seem highly unlikely to be responsible for the discrepancy between the measured and the modeled NO_x/HNO₃ ratios as proposed by model studies (11).

However, the reaction of adsorbed HNO₃ with gaseous NO does occur, with a lower limit to the reaction probability of $\gamma^{\text{NO}} \geq (6 \pm 2) \times 10^{-9}$ (2s). While this lower limit is relatively slow, such chemistry may occur over hours to days in the boundary layer of polluted urban atmospheres. Consider a column of air 1 cm × 1 cm and 38.5 m high, the height of the lowest box in a well-known airshed model (60). Using an NO concentration of 100 ppb that is found in polluted urban atmospheres, the rate of generation of additional NO₂ via the overall reaction 7 can be calculated to be 9×10^4 molecule cm⁻³ s⁻¹. In 1 h, an additional NO_x concentration of ~0.014 ppb would result from this renoxification. However, this assumes the surface is geometrically flat; this is certainly not the case for soil, where the available surface area can be much larger (e.g., ~1-15 m² g⁻¹) (61). We have measured the

mass per geometric area of a thin layer of sand to be 0.2 g cm^{-2} . With a surface area in the range of $1\text{--}15 \text{ m}^2 \text{ g}^{-1}$, this thin layer of sand with geometric area 1 cm^2 would have a surface for uptake and reaction of gases in the range of $(0.2\text{--}3) \times 10^4 \text{ cm}^2$ (i.e., a factor of 2000–30,000 greater than the flat geometrical area). If the $\text{HNO}_3\text{--NO}$ renoxification reaction occurred at the lower limit to the rate as measured in these laboratory studies, it would lead to the generation of additional NO_x of $\sim 30\text{--}400$ ppb, if transport of NO to the surface were not limiting. Diffusion and biological production of NO within the soil could also contribute to renoxification processes. On the other hand, the availability of HNO_3 on soils and other surfaces in the polluted boundary layer is not known but is likely to be less than that used in the present studies, and transport of NO to the surface from the boundary layer may be limiting.

Knipping and Dabdub (60) have shown that inclusion of renoxification reactions, specifically reaction 2, in the airshed model for the South Coast Air Basin in southern California may help to resolve some long-standing discrepancies between observations and model-predictions for species such as ozone. In this initial assessment carried out prior to the present experimental studies, the reaction probability was taken to be unity and the reaction limited by either the deposition rate of gas-phase HNO_3 or of turbulent diffusion/collision of nitric oxide with an idealized geometrically flat area at the earth's surface. While the reaction probability is likely substantially less than unity, the area at the surface available for such chemistry is much larger than the assumed flat surface as discussed above. These model studies gave much better agreement for the peak O_3 concentrations measured at the Central Los Angeles monitoring station and also predict the two ozone peaks commonly observed during the afternoon at downwind locations, unlike the base-case model. While it is not confirmed that the $\text{HNO}_3\text{--NO}$ reaction is indeed responsible for resolving the discrepancy between the model predictions and the field observations, it is intriguing and suggestive that such renoxification processes reproduce the observations in a manner that other known chemistry cannot.

Clearly, renoxification processes need to be considered further as potentially important in polluted urban atmospheres. In addition, the role of structures such as buildings, roads, etc. as well as natural materials such as soils and vegetation (SURFACE) in promoting heterogeneous reactions needs to be explored.

Acknowledgments

We are grateful to the California Air Resources Board (CARB) and the Graduate Studies Office of the University of California at Irvine for the support of this work. We also thank N. Saliba, V. Grassian, G. Lammel, and J. N. Pitts, Jr. for helpful discussions.

Literature Cited

- Finlayson-Pitts, B. J.; Pitts, J. N., Jr. *Chemistry of the Upper and Lower Atmosphere: Theory, Experiments, and Applications*; Academic Press: San Diego, CA, 2000.
- Grassian, V. H. *J. Phys. Chem. A* **2002**, *106*, 860.
- Hughes, L. S.; Allen, J. O.; Bhawe, P.; Kleeman, M. J.; Cass, G. R.; Liu, D. Y.; Fergenson, D. F.; Morrical, B. D.; Prather, K. A. *Environ. Sci. Technol.* **2000**, *34*, 3058.
- Diamond, M. L.; Gingrich, S. E.; Fertuck, K.; McCarry, B. E.; Stern, G. A.; Billeck, B.; Grift, B.; Brooker, D.; Yager, T. D. *Environ. Sci. Technol.* **2000**, *34*, 2900.
- Gingrich, S. E.; Diamond, M. L.; Stern, G. A.; McCarry, B. E. *Environ. Sci. Technol.* **2001**, *35*, 4031.
- Chatfield, R. B. *Geophys. Res. Lett.* **1994**, *21*, 2705.
- Singh, H. B.; Viezee, W.; Chen, Y.; Thakur, A. N.; Kondo, Y.; Talbot, R. W.; Gregory, G. L.; Sachse, G. W.; Blake, D. R.; Bradshaw, J. D.; Wang, Y.; Jacob, D. J. *J. Geophys. Res.* **1998**, *103*, 28237.
- WMO. *Scientific Assessment of Ozone Depletion: 1998*; World Meteorological Organization: Geneva, 1998.
- Gao, R. S.; Fahey, D. W.; Del Negro, L. A.; Donnelly, S. G.; Keim, E. R.; Neuman, J. A.; Teverovskaia, E.; Wennberg, P. O.; Hanisco, T. F.; Lanzendorf, E. J.; Proffitt, M. H.; Margitan, J. J.; Wilson, J. C.; Elkins, J. W.; Stimpfle, R. M.; Cohen, R. C.; McElroy, C. T.; Bui, T. P.; Salawitch, R. J.; Brown, S. S.; Ravishankara, A. R.; Portmann, R. W.; Ko, M. K. W.; Weisenstein, D. K.; Newman, P. A. *Geophys. Res. Lett.* **1999**, *26*, 1153.
- Osterman, G. B.; Sen, B.; Toon, G. C.; Salawitch, R. J.; Margitan, J. J.; Blavier, J.-F. *Geophys. Res. Lett.* **1999**, *26*, 1157.
- Lary, D. J.; Shallcross, D. E. *J. Geophys. Res.* **2000**, *105*, 11617.
- Perkins, K. K.; Hanisco, T. F.; Cohen, R. C.; Koch, L. C.; Stimpfle, R. M.; Voss, P. B.; Bonne, G. P.; Lanzendorf, E. J.; Anderson, J. G.; Wennberg, P. O.; Gao, R. S.; Del Negro, L. A.; Salawitch, R. J.; McElroy, C. T.; Hints, E. J.; Loewenstein, M.; Bui, T. P. *J. Phys. Chem. A* **2001**, *105*, 1521.
- Fairbrother, D. H.; Sullivan, J. D.; Johnston, H. S. *J. Phys. Chem. A* **1997**, *101*, 7350.
- Saliba, N.; Mochida, M.; Finlayson-Pitts, B. J. *Geophys. Res. Lett.* **2000**, *27*, 3229.
- Pitts, J. N., Jr.; Sanhueza, E.; Atkinson, R.; Carter, W. P. L.; Winer, A. M.; Harris, G. W.; Plum, C. N. *Int. J. Chem. Kinet.* **1984**, *16*, 919.
- Winer, A. M.; Biermann, H. W. *Res. Chem. Intermed.* **1994**, *20*, 423.
- Alicke, B.; Platt, U.; Stutz, J. *J. Geophys. Res.* **2002**, *107*, 8196, doi:10.1029/2002JD000075.
- Stutz, J.; Alicke, B.; Neftel, A. *J. Geophys. Res.* **2002**, *107*, 8192, doi:10.1029/2001JD000390.
- Mochida, M.; Finlayson-Pitts, B. J. *J. Phys. Chem. A* **2000**, *104*, 9705.
- Saliba, N. A.; Yang, H.; Finlayson-Pitts, B. J. *J. Phys. Chem. A* **2001**, *105*, 10339.
- Kiselev, A. V.; Lygin, V. I. *Infrared Spectra of Surface Compounds*; John Wiley & Sons: New York, 1975.
- Elmer, T. H. Porous and Reconstructed Glasses. In *Engineered Materials Handbook*; ASM International: Materials Park, OH, 1992; Vol. 4; p 427.
- Sumner, A. L.; Finlayson-Pitts, B. J. Manuscript in preparation, 2003.
- Pacific Environmental Services. *Background Report, AP-42 Section 6.8, Ammonium Nitrate Fertilizer*; U.S. Environmental Protection Agency: Washington, DC, 1996.
- Dedik, A. N.; Hoffmann, P.; Enslin, J. *Atmos. Environ.* **1992**, *26A*, 2545.
- Erel, Y.; Pehkonen, S. O.; Hoffmann, M. R. *J. Geophys. Res.* **1993**, *98*, 18423.
- Siefert, R. L.; Johansen, A. M.; Hoffmann, M. R.; Pehkonen, S. P. *J. Air Waste Manage. Assoc.* **1998**, *48*, 128.
- Zhu, X.; Prospero, J. M.; Millero, F. J. *J. Geophys. Res.* **1997**, *102*, 21297.
- Barney, W. S.; Finlayson-Pitts, B. J. *J. Phys. Chem. A* **2000**, *104*, 171.
- Brunauer, S.; Emmett, P. H.; Teller, E. *J. Am. Chem. Soc.* **1938**, *60*, 309.
- Low, M. J. D.; Ramasubramanian, N. *J. Phys. Chem.* **1966**, *70*, 2740.
- Adsorption on Silica Surfaces*; Papirer, E., Ed.; Marcel Dekker: New York, 2000; Vol. 90, 753pp.
- Cabot Corp. *Cab-O-Sil HS-5 Untreated Fumed Silica*; Cabot Corp: Tuscola, IL, 1999.
- Goodman, A. L.; Bernard, E. T.; Grassian, V. H. *J. Phys. Chem. A* **2001**, *105*, 6443.
- Finlayson-Pitts, B. J.; Wingen, L. M.; Sumner, A. L.; Syomin, D.; Ramazan, K. A. *Phys. Chem. Phys.* (in press).
- Shen, Z. X.; Kuok, M. H.; Tang, S. H. *Spectrochim. Acta* **1993**, *49A*, 21.
- Cziczo, D. J.; Abbatt, J. P. D. *J. Phys. Chem. A* **2000**, *104*, 2038.
- Fehsenfeld, F. C.; Ferguson, E. E.; Mosesman, M. *Chem. Phys. Lett.* **1969**, *4*, 73.
- Choi, J.-H.; Kuwata, K. T.; Haas, B.-M.; Cao, Y.; Johnson, M. S.; Okamura, M. *J. Chem. Phys.* **1994**, *100*, 7153.
- Hamman, E.; Lee, E. P. F.; Dyke, J. M. *J. Phys. Chem. A* **2000**, *104*, 4571.
- Fehsenfeld, F. C.; Howard, C. J. *J. Chem. Phys.* **1973**, *59*, 6272.
- Fehsenfeld, F. C.; Howard, C. J.; Schmeltekopf, A. L. *J. Chem. Phys.* **1975**, *63*, 2835.
- Cao, Y.; Choi, J.-H.; Haas, B.-M.; Johnson, M. S.; Okamura, M. *J. Chem. Phys.* **1993**, *99*, 9307.
- Cao, Y.; Choi, J.-H.; Haas, B.-M.; Okamura, M. *J. Phys. Chem.* **1994**, *98*, 12176.

- (45) Sunderlin, L. S.; Squires, R. R. *Chem. Phys. Lett.* **1993**, *212*, 307.
- (46) Kay, B. D.; Hermann, V.; Castleman, A. W. J. *Chem. Phys. Lett.* **1981**, *80*, 469.
- (47) Zhang, X.; Mereand, E.; Castleman, A. W. J. *J. Phys. Chem.* **1994**, *98*, 3554.
- (48) Gilligan, J. J.; Castleman, A. W. J. *J. Phys. Chem. A* **2001**, *105*, 5601.
- (49) Tao, F.-M.; Higgins, K.; Klemperer, W.; Nelson, D. D. *Geophys. Res. Lett.* **1996**, *23*, 1797.
- (50) Staikova, M.; Donaldson, D. J. *Phys. Chem. Chem. Phys.* **2001**, *3*, 1999.
- (51) McCurdy, P. R.; Hess, W. P.; Xantheas, S. S. *J. Phys. Chem. A* **2002**, *106*, 7628.
- (52) Lammel, G. *Formation of Nitrous Acid: Parameterization and Comparison with Observations*, Report No. 286; Max-Planck-Institut für Meteorologie: Hamburg, Germany, 1999; 36 pp.
- (53) Yang, H.; Finlayson-Pitts, B. J. *J. Phys. Chem.* **2000**, *105*, 1890.
- (54) Coleman, G. H.; Lillis, G. A.; Goheen, G. E. In *Inorganic Syntheses*; Booth, H. S., Ed.; McGraw-Hill: New York, 1939; Vol. 1, Chapter 5.
- (55) Martin, L. R.; Damschen, D. E.; Judeikis, H. S. *Atmos. Environ.* **1981**, *15*, 191.
- (56) Portland Cement Association. *Scientific Principles*; Skokie, IL, 1999.
- (57) BNZ Materials. *Silica Brick and Mortar and Insulating Fire Brick-Material Safety Data Sheet*, Littleton, CO, 1999.
- (58) Diamant, R. M. E. *Chemistry of Building Materials*; Business Books Limited: London, 1970.
- (59) USGS. *Sediment*; U.S. Geological Survey, National Park Service Department of Interior: Washington, DC, 1999.
- (60) Knipping, E. M.; Dabdub, D. *Atmos. Environ.* **2002**, *36*, 5741.
- (61) Hodson, M. E.; Langan, S. J.; Kennedy, F. M.; Bain, D. C. *Geoderma* **1998**, *85*, 1.
- (62) Cohn, H.; Ingold, C. K.; Poole, H. G. *J. Chem. Soc.* **1952**, 4272.
- (63) Querry, M. R.; Tyler, I. L. *J. Chem. Phys.* **1980**, *72*, 2495.
- (64) Goodman, A. L.; Underwood, G. M.; Grassian, V. M. *J. Phys. Chem. A* **1999**, *103*, 7217.

Received for review July 10, 2002. Revised manuscript received November 11, 2002. Accepted November 20, 2002.

ES020828G

The heterogeneous hydrolysis of NO₂ in laboratory systems and in outdoor and indoor atmospheres: An integrated mechanism

B. J. Finlayson-Pitts,* L. M. Wingen, A. L. Sumner, D. Syomin and K. A. Ramazan

Department of Chemistry, University of California, Irvine, Irvine, CA 92697-2025, USA.
 E-mail: bjfinlay@uci.edu; Fax: (949) 824-3168; Tel: (949) 824-7670

Received 2nd September 2002, Accepted 2nd December 2002
 First published as an Advance Article on the web 16th December 2002

The heterogeneous reaction of NO₂ with water on the surface of laboratory systems has been known for decades to generate HONO, a major source of OH that drives the formation of ozone and other air pollutants in urban areas and possibly in snowpacks. Previous studies have shown that the reaction is first order in NO₂ and in water vapor, and the formation of a complex between NO₂ and water at the air–water interface has been hypothesized as being the key step in the mechanism. We report data from long path FTIR studies in borosilicate glass reaction chambers of the loss of gaseous NO₂ and the formation of the products HONO, NO and N₂O. Further FTIR studies were carried out to measure species generated on the surface during the reaction, including HNO₃, N₂O₄ and NO₂⁺. We propose a new reaction mechanism in which we hypothesize that the symmetric form of the NO₂ dimer, N₂O₄, is taken up on the surface and isomerizes to the asymmetric form, ONONO₂. The latter autoionizes to NO⁺NO₃⁻, and it is this intermediate that reacts with water to generate HONO and surface-adsorbed HNO₃. Nitric oxide is then generated by secondary reactions of HONO on the highly acidic surface. This new mechanism is discussed in the context of our experimental data and those of previous studies, as well as the chemistry of such intermediates as NO⁺ and NO₂⁺ that is known to occur in solution. Implications for the formation of HONO both outdoors and indoors in real and simulated polluted atmospheres, as well as on airborne particles and in snowpacks, are discussed. A key aspect of this chemistry is that in the atmospheric boundary layer where human exposure occurs and many measurements of HONO and related atmospheric constituents such as ozone are made, a major substrate for this heterogeneous chemistry is the surface of buildings, roads, soils, vegetation and other materials. This area of reactions in thin films on surfaces (*SURFACE* = Surfaces, Urban and Remote: Films As a Chemical Environment) has received relatively little attention compared to reactions in the gas and liquid phases, but in fact may be quite important in the chemistry of the boundary layer in urban areas.

I. Introduction

It has been known for more than half a century that a number of reactions of nitrogen oxides that are slow in the gas phase do occur at significant rates on the surfaces of laboratory systems. One of the best known examples is the reaction of NO₂ hydrolysis, where the overall stoichiometry is represented by reaction (1):

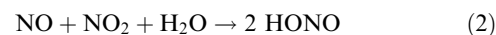


This reaction is of particular interest in atmospheric chemistry because it generates nitrous acid (HONO), a major source of OH in polluted urban atmospheres.^{1–12} Since OH initiates the chemistry that leads to the formation of ozone and other air pollutants, it is important to determine which OH precursors are significant in order to accurately model urban airsheds and to develop regional control strategies. A number of studies have shown that HONO is a major OH source when compared to other well known sources of OH such as the photolysis of O₃ and HCHO, and the dark reaction of ozone with alkenes; this is the case not only at dawn, but even when averaged over the entire day.^{3,7,11,12} The formation of HONO by reaction (1) indoors has also been observed^{13–21} and is of concern since it can lead to human respiratory tract irritation²² and can react with amines in air to form carcinogenic nitrosamines.²³

There are a number of excellent reviews of potential mechanisms of HONO formation in the troposphere (*e.g.*, refs. 4–7). While reaction (1) is believed to be a major contributor to

HONO formation in air, there are other sources, including direct emissions from fossil fuel combustion.^{14–17,20,24–26} Another potential source is the reaction of soot surfaces with NO₂.^{27–35} However, it appears that the soot surface deactivates with time, which would limit the amount of HONO that can be generated from this reaction. A recent study³⁶ suggests that it is the semi-volatile and/or water-soluble organics generated in diesel exhaust that lead to significant HONO formation from NO₂, rather than the soot surface itself.

Modeling studies combined with measurements of HONO and its precursors in urban areas suggest that the reaction (2) of NO, NO₂ and water is a HONO source.⁴

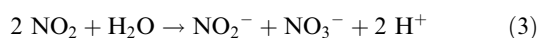


In contrast, the addition of NO to the NO₂–H₂O mixture in laboratory studies does not affect the reaction, and therefore it is generally thought that reaction (2) is not important.^{27,37–46}

The gas phase reaction of OH with NO also generates HONO. However, since most of the OH sources are photolytic, this reaction is most important during the day when HONO efficiently photolyzes back to OH + NO.⁸ Similarly, the reaction of HO₂ with NO₂ generates HONO, but is not likely to be a significant source of atmospheric HONO due to its small rate constant⁴⁷ and competing daytime photolysis.

Photochemical formation of HONO in snowpacks has been identified in the Arctic following irradiation of surface snow with either natural sunlight or a xenon arc lamp with a Pyrex glass filter ($\lambda > 280 \text{ nm}$).^{48,49} Zhou *et al.*⁴⁸ proposed that

photolysis of NO_3^- present in the snow forms predominantly O^- and NO_2 at the air–ice interface, with the NO_2 hydrolyzing to nitrite and nitrate ions in a reaction equivalent to reaction (1):



When the snow surface is acidic, NO_2^- is converted to HONO which then escapes to the gas phase. Despite the fast photolysis of HONO occurring during daylight hours, the researchers observed up to 10 ppt HONO near the surface under ambient conditions. The generation of OH in snowpacks, either through the reaction of O^- with water or the photolysis of HONO, is important since it leads to oxidation of organics and the generation of such species as HCHO.⁵⁰

Finally, the formation of HONO has been observed during sampling of ambient air through a “dirty” borosilicate glass sampling tube.⁵¹ The reaction leading to HONO is not entirely clear, but appears to require sunlight. Nitrous acid production was not observed immediately after cleaning of the sampling line, suggesting that a water-soluble species, such as nitric acid and/or nitrate, on the surface plays a role in the observed production of HONO. Photolysis of nitrate to form NO_2 , followed by reaction (1), was proposed as the source of HONO.

In summary, it is generally believed that reaction (1) is a significant source of HONO, and hence OH. Current urban airshed models often include a simple parameterization of reaction (1) based on rates observed experimentally in some laboratory systems. However, this treatment may not be appropriate given the complexity of the reaction, the important role of the surface and species adsorbed on it, and how the surface composition changes during experiments. It is clearly critical to understand the reaction on a molecular level in order to accurately include it in airshed models that are used to develop air pollution control strategies. In addition, understanding this chemistry will contribute to the elucidation of the photochemistry in snowpacks. Finally, this chemistry may occur on surfaces of airborne dust particles that are known to be transported globally and to play a role in the chemistry of the global troposphere.^{52–62}

A number of studies^{16,26,37,40–46,63–74} have established that reaction (1) is negligible in the gas phase but occurs in the presence of surfaces. Fig. 1 summarizes the results of a number of these studies in terms of the measured rates of reaction as a function of the surface-to-volume (S/V) ratio of the reaction cells used. This plot shows the combined formation rates of HONO plus NO (a secondary reaction product of HONO) normalized for the different initial NO_2 and water vapor concentrations used in the various studies. An increase in the rates with S/V is expected for a surface reaction where there are a given number of product molecules formed per second per unit surface area. For large reactors (small S/V), the product is diluted into a larger volume, giving a smaller increase in the product concentration per unit time compared to smaller reaction chambers. Thus, the trend to larger reaction rates with larger S/V ratios seen in the data shown in Fig. 1 is consistent with expectations for a heterogeneous reaction on the chamber surface.

While the experimental results are not uniformly in quantitative agreement, there are a number of common observations of NO_2 hydrolysis studies in the dark:

(1) Three gas phase products have been observed. The major gas phase product is HONO, but the yield is usually less than the 50% expected from reaction (1).^{13,21,40–46,67,70} NO is the other significant gaseous product;^{21,40–42,66,67} in some studies (e.g. Sakamaki *et al.*⁴⁰), NO was reported to be formed simultaneously with HONO, while in others (e.g. Pitts *et al.*⁴¹) it was observed only at longer reaction times. Small quantities of N_2O are also formed.^{45,46,70}

(2) The rate of generation of HONO has been reported in most studies of this reaction to be first order in nitrogen dioxide^{13,16,40–43,45,46,71} and first order in water vapor.^{40–43}

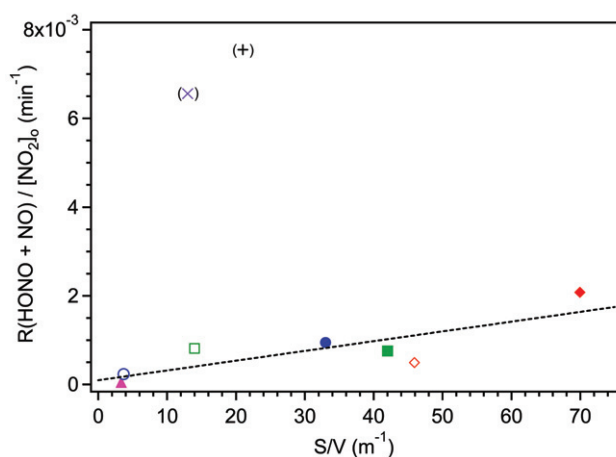


Fig. 1 Summary of some of the literature reported rates for the heterogeneous hydrolysis of NO_2 as a function of the surface-to-volume (S/V) ratio of the reactor. The y-axis is the total rate of HONO plus NO formation normalized to 1 ppm NO_2 and 50% relative humidity. ▲ Pitts *et al.*⁴¹ Teflon-coated chamber at 24 C and 50% RH (S/V = 3.4 m^{-1}); ○ Sakamaki *et al.*⁴⁰ PFA-coated chamber at 30 C and 49% RH (S/V = 3.7 m^{-1}); ● Sakamaki *et al.*⁴⁰ quartz cell at 22 C and 15% RH (S/V = 33 m^{-1}); □ Svensson *et al.*⁴² Teflon-lined chamber at 22 C and 54% RH (S/V = 14 m^{-1}); ■ Svensson *et al.*⁴² Teflon-lined chamber at 22 C and 29% RH with Teflon foil added (S/V = 42 m^{-1}); Jenkin *et al.*⁴³ Pyrex chamber at 23 C and 29% RH (S/V = 13 m^{-1}); + Wiesen *et al.*⁴⁵ Quartz reactor with dry, synthetic air (S/V = 21 m^{-1}); ◇ Data from this laboratory: 19.4 L glass cell at 23 C and 50% RH (S/V = 46 m^{-1}); ◆ Data from this laboratory: 7.4 L glass cell at 23 C and 50% RH (S/V = 70 m^{-1}).

(3) Nitric acid has not been observed in the gas phase but nitrate is measured in washings from the surface⁴² and on denuder surfaces,¹⁶ and molecular nitric acid has been observed on silica surfaces in the presence of NO_2 and water.^{72,73} Presumably, as the reaction proceeds, the surfaces become more acidic.

(4) The rates of NO_2 loss and HONO formation in clean chambers are higher than those in “conditioned chambers” (i.e. “dirty” chamber contaminated from previous experiments).^{41,42}

(5) The rates in conditioned chambers are relatively insensitive to the nature of the underlying surface. For example, Svensson *et al.*⁴² reported similar rate constants for HONO formation on glass and smooth FEP Teflon film, and Pitts *et al.*^{13,41} showed that the rates of HONO production in two environmental chambers and in a mobile home were relatively consistent over a wide range of initial NO_2 concentrations (0.05–20 ppm). The data in Fig. 1 also illustrate that the rates measured using different surfaces are relatively consistent, again suggesting that the nature of the underlying surface does not play a critical role in the reaction.

(6) Use of H_2^{18}O generates H^{18}ONO and, at very low water vapor concentrations, HON^{18}O is also generated. For example, Sakamaki *et al.*⁴⁰ showed that NO_2 reacts in a small quartz cell at room temperature with H_2^{18}O at 15% RH to generate exclusively H^{18}ONO . Svensson *et al.*⁴² reported a similar observation for relative humidities in the range of ~20–40%; however, at a relative humidity of ~4%, HON^{18}O was also formed.

Here we present new experimental data for the heterogeneous hydrolysis of NO_2 in laboratory systems and discuss them in light of these previous studies. We outline major features of a new mechanism for reaction (1) that is consistent not only with our experiments but also with many of the previous observations summarized above. It should be noted that, although there is firm experimental evidence for some steps in the proposed mechanism, there remain major gaps in our

understanding of some portions. This continues to be an active area of research in this laboratory and future studies will undoubtedly shed new insights into the chemistry of this complex system. It is our hope that, by presenting this proposed mechanism at this time, it will spur additional work on this heterogeneous chemistry and the various steps that comprise the overall reaction.

The studies reported here have been carried out using borosilicate glass, which is relevant to understanding the mechanism in laboratory systems. This is an essential first step for extrapolating to processes in urban airsheds. It should be noted that silicates themselves are atmospherically relevant as they are major components of building materials and soils.^{56,75–78} The surface area available in soils and buildings may be comparable to, or larger than, the surface area of airborne particles in the planetary boundary layer. Thus, it is expected that heterogeneous chemistry in the boundary layer, where measurements of HONO and other oxides of nitrogen are often made, will have a significant contribution from reactions on soils, buildings, roads, and other such materials.^{5–7} There is some evidence for this from field studies. For example, Harrison and coworkers^{7,79} observed fluxes of HONO upward from the surface when NO₂ concentrations were > 10 ppb, but downward fluxes at smaller NO₂ concentrations; they attributed this to competition between generation at the surface and the deposition of HONO. Andrés-Hernández *et al.*⁸⁰ concluded that the relatively large HONO/NO_x ratios they observed in Milan compared to less polluted non-urban regions were due to heterogeneous chemistry on urban surfaces such as buildings, aided by a low inversion layer.

In short, given the contribution of silicates to the composition of soils and many building materials, the chemistry discussed below may extrapolate in a reasonable fashion to the lowest portion of the atmosphere in urban areas. In addition, as discussed in Section V, this chemistry may occur on airborne dust particles that are transported globally. Finally, the mechanistic insights obtained from room temperature studies on surfaces will also aid in understanding the chemistry and photochemistry reported on ice surfaces.

We focus in this article on studies reported in the literature of heterogeneous NO₂ hydrolysis that have been carried out using water vapor, gas phase NO₂ and a solid surface. The potential relevance to the reactions on liquid aerosol particles, fogs and clouds is discussed briefly in Section V.

II. A new mechanism for HONO formation from the reaction of NO₂ with water on surfaces

Fig. 2 is a schematic diagram of the major components of our proposed mechanism. The key features are as follows:

1. The dimer of nitrogen dioxide, N₂O₄, is an important precursor surface species in the reaction.
2. The reactive surface species is proposed to be asymmetric dinitrogen tetroxide, ONONO₂, formed by isomerization of symmetric N₂O₄.
3. The asymmetric ONONO₂ autoionizes to generate NO⁺NO₃⁻; this is in competition with a back reaction with gas phase NO₂ to form symmetric N₂O₄. The NO⁺NO₃⁻ complex reacts with water to generate HONO that escapes, at least in part, from the surface, as well as nitric acid that remains on the surface.
4. The HNO₃ on the surface generates NO₂⁺, a well known reaction in concentrated solutions of HNO₃.
5. Nitric oxide is generated by the reaction of HONO with NO₂⁺. Nitrous acid also reacts with HNO₃ to generate NO⁺ on the surface.

We describe in the following sections a variety of experimental data from this laboratory and show that this mechanism is

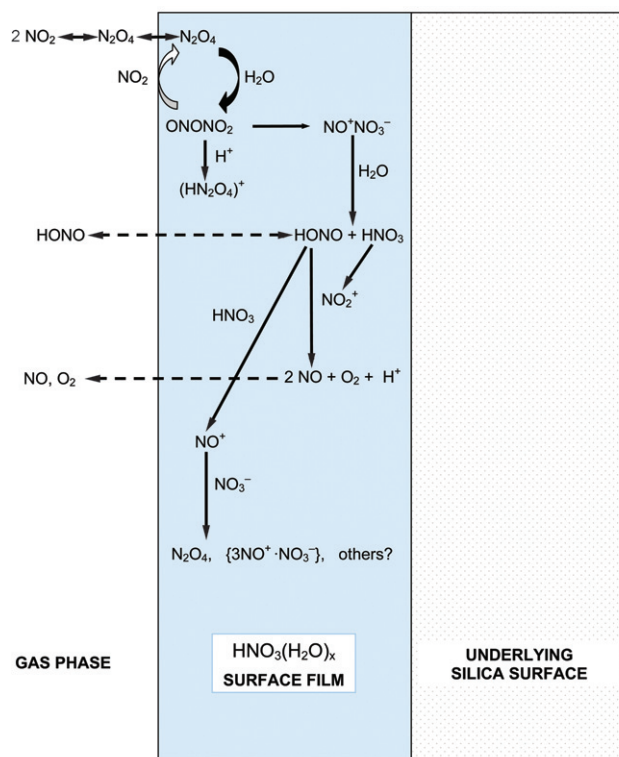


Fig. 2 Schematic diagram of proposed mechanism of heterogeneous hydrolysis of NO₂.

consistent with these data as well as with many observations from previous studies of the heterogeneous hydrolysis of NO₂.

III. Present and prior observations: Testing the mechanism

A. Products, intermediates, and mass balance

1. Gas phase products. Product formation in heterogeneous NO₂ hydrolysis experiments has been studied in this laboratory using Fourier transform infrared spectroscopy (FTIR) to measure gaseous species in two borosilicate glass long path cells with multi-reflection White cell optics.⁸¹ The experiments were carried out by first adding a low pressure of a dilute NO₂/N₂ mixture to the cell and then bringing the cell to atmospheric pressure at the desired relative humidity (~20%, 50%, or 80%) using the appropriate combination of flows of H₂O/N₂ and dry N₂. The reactants and products were measured by FTIR in the dark for reaction times up to 15 h.

The first cell used here had a volume of 7.4 L, a surface area of 0.31 m² and a surface-to-volume ratio of S/V = 42 m⁻¹; the base path is 0.8 m and the total pathlength used in these studies was 32 m. The second cell was 19.4 L in volume, with a surface area of 0.58 m² and a S/V of 30 m⁻¹; the base path in this apparatus is 1.0 m and the total pathlength used in these studies was either 84 m or 112 m. The surface areas and S/V cited are for the cells themselves and do not include the surface areas of the optics; the total area of the mirror mounts and mirrors is estimated to be ~40% of the cell surface area. When this additional surface is taken into account, the S/V for the 7.4 L cell is 70 m⁻¹ and that for the 19.4 L cell is 46 m⁻¹. The metal optics holders (but not the mirror surfaces themselves) were coated with halocarbon wax (Halocarbon Products, Inc., Series 1500) to prevent reactions with the metal.

Nitrogen dioxide was synthesized by combining an excess (> 2:1) of O₂ (Oxygen Service Co., 99.993%) with NO (Matheson, 99%) which had first been passed through a dry

ice–acetone bath (195 K) or ethanol–liquid N₂ bath (180 K) to remove HNO₃ and other impurities. The mixture was allowed to react in a 5 L glass bulb, then purified by condensing the mixture at 195 K and pumping away the excess O₂. Nitrogen was humidified by bubbling N₂ through Nanopure water (Barnstead, 18.2 MΩ cm) and diluting with dry N₂ (Oxygen Service Co, 99.999%).

In general, absorption spectra were quantitatively analyzed for each gaseous species using two approaches. The first was based on the net absorbances of the peaks at selected wavenumbers. The second used a least squares fitting procedure, MFC,⁸² which determines the ratio of the species in the spectrum of interest relative to a reference spectrum of known concentration. This fitting procedure uses all of the data over a selected spectral region, rather than the absorbance at a single peak height. MFC was used in conjunction with an in-house calibration or literature reference spectrum⁸³ at the same resolution and total pressure. Nitrogen dioxide was quantified using the band centered at 2910 cm⁻¹ for the MFC analysis as well as the net absorbance of the peak at 2917 cm⁻¹. Calibrations were carried out using an authentic sample of NO₂; although the 2910 cm⁻¹ band is much weaker than that in the 1600 cm⁻¹ region, it does not overlap with water absorption bands and hence provides more precise analysis. Nitrous acid was quantified using its ν₃ (*trans*-HONO) absorption at 1263 cm⁻¹ and the published effective cross section (base 10) of 3.7 × 10⁻¹⁹ cm² molecule⁻¹.⁸⁴ *Trans*-HONO is in equilibrium with the *cis* form, and the effective absorption cross section takes this ratio into account to give the total (*trans* plus *cis*) HONO concentration. The value of the effective cross section cited assumes the ratio of *trans/cis* at room temperature to be 2.3.⁸⁴ Nitrous oxide was quantified using the rotational line of the ν₃ band at 2236 cm⁻¹ with the calibration from an authentic sample of N₂O (Liquid Carbonic, 99.99%), or when using MFC, a published reference spectrum using the entire band centered at 2223 cm⁻¹ at the same resolution.⁸³

The small absorption lines of NO are particularly difficult to observe due to the strong water vapor absorptions in this region and the weak absorption cross section for NO in the infrared. Both the Q branch at 1876 cm⁻¹ and a second vibration–rotation line at 1900 cm⁻¹, which do not suffer from interference by water vapor lines, were compared with a calculated reference spectrum for quantification.⁸³ The detection limits in the 7.4 L cell were the following (in units of molecules cm⁻³): 5 × 10¹³ for NO₂, 1.5 × 10¹³ for HONO, 3.5 × 10¹³ for NO, and 2.5 × 10¹² for N₂O. In the 19.4 L cell, they were 2.8 × 10¹³ for NO₂, 6.2 × 10¹² for HONO, 4.3 × 10¹³ for NO, and 2.3 × 10¹² for N₂O.

Throughout the paper, we use a combination of units for concentration: molecule cm⁻³ or ppm for NO₂, HONO, NO and N₂O, and either relative humidity (RH) or molecule cm⁻³ for water vapor. Because concentrations have been reported both ways in the previous literature, we prefer to report our data using both conventions for ease of comparison with the various studies.

Typical concentration–time profiles for these experiments are shown in Fig. 3 at three different relative humidities. The experiments at ~20% and ~50% RH were carried out in the smaller cell (S/V = 70 m⁻¹) with an initial NO₂ concentration of 60 ppm. Runs were also carried out at 80% RH in the smaller cell, but there was a large uncertainty in quantification of the loss of NO₂ that may have been caused by significant amounts of liquid water at this high relative humidity on the optical mirrors as they aged. The experiment shown at 80% RH was carried out using the larger cell (S/V = 46 m⁻¹) and an initial NO₂ concentration of 100 ppm. The reaction occurs on the surface and hence depends on the S/V ratio of the reaction chamber; as discussed in more detail below, the rate of HONO formation also depends linearly on the initial NO₂ concentration. Experiments in these two cells under

conditions where the product of the S/V ratio and the initial NO₂ concentration are similar, as is the case for the data in Figs. 3a–c, should thus be directly comparable and, indeed, as discussed in more detail below, they are consistent.

In agreement with previous studies of this reaction,^{13,21,40–46,66–68,70} HONO and NO are the two major gaseous products observed. Small amounts of N₂O are also formed at the higher relative humidities and longer reaction times. The rates of loss of NO₂ and the formation of products clearly increase as the water vapor concentration increases. Under all conditions, nitrous acid increases initially, reaches a plateau, and then decreases. This behaviour suggests that HONO undergoes secondary chemistry in the cell.

The yields for each gaseous product were determined as a function of time and are also shown in Fig. 3d–f. The yield of HONO is much less than 50% of the NO₂ loss, particularly at longer reaction times where secondary chemistry becomes more important. The yield of NO relative to HONO increases with time, and NO becomes the major product after several hours. The formation of small amounts of N₂O is in agreement with the studies of Wiesen *et al.*⁴⁵ and Kleffmann *et al.*^{46,70} who reported N₂O formation during hydrolysis of NO₂ on the acidic surfaces of quartz reaction chambers and on acid–air interfaces using a bubbler apparatus.

For the overall reaction (1), the yield of gaseous HONO plus its secondary reaction products such as NO should be 50%. This is consistent with our measurements (Figs. 3d–f) when the experimental uncertainties, particularly in the NO concentrations, are taken into account. The scatter in the yield plots at shorter reaction times is due to two factors: (1) the products are present in concentrations near their detection limits, and (2) the change in the NO₂ concentration is small.

The variation in the yields of NO and HONO in the previous laboratory studies in the literature^{13,40–43,66,67} suggests that the nature of the surface film plays an important role in determining the relative amounts of NO and HONO generated. The initial yields of HONO approached 50% in the studies of Pitts *et al.*⁴¹ where the initial NO₂ concentrations were, for the most part, below 1 ppm. Sakamaki *et al.*⁴⁰ used a reaction chamber that was very similar in size (see Table 1) and surface materials, but observed significant yields of NO (about 30% of the HONO yields) even at short reaction times; however, their initial NO₂ concentrations were larger, from 0.78 ppm to 20 ppm. This was also the case for our studies, as well as those of a number of other researchers,^{42,66,67} which were carried out using initial NO₂ concentrations above one ppm. The use of higher reactant concentrations will result in more rapid accumulation of HNO₃ on the walls of the reactor and hence accelerate secondary surface reactions involving HNO₃. Perhaps relevant to this is the work of Febo and Perrino¹⁶ which, in contrast to the other studies, was carried out under flow conditions; they observed equimolar production of nitrite and nitrate, with the sum equal to the NO₂ loss. Under flow conditions, HONO would be swept away from the acidic surface as it is formed, minimizing secondary reactions on the walls. The body of evidence therefore suggests that the NO that is observed results from secondary reactions of HONO on the walls of the reactor that have become acidic due to the simultaneous generation of HNO₃ that remains on the surface.

2. Surface species. a. *N₂O₄*. Infrared spectroscopic studies show that adsorbed N₂O₄ is formed on the reaction surface immediately upon exposure of silica surfaces to gaseous NO₂ at room temperature.^{72,73} There is no evidence for detectable amounts of NO₂ adsorbed on the surface. This is reasonable since the Henry's law coefficient for N₂O₄ in water and sulfuric acid is approximately two orders of magnitude larger than that for NO₂.^{8,85–87} Although we show below that these reactions cannot be thought of as occurring in bulk aqueous

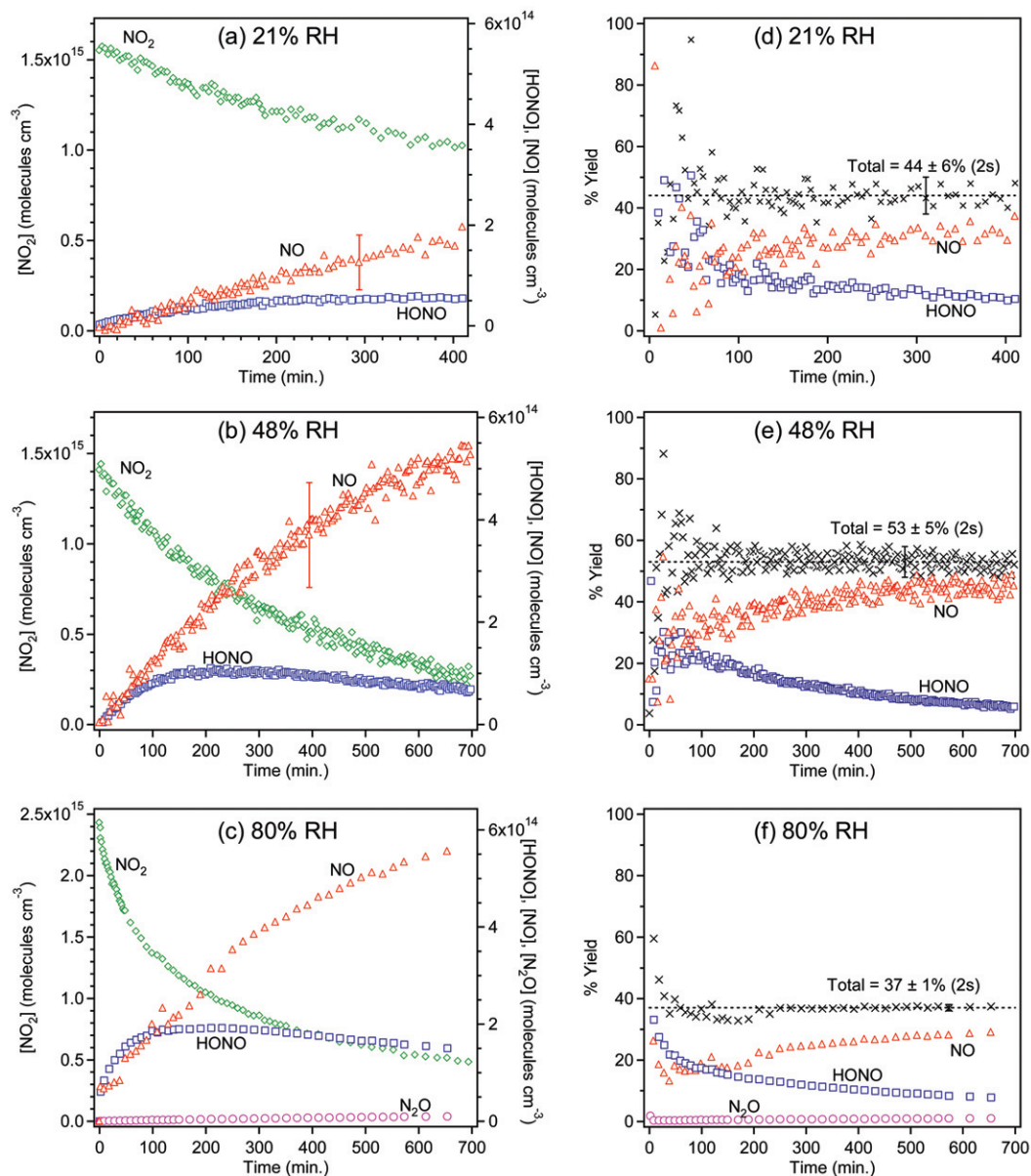


Fig. 3 Concentration–time profiles for NO_2 hydrolysis experiments in this laboratory at (a) 21% RH, $[\text{NO}_2]_0 = 1.5 \times 10^{15}$ molecules cm^{-3} , (b) 48% RH, $[\text{NO}_2]_0 = 1.4 \times 10^{15}$ molecules cm^{-3} , (c) 80% RH, $[\text{NO}_2]_0 = 2.5 \times 10^{15}$ molecules cm^{-3} . The corresponding yields of gas phase HONO, NO and N_2O , expressed relative to the measured losses of NO_2 , are shown in parts (d–f). As discussed in the text, the experiments at 21% and 48% RH were carried out in the 7.4 L cell and that at 80% in the 19.4 L cell.

solutions, the relative values of the Henry's law constants do indicate that the interaction of water with N_2O_4 is more favorable than with NO_2 . Chou *et al.*⁷⁴ have shown by *ab initio* calculations that complexes between N_2O_4 and one or two water molecules are stabilized by 4.3 kcal mol^{-1} and 11.5 kcal mol^{-1} , respectively, relative to separated N_2O_4 and water; the complexes of NO_2 with one or two water molecules were shown to be stabilized by only 0.9 kcal mol^{-1} and 8.3 kcal mol^{-1} relative to the separated reactants.⁷⁴ Thus, both the relative values of the N_2O_4 and NO_2 Henry's law constants and *ab initio* calculations show that N_2O_4 interacts more strongly with water and would be more likely present in the surface water film.

Although N_2O_4 is observed on the surface immediately upon exposure to NO_2 , it is not known how N_2O_4 interacts with the surface film. Possible interactions include association with one or more H_2O molecules,⁷⁴ with undissociated HNO_3 molecules, or with HNO_3 – H_2O complexes or hydrates. Nitric acid does appear to be involved as our experiments show that it enhances the amount of N_2O_4 on the surface. Fig. 4 shows the transmission spectra of clean pieces of porous glass (Vycor 7930, 14 mm diameter \times 0.24 mm thick discs of mass 59 mg

and an internal (BET) surface area of 250 $\text{m}^2 \text{g}^{-1}$, Advanced Glass and Ceramics, Holden, MA) exposed in a cell described elsewhere⁷² to NO_2 with and without prior adsorption of HNO_3 on the glass surface. The porous glass had been exposed to the water vapor in room air and not heated during the initial cell evacuation. Under these conditions, water remains adsorbed on the surface.

In Fig. 4a, the glass has been “conditioned” with dry gaseous HNO_3 by adding 2–3 Torr of HNO_3 vapor from above a mixture of 2:1 H_2SO_4 : HNO_3 (Fisher Scientific 95.7% H_2SO_4 , 69.9% HNO_3) to the cell, and then pumping it out; this procedure was repeated three times followed by pumping for 30 min before 1.2 Torr NO_2 was added. Fig. 4b is the spectrum for porous glass that was exposed to 1.3 Torr of gaseous NO_2 alone. In both cases, the cell was filled with N_2 to atmospheric pressure. The band at 1680 cm^{-1} is due to molecular nitric acid on the surface and that at 1740 cm^{-1} is due to adsorbed N_2O_4 .^{72,73,88,89} Fig. 4c is the difference spectrum, (a – 0.92b), where the factor 0.92 takes into account the slightly larger NO_2 pressure when the spectrum in Fig. 4b was taken. These data show that not only is N_2O_4 taken up on the porous glass

Table 1 Reanalysis of some kinetics data reported in the literature on heterogeneous NO₂ hydrolysis on the surfaces of laboratory systems (Teflon, glass, quartz, acid solutions, aerosol particles)

Reference	Type A plots		Type B plots ^a		Reactor type	Reported reaction order
	ln[NO ₂] vs. time	1/[NO ₂] vs. time	Slope of log d(-[NO ₂]/ dt) vs. log [NO ₂] ₀ (2s)	Slope of log d([HONO]/ dt) vs. log [NO ₂] ₀ (2s)		
England and Corcoran, 1974 ⁶⁶	Linear in first 500 min	Linear in first 500 min	N/A ^b	N/A	4.4 L Pyrex (S/V 36 m ⁻¹)	Authors reported second order in NO ₂ at 25–40 °C using NO ₂ decay at H ₂ O concentrations of (0.7–2.8) × 10 ¹⁷ cm ⁻³
Sakamaki <i>et al.</i> , 1983 ⁴⁰	N/A ^b	N/A	1.2 0.2	0.74 0.37	6065 L PFA-coated (S/V 3.7 m ⁻¹)	Authors reported first order in NO ₂ using NO ₂ decay rate or HONO and NO formation rates at 30 °C and [H ₂ O] of 2.3 × 10 ¹⁷ cm ⁻³
Pitts <i>et al.</i> , 1984 ⁴¹	N/A	N/A	1.0 0.2 ^c	0.85 0.15 ^c	5800 L Teflon-coated chamber (S/V 3.4 m ⁻¹)	Authors reported that slope of HONO formation in Type B plot was close to unity at 297 K and [H ₂ O] of 3.7 × 10 ¹⁷ cm ⁻³ and at 305 K and [H ₂ O] of 5.9 × 10 ¹⁷ cm ⁻³
Svensson <i>et al.</i> , 1987 ⁴²	N/A	N/A	1.1 0.04	0.59 0.25	153 L glass reactor lined with Teflon film (S/V 14 m ⁻¹)	Authors reported first order for NO ₂ decay at [H ₂ O] = 2.5 × 10 ¹⁶ cm ⁻³ using data after first 60 min of reaction
Jenkin <i>et al.</i> , 1988 ^{d 43}	N/A	N/A	1.2 0.5	N/A	19.8 L PTFE-coated glass cylinder with stainless steel endplates (S/V 13 m ⁻¹)	^d Authors reported first order for NO ₂ loss at 292 K and [H ₂ O] = 1.2 × 10 ¹⁷ cm ⁻³
Febo and Perrino, 1991 ^{e 16}	N/A	N/A	N/A	1.5 0.2	Frosted Pyrex glass flow reactor	^e Authors reported first order in NO ₂ by NO ₂ decay or HONO formation at 5 × 10 ¹⁷ cm ⁻³ H ₂ O
Wiesen <i>et al.</i> , 1995 ⁴⁵	Linear in first 50 min	Linear in first 50 min	N/A	N/A	64 L quartz reactor Pyrex cell (S/V 21 m ⁻¹) and bubbler connected to 11 L Pyrex cell (S/V 22 m ⁻¹)	Authors reported HONO formation was first order in NO ₂ in quartz reactor and dry synthetic air and when gases were passed through a bubbler containing various solutions
Harrison and Collins, 1998 ⁷¹	Linear in first 2 min	Linear in first 2 min	N/A	N/A	Flow tube in presence of aerosol particles	Authors reported NO ₂ loss is first order in NO ₂ at 279 K at [H ₂ O] = 2 × 10 ¹⁷ cm ⁻³
Kleffman <i>et al.</i> , 1998 ⁴⁶	Linear in first 100 min	Linear in first 100 min	N/A	N/A	64 L quartz reactor (S/V 21 m ⁻¹) and bubbler containing sulfuric acid/water solutions	Both NO ₂ decay and HONO formation were reported first order in NO ₂ on quartz surface at [NO ₂] = (0.05–5) × 10 ¹² cm ⁻³ and [H ₂ O] = (10 ¹² –10 ¹⁷ cm ⁻³). NO ₂ loss was first order when bubbled through sulfuric acid solutions. Authors reported that NO ₂ decay was second order in NO ₂ at high [NO ₂] and 248 K in bubbler apparatus
This work	Linear in first 200 min	Linear in first 200 min	1.6 0.2	1.2 0.4	20 L glass cell (S/V 30 m ⁻¹)	

^a Values for slopes calculated here based on data presented in those papers. ^b N/A = data not reported in paper in such a manner that this value could be calculated. ^c Calculated using the 297 K data. ^d Most experiments were performed at <10 Torr total pressure, with four performed at ~300 Torr. ^e The authors did not report the temperature; we presumed 25 °C to calculate that their RH ≈ 64%.

surface, but also that the amount adsorbed increases with the amount of nitric acid on the surface. This suggests that N₂O₄ is interacting with HNO₃ and/or HNO₃–H₂O water complexes on the surface, perhaps in addition to the interactions with H₂O.

In the long path cell studies shown in Fig. 3, surface species could not be measured and so it was not known if NO₂/N₂O₄ was taken up on the surface. However, given the rapid appearance of N₂O₄ on silica surfaces (Fig. 4 and refs. 72 and 73), it is

likely that a similar process occurs on the borosilicate glass cell walls.

N₂O₄ has generally been ignored as being important in the atmosphere because of its small concentrations and relatively slow reactions in the gas phase. For example, at an NO₂ concentration of 0.1 ppm (2.5 × 10¹² molecule cm⁻³), the equilibrium concentration of N₂O₄ is only 1.5 × 10⁶ molecule cm⁻³, based on the well-known 2 NO₂ ↔ N₂O₄ equilibrium constant.⁹⁰ Although our studies were carried out at much higher concen-

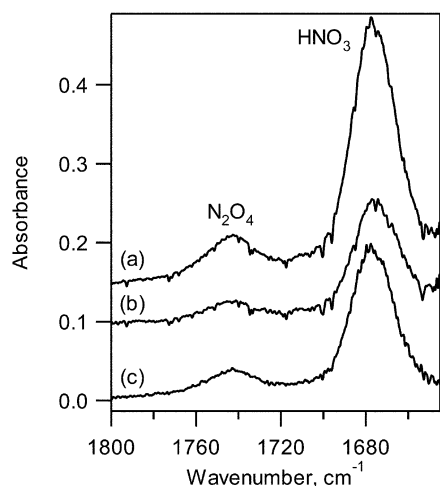


Fig. 4 Spectra of porous glass discs: (a) Exposed to gaseous HNO_3 followed by pumping and then adding 1.2 Torr NO_2 ; (b) porous glass exposed to 1.3 Torr NO_2 only; (c) difference spectrum (a - 0.92b). All experiments carried out in 1 atm N_2 using 64 scans at 1 cm^{-1} resolution. Background used for spectra was that of the unexposed porous glass.

trations of NO_2 , and hence N_2O_4 , than found in the atmosphere, they demonstrate that N_2O_4 is preferentially taken up on surfaces compared to NO_2 . Given that the kinetics on surfaces may be quite different than in the gas phase and that the relevant chemistry forming HONO in the atmosphere occurs rather slowly (e.g., overnight), it is reasonable that N_2O_4 could play a role under atmospheric conditions.

b. Nitric acid and nitric acid–water hydrates. While a number of groups report that HNO_3 production is not observed in the gas phase,^{16,40–42} a variety of both indirect as well as direct evidence indicates that HNO_3 is indeed formed and remains on the surface. For example, Svensson *et al.*⁴² rinsed the walls of their chamber with water after NO_2 hydrolysis experiments and analyzed the washings by ion chromatography (IC); the nitrate concentration was shown to be consistent with the stoichiometry of reaction (1). Febo and Perrino¹⁶ used a glass flow reactor to study the products of NO_2 hydrolysis. The HNO_3 and HONO that remained on the walls after reaction were collected and measured by IC as NO_3^- and NO_2^- , respectively, while gaseous HONO was measured using a chemiluminescence analyzer in combination with denuders to remove HNO_3 and HONO, or HNO_3 only. In their experiments, equal rates of formation of nitrite and nitrate were observed, and the sum was equal to the NO_2 decay rate.

More recently, infrared studies have confirmed the formation of HNO_3 and NO_3^- during the reaction of NO_2 on silica surfaces.^{72,73} For example, Goodman *et al.*⁷³ showed by transmission FTIR that addition of gaseous NO_2 to dehydrated silica particles (heated to 673 K) yields oxide-coordinated NO_3^- . In contrast, the use of hydrated silica particles, prepared by exposure to ≥ 10 Torr H_2O followed by evacuation (yielding a coverage of 0.08 H_2O monolayers), resulted in the formation of undissociated HNO_3 upon addition of gaseous NO_2 . The authors suggest that water on hydrated silica particles interacts with undissociated HNO_3 via hydrogen bonding which may be observed as a broad absorption in the 2700–3700 cm^{-1} region. Similar observations of the formation of undissociated HNO_3 during the reaction of NO_2 on porous glass were also made in this laboratory;⁷² the infrared cutoff of porous glass at $\sim 1550 \text{ cm}^{-1}$ did not allow the observation of nitrate ions, but subsequent studies using pressed discs of silica powder where the cutoff is extended to $\sim 1300 \text{ cm}^{-1}$ revealed small peaks due to NO_3^- .⁹¹

It should be noted that the surface nitric acid observed is largely undissociated HNO_3 which, as discussed below, has unique

reactivity compared to the dissociated H^+ and NO_3^- ions. Thin films of water on silica surfaces do not have the same spectroscopic signatures as bulk water, so it is perhaps not surprising to find undissociated HNO_3 associated with these thin water films. For example, transmission FTIR spectroscopy experiments on water uptake on borosilicate glass^{92,93} show that at the water vapor concentrations used in these experiments, one to twelve monolayers of water (corresponding to film thicknesses of 0.35 to 4 nm) would be present on the surface in the absence of nitric acid. These thin water films exhibit blue-shifted O–H stretching vibrations relative to bulk, liquid water, indicating that the thin films are less hydrogen-bonded than in the bulk liquid. This is similar to the observations of Ewing and coworkers on solids such as mica and NaCl, and has been interpreted as reflecting either a two-dimensional water network or islands of water on the surface.^{94–96} While it has been suggested that water films have properties approaching bulk water at approximately 3 water monolayers,⁹⁷ the data of Saliba *et al.*⁹² and Sumner *et al.*⁹³ show that the O–H stretch of adsorbed water is blue-shifted relative to bulk water even at 5 water monolayers. This suggests that it may be more appropriate to consider the mechanism of the NO_2 heterogeneous hydrolysis as occurring in a 2-D surface film or in small islands, rather than in a bulk, 3-D liquid.

However, this surface film is not simply comprised of water, since nitric acid is formed simultaneously during the reaction and remains on the surface. In addition, as discussed in more detail below, even after pumping and moderate heating, nitric acid from previous experiments remains on the surface. Thus, the thin film is, at the very least, comprised of nitric acid and water. An experimental observation common to researchers handling nitric acid in glass vacuum systems is that HNO_3 is very “sticky” and difficult to pump out, even with extensive heating and pumping. However, experiments in this and other⁹⁸ laboratories show that nitric acid can be readily pumped off dry silica surfaces. The role of water must be to form very stable nitric acid–water complexes or hydrates. Nitric acid is well known to form hydrates with water both in aqueous solution^{99–101} and on ice.^{102–105} In aqueous solution, as the concentration of nitric acid increases, the composition changes from the dissociated ions to the trihydrate and then the monohydrate, and finally pure HNO_3 .^{99–101} On ice, the dihydrate is also observed.^{102–105} Different forms of the monohydrate such as $\text{H}_2\text{O} \cdot \text{HONO}_2$, $(\text{H}_2\text{OH})^+ (\text{ONO}_2)^-$ and $4\text{HNO}_3 \cdot \text{H}_2\text{O}$ have also been observed using Raman spectroscopy.^{106,107}

There is also theoretical evidence for nitric acid–water complexes. *Ab initio* calculations of the 1:1 nitric acid–water complex in the gas phase have been carried out,^{108–110} showing that two hydrogen bonds form between HNO_3 and H_2O with a binding energy for the complex of 9.5 kJ mol^{-1} . Although such *ab initio* calculations are for a gas phase environment, these calculations show that undissociated HNO_3 is stabilized upon formation of the $\text{HNO}_3\text{--H}_2\text{O}$ complex. Studies of water clusters with HNO_3 have shown that four water molecules are required for dissociation of nitric acid.^{111–113} Thus, complexation of nitric acid with the relatively small amounts of water present in thin films on the surfaces, and limited dissociation to H^+ and NO_3^- is reasonable.

It should be noted that, in our experiments as well as those of other researchers, the reaction chambers are typically pumped on after each experiment, sometimes with heating. However, at least in the case of borosilicate glass, some nitric acid and water remains on the surface. As a result, the surface layer already contains adsorbed acid when the next experiment is initiated. This is likely responsible for the “dirty chamber” effect on the rates reported by some groups.^{41,42}

Experiments were conducted on porous glass to determine the relative strengths of interaction of HNO_3 and H_2O with a silica surface and how pumping affects the relative

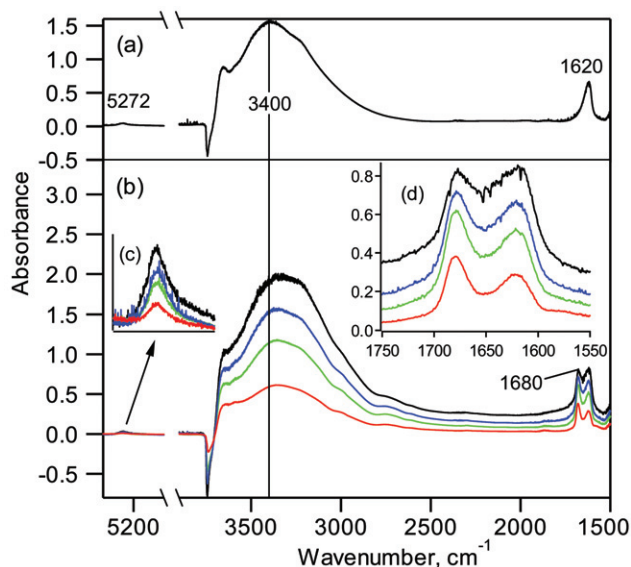


Fig. 5 Spectrum of porous glass exposed to (a) water vapor and (b) water vapor and nitric acid after pumping times of 0 s (black), 5 s (blue), 10 s (green), and 35 s (red). The insets show expanded regions for absorptions by (c) H₂O and (d) HNO₃, H₂O and complexes between the two.

magnitudes of water and nitric acid. Fig. 5a is a spectrum of water adsorbed on the porous glass, obtained by first heating the porous glass to 400 K to drive off adsorbed water, cooling to room temperature and then exposing to 10 Torr water vapor in 723 Torr N₂ for 30 min.; the gas phase water peaks have been subtracted. Absorption bands due to water at 1620 cm⁻¹ (ν_2 bending mode), 3400 cm⁻¹ (ν_1 and ν_3 stretching modes) and a weak combination band ($\nu_2 + \nu_3$) at 5272 cm⁻¹ are evident. The negative peak at 3750 cm⁻¹ is due to the free (non-hydrogen bonded) SiO-H stretch, indicating that free SiO-H groups decrease on exposure to water vapor. This is believed to be due to clustering of water to these groups *via* hydrogen bonding interactions; on pumping off the water, this peak recovers, indicating that the interaction is reversible.

Fig. 5b shows spectra of porous glass after it had been heated to 420 K, cooled and exposed to 1.5 Torr HNO₃ followed by 10 Torr of water vapor. The first spectrum (black) was taken 10 min later (the gas phase has been subtracted). The peak at 3400 cm⁻¹ has red-shifted by ~70 cm⁻¹ to 3330 cm⁻¹, and a new peak at 1680 cm⁻¹ appears. The latter is assigned to undissociated HNO₃.^{72,73,98} The peak at 1620 cm⁻¹ has broadened. *Ab initio* calculations¹⁰⁸⁻¹¹⁰ show that the formation of a 1:1 HNO₃-H₂O complex in the gas phase results in a band at ~3300 cm⁻¹ due to the hydrogen-bonded OH ν_1 stretch in nitric acid; this band is red-shifted by ~300 cm⁻¹ from the OH stretch in the uncomplexed gas phase HNO₃. As more water is complexed to nitric acid, this band continues to red-shift.¹¹⁰ These calculations are consistent with the infrared spectra of nitric acid hydrates, which typically have strong bands in this region.¹⁰²⁻¹⁰⁵ However, the bending mode of water in the 1600 cm⁻¹ region does not change significantly on binding to nitric acid, which is consistent with our observations.¹⁰⁸⁻¹¹⁰ We therefore assign the peaks at 3300 cm⁻¹ and 1620 cm⁻¹ in Fig. 5b to a combination of liquid water and nitric acid-water complexes.

The subsequent spectra were taken after pumping times of 5 s, 10 s and 35 s. During these initial stages of pumping, it can be seen that the water peak at 5272 cm⁻¹ decreases, indicating water is being pumped off the surface. The peaks at 1680 cm⁻¹ due to HNO₃ and 1620 cm⁻¹ due to water, or water complexed to nitric acid, also decrease; however, the 1620 cm⁻¹ band decreases more rapidly than that at 1680 cm⁻¹ (Fig. 5d). These

indicate a change in the composition of the surface film, consistent with the preferential removal of water, and may reflect a change from the trihydrate through the dihydrate to the monohydrate and perhaps ultimately species such as 4HNO₃·H₂O as observed in solid and liquid mixtures of HNO₃ and water by Raman spectroscopy.¹⁰⁶

The combination of data suggests that there are significant amounts of undissociated nitric acid on the surface, perhaps in part in the form of hydrates. In concentrated HNO₃ solutions, NO₂⁺ is also generated *via* a self-reaction of HNO₃:¹⁰¹



These reactions are in equilibrium so that, in the presence of sufficient water, NO₂⁺ converts back to HNO₃. Experimental studies¹¹⁴⁻¹¹⁸ have shown that, in the gas phase, this conversion of NO₂⁺ to HNO₃ occurs in clusters of NO₂⁺ with four or more water molecules.

A search was made for NO₂⁺ on porous glass during an NO₂ hydrolysis experiment and, for comparison, porous glass was exposed to gaseous HNO₃ alone. Fig. 6a shows the spectrum in the 2200 to 2400 cm⁻¹ region of porous glass upon exposure to 1.3 Torr NO₂ and addition of N₂ to atmospheric pressure; the porous glass had been exposed to room air and evacuated but not heated, so there are significant amounts of water on the surface to participate in the hydrolysis. The broad peak at 2297 cm⁻¹ is consistent with that reported in the literature for NO₂⁺.^{89,119,120} Fig. 6b is the spectrum in the same region of a similar piece of porous glass that had been exposed to HNO₃ and then the gas phase pumped off; the peak at 2297 cm⁻¹ is also present, as expected for NO₂⁺ formed from concentrated HNO₃. To confirm this assignment, a fresh piece of porous glass was exposed to ¹⁵N-labelled nitric acid; it is seen in Fig. 6c that the peak has red-shifted by 33 cm⁻¹, to 2265 cm⁻¹, confirming the assignment of this band as NO₂⁺.¹¹⁹

In summary, the composition of nitric acid-water thin films on silicate and other surfaces is clearly complex, but cannot be thought of as simply nitric acid-water aqueous solutions. The composition of these thin films under atmospheric conditions is not known, but clearly is an area that warrants both theoretical and experimental investigation. Despite the complexity, however, we have observed in laboratory studies many of the gas phase as well as surface intermediates and products proposed in the mechanism shown in Fig. 2. These include HONO and NO in the gas phase, and on the surface, HNO₃, water-nitric acid complexes, NO₂⁺ and N₂O₄.

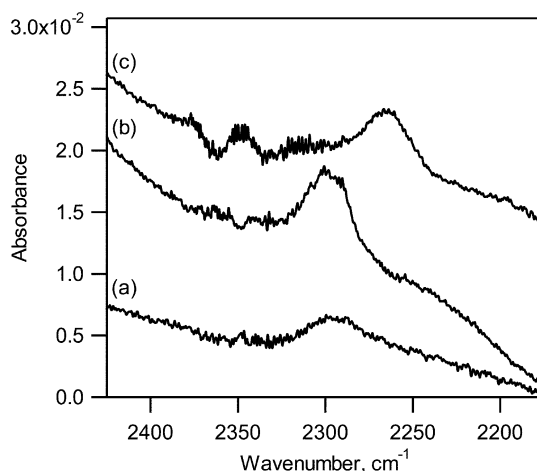
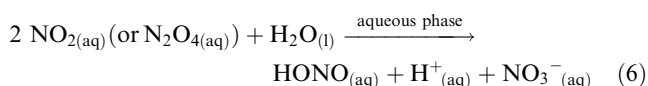


Fig. 6 Spectrum of NO₂⁺ on porous glass surface (a) during heterogeneous NO₂ hydrolysis; (b) after exposure to gaseous HNO₃, and (c) after exposure to H¹⁵NNO₃.

B. Kinetics

1. Rate of NO₂ hydrolysis reaction. It is clear from the combination of data discussed above that a thin film of water with nitric acid on the surface provides the reaction medium for heterogeneous NO₂ hydrolysis. Although the infrared data show that this film does not, at least spectroscopically, behave like a bulk liquid, it is worthwhile to compare the measured rates of HONO generation with those expected *if* the film could be treated as a bulk aqueous solution. The bulk aqueous phase kinetics for uptake and reaction of NO₂ in aqueous solutions are well known.^{85,86,132} It can be readily shown that the observed rates of HONO formation from NO₂ hydrolysis in our long path cell experiments as well as those reported in previous studies by other researchers are much larger than those predicted by bulk aqueous phase kinetics.

For example, consider a typical experiment carried out at 50% RH and an initial [NO₂] of 50 ppm in the 7.4 L long path cell (S/V = 70 m⁻¹). The number of water monolayers on the surface at 50% RH is ~3;^{92,93} taking monolayer water coverage to be 1.0 × 10¹⁵ molecule cm⁻², the available volume of water on the reaction chamber walls is ~5 × 10⁻⁷ L (assuming there is also water on the halocarbon wax coated optics mounts). The aqueous phase reaction of NO₂ with bulk liquid water has been studied in detail.^{85,86,132} As discussed by Schwartz and White,⁸⁶ studies of this reaction cannot distinguish between NO₂ and N₂O₄ as the reactant, and it can be written either way, with appropriate adjustment of the rate constant:



A recent measurement of the second order rate constant¹³² for NO₂ taken as the reactant is 3.0 × 10⁷ M⁻¹ s⁻¹. Using a Henry's law constant¹³² for NO₂ of 1.4 × 10⁻² M atm⁻¹, the concentration of aqueous phase NO₂ in equilibrium with 50 ppm gaseous NO₂ is 7.0 × 10⁻⁷ M. The calculated rate of HONO formation in the aqueous phase, proportional to the square of [NO_{2(aq)}], is thus 1.5 × 10⁻⁵ M s⁻¹. If it is assumed that all of this aqueous HONO escapes into the gas phase, the maximum rate of HONO formation would be 4 × 10¹² molecules s⁻¹ in a volume of 7.4 L, or 5 × 10⁸ molecules cm⁻³ s⁻¹. The average observed HONO formation rate in a typical long path cell experiment carried out at 50% RH and an initial NO₂ concentration of 50 ppm in the 7.4 L long path cell was ~2 × 10¹⁰ molecules cm⁻³ s⁻¹, a factor of 40 larger than expected based on chemistry in the bulk aqueous phase. When the simultaneous production of NO, which is at least in part from secondary reactions of HONO, is taken into account, the discrepancy is close to two orders of magnitude.

A similar conclusion can be reached from the data of other researchers, for example, from the larger (5800 L) chamber used by Pitts *et al.*⁴¹ A question is how much water would have been on the Teflon-coated walls of their chamber at 50% RH. In separate experiments in our laboratory on a halocarbon wax surface, the amount of water on the surface at 50% RH measured using transmission FTIR spectroscopy was about the same as that on glass.⁹³ This surprising result may reflect the roughness of the surface. For example, Rudich and coworkers¹³³ showed that irregular hydrophobic organic films took up more water than well-ordered films; this was attributed to condensation of water in the indentations in the surface. We therefore assume that the Teflon-coated surface of the large environmental chamber of Pitts and coworkers takes up water in the discontinuities on roughened hydrophobic surface in a manner similar to our measurements for a halocarbon wax coating. This assumption is supported by the similar rates in the generation of gas phase products between the studies of

Pitts *et al.*⁴¹ and ours, when differences in the S/V of the reactors are taken into account (see details in Section V, below).

Application of calculations similar to those described above for potential HONO formation in the aqueous phase on walls of the environmental chamber of Pitts and coworkers⁴¹ then shows that the observed HONO formation rate is about four orders of magnitude larger than expected for the aqueous phase reaction. For example, for an initial NO₂ concentration of 530 ppb and 50% RH (their run # 757), the calculated rate of gas phase HONO formation from a reaction in a bulk aqueous phase on the walls equivalent to 3 layers of water is 9 × 10⁻⁶ ppb min⁻¹, compared to their measured rate of 6 × 10⁻² ppb min⁻¹ of HONO.

These comparisons assume that the volume of water on the cell walls is not altered by the presence of HNO₃. However, this may not be the case, at least at low relative humidities. Bogdan and Kulmala¹³⁴ reported increased water uptake by pyrogenic silica powders under some conditions when exposed simultaneously to gas phase nitric acid. Thus, the amount of adsorbed water was 0.02 g per g of SiO₂ at 55% RH when exposed to pure water vapor, while 0.10 g H₂O per g of SiO₂ was adsorbed when exposed to the vapor over a 45% (w/w) HNO₃-H₂O solution whose relative humidity was estimated to be 53%. Svensson *et al.*⁴² observed that approximately a factor of two times more water was taken up on a Teflon surface at ~10% relative humidity when the Teflon had been first exposed to HNO₃. In both studies, however, there was no significant increase in water uptake at higher relative humidities.

These observations are consistent with surfaces retaining nitric acid even on pumping. Subsequent exposure to water vapor leads to uptake of water on the surface and the formation of nitric acid-water thin films. At the lower relative humidities, the increased water uptake may be related to the water needed to form a particular hydrate of nitric acid, *e.g.* the trihydrate. However, at the higher relative humidities, there may be sufficient water on the surface to dissociate the HNO₃, leading to water uptake that is similar to that for water alone.

However, with respect to the kinetics in the thin films, even a factor of five increase in water uptake measured for silica powders¹³⁴ does not reconcile the large discrepancies in the measured rates of HONO production compared to that calculated for reaction in a bulk aqueous layer on the surface.

2. Reaction order. Kinetics studies can be helpful in assessing which mechanisms are, or particularly are not, feasible based on the experimental data. The dependence of the rates of NO₂ loss and of product formation on the concentrations of the reactants has been studied by a number of groups.^{16,40-46,66,71} For reaction (1) as written, the *overall* rate law is given by eqn. (I):

$$\text{Rate} = R = -\frac{1}{2} \frac{d[\text{NO}_2]}{dt} = \frac{d[\text{HONO}]}{dt} = k[\text{NO}_2]^a [\text{H}_2\text{O}]^b \quad (\text{I})$$

If the reaction is first order in NO₂, then a plot of the initial rate of NO₂ loss or HONO formation against the initial NO₂ concentration should be linear. Similarly, the analogous plot as a function of the gas phase water concentration should be linear if the reaction is first order in water vapor. This analytical approach has been taken in many of the kinetics analyses of the heterogeneous NO₂ hydrolysis, and it is generally reported that the reaction is first order in NO₂ and first order in gaseous H₂O. We treat the dependence of the rates on water vapor first, followed by the dependence on the NO₂ concentration.

a. *Reaction order with respect to water vapor.* Fig. 7 shows the dependence of the initial HONO and NO rates of formation on the concentration of water vapor measured in this laboratory. Consistent with the earlier studies, the rates of HONO and NO formation increase with water vapor concentration.

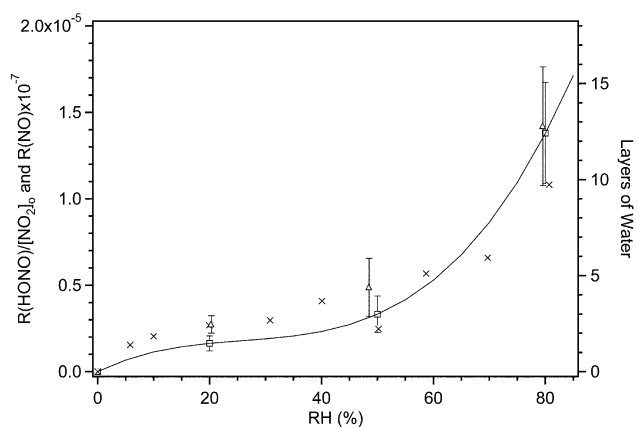


Fig. 7 Initial rates of HONO (\square) formation (in 19.4 L cell) and NO (\triangle) formation (in 7.4 L cell) as a function of relative humidity at 295 \pm 2 K. The NO rates have been multiplied by 10^{-7} to adjust to scale. The solid line is a fit through the combined data sets for the rates of HONO and NO formation. The number of effective layers of water measured on a smooth borosilicate glass surface⁹³ are shown for comparison (right axis and \times symbols).

However, the current studies were carried out to 80% RH, a higher water vapor concentration than used in most previous studies. While there is a significant increase in the rates of HONO and NO formation from 20 to 50% relative humidity, the increase from 50% to 80% RH is much larger than expected for a linear relationship. Also shown for comparison are recent measurements in this laboratory⁹³ of the uptake of water on borosilicate glass cover slips (0.13–0.17 mm thickness, 25 mm diameter, Micro Cover Glass, Number 1, VWR Scientific). It is clear that the shapes of plots of $d[\text{HONO}]/dt$ and $d[\text{NO}]/dt$ versus relative humidity are similar in shape to the water uptake isotherm. These results show that the rates of HONO and NO formation are determined by the amount of water on the surface, rather than the gas phase water concentration.

In previous studies, the rates of formation of HONO, and NO where they have been measured, have generally been reported to be linear in the concentration of water vapor,^{40–43,66} although Svensson *et al.*⁴² reported a steep increase in the rate of NO production at 77% RH ($[\text{H}_2\text{O}] = 5 \times 10^{17} \text{ cm}^{-3}$) in their experiments. The data of Pitts *et al.*⁴¹ for HONO generation increase more than expected based on a linear relationship for experiments at 305 K and 60% RH ($[\text{H}_2\text{O}] = 7 \times 10^{17} \text{ cm}^{-3}$), although they state that, within the scatter of the data, no firm conclusions can be drawn. Kleffmann *et al.*⁴⁶ observed that HONO formation was “almost independent” of water vapor at low NO_2 concentrations, and attributed this to an excess of water present on the reactor surfaces.

In short, over a limited range of relative humidities, the relationship between the rate of HONO formation and water vapor concentration appears to be linear. However, our data clearly show that, on a borosilicate glass surface, the rate of formation follows the shape of the isotherm for water uptake on the surface. This again is consistent with the mechanism in Fig. 2 in that it is water on the surface that is the reactant, rather than the collision of a water molecule from the gas phase with HONO precursors on the surface such as asymmetric ONONO_2 .

One important aspect of the amount of water on the surface is its impact on the dissociation of nitric acid. As discussed above, with small amounts of water on the surface, nitric acid is largely undissociated. This is important because it is clear that the chemistry of undissociated nitric acid compared to nitrate ions on surfaces is quite different. For example, gaseous NO reacts^{92,121–131} with undissociated HNO_3 on silica surfaces to generate HONO and NO_2 , but does not react with nitrate ions.¹³¹

b. Reaction order with respect to NO_2 . The reaction order with respect to NO_2 was examined from data such as those in Fig. 3 first by examining the rates of NO_2 decay. For a first order reaction, a plot of $\ln[\text{NO}_2]$ versus time should be linear, while for a second order reaction, a plot of $1/[\text{NO}_2]$ as a function of time should be linear. We designate these Type A plots. Fig. 8 shows typical data from this laboratory plotted in this manner. In all cases, plots of $\ln[\text{NO}_2]$ and $1/[\text{NO}_2]$ versus time are both reasonably linear in the initial stages of the reaction where secondary chemistry is less important. This precludes distinguishing between first order and second order kinetics in a definitive manner.

These results prompted us to examine the reaction order data from some earlier studies. Where available, data from our experiments and previous NO_2 hydrolysis studies were plotted in two different ways to determine the reaction order. The first, Type A, is as described above, in which either

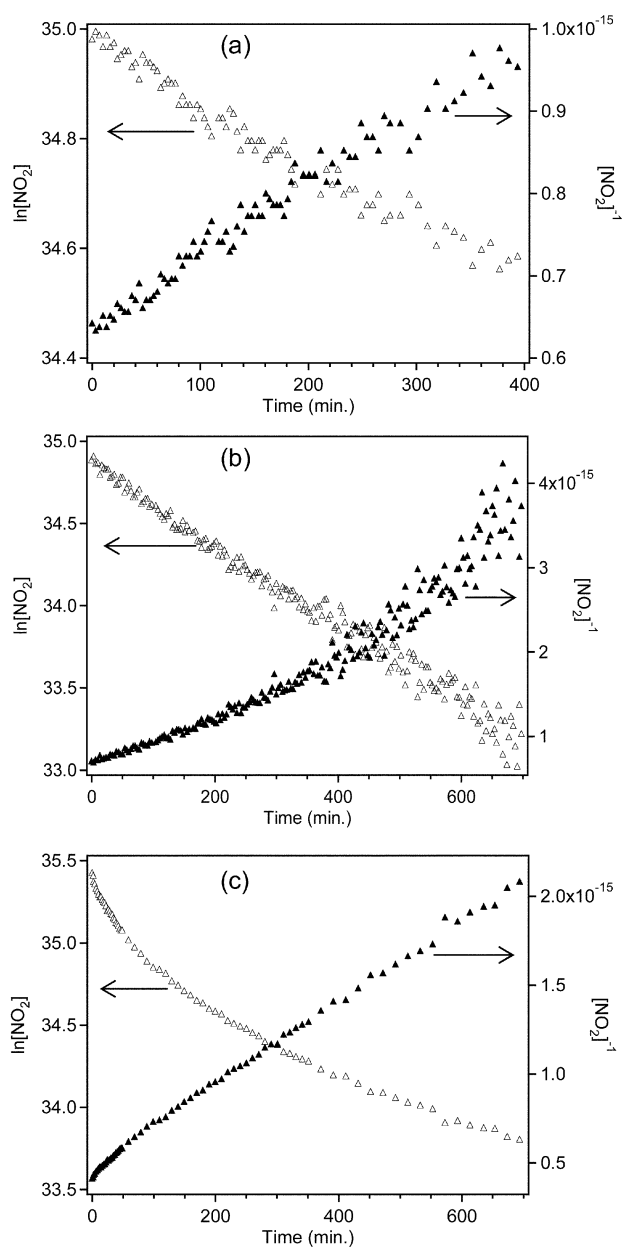


Fig. 8 First and second order Type A kinetics plots for the loss of NO_2 at (a) 21% RH, $[\text{NO}_2]_0 = 1.5 \times 10^{15} \text{ molecules cm}^{-3}$, (b) 48% RH, $[\text{NO}_2]_0 = 1.4 \times 10^{15} \text{ molecules cm}^{-3}$, (c) 80% RH, $[\text{NO}_2]_0 = 2.4 \times 10^{15} \text{ molecules cm}^{-3}$. As discussed in the text, the experiments at 21% and 48% RH were carried out in the 7.4 L cell and that at 80% in the 19.4 L cell.

$\ln[\text{NO}_2]$ or $1/[\text{NO}_2]$ are plotted *versus* time; these plots utilize the rate of NO_2 decay during an individual experiment.

A second approach utilizes the rate law, eqn. (I) above, where the reaction order can be obtained from plots of the log of the initial rate of NO_2 loss or of product formation *versus* log of the initial NO_2 concentration:

$$\log(R) = \log k + a \log [\text{NO}_2] + b \log [\text{H}_2\text{O}] \quad (\text{II})$$

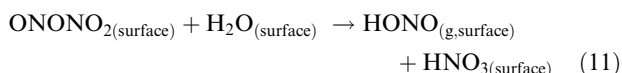
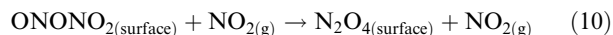
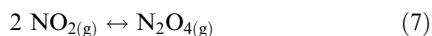
We designate these Type B plots; the reaction orders in NO_2 and H_2O , a and b , respectively, are obtained from the slopes of the appropriate log–log plots.

Table 1 summarizes our analysis of some of the previously reported laboratory studies of reaction (1) where sufficient data are available in the published paper for such an examination. For Type A plots, the time-dependence of the loss of NO_2 in a number of studies^{45,46,66,71} is similar to that reported here. That is, when we constructed Type A plots from their data, no clear distinctions between first and second order in NO_2 could be made, especially at early reaction times before secondary chemistry became apparent.

Type B plots could be constructed for four studies^{40–43} carried out in chambers similar to those used here. As Table 1 shows, the slopes of these Type B plots for the loss of NO_2 fall within the range from 1.0 to 1.2, supporting first order kinetics for the removal of NO_2 from the gas phase. The HONO data are more scattered, with slopes of the log–log plots falling in the range from 0.59 to 1.5. The lowest value, 0.59 ± 0.25 ($2s$) was obtained from the published rates which were calculated using the data after the first 60 min of reaction. This could be due to larger impacts of secondary chemistry on the apparent reaction rate. The largest value was obtained using a glass flow tube,¹⁶ that, as discussed in Section III.A.1, may have minimized the impact of secondary chemistry.

Fig. 9 shows Type B plots for experiments carried out in this laboratory in the 19.4 L glass long path cell. The data for HONO formation have an average slope of 1.2 ± 0.4 ($2s$), in agreement with previous studies in other laboratories in which HONO formation was reported to be first order in NO_2 .^{13,16,40–43,45,46,71} The reaction order for loss of NO_2 is somewhat higher, 1.6 ± 0.2 ; the reasons for the discrepancy between this and the values of ~ 1.0 (Table 1) are not clear.

Although the reaction requires a surface and water, as discussed above, it cannot be treated as if it occurred in an aqueous bulk water solution on the walls of the reactor. Rather, a thin film as shown in Fig. 2 is a more appropriate model for the medium in which this chemistry occurs. This mechanism predicts that HONO formation is first order in gas phase NO_2 despite N_2O_4 being a key precursor to HONO. This arises from the back reaction of asymmetric ONONO_2 with gas phase NO_2 . The key steps for HONO in Fig. 2 can be summarized as follows:



If the rate of reaction of ONONO_2 with NO_2 to regenerate N_2O_4 on the surface is faster than its reaction with water, (*i.e.* $k_{10}[\text{NO}_2] \gg k_{11}[\text{H}_2\text{O}]$), the steady-state concentration of ONONO_2 on the surface is given by:

$$[\text{ONONO}_2]_{\text{ss}} = \frac{k_9 K_7 K_8 [\text{NO}_2]^2}{k_{10} [\text{NO}_2]} = C [\text{NO}_2] \quad (\text{III})$$

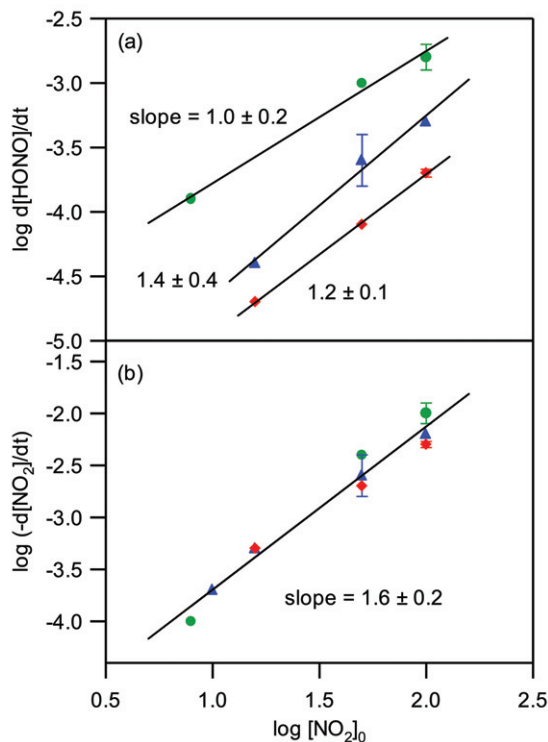


Fig. 9 Plots of (a) $\log(d[\text{HONO}]/dt)$ and (b) $\log(-d[\text{NO}_2]/dt)$ vs. $\log[\text{NO}_2]_0$ for experiments carried out in the 19.4 L glass long path cell in this laboratory at 20% (\blacklozenge), 50% (\blacktriangle), and 80% (\blacklozenge) RH. The slopes ($\pm 2s$), are reaction order in NO_2 calculated using the initial rates of HONO formation or NO_2 loss (see text).

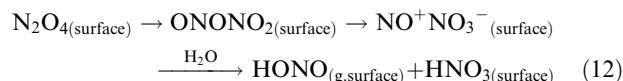
k_9 and k_{10} are the rate constants for reactions (9) and (10), K_7 and K_8 are the equilibrium constants for reactions (7) and (8), and C is the combination of rate and equilibrium constants $\{k_9 K_7 K_8 / k_{10}\}$. The rate of HONO generation is given by

$$\begin{aligned} \frac{d[\text{HONO}]}{dt} &= k_{11} [\text{ONONO}_2] [\text{H}_2\text{O}(\text{surface})] \\ &= k_{11} C [\text{H}_2\text{O}(\text{surface})] [\text{NO}_2] \quad (\text{IV}) \end{aligned}$$

and hence is first order in NO_2 . An alternate portion of the mechanism that would be consistent with HONO production being first order in NO_2 is also considered briefly in the following section.

IV. Mechanisms and models

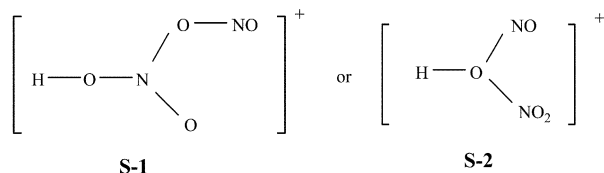
A key step in Fig. 2 is uptake of gaseous N_2O_4 on the surface and its isomerization to surface asymmetric ONONO_2 . This isomerization is known to occur in solid matrices at low temperatures or high pressures, on ice and in solution,^{101,135–150} (although one study¹⁵¹ observed only the symmetric form of N_2O_4 on ice films). Koel and coworkers^{148–150,152} proposed that this isomerization occurs *via* the free O–H groups on amorphous ice, and it is possible that a similar process occurs in the thin films studied here. Once formed, the asymmetric ONONO_2 can readily autoionize to nitrosonium nitrate, NO^+NO_3^- , and its reaction with water generates HONO and HNO_3 :



Experimental and theoretical studies^{153–155} of the reactions of gas phase clusters of hydrated NO^+ show that reaction to

generate HONO occurs with four or more water molecules bound to NO^+ .

Bands due to the asymmetric ONONO_2 have not yet been identified on silica surfaces at room temperature. This is not surprising, since the steady-state concentration of ONONO_2 is expected to be significantly smaller than that of symmetric N_2O_4 . In addition, given the presence of HNO_3 on the surface, ONONO_2 is likely protonated. Thus, Bernardi *et al.*¹⁵⁶ used a combination of mass spectrometry and theory to study the $[\text{HN}_2\text{O}_4]^+$ formed from the reaction of NO^+ with HNO_3 in the gas phase. The structure of the adduct is one of the structures shown below:

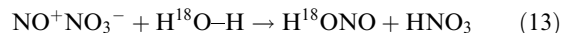


The mass spectral data were more consistent with structure **S-1**. These adducts are equivalent to protonation of the asymmetric ONONO_2 at either the nitro group or the bridging oxygen. Bernardi *et al.*¹⁵⁶ calculated that the proton affinities for ONONO_2 are large, 186 kcal mol⁻¹ for structure **S-1** and 177 kcal mol⁻¹ for structure **S-2**. The proton affinity¹⁵⁶ for N_2O_4 is also large, 166 kcal mol⁻¹. As discussed below, protonation of N_2O_4 and/or ONONO_2 on the surface may be responsible, at least in part, for decreasing the rate of HONO generation in chambers contaminated by the products of previous experiments, such as HNO_3 .

While we have shown the formation of NO^+ from the reaction of HONO with HNO_3 on the surface in Fig. 2 for simplicity, it is likely complexed to other species such as water and/or nitric acid. For example, the complex $3\text{NO}^+ \text{NO}_3^-$ has been observed^{101,157} by Raman spectroscopy in solutions of N_2O_4 in HNO_3 . Similar considerations apply to the other surface species. For example, in the gas phase, clusters of NO_3^- with HNO_3 and H_2O are well known^{106,158-161} and it seems likely that similar complexes would form on the surface. Oligomer $(\text{HNO}_3)_x$ chains as well as complexes such as $(\text{NO}_3 \cdot 3\text{HNO}_3)^-$ have been reported in liquid and solid anhydrous HNO_3 .^{106,162,163}

Given the apparent complexity of the species in the surface film, it would clearly be of great interest to detect intermediates such as asymmetric ONONO_2 (including the protonated form), autoionized NO^+NO_3^- , or other complexes of NO^+ on these surfaces.

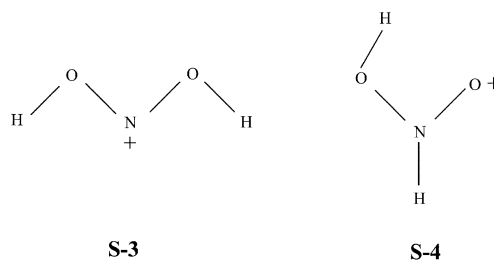
This mechanism for formation of HONO is also consistent with isotope labelling experiments. Sakamaki *et al.*⁴⁰ showed that NO_2 reacts in a small quartz cell at room temperature with H_2^{18}O at 15% RH to generate exclusively H^{18}ONO . Svensson *et al.*⁴² reported a similar observation for relative humidities in the range of ~20–40%; however, at a relative humidity of ~4%, HON^{18}O was also formed. The formation of H^{18}ONO is easily explained by the mechanism in Fig. 2. Once the asymmetric ONONO_2 has autoionized to NO^+NO_3^- , reaction of H_2^{18}O will lead to H^{18}ONO :



The formation of the HON^{18}O may be due to a proton-exchange reaction of HONO:



Ab initio calculations^{154,164} of protonated nitrous acid show that the most stable form is a cluster of NO^+ with water, $\text{NO}^+(\text{H}_2\text{O})$. However, there are two higher energy forms (by ~30–40 kcal mol⁻¹) corresponding to protonation at the terminal oxygen or at the nitrogen, respectively:

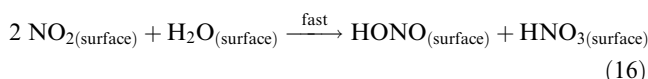


The observation of $^{18}\text{ONOH}$ only at very low relative humidities⁴² is not surprising in that the ratio of nitric acid to water on the surface is likely quite high, giving a very acidic surface film that would enhance reaction (14).

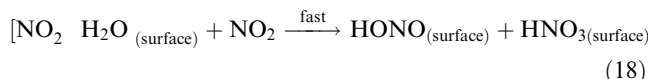
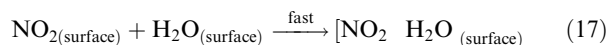
All of the previous studies^{13,16,40-43,45,46,71} reported that the formation of HONO was first order in NO_2 . This led to the conclusion that N_2O_4 cannot be the reactive species, since its concentration varies with $[\text{NO}_2]^2$. Based on experiments performed at 50% RH in large chambers (~4–6 m³) that were Teflon or Teflon-coated, Pitts *et al.*⁴¹ proposed several mechanisms consistent with the observed first order NO_2 kinetics. One hypothesis was that adsorption of NO_2 on the surface is rate-determining:



Formation of HONO was proposed to occur either by the direct reaction of surface-adsorbed NO_2 with water on the surface,

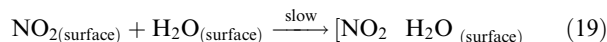


or through the formation of an NO_2 -water complex at the interface, followed by reaction with a second NO_2 molecule:



For both of these mechanisms, uptake of NO_2 on the surface is rate-determining.

An alternate proposed mechanism^{41,43} involved rapid uptake of NO_2 from the gas phase, with the slow formation of a surface NO_2 - H_2O complex as the rate-determining step:



followed by reaction (18). In all cases, the HONO is released into the gas phase while the HNO_3 was proposed to remain on the surface.

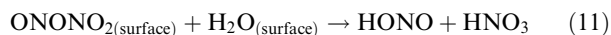
Further evidence for the formation of a complex of NO_2 with water at the interface was obtained in studies of the uptake of gaseous NO_2 on liquid water where the uptake was measured to be much faster than expected based on bulk phase solubility and reaction.^{165,166} However, direct measurement of surface species was not carried out in these studies.

Cheung *et al.*¹³² studied the uptake and reaction of NO_2 with liquid water in a falling droplet apparatus and a bubble apparatus. Similar experiments have in the past generated evidence for the formation of complexes at the air-water interface as part of the mechanism of reaction, *e.g.*, of gaseous Cl_2 with bromide ion in aqueous solution.¹⁶⁷ In the case of the NO_2 studies, Cheung *et al.*¹³² found no evidence for a reactive NO_2 complex at the interface. There is one report¹⁵¹ of an NO_2 - H_2O adduct on ice surfaces with only the symmetric N_2O_4 being observed; the reason for the discrepancy between this and the studies that have reported isomerization^{101,135-150} is unclear.

An analogous system involving SO₂ may be relevant for examining whether the formation of a complex of NO₂ with water at the interface is a viable mechanism for heterogeneous NO₂ hydrolysis. There are data from studies of the uptake of SO₂ into aqueous solutions^{168,169} and from sum frequency generation studies¹⁷⁰ that a complex of SO₂ exists at the interface and plays a role in its uptake and oxidation. In addition, a significant decrease in the surface tension of bisulfite solutions was reported and attributed to this complex.¹⁷⁰ However, ATR-FTIR studies of SO₂ uptake into thin water films on an infrared-transmitting crystal, interpreted with the aid of *ab initio* calculations, failed to find evidence for an interface complex of SO₂ with water.¹⁷¹ It may be that the surface complex was present at concentrations below the detection limit of 4 × 10¹⁴ cm⁻² or that in this case, the complex is an ion-water cluster,^{168,172,173} for which the detection limits were higher, rather than a complex with the unionized gas molecule.

Ab initio calculations^{170,171} give a binding energy for an SO₂-H₂O complex (the most stable “open-faced sandwich” structure in which the planes of SO₂ and H₂O molecules are parallel) of ~4–5 kcal mol⁻¹ compared to the separated reactants. Chou *et al.*⁷⁴ have calculated that the binding energy for NO₂ with one water molecule is only 0.90 kcal mol⁻¹. Thus, the interaction between NO₂ and one water molecule is weaker than between SO₂ and water (and the latter is not particularly strong). Based on this information, it seems unlikely that NO₂ would form a complex at the surface with water. Certainly, there is no definitive evidence in favor of such a complex at the interface of air with thin films of water or water-nitric acid on surfaces.

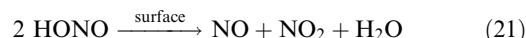
Based on this and the other evidence presented, we therefore favor the more complex, multi-step mechanism in Fig. 2. As discussed in the previous section, HONO generation by the mechanism in Fig. 2 will be first order in NO₂ if the conversion of ONONO₂ back to N₂O₄ by reaction with gas phase NO₂ is rapid compared to the reaction of ONONO₂ with water. It should be noted that, while Fig. 2 captures the major features of our proposed mechanism, there are alternatives to particular steps in the overall process that may also be consistent with the experimental observations. For example, one possibility is that there is a fixed amount of N₂O₄ that can be accommodated on the surface per unit area. In this scenario, N₂O_{4(surface)} is not in equilibrium with the gas phase dimer but rather, there is a maximum amount that the surface can hold; increased concentrations of the dimer in the gas phase would not lead to increased surface concentrations of N₂O₄ once the surface sites were filled. Under this scenario, the following reactions would also predict HONO generation that is first order in NO₂:



If reaction (20) were the rate-determining step and the concentration of N₂O_{4(surface)} was at its maximum, independent of gas phase N₂O₄, the steady-state concentration of ONONO₂ and hence the rate of generation of HONO would be first order in gas phase NO₂. In experiments using the porous glass surface and gas phase NO₂ concentrations in the 0.6–1.3 Torr range, the intensity of the 1740 cm⁻¹ infrared absorption band of N₂O₄ on the surface increased with the NO₂ pressure, suggesting that this alternate mechanism is less likely than that shown in Fig. 2. Because HNO₃ on the surface also impacts the amount of surface N₂O₄ as seen in Fig. 4, it has not yet been possible to definitively determine whether the surface N₂O₄ varies with the gas phase concentration of [NO₂] or [NO₂]², *i.e.* N₂O₄. However, it is possible that these porous glass experiments do not extrapolate directly to smooth glass because of the much larger internal surface area of the porous glass and pore geometry.¹⁷⁴ In addition, there is some

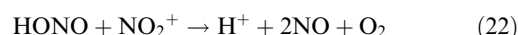
difference in the composition of the porous glass (96.3% SiO₂, 2.95% B₂O₃, 0.04% Na₂O and 0.72% Al₂O₃ + ZrO₂) compared to the smooth glass of the long path cells (81% SiO₂, 13% B₂O₃, 4% Na₂O and 2% Al₂O₃). Hence we cannot definitively rule out alternative steps such as reaction (20) in the overall mechanism. Clearly, much more work remains to be done to clarify each of the individual steps in the mechanism.

Nitric oxide has been observed in this and a number of other studies^{21,40–42,66,67} to be generated simultaneously with HONO, although Pitts *et al.*⁴¹ reported that NO was observed only at longer reaction times after an induction period. Since the concentration of HONO decreases at larger extents of reaction (Fig. 3), it is likely that secondary reactions of HONO on the cell walls generate NO. There have been a number of studies^{37,38,175–181} of the loss of HONO in laboratory reaction chambers that indicate that this chemistry also occurs on the reactor surfaces. The formation of both NO and NO₂ was observed in a manner consistent with reaction (21) in terms of the reaction products as well as second order kinetics in the initial HONO concentration:

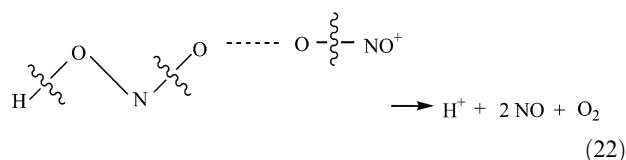


The production of NO by the bimolecular reaction of HONO on the surface is one possibility in the NO₂ hydrolysis system, *i.e.* HONO is generated in the gas phase and then undergoes secondary reaction (21) on the walls. In this case, production of NO would be expected to be a very sensitive function of the HONO concentration, and to have an induction time. While an induction time for NO generation was reported in the studies of Pitts *et al.*,⁴¹ NO was generated immediately in our experiments and those of Sakamaki *et al.*⁴⁰ and Svensson *et al.*⁴² A major difference between the latter experiments and those of Pitts *et al.*⁴¹ is the range of initial NO₂ concentrations used; in the former cases, NO₂ was typically in the 1–100 ppm range, whereas most of the Pitts *et al.*⁴¹ experiments were carried out in the sub-ppm range. At higher NO₂ concentrations, the reaction is faster and HNO₃ builds up more rapidly on the walls. This suggests that the secondary chemistry that converts HONO to NO on the surface involves either HNO₃ or species derived from it.

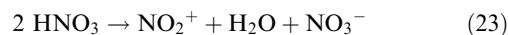
As shown earlier (Fig. 6), NO₂⁺ is present on the surface, as expected in the presence of concentrated HNO₃. We propose that HONO reacts on the surface with NO₂⁺ to form NO that is released to the gas phase:



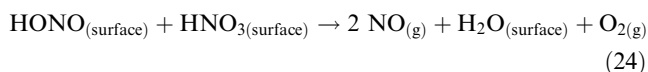
Reaction (22) is reasonable if NO₂⁺ attacks the terminal oxygen in HONO:



Combined with the net reaction (23) for NO₂⁺ production from HNO₃ (reaction (23) = reactions (4) plus (5) above),



the overall reaction for NO production is reaction (24):



Isotope labelling studies in which the oxygen of NO₂ is labelled would be worthwhile, since this mechanism predicts that labelled O₂ would be formed.

Crowley *et al.*¹⁸² reported the formation of both NO₂ and NO₃ in the gas phase when HNO₃ was added to an uncoated

quartz reactor. We have also observed the formation of NO_2 when porous glass treated with HNO_3 was left standing. Crowley and coworkers¹⁸² attributed this to the formation of NO_2^+ and its reaction with NO_3^- to generate N_2O_5 that then decomposed to $\text{NO}_2 + \text{NO}_3$. Similar chemistry may be occurring in heterogeneous NO_2 hydrolysis, although to the best of our knowledge, there is no evidence for N_2O_5 or NO_3 in the NO_2 system. A search for these species would be worthwhile. Interestingly, Crowley *et al.*¹⁸² did not observe NO_3 in liquid HNO_3 .

There are additional potential mechanisms that can convert HONO to NO. For example, theoretical studies¹⁸³ of the reaction of HONO with NO_2 show that this reaction in the gas phase has a large activation energy (32–33 kcal mol⁻¹ depending on whether it is *cis*- or *trans*-HONO). However, the mechanism may be quite different on highly acidic surfaces, involving for example, NO^+ . This reaction of NO_2 with HONO has been proposed to explain the production of NO inside a research house after injection of NO_2 .¹⁷

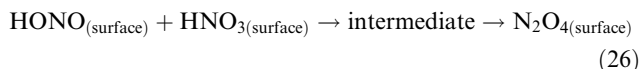
There may also be additional secondary chemistry that forms HONO at longer reaction times. For example, gaseous NO reacts with HNO_3 on silica surfaces to generate NO_2 as the major product.^{92,121–131} It is likely that HONO is first formed (reaction (25)),



and that HONO is then removed by secondary chemistry on the surface as discussed above. The generation of NO_2 in reaction (25) and the secondary HONO chemistry complicate interpretations of the kinetics and mass balance, particularly at larger extents of reaction, *i.e.*, higher initial concentrations and longer reaction times.

In order to provide an initial test of our proposed mechanism, we used the REACT version¹⁸⁴ of the ACUCHEM model¹⁸⁵ (REACT for Windows, Version 1.2, M. J. Manka, Alchemy Software, Wesley Chapel, FL, 2001) to predict the formation of HONO and NO, and the loss of NO_2 under the conditions of the experiments in Fig. 3. The gas phase chemistry is reasonably well known.^{90,186–188} This model does not explicitly treat uptake and reactions on surfaces, so the surface reactions summarized in Fig. 2 were parameterized as gas phase reactions. The surface reactions included in the model were (7)–(11), (22), (23), (25) and a reversible reaction that releases HONO from the surface into the gas phase. Rate constants for the surface reactions were adjusted within the constraints of the proposed mechanism (*e.g.*, the back reaction of ONONO_2 must be faster than its reaction with water) to obtain a best fit to the data for a typical experiment at 50% RH and an initial concentration of 60 ppm NO_2 , similar to the conditions in Fig. 3b. Based on our experimental observations described above, it was assumed that there was N_2O_4 and HNO_3 present on the walls initially. The model was then run for typical 20% and 80% RH experiments.

While this model gave reasonable fits to the HONO and NO production, NO_2 concentrations were over-predicted at longer reaction times. The addition of a reaction (26) of HONO with HNO_3 on the surface that generates an intermediate that slowly gives N_2O_4



gave a reasonable fit to all of the gas phase measurements. This reaction, which was proposed in earlier studies of the decomposition of nitric acid,¹⁸⁹ can be thought of as a reaction of NO_3^- with NO^+ formed from the reaction of HONO with the acid, *i.e.*, the reverse of the overall NO_2 hydrolysis reaction.

Fig. 10 shows the model predictions compared to the measured losses of NO_2 and production of HONO and NO at

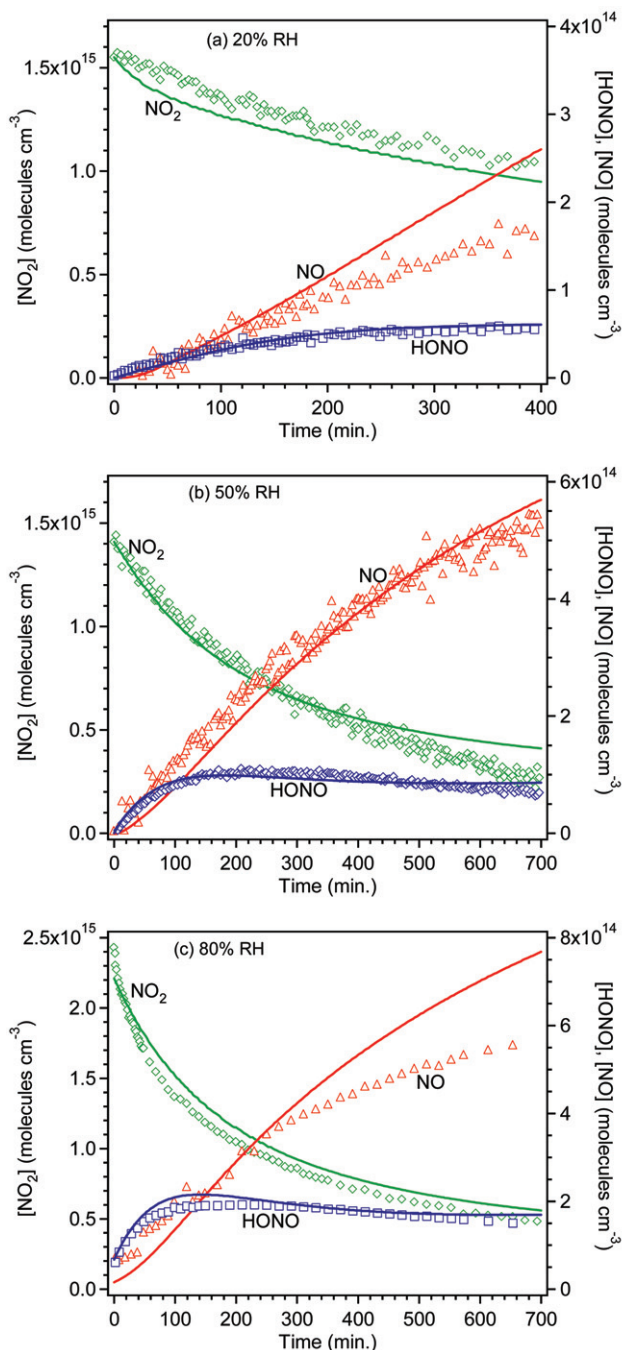


Fig. 10 Comparison of model predicted loss of NO_2 and formation of HONO and NO to experimental data for typical runs at (a) 20% RH, (b) 50% RH and (c) 80% RH.

20%, 50% and 80% RH. While the match is not perfect, it provides a reasonable fit, given the unknown rate constants and details of the mechanism. Furthermore, this mechanism predicts that the reaction order (obtained from a plot of log of the initial rate *versus* log of the initial NO_2 concentration) for the initial formation of HONO is in the range of 0.9 to 1.1 and that for loss of NO_2 is in the range of 1.8 to 2.1, in reasonable agreement with our measured values of 1.2–0.4 and 1.6–0.2, respectively. Further studies are planned using a model that is designed to treat both gas and surface species specifically in a heterogeneous chemical system.

Several studies have concluded that, in a “dirty” chamber, the nature of the underlying surface does not significantly alter the chemistry.^{41,42} This is not surprising if a thin surface film of nitric acid and water is the reactive medium in which the chemistry takes place. The underlying surface provides the support

for this film but apparently does not change its composition substantially, at least for relatively unreactive surfaces.

Finally, a common observation in the literature is that the initial rate of HONO formation and loss rate for NO₂ are faster on a clean surface. For example, Pitts *et al.*⁴¹ reported that the observed rate of HONO formation was doubled after cleaning their Teflon-coated evacuable chamber by the irradiation of Cl₂ and subsequent heating during evacuation for several hours. The HONO formation rate was no longer elevated after several more experiments were performed. Svensson *et al.*⁴² reported similar behavior for clean compared to contaminated surfaces. There are several possible explanations for this effect, based on our proposed mechanism. As discussed earlier, acid present on a contaminated surface is likely to protonate both N₂O₄ and/or ONONO₂; if protonation decreases the rates of conversion of N₂O₄ to ONONO₂, and/or the autoionization of ONONO₂ to NO⁺NO₃⁻, the rate of HONO generation would decrease. Another possibility is that nitric acid already present on the walls ties up some of the water on the surface in the form of nitric acid–water complexes. Hence the amount of “free” water available to play a role in isomerizing the N₂O₄ and to react with NO⁺NO₃⁻ to form HONO will be decreased, leading to reduced rates of HONO formation.

Our mechanism does not address the formation of N₂O. The available data^{45,46,70} strongly suggest that it is formed by secondary reactions of HONO on the acidic surface. Hyponitrous acid, HON=NOH, is known to decompose to N₂O over a wide pH range, including under highly acidic conditions,^{190,191} and HON is known to self-react in solution to form N₂O:^{192–195}



This suggests that the N₂O precursors (HON=NOH and/or HON) are formed by reactions of the protonated forms of HONO (structures S-3 and S-4 above) or possibly NO⁺, and that these generate N₂O. Similar chemistry has been proposed for the formation of N₂O under acidic conditions in the presence of SO₂.¹⁹⁶ Clearly, this area awaits further study.

V. Atmospheric implications

A. Polluted urban environments

An important aspect of atmospheric chemistry in the boundary layer of urban areas that has not received much attention is the heterogeneous chemistry occurring on buildings, structures, soils and vegetation. Such surfaces have been proposed in the past to be important substrates for heterogeneous NO₂ hydrolysis,^{5–7,79,80} but may also be important in other processes such as renoxification of nitric acid.^{92,129–131} Also consistent with reactions at the surface is the recent observation of increased HONO/NO₂ ratios at ground level compared to higher altitudes.²²⁰ There is also evidence that windows, for example, adsorb organics in urban areas,^{197,198} and may provide a support on which their oxidation occurs. This area of reactions in thin films on surfaces (*SURFACE* = Surfaces, Urban and Remote: Films As a Chemical Environment) has the potential to contribute significantly to the chemistry of this portion of the earth's atmosphere. The resulting impacts can be substantial, since the chemistry occurs in the physical location in which people are exposed to air pollutants. This is also the region in which many measurements of atmospheric species are taken for regulatory purposes, and hence the chemistry of the lower boundary layer significantly influences our understanding of atmospheric processes, the development of computer kinetics models, and their application to the promulgation of control strategies.

It is clear from our studies that the nature of the surface film is a key determinant of the kinetics and mechanism of the heterogeneous hydrolysis of NO₂. The experiments reported here

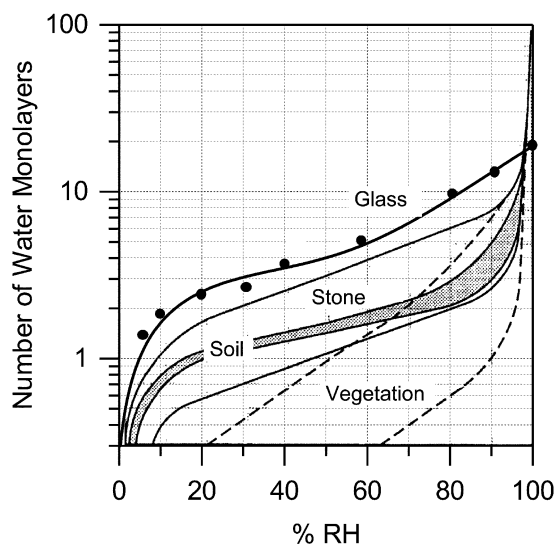


Fig. 11 Water uptake on some common materials found in the boundary layer. Adapted from Lammel.⁶

were carried out on borosilicate glass; many urban building materials contain silicates so that surface characteristics may be similar to the glass walls of laboratory reactors. Regardless, the evidence from the combination of the many different studies of this reaction suggests that the reaction is not very sensitive to the nature of the underlying surface. Based on the work presented here, one would expect the surface film of water and nitric acid to be the determining factor. Hence, it is the amount of water on the surfaces as a function of relative humidity that is likely to be important rather than the water vapor concentration or chemical nature of the underlying surface.

Fig. 11 shows a summary prepared by Lammel⁶ of the number of water layers taken up on various surfaces found in urban regions as a function of relative humidity. It is seen that the water uptake isotherms measured in this laboratory for borosilicate glass are similar to those for stone and soil materials. While vegetation takes up less water, a monolayer or more is present at relative humidities above 50%. Hence, all of these surfaces are likely to participate in HONO and NO formation in urban areas where significant NO₂ levels are present.

Our mechanism predicts that the asymmetric dimer ONONO₂ reacts with water to generate HONO, and the latter reacts to form NO in the presence of acid on the surface. As a result, the rate of NO formation from secondary HONO reactions should be sensitive to the relative concentrations of water and acid on the surface. Different amounts of acid on the walls of reaction chambers in laboratory studies may be the reason for different amounts of NO production relative to HONO reported in previous studies. It is not known what the form of nitric acid is on surfaces in urban environments nor what the ratio of HONO to NO production will be under typical atmospheric conditions. In addition, accurately representing the mechanism in Fig. 2 in airshed models will not be possible until the individual steps are known. Still, one can compare the rates of HONO and NO generation in various laboratory studies to obtain a likely range of maximum HONO production rates.

Fig. 12 shows such a comparison of the rates of HONO generation reported by Sakamaki *et al.*,⁴⁰ Pitts *et al.*,⁴¹ Svensson *et al.*,⁴² as well as in the present work. Different relative humidities, temperature and S/V ratios were used in the various studies. We have chosen data that were measured at 50% RH, or the closest RH studied to 50%, and normalized the reported rates of HONO generation for both the S/V ratio of 3.4 m⁻¹ and to the water vapor concentration of 3.6 × 10¹⁷ cm⁻³ used

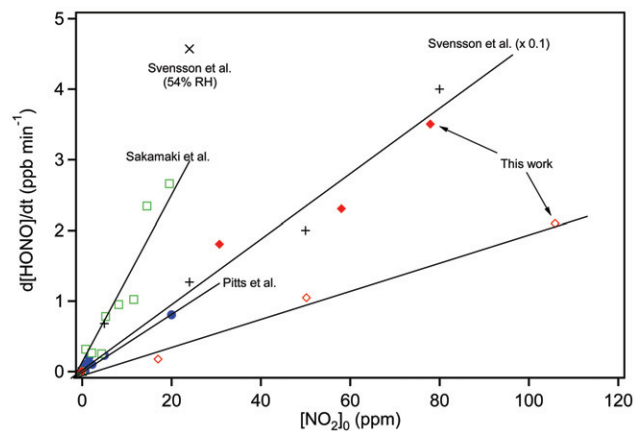


Fig. 12 Initial rates of generation of HONO measured in several studies, normalized to a S/V of 3.4 m^{-1} and water vapor concentration of $3.6 \cdot 10^{17} \text{ cm}^{-3}$ used in the studies by Pitts *et al.*⁴¹ ● Pitts *et al.*⁴¹ □ Sakamaki *et al.*⁴⁰ + Svensson *et al.*⁴² rates divided by 10; Svensson *et al.*⁴² experiment at 54% RH; ◇ this work, 19.4 L cell; ◆ this work, 7.4 L cell.

in the Pitts *et al.* studies.⁴¹ This normalization involved a simple multiplication of the reported rates of HONO generation by the S/V ratio ($R_{\text{HONO}} \cdot 3.4 \text{ m}^{-1}/(S/V \text{ used in that study})$) and by the ratio of water vapor in the Pitts *et al.*⁴¹ study to that in the comparison experiments.

A correction also needs to be made for different methods of HONO measurement. Nitrous acid was measured by FTIR in the studies of Sakamaki *et al.*⁴⁰ Svensson *et al.*⁴² and this work, but different absorption cross sections were used, giving different HONO concentrations for a given measured absorbance, which leads to different measured formation rates. In the Pitts *et al.* studies, HONO was measured by DOAS.⁴¹ The HONO infrared absorption cross section we used⁸⁴ was determined by simultaneous measurement of HONO concentrations by DOAS so our data should be directly comparable to those of Pitts *et al.*⁴¹ We have therefore corrected the rates of HONO formation reported by Sakamaki *et al.*⁴⁰ and Svensson *et al.*⁴² to our effective absorption cross section of $3.7 \cdot 10^{-19} \text{ cm}^2 \text{ molecule}^{-1}$ (measured for the *trans* form at 1264 cm^{-1} but taking into account the *cis* form in equilibrium with it); the values of the absorption cross sections used in the Sakamaki *et al.*⁴⁰ and Svensson *et al.*⁴² studies were $2.8 \cdot 10^{-19} \text{ cm}^2 \text{ molecule}^{-1}$ and $4.8 \cdot 10^{-19} \text{ cm}^2 \text{ molecule}^{-1}$, respectively.

Table 2 summarizes the slopes of the plots of HONO generation in Fig. 12, normalized to the initial NO_2 . Pitts *et al.*⁴¹ only observed NO at longer reaction times, and their initial rates of HONO production accounted for 40–50% of the NO_2 loss as expected if HONO were the only gas phase product. However, significant rates of NO production were observed simultaneously in this work and that of Sakamaki *et al.*⁴⁰ and Svensson *et al.*^{40,42} with the relative rates of NO

to HONO generation varying from about 0.3 to 1.0. Table 2 therefore also shows the estimated *total* rates of production of HONO plus NO.

Comparison of these laboratory rates of HONO production in Table 2 shows that the dependence of the rate of (HONO + NO) formation in the present studies is in reasonable agreement with that of Pitts *et al.*⁴¹ but smaller than measured by Sakamaki *et al.*⁴⁰ One reason for the latter discrepancy may be that their studies were carried out at a temperature of 30 C, about 5–10 higher than the other three studies (although Svensson *et al.*⁴² reported a negative temperature dependence). The rates of HONO generation reported by Svensson *et al.*¹²⁸ are substantially higher than those in the other three studies. The experiments used for the rate calculation were carried out at very small water vapor concentrations, 1000 ppm, which correspond to 3.8% RH at their temperature of 22 C; the correction to their data for the water vapor was more than an order of magnitude. Given the complex nature of the surface film, such a linear extrapolation may not be justified and hence the apparent discrepancy not surprising. Also shown is the result of a single experiment from their studies⁴² that was carried out at a relative humidity of ~50%; this is in better agreement with the other studies shown.

Given the very different chamber sizes (*i.e.*, S/V) and composition of the chamber walls, the agreement in the rates of production of HONO for our studies at 50% RH compared to those of Pitts *et al.*⁴¹ is quite good. The average HONO production rate per ppm of NO_2 at 50% RH from our study and that of Pitts *et al.*⁴¹ which were carried out at similar temperatures and relative humidities, is $4 \cdot 10^{-2} \text{ ppb min}^{-1} \text{ per ppm}$ of NO_2 , normalized to a S/V ratio of 3.4 m^{-1} . This corresponds to an emission rate from the chamber surface of $3 \cdot 10^{10} \text{ HONO cm}^{-2} \text{ min}^{-1}$ at an NO_2 concentration of 1 ppm.

For the purposes of examining whether this rate is consistent with concentrations of HONO measured in the boundary layer in polluted urban atmospheres, we shall assume an NO_2 concentration of 0.1 ppm. From the results of the laboratory studies, the emission rate of HONO will be $3 \cdot 10^9 \text{ HONO cm}^{-2} \text{ min}^{-1}$ at 50% RH and 0.1 ppm NO_2 . However, the surfaces on which the reaction occurs are not geometrically flat. Typical BET surface areas for soil¹⁹⁹ are $1\text{--}15 \text{ m}^2 \text{ g}^{-1}$. We have measured the mass of a quantity of sand (Norway Bay, Quebec) that would visually cover a known surface area with a very thin layer and find a coverage of 0.2 g of sand per cm^2 of geometric area. Thus, the available surface area of sand and soils per cm^2 of geometric area may be on the order of 2000–30 000 $\text{cm}^2 \text{ per cm}^2$ geometric area. The emission rate of HONO from 1 cm^2 geometric area would then be in the range of $(0.6\text{--}9) \cdot 10^{13} \text{ HONO min}^{-1}$. Taking the height of the boundary layer to be 38.5 m, the height often used in one airshed model for a polluted urban area,²⁰⁰ the total HONO concentration formed in 10 h (*e.g.* overnight) would be in the range of 40–600 ppb. However, this assumes that the reaction is not limited by diffusion of NO_2 to the soil surface, that the entire BET

Table 2 Comparison of rates of HONO generation in this work with some previous studies as a function of the initial NO_2 concentration

Reference	$\{1/[\text{NO}_2]_0\} \cdot d[\text{HONO}]/dt$ (ppb min^{-1} per ppm NO_2) ($2s$)	Typical ratio of initial rate of NO production to that of HONO	Approximate rate of production of HONO plus NO per ppm NO_2 (ppb min^{-1} per ppm NO_2)
This work (19.4 L cell)	(2.1 0.4) 10^{-2}	1.0	$4 \cdot 10^{-2}$
This work (7.4 L cell)	(4.2 1.2) 10^{-2}	1.0	$8 \cdot 10^{-2}$
Sakamaki <i>et al.</i> ⁴⁰	(14 4) 10^{-2}	0.3	$18 \cdot 10^{-2}$
Pitts <i>et al.</i> ⁴¹	(3.9 0.4) 10^{-2}	0	$4 \cdot 10^{-2}$
Svensson <i>et al.</i> ⁴²	0.43 0.14	0.6	0.7
Svensson <i>et al.</i> ⁴² at 54%RH	0.2	0.6	0.3

surface area is available for reaction, and that all of the HONO is released to the gas phase without any subsequent deposition or secondary reactions on the surfaces. Thus, while such calculations are quite approximate, they demonstrate that this chemistry is more than adequate to generate the typical range of HONO concentrations of a few ppb measured under such conditions, *e.g.*, see ref. 1–3,5–8,11,12

Zhou *et al.*⁵¹ have shown recently that there is an artifact formation of HONO when ambient air is sampled through a “dirty” glass manifold in the presence of sunlight. Our studies reported here were conducted in the dark, but they illustrate the complex nature of the surface film. The observations of Zhou *et al.*⁵¹ suggest that such surface films have some unique photochemistry that remains to be explored.

While this paper has focussed on the heterogeneous reaction of NO₂ with water, it should be noted that a similar reaction occurs with alcohols:^{201–203}



The organic nitrites such as CH₃ONO also photolyze readily,⁸ leading to the formation of HO₂ and OH *via* reactions of the alkoxy radical that is generated. This chemistry may become important if the use of alcohol fuels or additives to gasoline increases, particularly with the phase-out of MTBE as a fuel additive.

B. Airborne particles and clouds

There are a variety of solid airborne particles⁸ that could serve as substrates for this chemistry as well, including sea salt and windblown dust. It has been known for many years that dust particles that become airborne through windstorms can be transported long distances and may impact chemistry on a global scale.^{52–62} For example, dust particles remove oxides of nitrogen such as N₂O₅ that might otherwise lead to ozone formation. The present work and the previous studies of heterogeneous NO₂ hydrolysis suggest that the surfaces of SiO₂ in such particles may also help to generate OH *via* the formation of HONO. Indeed, increased HONO production has been observed during a dust storm in Phoenix, Arizona.²²¹

The components of dust particles include not only silicates, but also a number of other components such as Fe₂O₃, Al₂O₃, and TiO₂.⁸ Nitric oxide has been reported as the major gas phase product from the heterogeneous reaction of NO₂ on these surfaces in the absence of water vapor by Grassian and coworkers;^{204–208} HONO may be a major gaseous product when there are significant amounts of water on the surface. Børensén *et al.*²⁰⁹ reported the formation and subsequent loss of nitrite ions on the surface of Al₂O₃ during its reaction with NO₂ in the absence of water vapor and proposed that the loss was due to acidification of the surface that converts surface nitrite to gas phase HONO. However, gas phase products could not be directly measured in those studies.

Aerosol particles in urban areas have a complex composition and can act as condensation nuclei for fog and cloud formation. There is evidence from field studies for the generation of HONO in aerosols and clouds (*e.g.* see refs. 5–7, 80, 210–212). How the mechanism of formation of HONO in these liquid media is related to those in thin films on solid substrates such as those studied here is not known, but clearly an area of interest.

C. Indoors

Nitrous acid has been observed indoors in a number of studies (*e.g.*, see refs. 13–19,21). Although HONO is generated during combustion, for example in gas stoves and space heaters,^{14–17,20} it is clear that the heterogeneous hydrolysis of NO₂ on the materials inside homes plays a significant role. High levels of nitrogen dioxide are often found inside commercial facilities

such as ice skating rinks,²¹³ and hence formation of nitrous acid is expected in these cases as well.

The uptake of NO₂ on various materials used inside and outside buildings has been shown to vary over a wide range.^{21,214–216} In the studies of Spicer *et al.*,²¹⁵ wallboard, cement blocks, wool carpets, brick and masonite had the highest uptake rates, which may reflect their ability to adsorb water and form a surface film. These were greater than window glass by more than an order of magnitude. Similarly, Wainman *et al.*²¹ showed that carpets made of synthetic fibers increased both the NO₂ removal rate and the formation of HONO. Thus, HONO and NO production rates may be greater on residential materials compared to borosilicate glass used in the present studies. However, clearly one needs to understand the nature of the surface film on such materials in order to accurately extrapolate from laboratory studies to indoor air environments.

D. Snowpacks

Over the past few years, there have been some intriguing observations made regarding photochemistry in snowpacks. For example, Sumner and Shepson⁵⁰ reported the photochemical production of HCHO, and enhanced production of NO and NO₂ that is associated with light has also been observed.^{217–219} Zhou *et al.*⁴⁸ and Dibb *et al.*⁴⁹ measured HONO production in the Arctic snowpack, and this may be a major source of OH that leads to the formation of such species as HCHO. The mechanism proposed is the photolysis of NO₃[–] to generate NO₂, followed by the heterogeneous hydrolysis of NO₂ to form HONO. In this case, the chemistry may be similar to that proposed here for the reaction on silica surfaces at room temperature.

If the formation of HONO involves N₂O₄, it may be enhanced on the surface of ice due to the temperature dependence of the NO₂–N₂O₄ equilibrium. The temperature dependence of the equilibrium constant is known,⁹⁰ and it increases by a factor of 124 from a temperature of 298 K to 245 K, typical of the Arctic in the spring. This increase in the fraction of NO₂ that is N₂O₄ in the gas phase, combined with increasing solubility with decreasing temperatures, may therefore enhance the amount of N₂O₄ on the ice surface and hence the generation of HONO. Of course, the nature of the surface of ice, where a quasi-liquid layer exists, is quite different from that of a solid silicate that holds adsorbed water, so a direct extrapolation of the present results is not possible. However, there are likely to be substantial similarities in the chemistry so that understanding the room temperature reaction on silica surfaces will be helpful in elucidating the snowpack chemistry as well.

VI. Conclusions

The heterogeneous hydrolysis of NO₂ is an important source of OH radicals in urban atmospheres *via* its generation of HONO. An important aspect of such chemistry is that in the boundary layer closest to the earth's surface, it is the surfaces of soil, buildings, roads, vegetation, *etc.* that provide the solid support for these heterogeneous processes. *SURFACE* has received relatively little attention,^{5–7,80,197,198} but may play a significant role in the chemistry of the boundary layer.

Much of the chemistry in laboratory systems, and likely in urban atmospheres as well, is determined by the nature of the surface film which contains water, nitric acid and a variety of species derived from them, such as NO₂⁺. The composition of the surface film and how it changes with relative humidity and the gaseous concentrations of oxides of nitrogen are not known, but are clearly a critical area for future research.

Acknowledgements

We are grateful to the California Air Resources Board (Contract No. 00-323) and to the National Science Foundation (Grant No. ATM-0097573) for support of this work. Invigorating and illuminating discussions, as well as comments on this manuscript, by J. N. Pitts, Jr. are gratefully acknowledged. We thank G. Lammel for permission to show the data in Fig. 11, F.-M. Tao, N. Wright and R. B. Gerber for elaboration of theoretical calculations of NO_x interactions, and V. Grassian, A. Rivera-Figueroa, P. Farmer and J. C. Hemminger for helpful discussions. Finally, we gratefully acknowledge the expertise and advice of our glassblower, Jorg Meyer, without whose assistance this work would not have been possible.

References

- 1 D. Perner and U. Platt, *Geophys. Res. Lett.*, 1979, **6**, 917.
- 2 U. Platt, D. Perner, G. W. Harris, A. M. Winer and J. N. Pitts, Jr., *Nature*, 1980, **285**, 312.
- 3 A. M. Winer and H. W. Biermann, *Res. Chem. Intermed.*, 1994, **20**, 423.
- 4 J. G. Calvert, G. Yarwood and A. M. Dunker, *Res. Chem. Intermed.*, 1994, **20**, 463.
- 5 G. Lammel and J. N. Cape, *Chem. Soc. Rev.*, 1996, **25**, 361.
- 6 G. Lammel, "Formation of Nitrous Acid: Parameterization and Comparison with Observations," Report No. 286, Max-Planck-Institut-für Meteorologie, Hamburg, 1999, pp. 1–36.
- 7 R. M. Harrison, J. D. Peak and G. M. Collins, *J. Geophys. Res.*, 1996, **101**, 14429.
- 8 B. J. Finlayson-Pitts, J. N. Pitts, Jr., *Chemistry of the Upper and Lower Atmosphere: Theory, Experiments and Applications*, Academic Press, 2000.
- 9 C. L. Schiller, T. J. Locquiao and G. W. Harris, *J. Atmos. Chem.*, 2001, **40**, 275.
- 10 V. R. Kotamarthi, J. S. Gaffney, N. A. Marley and P. V. Doskey, *Atmos. Environ.*, 2001, **35**, 4489.
- 11 B. Alicke, U. Platt and J. Stutz, *J. Geophys. Res. Atmos.*, 2002, **107**, 8196.
- 12 J. Stutz, B. Alicke and A. Neftel, *J. Geophys. Res. Atmos.*, 2002, **107**, 8192.
- 13 J. N. Pitts, Jr., T. J. Wallington, H. W. Biermann and A. M. Winer, *Atmos. Environ.*, 1985, **19**, 763.
- 14 J. N. Pitts, Jr., H. W. Biermann, E. C. Tuazon, M. Green, W. D. Long and A. M. Winer, *J. Air Pollut. Control Assoc.*, 1989, **39**, 1344.
- 15 M. Brauer, P. B. Ryan, H. H. Suh, P. Koutrakis, J. D. Spengler, N. P. Leslie and I. H. Billick, *Environ. Sci. Technol.*, 1990, **24**, 1521.
- 16 A. Febo and C. Perrino, *Atmos. Environ.*, 1991, **25A**, 1055.
- 17 C. W. Spicer, D. V. Kenny, G. F. Ward and I. H. Billick, *J. Air Waste Manage. Assoc.*, 1993, **43**, 1479.
- 18 J. D. Spengler, M. Brauer, J. M. Samet and W. E. Lambert, *Environ. Sci. Technol.*, 1993, **27**, 841.
- 19 C. J. Weschler, H. C. Shields and D. V. Naik, *Environ. Sci. Technol.*, 1994, **28**, 2120.
- 20 Z. Vecera and P. K. Dasgupta, *Int. J. Environ. Anal. Chem.*, 1994, **56**, 311.
- 21 T. Wainman, C. J. Weschler, P. J. Liroy and J. Zhang, *Environ. Sci. Technol.*, 2001, **35**, 2200.
- 22 T. R. Rasmussen, M. Brauer and S. Kjaergaard, *Am. J. Crit. Care Med.*, 1995, **151**, 1504.
- 23 J. N. Pitts, Jr., D. Grosjean, K. van Cauwenbergh, J. P. Schmid and D. R. Fitz, *Environ. Sci. Technol.*, 1978, **12**, 946.
- 24 J. N. Pitts, Jr., H. W. Biermann, A. M. Winer and E. C. Tuazon, *Atmos. Environ.*, 1984, **18**, 847.
- 25 T. W. Kirchstetter, R. A. Harley and D. Littlejohn, *Environ. Sci. Technol.*, 1996, **30**, 2843.
- 26 R. Kurtenbach, K. H. Becker, J. A. G. Gomes, J. Kleffmann, J. C. Lörzer, M. Spittler, P. Wiesen, R. Ackermann, A. Geyer and U. Platt, *Atmos. Environ.*, 2001, **35**, 3385.
- 27 A. Gerecke, A. Thielmann, L. Gutzwiller and M. J. Rossi, *Geophys. Res. Lett.*, 1998, **25**, 2453.
- 28 M. Ammann, M. Kalberer, D. T. Jost, L. Tobler, E. Rossler, D. Piguet, H. W. Gaggeler and U. Baltensperger, *Nature*, 1998, **395**, 157.
- 29 J. Kleffmann, K. H. Becker, M. Lackhoff and P. Wiesen, *Phys. Chem. Chem. Phys.*, 1999, **1**, 5443.
- 30 C. A. Longfellow, A. R. Ravishankara and D. R. Hanson, *J. Geophys. Res.*, 1999, **104**, 13833.
- 31 M. Kalberer, M. Ammann, F. Arens, H. W. Gaggeler and U. Baltensperger, *Geophys. Res.*, 1999, **104**, 13825.
- 32 D. Stadler and M. J. Rossi, *Phys. Chem. Chem. Phys.*, 2000, **2**, 5420.
- 33 H. A. Al-Abadleh and V. H. Grassian, *J. Phys. Chem. A*, 2000, **104**, 11926.
- 34 C. Alcalá-Jornod, H. Van den Bergh and M. J. Rossi, *Phys. Chem. Chem. Phys.*, 2000, **2**, 5584.
- 35 F. Arens, L. Gutzwiller, U. Baltensperger, H. Gaggeler and M. Ammann, *Environ. Sci. Technol.*, 2001, **35**, 2191.
- 36 L. Gutzwiller, F. Arens, U. Baltensperger, H. W. Gaggeler and M. Ammann, *Environ. Sci. Technol.*, 2002, **36**, 677.
- 37 L. G. Wayne and D. M. Yost, *J. Chem. Phys.*, 1951, **19**, 41.
- 38 R. F. Graham and B. J. Tyler, *J. Chem. Soc., Faraday Trans. 1*, 1972, **68**, 683.
- 39 W. P. L. Carter, R. Atkinson, R. M. Winer and J. N. Pitts, Jr., *Int. J. Chem. Kinet.*, 1982, **14**, 1071.
- 40 F. Sakamaki, S. Hatakeyama and H. Akimoto, *Int. J. Chem. Kinet.*, 1983, **15**, 1013.
- 41 J. N. Pitts, Jr., E. Sanhueza, R. Atkinson, W. P. L. Carter, A. M. Winer, G. W. Harris and C. N. Plum, *Int. J. Chem. Kinet.*, 1984, **16**, 919.
- 42 R. Svensson, E. Ljungstrom and O. Lindqvist, *Atmos. Environ.*, 1987, **21**, 1529.
- 43 M. E. Jenkin, R. A. Cox and D. J. Williams, *Atmos. Environ.*, 1988, **22**, 487.
- 44 C. Perrino, F. DeSantis and A. Febo, *Atmos. Environ.*, 1988, **22**, 1925.
- 45 P. Wiesen, J. Kleffmann, R. Kurtenbach and K. H. Becker, *Faraday Discuss.*, 1995, **100**, 121.
- 46 J. Kleffmann, K. H. Becker and P. Wiesen, *Atmos. Environ.*, 1998, **32**, 2721.
- 47 G. S. Tyndall, J. J. Orlando and J. G. Calvert, *Environ. Sci. Technol.*, 1995, **29**, 202.
- 48 X. Zhou, H. J. Beine, R. E. Honrath, J. D. Fuentes, W. Simpson, P. B. Shepson and J. W. Bottenheim, *Geophys. Res. Lett.*, 2001, **28**, 4087.
- 49 J. E. Dibb, M. Arsenuault, M. C. Peterson and R. E. Honrath, *Atmos. Environ.*, 2002, **36**, 2501.
- 50 A. L. Sumner and P. B. Shepson, *Nature*, 1999, **398**, 230.
- 51 X. Zhou, Y. He, G. Huang, T. D. Thornberry, M. A. Carroll and S. B. Bertman, *Geophys. Res. Lett.*, 2002, **29**, 1681.
- 52 J. M. Prospero and R. T. Nees, *Science*, 1977, **196**, 1196.
- 53 J. M. Prospero, R. A. Glaccum and R. T. Nees, *Nature*, 1981, **289**, 570.
- 54 J. M. Prospero and R. T. Nees, *Nature*, 1986, **320**, 735.
- 55 F. J. Dentener, G. R. Carmichael, Y. Zhang, J. Lelieveld and P. J. Crutzen, *J. Geophys. Res.*, 1996, **101**, 22.
- 56 D. Gillette, *J. Exposure Anal. Environ. Epidemiol.*, 1997, **7**, 303.
- 57 X. Y. Zhang, R. Arimoto and Z. S. An, *J. Geophys. Res.*, 1997, **102**, 28041.
- 58 K. D. Perry, T. A. Cahill, R. A. Eldred, D. D. Dutcher and T. E. Gill, *J. Geophys. Res.*, 1997, **102**, 11225.
- 59 J. M. Prospero, *J. Geophys. Res.*, 1999, **104**, 15917.
- 60 Y. Zhang and G. R. Carmichael, *J. Appl. Meteorol.*, 1999, **38**, 353.
- 61 M. de Reus, F. Dentener, A. Thomas, S. Borrmann, J. Ström and J. Lelieveld, *J. Geophys. Res.*, 2000, **105**, 15263.
- 62 A. D. Clarke, W. G. Collins, P. J. Rasch, V. N. Kapustin, K. Moore, S. Howell and H. E. Fuelberg, *J. Geophys. Res.*, 2001, **106**, 32555.
- 63 J. Cathala and G. Weinrich, *Compt. Rend.*, 1952, **244**, 1502.
- 64 M. S. Peters and J. L. Holman, *Ind. Eng. Chem.*, 1955, **47**, 2536.
- 65 G. G. Goyer, *J. Colloid Sci.*, 1963, **18**, 616.
- 66 C. England and W. H. Corcoran, *Ind. Eng. Chem. Fundam.*, 1974, **13**, 373.
- 67 H. M. Ten Brink, J. A. Bontje, H. Spoelstra and J. F. van de Vate, "Atmospheric Pollution 1978", in *Studies in Environmental Science*, ed. M. M. Benarie, Elsevier, Amsterdam, 1978, vol. 1, pp. 1–239.
- 68 H. Akimoto, H. Takagi and F. Sakamaki, *Int. J. Chem. Kinet.*, 1987, **19**, 539.
- 69 A. Bambauer, B. Brantner, M. Paige and T. Novakov, *Atmos. Environ.*, 1994, **28**, 3225.
- 70 J. Kleffmann, K. H. Becker and P. Wiesen, *J. Chem. Soc., Faraday Trans.*, 1998, **94**, 3289.

- 71 R. M. Harrison and G. M. Collins, *J. Atmos. Chem.*, 1998, **30**, 397.
- 72 W. S. Barney and B. J. Finlayson-Pitts, *J. Phys. Chem. A*, 2000, **104**, 171.
- 73 A. L. Goodman, G. M. Underwood and V. H. Grassian, *J. Phys. Chem. A*, 1999, **103**, 7217.
- 74 A. Chou, Z. Li and F.-M. Tao, *J. Phys. Chem. A*, 1999, **103**, 7848.
- 75 R. M. E. Diamant, *The Chemistry of Building Materials*, Business Books Limited, 1970.
- 76 BNZ Materials, "Silica Brick and Mortar" and "Insulating Fire Brick—Material Safety Data Sheet", BNZ Materials, Inc., Littleton, CO, 1999.
- 77 USGS "Sediment", U.S. Geological Survey, National Park Service, Department of Interior, 1999.
- 78 Portland Cement Association, "Scientific Principles", Skokie, IL, 1999.
- 79 R. M. Harrison and A.-M. N. Kitto, *Atmos. Environ.*, 1994, **28**, 1089.
- 80 M. D. Andrés-Hernández, J. Notholt, J. Hjorth and O. Schrems, *Atmos. Environ.*, 1996, **30**, 175.
- 81 J. U. White, *J. Opt. Soc. Am.*, 1942, **32**, 285.
- 82 T. Gomer, T. Brauers, F. Heintz, J. Stutz and U. Platt, University of Heidelberg, 1995.
- 83 EPA Office of Air Quality Planning and Standards, Emission Measurement Center AEDC Calculated Spectra Technology Transfer Network Emission Measurement Center, 2002.
- 84 W. S. Barney, L. M. Wingen, M. J. Lakin, T. Brauers, J. Stutz and B. J. Finlayson-Pitts, *J. Phys. Chem. A*, 2000, **104**, 1692; W. S. Barney, L. M. Wingen, M. J. Lakin, T. Brauers, J. Stutz and B. J. Finlayson-Pitts, *J. Phys. Chem. A*, 2001, **105**, 4166.
- 85 S. E. Schwartz and W. H. White, "Solubility Equilibria of the Nitrogen Oxides and Oxyacids in Dilute Aqueous Solution", in *Advances in Environmental Science and Engineering*, ed. J. R. Pfaflin and E. N. Ziegler, Gordon and Breach Science Publishers, New York, 1981, vol. 4, pp. 1–45.
- 86 S. E. Schwartz and W. H. White, *Kinetics of Reactive Dissolution of Nitrogen Oxides into Aqueous Solution*, John Wiley and Sons, 1983, vol. 12, pp. 1–116.
- 87 S. Langenberg, V. Proksch and U. Schurath, *Atmos. Environ.*, 1998, **32**, 3129.
- 88 I. C. Hisatsune, J. P. Devlin and Y. Wada, *J. Chem. Phys.*, 1960, **33**, 714.
- 89 T. G. Koch, A. B. Horn, M. A. Chesters, M. R. S McCoustra and J. R. Sodeau, *J. Phys. Chem.*, 1995, **99**, 8362.
- 90 W. B. DeMore, S. P. Sander, D. M. Golden, R. F. Hampson, M. J. Kurylo, C. J. Howard, A. R. Ravishankara, C. E. Kolb and M. J. Molina, *Chemical Kinetics and Photochemical Data for Use in Stratospheric Modeling. Evaluation No. 12*, Jet Propulsion Laboratory, Pasadena, CA, 1997, vol. JPL Publ. No. 97-4.
- 91 A. Rivera-Figueroa and B. J. Finlayson-Pitts, 2002, unpublished data.
- 92 N. Saliba, H. Yang and B. J. Finlayson-Pitts, *J. Phys. Chem. A*, 2001, **105**, 10339.
- 93 A. L. Sumner and B. J. Finlayson-Pitts, 2003, in preparation.
- 94 M. Foster and G. E. Ewing, *Surf. Sci.*, 1999, **427/428**, 102.
- 95 M. C. Foster and G. E. Ewing, *J. Chem. Phys.*, 2000, **112**, 6817.
- 96 W. Cantrell and G. E. Ewing, *J. Phys. Chem. B*, 2001, **105**, 5434.
- 97 G. A. Parks, *J. Geophys. Res.*, 1984, **89**, 3997.
- 98 A. L. Goodman, E. T. Bernard and V. Grassian, *J. Phys. Chem. A*, 2001, **105**, 6443.
- 99 J. Chédin, *J. Chim. Phys.*, 1952, **49**, 109.
- 100 E. Högfeldt, *Acta Chem. Scand.*, 1963, **17**, 785.
- 101 C. C. Addison, *Chem. Rev.*, 1980, **80**, 21.
- 102 M. A. Tolbert and A. M. Middlebrook, *J. Geophys. Res.*, 1990, **95**, 22.
- 103 G. Ritzhaupt and J. P. Devlin, *J. Phys. Chem.*, 1991, **95**, 90.
- 104 R. T. Tisdale, A. J. Prenni, L. T. Iraci and M. A. Tolbert, *Geophys. Res. Lett.*, 1999, **26**, 707.
- 105 T. G. Koch, N. S. Holmes, T. B. Roddis and J. R. Sodeau, *J. Phys. Chem.*, 1996, **100**, 11402.
- 106 M. H. Herzog-Cance, J. Potier, A. Potier, P. Dhamelincourt, B. Sombret and F. Wallart, *J. Raman Spectrosc.*, 1978, **7**, 303.
- 107 M. P. Thi, M. H. Herzog-Cance, A. Potier and J. Potier, *J. Raman Spectrosc.*, 1981, **11**, 96.
- 108 F.-M. Tao, K. Higgins, W. Klemperer and D. D. Nelson, *Geophys. Res. Lett.*, 1996, **23**, 1797.
- 109 M. Staikova and D. J. Donaldson, *Phys. Chem. Chem. Phys.*, 2001, **3**, 1999.
- 110 P. R. McCurdy, W. P. Hess and S. S. Xantheas, *J. Phys. Chem. A*, 2002, **106**, 7628.
- 111 B. D. Kay, V. Hermann and A. W. J. Castleman, *Chem. Phys. Lett.*, 1981, **80**, 469.
- 112 X. Zhang, E. Mereand and A. W. J. Castleman, *J. Phys. Chem.*, 1994, **98**, 3554.
- 113 J. J. Gilligan and A. W. J. Castleman, *J. Phys. Chem. A*, 2001, **105**, 5601.
- 114 F. C. Fehsenfeld and C. J. Howard, *J. Chem. Phys.*, 1973, **59**, 6272.
- 115 F. C. Fehsenfeld, C. J. Howard and A. L. Schmeltekopf, *J. Chem. Phys.*, 1975, **63**, 2835.
- 116 Y. Cao, J.-H. Choi, B.-M. Haas, M. S. Johnson and M. Okamura, *J. Chem. Phys.*, 1993, **99**, 9307.
- 117 Y. Cao, J.-H. Choi, B.-M. Haas and M. Okamura, *J. Phys. Chem.*, 1994, **98**, 12176.
- 118 L. S. Sunderlin and R. R. Squires, *Chem. Phys. Lett.*, 1993, **212**, 307.
- 119 D. Forney, W. E. Thompson and M. E. Jacox, *J. Chem. Phys.*, 1993, **99**, 7393.
- 120 J. Agreiter, M. Frankowski and V. E. Bondybey, *Low Temp. Phys.*, 2001, **27**, 890.
- 121 J. H. Smith, *J. Am. Chem. Soc.*, 1947, **69**, 1741.
- 122 S. Jaffe and H. W. Ford, *J. Phys. Chem.*, 1967, **71**, 1832.
- 123 E. W. Kaiser and C. H. Wu, *J. Phys. Chem.*, 1977, **81**, 187.
- 124 G. E. Streit, J. S. Wells, F. C. Fehsenfeld and C. J. Howard, *J. Chem. Phys.*, 1979, **70**, 3439.
- 125 I. R. McKinnon, J. G. Mathieson and I. R. Wilson, *J. Phys. Chem.*, 1979, **83**, 779.
- 126 A. C. Besemer and H. Nieboer, *Atmos. Environ.*, 1985, **19**, 507.
- 127 D. H. Fairbrother, D. J. D. Sullivan and H. S. Johnston, *J. Phys. Chem. A*, 1997, **101**, 7350.
- 128 R. Svensson and E. Ljungström, *Int. J. Chem. Kinet.*, 1988, **20**, 857.
- 129 M. Mochida and B. J. Finlayson-Pitts, *J. Phys. Chem. A*, 2000, **104**, 9705.
- 130 N. Saliba, M. Mochida and B. J. Finlayson-Pitts, *Geophys. Res. Lett.*, 2000, **27**, 3229.
- 131 A. Rivera-Figueroa, A. L. Sumner and B. J. Finlayson-Pitts, *Environ. Sci. Technol.*, 2003, in press.
- 132 J. L. Cheung, Y. Q. Li, J. Boniface, Q. Shi, P. Davidovits, D. R. Worsnop, J. T. Jayne and C. E. Kolb, *J. Phys. Chem. A*, 2000, **104**, 2655.
- 133 Y. Rudich, I. Benjamin, R. Naaman, E. Thomas, S. Trakhtenberg and R. Ussyshkin, *J. Phys. Chem. A*, 2000, **104**, 5238.
- 134 A. Bogdan and M. Kulmala, *J. Colloid Interface Sci.*, 1997, **191**, 95.
- 135 L. Parts and J. T. Miller, *J. Chem. Phys.*, 1965, **43**, 136.
- 136 F. Bolduan and H. J. Jodl, *Chem. Phys. Lett.*, 1982, **85**, 283.
- 137 S. F. Agnew, B. I. Swanson, L. H. Jones and D. Schiferl, *J. Phys. Chem.*, 1983, **87**, 5065.
- 138 F. Bolduan, H. J. Jodl and A. Loewenschuss, *J. Chem. Phys.*, 1984, **80**, 1739.
- 139 L. H. Jones, B. I. Swanson and S. F. Agnew, *J. Chem. Phys.*, 1985, **82**, 4389.
- 140 D. A. Pinnick, S. F. Agnew and B. I. Swanson, *J. Phys. Chem.*, 1993, **96**, 7092.
- 141 X. Wang, Q. Zheng and K. Fan, *J. Mol. Struct.*, 1997, **403**, 245.
- 142 A. Givan and A. Loewenschuss, *J. Chem. Phys.*, 1989, **91**, 5126.
- 143 A. Givan and A. Loewenschuss, *J. Chem. Phys.*, 1989, **90**, 6135.
- 144 A. Givan and A. Loewenschuss, *J. Chem. Phys.*, 1990, **93**, 866.
- 145 A. Givan and A. Loewenschuss, *Struct. Chem.*, 1990, **1**, 579.
- 146 A. Givan and A. Loewenschuss, *J. Chem. Phys.*, 1991, **94**, 7592.
- 147 A. Givan and A. Loewenschuss, *J. Chem. Phys.*, 1991, **94**, 7562.
- 148 J. Wang, M. R. Voss, H. Busse and B. E. Koel, *J. Phys. Chem. B*, 1998, **102**, 4693.
- 149 J. Wang and B. E. Koel, *J. Phys. Chem.*, 1998, **102**, 8573.
- 150 J. Wang and B. Koel, *Surf. Sci.*, 1999, **436**, 15.
- 151 S. Sato, D. Yamaguchi, K. Nakagawa, Y. Inoue, A. Yabushita and M. Kawasaki, *Langmuir*, 2000, **16**, 9533.
- 152 X. Wang, Q.-Z. Qin and K. Fan, *J. Mol. Struct.*, 1998, **432**, 55.
- 153 F. C. Fehsenfeld, E. E. Ferguson and M. Mosesman, *Chem. Phys. Lett.*, 1969, **4**, 73.
- 154 J.-H. Choi, K. T. Kuwata, B.-M. Haas, Y. Cao, M. S. Johnson and M. Okamura, *J. Chem. Phys.*, 1994, **100**, 7153.
- 155 E. Hamman, E. P. F. Lee and J. M. Dyke, *J. Phys. Chem. A*, 2000, **104**, 4571.
- 156 F. Bernardi, F. Cacace, G. de Petris, F. Pepi and I. Rossi, *J. Phys. Chem. A*, 1998, **102**, 1987.
- 157 J. E. Harrar, L. P. Rigdon and S. F. Rice, *J. Raman Spectrosc.*, 1997, **28**, 891.
- 158 J. A. Davidson, F. C. Fehsenfeld and C. J. Howard, *Int. J. Chem. Kinet.*, 1977, **9**, 17.

- 159 N. Lee, R. G. Keesee and A. W. J. Castleman, *J. Chem. Phys.*, 1980, **72**, 1089.
- 160 S. Wlodek, Z. Luczynski and H. Wincel, *Int. J. Mass Spectrom. Ion Phys.*, 1980, **35**, 39.
- 161 R. D'Auria and R. P. Turco, "A Thermodynamic Kinetic Model for Ionic Cluster Formation. Growth and Nucleation"; The Proceedings of the Workshop on Ion-Aerosol-Cloud Interactions, CERN 2001-007, 118-138, 2001, 2001, CERN, Geneva.
- 162 M.-H. Herzog-Cance, A. Potier and J. Potier, *Can. J. Chem.*, 1985, **63**, 1492.
- 163 T. Jirsak and J. A. Rodriguez, *Langmuir*, 2000, **16**, 10287.
- 164 G. DePetris, A. D. Marzio and F. Grandinetti, *J. Phys. Chem.*, 1991, **95**, 9782.
- 165 J. L. Ponche, C. George and P. Mirabel, *J. Atmos. Chem.*, 1993, **16**, 1.
- 166 S. Mertes and A. Wahner, *J. Phys. Chem.*, 1995, **99**, 14000.
- 167 J. H. Hu, Q. Shi, P. Davidovits, D. R. Worsnop, M. S. Zahniser and C. E. Kolb, *J. Phys. Chem.*, 1995, **99**, 8768.
- 168 J. T. Jayne, P. Davidovits, D. R. Worsnop, M. S. Zahniser and C. E. Kolb, *J. Phys. Chem.*, 1990, **94**, 6041.
- 169 J. Boniface, Q. Shi, Y. Q. Li, J. L. Cheung, O. V. Rattigan, P. Davidovits, D. R. Worsnop, J. T. Jayne and C. E. Kolb, *J. Phys. Chem. A*, 2000, **104**, 7502.
- 170 D. J. Donaldson, J. A. Guest and M. C. Goh, *J. Phys. Chem.*, 1995, **99**, 9313.
- 171 H. Yang, N. J. Wright, R. B. Gerber and B. J. Finlayson-Pitts, *Phys. Chem. Chem. Phys.*, 2002, **4**, 1832.
- 172 Q. Shi, P. Davidovits, J. T. Jayne, D. R. Worsnop and C. E. Kolb, *J. Phys. Chem. A*, 1999, **103**, 8812.
- 173 S. M. Clegg and J. P. D. Abbatt, *J. Phys. Chem. A*, 2001, **105**, 6630.
- 174 L. D. Gelb and K. E. Gubbins, *Langmuir*, 1998, **14**, 2097.
- 175 R. A. Cox and R. G. Derwent, *J. Photochem.*, 1976/77, **6**, 23.
- 176 W. H. Chan, R. J. Nordstrom, J. G. Calvert and J. H. Shaw, *Chem. Phys. Lett.*, 1976, **37**, 441.
- 177 W. H. Chan, R. J. Nordstrom, J. G. Calvert and J. H. Shaw, *Env. Sci. Technol.*, 1976, **10**, 674.
- 178 C. England and W. H. Corcoran, *Ind. Eng. Chem. Fundam.*, 1975, **14**, 55.
- 179 E. W. Kaiser and C. H. Wu, *J. Phys. Chem.*, 1977, **81**, 1701.
- 180 H. M. Ten Brink and H. Spoelstra, *Atmos. Environ.*, 1998, **32**, 247.
- 181 A. A. Mebel, M. C. Lin and C. F. Melius, *J. Phys. Chem. A*, 1998, **102**, 1803.
- 182 J. N. Crowley, J. P. Burrows, G. K. Moortgat, G. Poulet and G. LeBras, *Int. J. Chem. Kinet.*, 1993, **25**, 795.
- 183 X. Lu, J. Park and M. C. Lin, *J. Phys. Chem. A*, 2000, **104**, 8730.
- 184 J. W. Bozzelli, *J. Chem. Ed.*, 2000, **77**, 165.
- 185 W. Braun, J. T. Herron and D. K. Kahaner, *Int. J. Chem. Kinet.*, 1988, **20**, 51.
- 186 W. Tsang and J. T. Herron, *J. Phys. Chem. Ref. Data*, 1991, **20**, 609.
- 187 S. P. Sander, R. R. Friedl, W. B. DeMore, D. M. Golden, M. J. Kurylo, R. F. Hampson, R. E. Huie, G. K. Moortgat, A. R. Ravishankara, C. E. Kolb and M. J. Molina, *Chemical Kinetics and Photochemical Data for Use in Stratospheric Modeling. Supplement to Evaluation No. 12. Update of Key Reactions. Evaluation No. 13*, Jet Propulsion Laboratory Pasadena, CA, 2000, vol. JPL Publ. No. 00-3.
- 188 R. Atkinson, D. L. Baulch, R. A. Cox, J. N. Crowley, R. F. Hampson, J. A. Kerr, M. J. Rossi and J. Troe, *Summary of Evaluated Kinetic and Photochemical Data for Atmospheric Chemistry*, Web version, 2001.
- 189 H. S. Johnston, L. Foering and J. R. White, *J. Am. Chem. Soc.*, 1955, **77**, 4208.
- 190 J. R. Buchholz and R. E. Powell, *J. Am. Chem. Soc.*, 1963, **85**, 509.
- 191 M. N. Hughes and G. Stedman, *J. Chem. Soc.*, 1964, 163.
- 192 M. J. Akhtar, J. A. Balschi and F. T. Bonner, *Inorg. Chem.*, 1982, **21**, 2216.
- 193 M. J. Akhtar, F. T. Bonner and M. N. Hughes, *Inorg. Chem.*, 1985, **24**, 1934.
- 194 D. A. Bazyliniski and T. C. Hollocher, *Inorg. Chem.*, 1985, **24**, 4285.
- 195 E. L. Loechler, A. M. Schneider, D. B. Schwartz and T. C. Hollocher, *J. Am. Chem. Soc.*, 1987, **109**, 3076.
- 196 M. Pires and M. J. Rossi, *Int. J. Chem. Kinet.*, 1997, **29**, 869.
- 197 M. L. Diamond, S. E. Gingrich, K. Fertuck, B. E. McCarry, G. A. Stern, B. Billeck, B. Grift, D. Brooker and T. D. Yager, *Environ. Sci. Technol.*, 2000, **34**, 2900.
- 198 S. E. Gingrich, M. L. Diamond, G. A. Stern and B. E. McCarry, *Environ. Sci. Technol.*, 2001, **35**, 4031.
- 199 M. E. Hodson, S. J. Langan, F. M. Kennedy and D. C. Bain, *Geoderma*, 1998, **85**, 1.
- 200 E. M. Knipping and D. Dabdub, *Atmos. Environ.*, 2002, **36**, 5741.
- 201 S. Koda, K. Yoshikawa, J. Okada and K. Akita, *Environ. Sci. Technol.*, 1985, **19**, 262.
- 202 H. Akimoto and H. Takagi, *Environ. Sci. Technol.*, 1986, **20**, 393.
- 203 H. Takagi, S. Hatakeyama, H. Akimoto and S. Koda, *Environ. Sci. Technol.*, 1986, **20**, 387.
- 204 T. M. Miller and V. H. Grassian, *Geophys. Res. Lett.*, 1998, **25**, 3835.
- 205 A. L. Goodman, T. M. Miller and V. H. Grassian, *J. Vacuum Sci. Technol.*, 1998, **16**, 2585.
- 206 G. M. Underwood, T. M. Miller and V. H. Grassian, *J. Phys. Chem. A*, 1999, **103**, 6184.
- 207 V. H. Grassian, *Int. Rev. Phys. Chem.*, 2001, **20**, 467.
- 208 V. H. Grassian, *J. Phys. Chem. A*, 2002, **106**, 860.
- 209 C. Børesen, U. Kirchner, V. Scheer, R. Vogt and R. Zellner, *J. Phys. Chem. A*, 2000, **104**, 5036.
- 210 J. Notholt, J. Hjorth and F. Raest, *Atmos. Environ.*, 1992, **26A**, 211.
- 211 J. N. Cape, K. J. Hargreaves, R. Storeton-West, D. Fowler, R. N. Colville, T. W. Choularton and M. W. Gallagher, *Atmos. Environ.*, 1992, **26A**, 2301.
- 212 K. Acker, D. Moller, W. Wiprecht, R. Auel, D. Kalass and W. Tschewenka, *Water Air Soil Pollut.*, 2001, **130**, 331.
- 213 M. Brauer, L. Lee, J. D. Spengler, R. O. Salonen, A. Pennanen, O. A. Braathen, E. Mihalikoa, P. Miskovic, A. Nozaki, T. Tsuzuki, S. Rui Jin, Y. Xu, A. Qing-Xiang, H. Drahonovska and S. Kjaergaard, *Air Waste Manage. Assoc.*, 1997, **47**, 1095.
- 214 H. Nishimura, T. Hayamizu and Y. Yanagisawa, *Environ. Sci. Technol.*, 1986, **20**, 413.
- 215 C. W. Spicer, R. W. Coutant, G. F. Ward, D. W. Joseph, A. J. Gaynor and I. H. Billick, *Environ. Int.*, 1989, **15**, 643.
- 216 P. Kirkitos and D. Sikiotis, *Atmos. Environ.*, 1996, **30**, 941.
- 217 R. E. Honrath, M. C. Peterson, S. Guo, J. E. Dibb, P. B. Shepson and B. Campbell, *Geophys. Res. Lett.*, 1999, **26**, 695.
- 218 A. E. Jones, R. Weller, E. W. Wolff and H. W. Jacobi, *Geophys. Res. Lett.*, 2000, **27**, 345.
- 219 A. E. Jones, R. Weller, P. S. Anderson, H.-W. Jacobi, E. W. Wolff, O. Schrems and H. Miller, *Geophys. Res. Lett.*, 2001, **28**, 1499.
- 220 J. Stutz, A. Geyer and S. Wang, EOS Trans. AGU, 2002, 83(47), Fall Meet. Suppl., abstract A12D-0180, presented at the Fall 2002 meeting of the American Geophysical Union.
- 221 S. Wang, C. W. Spicer, R. Ackerman, J. D. Fast and J. Stutz, EOS Trans. AGU, 2002, 83(47), Fall Meet. Suppl., abstract A51B-0056, presented at the Fall 2002 meeting of the American Geophysical Union.

HONO decomposition on borosilicate glass surfaces: implications for environmental chamber studies and field experiments

Dennis A. Syomin and Barbara J. Finlayson-Pitts*

Department of Chemistry, University of California, Irvine, CA 92697-2025.
E-mail: bjfinlay@uci.edu; Fax: +1 949 824 3168; Tel: +1 949 824 7670

Received 15th August 2003, Accepted 29th September 2003

First published as an Advance Article on the web 21st October 2003

Nitrous acid (HONO) is the major source of OH in polluted urban atmospheres, so an understanding of its formation and loss processes both in urban atmospheres and in laboratory systems is important. Earlier studies over a limited range of conditions showed that HONO is taken up and undergoes reaction on surfaces. We report here a comprehensive set of studies of the decay of HONO and the formation of gas phase products over a range of initial HONO concentrations (0.1–11 ppm) at 1 atm pressure in N₂ at 296 K and 0, 20 and 50% relative humidity (RH), respectively. The loss of HONO and increase in gas phase products were measured over time using long path FTIR spectroscopy. Studies were carried out in an unconditioned borosilicate glass cell and in the same cell after pretreatment with dry gaseous nitric acid. In the HNO₃-conditioned cell, the loss of HONO was first order at all values of relative humidity (RH), and NO₂ was the only significant gas phase product. For the unconditioned cell, the reaction order increased from first order at 0% RH to second order at 50% RH. The gas phase products at 0% RH were equal amounts of NO and NO₂. The yield of NO increased to > 90% at 50% RH while the yield of NO₂ decreased to ≤ 10%. For both the unconditioned and the HNO₃-treated cell, the rate of loss of HONO decreased with increasing RH. These results suggest that there is a competition between water, HONO and HNO₃ for surface sites. Displacement of HONO from the cell walls by water was observed in separate experiments. Possible mechanisms, and the implications for HONO formation in environmental chambers and in air, are discussed.

Introduction

Nitrous acid (HONO) is the major photochemical source of OH radicals in polluted urban atmospheres, both at sunrise and when averaged throughout the day.^{1–5} Although the origin of the HONO has been somewhat controversial, it is believed that the heterogeneous NO₂ hydrolysis, described by overall reaction (1), is likely to be the major source:^{6–11}



The nitrous acid is released to the gas phase; the nitric acid remains adsorbed on the surface.^{12,13} However, the yield of HONO measured in laboratory studies is generally less than expected from reaction (1), particularly in reactors with large surface-to-volume (S/V) ratios.^{10,14–24} This suggests either that some of the HONO reacts on the surface before it is released to the gas phase, or that it is released and subsequently reacts on the chamber walls.

Understanding the reactions of HONO on surfaces is important not only from a fundamental chemistry standpoint, but also for interpreting field and environmental chamber studies. Measurements of HONO and its precursor NO₂ in ambient air allow one to probe the contribution of heterogeneous reactions at the earth's surface to the production of HONO, and ultimately of OH, provided both the production and loss processes for HONO are understood.

In environmental chambers used to simulate reactions in air, the production of HONO has been observed from chamber walls,^{11,25–29} even when oxides of nitrogen have not been included in the reaction mixture. Additionally, there have been several studies of the loss of HONO in laboratory systems.^{18,30–35} Chan *et al.*^{30,31} studied the decomposition in

a stainless steel reactor ($S/V = 5.3 \text{ m}^{-1}$) at concentrations of HONO ranging from 2–9 ppm and at water vapor concentrations corresponding to 0.7–15% RH. They reported that the reaction is second order in HONO and occurs in the gas phase to generate NO and NO₂:



In a number of subsequent studies, other groups also observed NO and NO₂ as products, but concluded that the reaction occurred heterogeneously on the reactor walls. For example, Kaiser and Wu³² reported that the reaction occurred on the walls of a Pyrex reactor ($S/V = 63 \text{ m}^{-1}$) at RH from 0.2 to 5%, with a reaction order between one and two with respect to HONO. The rate of HONO loss decreased with increasing water vapor, with an apparent reaction order in water vapor of about –0.6. The production of NO and NO₂ were not consistent with reaction (2) alone and for analysis of the data, the reactions of HONO and NO with HNO₃ were included in their mechanism. These researchers found that prior exposure of the reactor walls to a mixture of NO, NO₂ and H₂O decreased the rate of HONO decomposition as the surface “aged”, but that coating the reactor surface with boric acid increased the decomposition rate. In a separate study, Kaiser and Wu³³ studied the loss of HONO in the reactor in the presence of HNO₃, and concluded that the chamber walls play a role in the reaction between HONO and HNO₃. They observed the reaction to be first order in HONO as well as gas phase HNO₃, and the reaction rate decreased when the water vapor pressure was increased from 0.1 to 5 Torr, corresponding to a RH from 0.5 to 22% RH.

Jenkin *et al.*¹⁸ studied the loss of HONO in a glass cell ($S/V = 13 \text{ m}^{-1}$) in conjunction with studies of the HONO

formation by reaction (1). They reported that the loss of HONO was first order at water vapor concentrations corresponding to 3.2 and 9.5% RH. Wallington and Japar³⁴ studied the decomposition of HONO in a similar reactor. They reported that the rate of disappearance of HONO increased in the presence of HNO₃ and could be modeled by a first order process in HONO. Ten Brink and Spoelstra³⁵ followed the loss of HONO in a Pyrex chamber at 80% RH. The decay of HONO was observed to be second order, with the major initial gas phase product being NO. At much longer reaction times (> 60 hrs), NO₂ was also observed as a product. They reported that the results were the same at 50% RH.

In summary, the preponderance of evidence shows that the loss of HONO in laboratory systems occurs *via* reactions on the chamber walls. This is in agreement with theoretical studies³⁶ of reaction (2), which show that this reaction in the gas phase should be very slow, with a rate constant of $10^{-25} \text{ cm}^3 \text{ molecule}^{-1} \text{ s}^{-1}$. Furthermore, the rate and mechanism might depend on the nature and amounts of co-adsorbed species, including water.

With the exception of the Ten Brink and Spoelstra experiments,³⁵ previous studies have been carried out at relative humidities that are much lower than those found in the troposphere. In addition, there has been no comprehensive study of the heterogeneous decomposition of HONO in which the concentrations of HONO and co-adsorbed species such as water and nitric acid were systematically varied over a wide range. We report here the results of such experiments, using the walls of a borosilicate glass chamber as the surface, as in many of the previous studies. However, this material is also relevant to many surfaces found in the boundary layer, since windows, buildings, concrete *etc.* have high silicate contents.^{10,37,38} We show that both water and HNO₃ compete with HONO for sites on the surface, which affects the kinetics, the products, and the mechanism of heterogeneous HONO uptake and reaction. This result has significant implications for HONO measurements in environmental chambers as well as in ambient air.

Experimental methods

Experiments were conducted at 296 K in a cylindrical, borosilicate glass, long-path cell equipped with a set of multi-pass optics of the White design.³⁹ Gas phase species were monitored using Fourier transform infrared spectrometry (Mattson, Research Series). The cell was 1.14 m in length, had an internal diameter of 0.15 m and a total volume $V = 19.4 \text{ L}$. The optical pathlength in these experiments was 72 m. The flanges and inner supports consist of anodized aluminum that were coated with a thin coating of halocarbon wax (Halocarbon Products, Inc., Series 1500) to prevent contact of HNO_x with the metal surfaces. The surfaces of the gold-coated mirrors were coated with a protective layer of silicon monoxide. The surface area (S) of the cell, without the internal supports and optics, is 0.58 m^2 ($S/V = 30 \text{ m}^{-1}$); when the surface area of the internal components is included, the total area is 0.89 m^2 ($S/V = 46 \text{ m}^{-1}$). We have shown in recent studies⁴⁰ that halocarbon wax takes up water in amounts similar to borosilicate glass over a broad range of relative humidities. Thus, for reactions occurring on the cell surfaces, such as those described here, the total area including the optics is most relevant.

In a typical experiment, 4–50 Torr of a mixture of HONO in N₂ was introduced into the cell from the HONO generator described below. The pressure was then brought up to 1 atm with nitrogen at the desired RH value. Nitrogen was used as the diluent gas to minimize the potential for thermal oxidation of nitric oxide in the system by oxygen. The relative humidity was adjusted by varying the ratio of humid and dry nitrogen during filling of the chamber. The humid

nitrogen was obtained by flowing N₂ gas through a bubbler containing Nanopure[®] water (Barnstead, 18.2 MΩ cm) and held at 296 K.

Concentrations of HONO, NO₂, and NO in the cell were measured as a function of time using FTIR spectroscopy. Spectra were collected at a resolution of 1 cm^{-1} , and 64 scans collected over 30 seconds were averaged for each data point. Gas phase HONO, NO₂ and NO were quantified by the net absorbance of their peaks at 1263, 2917 and 1875 cm^{-1} , respectively. Absolute concentrations of NO₂ and NO were based on calibrations using authentic samples in the cell. Nitrous acid concentrations were calculated from absorbances (base 10) using an effective cross section⁴¹ of $(3.7 \pm 0.4) \times 10^{-19} \text{ cm}^2 \text{ molecule}^{-1}$ at 1263 cm^{-1} . Use of the effective cross section gives the total HONO concentration (*cis* and *trans* isomers, which are in equilibrium). (The 1263 cm^{-1} band that was measured is only due to the *trans* form.)

Two sets of studies were carried out using different treatments of the surfaces of the cell. In the first series, the cell walls were conditioned with gas phase HNO₃ by introducing approximately 2 Torr of dry gaseous HNO₃ into the cell. After 15 min, the cell was evacuated with a diffusion-pump for several hours. The HONO and humid N₂ were then added as described above. In the second series, the cell walls were unconditioned. At the beginning of this set of experiments the cell was thoroughly rinsed first with distilled and then with Nanopure[®] water to remove soluble contaminants. Subsequent experiments in this series were carried out after simply evacuating the cell for several hours with a diffusion pump, due to the impracticality of disassembling the cell, rinsing it and realigning the optics for individual experiments.

Nitrous acid was synthesized by reacting hydrochloric acid with sodium nitrite:



Prior to reaction, the solid NaNO₂ (Aldrich, 99.5%) was exposed to humid N₂ (80–100% RH) for 15–20 min to moisten the salt surface. The flow of humid N₂ was then stopped and replaced by a flow of moist HCl in N₂, as obtained by flowing dry N₂ over the surface of an aqueous solution of HCl (Fisher, Certified ACS Plus, 12.1 M diluted 1:3 (v/v) with Nanopure[®] water).

Nitric acid used for conditioning the cell, and nitrogen dioxide and nitric oxide used for calibrations, were synthesized and purified as described elsewhere.¹⁰

Results

1. Experiments in an HNO₃-conditioned cell

Fig. 1 shows typical concentration–time profiles for HONO decay in an HNO₃ conditioned cell at 0 (Fig. 1a), 20 (Fig. 1c) and 50% RH (Fig. 1e), along with profiles for the gas phase products, NO and NO₂. Both NO₂ and NO are unavoidably present at the beginning of each experiment, due to HONO decomposition during its generation and handling in the glass manifold. This was particularly significant in experiments where the cell was conditioned with HNO₃ because the walls of the vacuum line used to introduce HONO into the cell had also been exposed to nitric acid. The data in Fig. 1 show that the only gas phase product observed in measurable yield is NO₂. The concentration of nitric oxide, present initially as an impurity, does not change significantly with time.

For each experiment, the initial rate of HONO loss and the corresponding rate of NO₂ formation were measured. The rate of HONO loss can be expressed by eqn. (1),

$$-\frac{d[\text{HONO}]}{dt} = k_d[\text{HONO}]^n \quad (1)$$

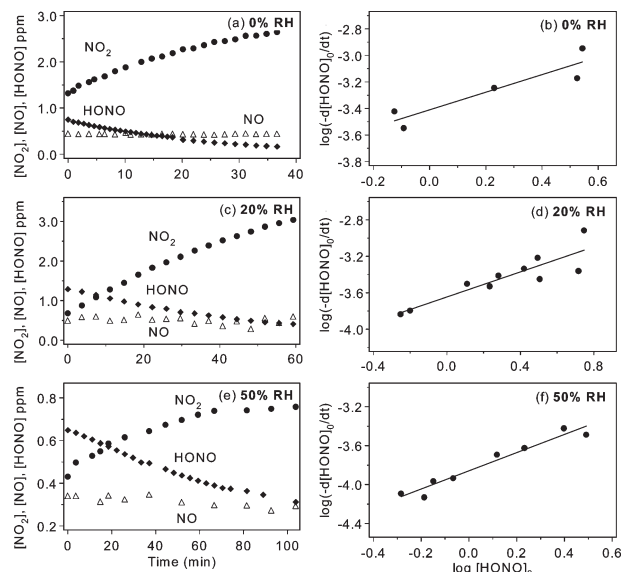


Fig. 1 Concentration–time profiles of HONO (\blacklozenge), NO_2 (\bullet) and NO (\triangle) and corresponding plots of $\log(-d[\text{HONO}]_0/dt)$ vs. $\log[\text{HONO}]_0$ for HONO decay experiments at 0% (a,b), 20% (c,d) and 50% RH (e,f) in the HNO_3 conditioned cell. Based on the known equilibrium constant for $2 \text{HONO} \rightleftharpoons \text{NO} + \text{NO}_2 + \text{H}_2\text{O}$,^{30,31} equilibrium is not attained within the reaction times used here.

where n is the reaction order with respect to HONO and k_d the rate constant for HONO loss. This assumes that other species than HONO are not involved in the HONO loss (or that if they are, their concentrations are constant). The reaction order and rate constants for HONO decay were obtained from the slope and intercepts respectively of log-log plots of the initial rate of HONO loss versus the initial HONO concentration:

$$\log(-d[\text{HONO}]_0/dt) = \log k_d + n \log[\text{HONO}]_0 \quad (\text{II})$$

Figs. 1b, d and f show the log-log plots for 0, 20 and 50% RH, respectively. In all cases the reaction is approximately first order in HONO.

The data are summarized in Table 1. The first order rate constants (k_d) for loss of HONO decrease by a factor of approximately three in the range from 0 to 50% RH. The yield of NO_2 formed relative to HONO removed is between two and three at 0 and 20% RH, but falls to one at 50% RH.

Table 1 Summary of HONO decomposition experiments

Conditioning of cell walls	RH (%)	No. of experiments	Range of initial $[\text{HONO}]_0$ (ppm)	Reaction order in $[\text{HONO}]_0$	First-order rate constant for HONO loss		Yield of NO_2^c		Yield of NO^d	
					k_d (units of 10^{-4} s^{-1})					
HNO_3	0	5	0.75–3.5	0.7 0.3 ^a	3.9 1.1 ^a	2.3 1.0 ^b	0			
	20	10	0.56–5.6	0.7 0.2	2.3 0.6	2.8 0.5	0			
	50	8	0.52–3.1	0.9 0.2	1.4 0.2	1.1 0.3	0			
Unconditioned	0	12	0.11–10.9	1.1 0.1	1.0 0.2	0.59 0.20	0.57 0.13 ^b			
	20	10	0.31–4.1	1.5 0.4	^e	0.26 0.26	0.67 0.56			
	50	7	1.3–10.9	1.8 0.4	^e	0.1 0.1	1.1 0.2			

^a Errors represent $2s$. ^b Errors represent 95% confidence limits (CL) using the t -test. The 95% CL is given by ts/\sqrt{N} where the standard deviation $s = \sqrt{\sum(x_i - x_{av})^2/(N-1)}$ and N is the number of data points in the mean. ^c For the HNO_3 -conditioned cell, the yield of NO_2 was calculated from the initial rates of NO_2 formation and HONO loss, i.e. from $\{d[\text{NO}_2]/dt\}/\{-d[\text{HONO}]/dt\}$. For the unconditioned cell where the rates of reaction were significantly slower, the yields were calculated from $\Delta[\text{NO}_2]/\Delta[\text{HONO}]$ at the end of each run; this was judged to be more accurate than using rates for the slower HONO losses. ^d The yields were calculated from $\Delta[\text{NO}]/\Delta[\text{HONO}]$ at the end of each run. ^e Since the reaction order is significantly greater than one, a first-order rate constant cannot be reported. However, as seen in Fig. 2, the rate of loss of HONO decreased with increasing RH.

2. Experiments in an unconditioned cell

Fig. 2a, c and e show typical concentration–time profiles for the decay of HONO and the formation of NO and NO_2 in the unconditioned cell at 0, 20 and 50% RH. At 0% RH, equal amounts of NO and NO_2 are produced. However, as the RH increases the relative yield of NO increases and that of NO_2 decreases.

Fig. 2b, d, and f shows the log–log plots (eqn. (II)) used to obtain the reaction order. The reaction is first order at 0% RH but changes to approximately second order at 50% RH. Table 1 also includes the data for these experiments. Because the reaction is first order only at 0% RH, the rate constant k_d is shown only for this set of experiments. However, it is clear from Fig. 2a, c and e that, as the RH increases, the rate of loss of HONO decreases.

Studies of the formation of HONO by the heterogeneous hydrolysis of NO_2 , reaction (1), were previously carried out in this cell at values of RH up to 80%.¹⁰ Based on these earlier experiments, HONO formation by heterogeneous NO_2 hydrolysis is negligible in comparison with the rate of HONO loss.

At low HONO concentrations (<0.9 ppm) and 50% RH in the unconditioned cell, HONO concentrations initially increased upon addition of the humid N_2 , rather than decreased as was the case under all other conditions. This suggests that water competes with HONO for surface sites and displaces some HONO that was previously adsorbed onto the walls into the gas phase. To test this point, experiments were carried out in which the cell was first exposed for one hour at 50% RH to 13 ppm HONO and then pumped for 60 min. Dry N_2 was added up to 1 atm pressure and the gas composition monitored for 9.5 h. No production of gaseous HONO was observed during this time. The cell was then pumped out and N_2 at 50% RH added. Fig. 3 shows the concentration–time profile for HONO. Clearly, HONO is being produced in the gas phase, and the only available source is displacement by the competitive adsorption of water on the surface.

Discussion

For the reaction in the cell that had been pretreated with HNO_3 , the reaction is approximately first order in HONO (Fig. 1), and NO_2 is the only gas phase product. Because the loss of HONO occurs on the surface of the cell, it is expected to be sensitive to the nature of the thin film of co-adsorbed

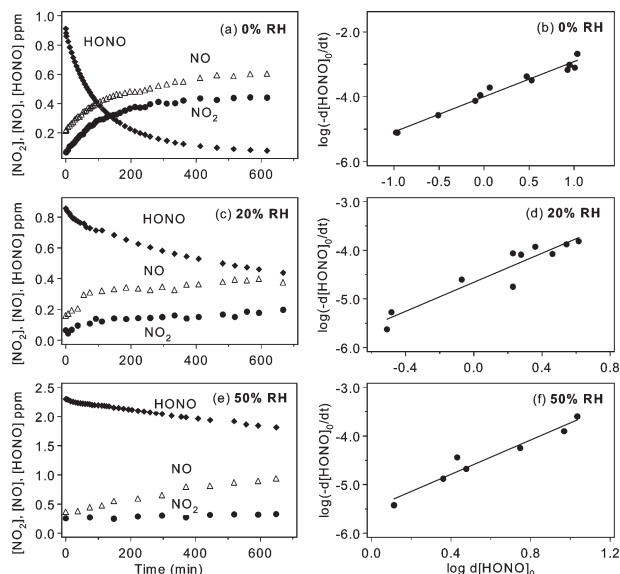
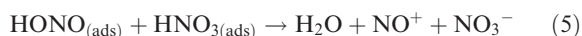


Fig. 2 Concentration–time profiles of HONO (◆), NO₂ (●) and NO (△) and corresponding plots of $\log(-d[\text{HONO}]_0/dt)$ vs. $\log d[\text{HONO}]_0$ of HONO decay experiments at 0% (a,b), 20% (c,d) and 50% (e,f) RH in the unconditioned cell. Based on the known equilibrium constant for $2 \text{HONO} \leftrightarrow \text{NO} + \text{NO}_2 + \text{H}_2\text{O}$,^{30,31} equilibrium is not attained within the reaction times used here.

species on the chamber walls. It is known from other studies in this laboratory that after exposing borosilicate glass to gas phase HNO₃, some of it remains adsorbed even after prolonged pumping.^{10,38,42} The form of the acid on the surface is not known, but it is likely to be, at least in part, complexed to water.¹⁰

The production of NO₂ as the only gas phase product in the experiments where the walls were conditioned with HNO₃ is consistent with the uptake of HONO on the chamber walls, followed by its protonation by adsorbed nitric acid:



If the HNO₃ adsorbed on the cell walls is constant, the rate of reaction of HONO should be first order in HONO, in agreement with observations.

Reactions (4)–(6) are the reverse of the heterogeneous hydrolysis of NO₂, reaction (1), which we recently proposed¹⁰ to occur *via* formation of the asymmetric NO₂ dimer:

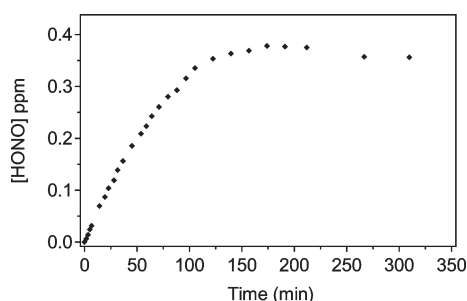
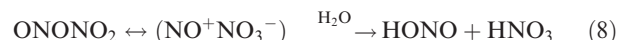


Fig. 3 Concentration–time profile of HONO in the HONO-conditioned cell at 50% RH and 1 atm in N₂. Before the experiment, the cell was exposed at 50% RH for 1 h to 13 ppm of HONO that contained 28 ppm of NO₂ and 60 ppm of NO as impurities. The cell was then pumped out before the water vapor–N₂ mixture was added.

The ONONO₂ then autoionizes and reacts with adsorbed water to generate HONO and HNO₃:



This sequence can be driven in reverse by high initial concentrations of HONO and HNO₃ as used in the present study. The stoichiometry from reactions (4)–(6) is expected to be $\Delta[\text{NO}_2]/\Delta[\text{HONO}] = 2$. Our measured yields of NO₂ are 2.3–1.0 and 2.8–0.5 at 0 and 20% RH, respectively; the latter value is slightly larger than anticipated on the basis of the proposed mechanism. The yield of NO₂ at 50% RH falls to approximately one, and no additional gas phase products are observed. This suggests that, for every two HONO molecules that are taken up on the surface, one reacts to form NO₂ *via* the mechanism described above, while one remains on the surface as undissociated HONO, as the dissociated form of HONO ($\text{H}^+ + \text{NO}_2^-$), or as some as yet unidentified involatile product.

Nitrogen dioxide is known^{43–46} to be generated in the decomposition of pure nitric acid, and indeed, some NO₂ formation was observed over time after the cell was pumped following the HNO₃ conditioning procedure. At 0% RH, the increase was small and represented less than 10% of the NO₂ formed in experiments where HONO was added. At 50% RH, significant amounts of NO₂ were generated, up to several ppm in 100 min. However, when HONO is present in the cell, its uptake and reaction with HNO₃ on the walls must compete with the generation of NO₂ from the self-reactions of adsorbed HNO₃. Thus, the NO₂ observed in the absence of HONO is an upper limit for the case where HONO is present. The fact that the yield of NO₂ falls to approximately one at 50% RH, compared to two at 0% RH, suggests that the contribution from the self-reactions of HNO₃ on the wall at the higher RH is not a major contributor to the measured NO₂ in the presence of added HONO.

A possible explanation for the low NO yields in the HNO₃-conditioned cell is that both NO and NO₂ are generated initially, but the NO reacts with adsorbed HNO₃,^{33,47–56}



Based on earlier experiments in this laboratory in a different cell,^{55,56} this process is expected to be too slow to be significant under the present experimental conditions. As a further check on this point, experiments were carried out at 0 and 50% RH in which 12 ppm of NO were added to the HNO₃ conditioned cell and the concentrations of gases monitored for 6 h. The observed rates of loss of NO and formation of NO₂ were confirmed to be too slow to be consistent with an initial formation of NO followed by reaction (9).

The data in Table 1 and in Figs. 1 and 2 show that the rate constant for HONO decomposition decreases with increasing relative humidity. As the partial pressure of water vapor increases, the amount of water on the surface increases relative to the amount of adsorbed nitric acid. The decreased rate constant at higher RH might be due to increased competition for the reaction of NO^+NO_3^- with water to generate HONO and HNO₃. Alternatively, or perhaps in addition, increased adsorbed water could change the nature of nitric acid on the surface. Nitric acid exists in the undissociated, molecular form at low RH on silica surfaces.^{12,13,57} Upon addition of water, dissociation to H^+ and NO_3^- occurs. This is consistent with gas-phase studies of complexes of nitric acid with water, where ionization of the acid occurs when there are four or more water molecules in the cluster with one nitric acid molecule.^{58–60} A decrease in the rate constant with increasing RH would also result if molecular HNO₃ is the reactant, while the dissociated ionic form, whose concentration increases with more water on the surface, is unreactive.

In the unconditioned cell, the reaction was first order in HONO (Fig. 2b) at 0% RH with a rate constant that was about a factor of four slower than in the HNO₃-conditioned cell. In this case, nitric oxide and nitrogen dioxide were generated in equal yields, in contrast to the HNO₃ conditioned chamber where NO₂ was the sole gas phase product. As the RH increases to 50%, the rate of HONO loss decreases, the reaction order increases and the product changes to NO with a yield greater than 90%. This is in contrast to the reaction on the HNO₃-conditioned cell walls where the reaction order remained one and NO₂ was the only product over the 0–50% range of RH.

We propose that the experimental observations in the unconditioned cell are attributable to competition between HONO and H₂O for the available surface sites. Thus, as the water vapor concentration increases, the coverage of surface-adsorbed water increases. This leads to a decrease in the amount of adsorbed HONO, and hence in the rate of reaction. This conclusion is supported by the data in Fig. 3, where the addition of water to a cell previously exposed to HONO and then pumped out leads to an increase in HONO in the gas phase.

Further, a competition between water and HONO for surface sites is consistent with the change in reaction order from one to two as the water vapor concentration increases. Thus, in a system where both HONO and H₂O can be adsorbed on a surface, the fraction of the surface covered by HONO (θ_{HONO}) is given by eqn. (III),⁶¹

$$\theta_{\text{HONO}} = \frac{K^{\text{HONO}}[\text{HONO}]}{1 + K^{\text{HONO}}[\text{HONO}] + K^{\text{H}_2\text{O}}[\text{H}_2\text{O}]} \quad (\text{III})$$

where K^{HONO} is the equilibrium constant for the surface uptake and desorption of HONO (*i.e.* $K^{\text{HONO}} = k_4/k_{-4}$ for reaction (4) above), $K^{\text{H}_2\text{O}}$ is the corresponding equilibrium constant for adsorption of water and [HONO] and [H₂O] are the gas phase concentrations. In the absence of water vapor, eqn. (III) becomes

$$\theta_{\text{HONO}} = \frac{K^{\text{HONO}}[\text{HONO}]}{1 + K^{\text{HONO}}[\text{HONO}]} \quad (\text{IV})$$

and if $K^{\text{HONO}}[\text{HONO}] \gg 1$, the fractional coverage of the surface by HONO becomes constant at one, *i.e.* the surface is saturated with HONO. In this case, the rate of reaction of gas phase HONO with adsorbed HONO is given by

$$-\frac{d[\text{HONO}]}{dt} = k'[\text{HONO}]_{\text{g}}[\text{HONO}]_{\text{ads}} = k'[\text{HONO}]S\theta_{\text{HONO}} = k'[\text{HONO}]S \quad (\text{V})$$

where k' is the rate constant for the gas-surface reaction and S is the surface density of one HONO monolayer (molecule per cm²). Because of the saturation of the surface by HONO, the reaction is predicted to be first-order in gas-phase HONO, which is consistent with our experimental observations.

At high relative humidities, water partially displaces HONO from the surface. Under conditions where $K^{\text{H}_2\text{O}}[\text{H}_2\text{O}] \gg K^{\text{HONO}}[\text{HONO}]$, eqn. (III) becomes

$$\theta_{\text{HONO}} = \frac{K^{\text{HONO}}[\text{HONO}]}{1 + K^{\text{H}_2\text{O}}[\text{H}_2\text{O}]} \quad (\text{VI})$$

The rate of reaction of gas phase HONO with adsorbed HONO is then given by eqn. (VII):

$$-\frac{d[\text{HONO}]}{dt} = k'[\text{HONO}]S\theta_{\text{HONO}} = \frac{k'K^{\text{HONO}}[\text{HONO}]^2S}{1 + K^{\text{H}_2\text{O}}[\text{H}_2\text{O}]} \quad (\text{VII})$$

That is, the loss of HONO from the gas phase decreases with increasing RH and becomes second order in HONO at constant RH, consistent with the experimental observations at 50% RH (Fig. 2e).

The fact that the rate appears to be between first and second order at intermediate relative humidities implies that the terms $K^{\text{HONO}}[\text{HONO}]$ and $K^{\text{H}_2\text{O}}[\text{H}_2\text{O}]$ are comparable under these conditions. Consider 20% RH, for example, where the water vapor concentration is about 5×10^3 ppm, and a 5 ppm HONO concentration. For the two terms $K^{\text{HONO}}[\text{HONO}]$ and $K^{\text{H}_2\text{O}}[\text{H}_2\text{O}]$ to be of comparable magnitude, K^{HONO} must be greater than $K^{\text{H}_2\text{O}}$ by a factor of approximately 10^3 .

The equilibrium constants for uptake of HONO and H₂O onto surfaces are related to the enthalpy and entropy of adsorption through the free energy. If it is assumed that the entropy of adsorption is similar for HONO and H₂O, then the ratio of the equilibrium constants is given by

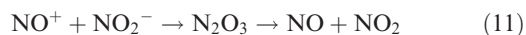
$$K^{\text{HONO}}/K^{\text{H}_2\text{O}} = \exp[-(\Delta H_{\text{ads}}^{\text{HONO}} - \Delta H_{\text{ads}}^{\text{H}_2\text{O}})/RT] \quad (\text{VIII})$$

where $\Delta H_{\text{ads}}^{\text{HONO}}$ and $\Delta H_{\text{ads}}^{\text{H}_2\text{O}}$ are the enthalpies of adsorption of HONO and water on the surface. If $K^{\text{HONO}}/K^{\text{H}_2\text{O}} \approx 10^3$, the difference between the enthalpies of adsorption of HONO and H₂O ($\Delta H_{\text{ads}}^{\text{HONO}} - \Delta H_{\text{ads}}^{\text{H}_2\text{O}}$) must be approximately -17 kJ mol⁻¹.

Thompson and Margey⁶² recently calculated enthalpies for formation of complexes of silica molecules (SiH₃OH or Si(OH)₄), taken as proxies for a silica surface, with HONO, water, HNO₃, NO₂ and N₂O₄. The enthalpy of formation for the complex of HONO with SiH₃OH was calculated to be -25.1 kJ mol⁻¹, and for the complex of H₂O with SiH₃OH, the enthalpy was calculated to be in the range from -15.5 to -23.2 kJ mol⁻¹, depending on the particular orientation of water to the silicate. This calculation shows that the difference in the enthalpies of adsorption for these complexes of HONO or H₂O should be in the range of $-(2-10)$ kJ mol⁻¹. The difference for binding of HONO compared to H₂O to Si(OH)₄ was also small, ≈ 2 kJ mol⁻¹. These differences are much smaller than our estimate of -17 kJ mol⁻¹. The apparent discrepancy could be due to several factors. First, the isolated SiH₃OH or Si(OH)₄ molecules used as proxies might not be truly representative of silica surfaces. This is particularly the case for borosilicate glass, which contains small amounts of oxides of metals such as Na, Zn, B, Al and Ti. Also, HONO may not adsorb in the molecular form by hydrogen bonding, as assumed in the calculations. For example, partial or full ionization to H⁺ and NO₂⁻ would provide strong electrostatic interactions, with larger associated heats of adsorption.

This work also predicted⁶² that nitric acid would form much stronger complexes with SiH₃OH and Si(OH)₄ than HONO. This might be the reason why HONO does not compete with HNO₃ for surface sites in the HNO₃-conditioned experiments, where the data are consistent with saturation of the surface sites by HNO₃.

The formation of equal amounts of NO and NO₂ as products is consistent with an autoionization reaction between gas-phase and adsorbed HONO:



Such autoionization reactions are known for HNO₃^{43–45} as well as for N₂O₅^{63–69} and N₂O₄ on ice.^{70–72} In the case of HONO, the relatively large enthalpy of adsorption on the surface relative to water as discussed above suggests that the adsorbed species might already be partially or fully ionized.

As the RH increases in the unconditioned cell, the yield of NO increases and that of NO₂ decreases. At 50% RH, the yield of NO is greater than 90% (Table 1 and Fig. 2e). These observations are similar to those of Ten Brink and Spoelstra,³⁵ who studied the decay of HONO in a pyrex chamber at 80% RH and 1–10 ppm HONO. Typical data in Fig. 3 of that paper show NO as the major gas phase product in the first 7 h of the reaction.

The mechanistic basis for the change in products as the RH increases in the unconditioned cell is not clear. In earlier studies¹⁰ of the NO₂ heterogeneous hydrolysis we reported that the yield of HONO was less than 0.5 as expected from reaction (1), and that the “missing HONO” was replaced by gas phase NO. We proposed that this was due to the reaction of HONO with NO₂⁺ on the surface,



If this is the source of NO in the present experiments in the unconditioned cell at 50% RH, the NO₂⁺ would have to be generated from adsorbed HONO if the reaction is to be second order as experimentally observed. However, a mechanism of formation of NO₂⁺ on the surface from HONO is not clear.

In summary, most of the experiments reported here are consistent with our proposed mechanisms. The only observation for which a clear explanation is not available is the change in the product distribution in the unconditioned cell from equal amounts of NO and NO₂ at 0% RH to primarily NO at 50% RH. Further work is underway to clarify the mechanisms responsible.

To the best of our knowledge, this is the first comprehensive study of HONO reactions on a borosilicate glass surface in which both the initial HONO concentration and the RH were varied over a relatively wide range, including the impact of coadsorption of HNO₃. The data reported here agree in large part with previous studies carried out over a more limited set of conditions. For example, Chan *et al.*^{30,31} reported that at low relative humidities in an unconditioned cell, NO and NO₂ are both generated and the rate of HONO loss decreases with RH, consistent with our experiments. We observed that the presence of HNO₃ increases the rate significantly and that the loss of HONO is first order under these conditions, in agreement with Kaiser and Wu³² and Wallington and Japar.³⁴ Reaction orders between one and two have been reported, depending on the conditions and presence of HNO₃.^{18,30–35} Our measured reaction orders are generally in agreement with these previous studies when comparisons are made under similar experimental conditions. For example, Jenkin *et al.*¹⁸ measured the rate of HONO decay in a glass chamber of similar size to the one used in these studies and reported the loss was first order at RH corresponding to 3.2 and 9.5% and the absolute value of the first order rate constant was $3.7 \times 10^{-4} \text{ s}^{-1}$. This is in excellent agreement with the value of $(3.9 \pm 1.1) \times 10^{-4} \text{ s}^{-1}$ measured in the present studies where the loss was also first order.

Finally, the results presented here provide some insight into laboratory studies of the heterogeneous hydrolysis of NO₂ in which yields of HONO have been frequently measured to be less than expected based on reaction (1). The observation of increasing yields of NO with decreasing HONO yields at intermediate to high relative humidities in such studies of reaction (1)^{10,14,15,17,23,24,73} is consistent with the formation of HONO followed by its conversion to NO on the “unconditioned” walls of the reactor as illustrated, for example, by the data in Fig. 2e.

Atmospheric implications

Nitrous acid production from the surfaces of environmental (“smog”) chambers used for studying atmospheric reactions has been observed in many studies using different chambers.^{25–29} This has been observed even when oxides of nitrogen have not been added during the experiment, implying that it must have arisen from contamination from previous experiments. Our studies show that the competition between water and HONO for surface sites leads to desorption of adsorbed HONO from the surface as the RH increases. This suggests that contamination of the walls of environmental chambers

in previous experiments leaves adsorbed HONO (or comparable species such as H⁺ and NO₂[−]) on the surface, and that HONO is displaced by water when the RH value is increased. Hence, if this point is accepted, generation of HONO in such chambers will be unavoidable once the chamber walls have been exposed to oxides of nitrogen. Consistent with this explanation is the observation that the rate of generation of HONO in such chambers increases with RH.²⁹

Nitrous acid has been measured in many field experiments, and it is clear from such studies that surface reactions act both as a source and as a sink for HONO. Separating the production and loss processes for HONO requires that the kinetics and mechanisms of this uptake be understood. In the tropospheric boundary layer there are a variety of surfaces of different chemical composition (*e.g.* vegetation, building materials *etc.*) available that might participate in uptake of HONO. Since many building materials are silicates,³⁷ our experiments using borosilicate glass are relevant to such surfaces in urban areas.

The results presented here suggest that the loss of HONO can vary from first to second order, depending on the RH and presence of reactive co-adsorbed species such as HNO₃. These experiments also show that HONO can be displaced from surfaces by water vapor, leading to an apparent increase in HONO as a function of RH. However, the formation of HONO from the NO₂ heterogeneous hydrolysis also increases with RH¹⁰ so that measurements of HONO at different RH may be affected both by the dependence of reaction (1) on water and by the displacement of HONO from the surface through preferential adsorption of water.

Stutz and coworkers⁷⁴ have measured HONO and NO₂ in urban areas and find that their data are consistent with a first-order loss of HONO at RH from 10 to 100%. This suggests that urban surfaces may have sufficient deposited HNO₃ (or other species that are reactive towards HONO) that the kinetics for the loss of HONO are determined by the collision rate of HONO with the surface.

Acknowledgements

We are grateful to the California Air Resources Board (Contract No. 00-323) and the National Science Foundation (Grant No. ATM-0097573) for support of this work. We would also like to thank K. A. Ramazan, L. F. Phillips, L. M. Wingen, J. N. Pitts Jr. and J. Stutz for helpful discussions.

References

- 1 A. M. Winer and H. W. Biermann, *Res. Chem. Intermed.*, 1994, **20**, 423.
- 2 B. Alicke, U. Platt and J. Stutz, *J. Geophys. Res.*, 2002, **107**, 10.1029/2000JD000075.
- 3 J. Stutz, B. Alicke and A. Neftel, *J. Geophys. Res.*, 2002, **107**, 10.1029/2001JD000390.
- 4 X. Zhou, K. Civerolo, H. Dai, G. Huang, J. Schwab and K. Demerjian, *J. Geophys. Res.*, 2002, **107**, 10.1029/2001JD001539.
- 5 B. Aumont, F. Chervier and S. Laval, *Atmos. Environ.*, 2003, **37**, 487.
- 6 G. Lammel and J. N. Cape, *Chem. Soc. Rev.*, 1996, **25**, 361.
- 7 G. Lamme, *Formation of Nitrous Acid: Parameterization and Comparison with Observations*, Report No. 286, Max-Planck-Institut für Meteorologie, Hamburg, 1999, pp. 1–36.
- 8 R. M. Harrison, J. D. Peak and G. M. Collins, *J. Geophys. Res.*, 1996, **101**, 14429.
- 9 V. R. Kotamarthi, J. S. Gaffney, N. A. Marley and P. V. Doskey, *Atmos. Environ.*, 2001, **35**, 4489.
- 10 B. J. Finlayson-Pitts, L. M. Wingen, A. L. Sumner, D. Syomin and K. A. Ramazan, *Phys. Chem. Chem. Phys.*, 2003, **5**, 223.

- 11 B. J. Finlayson-Pitts and J. N. Pitts, Jr., *Chemistry of the Upper and Lower Atmosphere: Theory, Experiments and Applications*, Academic Press, San Diego, 2000.
- 12 A. L. Goodman, G. M. Underwood and V. H. Grassian, *J. Phys. Chem. A.*, 1999, **103**, 7217.
- 13 W. S. Barney and B. J. Finlayson-Pitts, *J. Phys. Chem. A*, 2000, **104**, 171.
- 14 F. Sakamaki, S. Hatakeyama and H. Akimoto, *Int. J. Chem. Kinet.*, 1983, **15**, 1013.
- 15 J. N. Pitts, Jr., E. Sanhueza, R. Atkinson, W. P. L. Carter, A. M. Winer, G. W. Harris and C. N. Plum, *Int. J. Chem. Kinet.*, 1984, **16**, 919.
- 16 J. N. Pitts, Jr., T. J. Wallington, H. W. Biermann and A. M. Winer, *Atmos. Environ.*, 1985, **19**, 763.
- 17 R. Svensson, E. Ljungstrom and O. Lindqvist, *Atmos. Environ.*, 1987, **21**, 1529.
- 18 M. E. Jenkin, R. A. Cox and D. J. Williams, *Atmos. Environ.*, 1988, **22**, 487.
- 19 C. Perrino, F. DeSantis and A. Febo, *Atmos. Environ.*, 1988, **22**, 1925.
- 20 P. Wiesen, J. Kleffmann, R. Kurtenbach and K. H. Becker, *Faraday Discuss.*, 1995, **100**, 121.
- 21 J. Kleffmann, K. H. Becker and P. Wiesen, *Atmos. Environ.*, 1998, **32**, 2721.
- 22 J. Kleffmann, K. H. Becker and P. Wiesen, *J. Chem. Soc. Faraday Trans.*, 1998, **94**, 3289.
- 23 T. Wainman, C. J. Weschler, P. J. Lioy and J. Zhang, *Environ. Sci. Technol.*, 2001, **35**, 2200.
- 24 H. M. Ten Brink, J. A. Bontje, H. Spoelstra and J. F. van de Vate, in *Studies in Environmental Science*, ed. M. M. Benarie, Elsevier, Amsterdam, 1978, vol. 1, pp. 239.
- 25 W. P. L. Carter, R. Atkinson, A. M. Winer and J. N. Pitts Jr., *Int. J. Chem. Kinet.*, 1981, **13**, 735.
- 26 W. P. L. Carter, R. Atkinson, A. M. Winer and J. N. Pitts, Jr., *Int. J. Chem. Kinet.*, 1982, **14**, 1071.
- 27 F. Sakamaki and H. Akimoto, *Int. J. Chem. Kinet.*, 1988, **20**, 111.
- 28 W. A. Glasson and A. M. Dunker, *Environ. Sci. Technol.*, 1989, **23**, 970.
- 29 J. P. Killus and G. Z. Whitten, *Int. J. Chem. Kinet.*, 1990, **22**, 547.
- 30 W. H. Chan, R. J. Nordstrom, J. G. Calvert and J. H. Shaw, *Chem. Phys. Lett.*, 1976, **37**, 441.
- 31 W. H. Chan, R. J. Nordstrom, J. G. Calvert and J. H. Shaw, *Environ. Sci. Technol.*, 1976, **10**, 674.
- 32 E. W. Kaiser and C. H. Wu, *J. Phys. Chem.*, 1977, **81**, 1701.
- 33 E. W. Kaiser and C. H. Wu, *J. Phys. Chem.*, 1977, **81**, 187.
- 34 T. J. Wallington and S. M. Japar, *J. Atmos. Chem.*, 1989, **9**, 399.
- 35 H. M. Ten Brink and H. Spoelstra, *Atmos. Environ.*, 1998, **32**, 247.
- 36 A. A. Mebel, M. C. Lin and C. F. Melius, *J. Phys. Chem. A*, 1998, **102**, 1803.
- 37 R. M. E. Diamant, *The Chemistry of Building Materials*, Business Books Limited, London, 1970.
- 38 A. M. Rivera-Figueroa, A. L. Sumner and B. J. Finlayson-Pitts, *Environ. Sci. Technol.*, 2003, **37**, 548.
- 39 J. U. White, *J. Opt. Soc. Am.*, 1942, **32**, 285.
- 40 A. L. Sumner, E. J. Mehnke, Y. Dubowski, J. T. Newberg, R. M. Penner, J. C. Hemminger, L. M. Wingen, T. Brauers and B. J. Finlayson-Pitts, 2003, submitted.
- 41 W. S. Barney, L. M. Wingen, M. J. Lakin, T. Brauers, J. Stutz and B. J. Finlayson-Pitts, *J. Phys. Chem. A*, 2000, **104**, 1692;
- W. S. Barney, L. M. Wingen, M. J. Lakin, T. Brauers, J. Stutz and B. J. Finlayson-Pitts, *J. Phys. Chem. A*, 2001, **105**, 4166.
- 42 A. L. Sumner, Y. Dubowski, R. C. Hoffman, D. J. Gaspar, E. Menke, J. T. Newberg, R. M. Penner, J. C. Hemminger and B. J. Finlayson-Pitts, unpublished data, 2003.
- 43 C. C. Addison, *Chem. Rev.*, 1980, **80**, 21.
- 44 J. Chédin, *J. Chim. Phys.*, 1952, **49**, 109.
- 45 E. Högfeldt, *Acta Chem. Scand.*, 1963, **17**, 785.
- 46 J. N. Crowley, J. P. Burrows, G. K. Moortgat, G. Poulet and G. LeBras, *Int. J. Chem. Kinet.*, 1993, **25**, 795.
- 47 J. H. Smith, *J. Am. Chem. Soc.*, 1947, **69**, 1741.
- 48 S. Jaffe and H. W. Ford, *J. Phys. Chem.*, 1967, **71**, 1832.
- 49 G. E. Streit, J. S. Wells, F. C. Fehsenfeld and C. J. Howard, *J. Chem. Phys.*, 1979, **70**, 3439.
- 50 I. R. McKinnon, J. G. Mathieson and I. R. Wilson, *J. Phys. Chem.*, 1979, **83**, 779.
- 51 A. C. Besemer and H. Nieboer, *Atmos. Environ.*, 1985, **19**, 507.
- 52 R. Svensson and E. Ljungström, *Int. J. Chem. Kinet.*, 1988, **20**, 857.
- 53 D. H. Fairbrother, D. J. D. Sullivan and H. S. Johnston, *J. Phys. Chem. A*, 1997, **101**, 7350.
- 54 M. Mochida and B. J. Finlayson-Pitts, *J. Phys. Chem. A*, 2000, **104**, 9705.
- 55 N. Saliba, H. Yang and B. J. Finlayson-Pitts, *J. Phys. Chem. A*, 2001, **105**, 10339.
- 56 N. Saliba, M. Mochida and B. J. Finlayson-Pitts, *Geophys. Res. Lett.*, 2000, **27**, 3229.
- 57 A. L. Goodman, E. T. Bernard and V. Grassian, *J. Phys. Chem. A*, 2001, **105**, 6443.
- 58 B. D. Kay, V. Hermann and A. W. J. Castleman, *Chem. Phys. Lett.*, 1981, **80**, 469.
- 59 X. Zhang, E. Mereand and A. W. J. Castleman, *J. Phys. Chem.*, 1994, **98**, 3554.
- 60 J. J. Gilligan and A. W. J. Castleman, *J. Phys. Chem. A*, 2001, **105**, 5601.
- 61 R. I. Masel, *Principles of Adsorption and Reaction on Solid Surfaces*, John Wiley & Sons, New York, 1996.
- 62 K. C. Thompson and P. Margey, *Phys. Chem. Chem. Phys.*, 2003, **5**, 2970.
- 63 M. Mozurkewich and J. Calvert, *J. Geophys. Res.*, 1988, **93**, 15889.
- 64 A. Fried, B. E. Henry and J. G. Calvert, *J. Geophys. Res.*, 1994, **99**, 3517.
- 65 C. George, J. L. Ponche, P. Mirabel, W. Behnke, V. Scheer and C. Zetzsch, *J. Phys. Chem.*, 1994, **98**, 8780.
- 66 W. Behnke, C. George, V. Scheer and C. Zetzsch, *J. Geophys. Res.*, 1997, **102**, 3795.
- 67 G. N. Robinson, D. R. Worsnop, J. T. Jayne, C. E. Kolb and P. Davidovits, *J. Geophys. Res.*, 1997, **102**, 3583.
- 68 A. Wahner, T. F. Mentel, M. Sohn and J. Stier, *J. Geophys. Res.*, 1998, **103**, 31103.
- 69 F. Schweitzer, P. Mirabel and C. George, *J. Phys. Chem. A*, 1998, **102**, 3942.
- 70 J. Wang, M. R. Voss, H. Busse and B. E. Koel, *J. Phys. Chem. B*, 1998, **102**, 4693.
- 71 J. Wang and B. E. Koel, *J. Phys. Chem. A*, 1998, **102**, 8573.
- 72 J. Wang and B. E. Koel, *Surf. Sci.*, 1999, **436**, 15.
- 73 C. England and W. H. Corcoran, *Ind. Eng. Chem. Fundamen.*, 1974, **13**, 373.
- 74 J. Stutz, personal communication, 2003.

An upper limit to the concentration of an SO₂ complex at the air–water interface at 298 K: infrared experiments and *ab initio* calculations

Husheng Yang,^{†a} Nicholas J. Wright,^{ab} Aaron M. Gagnon,^{‡c} R. Benny Gerber^{*§ab} and Barbara J. Finlayson-Pitts^{*§a}

^a Department of Chemistry, University of California, Irvine, CA 92697-2025, USA

^b Department of Physical Chemistry and The Fritz Haber Research Center, The Hebrew University, Jerusalem, Israel 91904

^c Thermo Spectra-Tech, 230 Long Hill Cross Road, Shelton, CT 06484, USA

Received 2nd October 2001, Accepted 12th February 2002

First published as an Advance Article on the web 16th April 2002

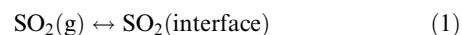
Unique reactions occurring at the interface between air and aqueous solutions are increasingly recognized to be of potential importance in atmospheric processes. Sulfur dioxide was one of the first species for which experimental evidence for the existence of a surface complex was obtained by several different groups, based on the kinetics of SO₂ uptake into aqueous solutions, large decreases in surface tension and second harmonic generation spectroscopic studies. The uptake has been proposed to involve an uncharged surface complex which subsequently converts into ionic species. We report here the results of a search for an uncharged SO₂ complex at or near the surface using attenuated total reflectance Fourier transform infrared spectrometry (ATR-FTIR) at 298 K guided by *ab initio* calculations of a 1:1 SO₂–H₂O complex. No infrared absorption bands attributable to such a complex of SO₂ were observed experimentally in the expected region, giving an upper bound of 4×10^{14} SO₂ cm⁻² to the concentration of neutral SO₂ molecules weakly sorbed to the surface in equilibrium with 1 atm SO₂(g). The implications for the nature of the surface species and previous observations are discussed.

Introduction

The uptake of gases into liquids, followed by diffusion and reactions in the liquid phase, is known to be important in a number of atmospheric processes. For example, the uptake of gaseous SO₂ into fogs and clouds followed by its oxidation by H₂O₂ and O₃ in the liquid phase is a major source of sulfuric acid in air.¹ However, there is an increasing body of experimental evidence that some gases may also undergo unique reactions at the air–water interface. In one of the first papers proposing this possibility, Jayne *et al.*² reported that the uptake of SO₂ into aqueous droplets could not be described without including a surface reaction involving an SO₂ complex at the interface; the conversion of this surface complex into H⁺ and HSO₃⁻ was proposed to determine the rate of uptake of SO₂. Donaldson and coworkers^{3,4} subsequently reported spectroscopic detection of an SO₂ surface complex in second harmonic generation spectroscopic studies of gas evolving from NaHSO₃ solutions. There was also a large reduction in the surface tension of these solutions and a saturation surface coverage of 5×10^{14} cm⁻² of an uncharged SO₂ surface complex was proposed. Additional examples of reactions of gases such as

Cl₂, Br₂, ClNO₂, ClONO₂ and OH with ions at the air–water or sulfuric acid solution interfaces, possibly *via* the formation of initial surface complexes, were subsequently reported,^{5–8} highlighting the importance of understanding the nature of such complexes at the air–water interface.

Boniface *et al.*⁹ reexamined the uptake and reactions of SO₂ in water and found that SO₂ reacts rapidly with OH⁻; the enhanced uptake observed in the earlier studies² at pH > 10 was shown to be due to this previously unrecognized reaction. However, a one-time uptake of SO₂ at pH < 2 was still observed and attributed to the formation of an SO₂ surface complex, with the number of available surface sites for SO₂ uptake being 10^{14} SO₂ cm⁻² as reported in the earlier studies.² Clegg and Abbati¹⁰ recently reported the uptake of gaseous SO₂ on ice surfaces at temperatures from 213 to 238 K. The measured uptake of SO₂ was observed to be consistent with the Jayne *et al.*² model, where the interfacial form of SO₂ [shown below as SO₂(interface)] involves interaction with a few water molecules at the surface, and the subsequent conversion to an ionic form determines the uptake:



Infrared spectroscopic measurements could be very useful in probing for the existence and nature of such interfacial species, and hence providing insight into its unique reactions at the interface. It can be inferred from the *ab initio* calculations by Bishenden and Donaldson¹¹ on the 1:1 SO₂:H₂O gas phase complex that there may be a red shift of 25 cm^{-1} in the ν_3

[†] Present address: Department of Chemistry, University of Idaho, Moscow, ID 83844-2343, USA

[‡] Present address: SensIR Technologies, 15 Great Pasture Road, Danbury, CT 06810-9931, USA

[§] Correspondence for theoretical calculations and experiments should be addressed to RBG (E-mail: bgerber@uci.edu) and BJFP (E-mail: bjfinlay@uci.edu; Fax: (949) 824-3168; Tel: (949) 824-7670), respectively.

asymmetric stretch of SO_2 on binding to water relative to the gas phase absorption, which occurs at 1361 cm^{-1} . One experimental approach for observing such a shifted absorption is the use of sum frequency generation (SFG) spectroscopic measurements which probes only the interface;^{12–15} however, covering the full range of infrared frequencies of interest is often not possible. Another approach is the use of single reflectance (SR) infrared spectroscopy which has been applied, for example, to monolayers of phospholipids at the air–water interface.^{16–22} This technique has the advantage that a wide range of infrared frequencies are measured. However, the infrared beam penetrates beyond the interface region into the bulk to a depth of the order of a few microns, depending on the frequency of the radiation and nature of the liquid; thus it probes the surface film, rather than just the interfacial region. As a result, if there are significant concentrations of dissolved compounds in addition to interfacial species, it can be difficult to separate the contributions of the interface species.

An alternate approach is attenuated total reflectance (ATR) combined with FTIR. ATR is an internal reflection technique in which light is directed into an infrared transmitting crystal. It strikes the interface at an angle greater than the critical angle and hence undergoes total internal reflection.²³ There is an evanescent wave that penetrates into the surrounding medium, with the depth of penetration depending on the angle of incidence and the indices of refraction of the crystal and the surrounding medium; typical depths of penetration are of the order of a few microns.²³ As a result, if single beam spectra with and without the absorbing species are ratioed, an absorption spectrum of infrared active species in the medium surrounding the crystal can be obtained. If the species adsorbs directly onto the crystal itself, it would also be detected. Such cells are normally used with liquids, and have proven particularly advantageous with aqueous solutions since the net path-length through the absorbing water solvent is minimized. ATR has also been used extensively with solids and their interactions with gases²⁴ and liquids.^{25,26} Horn and Sully^{27,28} applied ATR to study the uptake of gases onto ice surfaces²⁷ as well as the formation of sulfuric acid–water films when SO_3 and H_2O were co-condensed on a Ge crystal at $T \leq 250\text{ K}$. Thus, ATR has been demonstrated to be a highly useful technique for studying both bulk materials and thin films.

As a result, we have chosen this technique to study the chemistry in these water films at room temperature. Thin films of water can be formed on the ATR crystal by exposure to water vapor, and the thickness of the film can be determined from the water absorption bands. In this case, even though the evanescent wave probes on the order of a micron away from the interface, the absorbing film is $<30\text{ nm}$ in depth and determines the infrared absorption spectrum. If interfacial species are formed at the air–water interface in sufficient concentrations, they should also be detectable, since this small film thickness maximizes contributions to the infrared absorption by interfacial compared to dissolved species.

We report here a search for the previously proposed uncharged SO_2 –water complex in surface films of water solutions using attenuated total reflectance Fourier transform infrared spectroscopy (ATR-FTIR). For comparison, we have obtained transmission and single reflectance spectra of saturated aqueous solutions of SO_2 . To assist in our search for a complex, we have also carried out electronic structure calculations on the SO_2 – H_2O complex in the gas phase, both for the lowest energy configuration (which has a ‘sandwich’ type structure) and for a hydrogen-bonded structure of slightly higher (1.6 kcal mol^{-1}) energy (see Fig. 1). The combination of these approaches allows us to put an upper limit on the concentration of an SO_2 –water surface complex at the air–water interface of $4 \times 10^{14}\text{ SO}_2\text{ cm}^{-2}$, based on the experimental data

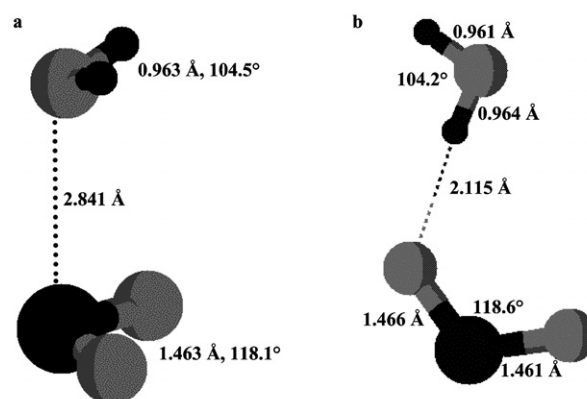


Fig. 1 Geometry of (a) the lowest energy and (b) a hydrogen-bonded configuration of the SO_2 – H_2O complex, calculated at the MP2/aug-cc-pvtz level.

and assuming its structure can be represented by a 1:1 SO_2 – H_2O or similar complex.

Experimental

Measurements using attenuated total reflectance

Experiments were carried out using two types of ATR probes: a fiber optic probe (Thermo Spectra-Tech, ATR Needle Probe) and a Tunnel cell[®] (Axiom Analytical, Inc., Irvine, CA). Most of the experiments reported here were carried out with the fiber optic probe that consisted of an infrared-transmitting chalcogenide (AsSeTe) fiber embedded in an epoxy support and polished to expose a portion of the fiber; the number of reflections is three. From the angle of incidence ($\theta = 45^\circ$) and the refractive index of chalcogenide ($n_1 = 2.8$), the depth of penetration (d_p) of the evanescent wave can be calculated²³ from $d_p = \lambda / [2\pi n_1 (\sin^2\theta - n_{21}^2)^{1/2}]$, where $n_{21} = n_2/n_1$ and n_2 is the index of refraction of the rarer medium surrounding the crystal. At 3400 cm^{-1} , d_p is $0.28\text{ }\mu\text{m}$ for air and $0.32\text{ }\mu\text{m}$ for water; at 1150 cm^{-1} , the corresponding values are $0.82\text{ }\mu\text{m}$ (air) and $0.94\text{ }\mu\text{m}$ (water), respectively. As discussed in detail later, the depth of penetration of the beam is much larger than the thickness of the water films deposited on the crystal. As a result, the evanescent wave probes not only the species dissolved in the film, but also any surface-adsorbed species present. In addition, for such thin films, the effective thickness, d_e , of the film and hence the relative intensities do not depend on wavelength, resulting in spectra that are very similar to transmission spectra (this is not the case for bulk materials, where the effective thickness depends on wavelength).²³

The probe was mounted in a borosilicate glass cell so that the infrared fiber could be exposed to gases in the cell under controlled conditions. The cell was attached to a conventional vacuum system for introducing gases, and to a 50 mL bulb containing water (Barnstead, Nanopure) which had been through a freeze–pump–thaw cycle. The probe was mated to a Mattson RS Series FTIR using a ‘Foundation’ transfer optic (Thermo Spectra-Tech) located in the sample compartment.

After the cell was pumped out, it was allowed to come to equilibrium with the water in the bulb. The water vapor pressure was not measured directly, but some condensation on the cell walls was observed visually. The presence of a thin water film led to a strong absorption at 3400 cm^{-1} that is characteristic of liquid water (ν_1).²⁹ Gaseous SO_2 (Matheson, Anhydrous) was then introduced into the cell to a measured total pressure and the single beam spectrum recorded. For comparison, a spectrum was also recorded with SO_2 added to the cell

in the absence of water vapor. In each case, a total of 1000 scans at 4 cm^{-1} resolution was used with the cell sealed off, *i.e.* in the static mode.

The thickness of the water film on the fiber optic surface was quantified in the following manner.²³ The reflectivity, R^N , for N reflections and weak absorptions is given by

$$R^N \cong 1 - N a d_e \quad (\text{I})$$

where d_e is the effective thickness, a parameter which reflects the coupling between the evanescent wave and the sample, and which can be related to the corresponding transmission spectrum for which $I/I_0 = e^{-a l}$ where l is the pathlength. The absorption parameter, a , is given by

$$a = (1 - R^N) \cong N a d_e \quad (\text{II})$$

and is measured in these experiments by measuring the reflectivity as the ratio of the single beam spectrum in the presence of the sample to that in the absence of the water film. (For ease of presentation, spectra are shown as absorbance ($\log I_0/I$) versus wavenumber.) Rather than using the intensity at one wavenumber, the band was integrated over the wavelength region $2800\text{--}3800\text{ cm}^{-1}$ and the optical constants from Bertie and Lan³⁰ applied to obtain the effective thickness, d_e . Taking 0.35 nm as the depth of one monolayer of water, the number of water layers was calculated as $d_e/0.35$. In these experiments, the water layers were sufficiently thick that the infrared spectrum was indistinguishable from that of bulk liquid water, in contrast to the case of 1–5 water layers where the spectrum shows that the water is significantly perturbed by the underlying surface.³¹ Therefore, application of the optical constants for liquid water are appropriate in the present experiments.

A second type of ATR experiment was carried out using the Tunnel cell[®] that consists of an $1/8''$ infrared-transmitting AMTIR (GeAsSe) crystal of length $1.5''$ situated in a cylindrical sample holder. For this particular cell, approximately 10 such internal reflections occur along the length of the rod. The cell was located in the sample compartment of a Mattson Galaxy FTIR spectrometer (Model 5020). The thin liquid water film was first formed on the crystal by flowing a stream of N_2 containing H_2O vapor at a given relative humidity and a total pressure of 1 atm through the cell. Some of the vapor condensed on the crystal, forming a thin film of liquid water which was again quantified using the liquid water infrared absorption at 3400 cm^{-1} . Gaseous SO_2 at approximately 1 atm pressure was then introduced into the cell and the spectrum recorded, again in the static mode. Comparison spectra using SO_2 in the absence of water were also measured. For these experiments, 1024 scans at 0.5 cm^{-1} resolution were recorded.

Measurement of transmission and single-reflectance FTIR spectra

For comparison to the ATR spectra, we also measured transmission spectra of the corresponding solutions. The transmission cell (McCarthy Scientific Co.) had CaF_2 windows and a $50\text{ }\mu\text{m}$ Teflon spacer. Spectra of water saturated with SO_2 and of NaHSO_3 (Fisher Scientific Certified ACS grade) were recorded at a resolution of 0.5 cm^{-1} and using a total of 1024 scans.

SR-FTIR spectra of saturated NaHSO_3 and SO_2 saturated water were measured in an apparatus similar to the one described previously³² but with a closed sample cell to prevent loss of gases. The infrared beam passed through a CaF_2 window to the surface where it is reflected by the liquid back through the CaF_2 window to an MCT detector. The resolution used for these studies was typically 0.5 cm^{-1} . Although lower resolution could have been used for the surface and bulk phase species, use of 0.5 cm^{-1} resolution optimized the identification

and subtraction of gas phase SO_2 from the spectra. A warm stream of nitrogen gas flow was directed onto the outside of the CaF_2 window in order to prevent condensation of water on the inside of the window; uptake of water or SO_2 into water films on the window was detectable in the single reflectance spectrum as positive absorbance signals superimposed on the differential-shaped peaks due to the bulk species, and because this complicated the data analysis, it was avoided.

Infrared reflectance spectra of bulk solutions contain contributions from species in the gas phase, in the top few microns of the liquid phase, and when present at sufficient concentrations, at the interface. The absorption bands for gas-phase species are similar to the peaks observed in a normal transmission spectrum, and were removed by subtracting an appropriate gas-phase reference spectrum. Reference spectra of SO_2 were taken in the same cell by introducing the gas into the cell and replacing the liquid solution with a reflecting mirror coated with gold and a protective overlayer of silicon monoxide. Although SO_2 has been observed to adsorb on gold³³ it is not known to adsorb on glass surfaces at room temperature and hence would not be expected to do so on the silicon monoxide coated mirror. The SR spectra were analyzed as described in earlier studies³² using the Kramers–Kronig (KK) transform^{34,35} to obtain the absorption coefficient (k) spectrum as a function of wavenumber.

In single reflectance spectra, the absorption bands responsible for the species in the bulk liquid appear as differential-shaped peaks. The Kramers–Kronig (KK) transform^{34,35} converts the reflectance spectrum into an absorption spectrum with positive bands similar to those obtained using transmission. If there is an interfacial layer between air and the bulk aqueous solution, the absorption bands for these species appear as negative peaks,^{16,18,19} and become differential in shape after application of the KK transform.

All measurements were carried out at $298 \pm 2\text{ K}$.

Results and discussion

Ab initio calculations

Calculations by Bishenden and Donaldson¹¹ suggest that the ν_3 asymmetric stretch for gas phase SO_2 at 1361 cm^{-1} may red-shift by as much as 25 cm^{-1} when SO_2 is complexed to one water molecule. To provide further guidance for our experiments, *ab initio* calculations were carried out for gaseous SO_2 as well as a 1:1 $\text{SO}_2\text{:H}_2\text{O}$ complex in the two configurations shown in Fig. 1. Fig. 1a is a ‘sandwich’ type structure and Fig. 1b is a hydrogen-bonded structure of slightly higher (1.6 kcal mol^{-1}) energy.

Table 1 compares our calculated harmonic frequencies for gas phase SO_2 and for both structures of the $\text{SO}_2\text{--H}_2\text{O}$ complex. All calculations were performed with the Gaussian 94 electronic structure³⁶ package at the MP2/aug-cc-pvtz level of theory. The agreement between the experimental frequencies and those calculated at this level of theory for $\text{SO}_2(\text{g})$ is good, and certainly sufficient to give us confidence in the theoretical method used. Blue shifts of 3 to 12 cm^{-1} are calculated when gas phase SO_2 forms the lowest energy 1:1 ‘sandwich’ complex with water shown in Fig. 1a. No significant differences in the relative band intensities are predicted for the complex compared to SO_2 itself. As discussed below, shifts for complexes of SO_2 with more than one water molecule but less than the bulk would be expected to fall between these two extremes; the calculations on the 1:1 complex and measurements of the spectrum in the bulk allow one to focus the experiments accordingly.

Interactions between SO_2 and water are weak compared to those between water molecules, which form a strong hydrogen-bonded network at the air–water interface, with some dan-

2c, indicating they are due to a species present in the top layer of the bulk solution. The same peaks are also present in a transmission spectrum of a similar solution that has been diluted by a factor of 10 (Fig. 2d), and are characteristic of the ν_3 and ν_1 modes of SO_2 in water, respectively.^{47,48} Also seen in Fig. 2d are weak, broad peaks at 1028 cm^{-1} due to HSO_3^- in equilibrium with $\text{SO}_2(\text{aq})$ and at 1060 cm^{-1} from $\text{S}_2\text{O}_5^{2-}$ in equilibrium with 2 HSO_3^- .^{48,49} From the known equilibrium constants,^{1,50,51} the concentrations for the solution in Fig. 2d are calculated to be $0.1\text{ M SO}_2(\text{aq})$, 0.04 M HSO_3^- and $1 \times 10^{-4}\text{ M S}_2\text{O}_5^{2-}$, with a pH of 1.4. As discussed in detail elsewhere,^{47,50} SO_2 is not strongly hydrated in aqueous solution so that its infrared spectrum is similar to that of liquid SO_2 .⁵² There was no evidence of differential-shaped peaks after application of the Kramers–Kronig transform, indicating that interfacial species, if they exist, were present at concentrations too small to be observable in these experiments.

The spectra in Fig. 2 clearly show the shift in the ν_3 asymmetric stretch from 1361 cm^{-1} for gas phase SO_2 to 1330 cm^{-1} when the SO_2 is surrounded by a number of water molecules in aqueous solution. The blue shift in the ν_1 symmetric stretch is small, several wavenumbers or less. Due to the different geometry and the smaller number of water molecules in contact with SO_2 for a surface complex, the vibrational shifts for surface-adsorbed SO_2 are likely to be smaller in magnitude than for SO_2 in bulk liquid water.

Thus, based on our theoretical calculations (Table 1), the experimentally observed shifts in argon matrices,^{44,45} and the position of this band in aqueous solution (Fig. 2), it is reasonable to expect the ν_1 symmetric stretch for the SO_2 surface complex with water will be within several wavenumbers of 1151 cm^{-1} . Because the corresponding absorptions of aqueous sulfur species are at 1152 cm^{-1} and are broad, a unique signal due to the surface species will be difficult to detect in this region. However, the combination of the theory and experimental data suggest that the ν_3 asymmetric stretch which appears at 1361 cm^{-1} for gaseous $\text{SO}_2(\text{g})$ will be shifted by $2\text{--}8\text{ cm}^{-1}$ for a surface species interacting with one water molecule. Presumably interactions with more than one water molecule, but less than the number in the bulk solution, will lead to shifts that are greater than 8 cm^{-1} but less than the 31 cm^{-1} for $\text{SO}_2(\text{aq})$. This is supported by the matrix infrared studies of Schriver *et al.*⁴⁵ who reported absorption bands not only for the 1:1 complex (Table 1) but also for the 2:1 $\text{H}_2\text{O}\text{--}\text{SO}_2$ complex. Compared to SO_2 in an Ar matrix,⁴⁴ the ν_3 asymmetric stretch of the 2:1 $\text{H}_2\text{O}\text{--}\text{SO}_2$ complex was red-shifted by 12 cm^{-1} , and the ν_1 was blue-shifted by 10 cm^{-1} , larger in both cases than for the 1:1 complex.

If the absorption band for the SO_2 surface complex was very broad, it would be difficult to detect. However, this is not likely to be the case. The width of the $\text{SO}_2(\text{aq})$ absorption band reflects a time-averaged set of changing interactions of SO_2 with a number of different water molecules. The surface complex is expected to interact simultaneously with fewer water molecules, on average, than $\text{SO}_2(\text{aq})$ in the bulk. The width of the absorption band for the surface complex, which reflects in part these changing interactions with water, would therefore not be expected to be significantly different than that of $\text{SO}_2(\text{aq})$. Because the gas phase does not contribute a measurable signal in ATR due to the small depth of penetration of the evanescent wave, and the absorption due to $\text{SO}_2(\text{aq})$ is shifted by 31 cm^{-1} , we expect that a signal from the shifted ν_3 asymmetric stretch of a surface SO_2 complex should be observable in our experiments.

ATR infrared experiments

To probe experimentally for the existence of a surface complex using ATR-FTIR, spectra were obtained using the fiber optic probe when SO_2 was present at 1 atm pressure in the absence

of water and then in its presence. Fig. 3a shows the spectrum obtained in the absence of water vapor. Weak peaks at 1330 and 1145 cm^{-1} are seen. Since there is little water present on the crystal under these conditions as evidenced by the absence of the strong band around 3400 cm^{-1} , these peaks must be due to SO_2 physisorbed on the crystal surface. The nature of physisorbed SO_2 is not clear, but the band positions are similar to those reported for liquid SO_2 ,⁵² 1338 and 1148 cm^{-1} , and gas phase clusters and thin film SO_2 at low temperatures,⁵³ 1330 and 1140 cm^{-1} . One possibility is that SO_2 exists on the surface in 2D “islands” involving $\text{SO}_2\text{--}\text{SO}_2$ interactions, similar to that reported for water at low coverages on salt^{54,55} and on borosilicate glass surfaces.³¹

Fig. 3b shows the spectrum when a similar pressure of SO_2 was added to the cell which had been allowed to equilibrate first with the bulb of liquid water. Peaks due to liquid water at 3400 and 1640 cm^{-1} are present. The peak at 1330 cm^{-1} has increased in intensity, and the 1145 cm^{-1} peak has broadened and shifted slightly to 1147 cm^{-1} .

With water present, gaseous SO_2 will dissolve to form $\text{SO}_2(\text{aq})$, HSO_3^- and SO_3^{2-} in the thin water film on the ATR crystal surface. From the 3400 cm^{-1} liquid water band, the effective thickness (d_e) of the water film is estimated as described above to be $2.8 \times 10^{-6}\text{ cm}$, corresponding to 80 monolayers of water. From the known equilibria and kinetics in water,^{1,50,51} equilibrium with gaseous SO_2 should be rapidly attained, with $\text{SO}_2(\text{aq})$ and HSO_3^- as the major sulfur species present in the water film. For the conditions of Fig. 3b, the concentrations of $\text{SO}_2(\text{aq})$ and HSO_3^- are calculated to be 1.05 M and 0.12 M respectively, and the pH is calculated to be 0.9. The increase in the 1330 cm^{-1} peak in the presence of water is therefore likely to be due to $\text{SO}_2(\text{aq})$ whose major absorption peak is at 1330 cm^{-1} (Fig. 2).⁵²

Fig. 4 shows an expanded region from 1400 to 1100 cm^{-1} for the experiment in Fig. 3b. Fig. 4a shows the difference between the spectrum with both SO_2 and water present and that when water was present alone before SO_2 was added. Fig. 4b shows the spectrum of SO_2 in the absence of water. Fig. 4c is the difference between Fig. 4a and 4b, showing the new bands that are formed when both water and SO_2 are present compared to SO_2 or water alone. Peaks at both 1330 and 1152 cm^{-1} are seen, as expected for $\text{SO}_2(\text{aq})$. Furthermore, they are in the same ratio, within experimental error, of those measured in the transmission and single reflectance spectra (Fig. 2c and d). Thus, when both water and SO_2 are present, $\text{SO}_2(\text{aq})$ is formed in the thin water film on the crystal surface, as expected.

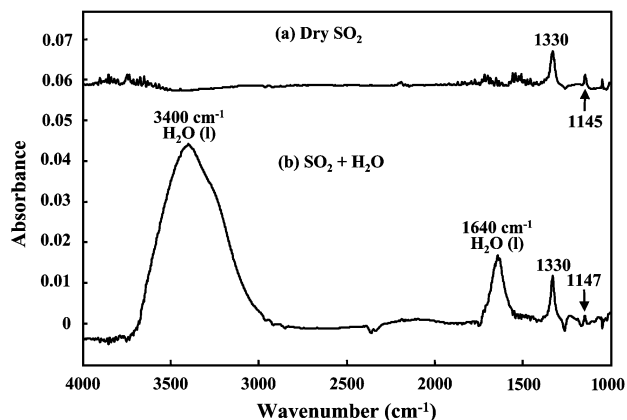


Fig. 3 ATR spectra in the presence of (a) 630 Torr $\text{SO}_2(\text{g})$ and (b) 645 Torr SO_2 added to the cell after the crystal had come to equilibrium with 24 Torr water vapor, forming a thin water film on the crystal. The equilibrium concentrations are calculated to be $1.05\text{ M SO}_2(\text{aq})$, 0.12 M HSO_3^- and $1 \times 10^{-3}\text{ M S}_2\text{O}_5^{2-}$, with a pH of 0.9.

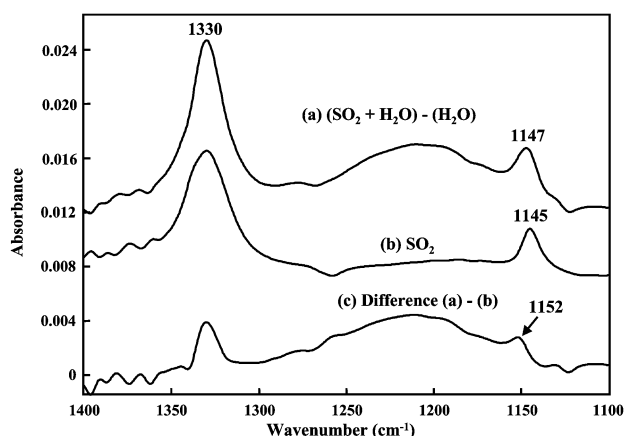


Fig. 4 Expanded region for experiment described in Fig. 3. (a) Spectrum in Fig. 3b after subtraction of the spectrum of water alone before the addition of gaseous SO_2 ; (b) spectrum of SO_2 alone as shown in Fig. 3a; (c) difference spectrum $4a - 4b$. The broad feature between the two SO_2 peaks at 1330 and 1152 cm^{-1} is likely to be due to small baseline shifts which are also manifested as similar broad features in other regions of the spectrum.

The fact that a peak remains at 1145 cm^{-1} when water is added to the cell suggests that even in the presence of water, some SO_2 continues to interact with the surface in a manner similar to the dry case, in addition to dissolved sulfur oxide species being formed in the water film. A question arises as to whether the 1330 and 1145 cm^{-1} bands observed in the presence of water could be assigned to an SO_2 complex of water at the interface. This seems unlikely since the shift of 30 cm^{-1} from 1361 to 1330 cm^{-1} appears to be characteristic of condensed phases or clusters where the SO_2 is surrounded by other SO_2 or water molecules. At the interface, SO_2 will not be surrounded in such 3D structures and hence, as our calculations and the matrix isolation experiments^{44,45} show, such a large shift is not expected for the surface complex.

With a water film of thickness $2.8 \times 10^{-6}\text{ cm}$, the volume of water over a 1 cm^2 area of the crystal surface is $2.8 \times 10^{-9}\text{ L}$. Given a concentration of $\text{SO}_2(\text{aq})$ of 1.05 M , there are 2×10^{15} SO_2 molecules per cm^2 dissolved in the water film and these give the increase in absorbance of 0.0046. Our detection limit of 0.001 (based on three times the peak-to-peak noise in this region) therefore corresponds to $4 \times 10^{14}\text{ cm}^{-2}$ for $\text{SO}_2(\text{aq})$. A second set of similar experiments gave a detection limit of $3 \times 10^{14}\text{ cm}^{-2}$. If the surface complex of SO_2 has a similar absorption coefficient, then it therefore should be detectable at levels $\geq 4 \times 10^{14}\text{ cm}^{-2}$ in these experiments. We believe that this is a conservative estimate, in that the 1152 cm^{-1} peak due to $\text{SO}_2(\text{aq})$ in Fig. 4c has a peak absorbance above the baseline of 0.001, equivalent to our stated detection limit, but is very clearly visible in the spectrum.

A careful examination of ATR spectra such as those in Fig. 4 revealed no new bands that were not attributable to $\text{SO}_2(\text{aq})$ or physisorbed SO_2 . There are no new bands between 1361 cm^{-1} where gas phase SO_2 absorbs and 1350 cm^{-1} , the region where the combination of calculations and matrix experiments suggest a 1:1 surface complex of $\text{SO}_2:\text{H}_2\text{O}$ should be observable. (The small peaks seen in the spectra in the 1400 to 1360 cm^{-1} region are due to incomplete subtraction of gas phase water due to changes in the purging of the sample compartment of the spectrometer.) Thus, this surface complex of SO_2 , if it exists, must be present at less than $4 \times 10^{14}\text{ cm}^{-2}$. It is reasonable to expect that if it interacted with several water molecules, it might be further red-shifted below 1350 cm^{-1} ; for example, the low temperature matrix studies^{44,45} suggest that the interaction with two water molecules would red-shift the

band by 12 cm^{-1} . Because of the tail of the $\text{SO}_2(\text{aq})$ band at 1330 cm^{-1} , this would be more difficult to observe but again, no detectable peaks are observed in this region.

Experiments were also carried out using the 10-reflection Tunnel cell[®] designed for use with liquid solutions. The results were essentially identical. That is, peaks at 1330 and 1145 cm^{-1} were observed with SO_2 in the absence of water, with the 1330 cm^{-1} peak being enhanced in the presence of water by an amount consistent with the formation of $\text{SO}_2(\text{aq})$ in the thin water film. In this case, the water film was only 18 monolayers thick so that the amount of $\text{SO}_2(\text{aq})$ on the crystal surface was significantly less than for the experiment shown in Fig. 3 using the needle probe, and the 1152 cm^{-1} peak was not observable. Analysis similar to that described above gives an upper limit to the 1:1 $\text{SO}_2:\text{H}_2\text{O}$ surface complex of $2 \times 10^{14}\text{ cm}^{-2}$, but this is considered to be less reliable because of the need to subtract a contribution from small amounts of gas phase SO_2 present in the light path in the sampling compartment due to leakage from the cell. However, it is noteworthy that in all respects the results were the same when a different ATR crystal and experimental system was used, ruling out unrecognized artifacts from a particular crystal surface.

Boniface *et al.*⁵⁶ observed a one-time uptake of SO_2 onto aqueous solutions at $\text{pH} < 2$, which based on the data of Jayne *et al.*,² corresponds to a saturation concentration of surface sites of 10^{14} cm^{-2} ; a surface complex at this concentration would not have been observable in our experiments. Donaldson *et al.*³ estimated a saturation surface coverage of 5×10^{14} SO_2 per cm^2 in their SHG and surface tension measurements of gases evolving from NaHSO_3 solutions, and proposed that this was due to an uncharged SO_2 surface complex. While this is only slightly larger than our detection limit, it seems likely from Fig. 4 that if an uncharged 1:1 SO_2 surface complex were present in our experiments at this concentration, it would have been observable.

Several groups^{2,10,51} have proposed that the uptake of SO_2 into water or ice occurs by the formation of a surface SO_2 complex that then dissociates into surface ionic species (eqns. (1) and (2) above). The expected absorption bands for such an ionic complex are not known but one might expect that they would be in the region of the HSO_3^- absorption bands. The weak, broad peak around 1028 cm^{-1} in Fig. 2d is due to HSO_3^- .^{48,49} From this spectrum, the molar extinction coefficient at 1028 cm^{-1} is estimated to be $2.8 \times 10^2\text{ M}^{-1}\text{ cm}^{-1}$, about half that for the 1330 cm^{-1} band of $\text{SO}_2(\text{aq})$. If a surface HSO_3^- exists and has an absorption coefficient similar to that for $\text{HSO}_3^-(\text{aq})$, our detection limit for the surface species would be about twice that for $\text{SO}_2(\text{aq})$, or $8 \times 10^{14}\text{ cm}^{-2}$.

In summary, no new peaks or significant shifts in sulfur dioxide peaks normally found in aqueous solutions were observed in any of the experiments, from which an upper limit to the concentration of a 1:1 SO_2 -water or similar complex at the air-water interface of $4 \times 10^{14}\text{ cm}^{-2}$ can be estimated.

Conclusions

Attenuated total reflectance Fourier transform spectrometry provides a powerful means of searching for surface complexes using well-developed and readily available spectroscopic methods. The inorganic species for which there is the greatest evidence from previous studies for the formation of a surface complex at the air-water interface is SO_2 , which is hypothesized to convert to an ionic form at the surface. A search for a 1:1 or similar neutral complex of SO_2 with water at the surface of aqueous solutions using this approach did not reveal any absorption bands attributable to such an interfacial species, from which concentrations higher than 4×10^{14} complexes cm^{-2} can be excluded with some confidence. Understanding the molecular form of this complex, if it exists,

is important for elucidating its role in the physical and chemical properties of the interface of aqueous solutions in the presence of SO₂, such as the reported reduction in surface tension. Future searches to elucidate the nature of this surface species need to be capable of detecting surface concentrations of the order of 10¹⁴ cm⁻² or less.

Acknowledgement

We are grateful to the California Air Resources Board for support of this work. We also thank P. R. Griffiths, R. A. Dluhy, D. J. Donaldson, C. Higgins, C. E. Kolb, D. R. Worsnop and P. Davidovits, S. Fleming and M. Doyle for helpful discussions, and D. J. Donaldson for providing a preprint prior to publication. This research was also supported in part by a grant from the Petroleum Research Fund administered by the American Chemical Society.

References

- B. J. Finlayson-Pitts and J. N. Pitts, *Chemistry of the Upper and Lower Atmosphere: Theory, Experiments and Applications*, Academic Press, San Diego, 2000.
- J. T. Jayne, P. Davidovits, D. R. Worsnop, M. S. Zahniser and C. E. Kolb, *J. Phys. Chem.*, 1990, **94**, 6041.
- D. J. Donaldson, J. A. Guest and M. C. Goh, *J. Phys. Chem.*, 1995, **99**, 9313.
- S. Izmailova, E. Bishenden and D. J. Donaldson, submitted for publication.
- D. R. Hanson and A. R. Ravishankara, *J. Phys. Chem.*, 1994, **98**, 5728.
- J. H. Hu, Q. Shi, P. Davidovits, D. R. Worsnop, M. S. Zahniser and C. E. Kolb, *J. Phys. Chem.*, 1995, **99**, 8768.
- C. George, W. Behnke, V. Scheer, C. Zetzsch, L. Magi, J. L. Ponche and P. Mirabel, *Geophys. Res. Lett.*, 1995, **22**, 1505.
- E. M. Knipping, M. J. Lakin, K. L. Foster, P. Jungwirth, D. J. Tobias, R. B. Gerber, D. Dabdub and B. J. Finlayson-Pitts, *Science*, 2000, **288**, 301.
- J. Boniface, Q. Shi, Y. Q. Li, J. L. Cheung, O. V. Rattigan, P. Davidovits, D. R. Worsnop, J. T. Jayne and C. E. Kolb, *J. Phys. Chem. A*, 2000, **104**, 7502.
- S. M. Clegg and J. P. D. Abbatt, *J. Phys. Chem. A*, 2001, **105**, 6630.
- E. Bishenden and D. J. Donaldson, *J. Phys. Chem. A*, 1998, **102**, 4638.
- K. B. Eiseenthal, *Annu. Rev. Phys. Chem.*, 1992, **43**, 627.
- K. B. Eiseenthal, *Acc. Chem. Res.*, 1993, **26**, 636.
- Y. R. Shen, *Annu. Rev. Phys. Chem.*, 1989, **40**, 327.
- Y. R. Shen, *Nature*, 1989, **337**, 519.
- R. A. Dluhy and D. G. Cornell, *J. Phys. Chem.*, 1985, **89**, 3195.
- R. A. Dluhy, B. Z. Chowdhry and D. G. Cameron, *Biochim. Biophys. Acta*, 1985, **821**, 437.
- R. A. Dluhy, *J. Phys. Chem.*, 1986, **90**, 1373.
- R. A. Dluhy, N. A. Wright and P. R. Griffiths, *Appl. Spectrosc.*, 1988, **42**, 138.
- R. A. Dluhy, M. L. Mitchell, T. Pettenski and J. Beers, *Appl. Spectrosc.*, 1988, **42**, 1289.
- R. A. Dluhy, K. E. Reilly, R. D. Hunt, M. L. Mitchell, A. J. Maunton and R. Mendelsohn, *Biophys. J.*, 1989, **56**, 1173.
- R. A. Dluhy, S. M. Stephens, S. Widayati and A. D. Williams, *Spectrochim. Acta, Part A*, 1995, **51**, 1413.
- N. J. Harrick, *Internal Reflection Spectroscopy*, Wiley Interscience Publishers, New York, 1967.
- P. Dumas, M. K. Weldon, Y. J. Chabal and G. P. Williams, *Surf. Rev. Lett.*, 1999, **6**, 225.
- M. I. Tejedor-Tejedor and M. A. Anderson, *Langmuir*, 1986, **2**, 203.
- A. J. McQuillan, *Adv. Mater.*, 2001, **13**, 1034.
- A. B. Horn and J. Sully, *J. Chem. Soc., Faraday Trans.*, 1997, **93**, 2741.
- A. B. Horn and K. J. Sully, *Phys. Chem. Chem. Phys.*, 1999, **1**, 3801.
- G. C. Pimentel and A. L. McClellan, *The Hydrogen Bond*, W. H. Freeman, San Francisco, 1960.
- J. E. Bertie and Z. Lan, *Appl. Spectrosc.*, 1996, **50**, 1047.
- N. Saliba, H. Yang and B. J. Finlayson-Pitts, *J. Phys. Chem. A*, 2001, **105**, 10339.
- H. Yang and B. J. Finlayson-Pitts, *J. Phys. Chem. A*, 2001, **105**, 1890.
- T. Wilke, X. Gao, C. G. Takoudis and M. J. Weaver, *J. Catal.*, 1991, **130**, 62.
- D. Krcho, *Kramers-Kronig Relations in Fourier Transform Infrared Spectroscopy of Semiconductors, The 3rd Biennial Engineering Mathematics and Applications Conference*, Adelaide, Australia, 1998.
- K. Ohta and H. Ishida, *Appl. Spectrosc.*, 1988, **42**, 952.
- M. J. Frisch, G. W. Trucks, H. B. Schlegel, P. M. W. Gill, B. G. Johnson, M. A. Robb, J. R. Cheeseman, T. Keith, J. A. Montgomery, K. Raghavachari, M. A. Al-Laham, V. G. Zakrzewski, J. V. Ortiz, J. B. Foresman, J. Cioslowski, B. B. Stefanov, A. Nanayakkara, M. Challacombe, C. Y. Peng, P. Y. Ayala, W. Chen, M. W. Wong, J. L. Andres, E. S. Replogle, R. Gomperts, R. L. Martin, D. J. Fox, J. S. Binkley, D. J. Defrees, J. Baker, J. P. Stewart, M. Head-Gordon, C. Gonzalez and J. A. Pople, *Gaussian 94*, rev. C.2, Gaussian, Inc., Pittsburgh, PA, 1995.
- M. C. Goh, J. M. Hicks, K. Kemnitz, G. R. Pinto, K. Bhattacharyya and K. B. Eiseenthal, *J. Phys. Chem.*, 1988, **92**, 5074.
- M. C. Goh and K. B. Eiseenthal, *Chem. Phys. Lett.*, 1989, **157**, 101.
- Q. Du, R. Superfine, E. Freysz and Y. R. Shen, *Phys. Rev. Lett.*, 1993, **70**, 2313.
- Q. Du, E. Freysz and Y. R. Shen, *Science*, 1994, **264**, 826.
- J. P. Devlin and V. Buch, *J. Phys. Chem.*, 1995, **99**, 16534.
- J. P. Devlin, C. Joyce and V. Buch, *J. Phys. Chem. A*, 2000, **104**, 1974.
- G. L. Richmond, *Annu. Rev. Phys. Chem.*, 2001, **52**, 357.
- D. Maillard, M. Allavena and J. P. Perchard, *Spectrochim. Acta*, 1975, **31A**, 1523.
- A. Schriver, L. Schriver and J. P. Perchard, *J. Mol. Spectrosc.*, 1988, **127**, 125.
- G. Herzberg, *Molecular Spectra and Molecular Structure. II. Infrared and Raman Spectra of Polyatomic Molecules*, D. Van Nostrand Company, Inc., Princeton, NJ, vol. II, 1945.
- M. Falk and P. A. Giguère, *Can. J. Chem.*, 1958, **36**, 1121.
- A. R. Davis and R. M. Chatterjee, *J. Solution Chem.*, 1975, **4**, 399.
- B. Meyer, M. Ospina and L. B. Peter, *Anal. Chim. Acta*, 1980, **117**, 301.
- F. A. Cotton and G. Wilkinson, *Advanced Inorganic Chemistry*, John Wiley & Sons, New York, 2nd edn., 1966.
- Q. Shi, P. Davidovits, J. T. Jayne, D. R. Worsnop and C. E. Kolb, *J. Phys. Chem. A*, 1999, **103**, 8812.
- R. H. Maybury, S. Gordon and J. J. Katz, *J. Chem. Phys.*, 1955, **23**, 1277.
- F. Fleyfel, H. H. Richardson and J. P. Devlin, *J. Phys. Chem.*, 1990, **94**, 7032.
- M. Foster and G. E. Ewing, *Surf. Sci.*, 1999, **427-428**, 102.
- M. C. Foster and G. E. Ewing, *J. Chem. Phys.*, 2000, **112**, 6817.
- J. Boniface, Q. Shi, Y. Q. Li, J. L. Cheung, O. V. Rattigan, P. Davidovits, D. R. Worsnop, J. T. Jayne and C. E. Kolb, *J. Phys. Chem. A*, 2000, **104**, 7502.

Reaction of Gaseous Nitric Oxide with Nitric Acid on Silica Surfaces in the Presence of Water at Room Temperature

N. A. Saliba, H. Yang, and B. J. Finlayson-Pitts*

Department of Chemistry, University of California, Irvine, Irvine, California 92697-2025

Received: June 19, 2001; In Final Form: August 27, 2001

The reaction of gaseous NO with HNO₃ on borosilicate glass in the presence of water was studied as a function of surface water coverage at 298 K and a total pressure of one atm in N₂. The loss of gaseous NO and the formation of NO₂ were measured in a long path cell using FTIR. The glass walls of the cell provided the surface upon which the chemistry occurred. Water coverages on thin glass cover disks were determined in a separate apparatus by measuring the intensity of the infrared band of liquid water at 3400 cm⁻¹. Approximately one monolayer was present on the surface at 20% RH and 12 monolayers at 100% RH. The rate of the reaction of NO with HNO₃ on the surface was the largest under conditions where approximately three surface monolayers of water were present on the surface. We propose a model for this reaction in which HNO₃, added first to the dry cell, hydrogen-bonds to the silanol groups on the surface. The first step in the reaction is believed to be HNO_{3(surface)} + NO_(g) → HONO_(surface) + NO_{2(g)}. Subsequently, HONO on the surface reacts with HNO₃ to generate solvated N₂O₄ as a product. Dissociation of N₂O₄ generates NO₂ as the final gas phase product. This chemistry is potentially important in “renoxification” of the boundary layer of polluted urban atmospheres where silica surfaces are plentiful in particles, soils and building materials, as well as globally in the free troposphere where dust particles are present.

I. Introduction

More than five decades of laboratory studies have shown that oxides of nitrogen react on surfaces in the presence of water. For example, Smith¹ noted during gas-phase studies of the reaction of NO with HNO₃ that there appeared to be a surface reaction dependent on water vapor. Such heterogeneous reactions may be potentially important in the atmosphere where oxides of nitrogen, present as air pollutants from combustion processes, are in contact with many surfaces in the form of suspended particles as soil, roads, buildings, and plants.

Despite the well-recognized occurrence of heterogeneous chemistry for the oxides of nitrogen, the kinetics and mechanisms of these reactions are not well understood. One difficulty arises in simultaneously measuring surface and gas-phase reaction species. However, recent infrared spectroscopic studies of heterogeneous hydrolysis of NO₂ on silica surfaces conducted by Grassian and co-workers² as well as by this laboratory,³ showed that this well-known^{4–16} reaction



produces N₂O₄ as a key intermediate on the surface. HNO₃ was also observed spectroscopically on the surface as hypothesized in the previous studies^{4–16} where only gas-phase measurements could be made, or nitrate ions measured in washings from the surface after reaction.

In subsequent studies, Mochida and Finlayson-Pitts¹⁷ showed that gaseous NO reacts with HNO₃ on a “wet” porous glass to generate nitrogen dioxide as the major gas-phase product, along with small amounts of gas-phase HONO. Thus, the mechanism

of the reaction was proposed in two steps as described below



followed by subsequent reactions such as



or



The net reaction is



If all reactants and products are in the gas phase, reaction 2 is close to thermoneutral. However, the free energy change for reaction 2 with typical atmospheric concentrations of the reactants and products is negative, so that it has been proposed to be potentially feasible on surfaces in the atmosphere.¹⁸

Nitric acid is known to be readily taken up on a variety of surfaces, e.g., soil and its components such as silica.^{19–22} Model studies^{23,24} suggest that this uptake could impact NO_x and O₃ in the troposphere. This process could also contribute to “renoxification” of the atmosphere and better reconcile field and modeling experiments,^{25,26} especially if HNO₃ produces photochemically reactive species such as NO₂ and HONO. Thus, a discrepancy has been reported between the measured ratio of [HNO₃]/[NO_x] ≈ 5 in the free troposphere and the values of 15–100 predicted by models.^{25,26} Although there are several hypotheses regarding the source of this discrepancy such as

* To whom correspondence should be addressed: E-mail bfinlay@uci.edu. Phone: (949) 824-7670. Fax: (949) 824-3168.

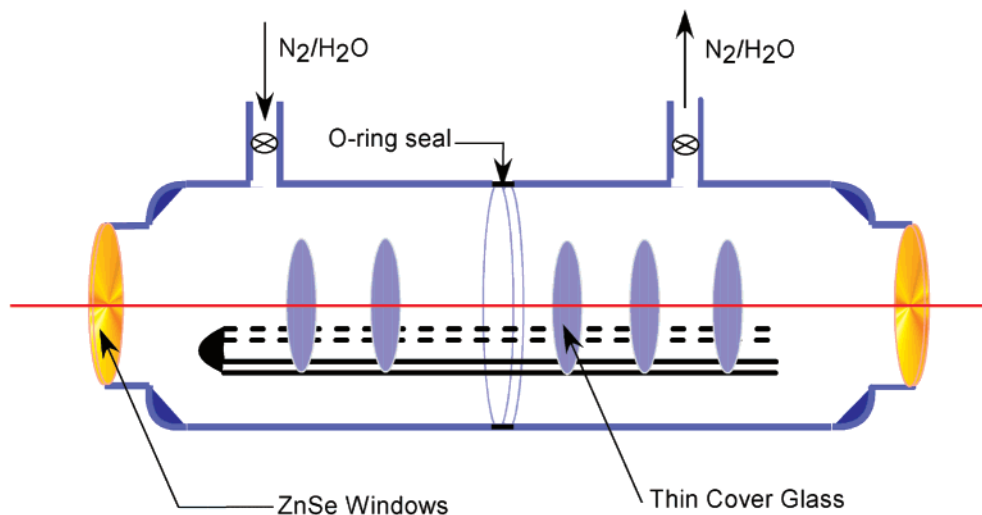


Figure 1. Cell used to measure water coverage on the borosilicate cover glass disks.

liquid-phase reactions of HCHO with HNO₃ in aerosols and cloud droplets, or reactions on soot,^{25–27} the cause remains unknown.

To better understand the uptake and potential reactions of HNO₃ on surfaces, we have carried out further studies of the reaction of gaseous NO with HNO₃ on a smooth borosilicate glass surface as a function of varying amounts of surface-adsorbed water. The relationship between the gas phase water vapor concentration and the amount of water on the surface was established in a newly designed experimental apparatus using transmission FTIR and thin cover glass disks. These studies provide insight into the reactive forms of nitric acid on the surface and the reaction mechanism. The atmospheric implications are discussed.

II. Experimental Section

A. Measurements of Water Coverage on Thin Borosilicate Glass Disks. The amount of liquid water adsorbed on thin cover glass disks at different relative humidities (RH) was determined by transmission infrared spectroscopy using the cell shown in Figure 1. The thin cover glass samples were thin Micro Cover Glasses (VWR Scientific, Inc.) with 0.13 to 0.17 mm thickness and 25 mm diameter. The cell, made of Pyrex glass, was 3.2 cm in diameter, 11 cm in length and capped with infrared-transmitting ZnSe windows. To increase the weak adsorbed H₂O signal, five disks of cover glass were placed in thin slots along a U-shaped glass rod, giving a total of 10 glass surfaces for water uptake.

A mixture of water vapor in N₂ at various relative humidities was generated by diluting a 100% RH stream, obtained by bubbling N₂ through Nanopure water (Barnstead, 18 MΩ cm), with dry N₂. The flow rates were controlled by calibrated Matheson TF 1050 flowmeters. Spectra were collected at 0.5 cm⁻¹ resolution with 1024 co-added scans and a total scan time of 14.5 min. A background spectrum was obtained after the cell and thin cover glass disks had been purged with dry N₂ for 24 h. Reference spectra of gas-phase water at different relative humidities were measured without the cover glass disks and subtracted before integration.

B. Reaction of Gaseous NO with HNO₃ On a Borosilicate Glass Surface. These experiments were performed in a long path infrared cell mounted vertically in the sample compartment of an FTIR spectrometer (Mattson, Cygnus) and equipped with an MCT detector. All experiments were carried out at 1 cm⁻¹

resolution with 150 co-added scans and a total scan time of 3.9 min. The cell consists of a borosilicate glass cylinder (10 cm diameter × 91.4 cm length) and two stainless steel rods holding the mirrors (Al with a silicon monoxide protective coating) which are attached to two stainless steel plates at each end of the cell. To avoid reactions of the gases with the stainless steel, the metal surfaces were coated with halocarbon wax (Halocarbon Products Corp., Series 1500). The optical base path length was 0.8 m, with a total path length of 38.4 m. The long path cell was wrapped in a dark cloth to prevent photolysis of reactants and products.

Dry, gaseous HNO₃ obtained from the vapor above an HNO₃/H₂SO₄ mixture (1:2 v:v) was first admitted to the cell. HNO₃ was allowed to adsorb onto the cell walls over five minutes. The remaining gas-phase HNO₃ was then pumped out, and this conditioning/adsorbing process was repeated at least three times. An NO concentration of (0.65–40) × 10¹⁵ molecule cm⁻³ was then added into the cell as a mixture with N₂. Initial relative humidities of 0, 20, 30, 40, 50 and 70% were obtained by adding a portion of dry N₂ followed by bubbling N₂ (100% humid) through a fritted glass immersed in water to give a total pressure of 1 atm. Gaseous reactants and products in the long path cell were measured using FTIR starting immediately after the addition of the reactants, for up to 350 min reaction time. Loss of NO and formation of gaseous NO₂ and HONO were measured using their absorption bands at 1876, 2900, and 1264 cm⁻¹, respectively.

Spectra of these species were quantitatively analyzed using a least-squares fitting procedure described in detail by Gomer et al.²⁸ The concentration of each species is determined relative to a reference spectrum of known concentration. Absolute concentrations for NO and NO₂ reference spectra were determined using calibrations of the pure gases. Nitrous acid was quantified using infrared cross sections for 1264 cm⁻¹ peak determined by Barney et al.^{29,30} in this laboratory.

Materials. HNO₃ was 70.1 wt % (Fisher) and H₂SO₄ was 95.8 wt % (Fisher). Nitric oxide (Matheson 99%) was purified by passing it rapidly through a liquid nitrogen trap. The N₂ was 99.999% (Oxygen Services Company) and used as received.

III. Results and Discussion

A. Water Coverage on Glass. Figure 2a shows typical infrared spectra in the 3800 to 2800 cm⁻¹ region where absorptions due to the stretching vibrations of water occur. The

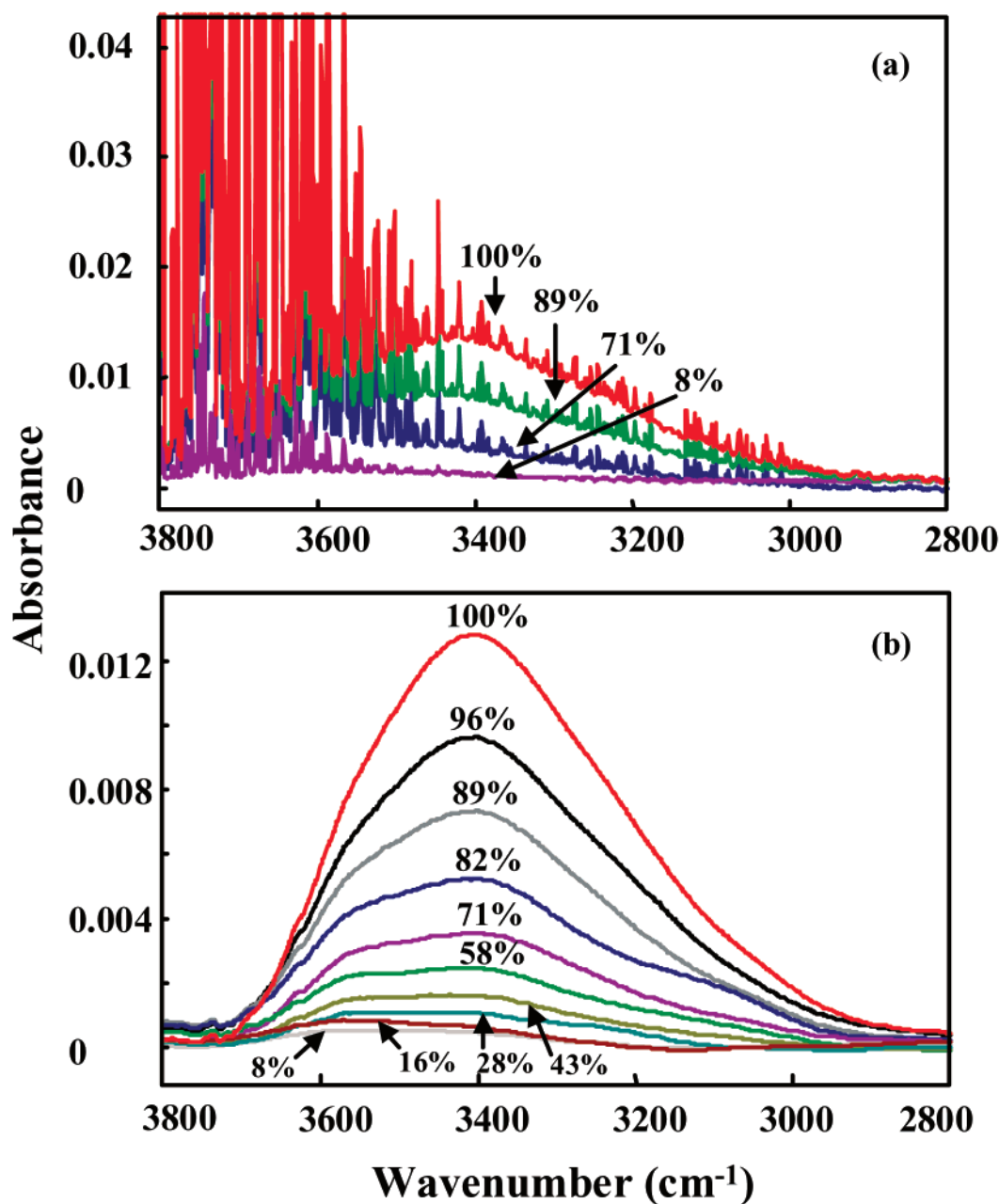


Figure 2. (a) Typical absorption spectra of water adsorbed on thin cover glass disks at different relative humidities and at room temperature; (b) spectra from (a) plotted at lower resolution (4 cm^{-1}) with gas-phase water subtracted and smoothing of the spectra.

ν_1 stretch of gas-phase water is centered at 3652 cm^{-1} and the asymmetric ν_3 stretch at 3756 cm^{-1} .³¹ These bands appear as a series of sharp rotational lines superimposed on a broad band centered at $\sim 3400\text{ cm}^{-1}$ at the highest water coverages. The broad band is due to liquid water, and is red-shifted by up to 200 wavenumbers compared to the gas phase due to intermolecular hydrogen bonding;³² the shift in band position from the gas to the liquid is also accompanied by an increase in the absorption coefficient.³²

Figure 2b shows more clearly the surface water band. These spectra were obtained by subtracting from Figure 2a the contribution from gas-phase water, converting the spectra to a lower resolution (4 cm^{-1} instead of 0.5 cm^{-1} which is adequate for this broad band), and smoothing them. These show that the surface water peak shifts from $\sim 3600\text{ cm}^{-1}$ to $\sim 3400\text{ cm}^{-1}$ as the water coverage increases, and at 100% RH, the spectrum becomes indistinguishable from that of liquid water. The shift

toward lower wavenumbers in the presence of more surface water reflects a trend in which water changes from strong interactions with the surface with some hydrogen-bonding to adjacent water molecules, to three-dimensional water hydrogen-bonding as is the case of the bulk liquid. This is similar to the effects observed by Ewing and co-workers^{33,34} on the infrared spectrum of water adsorbed on NaCl crystals, in which the center of the 3400 cm^{-1} band was red-shifted to 3500 cm^{-1} at submonolayer coverages.

The number of monolayers (ML) of adsorbed H_2O on glass as a function of relative humidity was calculated from the integrated absorbance, \tilde{A} (cm^{-1}), and the known integrated absorption coefficient for liquid water,^{33–35} $\bar{\sigma} = 6.1 \times 10^{-17}\text{ cm molecule}^{-1}$ (base 10)

$$ML = \tilde{A} / (1.0 \times 10^{15} N \bar{\sigma}) \quad (1)$$

where $N = 10$ is the number of thin cover glass surfaces and

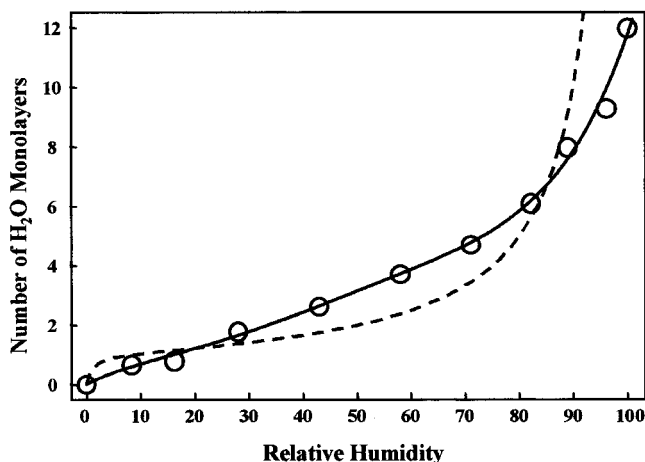


Figure 3. Number of monolayers of adsorbed H₂O on cover glass as a function of relative humidity. The solid line is a fit to the data and the dotted line shows a BET isotherm for multilayer adsorption.

1×10^{15} molecule cm⁻² is the surface density of one monolayer of water, based on an area per water molecule of 10 \AA^2 .³⁶ An integrated absorption coefficient of $\bar{\sigma} = 6.1 \times 10^{-17}$ cm molecule⁻¹ was used for all water coverages on the surface. In order to avoid systematic errors in determining the number of water layers that might be introduced by the smoothing procedure, the spectra used for quantification were the 0.5 cm^{-1} spectra (Figure 2a) but with the contribution of gas-phase water subtracted out. Figure 2 shows the blue shift in the absorption spectrum due to a strong interaction between water and the surface at low coverages; it is therefore expected that the absorption coefficient will also be smaller than that for bulk liquid water at these lower coverages. However, given the uncertainty inherent in estimating the correction factor for the absorption coefficient for such a perturbed liquid-surface system, we have used the bulk liquid water value at all coverages.

Figure 3 summarizes the number of monolayers of water on the glass surface as a function of the relative humidity. The data suggest a Type II isotherm³⁷ characteristic of multilayer adsorption. The dotted line shown in Figure 3 represents a fit for a BET isotherm of the form³⁷

$$\text{fractional coverage} = \frac{c_B RH}{(1 - RH)[1 + (c_B - 1)RH]} \quad (\text{II})$$

where $c_B = 100$ is a constant. We understand that although the fit could be improved with a multi-parameter model, the data in Figure 3 are adequate for determining the number of water layers under our experimental conditions.

Our data are consistent with literature reports of the uptake of water on glass,³⁸ particularly given the different analytical methods that were used and the different treatments under which the glass surfaces were prepared. It is interesting, for example, to note that in 1918 Langmuir reported that 4.5 layers of water were adsorbed on glass in air.³⁹ This would be consistent with ~70% RH in their laboratory.

There is a great deal of evidence that the first few layers of water on silica surfaces interact strongly with the surface and do not behave like bulk liquid water. At least the first three layers of water are known to be strongly perturbed.^{40–42} In addition, water is known to form clusters on the surface at low coverages, rather than forming a uniform thin film.^{40–43} As a result, in our experimental system, the water on the surface is better thought of as clusters at relative humidities at or below 50%. Therefore, one, two or three layers of water on the surface

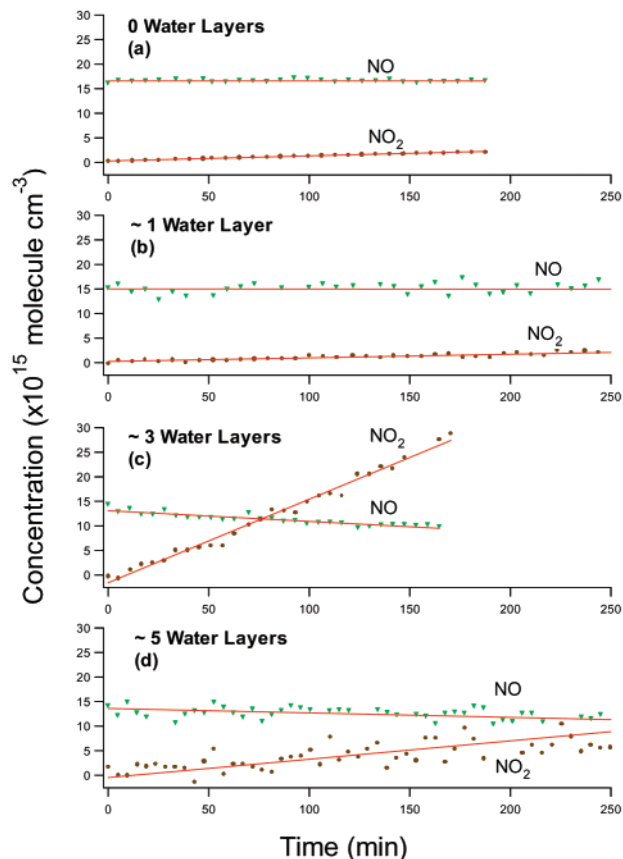


Figure 4. Decay of gas-phase NO and formation of NO₂ in the long path cell whose walls had first been exposed to HNO₃. (a) 0% RH and $[\text{NO}]_0 = 1.6 \times 10^{16}$ molecule cm⁻³ (b) 30% RH and $[\text{NO}]_0 = 1.4 \times 10^{16}$ molecule cm⁻³; (c) 50% RH and $[\text{NO}]_0 = 1.4 \times 10^{16}$ molecule cm⁻³; (d) 70% RH and $[\text{NO}]_0 = 1.4 \times 10^{16}$ molecule cm⁻³. The total pressure was 1 atm in N₂ at room temperature.

are used in the context of “equivalent numbers of layers” because the water is unevenly distributed.

We assume in the experiments with HNO₃ on the surface that preadsorbing HNO₃ on the glass does not alter the subsequent uptake of water. Although Bogdan and Kulmala⁴⁴ reported that HNO₃ and HCl do affect the uptake of water on silica powder, we did not observe an increase in the 5275 cm^{-1} combination infrared band of water on silica powder when it had been “dosed” with HNO₃ before exposure to water vapor.⁴⁵ (This band was followed to avoid interfering absorptions in the $3000\text{--}3500 \text{ cm}^{-1}$ region by HNO₃ itself).

B. Reaction of Gaseous NO with HNO₃–H₂O Thin Surface Films. Figure 4a shows the results of a typical experiment in which a mixture of NO in N₂ was added to the cell in the absence of water after dosing with HNO₃. There was no detectable loss of NO and only a slow formation of NO₂. This could be due to some thermal oxidation of NO by molecular oxygen impurities from small amounts of air leakage into the cell during these long experiments, or to a very slow reaction between NO and HNO₃ on the cell surface. With approximately one monolayer of water, a slightly higher rate of NO₂ formation was observed (e.g., Figure 4b). With three monolayers of water, the reaction was much faster, with measurable losses of NO and rapid formation of NO₂ (e.g., Figure 4c). However, with a further increase in water coverage to five layers (Figure 4d), the rate of formation of NO₂ again decreased.

The stoichiometry $\Delta[\text{NO}_2]/\Delta[\text{NO}]$ was calculated from the slopes of the lines obtained when NO and NO₂ were plotted as

TABLE 1: Summary of Long Path Cell FTIR Measurements of the Decay of NO and Formation of NO₂ in the Reaction of NO with HNO₃ Adsorbed on the Cell Walls at Different Water Coverages on the Surface

number of surface water layers (%RH)	experiment #	[NO] ₀ (10 ¹⁵ molecule cm ⁻³)	-d[NO]/dt (10 ¹³ molecule cm ⁻³ min ⁻¹)	d[NO ₂]/dt (10 ¹³ molecule cm ⁻³ min ⁻¹)	ΔNO ₂ /ΔNO ^a	average ± 2σ
1.9 (30)	1	4.0	0.12	0.35	2.9	3.8 ± 1.1
	2	7.2	0.14	0.47	3.3	
	3	9.5	0.46	2.5	5.4	
	4	15.0	0.63	2.2	3.5	
2.5 (40)	1	2.6	0.08	0.2	2.5	3.2 ± 0.6
	2	8.0	0.42	1.5	3.6	
	3	11.0	0.59	2.2	3.7	
	4	15.0	1.1	3.3	3.0	
3 (50)	1	0.65	0.095	0.35	3.7	3.3 ± 0.4
	2	3.2	0.36	1.1	3.0	
	3	7.0	0.91	2.6	2.8	
	4	8.2	2.0	7.1	3.6	
	5	14	4.3	15	3.5	
	6	22	7.3	20	2.7	
	7	40	11	40	3.6	

^a From the ratio of {d[NO₂]/dt}/{d[NO]/dt}.

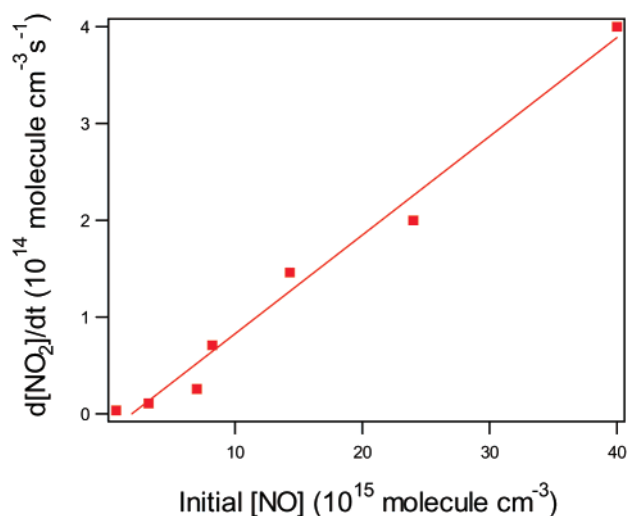


Figure 5. Rate of NO₂ formation as a function of initial NO concentration at 1 atm pressure in N₂ and 50% RH.

a function of time between 0 and 300 min for the runs where 2–3 layers of water were on the surface. Table 1 summarizes these data. The weighted average is $\Delta[\text{NO}_2]/\Delta[\text{NO}] = 3.3 \pm 1.0$ (2σ). Small concentrations of HONO ($\sim 10^{14}$ molecule cm⁻³) were detected at larger reaction times; for example, with an initial NO concentration of 2.2×10^{16} molecule cm⁻³ and three layers of surface water, HONO at 260 min was $\sim 2 \times 10^{14}$ molecule cm⁻³ compared to NO₂ at 4×10^{16} molecule cm⁻³. Because HONO was detectable when significant amounts of NO₂ had been formed, it may have been generated at least in part by the surface NO₂ hydrolysis reaction.^{2–16}

Figure 5 shows the rate of NO₂ formation in the long path cell as a function of the initial NO concentrations under conditions where three layers of surface water were present, indicating that the reaction generating NO₂ is first-order in NO.

To ensure that NO₂ formation was due to reaction 5, blank runs were also carried out in which NO was introduced alone into the clean cell whose walls had been cleaned by rinsing with Nanopure water. Spectra of NO in the cell at 0 and 50% RH were collected as a function of time; no significant formation of NO₂ was observed. Similarly, blank runs in which nitric acid alone was introduced into the cell at various RH also gave no reaction.

These experiments clearly show that the rate of the heterogeneous reaction of gaseous NO with HNO₃ on borosilicate glass depends strongly on the presence of water on the surface. The reaction was so slow as to be undetectable in the absence of water, but accelerated as the number of surface water layers approached three. With further increases in water, however, the rate again decreased.

Nitric acid is expected to hydrogen bond with the polar silanol groups (–Si–OH) at the silica surface.^{40,46,47} Independent evidence for this HNO₃–silica interaction was obtained⁴⁵ from the absorption spectrum of porous glass and silica before and after dosing with HNO₃. The sharp peak at ~ 3750 cm⁻¹ due to the O–H stretch of free (i.e., not hydrogen-bonded) –SiOH surface groups³² decreased upon adsorption of HNO₃ but recovered when HNO₃ was removed by extensive pumping. Thus, we attribute the decrease in the peak to a reversible hydrogen-bonding of HNO₃ to the silanol group. A similar change has been observed by Goodman et al.²¹ when silica powders were exposed to gaseous HNO₃. The strength of this hydrogen-bond can be estimated from ab initio calculations by Tao et al.⁴⁸ of the binding of nitric acid to water in the gas phase. The binding energy was estimated to be ~ 30 kJ mol⁻¹, with two hydrogen bonds formed between the molecules. A reasonable value for one hydrogen bond between water and nitric acid is therefore 15 kJ mol⁻¹, which lies in the range of 12–24 kJ mol⁻¹ reported for a variety of hydrogen bonds.³²

When small amounts of water are adsorbed on silica surfaces, it is believed to cluster on the surface rather than forming a uniformly distributed layer. This is attributed to an enthalpy of adsorption of water on water clusters that is greater than that for adsorption on an isolated silanol group (44 kJ mol⁻¹ vs 25 kJ mol⁻¹).⁴⁰ When nitric acid has been preadsorbed on the surface as in these experiments, water may cluster around the surface HNO₃. An alternate possibility is that water displaces HNO₃ from the silanol group onto the adjacent surface, but that HNO₃ remains in close proximity to the water now clustered around the –SiOH group; the latter is suggested by the greater strength of the hydrogen bond between water and the –SiOH group (25 kJ mol⁻¹) compared to that between nitric acid and water, estimated to be ~ 15 kJ mol⁻¹. When both water and nitric acid are present, water stabilizes HNO₃ by as much as 30 kJ mol⁻¹ relative to the gas phase, assuming two hydrogen-bonds to nitric acid are involved.

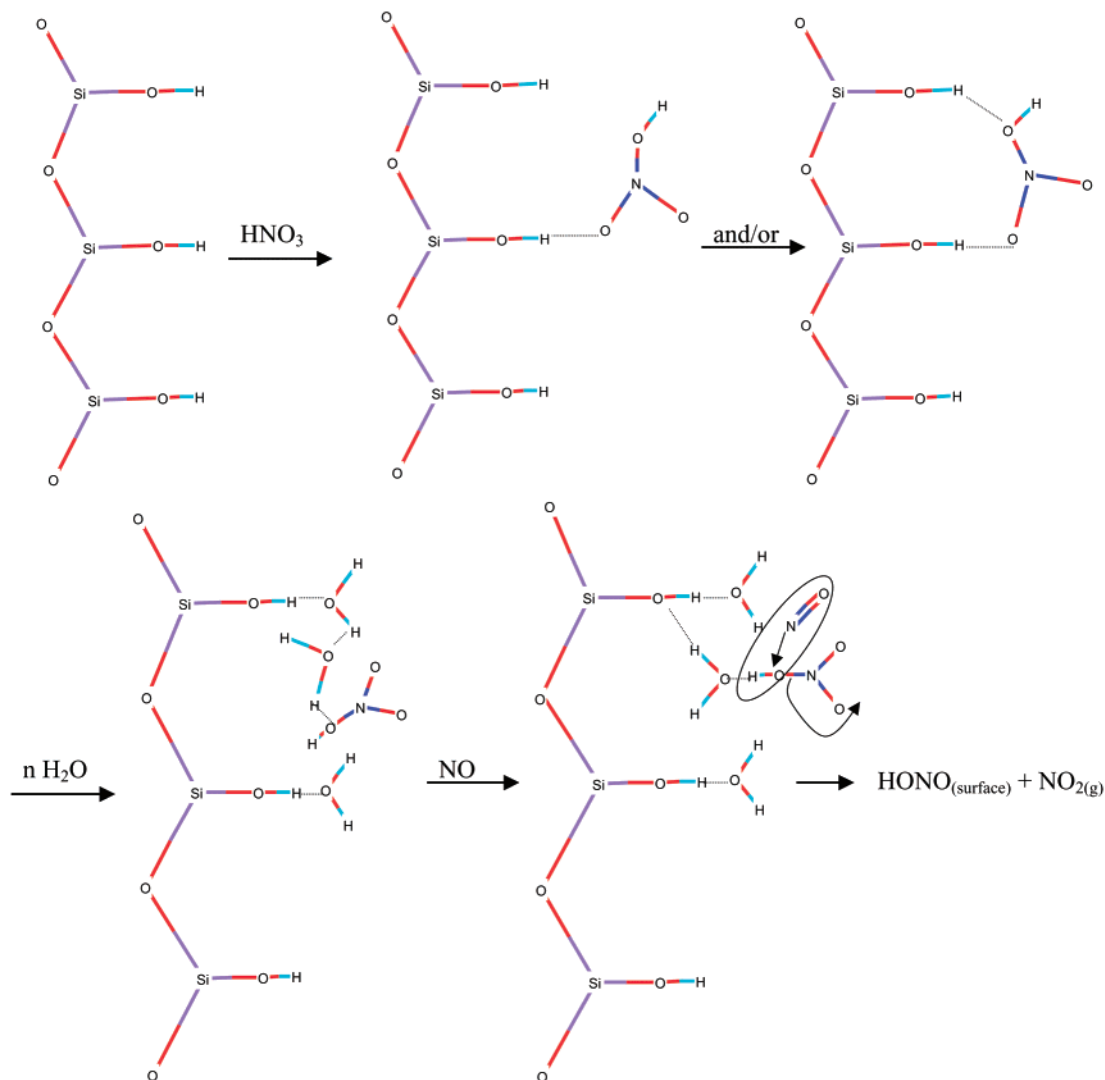


Figure 6. Model of reaction of HNO_3 with NO on a silica surface in the presence of water.

It is relevant that HNO_3 readily desorbs back into the gas phase in a dry cell but most of it remains on the surface where water is present. In a dry cell, the amount of HNO_3 desorbing into the gas-phase varies, depending on the condition of the cell walls. A typical peak absorbance of $\sim 0.3\text{--}0.6$ at 896 cm^{-1} is observed after dosing HNO_3 in a dry cell, compared to ~ 0.1 after water vapor is added. Figure 6 summarizes this model of nitric acid and water on the surface.

Gaseous NO introduced in the cell reacts with the adsorbed HNO_3 surrounded by water molecules to produce NO_2 and HONO



If the reactants and products in reaction 2 are in the gas phase, the standard enthalpy of reaction is $\Delta H_{298\text{K}}^0 = -1.4\text{ kJ mol}^{-1}$. However, our experiments show that in order for reaction 2 to occur, (i) HNO_3 must be on the surface, and (ii) water must be present. As discussed above, nitric acid hydrogen-bonded to the surface and to a water molecule is estimated to be stabilized compared to the gas phase³² by $\sim 30\text{ kJ mol}^{-1}$, making the reaction endothermic by $\sim 29\text{ kJ mol}^{-1}$.

However, water is also capable of solvating the reaction products. The Henry's Law constants, $49\text{ L mol}^{-1}\text{ atm}^{-1}$ for HONO compared to 1.4×10^{-2} for NO_2 ,^{19,49} show that nitrous acid interacts more strongly with water than does NO_2 , and

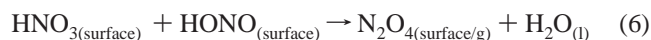
hence, solvation of HONO as it is formed should be particularly important. The difference between the enthalpy of formation⁵⁰ of HONO in the gas phase compared to solution (undissociated HONO) is 40 kJ mol^{-1} . This is more than sufficient to make the reaction between NO and surface hydrogen-bonded HNO_3 exothermic. The product NO_2 will be formed initially in the water cluster and solvation of this product will further increase the reaction exothermicity. Because NO_2 is much less soluble, it will be released to the gas phase as shown in Figure 6, whereas HONO remains on the surface to undergo further reaction with adsorbed nitric acid.

As discussed earlier, the subsequent chemistry of HONO on the surface may either be the reaction with another surface HNO_3 or the bimolecular reaction between two HONO molecules on the surface. Although neither can be firmly ruled out based on our experiments, the former seems more likely

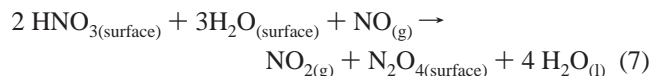


The enthalpy of this gas-phase reaction is $\Delta H_{298\text{K}}^0 = +39\text{ kJ mol}^{-1}$. Assuming, as discussed previously, that HNO_3 is stabilized by 30 kJ mol^{-1} , HONO is stabilized by 40 kJ mol^{-1} due to solvation, and the water is generated in the liquid state, the reaction enthalpy becomes $+65\text{ kJ mol}^{-1}$. However, it is mechanistically reasonable to suggest that the $\text{HONO} - \text{HNO}_3$ reaction initially generates N_2O_4 rather than 2NO_2 , and the

reaction then becomes



If the N_2O_4 product is in the gas phase, the standard enthalpy change for reaction 4 becomes $+8 \text{ kJ mol}^{-1}$. However, solvation of N_2O_4 as it is formed will stabilize this product, increasing the reaction exothermicity. N_2O_4 is much more soluble than NO_2 in water, with its Henry's Law constant¹⁹ being 2 orders of magnitude larger than that for NO_2 . As an upper limit, we estimate an additional gain of 29 kJ mol^{-1} based on the difference between gaseous and liquid N_2O_4 . Dissociation of N_2O_4 then releases NO_2 into the gas phase. Given the critical role played by water, the most accurate representation of the overall reaction may be



This model is consistent with the work of Bogdan and co-workers^{44,51,52} who studied the uptake of nitric acid and water on silica powders. They reported that the concentration of nitric acid was larger in the layers adjacent to the silica surface⁵¹ and that the enthalpies of fusion of microdroplets of nitric acid and water on these surfaces are lower than for the bulk acid–water solutions.⁵² Thus, nitric acid and water on silica surfaces cannot be treated as bulk aqueous systems.

The reaction with five layers of water present on the surface (Figure 4) is much slower than that with two to three layers of water. This is likely due to the fact that water behaves like a bulk liquid at these higher coverages.^{40–42} Thus, under these conditions the surface water may more closely resemble a bulk aqueous solution of nitric acid, rather than surface-adsorbed clusters as proposed in the model in Figure 6. Nitric acid is well-known to dissociate in dilute aqueous solutions, even on surfaces. Supporting this possibility is the observation by Goodman et al.²¹ and by this laboratory⁴⁵ that addition of water vapor at high relative humidities when HNO_3 is adsorbed on silica leads to a decrease in the molecular nitric acid peak and an increase in nitrate ion peaks. At the other extreme, if the film is highly concentrated in nitric acid, molecular HNO_3 associates with water molecules to form hydrates.^{53–59} Under these conditions, the vapor pressure of nitric acid in equilibrium with the solution is quite high (of the order of Torr)⁵⁶ and less nitric acid may remain on the silica surface for reaction.

Atmospheric Implications. Silica surfaces are ubiquitous in the troposphere in the form of dust particles, soil and building materials. Nitric acid is well-known to be readily taken up by such surfaces.^{19–22} The studies presented here suggest that the sticking of nitric acid to such surfaces is more efficient in the presence of surface water; given that water vapor is always present in the lower atmosphere, this will not be a limiting factor under atmospheric conditions. Our studies show that with the appropriate amount of water on the surface, HNO_3 can potentially be converted into NO_2 . Such “renoxification” has significant implications for the chemistry of both the free troposphere and polluted urban areas. In order for such chemistry to occur, there must be sufficient water on the surface to stabilize the HNO_3 and to solvate the reaction products. On the other hand, if there is so much water on the surface that it behaves like a bulk liquid and the nitric acid is largely dissociated, the reaction does not occur. The data presented here with approximately three surface monolayers of water imply that the reaction probability for loss of NO on the cell walls under these conditions is of the order of 10^{-8} . However, this cannot be

directly applied to the atmosphere because the actual form of nitric acid on the cell walls and how that relates to atmospheric conditions is not known. Understanding the amounts of water on surfaces in the lower atmosphere and the form of surface nitric acid are key to assessing the importance of this chemistry under various atmospheric conditions. Increased reactive surface areas of soils⁶⁰ compared to the geometric surface area at the earth's surface must also be taken into account. Finally, the reaction kinetics of NO with the nitric acid–water clusters needs to be directly assessed. Such studies are currently underway in this laboratory.

IV. Conclusions

Gaseous nitric oxide reacts at room temperature with nitric acid on a glass surface in the presence of water. The major gaseous product is NO_2 , with the overall reaction stoichiometry corresponding to 3 NO_2 produced per NO reacted. The reaction is first order with respect to NO. These experimental observations are consistent with the overall reaction $2 \text{HNO}_{3(\text{surface})} + \text{NO}_{(\text{g})} \rightarrow 3 \text{NO}_{2(\text{g})} + \text{H}_2\text{O}_{(\text{l})}$. However, the presence of water on the surface is critical. Its role is likely to solvate the HONO and N_2O_4 products generated in two steps that make up the overall reaction. We propose a model in which HNO_3 is hydrogen-bonded to the surface in close proximity to water. As a result, the overall reaction may be better represented as follows: $2 \text{HNO}_{3(\text{surface})} + 3\text{H}_2\text{O}_{(\text{surface})} + \text{NO}_{(\text{g})} \rightarrow \text{NO}_{2(\text{g})} + \text{N}_2\text{O}_{4(\text{surface})} + 4 \text{H}_2\text{O}_{(\text{l})}$. This chemistry is potentially important in “renoxification” of HNO_3 in the boundary layer of polluted urban atmospheres where silica surfaces are plentiful in particles, soils and building materials, as well as globally in the free troposphere where dust particles are present.

Acknowledgment. We are grateful to the California Air Resources Board for support of this work. We also thank J. N. Pitts, Jr. for helpful discussions and encouragement to study these heterogeneous systems, V. H. Grassian, G. E. Ewing, D. Tobias and P. Jungwirth for providing preprints prior to publication and for helpful discussions, and J. Meyer for technical assistance.

References and Notes

- (1) Smith, J. H. *J. Am. Chem. Soc.* **1947**, *69*, 1741.
- (2) Goodman, A. L.; Underwood, G. M.; Grassian, V. H. *J. Phys. Chem. A* **1999**, *103*, 7217.
- (3) Barney, W. S.; Finlayson-Pitts, B. J. *J. Phys. Chem. A* **2000**, *104*, 171.
- (4) Sakamaki, F.; Hatakeyama, S.; Akimoto, H. *Int. J. Chem. Kinet.* **1983**, *15*, 1013.
- (5) Pitts, J. N.; Sanhueza, E.; Atkinson, R.; Carter, W. P. L.; Winer, A. M.; Harris, G. W.; Plum, C. N. *Int. J. Chem. Kinet.* **1984**, *16*, 919.
- (6) Svensson, R.; Ljungstrom, E.; Lindqvist, O. *Atmos. Environ.* **1987**, *21*, 1529.
- (7) Jenkin, M. E.; Cox, R. A.; Williams, D. J. *Atmos. Environ.* **1988**, *22*, 487.
- (8) Febo, A.; Perrino, C. *Atmos. Environ.* **1991**, *25A*, 1055.
- (9) Bambauer, A.; Brantner, B.; Paige, M.; Novakov, T. *Atmos. Environ.* **1994**, *28*, 3225.
- (10) Mertes, S.; Wahner, A. *J. Phys. Chem.* **1995**, *99*, 14 000.
- (11) Harrison, R. M.; Peak, J. D.; Collins, G. M. *J. Geophys. Res.* **1996**, *101*, 14 429.
- (12) Lammel, G.; Cape, J. N. *Chem. Soc. Rev.* **1996**, *25*, 361.
- (13) Kleffmann, J.; Becker, K. H.; Wiesen, P. *Atmos. Environ.* **1998**, *32*, 2721.
- (14) Kleffmann, J.; Becker, K. H.; Wiesen, P. *J. Chem. Soc., Faraday Trans.* **1998**, *94*, 3289.
- (15) Harrison, R. M.; Collins, G. M. *J. Atmos. Chem.* **1998**, *30*, 397.
- (16) Wingen, L.; Yang, H.; Sumner, A. L.; Finlayson-Pitts, B. J., in preparation, **2001**.

- (17) Mochida, M.; Finlayson-Pitts, B. J. *J. Phys. Chem. A* **2000**, *104*, 9705.
- (18) Fairbrother, D. H.; Sullivan, D. J. D.; Johnston, H. S. *J. Phys. Chem. A* **1997**, *101*, 7350.
- (19) Finlayson-Pitts, B. J.; Pitts, J. N. *Chemistry of the Upper and Lower Atmosphere: Theory, Experiments and Applications*; Academic Press: New York, 2000.
- (20) Padgett, P. E.; Bytnerowicz, A. *Atmos. Environ.* **2001**, *35*, 2405.
- (21) Goodman, A. L.; Bernard, E. T.; Grassian, V. H. *J. Phys. Chem. A* **2001**, *105*, 6443.
- (22) Hanisch, F.; Crowley, J. N. *J. Phys. Chem. A* **2001**, *105*, 3096.
- (23) Dentener, F. J.; Carmichael, G. R.; Zhang, Y.; Lelieveld, J.; Crutzen, P. J. *J. Geophys. Res.* **1996**, *101*, 22.
- (24) Underwood, G. M.; Song, C. H.; Phadnis, M.; Carmichael, G. R.; Grassian, V. H. *J. Geophys. Res.* **2001**, *106*, 18055.
- (25) Chatfield, R. B. *Geophys. Res. Lett.* **1994**, *21*, 2705.
- (26) Hauglustaine, D. A.; Ridley, B. A.; Solomon, S.; Hess, P. G.; Madronich, S. *Geophys. Res. Lett.* **1996**, *23*, 2609.
- (27) Lary, D. J.; Lee, A. M.; Toumi, R.; Newchurch, M. J.; Pirre, M.; Renard, J. B. *J. Geophys. Res.* **1997**, *102*, 3671.
- (28) Gomer, T.; Brauers, T.; Heintz, F.; Stutz, J.; Platt, U. *University of Heidelberg* 1995.
- (29) Barney, W. S.; Wingen, L. M.; Lakin, M. J.; Brauers, T.; Stutz, J.; Finlayson-Pitts, B. J. *J. Phys. Chem. A* **2000**, *104*, 1692.
- (30) Barney, W. S.; Wingen, L. M.; Lakin, M. J.; Brauers, T.; Stutz, J.; Finlayson-Pitts, B. J. *J. Phys. Chem. A* **2001**, *105*, 4166.
- (31) Herzberg, G. *Molecular Spectra and Molecular Structure. II. Infrared and Raman Spectra of Polyatomic Molecules*; D. Van Nostrand Company, Inc.: Princeton, N. J., 1945; Vol. II.
- (32) Pimentel, G. C.; McClellan, A. L. *The Hydrogen Bond*; W. H. Freeman: San Francisco, 1960.
- (33) Foster, M.; Ewing, G. E. *Surf. Sci.* **1999**, *427/428*, 102.
- (34) Foster, M. C.; Ewing, G. E. *J. Chem. Phys.* **2000**, *112*, 6817.
- (35) Weis, D. D.; Ewing, G. E. *J. Geophys. Res.* **1996**, *101*, 18 709.
- (36) Chattoraj, D. K.; Birdi, K. S. *Adsorption and the Gibbs Surface Excess*; Plenum Press: New York, 1984.
- (37) Masel, R. I. *Principles of Adsorption and Reaction on Solid Surfaces*; Wiley: New York, 1996.
- (38) Frazer, J. H. *Phys. Rev.* **1929**, *33*, 97.
- (39) Langmuir, I. *J. Am. Chem. Soc.* **1918**, *40*, 1361.
- (40) Iler, R. K. *The Chemistry of Silica*; Wiley: New York, 1978.
- (41) Icenhower, J. P.; Dove, P. M. Water Behaviour at Silica Surfaces. In *Adsorption on Silica Surfaces*; Papirer, E., Ed.; Marcel Dekker: New York, 2000; Ch. 9.
- (42) *Adsorption on Silica Surfaces*; Papirer, E., Ed.; Marcel Dekker: New York, 2000; Vol. 90.
- (43) Bogdan, A. Fumed Silica as a Host for Study of the Large Surface-to-Volume Ratio Problems in Finely Divided Aqueous Systems: Implications for the Atmosphere. In *Adsorption on Silica Surfaces*; Papirer, E., Ed.; Marcel Dekker: New York, 2000.
- (44) Bogdan, A.; Kulmala, M. *J. Colloid Interfac. Sci.* **1997**, *191*, 95.
- (45) Sumner, A. L.; Ramazan, K.; Rivera, A.; Finlayson-Pitts, B. J. **2001**, unpublished results.
- (46) Chuang, I.-S.; Kinney, D. R.; Bronnimann, C. E.; Ziegler, R. C.; Maciel, G. E. *J. Phys. Chem.* **1992**, *96*, 4027.
- (47) Bronnimann, C. E.; Zeigler, R. C.; Maciel, G. E. *J. Am. Chem. Soc.* **1988**, *110*, 2023.
- (48) Tao, F.-M.; Higgins, K.; Klemperer, W.; Nelson, D. D. *Geophys. Res. Lett.* **1996**, *23*, 1797.
- (49) Cheung, J. L.; Li, Y. Q.; Boniface, J.; Shi, Q.; Davidovits, P.; Worsnop, D. R.; Jayne, J. T.; Kolb, C. E. *J. Phys. Chem. A* **2000**, *104*, 2655.
- (50) Wagman, D. D.; Evans, W. H.; Parker, V. B.; Schumm, R. H.; Halow, I.; Balley, S. M.; Churney, K. L.; Nuttall, R. L. *J. Phys. Chem. Ref. Data* **1982**, *11*, Suppl. No. 2.
- (51) Bogdan, A.; Kulmala, M.; Gorbunov, B.; Kruppa, A. *J. Colloid Interfac. Sci.* **1996**, *177*, 79.
- (52) Bogdan, A.; Kulmala, M. *Geophys. Res. Lett.* **1999**, *26*, 1433.
- (53) Redlich, O.; Bigeleisen, J. *J. Am. Chem. Soc.* **1943**, *65*, 1883.
- (54) Redlich, O. *Chem. Rev.* **1946**, *39*, 333.
- (55) Miles, F. D. *Nitric Acid Manufacture and Uses*; Oxford University Press: London, 1961.
- (56) Davis, W. J.; DeBruin, H. J. *J. Inorg. Nucl. Chem.* **1964**, *26*, 1069.
- (57) Schwartz, S. E.; White, W. H. Solubility Equilibria of the Nitrogen Oxides and Oxyacids in Dilute Aqueous Solution. In *Advances in Environmental Science and Engineering*; Pfafflin, J. R., Ziegler, E. N., Eds.; Gordon and Breach Science Publishers: New York, 1981; Vol. 4; p 1.
- (58) Koller, J.; Hazdi, D. *J. Mol. Structure* **1991**, *247*, 225.
- (59) Molina, M. J.; Zhang, R.; Wooldridge, P. J.; McMahon, J. R.; Kim, J. E.; Chang, H. Y.; Beyers, K. D. *Science* **1993**, *261*, 1418.
- (60) Hodson, M. E.; Langan, S. J.; Kennedy, F. M.; Bain, D. C. *Geoderma* **1998**, *85*, 1.